Design and Synthesis of Novel Probes for the Monitoring of Potential Drug Targets in Sphingolipid Metabolism

Dissertation

Zur Erlangung des akademischen Grades
Doctor rerum naturalium
(Dr. rer. nat.)
im Fach Chemie

eingereicht an der

Mathematisch-Naturwissenschaftlichen Fakultät

der Humboldt-Universität zu Berlin

von

M.Sc. Zainelabdeen Hassep Mohamed Ahmed

Präsidentin der Humboldt-Universität zu Berlin
Prof. Dr.-Ing. Dr. Sabine Kunst

Dekan der Mathematisch-Naturwissenschaftlichen Fakultät
Prof. Dr. Elmar Kulke

Gutachter/in:

1. Prof. Dr. Christoph Arenz
2. Prof. Dr. Dorothea Fiedler
3. Prof. Dr. Michael Schäferling

Berlin, 2020

Tag der mündlichen Prüfung: 10. November 2020

Die vorgelegte Dissertation entstand in der Zeit von Oktober 2015 bis August 2020 am Institut für Chemie der Humboldt-Universität t zu Berlin.

Table of Contents

Kurzfassung

Ziel dieser Arbeit ist die Entwicklung neuer chemischer Sonden zur Überwachung der Aktivität von ASM sowohl in vitro als auch in vivo. Darüber hinaus wurde auch die Optimierung der angegebenen Sonden (besser: bereits publizierter Sonden) durchgeführt. Im ersten Teil dieser Studie wurden zwei Eu-Komplexe ausgehend von handelsüblicher Chelidaminsäure synthetisiert und führten zu einer guten Ausbeute mit hoher Reinheit. Die synthetisierten Sonden **4-D**$^+$ und **5-D**$^+$ wurden zum Nachweis verschiedener Phosphate und Carboxylatspezies verwendet. Sie wurden zur Überwachung der ASM-Aktivität durch den Nachweis des enzymatisch freigesetzten Phosphorylcholins (PC) eingesetzt. Trotz der vielversprechenden Abnahme der Lumineszenz von **4-D**$^+$ als Reaktion auf das anorganische PC zusätzlich zur Simulationsreaktion zur Änderung des SM / PC-Verhältnisses wurde in allen enzymatischen homogenen und heterogenen Experimenten ein allgemeiner Löscheffekt beobachtet. Der **5-D**$^+$ Komplex könnte zur Überwachung des ATP-hydrolysierenden Apyrase-Enzyms in Echtzeit verwendet werden.

Im zweiten Teil dieser Studie wurden verschiedene FRET- und monomarkierte ASM-Sonden entworfen und synthetisiert. Eine neuartige FRET-Sonde mit einem besseren 2P-anregbaren Cumarinderivat zeigte eine etwa 20% Steigerung der Cumarinintensität im Vergleich zum alten Cumarinderivat. Eine neue Generation von ASM-Sonden mit einer quaternären Ammoniumgruppe, die das natürliche Substrat nachahmt, wurde ebenfalls entworfen und synthetisiert. Alle neuen quaternären Sonden wurden als ASM-Substrate nachgewiesen und zeigten unterschiedliche kinetische Parameter. Sie zeigten höhere Umsatz-K_{cat}-Werte im Vergleich zur nicht quaternären Sonde. Die meisten neuen Sonden zeigten auch höhere Spezifitätskonstanten gegenüber dem ASM-Enzym.

Abstract

Sphingolipids are a family of bioactive signalling molecules. Besides their role in cellular structure, sphingolipids act as key regulators of many cellular functions including cell proliferation, differentiation, and apoptosis. The acid sphingomyelinase (ASM) catalyses the hydrolysis of sphingomyelin (SM) to ceramide, a metabolic hub of sphingolipid metabolism, and phosphoryl choline. Due to the lack of biochemical analytical tools, the molecular details of acid sphingomyelinase activity are still not fully discovered, and the development of pharmacological inhibitors is also hampered. The scope of this work is to develop new chemical probes for monitoring the activity of ASM both *in vitro* and *in vivo*.

In the first part of this study, two Eu complexes **4-D**$^{+}$ and **5-D**$^{+}$ (**Figure 1**) were synthesized starting from commercially available chelidamic acid and resulted in a good yield with high purity. The two probes were designed to have a positive charge that promotes binding with phosphates. The synthesized probes were used for detecting different phosphates and carboxylate species. The response of the two probes toward the studied phosphates was dramatically different, confirming the effect of structural and geometrical differences on the luminescence response.

The probes were applied for the monitoring of the ASM activity through the detection of the enzymatically released phosphocholine (PC). In the optimization steps, the **4-D**$^{+}$ revealed a promising luminescence decrease in response to the inorganic PC in addition to the SM/PC ratio change simulation reaction. A general quenching effect was observed in both of the homogeneous and heterogeneous enzymatic experiments and this was attributed to the ASM acetate buffer. Other trials for the monitoring of neutral sphingomyelinase 2 (nSMase 2) could not prove the ability of the probes to monitor the phosphates (SM & PC) ratio change in the complex enzymatic reaction media despite the obvious ability in the simulation reaction containing the phosphates only. However, the **5-D**$^{+}$ complex could be used for the monitoring of the ATP hydrolyzing Apyrase enzyme in a real-time pattern and could differentiate between the effect of an 8 fold range of different enzyme concentrations.

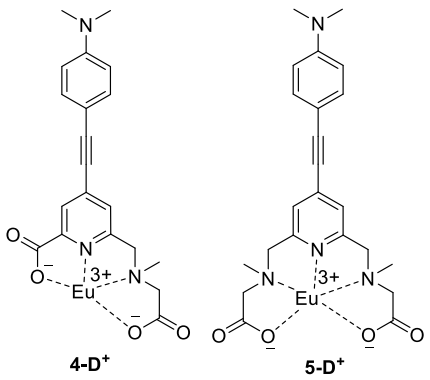

Figure 1. Structures of the Eu-Complexes.

In the second part of this study, different FRET and mono-labelled ASM probes were designed and synthesized (**Figure 2**). A novel FRET probe **ZP-403** with a better 2P-excitable coumarin derivative was synthesized to make use of the 2P excitation advantages in monitoring of ASM in biological samples.

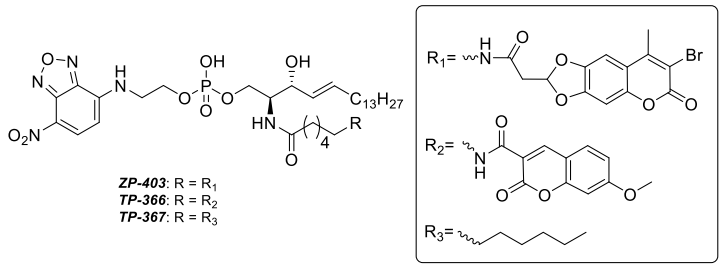

Figure 2. Structural elucidation of the ASM probes with a secondary amino group which were prepared in this study.

This probe was confirmed as an ASM substrate with a 10-fold coumarin fluorescence intensity turnover and could be used for the detection of ASM inhibitors. The quantification of the 2P excitability difference using silica beads labelled with the probe showed about 20% enhancement of the coumarin intensity compared to that of **TP-366**. The reported probes **TP-366** and **TP-367** were also resynthesize for high throughput screening and ASM monitoring in live cells studies.

A new generation of ASM probes containing a quaternary ammonium group which mimics the natural substrate were also designed and synthesized. A phosphorylation strategy which allows the insertion of a quaternary ammonium moiety in addition to a terminal alkyne group was applied. Two FRET probes **ZQP-407** and **ZQ$_2$P-410** were synthesized which can be excited in the ultraviolet and visible light range respectively. Another fluorescein mono-labelled probe **ZQ$_3$P-411** was also synthesized (**Figure 3**). All three probes were proven as ASM substrates and revealed varying kinetics parameters. All novel quaternary probes revealed higher turnover K_{cat} values when compared to the **ZP-403** probe. All of the novel probes displayed higher specificity constants k_{cat}/K_M toward the ASM enzyme except the **ZQ$_2$P-410** probe.

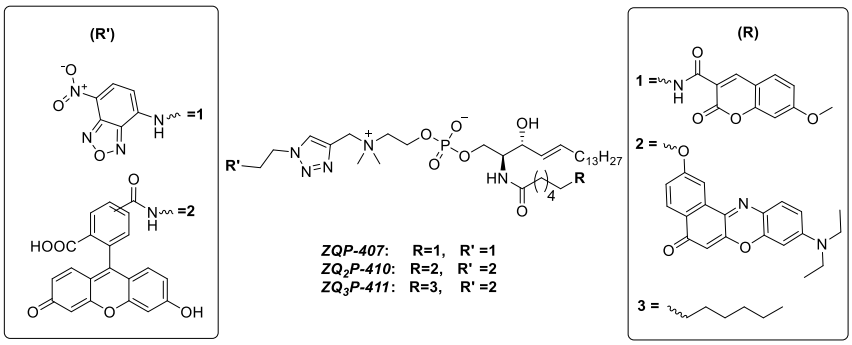

Figure 3. Structure elucidation of the ASM probes with a quaternary ammonium group which were prepared in this study.

List of abbreviations

2PE	Two-photon excitation
ACN	Acetonitrile
ADP	Adenosine diphosphate
alk-SMase	Alkaline sphingomyelinase
AMP	Adenosine monophosphate
aq.	Aqueous
ar	Aromatic
ASM	Acid sphingomyelinase
ATP	Adenosine triphosphate
Boc	tert-Butyloxycarbonyl
Boc_2O	di- tert-butyloxycarbonyl
br. s	Broad singlet (NMR)
BSA	Bovine serum albumin
Calc.	Calculated
CDase	Ceramidase
cDNA	Complementary DNA
Cer	Ceramide
CerS	Dihydroceramide synthase
CERT	Ceramide transporter
conc.	Concentrated
d	Doublet (NMR)
DCC	N, N′-dicyclohexylcarbodiimide
DCC	1,3-Dicyclohexylcarbodiimide
DCM	Dichloromethane
dd	Doublet of doublet (NMR)
dhCer	Dihydroceramides
DIBAL-H	Diisobutylaluminum hydride
DIPEA	N-N‟-Diisopropylethylamine
DMAP	4-Dimethylaminopyridine
DMAP	4-dimethylaminopyridine
DMF	N,N-Dimethylformamide
DMSO	Dimethylsulfoxide
dt	Doublet of trip et (NMR)
EDTA	Ethylenediaminetetraacetic acid
em	Emission
equiv	Equivalent
ER	Endoplasmic reticulum
et al.	et alia
EtOAc	Ethylacetate
EtOH	Ethanol
Ex	Excitation
FACS	Fluorescence activated cell sorting
FRET	Förster resonance energy transfer
GluCer	Glucosylceramide
H	Hour (s)
HeLa	Human cervical cancer cell line
HOBt	1-Hydroxybenzotriazole hydrate
HOSu	N-Hydroxysuccinimide

HPLC	High-performance liquid chromatography
HRMS	High-resolution mass spectrometry
HTS	High throughput screening
J	Coupling constant [Hz]
k_{cat}	Catalytic constant
K_M	Michaelis constant
KO	(ASM) knockout
LLCs	Luminescent lanthanide (III) complexes
Ln	Lanthanide (III)
L-SMase	Lysosomal sphingomyelinase
m	Meta
M	Molarity (mol/L)
m	Multiplet (NMR)
m/z	Mass/Charge ratio
Me	Methyl
MEF	Mouse Embryonic Fibroblasts
MeOH	Methanol
MHz	Megahertz
min	Minutes
ml	Milliliter
MOM	Methoxymethyl
MS	Mass spectrometry
NaOAc	Sodium acetate
NBD	7-Nitrobenzo-2-oxa-1,3-diazole amine
NBD-Cl	4-chloro-7-nitrobenzo-2-oxa-1,3-diazole
NBS	N-bromo succinimide
NMR	Nuclear magnetic resonance
NPD	Niemann–Pick disease
NR	9-Diethylamino-5-oxo-5H-benzo[a]-phenoxazin-2-yl-
n-SMase	Neutral sphingomyelinase
OE	Over expression
PBS	Phosphate buffered saline
PC	Phosphorylcholin
PC	Phosphatidylcholine
Ph	Phenyl-
ppm	Parts per million (NMR)
q	Quartet (NMR)
quant.	quantitative
RT	Room temperature
R_f	Retardation factor
s	Singlet (NMR)
S1P	Sphingosine-1-phosphate
SAPs	Sphingolipid activator proteins
SLs	Sphingolipids
SM	Sphingomyelin
SMases	Sphingomyelinases
SMPD1	Sphingomyelin phosphodiesterase 1
SPT	Serine palmitoyl transferase
S-SMase	Secreted sphingomyelinase
t	Triplet (NMR)

TBAF	Tetrabutylammonium fluoride
TBDPS	tert-Butyldiphenylsilyl
TBDPS	tert-Butyldiphenylsily
TBLAH	Tri-tert-butoxyaluminumLithium hydride
*t*Bu	tert-Butyl-
TFA	Trifluoroacetic acid
THF	Tetrahydrofuran
TLC	Thin layer chromatography
Tris	Tris(hydroxymethyl)aminomethane
Tris-HCl	Tris(hydroxymethyl)aminomethane hydrochloride
UPLC	Ultra-performance liquid chromatography
UV	Ultraviolet
V_{max}	Maximum catalytic velocity
δ	Chemical shift [ppm]

1 Introduction

1.1 Sphingolipids

Sphingolipids SLs were initially discovered in the 1880s by J. L. W. Thudichum while studying the lipid composition of the brain and were named after the Greek mythological creature 'Sphinx' because of their enigmatic nature[1]. Sphingolipids were considered for a long time to be essential only as structural components of the cellular membranes[2–4]. It is shown by calculation that sphingolipid is a major part of the surface monolayer, in addition to protein, cholesterol, and phosphatidylcholine[5]. However, intensive research over the last recent decades has established that Sphingolipids are both structural and functional lipids. Alongside playing structural functions in cellular membranes, some metabolites, including ceramide (Cer), sphingosine, and sphingosine-1-phosphate (S1P), have drawn attention as bioactive signaling molecules implicated in the regulation of cell growth, differentiation, senescence, and apoptosis[6–8]. Moreover, SLs have been reported to play a crucial role in infectious diseases [9–11], Major Depression/Psychiatric disorders[12,13], various cancers, immune function, cardiovascular disorders, and skin integrity[14].

1.1.1 Structure

Sphingolipids are various classes of lipids with a varying degree of hydrophobic and hydrophilic properties. They contain a sphingoid base, N-linked to a fatty acid, and, in some of them, O-linked to a charged group. The Sphingoid base is the hydrophobic backbone of sphingolipids and consists of a long chain aminodiol which encompasses a wide array of 2-amino-1,3-dihydroxyalkanes or -enes with (2S,3R)-erythro stereochemistry[15,16]. Sphingoid bases vary in alkyl chain length, the position and number of double bonds and hydroxyl groups, and other features[17].

Sphingosine, sphinganine, and phytosphingosine are the most frequent basic sphingolipids in mammalian tissues and found also in yeast and plants. These species can be either with a free amino group or with N-acylated variable fatty acids generating a diverse ceramide species. The headgroups range in complexity from a simple H in ceramide to highly complex glycoconjugates[18] (**Figure 4**).

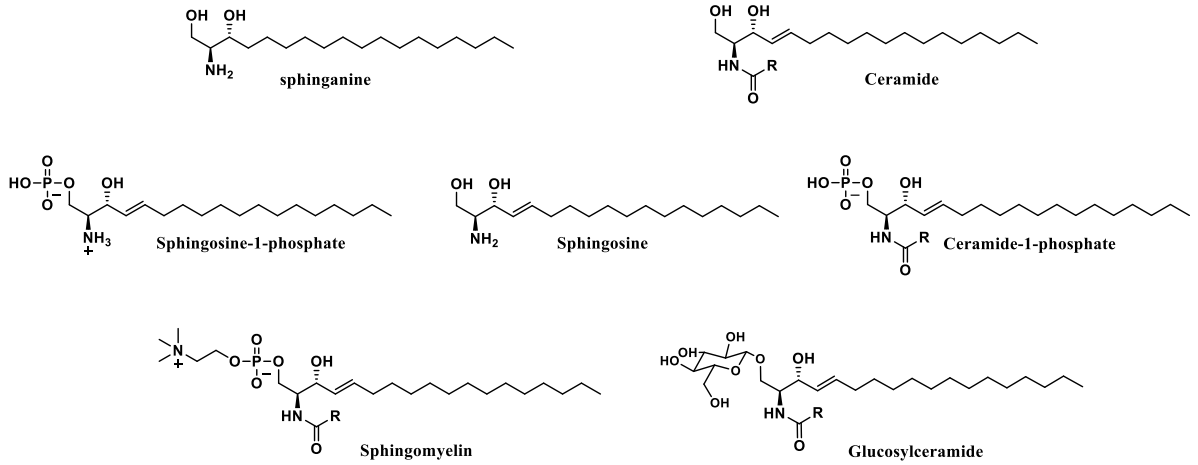

Figure 4. Structural diversity of SLs Compared to the structurally basic Sphingosine. R = different acyl chains[19].

1.1.2 Sphingolipids metabolism

Sphingolipid metabolism occurs mainly in eukaryotes but is also found in the *Sphingomonas* bacterial genus. The metabolic entry point of sphingolipid metabolism which forms the first sphingolipid in the *de novo* pathway is serine palmitoyltransferase SPT. S1P lyase is the unique exit point which breaks down S1P into non-sphingolipid molecules. In between, The SLs metabolic pathway displays a complex network of reactions resulting in the formation of a variety of SLs, with Ceramide as the central molecule of SLs biosynthesis, catabolism, and as precursors of complex SLs [6,7,20]. Ceramide biosynthesis is complex and involves at least three pathways; *de novo* biosynthesis pathway, Sphingomyelin (SM) cycle, and salvage pathway (**Figure 5**).

1.1.2.1 *De novo* biosynthesis

The *de novo* pathway starts in the endoplasmic reticulum (ER) with the condensation of L-serine and palmitoyl-CoA catalyzed by SPT to generate 3-ketodihydrosphingosine and this step is considered to be the rate-limiting step for this pathway. 3-Keto-dihydrosphingosine is subsequently reduced to form dihydrosphingosine (sphinganine), which is then N-acylated with various fatty acids of different chain lengths and/or differing degrees of saturation to produce dihydroceramides (dhCer). The latter reaction is catalyzed by one of six different dihydroceramide synthase (CerS1-6), each with specific fatty acyl-CoA chain length preference. Most dhCer are then desaturated by dhCer desaturase, generating a 4,5-trans-double bond to form Ceramides.[6,21] Ceramide is then transported to the Golgi apparatus by vesicular or protein-facilitated transport (ceramide transporter (CERT)) for the subsequent formation of complex sphingolipids.

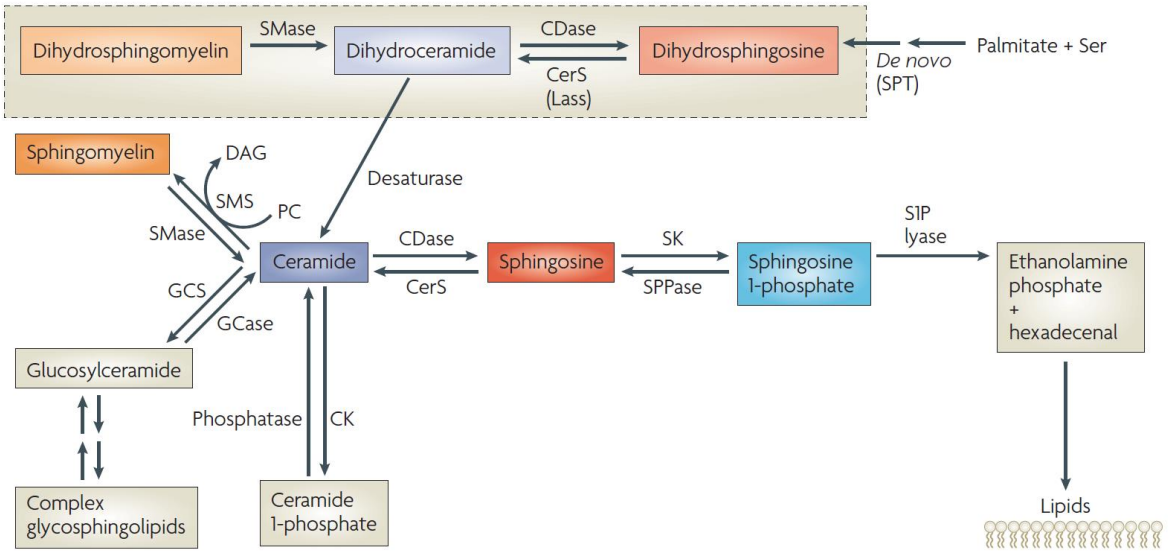

Figure 5. Bioactive Sphingolipid metabolic pathways. CDase, ceramidase; CK, ceramide kinase; DAG, diacylglycerol; GCase, glucosyl ceramidase; GCS, glucosylceramide synthase; PC, phosphatidylcholine; SK, sphingosine kinase; SMase, sphingomyelinase; SMS, sphingomyelin synthase; SPPase, sphingosine phosphate phosphatase; SPT, serine palmitoyl transferase.[7]

1.1.2.2 Sphingomyelin cycle

The sphingomyelin cycle is the second major metabolic pathway for ceramide generation. This pathway, which occurs mainly in the plasma membrane and mitochondria, involves the hydrolysis of phosphodiester bonds in sphingomyelin by alkaline, acid or neutral sphingomyelinases (SMases) to provide ceramide and phosphorylcholine.[22,23]

1.1.2.3 Salvage pathway

Furthermore, ceramide can also be generated from the lysosomal degradation of complex sphingolipids, mainly sphingomyelin and glycosphingolipids which are broken down eventually to sphingosine. Sphingosine can leave the lysosome and re-enter pathways for synthesis of ceramide through re-acylation reactions. This latter pathway is called recycle or salvage pathway and involve several key enzymes like SMases and glycosphingolipids hydrolases.[19,22,24]

1.1.3 Compartmentalization of metabolites and enzymes of the SLs pathways

The enzymatic reactions of SLs metabolism are distributed throughout different cellular compartments as presented in **Figure 6**. *De novo* Cer synthesis occurs on the cytosolic surface of the ER and possibly in ER-associated membranes, such as the perinuclear membrane and mitochondria-associated membranes.[6]

The synthesis of more complex SL metabolites like SM and Glucosylceramide (GlcCer) occurs in the Golgi apparatus and therefore Cer is transported from the endoplasmic reticulum to the Golgi apparatus through two known pathways. First, by the CERT where SM is formed from the transported Cer. Second, the vesicular transport of Cer on which the synthesis of GlcCer is based. Subsequently, the transport protein FAPP2 delivers GlcCer as a precursor for glycosphingolipid (GSL) synthesis. In contrast to luminally/extracellularly oriented SM and complex GSLs, Both Cer and GlcCer are synthesized on the cytosolic face. [25]

The complex SLs, SM, and GSLs are then transported to the plasma membrane via vesicular trafficking. There, SM can be metabolized by SMases to Cer, and accordingly other bioactive lipids.

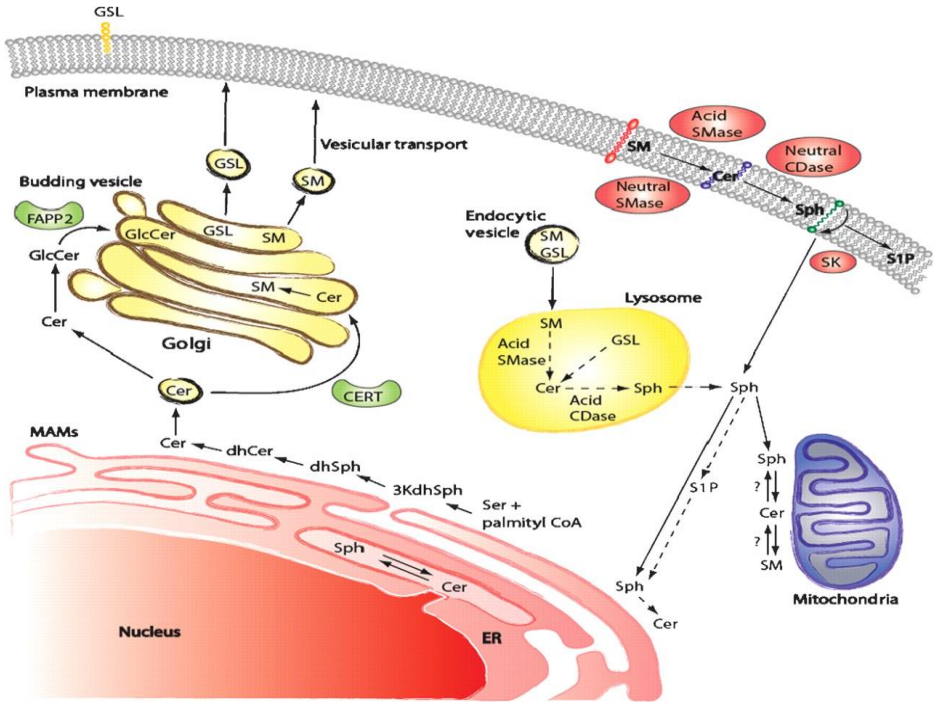

Figure 6. Compartmentalization of SL pathway metabolites and enzymes. 3KdhSph, 3-keto-dihydrosphingosine; dhSph, dihydrosphingosine; MAMs, mitochondria associated membranes.[6]

SLs recirculation from the plasma membrane may occur through the endosomal pathway. In the lysosomal compartment, SM and GSL are metabolized to Cer which is subsequently degraded by acid ceramidase CDase to form sphingosine. Due to its positive charge, the salvaged sphingosine can leave the lysosome and dissolve adequately in the cytosol to move between membranes, including the ER, where it would be available for recycling.[6,19]

1.2 Sphingomyelinases

1.2.1 Sphingomyelin

Sphingomyelin SM is the most abundant complex sphingolipid in mammalian cells and represents about 85% of all sphingolipids in humans. It has an essential role in eukaryotic cell viability as evidenced by the inability of mammalian or yeast cells to survive in culture when they are unable to produce SM.[26] SM is preferentially concentrated in the outer leaflet of the plasma membrane. Its high packing density and affinity for sterols provide a rigid barrier to the extracellular environment and play a role in the formation of lipid rafts which are specialized areas in cellular membranes with important functions in signal transduction and membrane trafficking. [27]

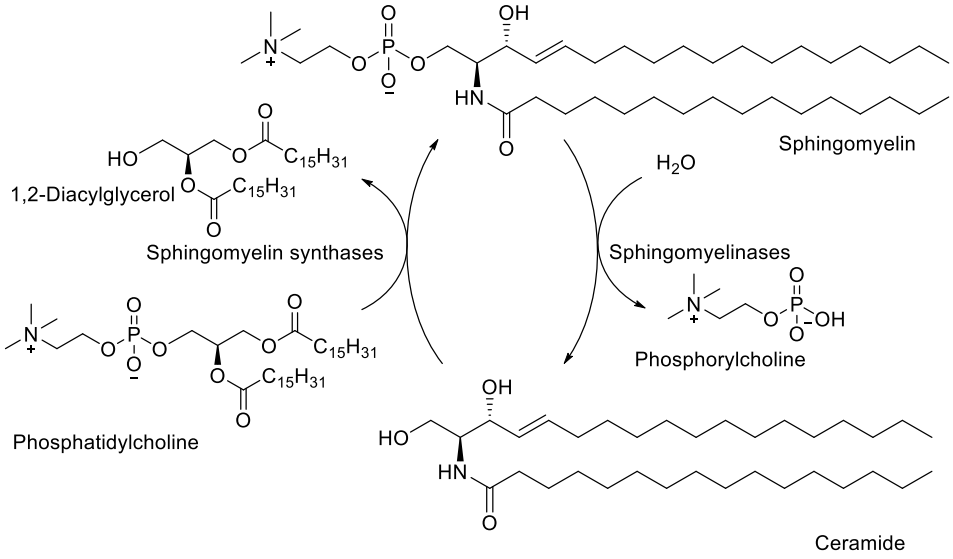

Figure 7. The sphingomyelin cycle demonstrating the essential enzymes and byproducts.

Structurally, SM consists of a ceramide unit with a phosphorylcholine (PC) moiety attached to position 1 of the sphingoid base component. SM obtained from natural sources, such as eggs or bovine brains, contains fatty acids of various chain lengths. Palmitic acid (16 C) and stearic acid (18 C) are the most abundant fatty acid component of SM [28,29]. The SM content in a cell is strictly regulated by the enzymes of SM metabolic pathways whose activities create a balance between SM synthesis and degradation (**Figure 7**). SM is an essential modulator of plasma membrane properties (due to the structural variability) which influences the membrane gathering of proteins involved in cellular proliferation, growth, and apoptosis as well as being an important source of ceramide. So its levels are critical for cell function.[30]

1.2.2 Sphingomyelinases subtypes

Sphingomyelinases SMases (Sphingomyelin phosphodiesterases) catalyze the reaction of SM hydrolysis. They hydrolyze the phosphodiester bond of SM to generate Cer and PC. Three types of SMases can be distinguished based on optimal pH values required for their activation: acid (ASM), alkaline (alk-SMase), and neutral (n-SMase) as presented in **Table 1**[30–32]. They differ not only in their optimum pH but also their dependence on the presence of divalent cations and subcellular localization.[33]

1.2.3 Acid Sphingomyelinase

Acid sphingomyelinase (ASM) is a sphingomyelin hydrolyzing enzyme that works optimally at acidic pH [34]. After reporting that the deficiency of ASM was responsible for the rare, recessively inherited lysosomal storage disorder, Niemann–Pick disease (NPD), intensive efforts to purify and characterize it were stimulated[35–38]. Because the acidic pH optimum of the enzyme in vitro (4.5 and 5.0), as well as the fact that the majority of storage material in NPD patients was found in lysosomes and/or late endosomes, the enzyme was classified as a lysosomal protein[39]. In the late 1980s and early 1990s, complementary DNA (cDNA) and gene encoding of ASM (designated Sphingomyelin phosphodiesterase 1 ‘’SMPD1’’) were cloned[40,41]. Later, a zinc-dependent, secreted form of ASM that also was encoded by the SMPD1 gene was identified[42,43]. The biological function of the secreted form remained unknown but There is now growing evidence suggesting that this ASM form may play a role in atherosclerosis, cell surface signaling, and host inflammation [33,44,45].

Group	**Acid sphingomyelinases**		**Neutral sphingomyelinases**			**Alkaline sphingomyelinase**
Gene	SMPD1	SMPD1	SMPD2	SMPD3	SMPD3	NPP7
Protein	Lysosomal acid sphingomyelinase (l-ASM)	Secreted acid sphingomyelinase (s-ASM)	Neutral sphingomyelinase 1 (NSMase1)	Neutral sphingomyelinase 2 (NSMase2)	Neutral sphingomyelinase 3 (NSMase3)	Alkaline sphingomyelinase (bSMase)
Cellular Compartmentalization	Lysosomes/endosomes, Outer plasma membrane	Extracellular	ER	Golgi, Plasma membrane	ER, Golgi, Plasma membrane	Extracellular in intestines and liver
Biochemical properties	pH 5 optimum	Zn^{2+}, pH 5 optimum	Mg^{2+}, pH 7.4 optimum			pH 8.5 optimum
Biological effects	- Post-IR cell death, contractile dysfunction - Vascular tone constriction - Oxidized phospholipids -induced apoptosis		-	- Growth - TNF-, ROS-, oxLDL - Induced proliferation	- TNF-, IL-1, hypoxia/ reoxygenation - Induced apoptosis	- Dietary SM digestion and ceramide formation[46]
Pathophysiology	- Niemann-Pick disease[47] - Atherosclerosis	- Niemann-Pick disease[47] - Atherosclerosis - Heart failure	-	-Atherosclerosis[48]	- Atherosclerosis - Heart failure	- Colon carcinogenesis[49]
Biological/pharmacological inhibitors	Glutathione, D609, Desipramine[50], NB6, L-Carnitine, ARC-39		Glutathione[51],	Cambinol[52] , Glutathione[51], Scyphostatin, GW4869[53]		Phosphatidylserine , Phosphatidylinositol ,TX100[54,55]

Table 1. Different Sphingomyelinases and their characters. I/R, ischemia/reperfusion [32,56]

The following studies revealed that the L-SMase seems well suited to operate at the low pH of the endo-lysosomal compartment while S-SMase is proposed to participate in SM hydrolysis at the neutral pH of the extracellular milieu or in association with lipoproteins in serum.[57] This is because an increase of the pH only alters the substrate affinity i.e. the K_m value of the enzyme while the activity (V_{max}) of the ASM is not affected. The substrate affinity, however, is regulated by the presence of extracellular factors such as LDL or by membrane co-factors that might compensate for the reduction of substrate affinity restoring ASM activity even at neutral pH values.[58]

Furthermore, both S-SMase and L-SMase were demonstrated to be zinc metalloenzymes. The apparent differences in zinc-dependence of the lysosomal and secreted ASM forms were due to differential cellular trafficking that either exposed or sequestered the enzyme from cellular pools of zinc[44,57]. The Zn^{2+}-independency of L-SMase can be explained by the fact that this form of the enzyme, as isolated from cell homogenates, is already saturated with Zn^{2+} and thus requires no exogenous Zn^{2+} for enzymatic activity[59]. Furthermore, as is often the case with zinc-metalloenzymes, Zn^{2+}-bound L-SMase cannot be readily stripped of its metal by short-term EDTA treatment [45].

1.2.4 Niemann–Pick disease

By the late 1960s, it was reported that the deficiency of ASM is the cause of the recessively inherited rare lysosomal storage disorder, Niemann–Pick disease (Types A and B NPD). Both forms of NPD are caused by recessive mutations in the ASM encoding gene SMPD1[60–64]. Type A NPD is an infantile form of ASM deficiency, characterized by a rapidly progressive neurodegenerative course that leads to death by age 2–3. In contrast, Type B NPD is the later-onset form in which patients show limited or no neurological symptoms but may exhibit severe and progressive visceral organ deformities, including hepatosplenomegaly, pulmonary insufficiency, and cardiovascular disease. Types A and B NPD are differently clinically presented most likely due to small differences in the amount of residual ASM activity [60]. The clinical findings in NPD are most likely related to lipid storage in lysosomes and/or endosomes. The recent data which reveal the important role of ASM in membrane formation and function propose that the functional shortage of the enzyme at the cell surface also could contribute to the pathophysiology of NPD as well [58,60].

Unlike NPD types A and B, which result from mutations in SMPD1, Niemann–Pick disease type C results from mutations in NPC1 and NPC2. It is also a lipid storage disease that can present in infants, children, or adults [65–67]. NPC1 and NPC2 encode in cholesterol trafficking involved proteins in the endo-lysosomal compartment, and mutation of either of these proteins results in massive accumulation of unesterified cholesterol in perinuclear lysosomes[68]. Fibroblasts from NPD-C patients exhibit marked inhibition of aSMase activity in cellular extracts despite the absence of genetic aberrations in SMPD1[69,70]. This Loss of aSMase activity occurs via post-translational mechanisms and is a direct result of the accumulation of cholesterol in the endo-lysosomal compartment. Whether the functional loss of ASM activity is a result of altered trafficking (e.g. cholesterol influences trafficking of ASM precursor), or via direct action on the enzyme is unclear [44].

1.2.5 Structure and catalytic mechanism of the acid sphingomyelinase

ASM is synthesized and differentially modified post-translationally in the endoplasmic reticulum and Golgi to yield distinct lysosomal and secreted forms[71]. ASM has an NH_2-terminal ER signal sequence that is sufficient for the co-translational introduction of the nascent precursor polypeptide into the endoplasmic reticulum (**Figure 8A)**. Mutated human ASM lacking a signal peptide results in the production of a non-glycosylated, cytosolic protein that lacks enzyme activity in cellular extracts, and is not secreted[72]. Next to the signal peptide, The primary structure of the N-terminal of ASM contains a saposin-like (SAP) domain extending from amino acid 89–165[73]. SAPs (sphingolipid activator proteins) are non-enzymatic glycoproteins predominantly found in the acidic compartment and function to facilitate degradation of various sphingolipids via mobilizing lipids from membranes, thus exposing substrates to the active site of the respective enzyme[44,74].

The SAP domain is separated from the catalytic domain and thus has been postulated within ASM functions to be as an intramolecular activating region for SM hydrolysis[44]. The linker connecting ASM_{cat} to ASM_{sap} is proline-rich and mostly rigid, wrapping itself around the catalytic domain as an L-shaped strap[71]. The presence of the SAP domain and proline-rich linker distinguishes ASM from all the other structurally known proteins[75].

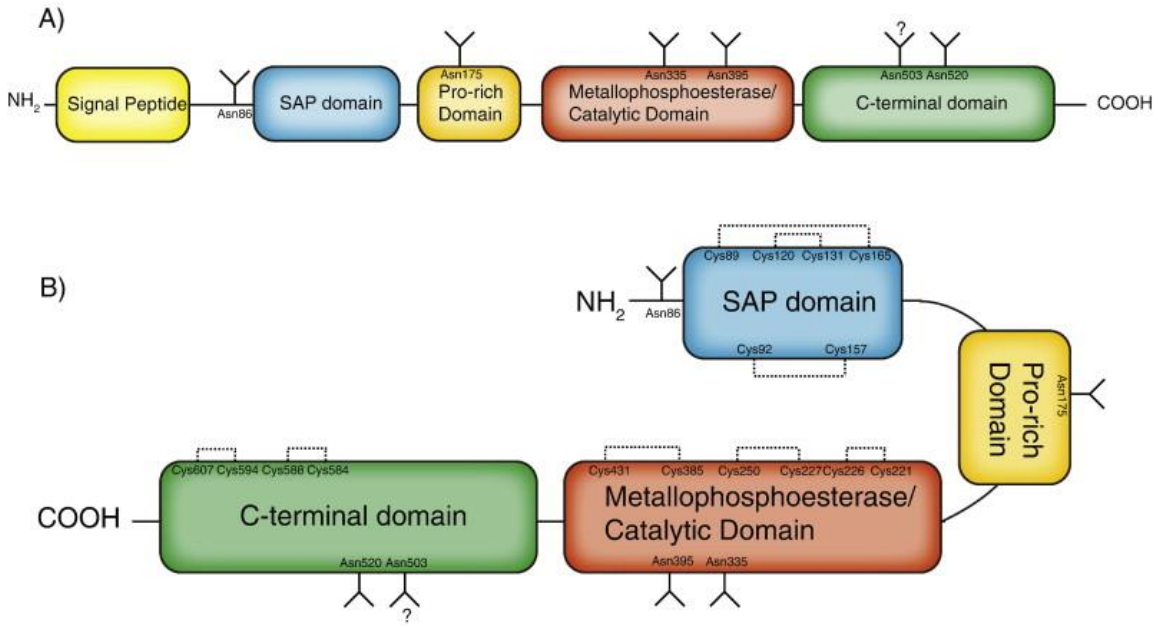

Figure 8. Structure of acid sphingomyelinase. **A**) Primary structure of ASM polypeptide. **B**) Stylized conformation of mature ASM. Domain structure, N-glycosylation sites, and disulfide bridges are shown. Signal peptide (amino acids 1–46), SAP domain (89–165), Pro-rich domain (166–198), metallophosphoesterase/catalytic domain (199–461), C-terminal domain (462–629). N-glycosylation sites (Asn86, Asn175, Asn335, Asn395, Asn503, Asn520). Disulfide bridges (Cys89–Cys165, Cys92–Cys157, Cys120–Cys131, Cys221–Cys226, Cys227–Cys250, Cys385–Cys431, Cys584–Cys588, Cys594–Cys607). [44]

The catalytic domain adopts a metallophosphatase fold and belongs to the calcineurin-like phosphoesterases structural family and resembles recent structures of the ASM-like protein[71,75,76]. The ASM metallophosphatase domain is featured with the long β stranded loops which extends toward the zinc ions. Beside mediating zinc and substrate binding, these loops form the interfaces to the proline-rich linker, saposin, and C-terminal domains[75].

The active site in ASM defines a stringently specific for zinc and the sphingomyelin phosphate group. The two zinc ions are coordinated by Asp206, His208, Asp278, Asn318, His425, His457, His459, and the catalytic water molecule. During the substrate recognition, it is speculated that - as with other phosphoesterases from the calcineurin-like superfamily- the dimetal zinc center coordinates the two unesterified oxygen atoms of the substrate phosphodiester as well as the nucleophilic water (**Figure 9**). Following that, the hydroxide initiates a nucleophilic attack on the phosphorus of sphingomyelin. The arrangement of the active site allows the phosphate oxygen on the ceramide side to extract a proton from either His319 of His282. The His282 imidazole ring is stabilized by π–π stacking interaction with Tyr488 and polar interaction to the Asp251 carboxylate group, while the His319 is involved in

water-mediated hydrogen bonding. As a result, H319 is a more energy favored hydrogen donor in the reaction.

It is proposed that the imidazole ring on H319 is the source of the proton to the oxyanion of the ceramide leaving group. The solvent accessibility allows quick exchange of protons on both H319 and the nucleophile water in the regeneration step. Consistent with this hypothesis, mutation of H319 to tyrosine causes severe ASMD[75–77].

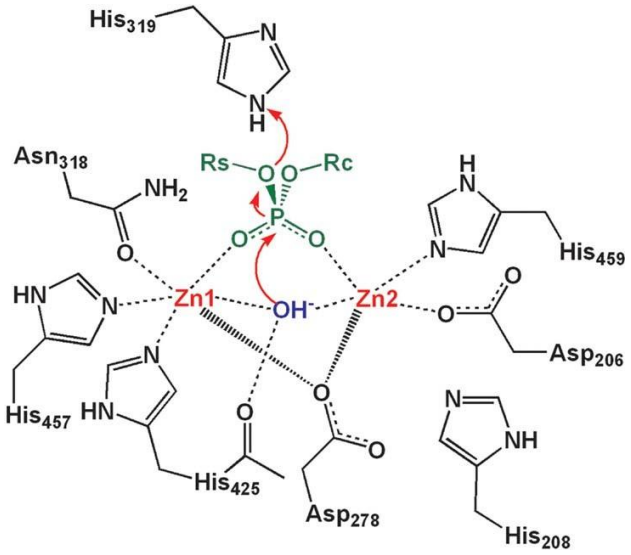

Figure 9. Proposed catalytic mechanism for the hydrolysis of phosphodiesters by ASM[78].

The last domain is the C-terminal domain which contributes to the stabilization of the active site conformation[75]. The relevance of C-terminal modification in the context of the maturation of S-ASM and L-ASM is still not fully discovered. However, given that C-terminal processing for other lysosomal enzymes like acid β-glucosidase and cathepsin D has been reported, C-terminal modification of Cys629 may serve as a cellular mechanism of ASM maturation/activation[44,79].

The presence of eight intramolecular disulfide bonds is a characteristic structural feature of ASM (**Figure 8**). Most of the disulfides in ASM are solvent accessible and therefore the exposure of these residues may make ASM sensitive to redox conditions[51,80]. Only sixteen of ASM's seventeen cysteine residues are involved in disulfide bond formation. Deletion or oxidation of the unbridged, carboxyterminal Cys629 resulted in a 4–5-fold increase in ASM activity[44].

There are six predicted N-glycosylation sites in the ASM polypeptide chain (**Figure 8**), of which five are utilized (Asn86, Asn175, Asn335, Asn395, and Asn520 — not Asn503)[44]. Elimination of the four N-terminal glycosylation sites doesn't affect lysosomal targeting,

processing, or enzymatic activity. However, removal of the two C-terminal N-glycosylation sites hinders the maturation of the enzyme.

Rapid cleavage of the primary translation polypeptide to an enzymatically inactive protein was observed in case of the absence of the fifth glycosylation site, whereas deletion of glycosylation site six led to the formation of an inactive ASM precursor[81]. In addition to mediating proper folding and trafficking, the glycosylation of ASM is believed to has a protective role to prevent destruction in the harsh environment of the lysosome. Glycosylation may also be important for maintaining the mature enzyme in an active conformation, as in vitro glycosidase treatment results in loss of activity[82,83].

1.2.6 Sphingomyelinase assays

Considering the broad variety of different cellular events where sphingomyelinases are involved, they have emerged as a new drug target for the treatment of atherosclerosis, ischemia/reperfusion injury, lung inflammation, diabetes, and obesity, as well as rare and neglected diseases such as pathogen infection (Neisseria gonorrhoeae) and Niemann Pick Disease types A and B. One of the prerequisites for a detailed study of the enzyme and the search for pharmacological inhibitors is a sensitive and selective determination of the ASM activity in biological samples (tissue homogenate, serum, urine, etc.). Thus, the need for a valuable, reliable, and rapid method for determination of sphingomyelinase (SMase)-activity is highly imperative.[56,84,85] Over the years, a significant amount of effort has been dedicated to develop an ASM activity assay for the screening and diagnosis of NPD A and B and other Smase related biological events[86]. Several SMase screening assays have been reported including fluorogenic, colorimetric, and radioactive assays[87–91].

1.2.6.1 Radioactive Sphingomyelinase assay

Historically, radioactive assay of SMases is considered as one of the earliest established characterization methods[92]. The principle of this method is to use a radiolabeled sphingomyelin, with a ^{14}C-label on the phosphocholine[93], as a substrate for the enzyme. After incubation of the substrate with the enzyme, the labeled phosphocholine can be separated from the remaining, unhydrolyzed sphingomyelin by extraction with a mixture of chloroform and methanol. The intact sphingomyelin and ceramide are captured in the organic phase, whereas the labeled product, phosphocholine is very polar and therefore soluble in water, partitions to the upper aqueous phase. Radioactivity in an aliquot of the upper phase can be counted in a liquid scintillation counter as a relative measure of sphingomyelin hydrolysis[88,94].

Alternative methods to the chloroform/methanol extraction process were explored to eliminate the dangers associated with chloroform and methanol on both the operators and the equipment. As phenyl-sepharose beads could capture the hydrophobic, lipophilic components of the ASM reaction they were thus used for their ability to separate unreacted hydrophobic sphingomyelin substrate from the radiolabeled phosphorylcholine product. The advantages of this bead-based extraction method were its lower cost, as well as its ability to screen for inhibitors of ASM without exposure to organic solvents[87]. Related to the radiolabeling based analysis, radiolabeled dihydrosphingomyelin[95], [^{3}H]ceramide-labeled sphingomyelin[96] and sphingomyelin (choline-methyl- ^{3}H)[87] were also used for sphingomyelinases monitoring. In addition to the price and the high equipment/safety demands[97], this assay also includes an aqueous/organic separation step. So, it is heterogeneous which excludes the possibility of real-time tracking of the reaction. Despite that, the unequaled advantage of radiolabeling is the use of a substrate that behaves biologically exactly like its natural substrate.

1.2.6.2 Chromogenic Sphingomyelinase assay

Due to the forenamed drawbacks of the radiochemical assay, an early need for alternative methods has emerged. The moderate outlay in equipment and the simple implementation predestine spectroscopic techniques for assay development[98]. This is particularly true for screening applications, i.e. the routine testing of large substance libraries for biologically active molecules (inhibitors etc.)[99,100]. The growing interest of ASM as a diagnostically relevant analyte, therefore, encouraged the development of synthetic, chromogenic or fluorogenic alternative substrates that indicate the activity of the enzyme through the formation of colored or fluorescent compounds[86].

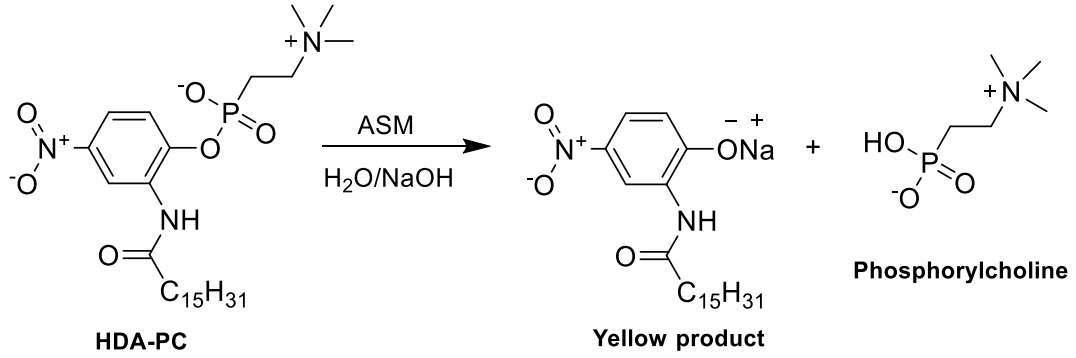

Scheme 1. Cleavage of 2-hexadecanoylamino-4-nitrophenylphosphorylcholine(HDA-PC) by ASM[101].

Early methods applied artificial chromogenic substrates, such as 2-hexadecanoylamino-4-nitrophenylphosphorylcholine (HDA-PC). It is dissimilar to sphingomyelin only by having an aromatic ring instead of a long aliphatic chain and a nitro group replacing the primary hydroxyl one carbon removed[102,103]. When HDA-PC is incubated with pure ASM or various tissue preparations, phosphorylcholine is enzymatically cleaved from the molecule. Sufficient sodium hydroxide solution is then added to produce a yellow color with 2-N-acylamido-4-nitrophenol, the other product of the reaction as in **Scheme 1**. Quantitation of the sphingomyelinase activity in the various preparations can be derived through the determination of the color intensity. A potential pitfall of using HDA-PC for the laboratory diagnosis of patients with sphingomyelinase deficiency is a false negative result, e.g. normal enzyme activity with the laboratory test in patients where this enzyme is deficient under physiological conditions *in vivo*. However, it is generally agreed that the technical advantages of these assays outweigh the risk of missing a diagnosis owing to false-normal enzyme activity[104,105].

1.2.6.3 Fluorogenic Sphingomyelinase assay

As the fluorescence is much more sensitive in addition to the fact that the absorption of the sample matrix is usually considerable, a new fluorogenic assay was developed for accurate determination of the ASM activity[105]. In this assay the non-fluorescent 6-Hexadecanoylamino-4-methylumbelliferylphosphorylcholine (HMU-PC) is used as a specific substrate for ASM. Upon cleavage of HMU-PC with ASM as in **Scheme 2**, the fluorescent 6-hexadecanoyl-4-methylumbelliferone (HMU) is released and quantified as a measure of the ASM activity[85].

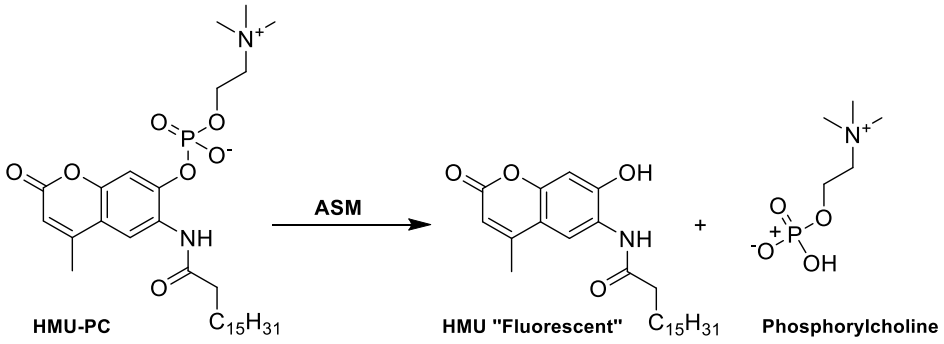

Scheme 2. Cleavage of 6-Hexadecanoylamino-4-methylumbelliferylphosphoryl choline (HMU-PC) by ASM.

The commercial frequently used amplex red® assay is a coupled enzyme assay including a four-step enzymatic procedure. First, sphingomyelinase is used to hydrolyze the sphingomyelin present in test samples to ceramide and phosphorylcholine. After the action of alkaline phosphatase, which hydrolyzes phosphorylcholine to choline, choline is oxidized by choline oxidase to betaine and H_2O_2.

Finally, H_2O_2, in the presence of horseradish peroxidase, reacts with dihydroxyphenoxazine (Amplex® Red; AR) to generate the highly fluorescent product resorufin[52,106,107] as demonstrated in **Scheme 3**. If ASM is to be assayed, pH adjustment is required after initial sphingomyelin breakdown[108], which further complicates the assay. Not only does its dependence on three consecutive enzymatic conversions predispose this assay to false inhibitor hits, but also absorption or emission of light by the compounds to be tested.

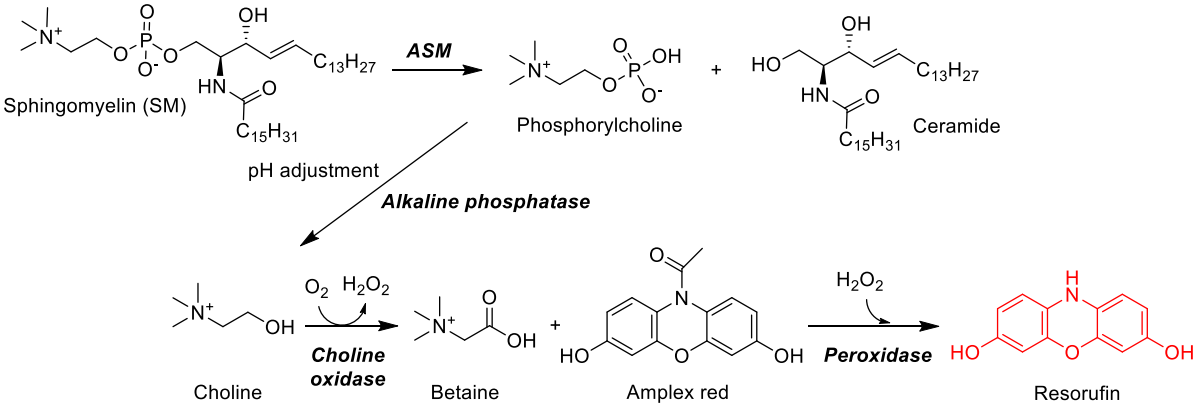

Scheme 3. Schematic representation of the Amplex® red based ASM assay.

Another fluorescence-based approach was suggested by Gaudino *et al.* to develop a more efficient sphingomyelinase assay. They proposed a sphingomyelin derivative that could be attached to a solid support via the ceramide moiety and that contained a fluorescent tag in the phosphocholine moiety (**Figure 10**). The ceramide portion of this substrate, when cleaved by sphingomyelinase, would be retained on the solid support along with unreacted starting material while fluorescently labeled phosphocholine would go into the solution phase. The solution phase could then be removed and phosphocholine content measured spectrophotometrically. Solid-phase attachment of sphingomyelin was envisioned as occurring via a biotin/avidin (or streptavidin) interaction[109]. A solid conclusion is difficult to be derived from this study due to the small number of derivatives examined but it can be said that all the three derivatives are ASM substrates to different extents. Compound A with the minimal structural deviation from the natural substrate was cleaved by ASM at 77% of the rate observed for ^{14}C-sphingomyelin. However, derivatives B and C modified with a biotin anchor also had acceptable hydrolysis rates, which are about three to six times lower than those of the natural substrate.

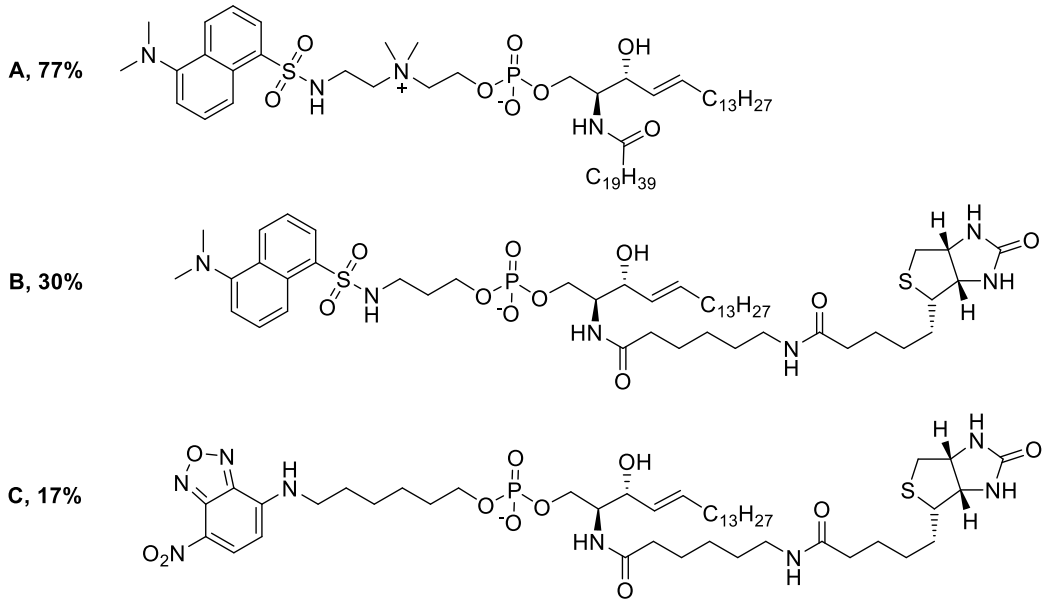

Figure 10. Sphingomyelin analogues developed by Gaudino et al. and their cleavage rate compared to ^{14}C-sphingomyelin[109].

The relative positioning of the ammonium group in Compound A and the ammonium group in sphingomyelin to the cleavage site is identical, therefore this cleavage rate study suggests that for human placenta acidic sphingomyelinase, the ammonium group of sphingomyelin is important but not absolutely essential for substrate recognition. Modifications of the head group with a significantly larger space requirement compared to choline were also tolerated. Follow-up studies combining both the ammonium group and biotin anchor were not published, which is why it must be assumed that the material was inferior to the previous methods.[56,109]

Some fatty acid-labeled fluorescent sphingomyelin analogs were also developed and used for several SMases[110] where both the substrate and the product usually remain in the hydrophobic fraction and have to be separated by either thin layer chromatography (TLC) or by other chromatographic methods like high performance liquid chromatography (HPLC)[111]. Different mass spectroscopy based methods were also reported for ASM activity quantification. Some of them were reported as robust and suitable for laboratory diagnosis of Niemann Pick disease[112–114].

The recent X-ray characterization of the enzyme[71] provides a reliable structural basis for a targeted synthesis of pharmacologically interesting inhibitors of ASM (rational drug design). This also increases the demand for a high-throughput, homogeneous assay to be able to evaluate these new substances efficiently. Arenz et al. are working on the development of FRET-based ASM probes in an attempt to compensate for the absence of a homogeneous ASM assay for more than 50 years of research.

1.2.6.4 Sphingomyelinase FRET substrates

Förster resonance energy transfer (FRET) is the radiation-free transfer of energy from one fluorescent dye to another. The main prerequisites for this transfer are the spectral overlap of the emission spectra of the donor dye with the excitation spectra of the acceptor dye and the spatial proximity of these dyes. Once a FRET pair has been defined, the first dye (FRET donor) with the shorter excitation wavelength is exited. If the FRET efficiency is high enough, the donor dye will transfer all its emission energy to the FRET acceptor, which is then excited and emits fluorescent light at a wavelength higher than the emission wavelength of the donor dye. Therefore, in an ideal FRET pair, the FRET donor is excited, but only the FRET acceptor is emitting fluorescent light. In a setup in which the enzyme or process of interest will form a FRET pair or destroy an existing FRET setup, the change in fluorescence will affect both dyes in way that the emission of one dye is increased, while the fluorescence intensity in the second dye is decreasing. Since both effects are contrariwise, they both contribute to the responsiveness and thus to the sensitivity of the probe. Furthermore, the ratio of both fluorescence intensities is not dependent on the absolute but only of the relative concentrations of the intact FRET system on the one side and the free independent dyes on the other side. The latter feature also known as “ratio-imaging” is a significant advantage over quenched probes or turn-on probes, in which the observed absolute fluorescence intensity is dependent on many factors like cellular delivery or export and thus not indicative of the cleavage (or formation) ratio (**Figure 11**). [115]

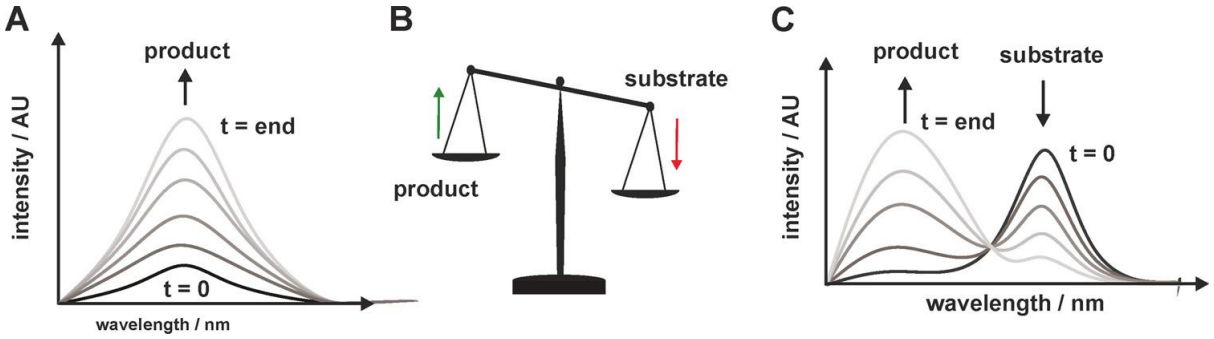

Figure 11. Illustration of the concept of ratio imaging. A) Time response of a turn-on probe, often allowing only qualitative information B) Increase in product fluorescence with a concomitant decrease in substrate florescence indicates the relative cleavage rate of probe molecules C) Time response of a typical FRET probe cleavage, providing relative cleavage rates and thus quantitative information.[115]

Some impressive examples of FRET pair formation exist in the field of small analyte determination like Ca^{2+}, which can be sensed by a tandem fusion protein of calmodulin with two different fluorescent proteins[116]. Small molecule sensors have been described for reactive specimen like cellular thiols, as exemplified in **Figure 12A** [117]. A few substrates that exhibit fluorescence resonance energy transfer (FRET) have been synthesized and used successfully in the past to monitor enzyme activities[118]. An example includes probe **CPF4** for monitoring phosphodiesterase activity [119] (**Figure 12B)**. The first FRET probe in the lipid field has been described by Wichmann et al., who synthesized a FRET probe for phospholipase A2 (PLA2)[120]. The molecule mimicking phosphatidylcholine contained an NBD dye as FRET donor in the acyl portion, while a Nile Red dye was used as a FRET acceptor in the second lipid tail as in **Figure 12C**. This probe showed an impressive 70-fold FRET response upon cleavage and was used to monitor PLA2 activity in live cells [118]. The specificity of the probe for PLA2 was ensured by replacing the SN1 ester bond with an inert ether linkage, making cleavage of the probe by PLA1 impossible. [115]

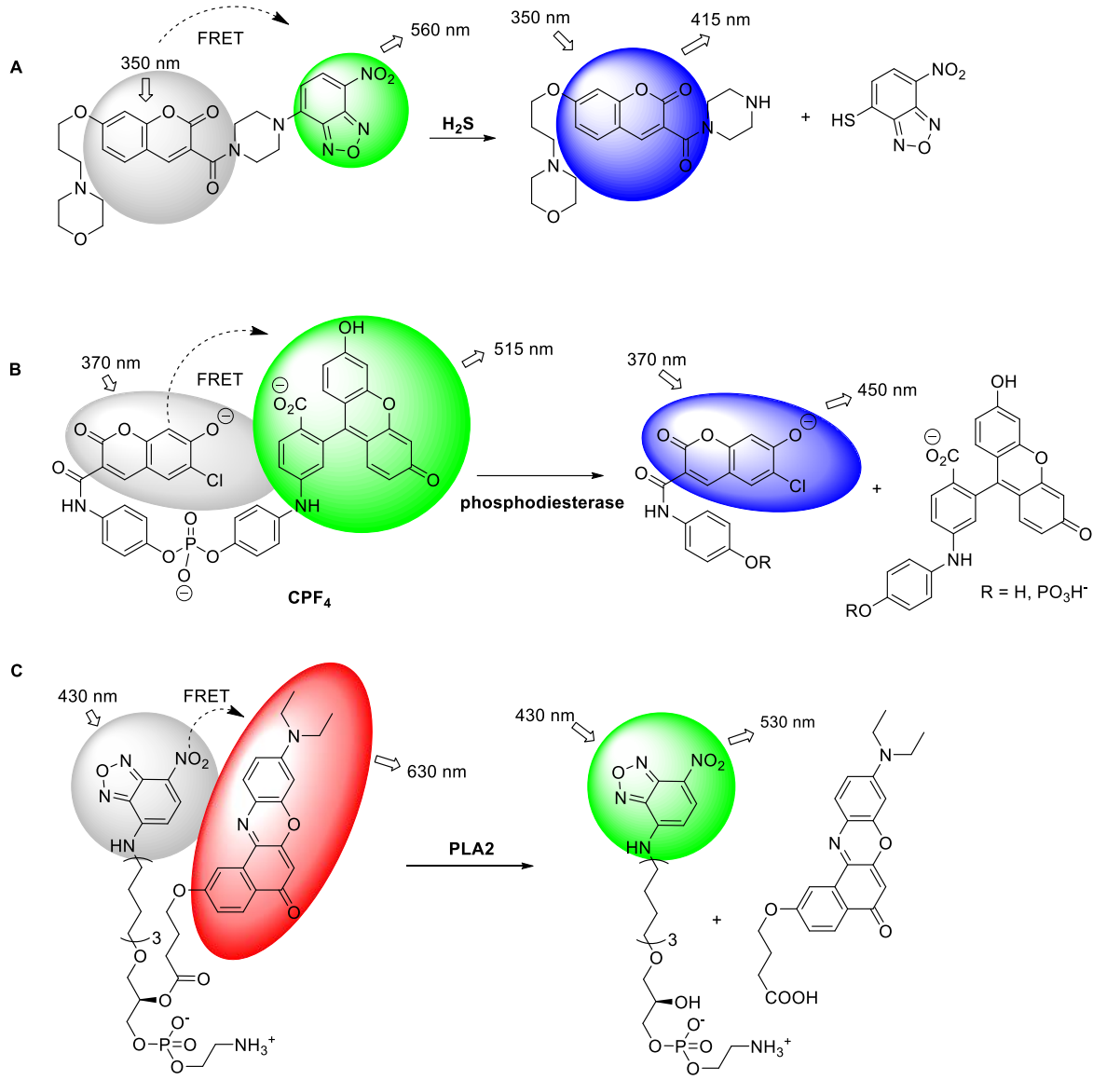

Figure 12. Examples for FRET probes for enzymes monitoring. **A**) FRET probe for fast Thiol-Quantification Assay of Glutathione Reductase. **B**) FRET probe **CPF4** for monitoring phosphodiesterase activity. **C**) FRET probe for phospholipase A2 (PLA2).[115]

To further extend the applicability of FRET probes, an acid sphingomyelinase FRET-probe was designed by Pinkert et al.[121] using the previously described NBD/Nile Red pair[122]. In contrast to ceramide, where both dyes inherently had to be incorporated into both lipid tails, the choline head was modified with the relatively polar NBD and the membrane-resident part with Nile Red, respectively (**Figure 13A**). Although the resulting sphingomyelin analogue was readily cleaved by recombinant human ASM (rec ASM), only a low ratio change was observed. While the acceptor Nile Red fluorescence declined by a factor of 3-fold, a concomitant change in donor NBD fluorescence was not observed (**Figure 13 B**), which was obviously due to the quenching of NBD fluorescence in the aqueous environment.

To make use of the NBD quenching effect after probe cleavage, a second probe was synthesized in which NBD was the FRET acceptor. For this setup, a coumarin dye was selected as a suitable FRET donor. Indeed, upon cleavage of this probe, an increase in coumarin fluorescence was accompanied by a very effective decline of the NBD fluorescence (**Figure 13C**) yielding an about 80-fold ratio change [121]. Before its application in cell-based assays, the probe was thoroughly tested. The probe allowed differentiation of different rec ASM concentrations over 3 orders of magnitude and incubation with different inhibitors of acid sphingomyelinase[123,124] showed a dose-dependent inhibition of the FRET change as presented in **Figure 13D**.

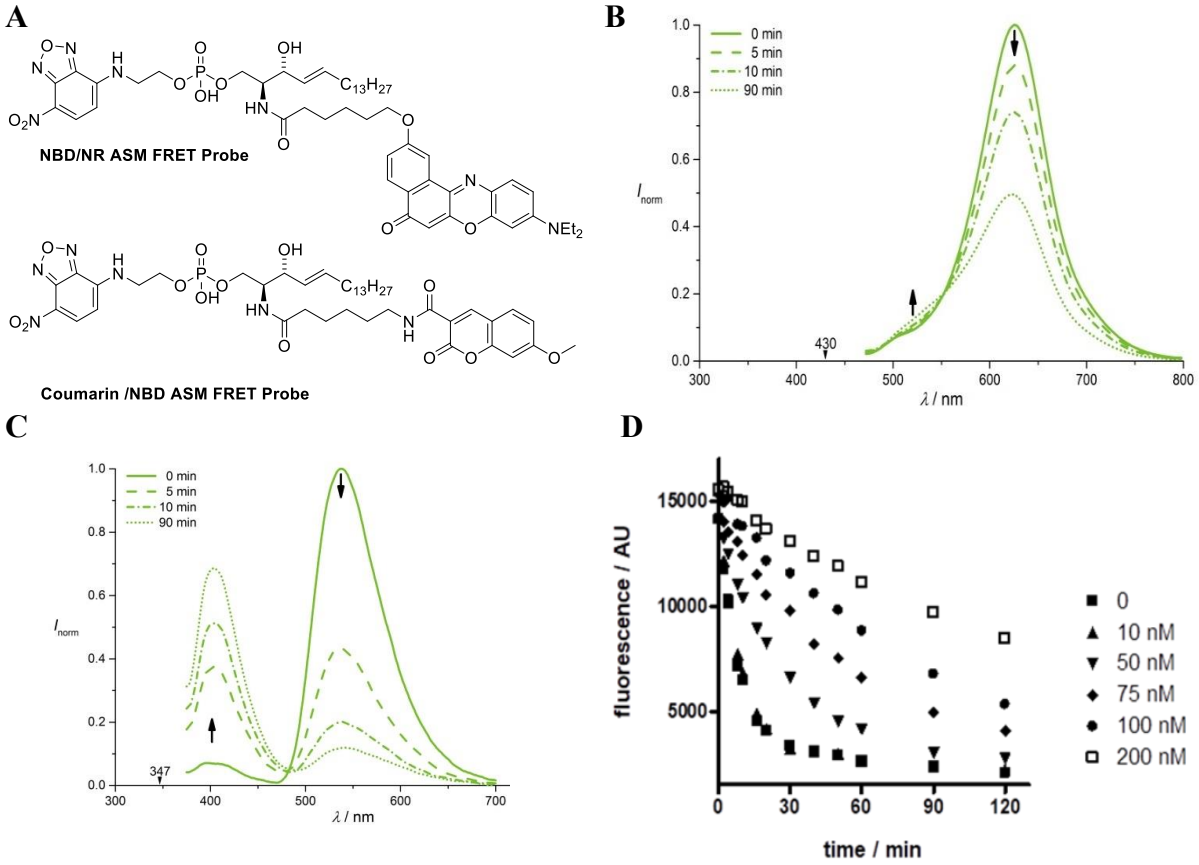

Figure 13. A) Structures of FRET probes developed by Pinkert et al. B) Fluorescence change of NBD/NR FRET probe upon incubation with ASM. C) Fluorescence change of probe Coumarin/NBD in presence of ASM. D) NBD fluorescence of the second probe in presence of ASM and different inhibitor concentrations.[115]

The second FRET probe was converted into a BSA complex and its cleavage was monitored in different cell types. All experiments showed an apparent probe cleavage, for at least 48 h. Overexpression of ASM in wildtype Mouse Embryonic Fibroblasts (MEFs) however significantly increased FRET change, showing that different ASM levels can be differentiated under live cell conditions.

In a recent study, Kappe et al. presented a developed form of the ASM FRET probes to address the shortcoming of ultraviolet (UV) excitation range of the former Coumarin/NBD probe. A new attempt towards a FRET substrate excitable in the visible range was made. BODIPY dye was introduced into the fatty acid part and a relatively polar fluorescein (FAM) residue (Ex. 485 nm/ Em. 518 nm) into the choline analogue head group to keep the polarity and membrane anchoring as close as possible to nature (**Figure 14A**).[125]

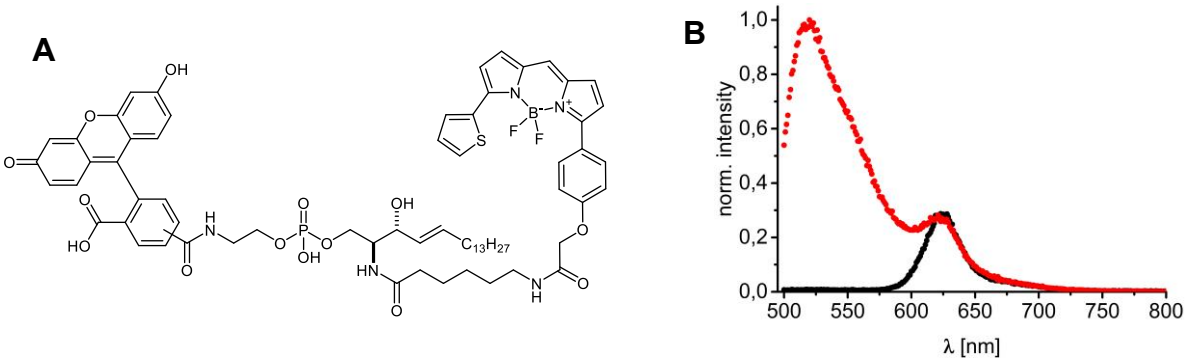

Figure 14. **A**) Structure of the visible range FRET probe. **B**) The Probe (Ex. 485 nm) before (black) and after (red) incubation with ASM.[125]

Upon incubation of a micellar solution of the novel substrate with rec ASM, the BODIPY acceptor fluorescence appeared to be almost unchanged, similarly to results with the Nile red containing probes[121,122]. Surprisingly, the fluorescence of FAM increased significantly by more than 100-fold as in **Figure 14B**. The new substrate enabled also differentiating between different concentrations/activities of ASM and allows for the first time to monitor relative sphingomyelinase activities of intact living cells by flow cytometry.

1.2.6.5 Two-photon excitation microscopy for the study of living cells

The effective sensitivity of fluorescence microscopy in live cells is limited by out of focus background signal, photobleaching and cells are prone to phototoxicity, especially when a short

wavelength is used. A further limitation is that in many biological specimens, autofluorescence is a large problem that excitation/emission filters might not completely get rid of[126]. This out of focus background and autofluorescence signal introduce a diffuse background fluorescence without any spatial information encoding, and therefore act to reduce the image contrast[127].To reduce the limitation of imaging extended samples and enable high-resolution 3-D imaging, the confocal microscope was developed with a confocal pinhole used to get rid of the out-of-focus background and produce a higher signal-to-noise ratio in the final image which corresponds to a thin (<1 μm) "optical section" (**Figure 15**)[128].

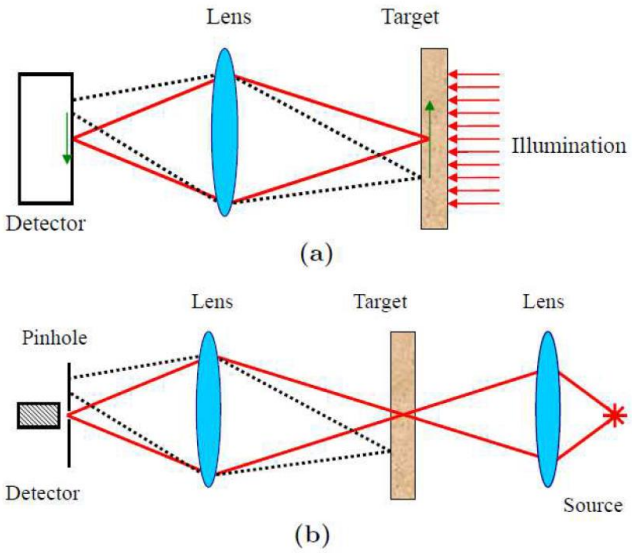

Figure 15. Different types of microscopy: (a) wide-field microscopy; (b) confocal microscopy.[129]

Two-photon excitation (2PE) microscopy is an advanced alternative to confocal microscopy that provides clear superiority for three-dimensional imaging. The main advantage of 2PE is the high localization of the excitation area (**Figure 16**) and the full detection of the emitted light because the full sensitive area of the detector is used in contrast to confocal microscopy. This allows the application of 2PE to thick, intact tissues such as brain slices, embryos, whole organs, and live animals (intra-vital imaging).[127,130]

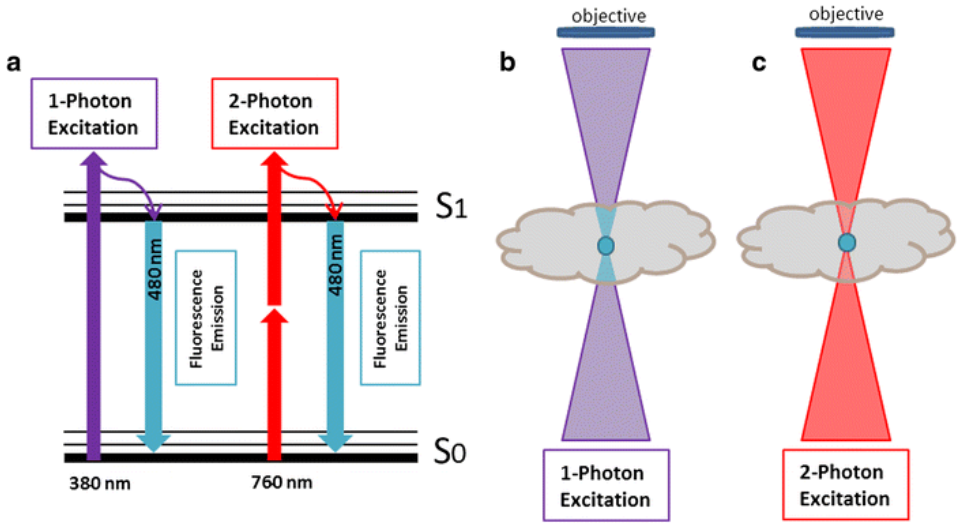

Figure 16. a) Simplified Jablonski scheme for one-photon (exemplified by 380 nm) and two-photon excitation. Fluorescent emission (cyan) within a biological sample in response to b) one-photon, c) two-photon excitation.[131]

The first prediction of two-photon absorption was by Göppert-Mayer (1931)[132]. She proposed that one atom or molecule should be capable of absorbing two photons simultaneously within $10x^{-16}$–$10x^{-17}$ s. The unit of two-photon absorption cross-section (GM) is named in her honor (1 GM = 10^{-50} cm^4 s $photon^{-1}$). Because it is a rare event at ordinary light intensities, it was only in the 1960s, after the development of laser sources, that the prediction could be verified[132]. The main difference between one-photon absorption (1PA) and two-photon absorption (2PA) is the ability to approach highly energetic excited states using relatively low-energy photons (**Figure 16**), and the I^2 dependence of the process which allows for excitation of a chromophore with a high degree of spatial selectivity in three dimensions using a tightly focused beam[133], whereas 1PA depends linearly on the intensity[132].

Molecules with a large two-photon absorption cross-section (σ) are in great demand for a variety of applications, including 2P fluorescence microscopy, optical limiting, three-dimensional optical data storage, and two-photon induced biological caging studies[134]. Exploring molecules that exhibit intense 2PA to open new pathways into its use and broaden existing 2PA applications is also a scientific challenge to explore the limits of the 2PA cross-section (σ) and to understand the structure-property relationships. Toward this goal, many research groups have done extensive research over the past decades[133–142]. The field of sphingolipids in general and sphingomyelinases monitoring especially are also in high need of developing new probes that can readily obey 2PE for deeper and clearer imaging and thus better understanding of the related biological events and pathological disorders.

1.3 Application of lanthanide luminescence in probing biological species

1.3.1 Luminescent lanthanide (III) complexes overview

Luminescent lanthanide (Ln) (III) complexes (LLCs) are getting increased attention in a wide range of bioanalytical applications, particularly those of europium(III) and terbium(III). Those lanthanide-based luminescent probes are particularly attractive for their long luminescence lifetimes. This long decay times offer a tremendous advantage for the time-gated measurement of biological samples wherein interfering short-lived autofluorescence and scattering is suppressed, drastically improving signal-to-noise ratio and increasing overall probe sensitivity. Compared to the conventional organic fluorophores, Ln(III) complexes offer several other advantages for use in biological applications. This includes a large separation between absorption and emission spectra which minimize the excitation light interference. They also exhibit a line-like emission spectra with clearly defined bands, allowing ratiometric analyses[143–145] . Because of their unrivaled aforementioned photophysical properties, LLCs are particularly useful as energy donors for FRET systems allowing much longer emission lifetimes to be observed for a conventional organic fluorophore, following excitation from a lanthanide donor[146].

Lanthanides possess intrinsic luminescence that originates from f−f electron transitions in the $4f^n$ shell of the $[Xe]5s^25p^6$ configuration and offer unique properties for optical imaging contrast agents that overcome current limitations of their organic homologous. First, due to shielding from the chemical environment by the filled, energetically lower 5s and 5p sub-shells, the 4f orbitals do not directly participate in chemical bonding. Thus, the emission wavelengths of lanthanides are minimally disturbed by the surrounding matrix and ligand field, resulting in sharp, line-like emission bands with the same fingerprint wavelengths and narrow peak widths of the corresponding free Ln(III) salts. Second, the f−f transitions are formally forbidden by the spin and Laporte rule making the direct excitation of Ln(III) ions is very inefficient but feature long excited-state lifetimes in the milli- to microsecond range. This property lends luminescent lanthanides to time-gated or time-resolved live-cell or in vivo imaging. Such an approach enhances signal-to-noise ratios through the elimination of interferences from scattering and short-lived autofluorescence of biological constituents as already mentioned. Finally, because the differences in electronic properties between the different Ln(III) ions reside in the shielded 4f orbitals, varying the metal center imposes minor effects on the chemical properties of the Ln(III) complex, allowing for facile multiplexing for ratiometric or multimodal applications.[143,147]

1.3.2 The antenna effect

The lanthanide ions (f-f transitions) have very weak absorption coefficients (ε), which makes direct photo-excitation of the lanthanide ions difficult. Intense light sources such as lasers are required to achieve the excited states of Ln(III) ions by direct excitation and are impractical for the majority of biological imaging. However, this can be overcome by using the large absorption cross-section of the organic chromophores and the energy transfer from organic chromophores to lanthanide ions.[143,147]

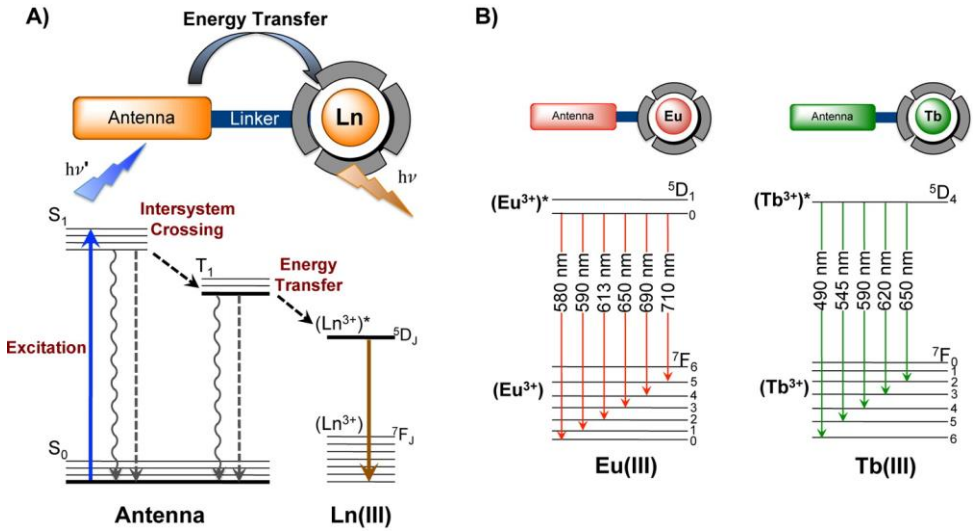

Figure 17. **A**) General architecture of luminescent lanthanide complexes showing the antenna effect: Excitation light excites the antenna, followed by energy transfer to the Ln(III) ion, which consequently emits light (upper). Jablonski Energy Diagram of Absorbance Energy Transfer Emission (AETE) mechanism for a Ln^{3+} complex (lower). **B**) Luminescent 4f−4f transitions of europium and terbium complexes and commonly observed emission wavelengths to emit red and green light, respectively.[143]

Thus, to design highly luminescent Ln^{3+} complexes, Weissman [148], first noticed the sensitization process in which the energy transfer takes place from coordinated ligands to the central metal ion. Light absorbed to the short-lived singlet excited state of the antenna (S0 → S1) can undergo non-radiative intersystem crossing to the longer-lived triplet excited state (S_1 → T_1). The non-radiative energy transfer from the T_1 state of the antenna to the lowest ^5D_J excited state of the lanthanide is the sensitization step resulting in metal-centered luminescence (**Figure 17A**). Energy transfer can also occur directly from the S_1 state, but energy transfer from the T_1 state is generally accepted as the mechanism due to its long lifetime. Final transitions from the ^5D_J excited state to the ^7F_J ground state of the lanthanide emit photons characterized by a series of specific bands in the visible (Eu(III) and Tb(III)) and near-IR (Dy(III) and Sm(III)) wavelengths (**Figure 17B**) .[143,144]

The nature of the sensitizing group can be particularly useful in designing responsive lanthanide probes, as changes to the antenna can modulate its absorption or energy transfer properties. These changes can result from irreversible reaction with biological analytes or reversible non-covalent interactions, disturbing the singlet or triplet excited states of the antenna.[144]

1.3.3 Design strategies for reactivity based lanthanide probes

According to the previous sections, the luminescence of lanthanides is depending on the next four parameters:[149,150]

1- The efficiency of the antenna's triplet excited state population.
2- The energy of the triplet excited state of the antenna relative to the ^5D excited state of the lanthanide ion.
3- The distance between the antenna and the lanthanide ion.
4- The number of coordinated water molecules.

Accordingly, these parameters can be manipulated to rationally design responsive luminescent probes.

1.3.3.1 Modulating luminescence via the Antenna−Ln distance

The energy transfer from the triplet excited state of the antenna to the metal ion drives to the sensitization of lanthanide complexes. The distance-dependence of this energy transfer process was exploited to modulate luminescence by altering the distance between the antenna and the metal center[143]. Distance modulation through analyte binding can be either by bringing the antenna in close proximity to the lanthanide ion as figured in **Figure 18A**, conjugating the antenna to the lanthanide complex as in **Figure 18B**, thereby starting the sensitization, or displacing a weakly coordinated antenna, thereby turning off the lanthanide's luminescence as in **Figure 18C** [151].

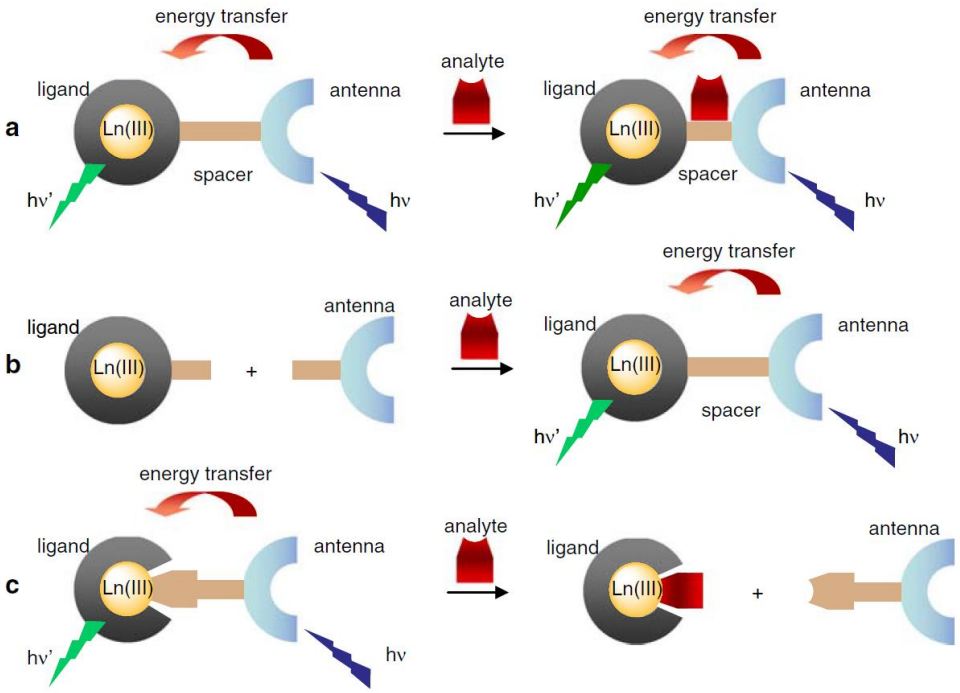

Figure 18. Modulating luminescence via the Antenna−Ln distance.[151]

An example of this class of sensors is the peptidic terbium probe synthesized by Schneider et al. for the luminescent determination of environmental redox potential. The linker contained a peptide sequence with a moderate propensity for β-sheet formation with cysteines that could respond to the environment (**Figure 19A**). Under reducing conditions, the cysteines remain protonated and the peptide prefers a flexible conformation with a long antenna−Ln distance and thus a weakly luminescent species. In contrast, oxidizing conditions induced disulfide bond formation between the cysteines and stabilized a β-sheet conformation, thereby bringing the antenna near the lanthanide and producing a highly luminescent species.[152]

Based on the advantage of the catalytic role of copper(I) in Huisgen 1,3-dipolar cycloaddition ("click") reactions, Viguier and Hulme designed a "turn-on" probe by attaching an alkyne-containing europium complex to a dansyl azide antenna. The covalent bonding of the antenna near the metal ion resulted in a 10-fold enhancement of luminescence compared to the free Eu(III) chelate (**Figure 19B**). This sensor could be a promising example of how components of existing synthetic methodologies will be manipulated for imaging applications. [153]

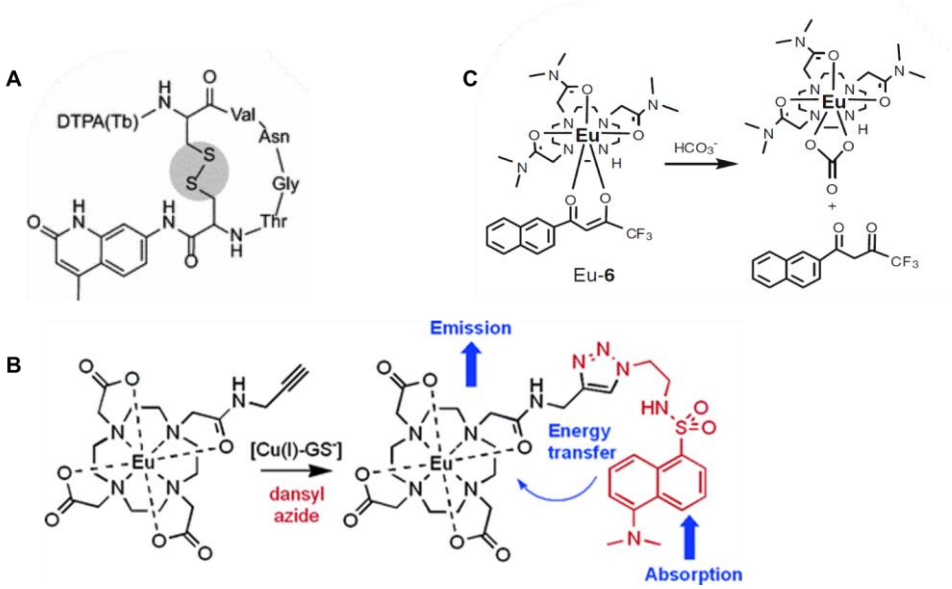

Figure 19. Examples of luminescent lanthanide sensors based on Modulating luminescence via the Antenna−Ln distance.

A "turn-off" luminescent europium complex was developed by Gunnlaugsson et al. in which displacement of a coordinated antenna by an analyte results in a sensor that senses anions via a displacement assay. The phenyl or naphthyl antennae are linked to a labile β-diketonate ligand. Displacement of the β-diketonate by a stronger chelating anion decreases the luminescence intensity of the europium as in **Figure 19C**.[154]

1.3.3.2 Modulating luminescence via coordinated water molecules

The long lifetimes of the ^5D excited states of the lanthanides render them particularly susceptible to quenching via nonradiative energy transfer to nearby O–H and N–H oscillators of lower energy. Since the fourth overtone of the O–H oscillator of water is slightly lower in energy than the excited ^5D states of europium and terbium, water molecules coordinated to these lanthanides are excellent quenchers of the metal's luminescence[151]. Therefore, in luminescent applications, lanthanides are typically chelated with multidentate ligands which protect the metal center from solvent coordination. Chelators such as EDTA derivatives, crown ethers, BAPTA (1, 2-bis(o-aminophenoxy)ethane-N, N, N', N'-tetraacetic acid), aza crown ethers or cryptands are frequently used as recognition elements for metal ions[155]. For biological imaging, chelation attenuates the toxicity of free lanthanide ions[143]. Since lanthanide ions typically adopt coordination numbers of between 8 and 9 in aqueous solution, the number of coordinated water molecules is readily governed through ligand design[156].

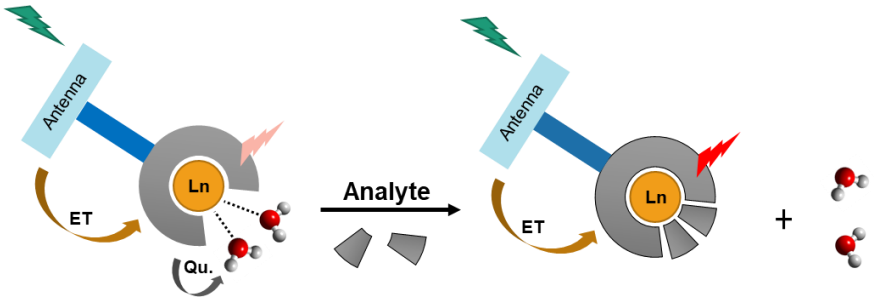

Figure 20. Modulating the luminescence of lanthanide complex via displacement of coordinated water molecules. ET : Energy transfer ; Qu: Quenching.

If the Ln(III) coordination sphere is not fully saturated, water molecules will occupy the free coordination sites, resulting in quenching of luminescence. The quenching effect of bound water molecules can be utilized for the design of responsive Ln(III) complexes, wherein water molecules coordinated on the lanthanide ion can be readily displaced by hard anions such as carboxylates and phosphates[151,156]. Therefore, in principle, a lanthanide complex comprising an antenna and one or more open coordination sites can be used as a turn-on sensor for hard, preferably polydentate, anions. In the off state, the open coordination sites will be filled with exchangeable water molecules that will quench the emission of the lanthanide. Displacement of these coordinated water molecules by hard anions eliminates this quenching, thereby increasing luminescence from the lanthanide as sketched in **Figure 20**. One should note that lanthanides are hard, oxophilic ions that preferentially bind carboxylates and phosphates, thereby limiting the number of analytes that can be targeted using this approach[151].

Based on the fact that anions are ubiquitous throughout biological systems, their determination is an essential tool in environmental monitoring. The presence of anions plays an important role in biomedical and catalytical processes, whilst pollutant anions have been linked to eutrophication of rivers (from the overuse of phosphate-containing fertilizers) and carcinogenesis (metabolites of nitrate)[157]. Therefore, the design of anion-sensitive probes with sufficient sensitivity and selectivity is a demanding task in analytical sciences and chemical sensor technology [158]. Primarily, probes for the detection of biologically relevant anions such as phosphates, acetate, carbonate, or halides were in the focus over the past years [159,160]. The problem in using this approach to detect oxoanions is achieving sufficient selectivity over other oxoanions also present in the media. pH-dependence of analyte speciation and binding affinity must be carefully taken into consideration.

Stephan Butler reported two water-soluble luminescent probes $\mathbf{[Eu.L^{1-2}]^{+}}$, each capable of binding and sensing fluoride in pure water samples, with minimal interference from other anions.

Fluoride binds reversibly to each probe, displacing the coordinated water (**Figure 21 A**), resulting in a 9-fold enhancement in the overall emission intensity and dramatic changes in emission spectral form.[161]

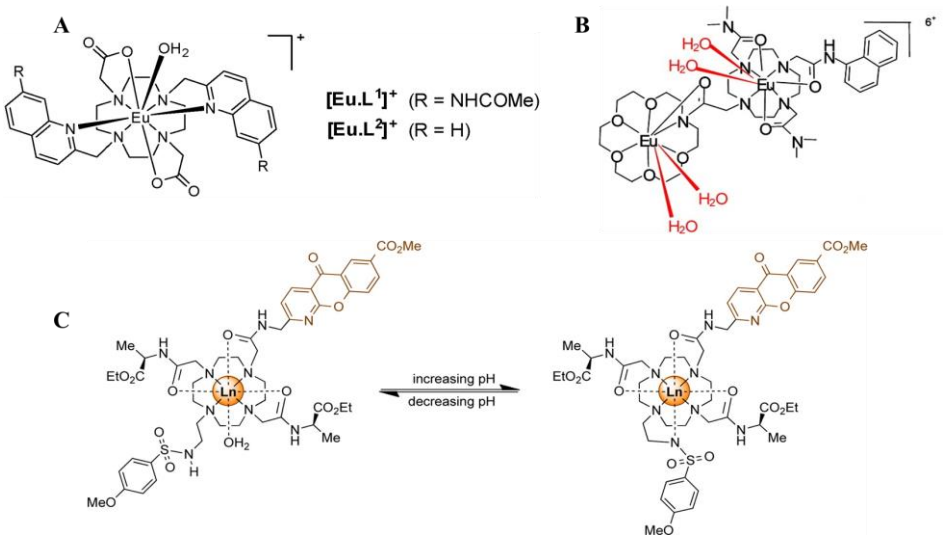

Figure 21. luminescent lanthanide sensors based on modulating the luminescence of lanthanide sensors via the number of coordinated water molecules. A) Europium complexes for quantitative determination of fluoride in pure water[161]. B) Europium sensor for the selective luminescent detection of malonate[162]. C) A pH-responsive lanthanide luminescent probe[143].

Some selectivity for oxoanions has been achieved in water as reported by The Gunnlaugsson group. They developed a bismacrocyclic dinuclear europium sensor (**Figure 21B**) for the selective luminescent detection of malonate. In pH 6.5 solutions, small dicarboxylic acids such as succinic, malonic, aspartic, or glutaric acid were shown to be bind also. However, only malonic acid gave rise to selective Eu(III) luminescent enhancements, as the emission was reduced for all of the other acids.[162]

Parker and coworkers developed a pH-sensitive europium sensor based on the intramolecular displacement of a bound water molecule following the deprotonation of the sulfonamide antenna. Under acidic conditions, the complex coordinates two water molecules that quench the luminescence of the europium. However, at alkaline pH, deprotonation of the sulfonamide enables direct coordination of the lanthanide by the nitrogen (**Figure 21C**). The concomitant displacement of both inner-sphere water molecules results in a significant increase in europium luminescence.[163]

Several more examples have emerged that demonstrate the potential of bound water displacement in biological applications and due to space limitations, the reader is referred to additional examples provided in different review articles.[164–167]

1.3.3.3 Modulating luminescence via direct coordination of the antenna or modulation of the Antenna Excited State

Effective sensors can be designed by combining both previous principles if one targets a chromophore that is directly capable of coordinating the lanthanide. The use of a stable lanthanide complex with one or more open coordination sites is required and the targeted analyte should be both an effective sensitizer and a hard ligand.[151]

Coordinately unsaturated terbium complexes possess two labile metal-bound water molecules were designed according to this strategy by Gunnlaugsson *et al*[168]. Water molecules can be displaced when terbium chelates aromatic carboxylic anions such as salicylic acid in water, which gives rise to a significant increase in the Tb(III) luminescence.

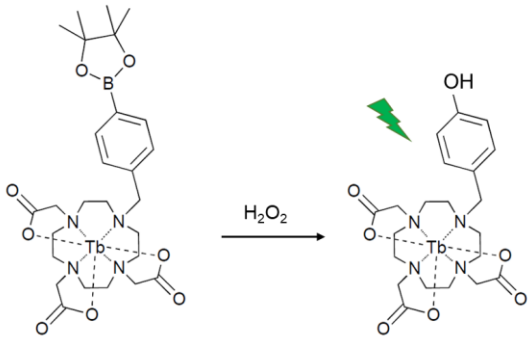

Figure 22. Caged antenna approach for the detection of hydrogen peroxide.

Altering the antenna excited state through chemoselective reactions with analytes is a promising approach for detecting reactive small molecules like hydrogen peroxide, and nitric oxide. Lippert et al. developed lanthanide-based luminescent probes for the detection of hydrogen peroxide (H_2O_2) in living systems as shown in **Figure 22**. The chemoselective reaction of these caged antenna probes with H_2O_2 activated the formation of the sensitizer and enhanced the luminescent intensity by 6-folds[169].

Some other strategies are relying on modulating the luminescence of a complex by altering the triplet state T_1 of the antenna through an analyte triggered chemical modification. This approach requires an antenna that can selectively react with the desired analyte to give a product that has a triplet state of substantially different energy from the pre-antenna[151,170].

2 Objectives of the present work

The overall aim of the present study was the synthesis and characterization of novel chemical tools for the *in vitro* and *in vivo* investigation of lipid metabolism. The main focus was on the monitoring of the acid sphingomyelinase, a key enzyme in the sphingolipid signaling network.

2.1 Design and synthesis of novel Europium complexes for ASM monitoring

Luminescent lanthanide complexes (LLCs) are widely used probes implemented for phosphate anion detection. Our goal was to apply this approach for monitoring the ASM cleavage product, phosphocholine (PC), as a measure of ASM activity. We hypothesized that the released PC can displace the coordinating water molecules on the metal sphere and give rise to luminescence enhancement which can be further quantitively correlated to the ASM activity (**Figure 23**).

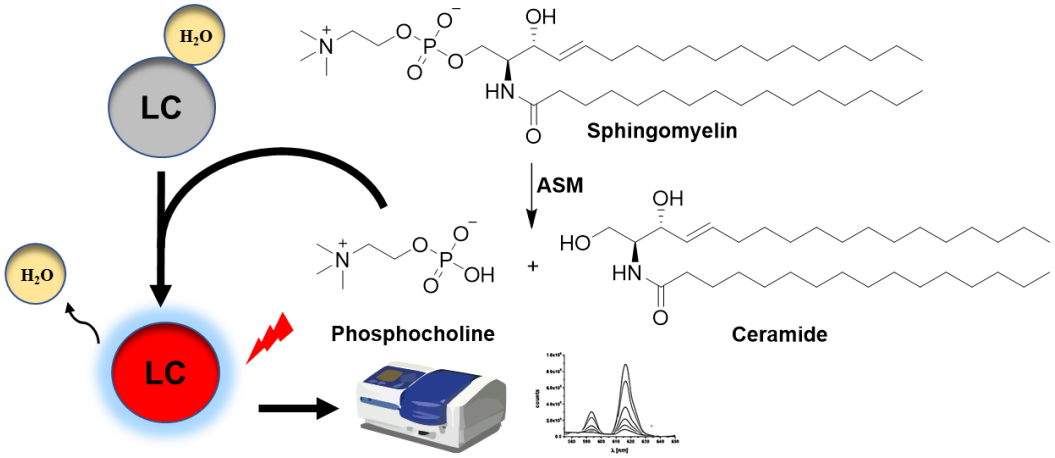

Figure 23. Hypothesis of ASM monitoring using LLCs.

2.2 Design, synthesis and characterization of ASM FRET probes

Our goal was to achieve the design and synthesis of ASM-FRET probes (**Figure 24**) for better ASM monitoring and quantification in addition to broadening the applications for the already synthesized probes.

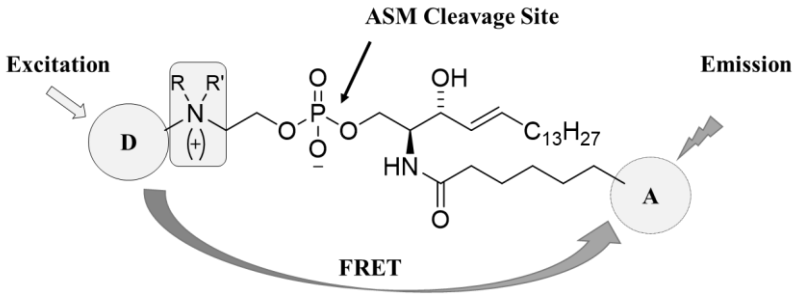

Figure 24. General structure for the ASM FRET probes. D: FRET donor, A: FRET acceptor, R&R': H or CH_3.

2.2.1 ASM-FRET probe with better two photon excitability

Given the advantages of 2PE microscopy, a novel and more efficient 2P excitable FRET probe was envisioned. Our goal was to use the recently reported[171] bromo-coumarin moiety with its significantly high 2PE cross-section as a FRET donor to enhance the 2P-excitability of the probe (**Figure 25**). In addition, the red shift of the new coumarin could result in a better donor/acceptor spectral overlap and accordingly a more efficient energy transfer.

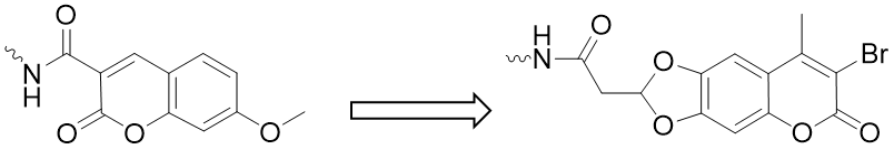

Figure 25. Envisioned FRET-donor modification for better 2P- excitability.

2.2.2 Sphingomyelinase-FRET probes with quaternary ammonium center

Due to the importance of the ammonium group[109] for the recognition and thus hydrolysis of sphingomyelin analogues by sphingomyelinases, we hypothesized that a sphingomyelin mimicking FRET probe with a quaternary ammonium group (**Figure 24**) would be highly recognizable and rapidly cleavable. It could also be a substrate not only for ASM but may be for nSMases and other comparable sphingomyelinases.

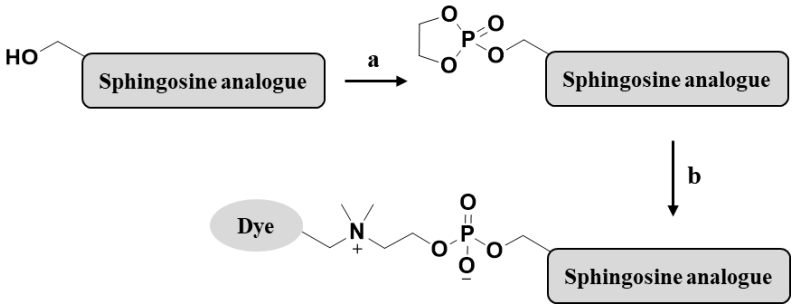

Figure 26. Partial schematic representation of the envisioned synthesis of an ASM-FRET probe with a quaternary ammonium group. a: phosphorylation, b: Quaternization and labelling, Dye: could be the FRET donor or acceptor.

The synthetic goal was to apply a sphingosine phosphorylation strategy which enables the insertion of a quaternary ammonium group accompanied/or followed by the labeling with the fluorescent dye as schemed in **Figure 26**. Incorporation of a terminal functional group like alkyne functionality can serve as a bioorthogonal handle for the introduction of a wide range of fluorophores or other labeling agents using aqueous phase chemistry.

2.2.3 Synthesis of the originally reported probes for novel applications

A high throughput screening (HTS) for potential ASM inhibitors was planned using the reported ASM FRET probe[121]. For this purpose, a more economically affordable upscaling of the synthesis was envisioned.

The reported NBD mono-labelled probe[56] was proved as an *in vitro* ASM turn-off probe. Resynthesis and testing of this probe as a potential *in vivo* ASM quenched probe for studying inhibitors and ASM deficient cells were envisioned.

3 Results and Discussion

3.1 5- and 4- dentate europium Complexes for anion sensing and their applicability to enzymatic dephosphorylation reactions

As discussed in section **1.3**, luminescent lanthanide complexes (LLCs) are promising tools for phosphate species detection. They are characterized by their long luminescence lifetimes which makes them suitable for the time-gated measurement of biological samples wherein interfering short-lived autofluorescence and scattering are suppressed. They also exhibit large separation between absorption and emission spectra and line-like emission spectra with clearly defined bands. This behavior minimizes the excitation light interference and allows ratiometric analysis [143–145]. As phosphocholine PC is the cleavage product of SM hydrolysis by ASM, we proposed that the quantitative detection of this PC using LLCs can be a good monitoring tool for ASM. For this purpose, we designed and synthesized two Eu complexes and tested them for the detection of different phosphate species including PC. Their applicability to enzymatic dephosphorylation reactions was also studied.

3.1.1 Synthesis of the 5-dentate europium complex

The 5-dentate **5-D**$^{+}$ complex was prepared in seven steps starting from commercially available chelidamic acid (**Scheme 4**). In the first step, diethyl 4-bromopyridine-2, 6-dicarboxylate **101** was synthesized by heating chelidamic acid with phosphorus pentabromide followed by the esterification with ethanol. The yield was 90% which is comparable with the reported data[172–175]. In general, this reaction consists of two steps, bromination, and esterification and they are easily exchangeable with a neglected yield difference[176,177]. The ester groups were then reduced with $NaBH_4$ to yield 4-Bromo-2, 6-pyridine-dimethanol **102**[178]. The reported purification led to very low yield (~15%) and the trials of using column chromatography for purification failed due to the dissolution of silica in the highly polar mobile phase needed to elute such a polar chelating compound. Finally, the continuous extraction with chloroform for one day (Soxhlet extraction) resulted in a 70% yield. 4-Bromo-2, 6-pyridine-dimethanol **102** was then transformed to bromomethyl functions using phosphorous tribromide to yield the tri-brominated intermediate **103** in 68% yield[179]. This strategy of reduction/bromination before the cross-coupling (step e in **scheme 1**) was followed to avoid any possible side reactions such as bromination of the triple bond which can occur in case of the active brominating reagents such as PBr_3. [180]

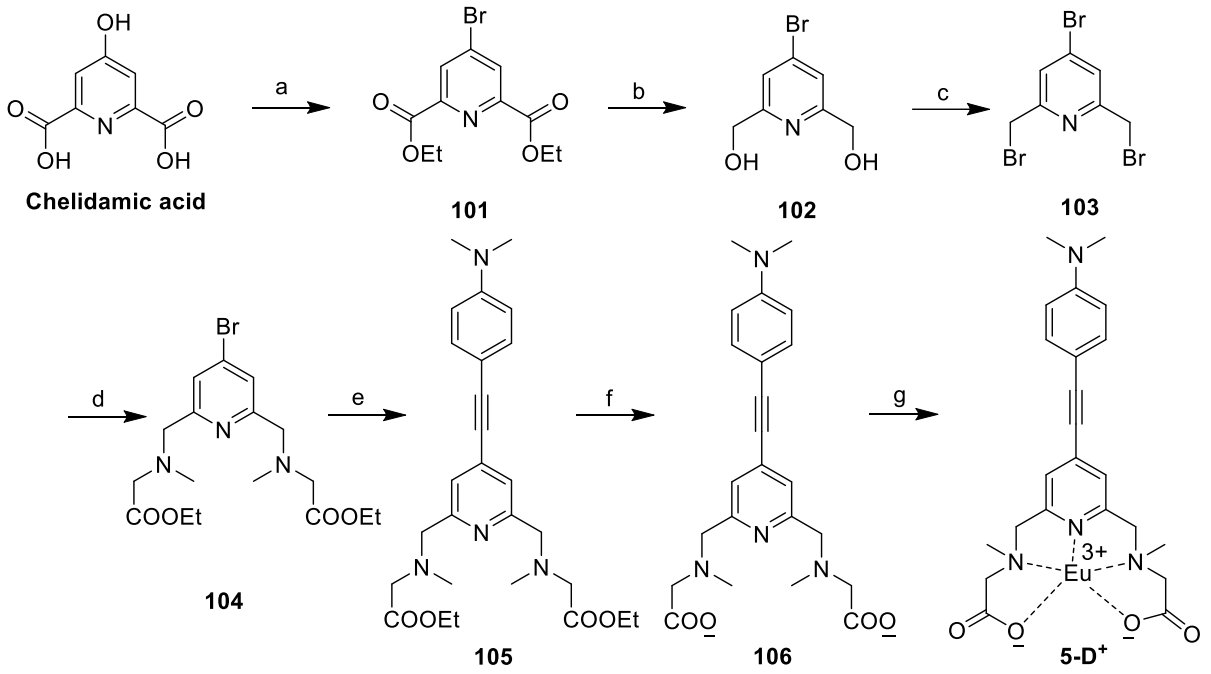

Scheme 4. Synthesis of the 5-D$^+$ complex. a) PBr_5, 90 °C, 2.5h, 0°C, EtOH, 90%; b) $NaBH_4$, EtOH, 0 °C, -80°C, 12h, Soxhlet extraction, 70%; c) PBr_3, $CHCl_3$, 62°C, 4h, 68%; d) Ethyl 2-(methylamino)acetate hydrochloride, K_2CO_3, CH_3CN, 83°C, 4h, 72%; e) 4-ethynyl-N,N-dimethylaniline, THF, $Pd(PPh_3)_2Cl_2$, CuI, Et_3N, 3h, RT , 50%; f) KOH, MeOH, 65°C, 3h, 89%; g) $EuCl_3 \cdot 6H_2O$, H_2O, pH 5 - 6.5, 2h, RT.

The symmetric ethyl 2-(methylamino)acetate chelating arms were introduced by reaction with a four-fold excess of ethyl-2-(methylamino) acetate following the procedure of similar coupling[181] to afford compound **104** in a good yield. The time and number of equivalents were enough to fully substitute both sides and thus no unsubstituted or singly substituted byproducts were detected. The structure of this new compound was confirmed using ^1H and ^{13}C NMR (see experimental) which revealed doubly integrated intensity for each peak in case of ^{1}HNMR and number of peaks which are half of the number of the common carbon atoms in ^{13}C NMR due to the symmetry of the structure.

The antenna chromophore ligand **105** was obtained via Sonogashira coupling of **104** with 4-ethynyl-*N*, *N*-dimethylaniline. During the first trials following similar coupling procedures [182,183] which include refluxing for overnight and a relatively higher palladium catalyst concentration, two main problems were faced: the first one is the very low yield due to the formation of the homocoupling byproduct and the second is the difficulty of the product purification from the catalyst side product triphenylphosphine oxide (**Figure 27**). To minimize the formation of the homocoupling product, 4-ethynyl-N, N-dimethylaniline was added drop-wisely at 0°C and then the reaction was stirred at room temperature for only 4 h.

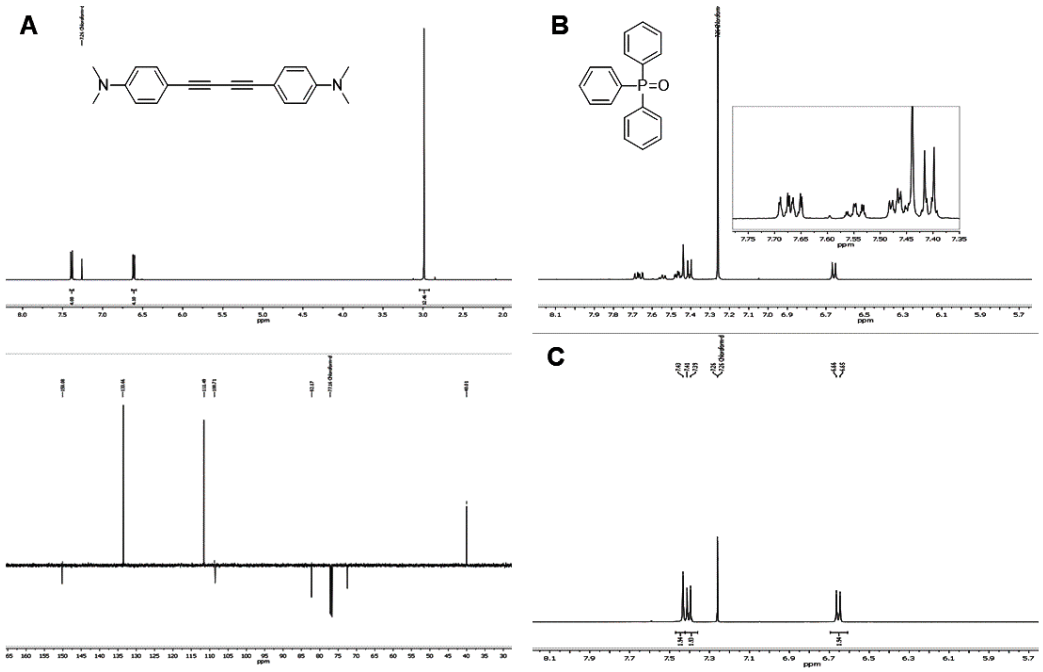

Figure 27. Cross coupling Reaction. A) Homocoupling product structure and NMR characterization after isolation from the product **105** reaction mixture; B) triphenyl phosphine oxide structure and interference with the ^{1}H-NMR spectrum of compound **105**; C) ^{1}H-NMR spectrum aromatic section of compound **105** after optimization and purification.

With this strategy combined with using the least possible equivalents of the palladium catalyst, the yield of the product was improved to 50%, and the resulting triphenylphosphine oxide could be highly minimized and removed with column chromatography. The ethyl esters were then hydrolyzed to get the free carboxylate moieties. Both acidic and alkaline hydrolysis were tried but finally, the alkaline hydrolysis was considered for its better yield and ease of isolation of the product **106**. The 5-dentate ligand was directly complexed with $EuCl_3 \cdot 6H_2O$ in aqueous solution affording the 5-dentate complex **5-D**$^{+}$ which was used for the next fluorescence studies in solution form without further purification.

3.1.2 Synthesis of the 4-dentate europium complex

The 4-dentate **4-D**$^{+}$ complex was prepared in six steps starting from the previously prepared intermediate **101 (Scheme 5**). **101** was partially reduced to the corresponding alcohol **107** following the previous reduction procedure but with only 1.14 equivalent of $NaBH_4$. The reaction mixture was stirred for only 1h at room temperature to avoid full reduction of the starting compound. The bromination of the former product revealed compound **108** in a very good yield. The ethyl 2-(methylamino) acetate chelating arm was introduced similarly by reaction with ethyl-2-(methylamino) acetate resulting in **109**.

The previously established Sonogashira coupling conditions were used also to get the antenna chromophore ligand **110** with a 10% higher yield. Alkaline hydrolysis of the ethyl esters gave the product **111** in a 90% yield which was then complexed with Europium following the same previous procedure to get the **4-D**$^{+}$.

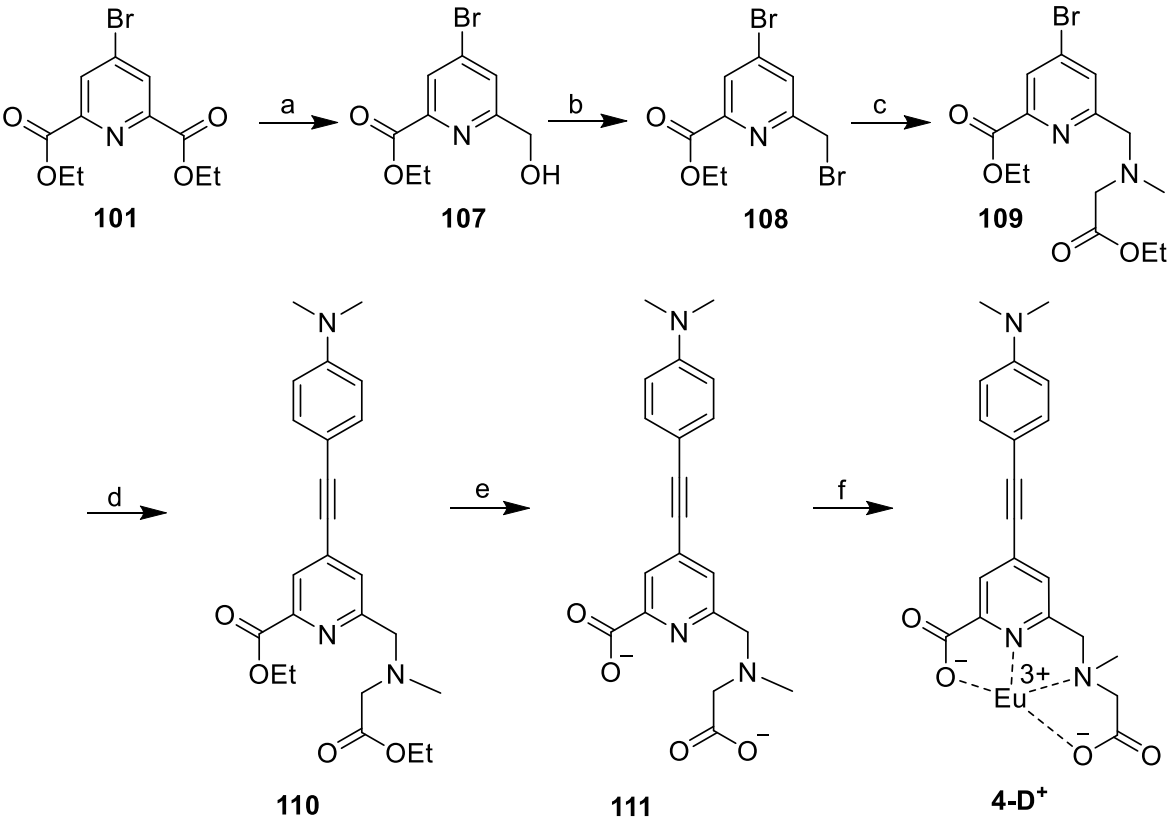

Scheme 5. Synthesis of the 4-D^{+} complex. a) $NaBH_4$, EtOH, RT, 1h, 38%; b) PBr_3, DMF , RT, 3h, 95%; c) Ethyl 2-(methylamino)acetate hydrochloride, K_2CO_3, CH_3CN, 83°C, 18h, 60%; d) 4-ethynyl-N,N-dimethylaniline, THF, $Pd(PPh_3)_2Cl_2$, CuI, Et_3N, 5h, RT , 60%; e) KOH, MeOH, 65°C, 3h, 90%; f) $EuCl_3 \cdot 6H_2O$, H_2O,pH 5 - 6.5, 2h, RT.

3.1.3 General properties of the europium complexes

The spectral properties of the europium complexes were measured by *Prof. Michael Schäferling* and are summarized in **Table S 1**, including the absorption maxima and molar absorption coefficients ε. The number water molecules q(H_2O) in the first coordination sphere of europium is calculated on the basis of difference of the mean lifetimes τ_M in H_2O and D_2O, according to the equation derived by *Supkowski* and *Horrocks:*[184]

$$q(H_2O) = 1.11[\tau_M^{-1}(H_2O) - \tau_M^{-1}(D_2O) - 0.31]$$

The calculated values for q(H_2O) clearly indicate the increasing number of coordinated water molecules by reducing the binding sites of the ligand. These are in good correlation to the theoretical quantities of four and five bounding water molecules for five and four-dentate complexes, respectively (based on a maximum number of nine binding sites for Eu^{3+})[185186]. It is obvious that the mean lifetimes in water decrease with the number of free binding sites at the europium center due to increased coordination of quenching water molecules. On the other hand, the mean lifetimes in D_2O increase from **5-D**$^+$ to **4-D**$^+$. In absence of quenching water molecules, the efficiency of the energy transfer from antenna chromophore to europium is the most important factor.

In the case of **4-D**$^+$, one binding carboxylic acid group is directly attached to the pyridine ring. This causes closer coordination of the europium to the antenna chromophore compared to **5-D**$^+$ with the longer ethyl 2-(methylamino) acetate binding arms**,** thus leading to a more efficient energy transfer. This is in accordance with the previous observations[181]. Competing radiationless deactivation processes are minimized with shorter europium-ligand distances. Correspondingly, the asymmetric five dentate complex with a shorter binding arm described in the previous reference[181] had a significantly longer lifetime in D_2O than **5-D**$^+$. The higher efficiency of the energy transfer with shorter binding arms leads to an increasing intensity of the 617 nm emission of Eu^{3+} from **5-D**$^+$ to **4-D**$^+$ with relative intensities of 1:5 respectively (time-gated detection). **Figure S 3** in the Supporting Information shows the fluorescence spectra of the corresponding ligands before and after the complexation of Eu^{3+}. They also indicate the increasing energy transfer efficiency.

3.1.4 Luminescence response of the 5-dentate complex (5-D^+)

The effect of different phosphate anions on the luminescence intensity of 5-$\mathbf{D}^+$ was studied. Variable effects, which occur in all cases immediately were noticed as in **Figure 28**. ATP has the highest increasing effect on the luminescence intensity of 5-$\mathbf{D}^+$ compared to the other anions. Two-fold excess of ATP resulted in a twenty-fold increase of luminescence intensity while saturation of the effect was observed at higher concentrations. Selective response of the **5-$\mathbf{D}^+$** to di- and tri-phosphates could be observed at ratios higher than 1:5 (anion:**5-$\mathbf{D}^+$**).

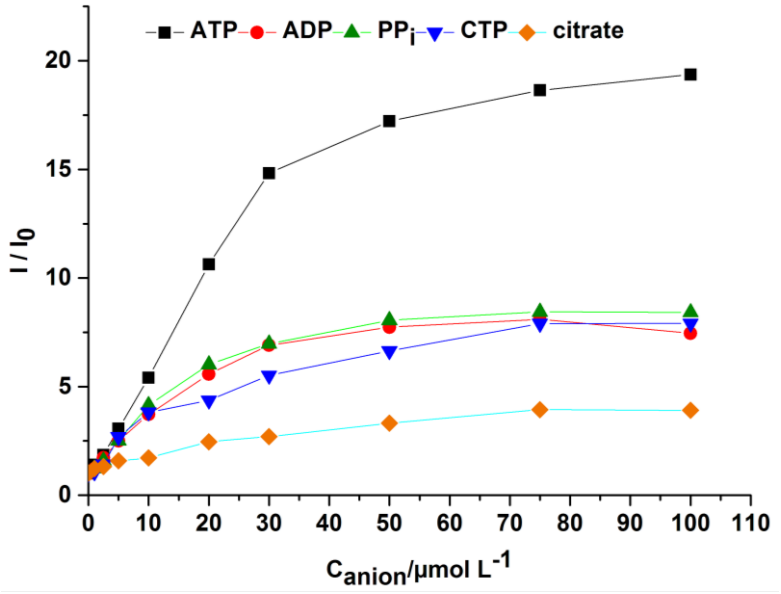

Figure 28. The Normalized luminescence responses (I/I_0) of **5-$\mathbf{D}^+$** to ATP, ADP, CTP, PPi and citrate in TRIS buffer (pH 7.4). (Conc. of **5-$\mathbf{D}^+$** =50 µmol L^{-1}), I_0 is the luminescence intensity in the absence of phosphate; λ_{ex} = 345 nm, λ_{em} = 618 nm; time-resolved measurement, Lag time: 100 µs, signal integration time: 400 µs.

To study the effect of the nucleoside part on the luminescence intensity change, we compared the effect of two different triphosphates moieties (ATP and CTP) and two different diphosphate moieties (ADP and PP_i). The difference was significant comparing ATP and CTP while in the case of ADP and PP_i no significant difference was observed. It was concluded that the overall effect is a combination of both the number of phosphate groups and the size of the nucleoside part (in addition to other factors), but the dominant contribution of effect is that the number of phosphates. Comparing the effect of AMP and P_i as in **Figure 29** revealed that the presence of the nucleoside part in AMP neutralized the strong decrease of the luminescence intensity caused by P_i which seems to interfere with the energy transfer between The europium and the antenna chromophore.

Assessment of the effect of citrate as a carboxy anion on the luminescence intensity of the **5-D**$^+$complex revealed an intensity triplication by the addition of an equimolar amount of citrate. 2:1 ratio of citrate to **5-D**$^+$ increased the luminescence intensity by about four-folds.

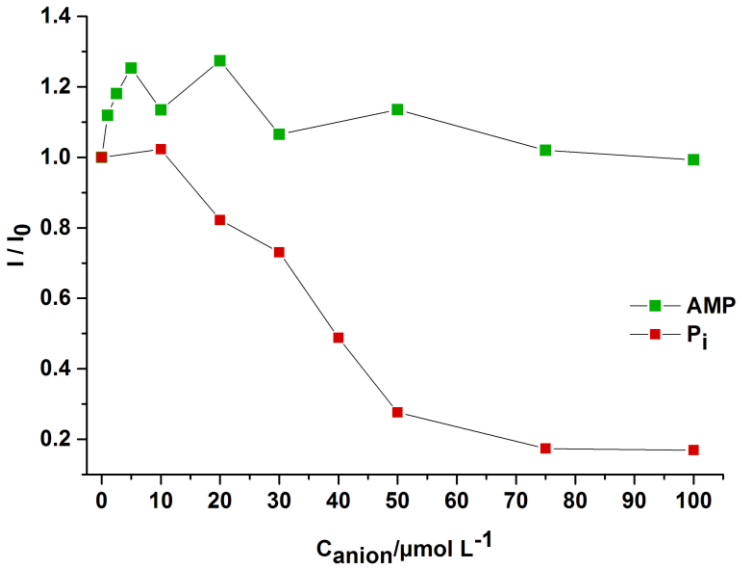

Figure 29. The Normalized luminescence responses (I/I_0) of **5-D**$^+$ to AMP and phosphate (Pi) in TRIS buffer (pH 7.4). (Conc. Of **5-D**$^+$=50 µmol L^{-1}), I_0 is the luminescence intensity in the absence of phosphate; λ_{ex} = 345 nm, λ_{em} = 618 nm; time-resolved measurement, Lag time: 100 µs, signal integration time: 400 µs.

For purposes of assay transfer and better applicability, the reproducibility of the response was assessed using different plate readers in two different institutes and the results were identical to a higher extent. **Figure S 4** in the Supporting Information shows the effect of ATP on the luminescence Intensity of **5-D**$^+$ using two different microplate readers.

3.1.5 Luminescence response of the 4-dentate complex (4-D$^+$)

A significant change in the response behavior to the different anions was observed due to the additional free binding site at the **4-D**$^+$ complex. Compared to a twenty-fold increase in the case of the **5-D**$^+$ complex, only a three-fold increase in the luminescence intensity could be observed after the addition of a two-fold excess of ATP to the **4-D**$^+$ complex (**Figure 30**). Accordingly, the slope of the linear fit in the concentration range from 0 to 30 µmol L^{-1} ATP is less steep and the LOD for ATP determination amounts 3.6 µmol L^{-1} (for c = 50 µmolL^{-1} of **4-D**$^+$). Only a two-fold increase of luminescence intensity was observed after adding the same amount of ADP which figures out the significant effect of the number of phosphate groups. With its different nucleoside part, CTP afforded about a 2.5-fold increase in the luminescence intensity. PP_i unexpectedly resulted in a decreased luminescence intensity to half of the initial value at a molar ratio of 1: 5 PP_i: **4-D**$^+$ complex.

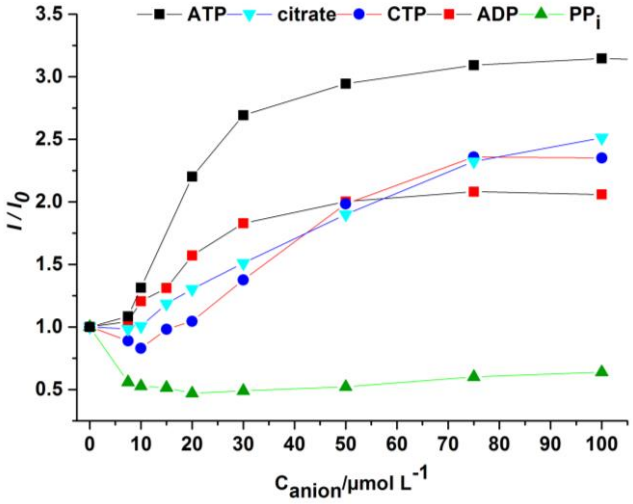

Figure 30. The Normalized luminescence responses (I/I_0) of **4-D**$^+$ to ATP, ADP, CTP, PPi and citrate in TRIS buffer (pH 7.4). (Conc. Of **4-D**$^+$ =50 µmol L^{-1}), I_0 is the luminescence intensity in the absence of phosphate; λ_{ex} = 345 nm, λ_{em} = 618 nm; time-resolved measurement, Lag time: 100 µs, signal integration time: 400 µs.

Anions with a single phosphate group (P_i and AMP) revealed a significant decrease of the luminescence intensity, regardless of the presence or absence of the nucleoside (**Figure 31**). This opposite effect of PP_i and monophosphates proposes a different explanation for the luminescence response than the replacement of coordinating water molecules. Most likely, the interference of the coordination of europium to the ligand and consequently the energy transfer by these anions. With β-diketonate ligands a displacement of the ligand was found after the addition of PP_i or ATP, generating a luminescence decrease[187]. This was also observed using tetracycline as sensitizing ligand[188].

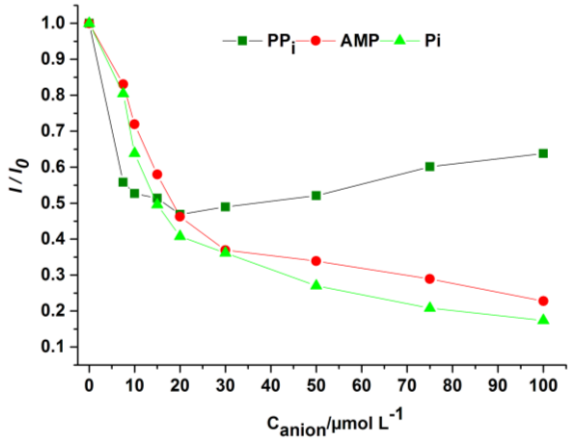

Figure 31. The Normalized luminescence responses (I/I_0) of **4-D**$^+$ to PPi, AMP and Pi in TRIS buffer (pH 7.4). (Conc. Of **4-D**$^+$ =50 µmol L^{-1}) I_0 is the luminescence intensity in the absence of phosphate; λ_{ex} = 345 nm, λ_{em} = 618 nm; time-resolved measurement, Lag time: 100 µs, signal integration time: 400 µs.

3.1.6 Optimization of the phosphate complex reaction for monitoring the acid sphingomyelinase activity

Inspired by the response of the synthesized complexes to different phosphate species, we commenced to optimize the application of the complexes to be used for monitoring the acid sphingomyelinase activity.

3.1.6.1 Luminescence response of 4-D$^+$ and 5-D$^+$ complexes to phosphorylcholine

The effect of phosphorylcholine PC, the phosphate species which results from the enzymatic cleavage of sphingomyelin, on both **4-D$^+$** and **5-D$^+$** was studied using the standard condition for the previously studied anions (**Figure 32 A**). The response of the **5-D$^+$** complex to an increasing concentration of phosphorylcholine was not significant in general although it showed a slightly decreasing change of the luminescence intensity in the lower concentration range. On the other hand, the change of the luminescence intensity of the **4-D$^+$** complex upon addition of increasing concentration of phosphorylcholine was significant and comparable to the effect of AMP, Pi in **Figure 31**. The addition of an equimolar amount 1:1 ratio of phosphorylcholine to **4-D$^+$** decreased the luminescence intensity to about one fifth of the initial intensity.

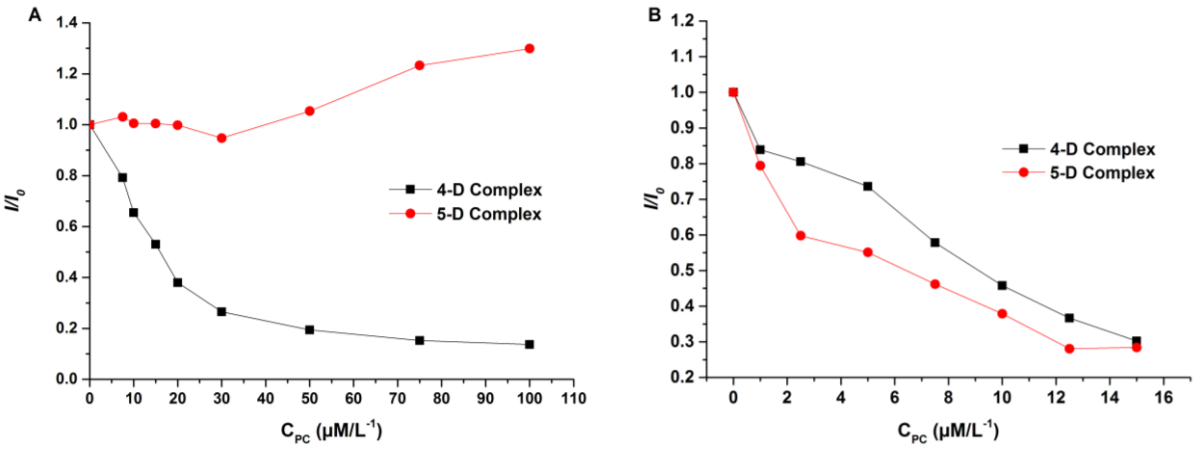

Figure 32. Normalized luminescence responses (I/I_0) of **4-D$^+$** and **5-D$^+$** to PC. **A**) Conc. Of Complex =50 µmol L^{-1} **B**) Conc. of Complex =10 µmol L^{-1} . TRIS buffer (pH 7.4), I_0 is the luminescence intensity in the absence of PC; λ_{ex} = 345 nm, λ_{em} = 618 nm; time-resolved measurement, Lag time: 100 µs, signal integration time: 400 µs.

To use a more realistic concentrations for an enzymatic reaction, a new experiment with a lower concentration scale of both the complexes (10 µmol L^{-1}) and the tested phosphorylcholine (0-15 µmolL^{-1}) were used keeping the same other conditions of the previous experiment. Interestingly, both complexes showed a similar behavior at this concentration scale (**Figure 32 B**).

For quenching 50% of the luminescence intensity of the **4-D**$^{+}$, 0.9:1 ratio of phosphorylcholine to complex was needed while only 0.6:1 ratio was needed in the case of the **5-D**$^{+}$. Because of the stability of response to phosphorylcholine in the case of **4-D**$^{+}$ in both concentration scales, it was selected for the next optimization step.

3.1.6.2 The effect of the acidic pH on the responsiveness of the 4-D^{+} Europium complex

Because the pH optimum of the acid sphingomyelinase *in vitro* was between 4.5 and 5.0 [60], our next optimization step was to check the validity of the **4-D**$^{+}$ complex response at this acidic pH range. A general decrease of the luminescence intensity was observed before the addition of phosphorylcholine (**Figure 33A**). It is reported that in case of the complexation of metal ions with acidic ligands like carboxylates, the complexation process is accompanied by deprotonation of ligand [189]. So, this luminescence quenching can be referred to the suppression of deprotonation at this acidic pH and thus the decrease of complexation efficacy. Despite this general intensity decrease, the behavior of the **4-D**$^{+}$ complex was similar to that at pH 7.4 upon addition of different concentrations of phosphorylcholine. 50% luminescence intensity decrease of the **4-D**$^{+}$ was observed at 0.75:1 molar ratio of phosphorylcholine to the complex.

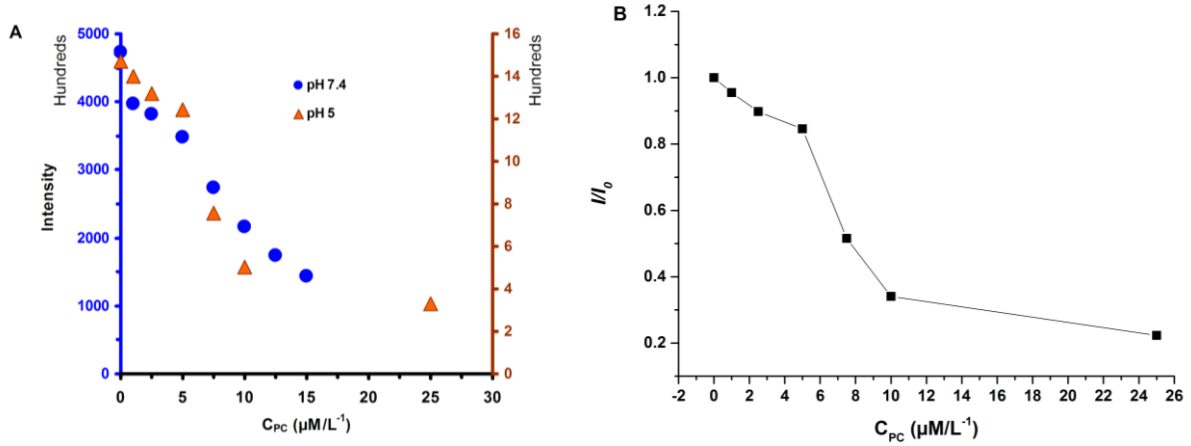

Figure 33. A) luminescence responses of **4-D**$^{+}$ to PC at pH 7.4 (blue) and pH 5 (brown); **B**) Normalized luminescence responses (I/I_0) of **4-D**$^{+}$ to PC at pH 5; Conc. Of **4-D**$^{+}$=10 μmol L^{-1} ; λ_{ex} = 345 nm, λ_{em} = 618 nm, time-resolved measurement, Lag time: 100 μs, signal integration time: 400 μs.

3.1.6.3 Simulation of the acid sphingomyelinase hydrolytic reaction

As the acid sphingomyelinase hydrolytic reaction contains two phosphate species, sphingomyelin SM and phosphorylcholine PC with a ratio that changes during the enzymatic reaction, the need to simulate this reaction and expect the kinetic complex response is essential.

The first step was to study the effect of sphingomyelin as a phosphate-containing molecule on the luminescence intensity of the **4-D**$^{+}$ complex and then using a series of different SM/PC ratios starting from 100%SM (to simulate the starting concentration) till 100% PC (to simulate the completion of the enzymatic reaction).

The addition of 1:1 molar ratio of sphingomyelin to the **4-D**$^{+}$ complex revealed about 1.4 folds increase of the luminescence intensity of the complex (**Figure 34 A**). So, we have now two opposite effects of both sphingomyelin and phosphorylcholine which mean theoretically that after the addition of sphingomyelin to the complex and waiting until reaching the stable intensity of the mixture, the enzymatic cleavage resulting in phosphoryl choline could be then monitored by following the decreasing effect of this phosphorylcholine on the luminescence intensity of the complex.

Figure 34 B shows the simulation reaction of ASM in which we started the measurement after the addition of sphingomyelin and getting a stable intensity which considered as I_0. Then as expected, 1:4 PC/SM ratio (simulate 20% cleavage) resulted in a 10% intensity decrease and a 2:3 PC/SM ratio (simulate 40% cleavage) resulted in about 30% luminescence intensity decrease. Using increased portions of phosphorylcholine (simulating 60% and 80 % cleavage), a different behavior was observed where a 1,13 folds intensity increase compared to I_0 and a comparable intensity to I_0 were observed respectively. This means that at these ratios the combination of both phosphates has a different mechanism of action which results in an overall increase of intensity. Finally, as already established, simulating 100% cleavage by the addition of only phosphorylcholine reveals about 50% intensity quenching.

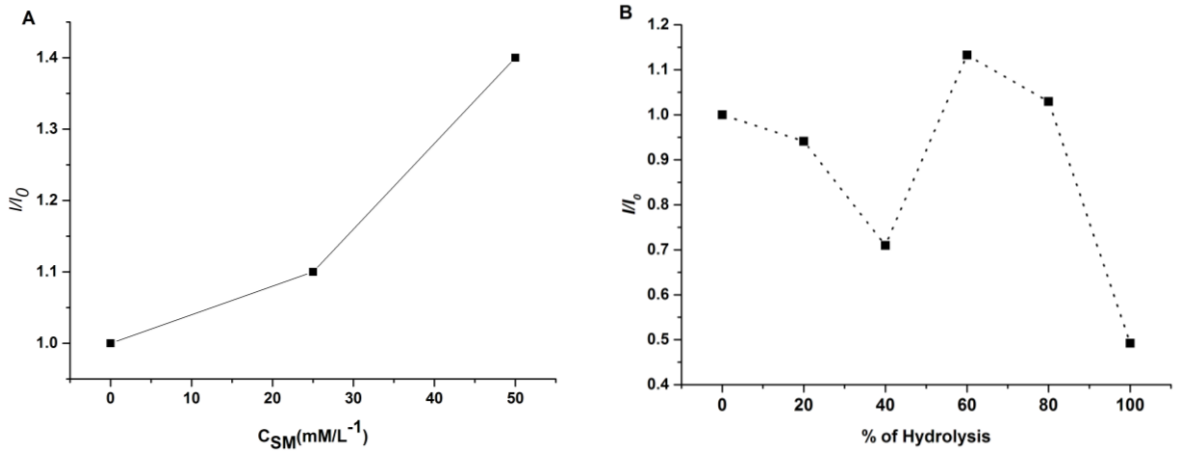

Figure 34. **A**) Normalized luminescence responses (I/I_0) of **4-D**$^{+}$ to SM at pH 5, Conc. of **4-D**$^{+}$=50 µmol L^{-1}; **B**) Simulation reaction of ASM and the normalized response of **4-D**$^{+}$ to the PC/SM mixture at pH 5;Conc. of **4-D**$^{+}$=10 µmol L^{-1}. λ_{ex} = 345 nm, λ_{em} = 618 nm, time-resolved measurement, Lag time: 100 µs, signal integration time: 400 µs.

Although the simulation reaction revealed a non-steady overall response of the **4-D**$^{+}$ complex to the ASM phosphate mixture, it still has a linear response in the first part which simulates till about 40% cleavage of sphingomyelin. Based on the already collected findings, we decided to go forward directly to the enzymatic reaction to test the applicability of the assay before putting more effort into the detailed optimization.

3.1.6.4 Monitoring the ASM cleavage reaction using the 4-D^{+} complex

After studying the effect of different parameters related to the acid sphingomyelinase enzyme reaction on the **4-D**$^{+}$ complex, we started to use this complex for monitoring the activity of this sphingomyelin cleaving enzyme. The strategy was to add our luminescent complex to the enzyme buffer, adding the enzyme-substrate (SM), waiting until we get the maximum intensity increase and then adding the enzyme to the mixture and measuring the luminescence intensity in a real-time pattern. Applying this strategy, we noticed a time-dependent decrease of the luminescence intensity independently from the presence of the enzyme or the substrate as in **Figure 35**. In the experiment where the enzyme was added to the complex and the substrate mixture, a time dependent decrease of intensity was observed which was the same situation in case of the complex only and the complex plus substrate mixture. This means that the decrease of the intensity is either not a response to the enzymatic reaction only or not a response to the enzymatic reaction at all.

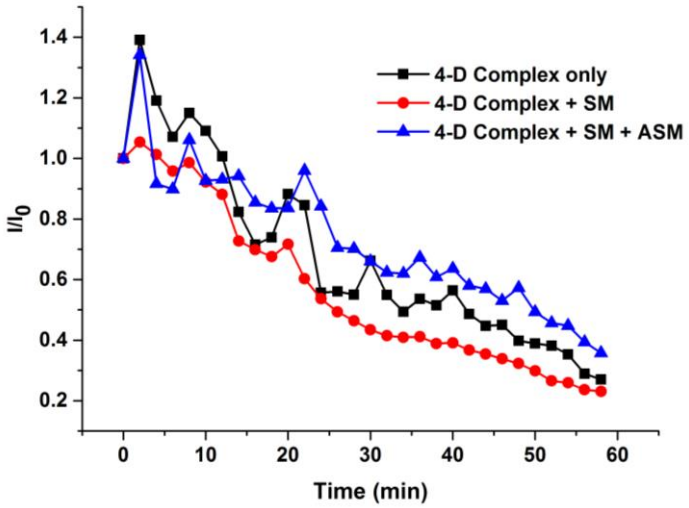

Figure 35. Monitoring the ASM cleavage reaction using the **4-D**$^{+}$ complex. Conc. of SM=10 µmol L^{-1}; Conc. of ASM =2µgm L^{-1}; Conc. of **4-D**$^{+}$=10 µmol L^{-1}; ASM buffer: (0.1 M NaOAc pH 5.0, 150 mM NaCl, 0.1 mM $ZnSO_4$, 0.1% TritonX-100); λ_{ex} = 345 nm; λ_{em} = 618 nm; time-resolved measurement; Lag time: 100 µs; signal integration time: 400 µs.

The only variable in this experiment was the enzyme buffer which seems to have a strong quenching effect on the complex luminescence intensity. To confirm this assumption, a new experiment to study the luminescence intensity stability of the **4-D**$^{+}$ complex in the acid sphingomyelinase buffer was done as in **Figure 36**.

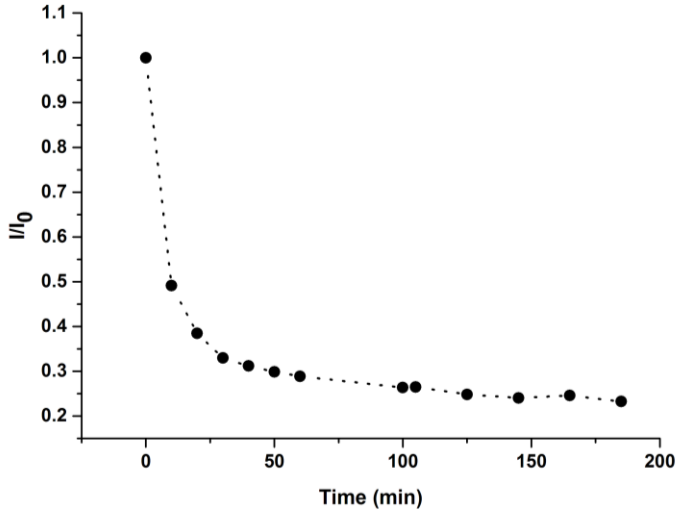

Figure 36. The luminescence intensity stability of the **4-D**$^{+}$ complex in the acid sphingomyelinase buffer; Conc. of **4-D**$^{+}$=50 µmol L^{-1}; ASM buffer: (0.1 M NaOAc pH 5.0, 150 mM NaCl, 0.1 mM $ZnSO_4$, 0.1% TritonX-100); λ_{ex} = 345 nm; λ_{em} = 618 nm; time-resolved measurement; Lag time: 100 µs; signal integration time: 400 µs.

As expected, after about 10 minutes of incubating the complex with the buffer, 50% quenching was observed. And after 1 hour, 70% of the luminescence intensity was quenched due to the buffer constituents. The exact interacting buffer constituent/s with the **4-D**$^{+}$ complex was not defined although the interaction of Zinc(II) and Triton X with the Europium(III) complexes is reported [190191]. The quenching effect of acidic pH was excluded in this case because in our previous optimization experiments this quenching wasn't time-dependent. As the applicability of the assay looks limited, we did not deeply investigate the cause of this quenching.

3.1.6.5 Heterogenous assay of the acid sphingomyelinase using the 4-D^{+} complex

As a last trial we tried to apply the europium complex luminescence intensity change for monitoring the activity of the acid sphingomyelinase in a heterogeneous manner. Because our trials to use the complex as an internal probe during the enzymatic reaction was not successful, we used the established strategy for monitoring the sphingomyelinases activity in which the substrate incubated with the enzyme, then the released phosphorylcholine can be separated from the remaining, unhydrolyzed sphingomyelin by extraction with a mixture of chloroform and methanol.

Thus, the un-cleaved sphingomyelin and the resulted ceramide are captured in the organic phase, whereas the phosphorylcholine, partitions to the upper aqueous phase which can be separated and measured depending on the nature of the assay as a relative measure of sphingomyelin hydrolysis[94,192].

We Applied the same procedures and separated the aqueous phase from different experiments containing different controls and different acid sphingomyelinase concentrations. Then we tested the effect of this phosphorylcholine containing aqueous phases on the luminescence intensity of the europium complex (**Figure 37**).

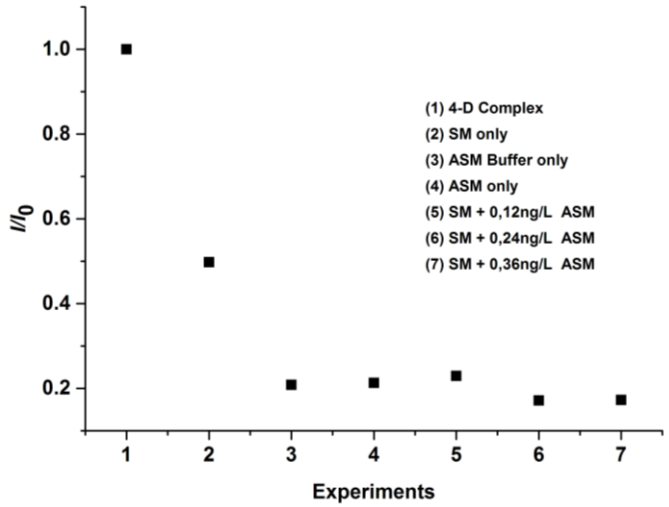

Figure 37. Heterogenous assay of acid sphingomyelinase using the **4-D**$^{+}$ complex. TRIS buffer (pH 7.4); I_0: Luminescence intensity of **4-D**$^{+}$ complex only; λ_{ex} = 345 nm; λ_{em} = 618 nm; time-resolved measurement; Lag time: 100 µs; signal integration time: 400 µs.

Unfortunately, we observed that the addition of the aqueous phase solution to the complex caused a luminescence quenching which is the same with the three different enzyme concentrations. This means that the differentiating power of the probe between the three different experiments with their different phosphorylcholine concentrations is not significant. The control experiments with either the enzyme or the enzyme buffer only revealed the same quenching behavior which excludes any probability of phosphorylcholine contribution in this luminescence change. This quenching was also observed with the control experiment containing only the substrate (sphingomyelin) which should remain in the organic phase after the extraction process. These observations enhance the assumption of the interference of the acid sphingomyelinase reaction buffer with the complex/phosphate reaction.

3.1.6.6 Monitoring the activity of neutral sphingomyelinase 2 using the 5-D$^+$ complex

Due to the relative similarity between the buffers of both nSMase 2 and that of our primary experiments in addition to the pH 7.4, we tried monitoring the nSMase 2 activity using our europium complexes. Firstly, we checked the stability of both **4-D$^+$** and **5-D$^+$** complexes in the nSMase 2 Buffer as in **Figure 38**. Both complexes revealed good luminescence stability over time with a slight decrease in intensity in the case of the **4-D$^+$** complex.

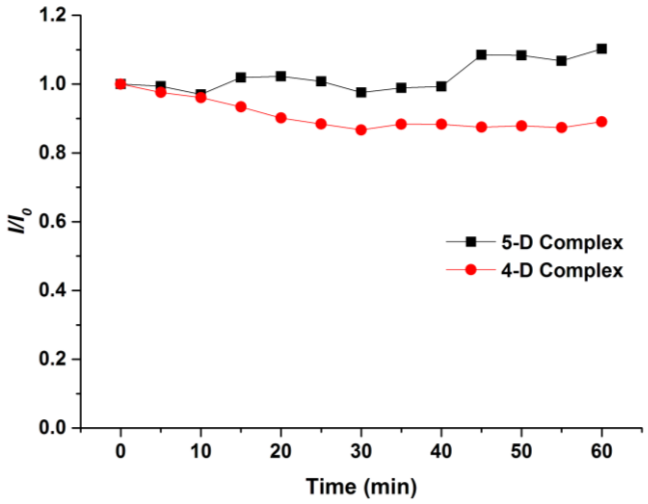

Figure 38. Stability of **4-D$^+$** and **5-D$^+$** complexes in nSMase 2 Buffer over time. nSMase 2 buffer: 50 mM M Tris/HCl pH 7.4, 150 mM NaCl, 0.1% TritonX-100, 5 mM $MgCl_2$; Conc. of **4-D$^+$**& **5-D$^+$** =5 µmolL^{-1}; I_0: Luminescence intensity of **4-D$^+$**& **5-D$^+$** complex at T_0; λ_{ex} = 345 nm; λ_{em} = 618 nm; time-resolved measurement; Lag time: 100 µs; signal integration time: 400 µs.

The next experiment was the simulation of the nSMase 2 reaction in which different ratios of PC/SM simulating the cleavage progress of the substrate SM were added to the **5-D$^+$** complex in the nSMase 2 buffer to check the response of the complex toward the cleavage progress. A scale of PC/SM ratios starting from SM only till PC only was tested and the results were presented in **Figure 39**. The behavior of the complex with the ratio change was like that of the **4-D$^+$** complex with the ASM simulation reaction (**Figure 34 B**). A linear luminescence intensity decrease was observed with the virtual percentage of cleavage till 40%. At this percentage about only 50% of the initial luminescence intensity was detected.

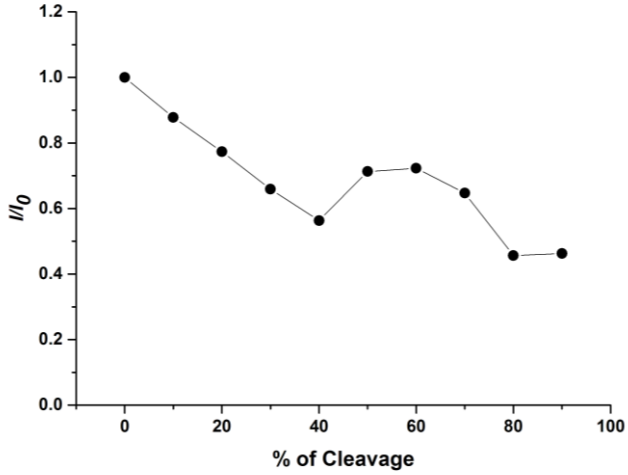

Figure 39. Simulation reaction of nSMase 2 and the normalized response of **5-D**$^{+}$ to the PC/SM mixture in nSMase 2 Buffer ;Conc. Of **5-D**$^{+}$=5 µmolL^{-1}; I_0: Luminescence intensity of **5-D**$^{+}$ complex + SM (5 µmolL^{-1}); λ_{ex} = 345 nm, λ_{em} = 618 nm, time-resolved measurement, Lag time: 100 µs, signal integration time: 400 µs.

After this ratio, the increase in PC portion to 50% caused a reverse response in which the luminescence intensity started to increase giving only a 30% intensity decrease corresponding to the initial 0% cleavage. This reverse response retreated by a 70% virtual cleavage and with an 80% virtual cleavage reached about 45% intensity decrease of luminescence. This linear response till the 40% virtual cleavage is a promising sign to use this setup for the monitoring of nSMase 2 activity *in vitro*.

The nSMase2 reaction was carried out starting with the addition of the complex to the enzyme buffer followed by the substrate sphingomyelin and then waiting till the luminescence intensity is stable. The enzyme was added to the mixture and the luminescence intensity was measured at 5 minutes interval as presented in **Figure 40**. Unfortunately, the results revealed a loss of differentiating ability of the probe neither between the enzymatic reactions and the controls nor between the enzymatic reactions with different enzyme concentrations. The validity of the enzyme was confirmed using NBD-labeled sphingomyelin commercially available substrate. Also, higher enzyme concentrations and longer reaction times were tried without any significant change in the results.

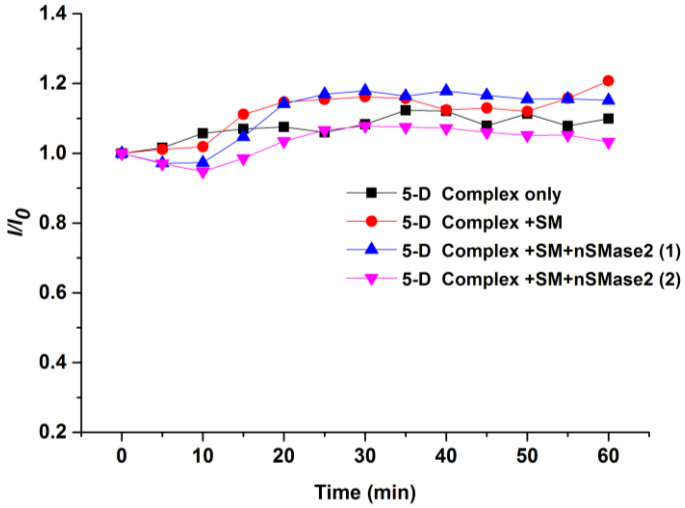

Figure 40. Monitoring the nSMase2 cleavage reaction using the **5-D$^+$** complex. Conc. of nSMase2 = (1) 30 µgmL^{-1}, (2) 60 µgmL^{-1}; Conc. of **5-D$^+$**=5 µmol L^{-1}; Conc. of SM =5 µmol L^{-1} ;nSMase2 buffer: (50 mM M Tris/HCl pH 7.4, 150 mM NaCl, 0.1% TritonX-100, 5 mM $MgCl_2$); λ_{ex} = 345 nm; λ_{em} = 618 nm; time-resolved measurement; Lag time: 100 µs; signal integration time: 400 µs.

After these different optimization steps and according to the results obtained it was concluded that this europium complexes-based sphingomyelinases assay is not applicable due to the limited specificity of the complexes response and the complex nature of the enzymatic reactions media in regards of interfering ions and pH ranges.

3.1.7 Applicability of the 5-D$^+$ to apyrase enzyme assay

Due to the significant response of the **5-D$^+$** to the interaction with ATP and the significant difference in response between ATP, AMP, and Pi, the applicability of the response for real-time monitoring of enzymatic conversion of ATP by apyrase enzyme was evaluated. Apyrase decomposes ATP to AMP and phosphate according to **Equation 1**.

ATP — (apyrase) → AMP + 2 P_i **Equation 1**

Apyrase is frequently used in neurobiological studies due to the wide role of ATP as a neurotransmitter. It is also reported that apyrase can protect against allergic airway inflammation by decreasing the chemotactic migration of dendritic cells (DCs). Apyrase enzyme is currently used in cancer and platelet aggregation studies in humans, as well as herbicide resistance in plants. Apyrase inhibitors are investigated for their use to defeat tumors and overcome herbicide resistance. ATPase activity monitoring is often based on radiolabelled phosphorous or colorimetric-based phosphate detection.

However, these detection methods have limitations, as radioactive assays are exhausting and release hazardous waste, while colorimetric assays are often limited with background interference and signal stability. Thus a luminescence-based assay would provide a useful alternative. [193–195]

The apyrase reaction buffer was firstly used to study the effect of both high salt concentrations (50 µmol L^{-1} NaCl and 5 µmol L^{-1} $CaCl_2$) and a lower pH value (6.5) on the response of the **5-D**$^+$ complex to the corresponding anions ratio change. The interference of high salt concentrations on the sensing of anions by luminescent probes is known to be a fundamental problem[181]. Lower pH values are known to affect the degree of ionization of the ligand carboxyl groups and accordingly the complex integrity as previously addressed in this study. Although the extent of the luminescence response was generally decreased in the apyrase reaction buffer, the model calibration curve for the apyrase reaction remained the same as in TRIS buffer (**Figure 41**). However, this simulation is too simple and cannot be applied as a real calibration curve for a quantitative determination of apyrase activity, as the phosphate anions are released in two steps and different amounts of ADP are present in the reaction mixture[196].

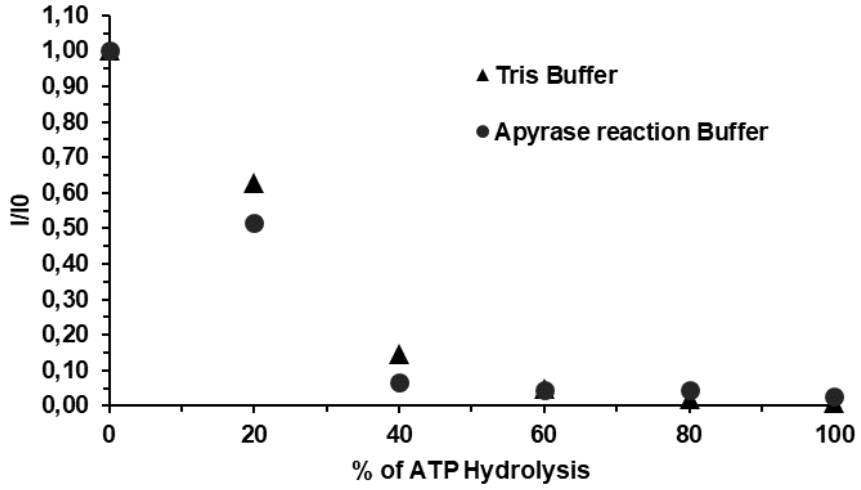

Figure 41. Normalized luminescence intensities (I/I_0) of **5-D**$^+$ (c=50 µmol L^{-1}) in TRIS and apyrase buffer in the presence of different mole fractions of ATP / AMP+2 P_i.

The real-time monitoring of the hydrolysis of ATP by four different concentrations of the apyrase enzyme indicated by the decreasing luminescence of **5-D**$^+$ complex is presented in **Figure 42**. The enzyme concentrations are denoted as activities in U per well (volume/well =100 µl) as specified by the manufacturer. Thus, the turnover of the enzymatic reaction is directly expressed as a change in the luminescence intensity.

The intensities were measured approximately every 120 second. For better comparability, the normalized intensities I/I_0 are displayed, with I_0 as the value of the initial signal directly after the addition of the apyrase enzyme.

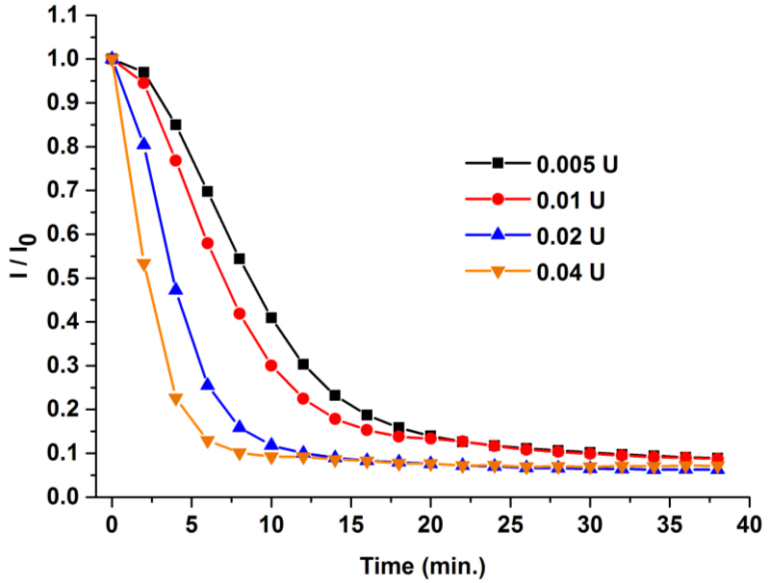

Figure 42. Real-time monitoring of the luminescence intensity decrease due to the hydrolysis of ATP (initial concentration 50 µmol L^{-1}) by different apyrase concentrations indicated by **5-D**$^+$ (50 µmol L^{-1}). I_0 is the intensity at T_0 (apyrase buffer pH 6.5). Temperature = 30 °C.

Apyrase activities lower than 0.005 U could not be distinguished through the time-trace of the signal decrease. For higher enzyme concentrations, increasing enzymatic activities can be correlated to the change of the initial reaction rate expressed as a signal drop per minute (Δ I/min) calculated after four minutes reaction time (**Table 2**).

Activity of added apyrase [U]	Calculated initial reaction rate* [Δ I Min^{-1}]
0.005	0.038
0.01	0.058
0.02	0.130
0.04	0.200

Table 2. Kinetic evaluation of the apyrase assay with **5-D**$^+$; *After 4 minutes reaction time.

The effect of the apyrase enzyme itself on the complex luminescence intensity was studied and showed no observable change. The enzymatic activity effect on the complex luminescence was confirmed by the parallel testing of the denatured enzyme as a control which showed no change of the complex luminescence intensity over the assay time (**Figure 43**).

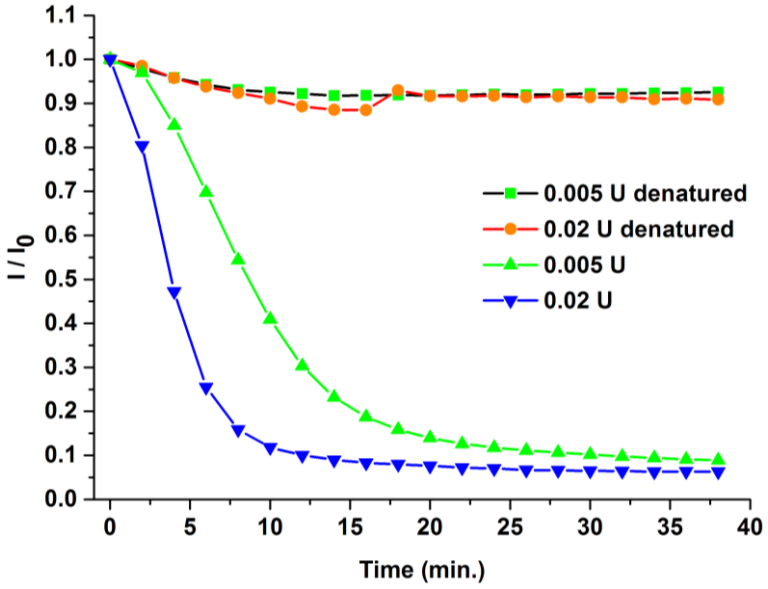

Figure 43. Real-time monitoring of the luminescence intensity decrease due to the hydrolysis of ATP (initial concentration 50 µmol L^{-1}) by different apyrase concentrations compared to the same denatured enzyme concentrations indicated by **5-D**$^{+}$ (c=50 µmol L^{-1}). I_0 is the intensity at T_0 (Apyrase buffer pH 6.5).

3.1.8 Conclusion

In this project, two Eu complexes were synthesized starting from the commercially available chelidamic acid in a good and pure yield (**Figure 44**). The two probes were designed to have a positive charge that can promote the binding with the phosphates. The synthesized probes **4-D**$^+$ and **5-D**$^+$ used for detecting different phosphates and carboxylate species. The response of the two probes toward the studied phosphates was dramatically different which confirms the effect of structural and geometrical differences on the luminescence response. Two-fold excess of ATP resulted in a twenty-fold increase of the **5-D**$^+$ luminescence intensity while only a three-fold increase in the luminescence intensity could be observed after the addition of a two-fold excess of ATP to the **4-D**$^+$ complex.

The effect of the nucleoside part and the number of phosphate groups could also be detected with the probes. The most obvious difference in the response to phosphates between the two probes was with pyrophosphates PP_i. PP_i unexpectedly resulted in a decreased luminescence intensity to half of the initial value at a molar ratio of 1: 5 PP_i: **4-D**$^+$ complex while resulted in about 5-folds increase at the same ratio with the **5-D**$^+$ complex. The monophosphates (Pi &AMP) had a clear quenching effect of both probes except in the case of AMP with the **5-D**$^+$.

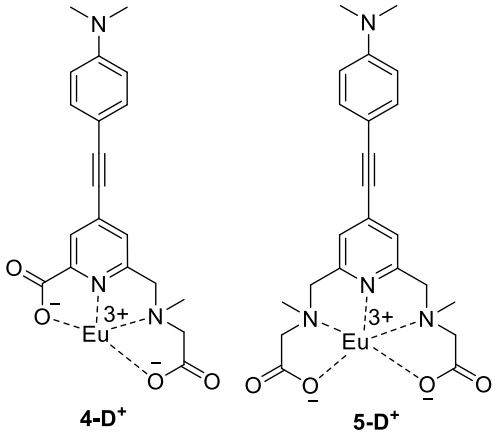

Figure 44. Synthesized Eu-Complexes.

The probes were then applied for the monitoring of the ASM activity through the detection of the enzymatically released phosphorylcholine (PC). In the optimization steps, the **4-D**$^+$ revealed a promising decreasing response to the inorganic PC at both pH 7.4 and 5 in addition to the SM/PC ratio change simulation reaction. In the real enzymatic reaction, a general quenching effect was observed in all the experiments and this was attributed to the ASM acetate buffer. In a heterogenous experiment setup, similar quenching was observed without any enzymatic detection ability. Other trials for the monitoring of nSMase 2 could not prove the ability of the probes to monitor the phosphates (SM & PC) ratio change in the complex enzymatic reaction media despite the obvious ability in the simulation reaction containing the phosphates only. However, the **5-D**$^+$ complex could be used for the monitoring of the ATP-hydrolyzing Apyrase enzyme in a real-time pattern and could differentiate between the effect of an 8 fold range of different enzyme concentrations.

3.2 Design, synthesis and characterization of ASM FRET probes

3.2.1 Stereoselective synthesis of protected sphingosine

The synthesis of the protected sphingosine was achieved following the previously established procedures[121] (**Scheme 6**). Tert-butoxycarbonyl (Boc) protection of the commercially available L-serine followed by the Weinreb amide formation and the protection of the primary hydroxyl group with tert-Butyldiphenylsilyl (TBDPS) produced **203** in a very good yield in three steps. The introduction of a vinyl group with the Grignard reagent provided vinyl ketone **204** in 65% yield. *Anti*-selective reduction [197] of the obtained α,β-unsaturated ketone **204** using Tri-tert-butoxyaluminohydride (TBLAH) in Ethanol/THF mixture at −84 °C revealed the desired vinyl alcohol (anti-product) **205** in 80% yield as a sole stereoisomer.

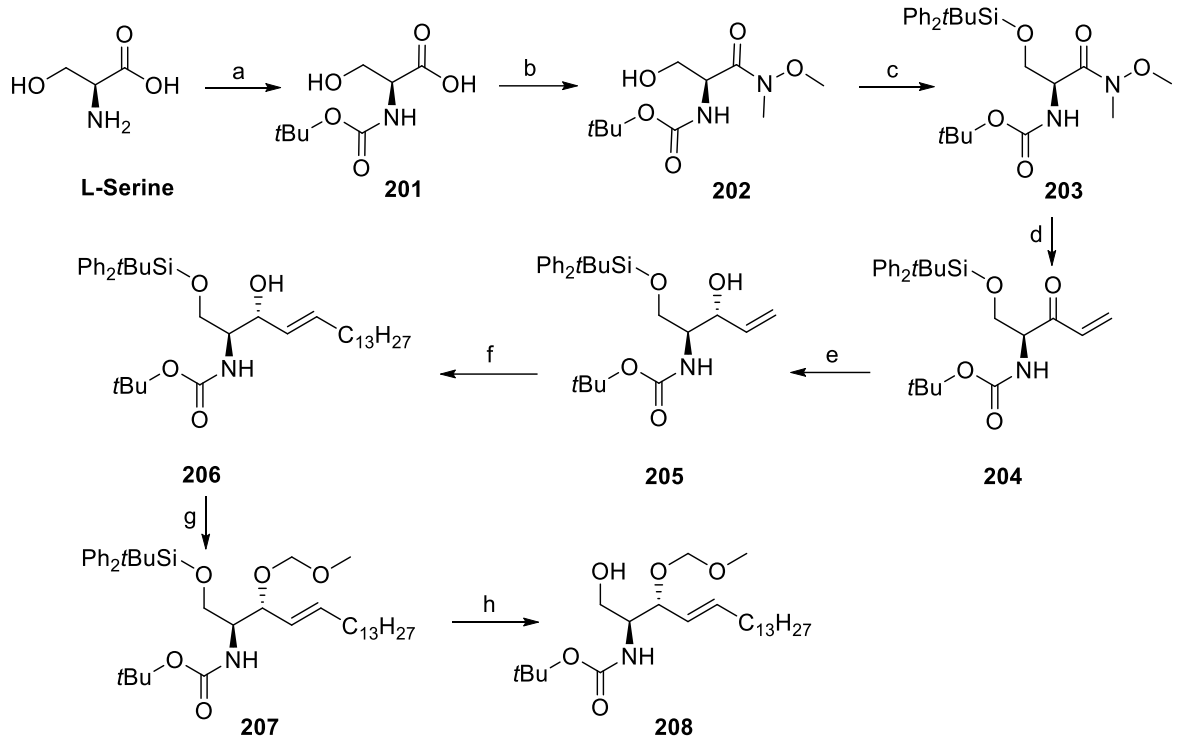

Scheme 6. Stereoselective synthesis of the protected Sphingosine; a) Boc_2O, NaOH, 1,4-dioxane/H_2O, 0°C then RT, 20h, 90%; b) NMM, dry DCM, HNMeOMe, EDC, -15°C, 1.5h, 75%; c) Imidazole, DMAP, dry DCM, Ph_2tBuSiCl, RT, 24h, 87%; d) VinylMgBr, dry THF, -15°C, 5h, 65%; e) TBLAH, dry THF/dry EtOH (1:10), -84°C, 4h, 80%; f) 1-pentadecene, Grubbs 2nd, dry DCM, reflux, 4 h, 63.5%; g) MOMCl, dry DCM, DIPEA, 0°C then RT, 20h, 72%; h) TBAF, THF, RT,3h, 88%.

The cross-metathesis coupling reaction between the vinyl alcohol **205** and 1-pentadecene using the Grubbs catalyst second generation in dichloromethane generated the skeleton of the natural sphingosine with the primary hydroxyl group and the amino group protected **206** in a moderate yield taking in consideration the possible by-products of the *E*-stereoisomer, homometathesis product and the *α,β*-saturated ketones[198].

To avoid any interferences through the secondary hydroxyl group, it was protected using Chloromethyl methyl ether in presence of DIPEA to give the fully protected sphingosine **207** which then was prepared for the next phosphorylation steps by deprotection of the primary hydroxyl group using Tetrabutylammonium fluoride (TBAF) to get the target compound of this synthetic stage **208**.

3.2.2 Synthesis of the phosphodiesters

After preparation of the protected sphingosine intermediate **208** as discussed in the last section we started with the synthesis of the phosphodiesters of the target sphingomyelin analogs (**Scheme 8**). For the first targeted 2P excitable FRET probe, the same strategy established for the synthesis of the first generation of FRET probes[121] was followed. In this reaction the asymmetric phosphodiester **211** was synthesized through the reaction between the intermediate **208** and 2-Phthalimidoethyl phosphorodichloridate **210** which was synthesized according to **Scheme 7**.

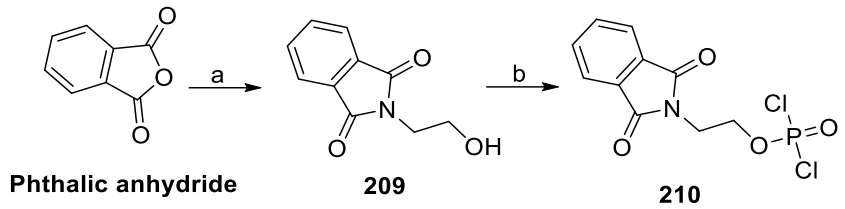

Scheme 7. Synthesis of 2-Phthalimidoethyl phosphorodichloridate. a) 2-aminoethanol, DMF, Reflux, 24 h, 79%; b) $POCl_3$, Dry toluene, Reflux, 4h, 70%.

The phthalimide protected diphosphate ester **211** was synthesized in good yield with a high purity and then the phthalimido protection was cleaved using hydrazine hydrate giving the sphingomyelin analogue **212** with the free terminal amino group ready for the coupling of the fluorophores.

To get a sphingomyelin analogue containing a quaternary ammonium group for a higher substrate similarity and thus better recognition and rapid cleavage, the reagent 2-chloro-2-oxo-1,3,2- dioxaphospholane was used for the synthesis of the diphosphate ester. This reagent is reported for the synthesis of sphingomyelin analogs containing quaternary ammonium group[199,200].

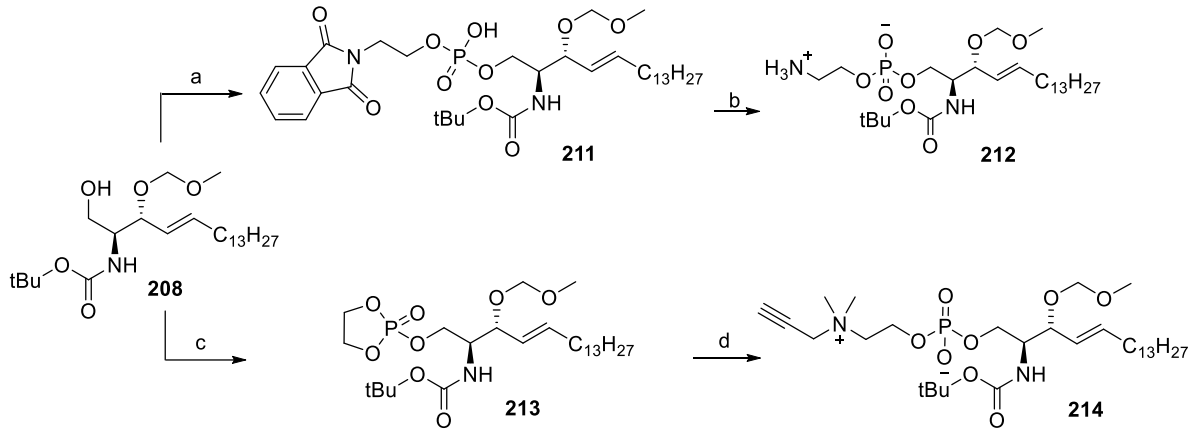

Scheme 8. Synthesis of the phosphodiesters of the target sphingomyelin analogs. a) dry DCM, 0°C, RT, 4 h, H_2O, 85 %; b) Hydrazine hydrate 64%, MeOH/$CHCl_3$ (1:1), RT, 4.5 h, 82%; c) EtN_3, DMAP , 2-chloro-2-oxo-1,3,2- dioxaphospholane, dry toluene, 0°C, 1h, used directly; d) N,N-Dimethylpropargylamine, dry MeCN, 80°C , 24 h, 50%.

The primary alcohol group of **208** reacted with 2-chloro-2-oxo-1,3,2 dioxaphospholane in the presence of triethylamine and a catalytic amount of 4-dimethylaminopyridine (DMAP) in toluene to produce the phosphate triester intermediate **213**. Compound **213** is sensitive to moisture and was used directly in the next reaction without further purification. The five-membered ring in **213** was then opened by N, N-Dimethylpropargylamine, in a sealed pressure tube at 80°C for 24 hours, leading to the sphingomyelin analogue **214**.

Getting out the sphingomyelin analogue **214** in a highly pure form was highly challenging and we couldn't get it in sufficient purity using the chromatography conditions described by Sandbhor et al. [200]. The high purity of this intermediate is critical because of the excess amount of N, N-Dimethylpropargylamine used during the synthesis which -if remains as an impurity with **214**- would highly compete with the next alkyne azide click reaction especially with the low steric hindrance compared with the target reactant **214**. Fortunately, using the reported chromatography conditions [201] in which a triple mixture of $CHCl_3$/MeOH/NH_4OH with varying ratios was used as a mobile phase allowed us to get the target compound **214** in a very pure form as confirmed by the mass and NMR data (**Figure 45**).

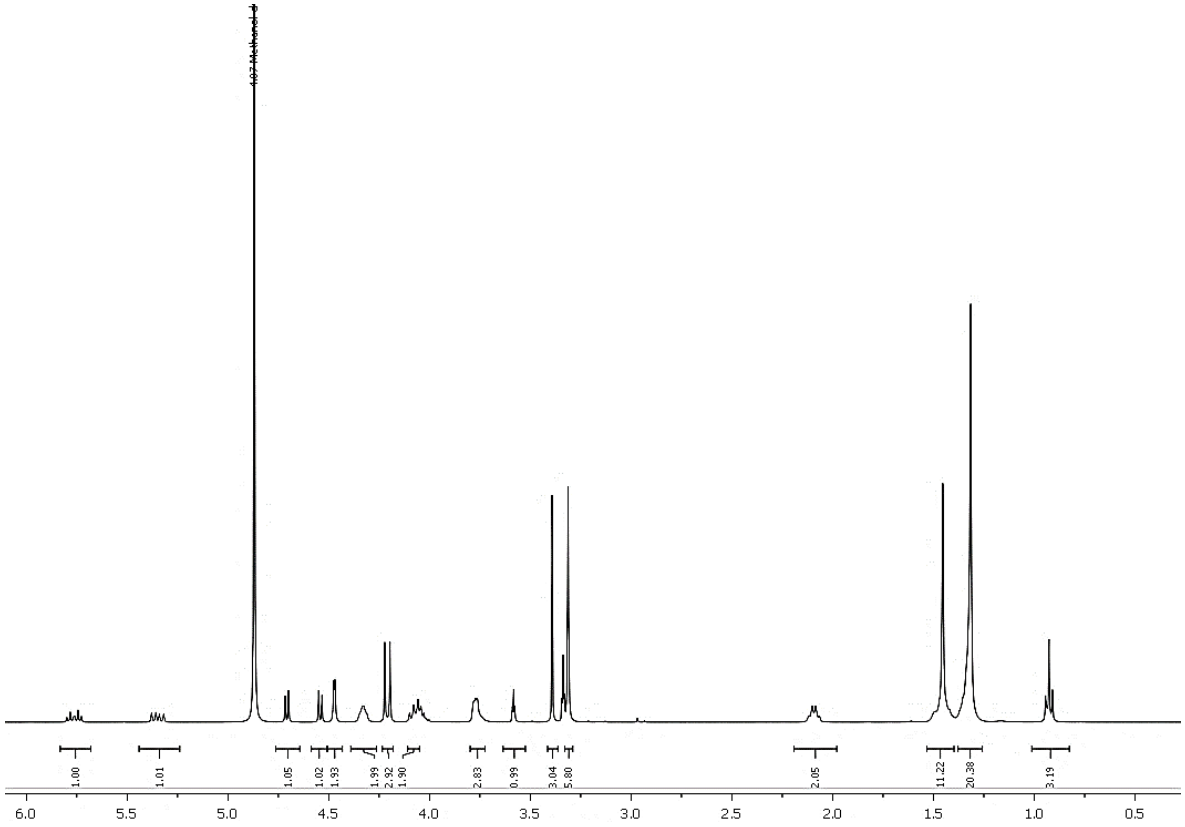

Figure 45. ^{1}H-NMR-Spectrum of compound **214** in CD_3OD.

With this strategy we preserved the ammonium functionality of the sphingomyelin phosphocholine moiety and incorporated an alkyne functionality that serves as a bioorthogonal handle for the introduction of a wide range of fluorophores or other labeling agents with aqueous phase chemistry.

3.2.3 Synthesis of the bromo coumarin dye

Benzyl propiolate **301** was synthesized through the Steglich esterification of propiolic acid with benzyl alcohol in the presence of N, N′-dicyclohexylcarbodiimide DCC and a catalytic amount of 4-dimethylaminopyridine DMAP[202]. Using such mild esterification conditions yielded the ester in a highly pure yield which is comparable to the highest reported yields for this benzylic esterification of the propiolic acid[203204]. The ester **301** was then reacted with the commercially available 6,7-dihydroxy-coumarin in the presence of DMAP to yield the intermediate **302 (Scheme 9**). The cyclic addition of catechols to terminal and internal alkynes is reported[205] but the first time to be applied to coumarin was reported by Wessig et al.[171]. This 1,3-dioxolocoumarin intermediate was synthesized in a nearly quantitative yield.

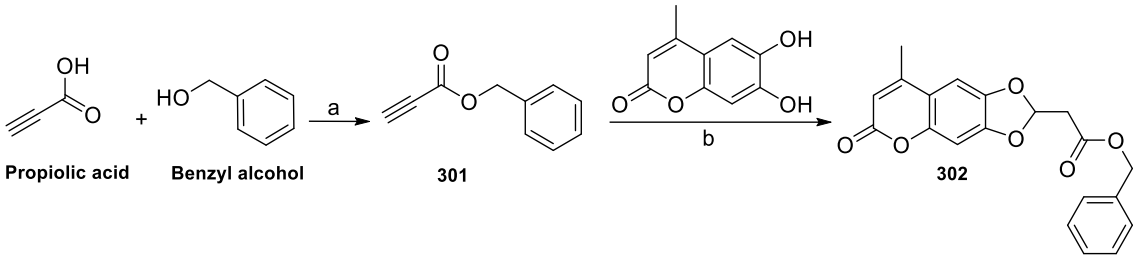

Scheme 9. Synthesis of the intermediate **302** a) DCC, DMAP, DCM,12h, 80%; b) DMAP, dry DCM, 7h, 97%

To synthesize the brominated coumarin dye, the intermediate **302** was brominated using the low density and easily handled N-Bromo succinimide NBS which provided the product in a quantitative yield. Bromine and dioxane dibromide were reported to be used also for bromination of similar coumarins[206,207]. The brominated coumarin **303** was then catalytically hydrogenated to get the free coumarin carboxylic acid **304** which couldn't be isolated in a pure form due to a resistant impurity (**Scheme 10**). Further investigation of the mass and NMR data of the mixture revealed that in addition to the target product **304** another portion of the debrominated acid **305** was formed during the hydrogenation reaction. The ^{1}H-NMR of the product mixture showed a 1:3 debrominated: brominated product as the arrows in the lower spectrum in **Figure 46** shows. The aromatic dehalogenation during catalytic hydrogenation is reported[180,208] and the rate depends on different reaction parameters[209,210] from which plays the pH a significant role[211].

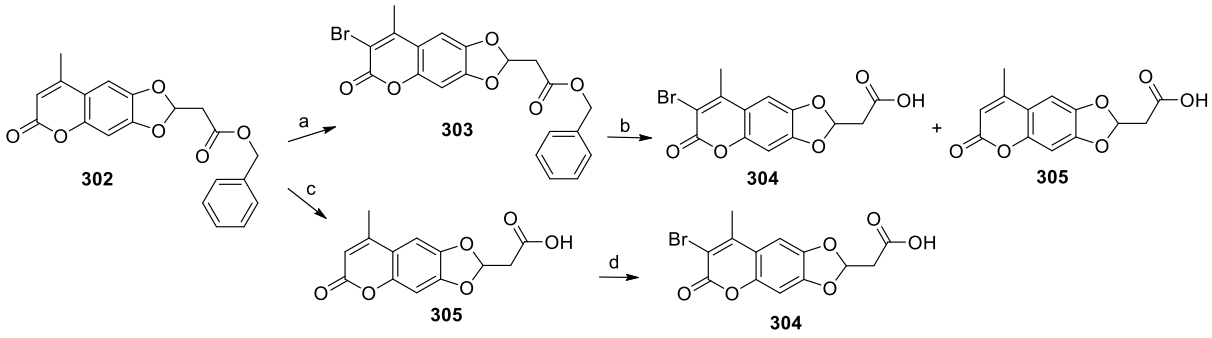

Scheme 10. Synthesis of the target bromo coumarin **304.** a) NBS, NaOAc, dry ACN, 12h, Quan. yield ; b) Pd/C, H_2 (1 atm) ,dry THF, 12h, 75%; c) Pd/C, H_2 (1 atm), dry THF, 12h, 65% ;d) NBS, NaOAc, dry DMF,12h, 50 %.

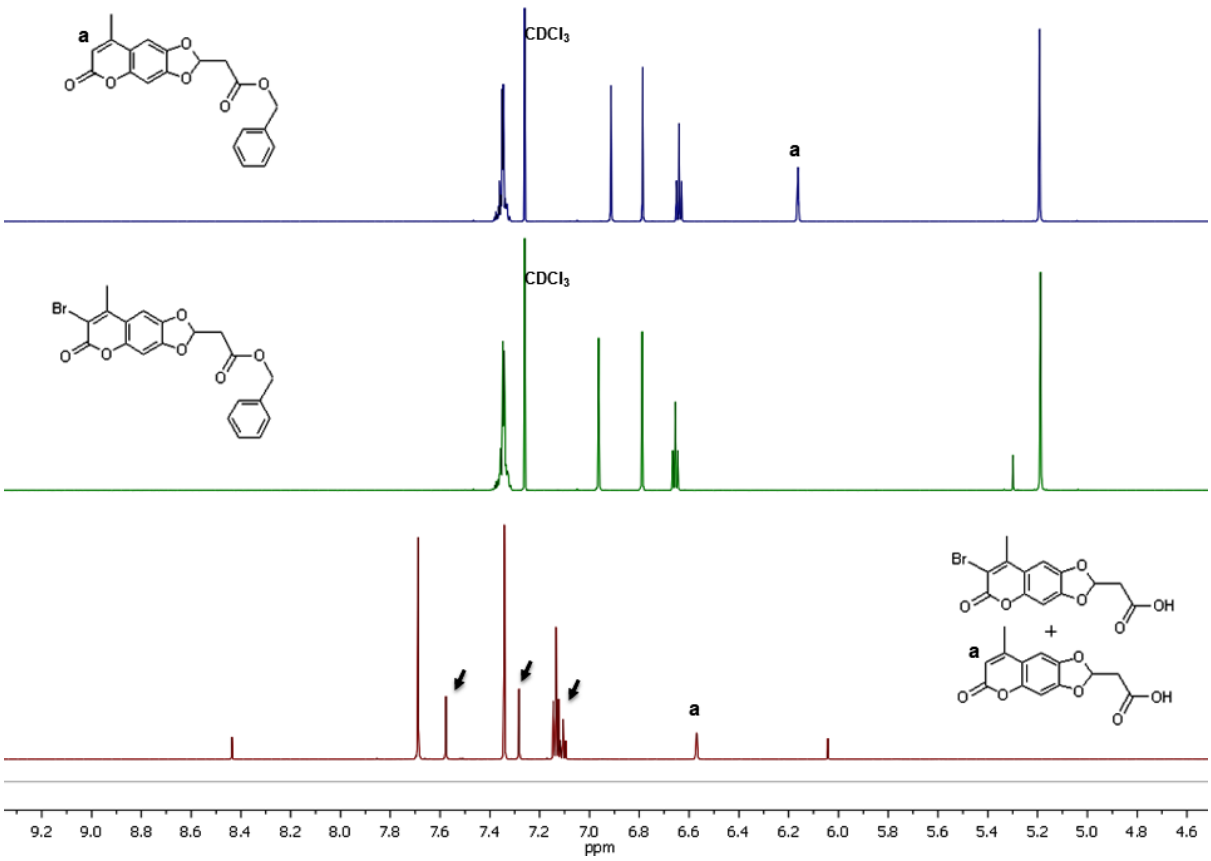

Figure 46. ^{1}H-NMR spectra (cutted section) comparison of compounds **302-305** revealing the disappearance of the coumarin proton **a** after bromination and reappearance again after the catalytic hydrogenation.

To avoid this debromination reaction and to get a pure product for the next steps, a new synthetic order was followed (steps c and d in **Scheme 10**). We decided to hydrolyze the benzyl ester of **302** to get the free nonbrominated acid **305** then this free acid can be brominated using the same previous conditions for bromination to get the target brominated coumarin carboxylic acid **304**. The challenge with this modified pathway (**Scheme 10**) was the purification of this polar free acid through two consecutive steps. The product was collected in a pure form as confirmed with NMR (**Figure 47**) and mass data.

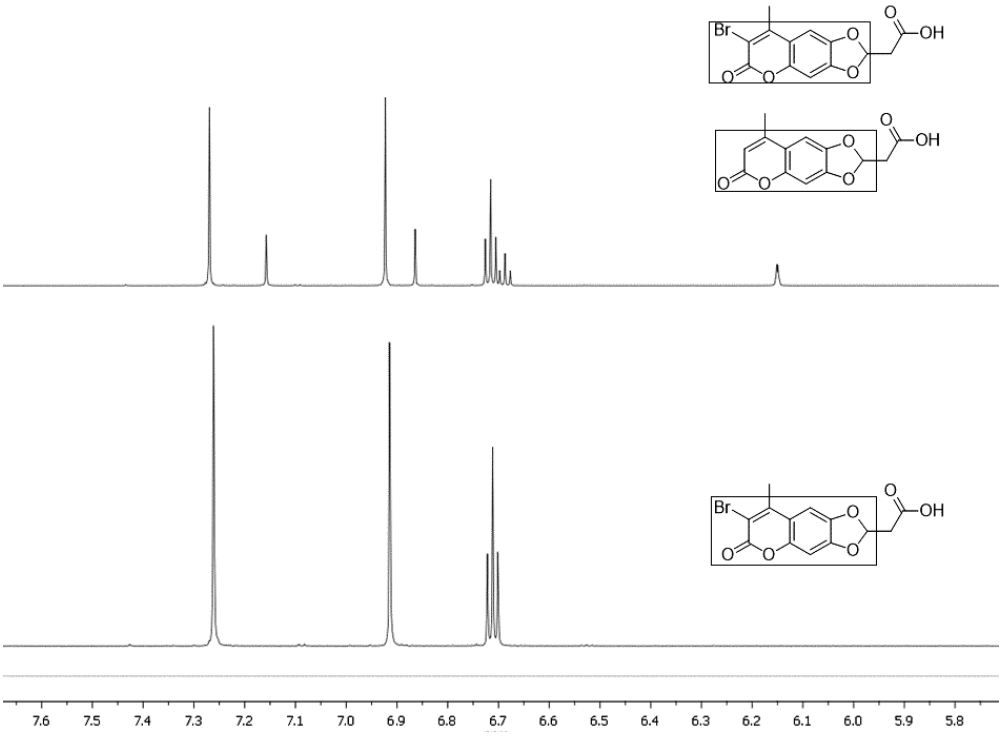

Figure 47. [1]H-NMR spectra (cutted section for the surrounded part of structure) comparison between the products of the 1st (upper) and 2nd (lower) pathways in **Scheme 10**.

Having the Bromo-coumarin carboxylic acid **304** in pure form, the next step was to couple it with a six-carbon atom linker. This six-carbon atom linker should be linked via an amide bond between the coumarin carboxylic acid and the amino group of 6-aminohexanoic acid 6-AHA. The carboxylic group of 6-AHA is challenging for such a coupling, but it is required for the final coupling with the FRET acceptor carrying intermediate. To achieve this reaction and get a good yield/ purity balance we tried several pathways according to **Scheme 11**.

In the first trial (a &b in **Scheme 11**), the acid **304** was activated in situ using Hydroxybenzotriazole (HOBt) and coupled directly with the methyl ester of 6-aminohexanoic acid in presence of EDC.HCl. The intermediate compound **306** was produced after 24 hours reaction time and column purification in a yield of 30%. This yield is relatively low taking into consideration the next methyl ester hydrolysis step. This ester alkaline hydrolysis was achieved using lithium hydroxide and provided the target free acid **307** in a 30% yield after column chromatography purification.

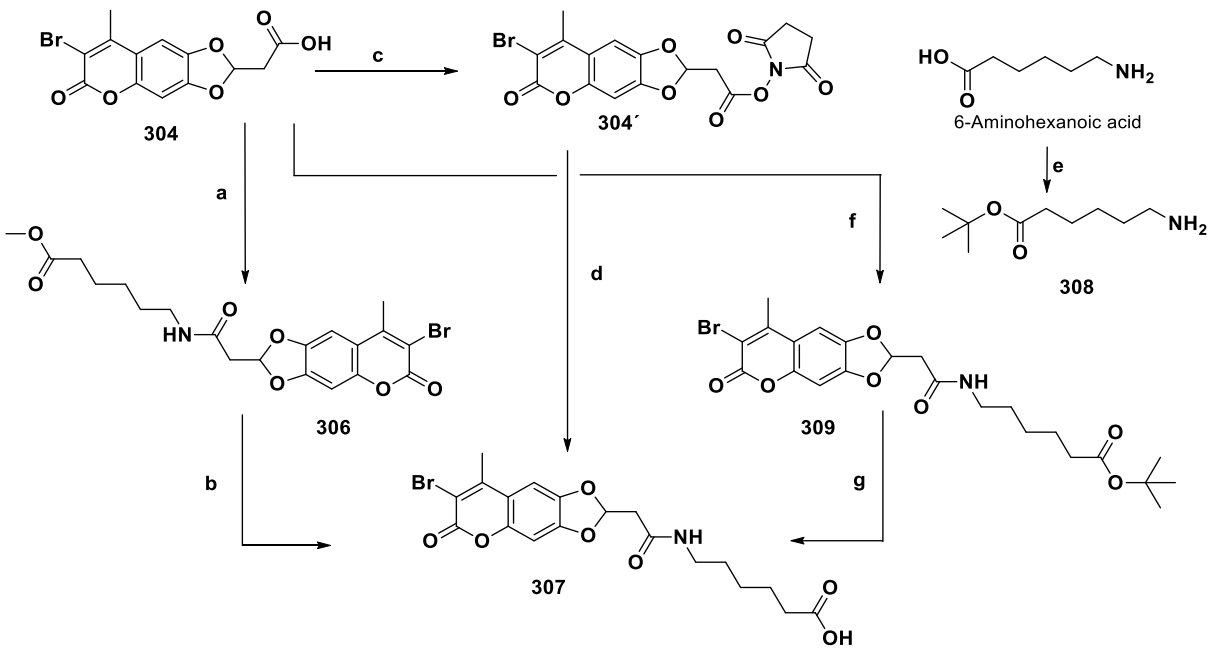

Scheme 11. Different pathways for the synthesis of the target compound **307**. a) Methyl 6-aminohaxanoate, dry DCM , EDC.HCl , HOBt, RT, 24h, 30%; b) dry THF, LiOH (in H_2O), rt, 3 h, 30%; c) DMAP, NHS, EDC , dry DCM,0°C then RT, 22h, isolated and used without purification; d) 6AHA, dry DCM, DIPEA, 0°C then RT, 22h, 45%; e) Thionyl chloride, 2h, $NaHCO_3$ in t-BuOH, 2h, 75%; f) **308**, dry DCM, EDC.HCl, HOBt, RT, 20h, 75%; g) TFA, dry DCM, RT, 3h, 80 %.

Due to the low yield of the first pathway, we shifted to another pathway (c&d in **Scheme 11**) where the acid **304** was activated using N-Hydroxysuccinimide (NHS) in the presence of DMAP and EDC. The complete conversion of the acid to the active ester was confirmed by TLC and UPLC-MS. Then the active ester was extracted and dried to be used directly for coupling without further purification. Coupling of this active ester with 6AHA in the presence of DIPEA revealed the target product **307** after 22 hours reaction in 45% yield over the two steps. So, in this alternative pathway, an increase of 36% in yield was accomplished through minimizing the purification steps from two columns to only one and avoiding the alkaline ester hydrolysis step.

The purification of the final free acid **307** through column chromatography is the major yield-reducing step. So, we thought about another pathway in which the final free acid **307** can be obtained in a pure form without the need to column chromatography. This can be achieved by the coupling with the t- butyl ester of the aminohexanoic acid which can be easily cleaved later by trifluoracetic acid. To apply this pathway, the t-butyl ester of 6-aminohexanoic acid was synthesized as reported[212] by esterification of 6-aminohexanoic with t-butyl alcohol to get the ester **308** in 75% yield.

Then the ester was coupled to the free acid **304** after in situ activation to get **309** in 75% yield. Finally, the t-butyl ester of **309** was hydrolyzed using trifluoracetic acid TFA providing a 60% yield of the pure product **307** over the two steps after simple evaporation of the solvent without the need to further purification. This product **307** was then activated using N-hydroxysuccinimide EDC.HCl to get the active ester **310** ready for the final coupling.

3.2.4 Synthesis of 7-methoxy-coumarin-3-carboxylic acid

A more economically affordable synthesis of the coumarin fluorophore of the previously synthesized probe [121] was targeted for a larger scale synthesis to be used for the high throughput screening study. In this project, the commercially available previously used 7-methoxy-coumarin-3-carboxylic active ester **313** was synthesized starting from commercially available cheap starting materials (**Scheme 12**). Formylation of 3-methoxyphenol was achieved selectively at the ortho position of the hydroxy group through the electrophilic aromatic substitution reaction using paraformaldehyde in the presence of magnesium chloride and triethyl amine as a base. The 4-methoxysalicylaldehyde **311** was obtained in a 98.5 % yield which is comparable to the reported yields[213,214].

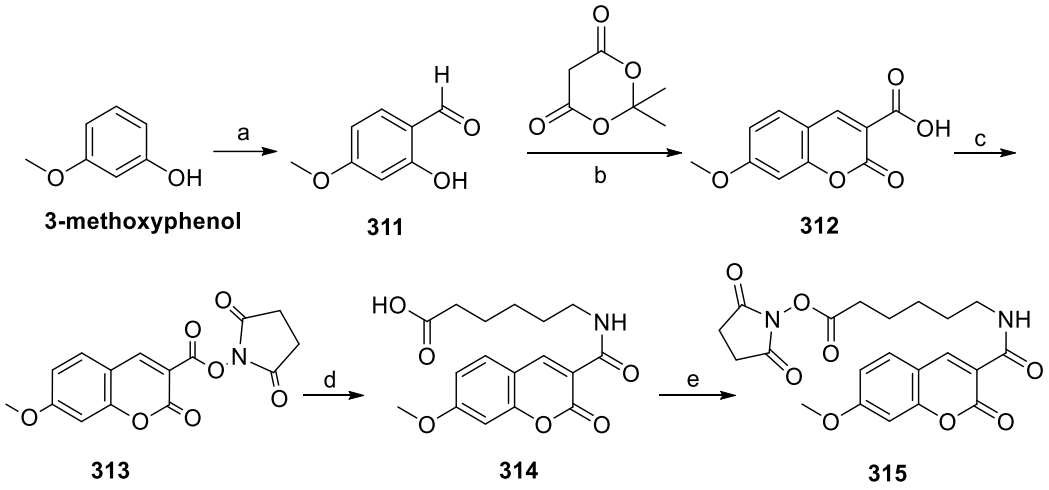

Scheme 12. Synthesis of 7-methoxy-coumarin-3-carboxylic acid based fluorophore. a) $MgCl_2$, dry THF, Et_3N, Parafomaldehyde, Reflux, 12h, 98.5%; b) Meldrum's acid, Dist. H_2O, NaN_3, rt, 1h, quantitative yield; c) N-hydroxysuccinimide, dry DMF, 0°C, 1 h, DCC, RT , 2.5 h, 56%; d) 6-aminohexanoic acid, dry DMF, DIPEA, rt, 12h, 90%; e) dry DCM, DMAP, N-hydroxysuccinimide, EDC, RT,12h, used without purification.

7-Methoxycoumarin-3-carboxylic Acid **312** was then synthesized through Knoevenagel condensation and intramolecular cyclization of 4-methoxysalicylaldehyde **311** with Meldrum's acid using sodium azide as a catalyst.

This reported method is highly advantageous concerning costs, environmental hazards, ease of handle, and efficient also for the large-scale synthesis without the use of toxic solvents and tedious column chromatographic purification[215]. 7-methoxy-coumarin-3-carboxylic active ester **313** was obtained in a moderate yield using N-hydroxysuccinimide and DCC according to the reported method[216]. This active ester was then coupled with 6-aminohexanoic acid in the presence of DIPEA to get the product **314** in a 90% yield. The coumarin labeled hexanoic acid **314** was then activated using the N-hydroxysuccinimide and EDC and the active ester **315** was isolated and used for the next coupling without further purification.

3.2.5 Synthesis of the NBD derivatives fluorophores

For the preparation of the 2P excitable FRET probe, NBD-Cl will be directly coupled with the free primary amino group of the phosphodiester sphingomyelin analogue **212** as will be discussed in the next steps. For a quaternary ammonium group-containing FRET probes, different NBD dye derivatives were prepared as presented in **Scheme 13**. Our starting goal was to synthesize the NBD derivative **316** with the terminal N, N dimethyl group to be used directly instead of N, N-Dimethylpropargylamine in **Scheme 8**. The product **316** was synthesized by treating NBD-Cl with N, N-dimethyl ethyl-1,2-diamine under basic condition according to the reported procedures[217].

For the azide/alkyne click reaction-based coupling, two different NBD azido derivatives were synthesized. The first simple NBD-N_3 **317** was simply synthesized through the reaction of NBD-Cl with sodium azide in a H_2O/acetone medium. The product isolated in a highly pure good yield comparable to the reported yield[218].

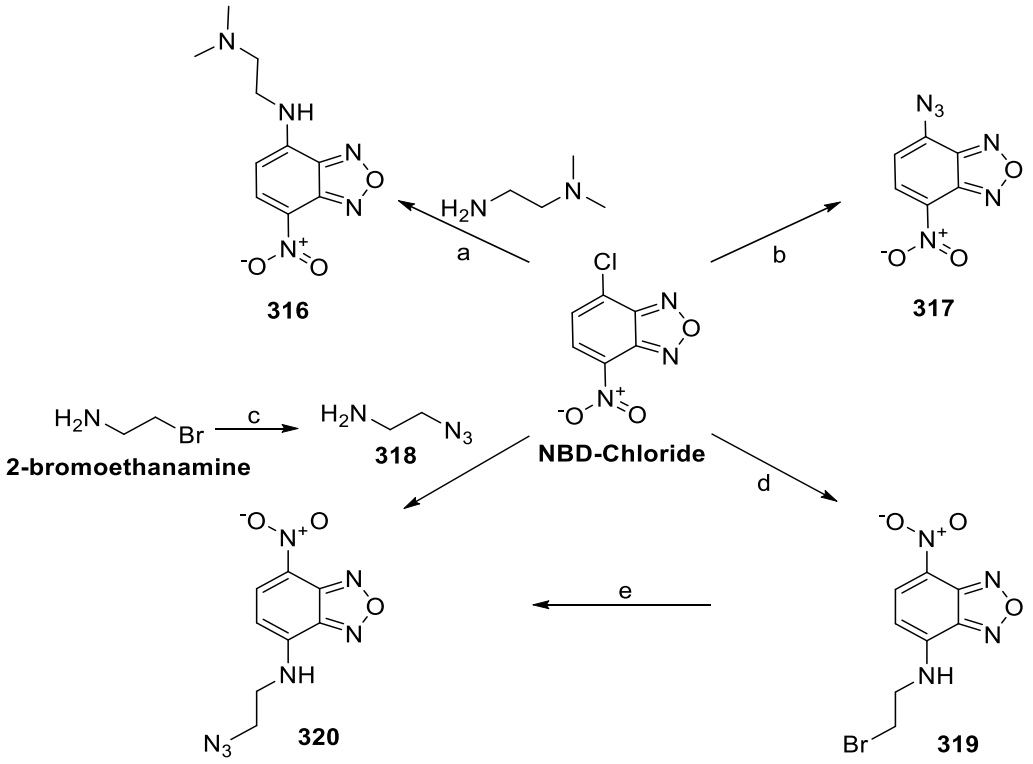

Scheme 13. Preparation of different NBD based fluorophores. a) $NaHCO_3$, MeCN, 60°C,15 min, 64%; b) NaN_3, H_2O/acetone (1:1), RT, 15 min. , 90%; c) NaN_3, H_2O, 75°C, 12h, 42%; d) 2-bromoethylamine.HBr, Dry EtOH, 70 °C, 4h, 70%; e) NaN_3, DMF, 80 °C for 4 h then RT for 15h, 93%.

The second NBD azido derivative **320** containing a two-carbon linker between the NBD and the azide group. It was suggested as an alternative for the NBD-N_3 **317** in an attempt to exclude any possible steric hindrance based unreactivity during the azide/alkyne click reaction. The first suggested pathway for the synthesis of **320** was through the preparation of 2-azidoethanamine **318** from 2-bromoethanamine followed by its coupling with NBD-Cl under basic conditions. Due to the extraction challenge and the low yield of **318** and also the reported low yield of the next coupling reaction with NBD-Cl[219], another pathway[220] was selected in which NBD-Cl was substituted with 2-bromoethylamine to get the intermediate **319** in a good yield which then was reacted with sodium azide to give the target compound **320** in a 93% yield.

3.2.7 Synthesis of the visible light range fluorophores

For the visible light range excitable FRET probe a Fluorescein /Nile red dye pair was suggested according to the excitation/emission wavelengths data. For the azide/alkyne click reaction-based coupling, a Fluorescein derivative functionalized with an azido group **321** was synthesized according to the reported method[221].

The Fluorescein was converted in situ to the N-hydroxysuccinimidyl (NHS) active ester and then coupled with the 2-azidoethanamine **318** to get the N-(2-azidoethyl)-5(6)-fluorescein-carboxamide **321** in 80%yield (**Scheme 14**).

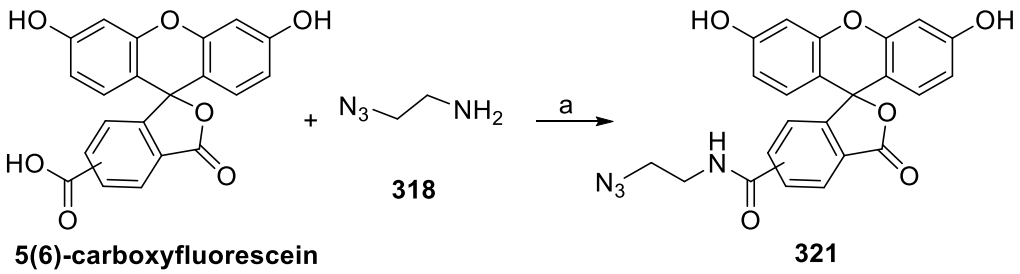

Scheme 14. Synthesis of N-(2-azidoethyl)-5(6)-fluorescein-carboxoamide. a) Et_3N, TSTU, DMSO, RT, 12h, 80%.

The previously synthesized Nile red (NR) labeled hexane acid [121] was activated to N-hydroxysuccinimidyl (NHS) ester derivative **322** (**Scheme 15**) and used directly for the next coupling.

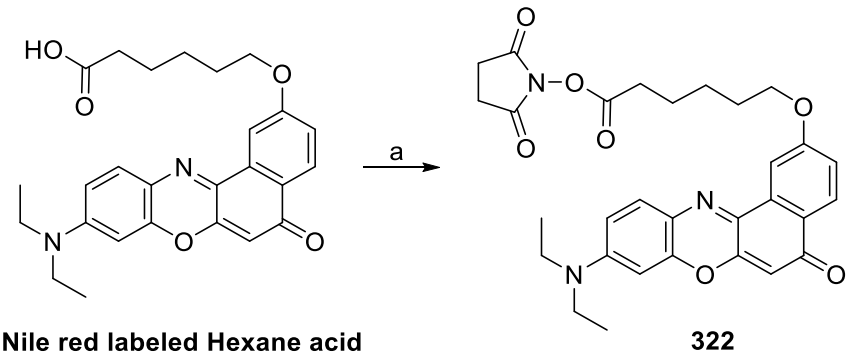

Scheme 15 Synthesis of Nile red labeled Hexanoic acid active ester. a) HOSu, DMAP, EDC, dry DCM, 0°C then RT, 4.5h, used without purification.

3.2.8 Coupling of the fluorescent dyes

The last stage of our synthetic pathway was the coupling of the previously synthesized dyes with the sphingomyelin analogues **212** and **214** to get the target final FRET probes

3.2.8.1 FRET probes with secondary amino group

The acceptor dye NBD was coupled to the phosphoryl choline part of the sphingomyelin analogue **212** according to the reported methods under basic conditions to get the NBD-labeled intermediate **401** in 85% yield according to **Scheme 16**. For the final coupling of the different FRET donor coumarin dyes, both the MOM-protected hydroxyl group and the Boc-protected amino group were deprotected using concentrated hydrochloric acid.

The active esters **310**, **315,** and Lauric acid N-hydroxysuccinimide ester could be then coupled to the free amino group of **402** under basic condition giving the target final FRET probes **ZP-403** and **TP-366** and the NBD-labeled SM analogue **TP-367** respectively in reasonable yields.

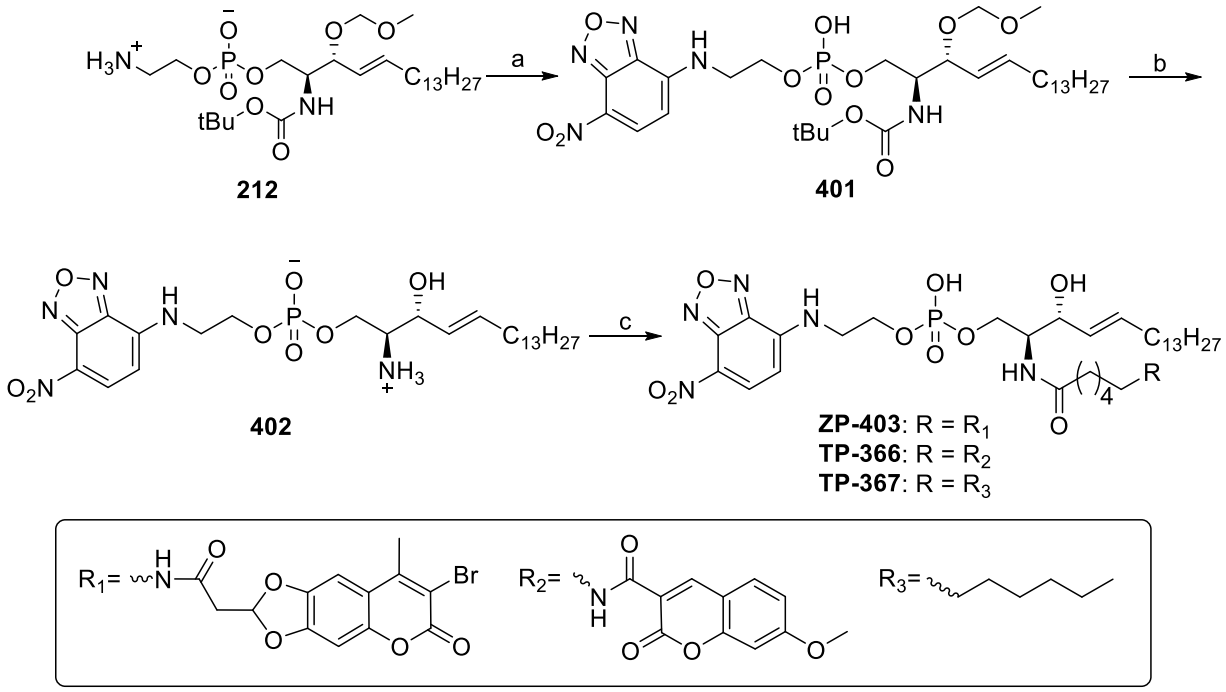

Scheme 16. Coupling of the fluorescent dyes and synthesis of the final FRET Probes. a) NBD-Cl, DIPEA, MeOH/$CHCl_3$ (1:3), RT, 4 h, 85%; b) 4 M HCl (in 1,4-dioxan), MeOH, 70°C, 2 h, Used directly without further purification; c) dry DIPEA, dry DCM, **310**, **315** or Lauric acid N-hydroxysuccinimide ester, RT, 24 h, 39%, 24%, and 45% respectively.

3.2.8.2 FRET probes with a quaternary ammonium group

Our primary strategy concerning this generation of ASM FRET probes was to keep it as similar as possible to the natural substrate. We started our trials of coupling using the N, N dimethylamino-functionalized NBD derivative **316** directly to nucleophilically open the five-membered phosphate triester ring of the intermediate **213**. The proposed product is the NBD Labeled intermediate **404** with only the dye labeling modification compared to the natural substrate (**Scheme 17**). Unfortunately, this reaction did not work even after different optimization trials like Time, Temperature, molar ratios, or catalyst [222] modifications. This inactivity is probably due to the increased steric bulk of nucleophile **316** as reported for similar reactions[200].

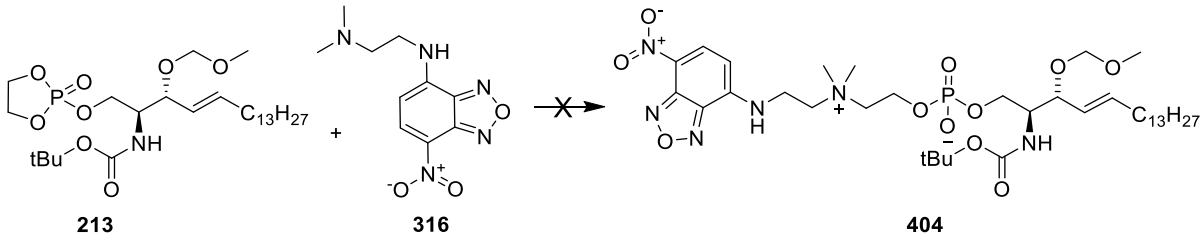

Scheme 17. Direct coupling trial of NBD for higher substrate similarity.

The next trial was to couple the FRET donor dye NBD through azide/alkyne click reaction between the azido functionalized NBD and the terminal alkyne functionalized intermediate **214**. For a minimized modification from the natural substrate, a direct azido functionalized NBD **317** was used for the click reaction with the alkyne intermediate **214** (**Scheme 18**). The reaction did not work even after different optimization trials regarding the solvent, reaction time, and molar ratios. Using the Cu(I) stabilizer Tris[(1-benzyl-1H-1,2,3-triazol-4-yl)methyl]amine TBTA for stabilizing the catalytic Cu(I) towards disproportionation and oxidation thus enhancing its catalytic effect in the azide-acetylene cycloaddition[223] made, unfortunately, no difference. Although it did not work with us, conversion of the azide **317** to triazoles is already reported but luckily this conversion caused a significant quenching effect upon triazole formation[224].

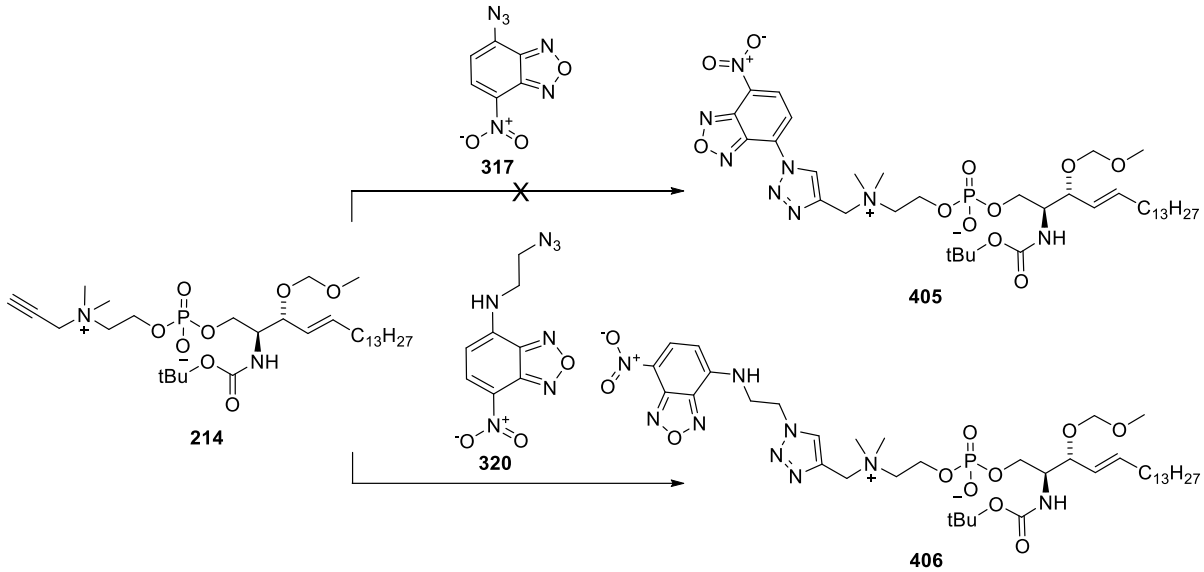

Scheme 18. Coupling of NBD through azide/alkyne click reactions; Reagents : t-BuOH/H_2O (4:1), sodium ascorbate & $CuSO_4.5H_2O$, RT, 48h.

The azide/alkyne click reaction was then repeated using a new azido functionalized NBD **320** in which the azido group was separated from the NBD nucleus through a 2 carbon linker. In our first trials of this pathway, the primary challenge was the purity of the alkyne **214**.

The primary trials before getting the alkyne **214** completely pure revealed the rapid formation of a side product on behave of the target compound **406**. Investigation of the mass and NMR data of this side product (**Figure 48**) reveals the click reaction product between the azide **320** and the N, N-Dimethylpropargylamine which was used in excess in the previous step and was not completely removed through the initial purification trials of **214**.

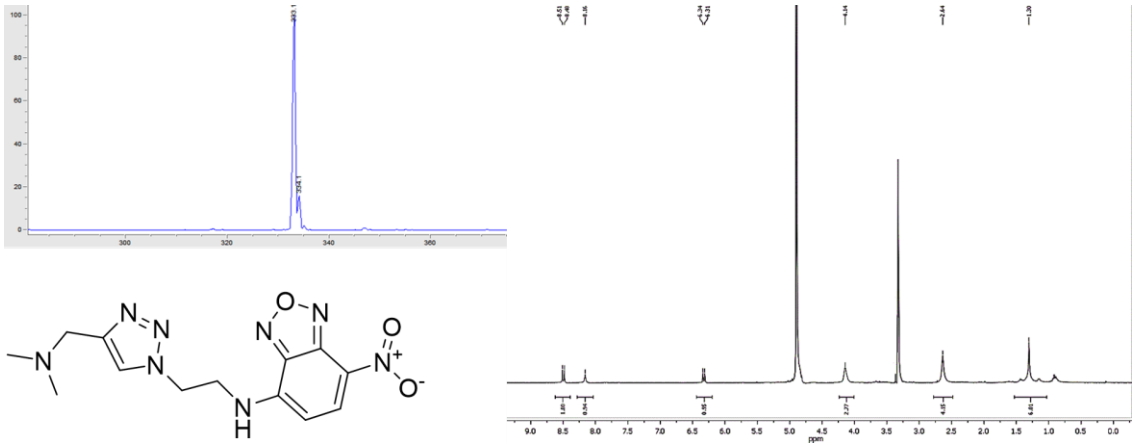

Figure 48. Structure, mass and ^{1}H-NMR spectrum of the click reaction side product.

After the complete removal of the N, N-Dimethylpropargylamine traces, and repeating the click reaction between the azide **320** and the pure alkyne **214**, the target triazole **406** could be isolated in an 83% yield. The amino and hydroxyl group of This NBD labeled intermediate **406** were then deprotected using concentrated hydrochloric acid and finally coupled with the coumarin labeled hexanoic acid active ester **315** to give the target FRET probe **ZQP-407** in 30% yield (**Scheme 19**).

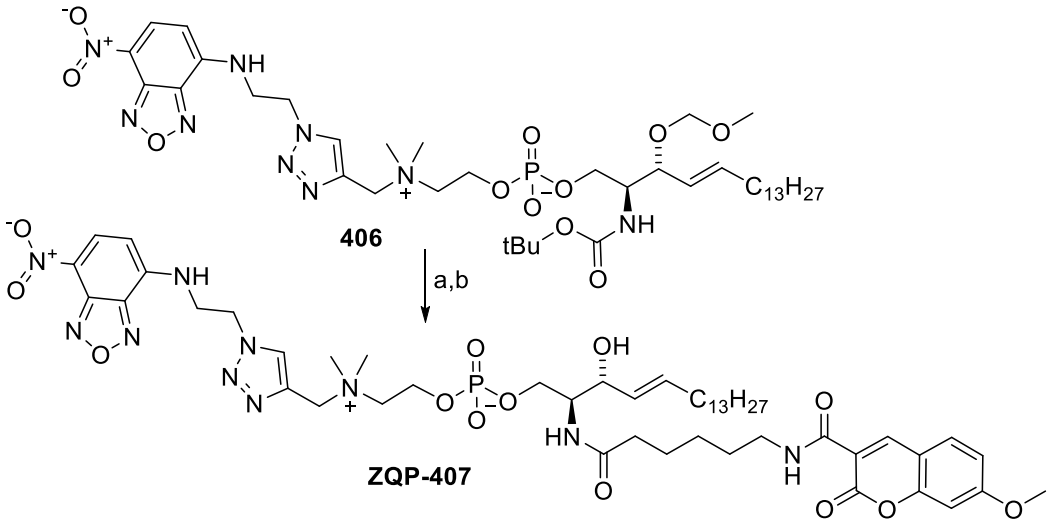

Scheme 19 Synthesis of the final FRET probe **ZQP-407**. a) 4 M HCl (in 1,4-dioxan), MeOH, 70°C, 2 h, Used directly without further purification; b) dry DIPEA, dry DCM, **315**, RT, 48 h, 30%.

3.2.8.3 FRET probes with a quaternary ammonium group and visible light range dyes

The alkyne functionality of the sphingomyelin analogue **214** serves as a tool for the introduction of a wide range of fluorophores or other labeling agents with aqueous phase click chemistry. So, we decided to extend our scope of the quaternary ammonium center containing probes to involve a visible light range dyes for either a FRET or simply mono-labeled probes (**Scheme 20**). Encouraged by the interesting results of our fluorescein containing FRET probe [125], we decided to include it in our target FRET probe aiming to combine the advantages of both higher substrate similarity and the cell-friendly visible light excitation ranges.

Using the established click reaction conditions, we managed to label our sphingomyelin analogue **214** with fluorescein and got the triazole intermediate **408** in a 54% yield. For the final coupling of the FRET acceptor dye Nile red or the fatty acid only, the intermediate **408** was deprotected using concentrated Hydrochloric acid and the free amino group was then coupled with the active ester of either Nile red -labeled hexanoic acid **322** or the Lauric acid to get the final FRET probe **ZQ$_2$P-410** or the fluorescein -mono labeled probe **ZQ$_3$P-411**.

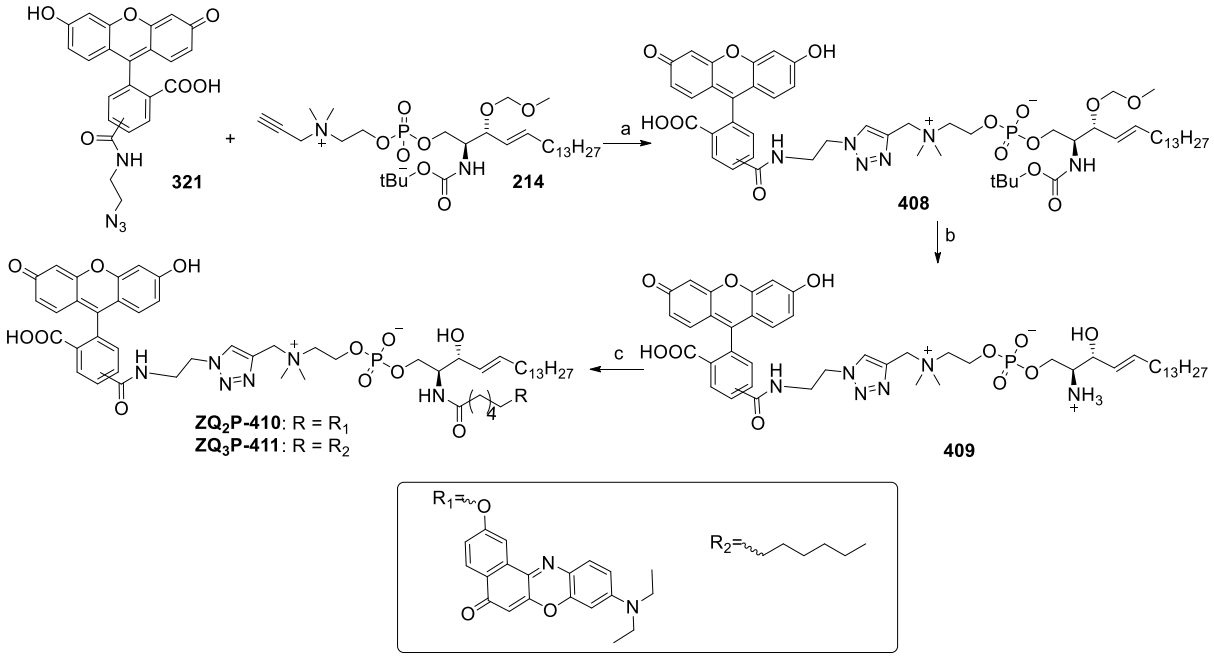

Scheme 20. Synthesis of the Final FRET and mono labeled quaternary probes with Visible light range chromophores. a) DMSO/H_2O (3:1), sodium ascorbate & $CuSO_4.5H_2O$, RT, 48h, 54%; b) 4 M HCl (in 1,4-dioxan), MeOH, 70°C, 3 h, Used directly without further purification; c) dry DIPEA, **322** or Lauric acid N-hydroxysuccinimide ester, dry DCM, RT, 72 h or 12h, 69% or 68% respectively.

3.2.8.4 Synthesis of the reference coumarin labeled ceramide analogue

For the comparative analytical purposes, the acid sphingomyelinase cleavage product of the FRET probe **ZP-403** was synthesized. This coumarin labeled ceramide analogue **413** was obtained starting from the previously synthesized protected sphingosine analogue **208** according to **Scheme 21**. After deprotection of the secondary hydroxyl and amino group, the active ester of the Bromo coumarin labeled hexanoic acid **310** was coupled with the free amino group of **412** under basic conditions to give the target reference ceramide analogue **413** in 90% yield.

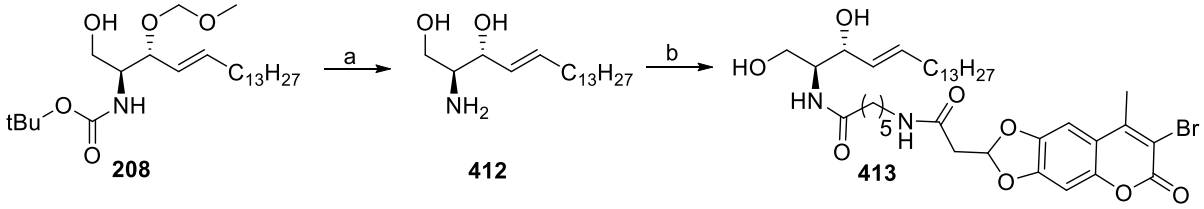

Scheme 21. Synthesis of the coumarin labeled ceramide analogue **413**. a) 4 M HCl (in 1,4-dioxan), MeOH, 70°C, 2 h, Used directly without further purification; b) dry DIPEA, **310**, dry DCM, RT, 12 h, 90% over two steps.

3.2.9 Fluorescence spectrophotometric characterization

3.2.9.1 Characterization of the FRET probe ZP-403

A FRET probe containing the bromo-coumarin derivative as donor was reported but with another acceptor dye[171]. And a coumarin/NBD FRET system was also reported by our group[121] but with a non-brominated coumarin derivative. So the fluorescence characters of the probe **ZP-403** with the new coumarin derivative were studied to check the formation of a FRET system between the new dye pair NBD and bromo-coumarin combination within the new molecule setup (**Figure 49**).

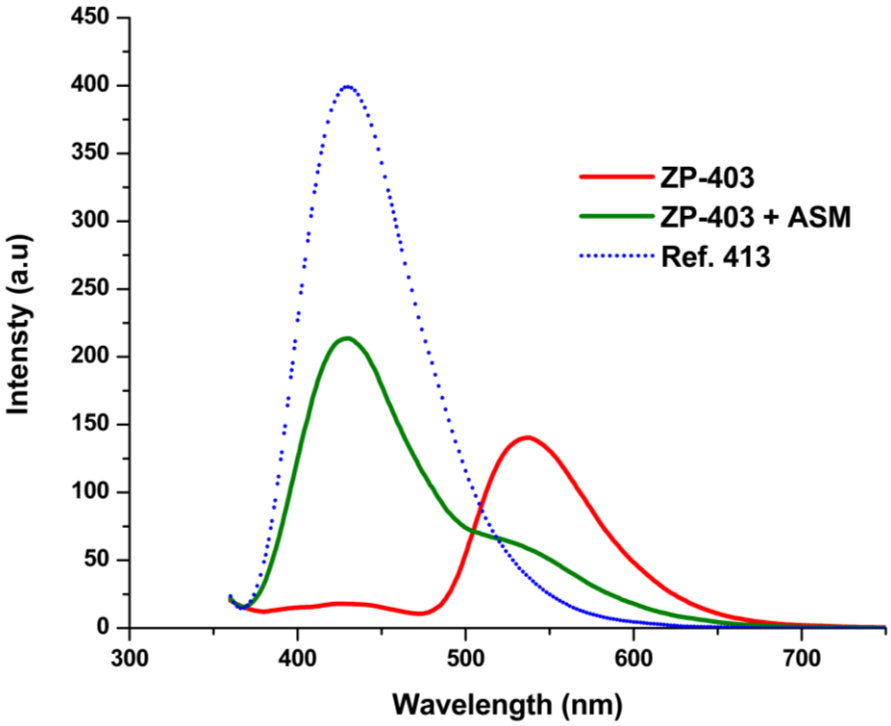

Figure 49. Fluorescence Emission spectrum for the probe **ZP-403** before and after the incubation with ASM (0.2 µg/ml) and the emission spectrum of the reference ceramide derivative probe **413**; Probes concentration= 1µM, ASM buffer, Ex :347 nm, $t_{incubation}$=17 h.

Excitation of the **ZP-403** Bromo-coumarin dye at 347 nm wavelength resulted in a main strong NBD emission peak at about 536 nm and only a very tiny residual of the coumarin emission at 430 nm. This means that a FRET system formed between the new bromo-coumarin dye as a donor and NBD as an acceptor. This FRET system resulted in a nearly complete transfer of the donor dye emission energy to the acceptor dye.

The next character to be studied was the cleavage of the FRET probe **ZP-403** with ASM. Enzymatic cleavage is a critical step for the enzymatic assays using artificial substrates because the modifications of the natural substrate can lead to either lower recognition or may be a complete unrecognized substrate.

In our case, although similar FRET probes for the ASM were already reported with similar dye pairs, this cannot be a guarantee for the recognition of the new FRET probe by the enzyme because some minor structural differences can lead to major enzymatic binding differences.

Incubation of the new probe with the recombinant enzyme under the established condition overnight has revealed a fluorescence intensity change in the form of decreasing fluorescence intensity of the FRET acceptor emission peak by about two thirds and increasing the FRET donor emission peak by about 10-folds (**Figure S 5**). This pattern of fluorescence intensity change means that the FRET system was destroyed by the enzyme under these conditions and thus the new FRET probe **ZP-403** is a substrate for the ASM enzyme.

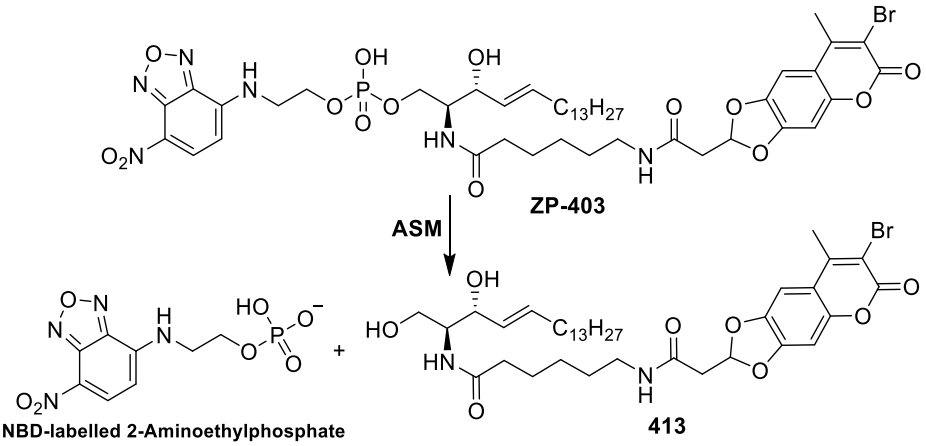

Scheme 22. Enzymatic cleavage of the **ZP-403** FRET probe by ASM.

For more confirmation of the enzymatic cleavage, the fluorescence of the synthesized cleavage product **413** (**Scheme 22**) was studied under the same condition in order to be used as a reference. The newly growing peak through the enzymatic cleavage showed the same maxima as the reference cleavage product (**Figure 49**).

The real-time enzymatic cleavage in terms of fluorescence change was studied using both the specific wavelengths measuring kinetic tool and the full scanning at different time points. Both showed a time-dependent change with most of the intensity change in the first two hours as in **Figure 50**. From this kinetic study also, it was reconfirmed that the fluorescence intensity change of the donor coumarin dye was higher than that of the acceptor NBD dye. As the emission of the new coumarin dye is red-shifted by about 25 nm, better overlap between both dyes could be achieved. The lower fluorescence change of the NBD compared to the previously reported probe could be explained by this close overlapping in which the increased fluorescence of the closely neighboring coumarin peak counteracts the fluorescence decrease of NBD.

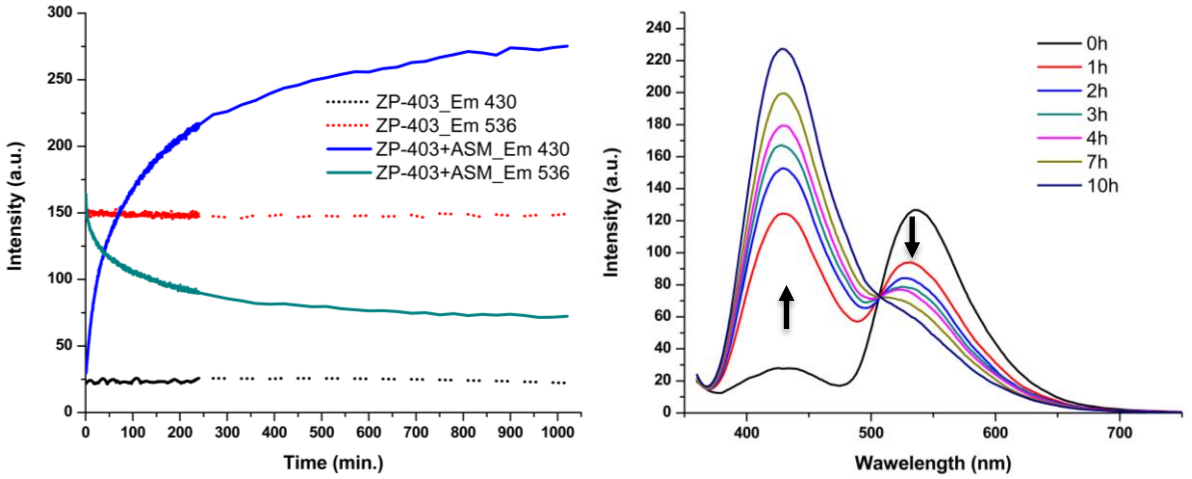

Figure 50. Real time fluorescence intensity changes during the enzymatic reaction; **left**: Intensities at selected wavelengths; **right**: full spectrum after addition of ASM (0.2 µg/ml) . Probe concentration= 1µM, ASM buffer.

This study also showed the stability of the probe **ZP-403** over the time course of the experiment. The control experiment in which the probe was incubated in the reaction buffer without enzyme showed no change over time. This stability against fluorescence quenching excludes the interference with the fluorescence change resulted from the enzymatic cleavage and also excludes the concerns regarding the stability of the acetal group of the new coumarin in this acidic pH[225].

After the primary characterization of the FRET probe **ZP-403** and the confirmation of the presence of a FRET system and cleavability by the acid sphingomyelinase, the probe was then tested in a more complex environment than the pure recombinant enzyme. For this purpose, a Hela cell lysate was used instead of the recombinant enzyme (**Figure 51**). In the trial where the pH was adjusted to 5 (pH optima for the ASM), a significant cleavage was noticed as compared to the control experiment with the probe only. While in another trial under a pH value of 7 (the pH optima for the neutral sphingomyelinase) no cleavage was detected even after a longer time than the presented in **Figure 51**.

Full scanning comparison before and after the incubation time revealed also the same results with a slight decrease in fluorescence intensity of the FRET peak at 536nm at pH7 which is not related to the enzymatic activity when we take in consideration the stability of the FRET donor peak at 430nm. From this experiment we could conclude that the probe **ZP-403** can be used in a complex cellular media and it is specific for the acidic range sphingomyelinase enzyme.

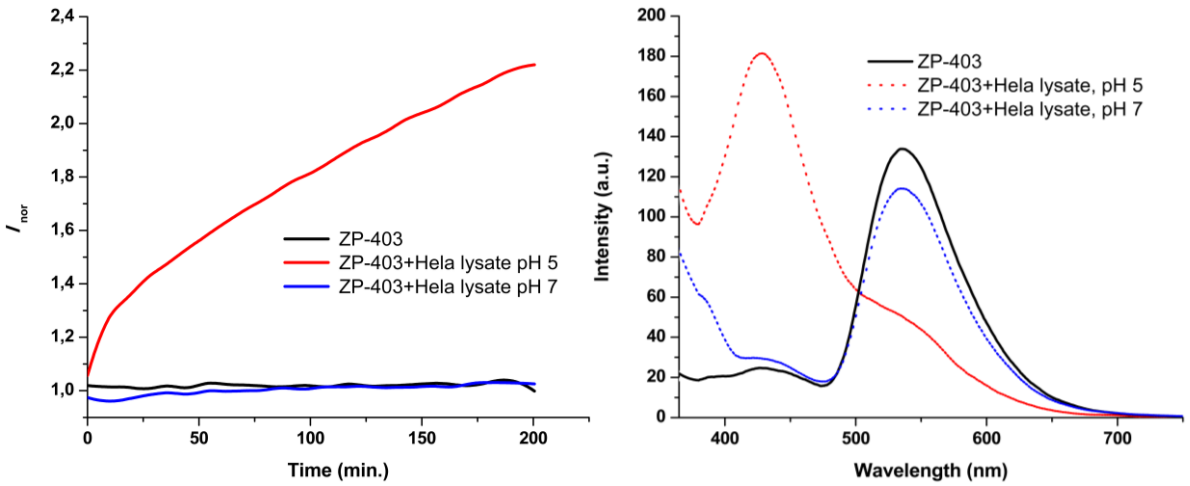

Figure 51. FRET probe **ZP-403** cleavage using cell lysates at different pH values. **Left**: kinetic study, Ex_347, Em_430, ASM buffer, $I_{nor}= I/I_0$; **Right**: full spectrum scanning after incubation, Ex_347. Probe concentration= 1µM.

For a further check of the probe selectivity, another experiment using both ASM knocked out MEF cell lysate and recombinant nSMase2 enzyme. The fluorescence intensities at 536nm could be presented in **Figure 52**. Neither with the ASM knocked out lysate nor with the recombinant nSMase 2, a cleavage was detected. Under the same experiment condition, a parallel experiment with ASM revealed a significant fluorescence intensity decrease as a result of the probe cleavage.

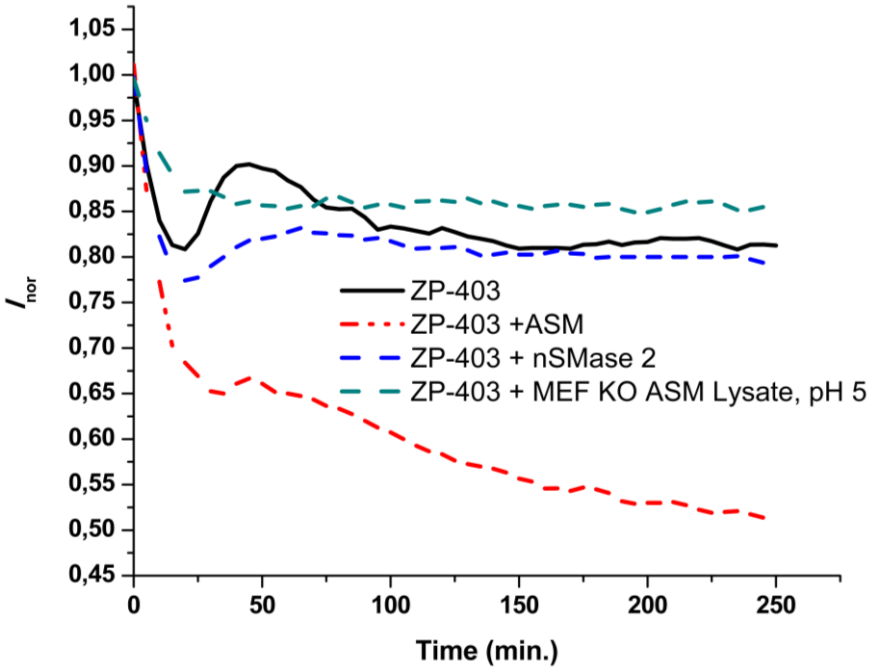

Figure 52. FRET probe **ZP-403** cleavage study using ASM Ko MEF lysate and recombinant nSMase 2; Ex_347, Em_536, ASM buffer, $I_{nor}= I/I_0$, Probe concentration= 1µM, Concentration of ASM (0.2 µg/ml).

At this stage, the probe **ZP-403** was confirmed as a FRET probe which can be cleaved selectively with the acid sphingomyelinase in both recombinant and lysate form in a real time manner and this cleavage can be monitored through either the donor , acceptor or both fluorescence channels.

3.2.9.2 Detection of ASM inhibitors using ZP-403

Enzymes are superior targets for drug discovery research not only because their catalysis is essential for all life processes and are commonly modified in various disease states but also, the geometry and chemistry of the enzymes' binding sites are highly well-suited for interactions with small, drug-like molecules[226]. The same attention is paid to the ASM enzyme due to the lack of selective, potent, and drug-like inhibitors for it[227].

As the development of new analytical tools is a key route toward the discovery and optimization of enzyme inhibitors, our main target during the development of ASM FRET probes was to use them for screening for inhibitors. The ability of **ZP-403** to detect the inhibitors of ASM was primarily studied using a reported phosphoinositide inhibitor[121].

In the experiment with the ASM inhibitor, a significant decrease was observed in the fluorescence change rate compared to the experiment without the inhibitor (**Figure 53**). This means that our setup is suitable for the detection of the inhibitory actions on the enzyme.

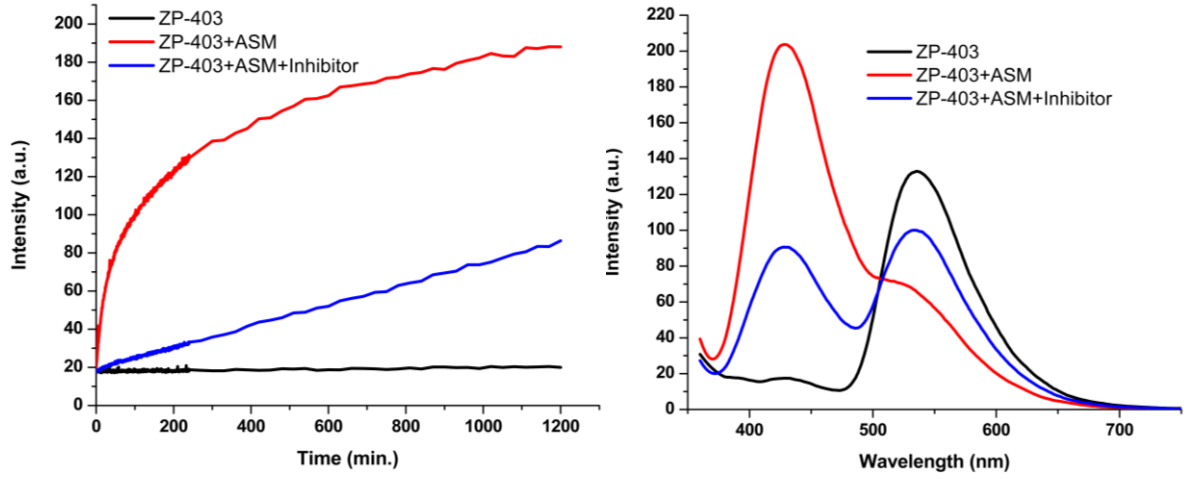

Figure 53. The effect of ASM inhibitor on the fluorescence change of **ZP-403** during the enzymatic cleavage; **left**: kinetic study, Ex_347, Em_430; **Right**: full spectrum scanning, Ex_347; ASM buffer, Probe concentration= 1µM, Concentration of ASM (0.2 µg/ml), Inhibitor= ASM inhibitor 1-O-hexadecylsulfonyl-myo-inositol-3,5-bisphosphate (500nM).

To check the ability of the assay to differentiate between different inhibitor concentrations, a new experiment was done where different inhibitor concentrations were tested in parallel (**Figure 54**).

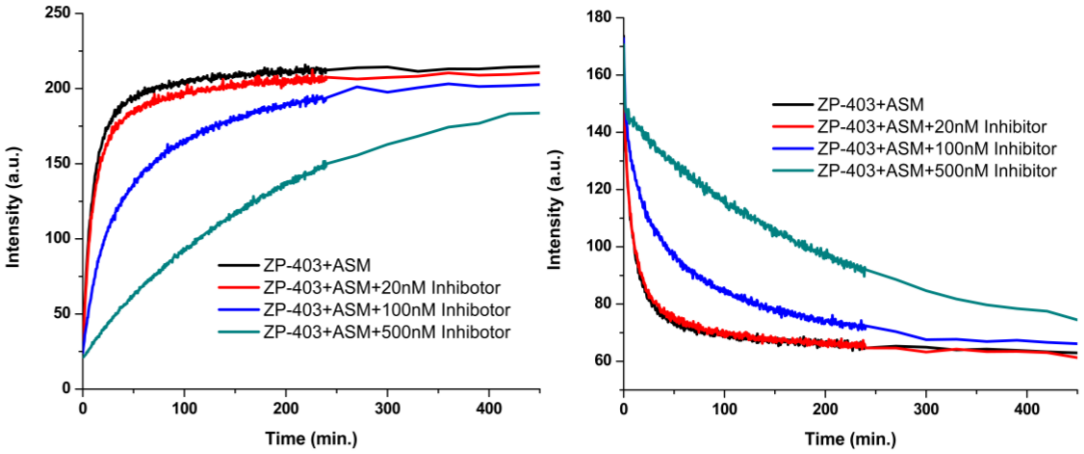

Figure 54. Effect of different inhibitor concentrations on the FRET probe **ZP-403** cleavage by ASM; **Left** : kinetic study, Ex_347, Em_430; **Right**: kinetic study, Ex_347, Em_536. ASM buffer, Probe concentration= 1µM, Concentration of ASM (0.2 µg/ml), Inhibitor= ASM inhibitor 1-O-hexadecylsulfonyl-myo-inositol-3,5-bisphosphate.

In both FRET donor and acceptor channels the action of a 20 nM to 500 nM inhibitor concentration range could be detected and differentiated. These results mean that the probe **ZP-403** is a promising screening tool for ASM inhibitors with flexibility regarding the available wavelengths filters. Based on the previous results, the effect of the inhibitor was also tested using Hella cell lysate instead of the recombinant enzyme as in **Figure 55**. The assay under these conditions was also able to significantly detect the effect of the inhibitor on the activity of ASM.

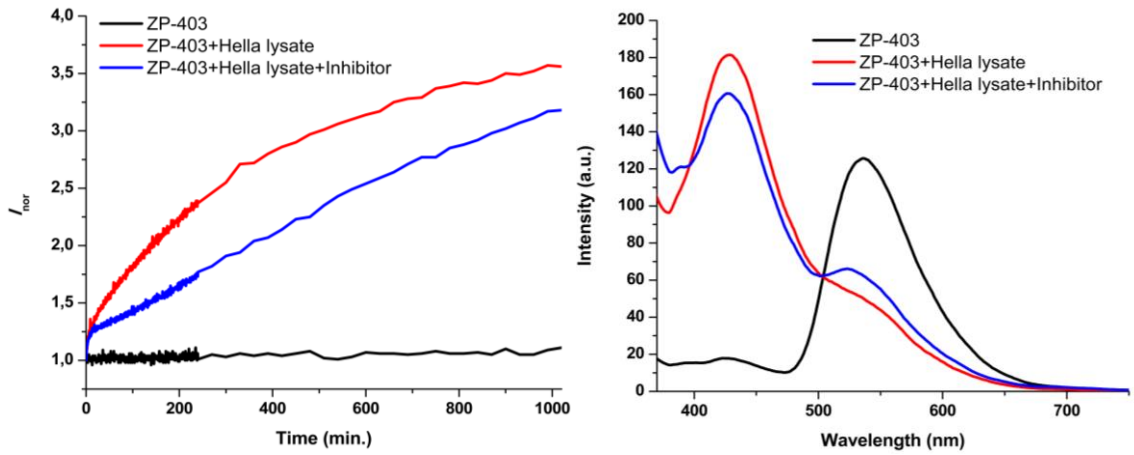

Figure 55. Testing the inhibitory action on ASM in cell lysate mixture; **Left**: kinetic study, Ex_347, Em_430; **Right**: full spectrum scanning, Ex_347; ASM buffer, Probe concentration = 1µM, Inhibitor = ASM inhibitor: 1-O-hexadecylsulfonyl-myo-inositol-3,5-bisphosphate (100nM).

As the level of an enzyme activity is a critical factor concerning its biological functions and the related pathological conditions, the developments of efficient assays for monitoring this level/activity is of high need in both diagnostic and drug discovery research areas. Our enzyme of interest acid sphingomyelinase is involved in the regulation of cell fate and signaling via hydrolysis of sphingomyelin to form ceramide. The increased activity of the lysosomal form has been associated with various pathological conditions[228] while the severe deficiency in sphingomyelinase activity in tissues causes NPD types A and B[229].

Because of the importance of ASM level monitoring, the FRET probe **ZP-403** was then used to monitor the effect of different ASM concentrations. Using our established setup with these different enzyme concentrations revealed different fluorescence change rates which could be also monitored through both FRET probe donor and acceptor channels (**Figure 56**).

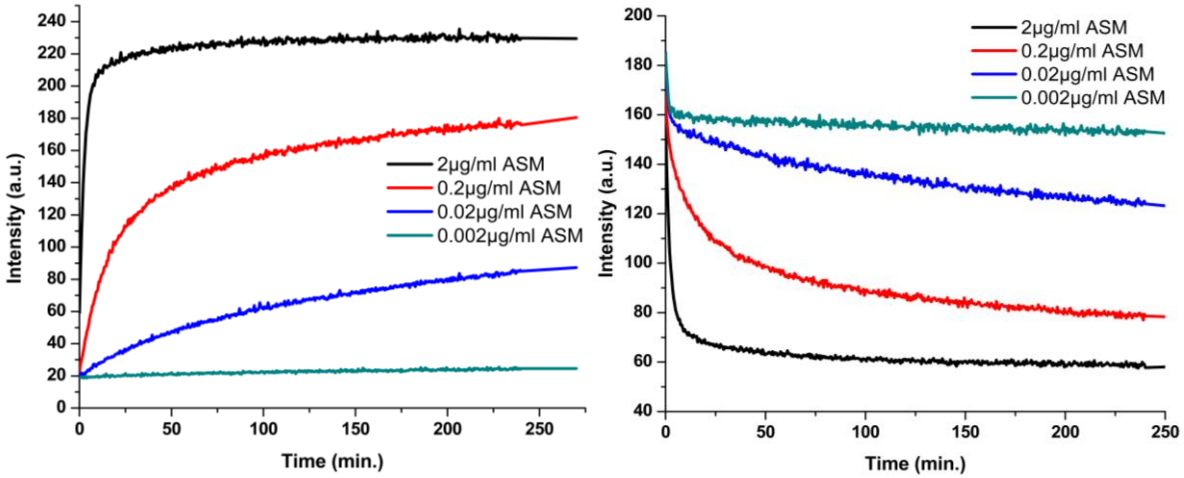

Figure 56. Effect of different ASM concentrations on the cleavage rate of the FRET probe **ZP-403**; **Left**: kinetic study, Ex_347, Em_430; **Right**: kinetic study, Ex_347, Em_536. ASM buffer, Probe concentration= 1µM.

With the lowest concentration (0.002µg/ml) used from ASM, a very slight change was observed over the experiment time (270 min.). While with the highest concentration used (2µg/ml), the reaction plateau was achieved in about 30 minutes. The two other used concentrations showed also a concentration-dependent cleavage rate as demonstrated with the fluorescence intensity change for both the coumarin donor dye (430 nm) and NBD acceptor dye (536nm).

3.2.9.3 Two-photon excitation fluorescence microscopy study

The main target of the **ZP-403** probe design and synthesis was to improve the 2P excitability through the newly included bromo-coumarin derivative. So after the synthesis and the primary characterization, the next step was to practically evaluate the effect of this modification on the 2P excitability compared to the old version coumarin containing probe **TP-366**. This comparative study was accomplished using a Two-photon excitation fluorescence microscopy which will be most probably the future analytical instrument for any live cell application studies.

For this purpose the two FRET probes were loaded on silica gel beads through mixing the probe containing freshly prepared liposomes in a 1:1 ratio with defatted Silica Gel 60M (0.04-0.063 mm) 10mg/ml and then the incubation for 1 hour at room temperature. Afterward, the beads were separated from the unbound liposomes by standing for 20 minutes then centrifugation for 2 min. The beads were washed with PBS (0.5 x) two times and resuspended in the same amount of PBS (0.5 x) buffer as the 1:1 mixture of liposomes and beads. The resuspended beads were stored at 4°C.

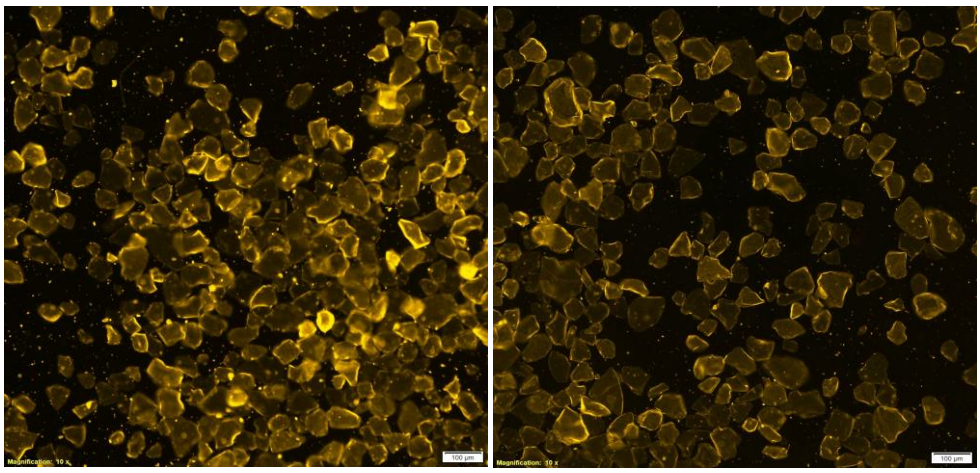

Figure 57. Primary fluorescence microscopy visualization of the FRET probes labeled silica beads **ZP-403** (left) and **TP-366** (right).NBD excitation/emission filter.

The FRET probes labeled beads act as a cellular lipid membrane but without any enzymatic activity which is important for our comparative study to exclude any cellular uptake or enzymatic cleavage rate differences. The primary visualization of the FRET probes labeled beads through the NBD excitation and emission using epifluorescence microscope (**Figure 57**) showed enough bead coating with a good resolution.

All microscopy images and quantifications in the next chapter have been recorded by *Dr. Cosima Rhein*, University of Erlangen. In the first 2P excitability experiment, the silica beads coated with **ZP-403** were excited at 720 nm which is the 2P excitation wavelength for the bromo-coumarin FRET donor dye (1P excitation ~350 nm). At this wavelength, the beads could be sufficiently excited and revealed the emission fluorescence of the intact FRET probe which could be also got through the direct excitation of the NBD dye. The 2P excitability of the FRET probe was proven by merging both the coumarin 2P excitation results with that of the direct NBD excitation which were identical (**Figure 58**).

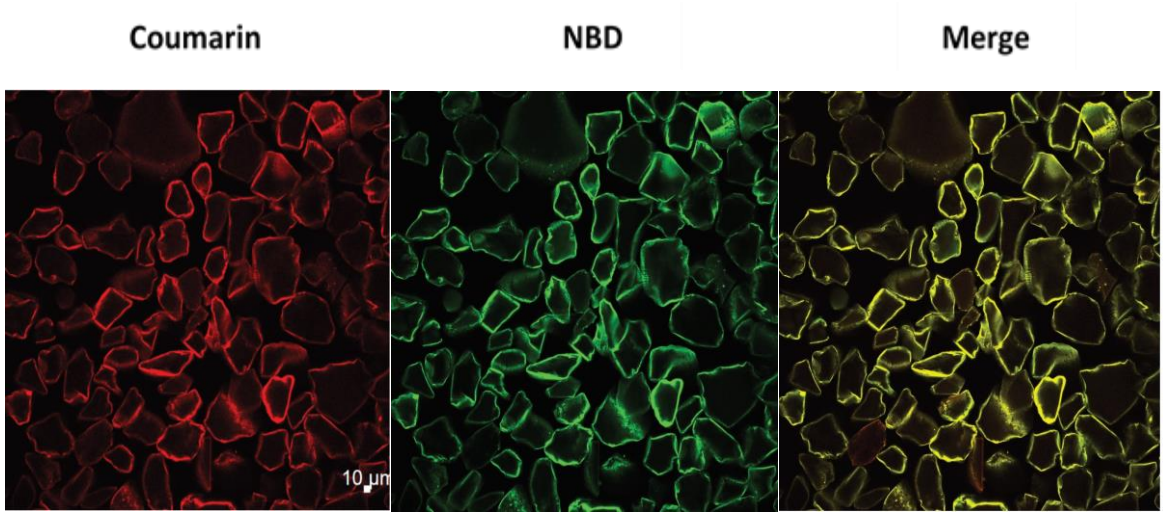

Figure 58. Fluorescence microscopy graphs of the lipid beads coated with **ZP-403** labeled liposomes. from left to right: Coumarin after two-photon excitation 720nm, NBD after two-photon excitation at 870 nm and the merge of both graphs. The white bar corresponds to 10 µm.

From this experiment we could conclude that the new bromo-coumarin dye can be excited using 2P excitation wavelengths and the FRET system can be also detected under this setup using those static platform beads. In the next step, the FRET probe **ZP-403** was applied as BSA-complex to Human H4 neuroglioma cells overexpressing ASM for 2 hours at a final concentration of 1 µM and then the cells were studied microscopically. Two-photon excitation of the bromo-coumarin at 720 nm resulted in the detection of the uncleaved probe that indicates sphingomyelin. Direct excitation of NBD revealed also the same emission fluorescence of the intact probe and this was further confirmed by merging both shots (**Figure 59**).

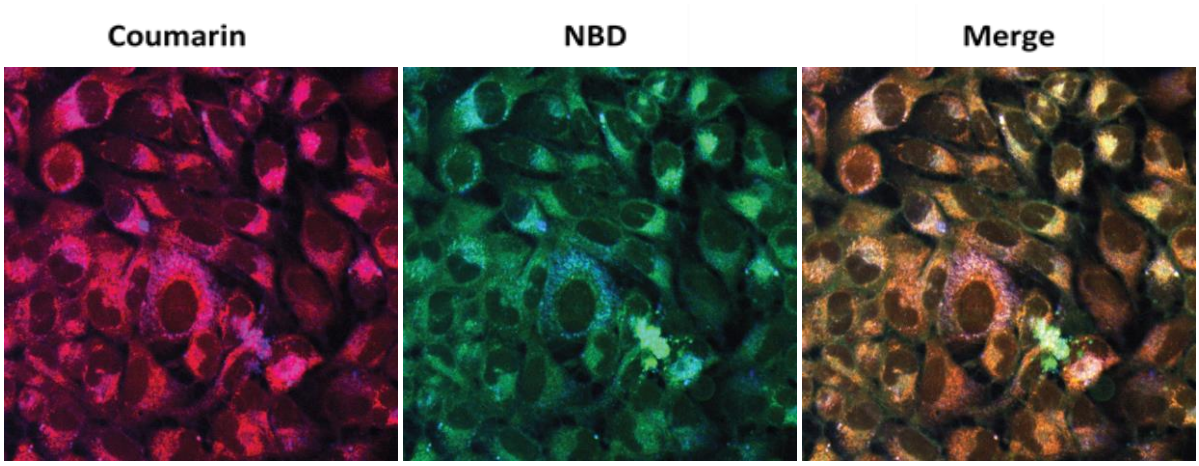

Figure 59. FRET substrate **ZP-403** in Human H4 neuroglioma cells. from left to right: Coumarin after two-photon excitation 720nm, NBD after two-photon excitation at 870 nm and the merge of both graphs.

From this experiment the cellular uptake of the FRET probe **ZP-403** as a BSA-complex could be confirmed. Also, the 2P excitation of the new coumarin and the detection of the FRET emission fluorescence in live cells was confirmed. As the target of the new probe, **ZP-403** was to improve the 2P excitability compared to the first generation probe **TP-366** for a more live-cell studies suitability, we tried to check the impact of the expected difference between the two probes directly in cells in terms of ease of detect, brightness or low beam energy needs. The idea was to excite the cells which were previously incubated with the probes with different laser powers and check if the expected difference in the 2P excitability will be able to compensate the laser power difference or not (**Figure 60**).

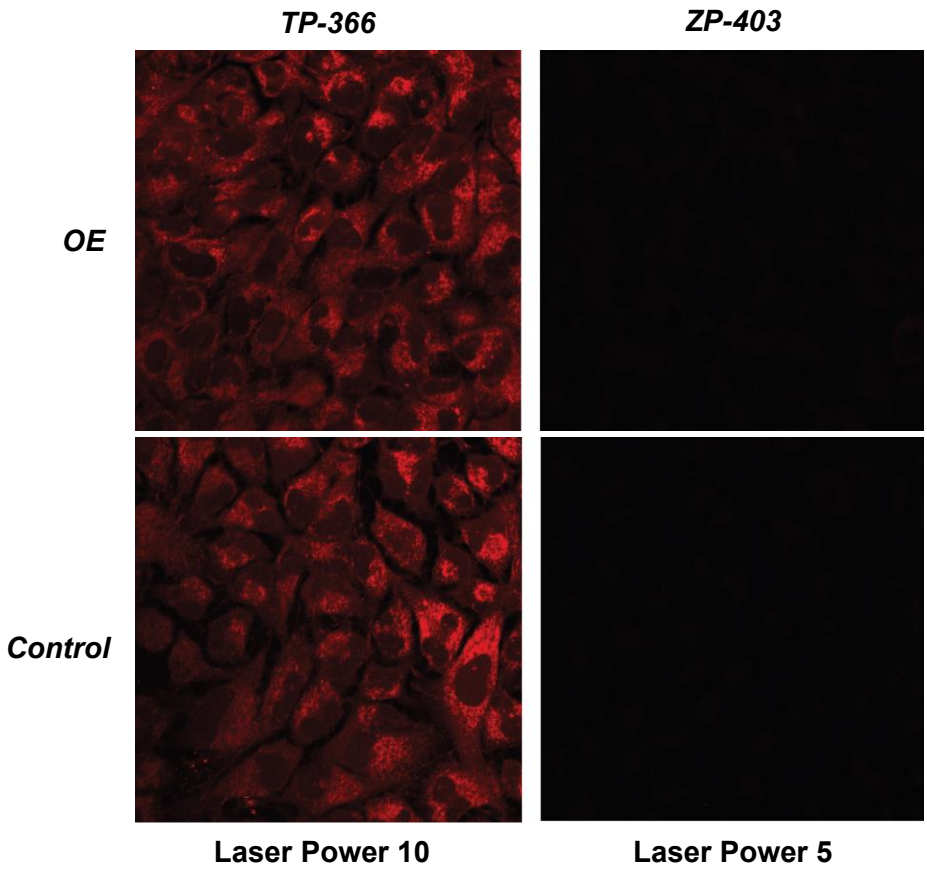

Figure 60. Direct comparison of the 2P excitability of **ZP-403** and **TP-366** FRET probes in live cells using different laser powers. OE: Human H4 neuroglioma cells overexpressing ASM; Control: Human H4 neuroglioma cells; FRET probes applied as BSA-complex for 2h before imaging.

Assuming a significant difference between the probes, **ZP-403** was excited using half of the laser power 10 used for **TP-366**. Under this setup the FRET probe **ZP-403** couldn't be detected at all compared to **TP-366** as presented in the upper part of **Figure 60**. To exclude the effect of the ASM overexpression in the tested cells, the experiment was repeated using normal Human H4 neuroglioma cells. The same results were obtained which excluded our assumption of 2P excitability improvement in the >2 fold range.

For a precise quantification of the difference between the two FRET probes **TP-366** and **ZP-403**, a new beads model was prepared in which the beads were coated with liposomes containing 1:1 mixture of the FRET probe and its coumarin containing cleavage product. The selection of the beads and not the cells was to exclude any uptake variations in case of using live cells. The use of a mixture of the intact FRET probe and its cleavage product is to get a cleavage-mimicking setup. In this setup, we can measure the direct coumarin emission (which is mainly quenched in the FRET system) for the free cleavage product in the presence of the intact probe.

The beads were excited with three different laser powers (3,5,10) and pixel intensities were measured for both FRET emissions (350 nm (2P) >> 560 nm and 350 nm (2P) >> 420 nm) and the direct NBD (480 nm >> 560 nm) which should be the same for both probes and can be used as an internal standard for normalization. Three shots were taken for each laser power and from each picture 3 beads were analyzed. Comparing the FRET NBD intensities (350 nm (2P) >> 560 nm) normalized to the direct NBD of both probes at the different laser powers did not reveal any significant difference between them (**Figure 61**).

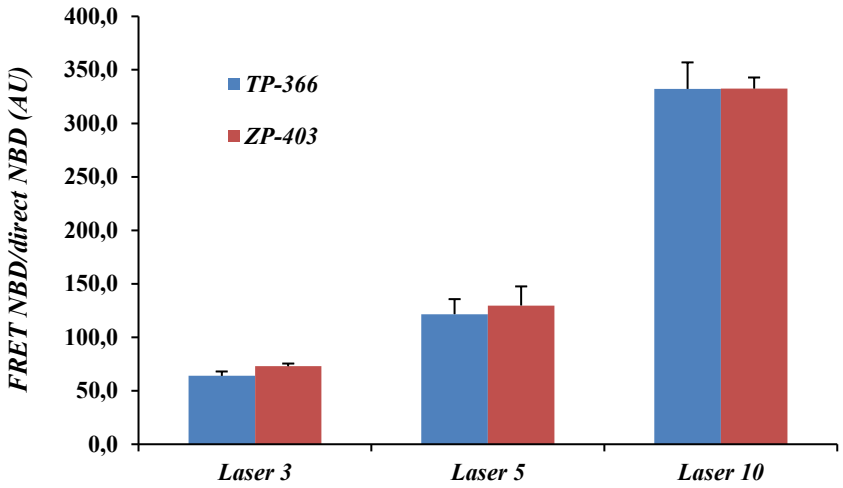

Figure 61. Comparative study between the FRET probes **ZP-403** and **TP-366** using the emission of direct NBD excitation as internal standard for normalization. FRET emission: Ex_350 nm (2P) >> 560; NBD emission : Ex_480 nm >> 560 nm).

In an actual cell experiment, the progress of the coumarin signal would be followed as a monitor for the cleavage of the probe. In the next experiment, it was checked whether the **ZP-403** probe would be brighter or more intense in the coumarin channel. Using the same setup of the previous experiment, the coumarin signal (mainly of the cleaved probe portion) was measured and normalized to the direct NBD, which should be the same for both probes. Interestingly in this experiment a difference between the two beads could be detected and it is increasing with the increase of the laser power to reach about 20% difference at laser power 10 (**Figure 62**).

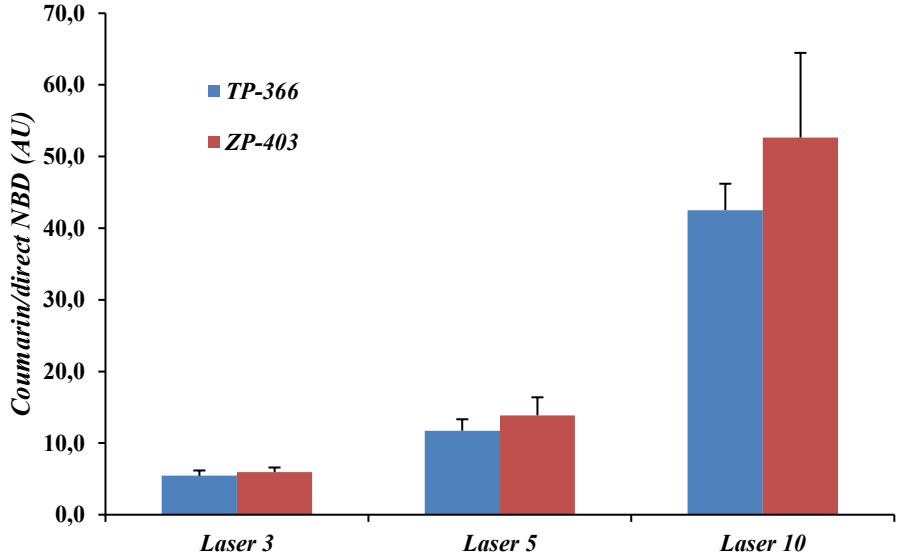

Figure 62. Comparison study between the beads containing 1:1 ratio **ZP-403** to its cleavage product **413** with the beads of **TP-366** and its cleavage product using the emission of direct NBD excitation as internal standard for normalization. Coumarin emission: Ex_350 nm (2P) >> 420 nm.

With these results we concluded that the inclusion of the bromo-coumarin derivative in the FRET system for ASM can to an acceptable extent improve the 2P excitability and thus the brightness of the probe during the monitoring of the cleavage reaction. This improvement could be mainly noticed in the channel of coumarin emission which revealed also in the primary characterization experiments about 10-fold intensity change over the course of the reaction time.

3.2.9.4 Live cells study of NBD-labeled SM analogue TP-367

The probe **TP-367** was reported by our group and primarily tested *in vitro*. It revealed a fluorescence turn off pattern upon cleavage with ASM. In this study the resynthesized probe was tested *in vivo* using the flow cytometry approach by *Dr. Gita Naseri*. To test the detection ability of this probe; regular HEK293 cells were treated with it and the fluorescence outputs were measured at different time points (**Figure 63**) . The cells treated with the probe **TP-367** for 16 hours showed significant lower green fluorescence (~ 3-fold) compared to cells pre-treated with the ASM inhibitor ARC39. In contrast to the turn on FAM/BODIPY FRET probe[125], **TP-367** showed maximum fluorescence in its intact form, when ASM activity is low thus was confirmed as an *in vivo* turn off probe. With this results the probe was confirmed as an orthogonal probe and a unique ASM assay has been developed. This assay is fast and valid as it measures the activity of the enzyme in living cells and not after lysis or in artificial buffer environments.

We expect that HEK293 cells carrying mutated *SMPD1* will behave like the inhibitor treated cells and a facile FACS mediated selection of these cells will thus be possible.

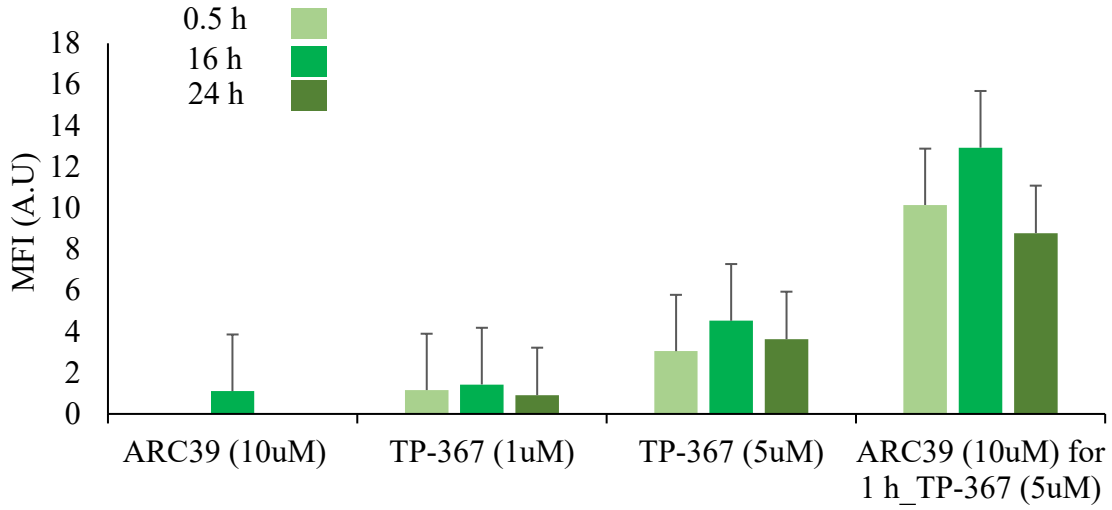

Figure 63. ASM activity assay using the probe **TP-367**. The data was normalized to the fluorescence intensity of cells treated with DMSO. Data are geometric means ± SD of the fluorescence intensity obtained from three cultures, each derived from an independent HEK293 culture and determined in three technical replicates. MFI: mean of fluorescence intensity.

3.2.9.5 Characterization of the quaternary ammonium containing FRET probes

The first quaternary ammonium group-containing FRET probe **ZQP-407** was tested regarding the presence of a FRET system although the FRET dye pair is already tested and reported [121]. As presented in **Figure 64**, the donor coumarin dye was excited and the emission was scanned over a wide range. A neglectable fluorescence was noticed at the emission wavelength of the coumarin while the main fluorescence intensity was detected at the emission maxima of the acceptor NBD dye. This means that the emission energy was successfully transferred to the NBD forming a FRET system with a high efficiency. The stability of the probe in the ASM reaction buffer was also studied. It revealed good stability regarding the fluorescence intensity after 18 hours of incubation. Thus, a stable FRET probe under the ASM reaction conditions was confirmed through this primary characterization.

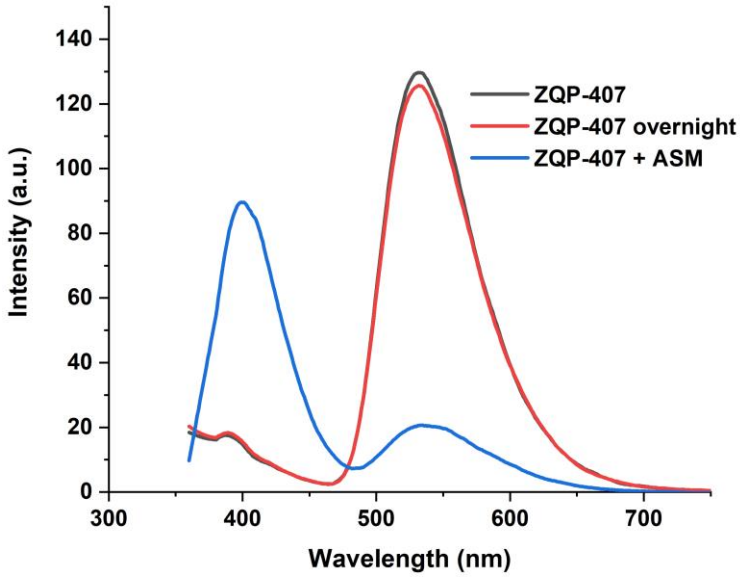

Figure 64. Fluorescence Emission spectrum for the probe **ZQP-407** before and after the incubation with ASM (0.2 µg/ml); Probes concentration= 1µM, ASM buffer, Ex :347 nm, $t_{incubation}$=18 h.

Although the target of the design of the probe **ZQP-407** was to achieve higher recognition through higher substrate similarity, there is still a possibility to be unrecognized and thus uncleavable by the enzyme due to the structural modification. Therefore, the recognition and cleavage of the probe with the ASM was studied. To figure this out, the probe was incubated with the recombinant ASM for 18 hours and the fluorescence behavior was compared with that before the addition of the enzyme (**Figure 64**). The FRET acceptor peak at ~ 536nm was significantly decreased while that of the donor emission was also significantly increased. This change means that the probe was hydrolyzed by the ASM and accordingly the FRET system pattern was cleaved. A time dependent change of both donor and acceptor dyes fluorescence with an obviously faster rate compared to the previously studied probes was observed (**Figure 65**). Effect of different ASM concentrations on the cleavage rate of the FRET probe **ZQP-407** was also studied and the results are displayed in **Figure S 6**.

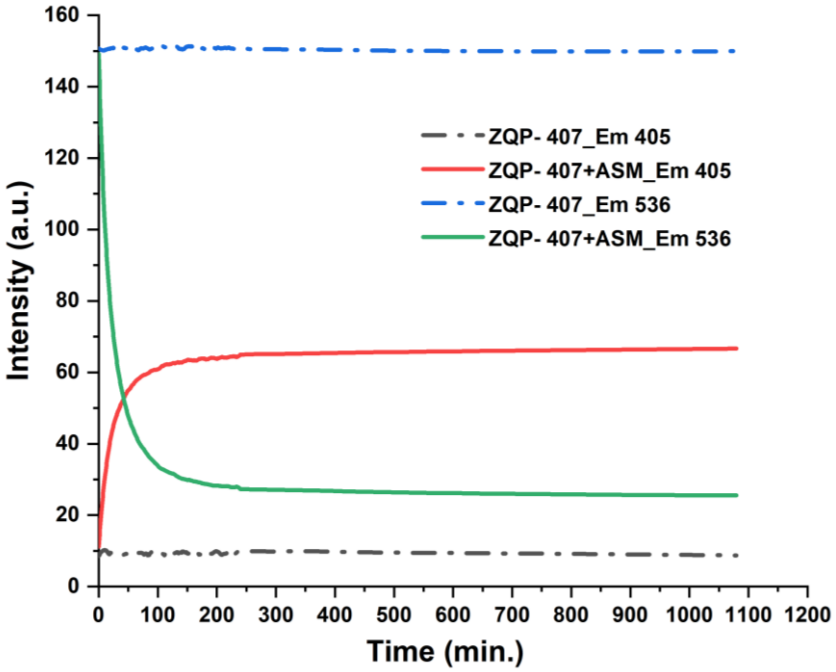

Figure 65. Real time fluorescence intensity changes during the enzymatic cleavage of **ZQP-407;** ASM (0.2 µg/ml), Probe concentration= 1µM, ASM buffer, Ex :347 nm.

The second probe **ZQ$_2$P-410** containing fluorescein as a donor and Nile red as an acceptor was also studied to check the presence of a FRET system and the cleavability with the ASM enzyme (**Figure 66**). Upon exciting the fluorescein, a main emission peak at 624 nm was detected which is the emission maxima for the acceptor dye Nile red. This mean that a FRET system was formed as expected from the spectral overlap of the dye pair. Then upon incubation of the probe with the ASM enzyme, a significant fluorescence intensity increase of the fluorescein dye was observed while only a minor decrease was observed with the fluorescence of the Nile red dye with the major change occurred at the first one hour as presented in **Figure 66**. This change of fluorescence intensities means that the FRET system can be cleaved by the ASM and the only minor change of the Nile red fluorescence can be explained through counteracting of the fluorescence decrease by the increasing fluorescence of the closely neighboring fluorescein peak as reported in previous probes[121,122].

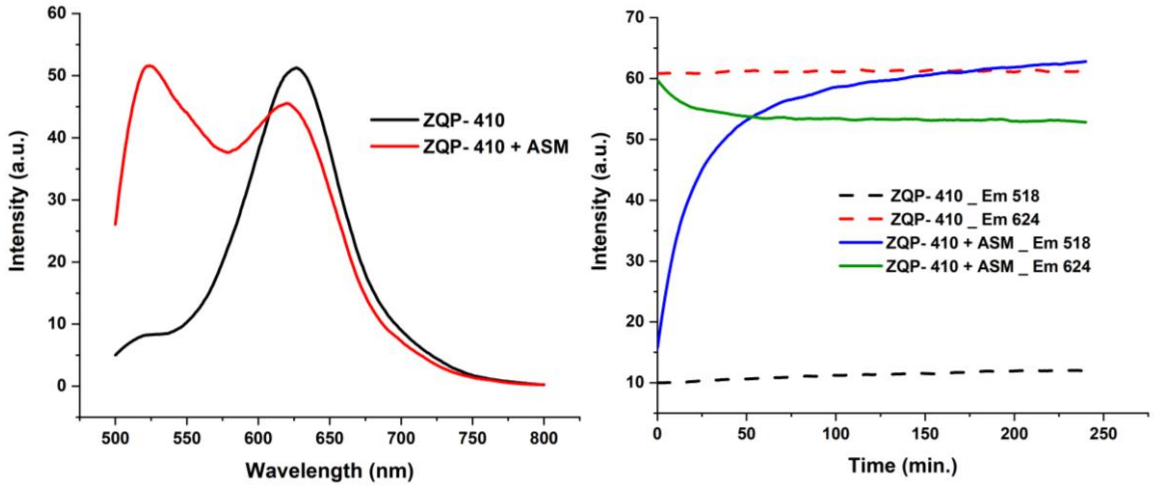

Figure 66. **Left**) Fluorescence Emission spectrum for the probe **ZQ$_2$P-410** before and after the incubation with ASM; **Right**) Real time fluorescence intensity changes during the enzymatic cleavage. ASM (0.2 µg/ml); Probes concentration= 1µM, ASM buffer, Ex :485 nm, $t_{incubation}$=4 h.

The fluorescein mono-labeled probe **ZQ$_3$P-411** was also tested as new a substrate for the ASM enzyme and the fluorescence change was monitored over four hours (**Figure 67**). Due to the combination of both quaternary ammonium group and the mono-labelling, the cleavage rate is higher than that for the other probes and the plateau was reached after about one hour reaction time. About 3.6 fold fluorescence increase was detected revealing that the probe is a significantly rapidly cleaved turn on probe.

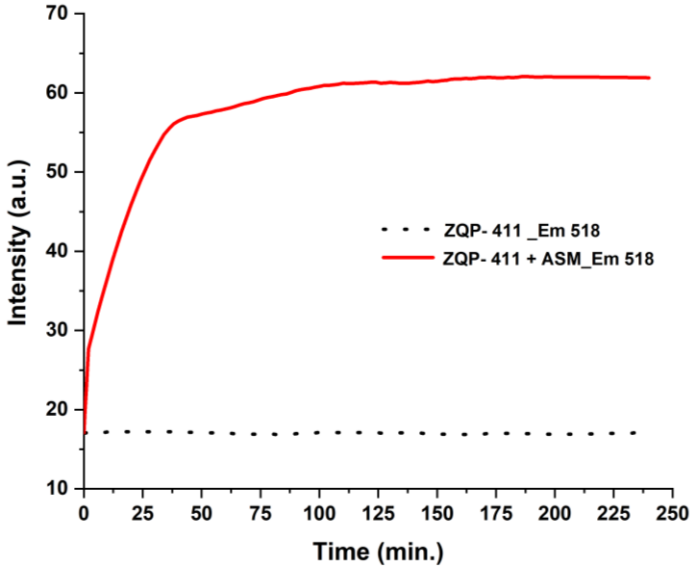

Figure 67. Real time fluorescence intensity change during the enzymatic cleavage of **ZQ$_3$P-411**. ASM (0.2 µg/ml); Probes concentration= 1µM, ASM buffer, Ex :485 nm.

3.2.10 Kinetic parameters of the new fluorescent probes as substrates for ASM

Detailed experiments for the determination of kinetic parameters of the newly synthesized probes as a substrate for ASM were carried out (**Table 3**). According to our driving hypothesis, we expected that the novel quaternary ammonium-containing probes would better mimic the natural sphingomyelin and thus should be better substrates for ASM. The substrate concentration needed for half-maximum catalytic velocity is the Michaelis constant K_M and it represents the enzyme's affinity to a given substrate. In contrast, the maximum catalytic velocity V_{max} is a measure for the enzyme's ability to cleave a given substrate, assumed that all the existing enzyme is saturated by the substrate. Thus, the ideal substrate should have low K_M and high V_{max} values[230]. Evaluation of the kinetic parameters of the probes showed that all the quaternary probes have higher V_{max} values than the non-quaternary **ZP-403** while only the probe **ZQP-407** has a lower K_M value than **ZP-403**. Between the quaternary probes, ASM has the highest affinity to **ZQP-407** followed by the mono-labeled one **ZQ$_3$P-411**.

Code	Structure	V_{max}	K_M	K_{cat}	k_{cat}/K_M
ZP-403	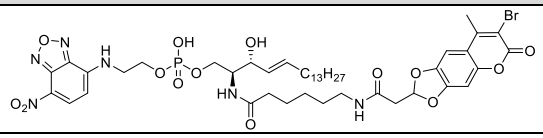	36,9	8	61,5	7,7
ZQP-407	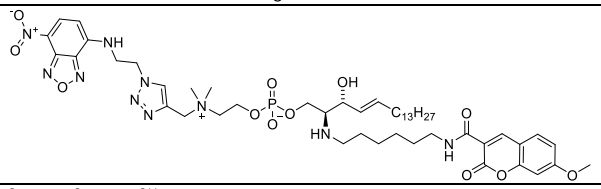	74,6	7	373,0	53,3
ZQ$_2$P-410	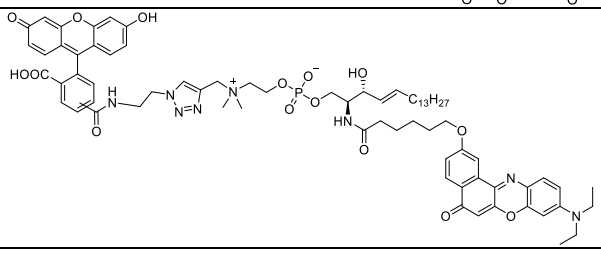	59,2	299,7	296,0	0,98
ZQ$_3$P-411	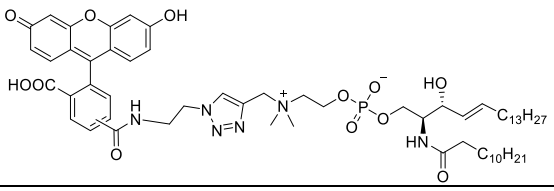	161,3	22,6	806,5	35,7

Table 3. kinetic parameters of the new fluorescent Probes as substrates for ASM. V_{max}=µmol/ (mg. h), K_M= µM, K_{cat} =V_{max}/ [ASM], k_{cat}/K_M = specificity constant. For the determination of kinetic parameters, the substrate concentration was varied from 0.25 to 50 µM at fixed concentration of ASM enzyme under standard assay condition (pH 4.5). All the kinetic parameters are determined from the Lineweaver-Burk plots and each data point in the plot represents Mean from three independent experiments (**Figure S 8**-**Figure S 23**).

The FRET probe **ZQ$_2$P-410** showed the lowest affinity which can be attributed to the large size of the labelling dyes (Fluorescein and Nile red) and the longer linker chain length which is reported to influence the phosphorylation of sphingosine derivatives by sphingosine kinases[230]. These affinity diminishing factors could not be compensated be the presence of the quaternary center or the reported superiority of NR in lipid mediums and membranes[231].

To understand the comparative specificity of the different probes to ASM enzyme active site, the specificity constant, the ratio of K_{cat} to K_M, was calculated. the specificity constants of all the quaternary probes except **ZQ$_2$P-410** were higher than **ZP-403** for the hydrolysis by ASM. In an agreement with the K_M values, **ZQ$_2$P-410** showed the lowest value for the specificity constant. The unexpected high V_{max} value for the **ZQ$_2$P-410** can be explained at least in part as an inherent result of the fluorescein's biophysical properties. The kinetic parameters of the probe **ZQ$_3$P-411**-except the value of K_M- are in accordance with our expectation as it is only mono-labelled in addition to the presence of the quaternary ammonium group which make the probe highly mimicking the natural substrate.

From this study we can conclude that the inclusion of the quaternary centre has a positive impact on the recognition and cleavage rate of the probe with the ASM. But the overall comparison between the different probes revealed also that the final behaviour is a sum of different factors including the intrinsic dye's characters.

3.2.11 Conclusion and outlook

In the second part of this study, different FRET and mono-labelled ASM probes were designed and synthesized in addition to the re-synthesis of the previously reported probes (**Figure 68**). The first goal was to resynthesize the reported probes **TP-366** and **TP-367** for a high throughput screening and a Fluorescence activated cell sorting (FACS) studies. **TP-366** was resynthesized in a higher scale using a self-prepared more affordable coumarin derivative from cheap starting materials. A new FRET probe with a better 2P-excitable coumarin derivative was also targeted and synthesized to make a use of the 2P excitation advantages in the monitoring of ASM in the biological samples.

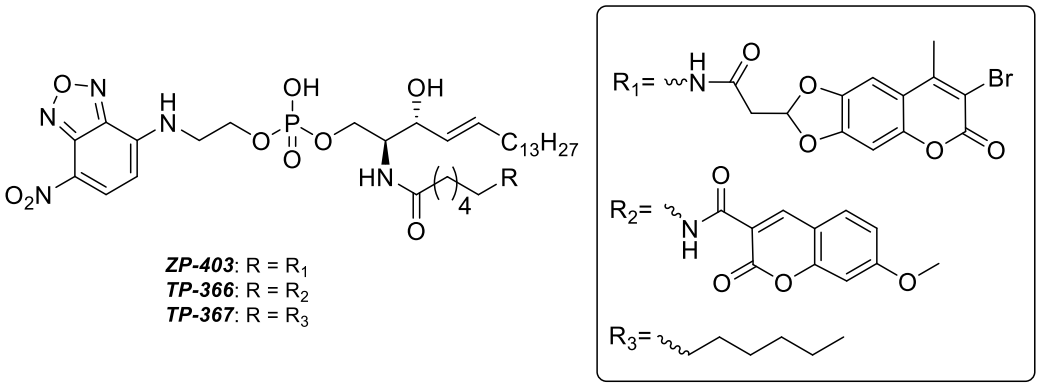

Figure 68. Structural elucidation of the ASM probes with a secondary amino group which were prepared in this study.

The new coumarin moiety was synthesized in a high and pure yield after modification of the reported method and used for the synthesis of the probe **ZP-403**. This probe was confirmed as an ASM substrate with a 10-fold coumarin fluorescence intensity turnover and could be used for the detection of ASM inhibitors. The FRET probe **ZP-403** was also confirmed to be a specific substrate for only the acid sphingomyelinase and not for the neutral phenotype. 2P-Fluorescence microscopy study revealed enough cellular labelling and detection. The quantification of the 2P excitability difference using a static silica beads labelled with the probe showed about 20% enhancement of the coumarin intensity compared to that of **TP-366** using the direct NBD emission intensity as an internal standard.

Based on the known importance of the quaternary ammonium for the sphingomyelin recognition and cleavage by the sphingomyelinases, we also designed and synthesized a new generation of ASM probes containing a quaternary ammonium group which mimics the natural substrate (**Figure 69**). A phosphorylation strategy which allow the insertion of a quaternary ammonium in addition to a terminal alkyne group was applied.

The terminal alkyne functionality serves as a bioorthogonal handle for the introduction of a wide range of fluorophores or other labeling agents with aqueous phase chemistry. With this synthetic pathway we synthesized two FRET probes **ZQP-407** and **ZQ$_2$P-410** which can be excited in the ultraviolet and visible light range respectively. Another fluorescein mono-labelled probe **ZQ$_3$P-411** was also synthesized. All the three probes were proven as ASM substrates and revealed a varying kinetics parameters. All the new quaternary probes revealed higher turnover Kcat values compared to the probe **ZP-403**. Except **ZQ$_2$P-410**, all the new probes has higher specificity constants toward the ASM enzyme.

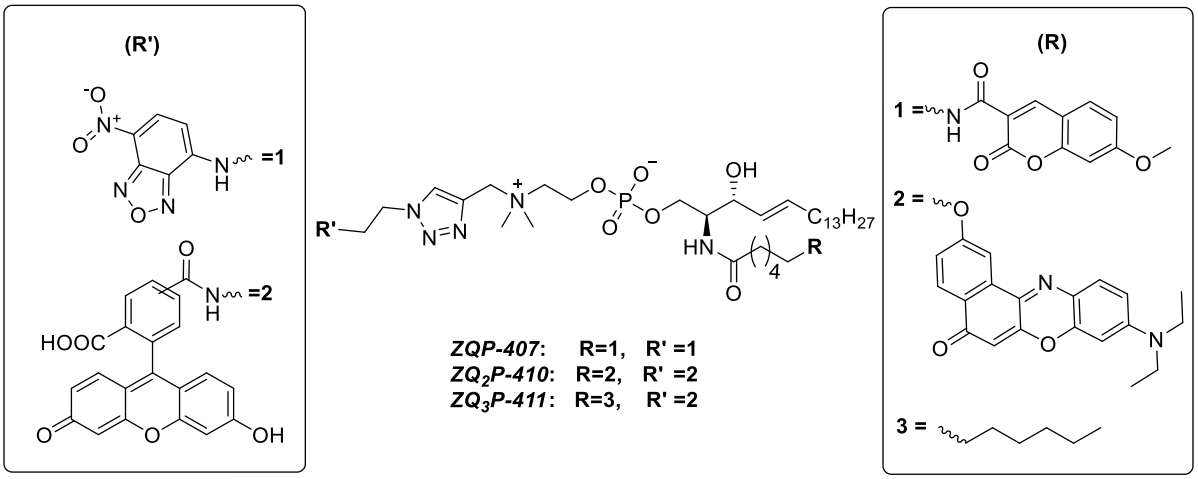

Figure 69. Structure elucidation of the ASM probes with a quaternary ammonium group which were prepared in this study.

According to the results of the current study, a sphingomyelin-mimicking FRET probe containing a quaternary center with a minimum structural deviation from the natural substrate would has the best kinetic characters. Applying a synthetic pathway which could allow the formation of a quaternary nitrogen with direct attachment to the FRET dye (**Figure 70**) would exclude the possible drawbacks of the extra triazole ring on the recognition and cleavage rate. Such a probe could be also recognized by the other sphingomyelinase phenotypes like n-SMase2 and other comparable sphingomyelinases for which the available analytical tools are highly limited.

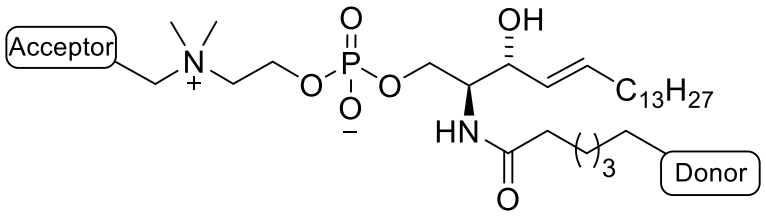

Figure 70. Proposed Structure for a Future sphingomyelin-mimicking FRET probe. Donor and acceptor positions are exchangeable.

The *in vivo* studies are of high importance for addressing the undiscovered issues regarding the biology of the ASM in addition to the related pathological disorders. For these *in vivo* studies, the cellular uptake of the chemical probes is a critical factor. Several strategies are applied to improve the cellular uptake of the small molecules like the masking of the ionizable groups with easily *in vivo* cleavable protecting groups. Regarding our FRET probes, we hypothesize that the temporary masking of the phosphate negatively charged hydroxyl group with an enzymatically cleavable protecting group like the acetoxymethyl group (**Figure 71**) would enhance the cellular permeation.

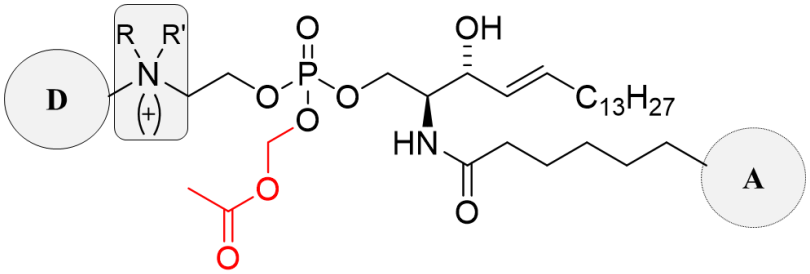

Figure 71. Proposed acetoxymethyl protection of the phosphate hydroxyl group for cellular permeation enhancement. D: FRET donor, A: FRET acceptor.

4 Experimental section

4.1 General description of chemical reactions methods

Unless otherwise specified, all reactions were carried out in oven-dried (>120 °C) glassware equipped with a magnetic stir bar and a rubber septum under a positive pressure of argon. Air- or moisture-sensitive reagents were transferred to the reaction vessel under positive pressure of argon via syringe or stainless steel cannula. Reactions were run at room temperature (20-25 °C) unless otherwise noted in the experimental procedure and reported reaction temperatures refer to the external temperatures measured for the bath in which the reaction vessel was immersed. Heating was obtained through the use of a silicone oil bath. For reactions run below room temperature, the term "0°C" refers to an ice-water bath, "-20 °C" refers to a slurry of sodium chloride and ice-water bath and "-78°C" refers to a bath of acetone and dry ice. Intermediate temperatures were obtained by the careful addition of dry ice to an acetone bath at periodic intervals to maintain the desired temperature. "Concentration" refers to the removal of solvent using a rotary evaporator equipped with a vacuum pump. Removal of residual solvents was accomplished by evacuation of the container for a period of 10-20 hours using a high vacuum line.

4.2 Reagents and solvents

Unless otherwise specified, all the commercially available reagents were purchased from Sigma-Aldrich, Fluka, Acros or TCI and used without any further purification. Air and/or moisture sensitive reactions were carried out in well dried glassware under argon atmosphere with dry, freshly distilled solvents using standard syringe-cannula/septa techniques. All the solvents were used after distillation by standard methods. The petroleum ether used throughout this work had a boiling range of 40–60°C. All corresponding glassware was oven dried and/or carefully dried in the line with a flameless heat gun. Reaction progress was monitored with analytical normal-phase thin layer chromatography (NP TLC). All synthesized compounds were purified to homogeneity as judged by TLC analysis, mass spectrometry (MS) analysis and nuclear magnetic resonance spectroscopy (NMR) analysis.

4.3 Buffers & media

Tris-HCl buffer: (50 mM M Tris/HCl pH 7.4).

Apyrase Storage buffer : 20 mM MES , 50 mM NaCl ,0.1 mM $CaCl_2$,1 mM DTT ,0.1% Tween® 20 ,50% Glycerol ,pH 6.5 , 25°C.

Apyrase Reaction buffer: (50 mM NaCl, 1 mM DTT, 0.05% Tween® 20, 20 mM MES, 5 mM $CaCl_2$ (pH 6.5).

ASM buffer: 0.1 M NaOAc, pH 5.0, 150 mM NaCl, 0.1 mM $ZnSO_4$, 0.1% TritonX-100.

NSM buffer: 50 mM M Tris/HCl pH 7.4, 150 mM NaCl, 0.1% TritonX-100, 5 mM $MgCl_2$.

Lysis buffer: 0.2 M sucrose, protease inhibitor cocktail w/o EDTA.

Elution buffer: 50 mM Tris/HCl pH 7.6, 1 M NaCl, 0.1 mM $ZnCl_2$, 0.4% β-octyl glucopyranoside (w/v).

Culture medium: DMEM, 10% FCS, 1% penicillin/streptomycin (Biochrom).

4.4 Chromatography

Thin-layer chromatography (TLC) was performed using silica gel 60 F254 (Merck (Darmstadt, Germany)) and the compounds were detected with UV light (254 nm/366 nm) and/or by spraying the plates with ninhydrin solution (3 w% in EtOH) or $KMnO_4$ solution (2 g of $KMnO_4$ in 200ml 0.5% K_2CO_3 aqueous solution) followed by heating.

Preparative TLC was performed on preparative silica gel 60 plates 20 cm x 20 cm with concentrating zone (Merck (Darmstadt, Germany)). After scraping off product bands, the silica was removed by extraction with the development solvent followed by 0.45 µm filtration. Binder was removed by dissolution of the product in pure MeOH and washing it twice with isooctane.

Flash chromatography was performed manually using glass columns of different size packed with Silica Gel 60M (0.04-0.063 mm) as stationary phase. Solvent ratios for chromatography and R_f values are reported in v/v% ratios. Solvents were evaporated under reduced pressure while maintaining the water bath temperature between 40 and 45°C.

4.5 Spectroscopic data

4.5.1 Nuclear magnetic resonance spectroscopy

NMR spectra (^{1}H, ^{13}C, APT and ^{31}P) were recorded in $CDCl_3$, CD_3OD, CD_3CN, D_2O, $(CD_3)_2CO$, $(CD_3)_4Si$ or mixtures of those on Bruker (Rheinstetten, Germany) Avance DPX-300, AvanceII-300, Avance400, AvanceIII-500 or Avance600 at 25°C. Chemical shifts are given in ppm with respect to TMS as external standard (^{1}H, APT, ^{13}C, $\delta = 0.00$) with calibration against the residual solvent signal, internal TMS or 85% H_3PO_4 (^{31}P, $\delta = 0.00$) as external standard. Compounds were measured as a solution in deuterated methanol (MeOD), deuterated chloroform ($CDCl_3$) or deuterated water (D_2O), unless otherwise indicated. Peak multiplicities are designed by the following abbreviations: s = singlet; d= doublet; t = triplet; q = quartet; dd = doublet of doublets, ddd = doublet of doublet of doublets, dt = doublet of triplets, qd = quartet of doublets, m = multiplet; br = broad. The coupling constants (J) are quoted in hertz (Hz). The reported chemical shifts are tabulated in the following format: δ (ppm) (multiplicity, coupling constant (s), number of protons). The measurements were done by hand or by Mrs. A. Thiesies , Mrs. K. Pfaff, J. Hildebrandt or H. Steingräber.

4.5.2 Mass spectroscopy (MS and HRMS)

High-resolution mass spectroscopy (HRMS) experiments were recorded on a Hewlett-Packard GCMS 5995-A mass spectrometer equipped with standard electrospray ionization (ESI) in the positive and negative ion detection modes. The major observable molecular ion and clusters have been reported.

4.5.3 UPLC−MS analyses

UPLC was performed on a 1290 Infinity series system (Agilent Technologies, Santa Clara, US) using Zorbax RRHD C18 Eclipse Plus 2.1x50 mm, 1.8 Micron column, UV/Vis detector and either FLD or Agilent 6120 quadrupole LC/MS (ESI+/-). UPLC-MS was carried out using mixtures of solvent A (99.9% H_2O + 0.1% FA) and B (99.9% MeOH + 0.1% FA) with gradient 1 (5% B in A to 95% B in A in 2 min) or isocratic (85% B in A) with a flow of 0.6 mL/min at 20°C.

4.5.4 Absorption and fluorescence/luminescence spectroscopy

Europium complexes: Absorption spectra for the europium complexes were recorded with a Specord 210 from Analytik Jena. Luminescence emission spectra (not corrected) and lifetime (decay) measurements were carried out in quartz cuvettes with a Edinburgh Instruments spectrofluorometer FSP-920 equipped with a µ-flash lamp 920H and a red extended photomultiplier tube (R2658P) from Hamamatsu. The delay time between subsequent measurement cycles was adjusted to 200 µs. The excitation pulse was 20 µs.

Time-resolved luminescence intensities (delay time: 100 µs, integration time: 400 µs) in presence of anions were recorded with a Tecan Infinite F200 Pro microwell plate reader. The excitation wavelength was 345 nm, the detection wavelength 618 nm. All measurements were performed 2 min after addition of the anions in 96-microwell plates with transparent flat bottom from Greiner Bio One in three replicates. The final sample volume was 100 µL in each well, containing 50 µmol L^{-1} (unless otherwise specified) of the europium complexes and the corresponding concentration of anions in 25 mM Tris-HCl buffer (pH 7.4).

FRET Probes: Fluorescence spectra were recorded with a Cary Eclipse spectrometer (Varian, Palo Alto, US) at a constant 37°C in 3 mL 1x1 cm quartz cuvettes. Unless otherwise specified, the slot widths were 5 nm and the scan rate 600 nm min^{-1}. The optical density at the wavelength used was less than 0.05 in each experiment.

The data obtained were corrected for background and volume, normalized and plotted using OriginLab OriginPro 9.1G software and Microsoft Excel (2007 &2010).

4.6 Assay Protocols

4.6.1 ASM/ nSMase 2 homogenous assay using Eu complex

The ASM assay was carried out using Victor 1420 Multilabel counter from Wallac, Perkin–Elmer Life and Analytical Sciences (Wellesley, MA). By diluting the required amount of **4-D$^+$/ 5-D$^+$** in ASM / nSMase 2 buffer, to achieve the desired final concentrations. The sequence of reagents addition was **4-D$^+$/ 5-D$^+$** (10/5µM), SM (10/5µM) then waiting till reaching stable luminescence intensity. Finally, the ASM enzyme (2µgmL^{-1}) / nSMase 2(30, 60 µgmL^{-1}) was added to give a final volume of 100 µL per well. The measurement was started after 1 min at 25°C. The mean intensities from three parallel runs are always displayed.

4.6.2 ASM heterogenous assay using 4-D$^+$Eu complex

After incubation of sphingomyelin (20 µl of 25 µM) with different concentration of ASM (in 80µl ASM buffer) at 37 °C for 1 h, the reaction was stopped by adding 1.5 ml of chloroform/methanol (1:1). Phases were separated by centrifugation at 2000 × g for 5 min. Quantitation of the amount of released phosphocholine was determined by adding 10 µl of the upper phase to 90 µl of **4-D$^+$** complex (to give a final 5 µM concentration). The measurement was started after 1 min at 25°C. The mean intensities from three parallel runs are always displayed.

4.6.3 Apyrase assay

Apyrase (recombinant, E. coli) and apyrase reaction buffer were obtained from New England Biolabs (NEB). The apyrase assay was carried out using Victor 1420 Multilabel counter from Wallac, Perkin–Elmer Life and Analytical Sciences (Wellesley, MA) by diluting the required amount of **5-D$^+$** and apyrase in TRIS or apyrase buffer, respectively, to achieve the desired final concentrations. The sequence of reagents addition was **5-D$^+$** (50µM), ATP (50µM), followed by dilution with apyrase buffer. Finally, the apyrase enzyme was added to give a final volume of 100 µL per well. The measurement was started after 1 min at 25°C. The mean intensities from three parallel runs are always displayed.

4.6.4 ASM fluorescence assay (cuvette)

All spectra were recorded at 37°C with magnetic stirring, all slit widths were 5 nm, PMT voltage was 700 V, if not stated otherwise. ASM or NSM buffer (usually 2970 µL) was filled into quartz cuvettes (1x1 cm, 3 mL) and blank spectra were recorded. The FRET Probe (0.5 mM in DMSO, usually 6 µL giving final 1 µM) was added and initial static spectra were recorded. Then, recombinant human ASM from insect cells (usually 24 µL 0.0625µg/µL ASM in elution buffer) was added simultaneously to the cuvette(s), which were stoppered tightly and placed in a multicell holder. After 30 sec of preincubation, data points (depending on the maxima of the tested probe dyes) or complete spectra were recorded in time intervals. After reaction completion, final spectra were recorded and the reactions were stopped by addition of 500 µL MeOH, optionally followed by lipid extraction using the Folch method[232]. If lysates were used, blanks and initial spectra were recorded with 9/10 of total reaction volume, before additional buffer and lysates (usually 35-100 µL) were added. Fluorescence data was corrected (time, blank, volume), normalized and plotted using OriginLab, OriginPro 9.1G, and Microsoft Excel (2007 &2010) software.

4.6.5 Fluorescence ASM assay (96 well plate) & Fluorescence microscopy

The assay was done in non-binding black clear-bottom 96-well microplate (greiner bio-one) using Victor 1420 Multilabel counter from Wallac, Perkin–Elmer Life and Analytical Sciences (Wellesley, MA). Recombinant ASM was also diluted using assay buffer to reach the desired concentration. The assay is done by adding 20 µl of the FRET probe solution and finally the addition of 80 µl of the recombinant enzyme solution. The plate is then sealed using transparent plastic cover. Measurements are done at room temperature. Fluorescence is measured from the bottom (measurement height: 8 mm) using the suitable excitation and emission filters with CW-lamp energy 3096. The device is also set to mix the contents of the assay by 5 mm orbital shaking for 1 seconds before each measurement.

The BSA-complexed FRET probes were added to the Human H4 neuroglioma cells media for 2 h at a final concentration of 1µM. ASM overexpression increased ASM activity 5-fold over control as measured in a parallel experiment using thin layer chromatography. Cells were washed with PBS and live cell microscopy was performed on a Zeiss LSM 880 NLO equipped with a 680–1300 nm tunable and fixed 1040 nm 2-photon laser from Newport Spectra Physics and the ZEN 2010 software (Carl Zeiss MicroImaging). The same Microscopy set up was used for imaging the beads labeled with the probes containing liposomes [56]. Liposomes were done by Dr. Housam Haj Hamdo and the microscopy imaging was done by Dr. Cosima Rhein.

4.7 Preparation of recombinant ASM

Human acid sphingomyelinase (ASM) was expressed in insect Sf9 cells and purified to homogeneity similar to method described by LANSMANN et al. [233]. The recombinant enzyme purified in the presence of Zn^{2+} (0.1 mM) had an activity of 23 nmol h^{-1} ml^{-1} as determined in a micellar assay system. The work was done by Mrs. S. Diederich.

4.8 Cell culture

Adherent HeLa cells, WT or ASM-KO-MEF cells were cultured in 25 cm ^{2} culture flasks in culture medium (see above, with phenol red) at 37 °C, 5% CO_2. For cell splitting, the (confluent) cells were washed twice with PBS, covered with 500 µL trypsin / EDTA and trypsinized at 37 ° C for 3 min. The cells were knocked off the bottom of the dish and the trypsin was inactivated by addition of 2.5 ml of culture medium. The cells were uniformly suspended, 1/12 of the volume (250 µL) transferred to a new culture flask, filled with 6 mL of new culture medium and further incubated. For microscopy purposes, 1/12 of the cell suspension (250 µL) was transfered into 35 mm MatTek glass bottom dishes and completed to 2 mL of imaging medium or 1/20 of the volume (150 µL) in ibidi µ-slides and the Volume completed to 230 µL. The sealed culture vessels were re-incubated. The work was done by Mrs. S. Diederich.

4.9 Cell lysis

In order to obtain cell lysates for cuvette assays, the content of two 75 cm^2 culture flasks was washed with 2x PBS, trypsinized for 5 min and 5 mL DMEM with 10% FBS without phenol red was added. The cell suspensions were combined in a centrifuge tube and centrifuged with 4000 rpm for 10 min at 4°C. The supernatant was removed and the pellet was resuspended in 1 mL PBS. Centrifugation was repeated with 3000 rpm for 5 min at 4°C. The supernatant was removed and the pellet was resuspended in 325 µL 0.4 M aq. sucrose and 325 µL 2x concentrated protease inhibitor stock solution. The suspension was lyzed for 5-10 min at 4°C using ultrasonication. The total protein content was determined using a colorimetric assay (Pierce™ BCA Protein Assay Kit, Thermo Fisher Scientific). The lysates were stored on ice or dip frozen in liquid nitrogen before prolonged storage at -20°C. The work was done by Mrs. S. Diederich.

4.10 Chemical Synthesis

4.10.1 Chemical Synthesis of the 5-dentate europium complex

Diethyl 4-bromo-2,6-pyridinedicarboxylate (101)

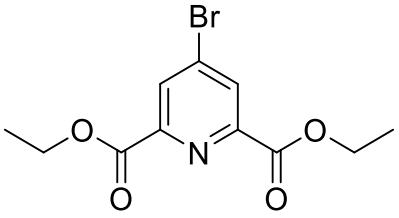

Chelidamic acid monohydrate (1.4 g, 6,9 mmol,1 eq.) and phosphorus pentabromide (15 g, 34.8 mmol, 5 eq.) were heated to 90 °C under dry condition, Till the solids formed a melt. This mixture was stirred at 90 ° C for 2.5 h. After the solution was cooled, 10 mL hloroform was added, and the solution was stirred for 5 min and filtered. The filtrate was chilled in an ice bath and 60 mL ethanol was slowly added to the solution. The solution was concentrated, and the oily residue was triturated with ice water to give a white precipitate. Purification with SiO_2 column chromatography (3:9→5:95 Aceton/Cyclohexan) afforded a white crystalline solid (1.9 g, 90%).

^{1}H-NMR (500 MHz, $CDCl_3$) δ 8.42 (s, 2H, CH_{ar}), 4.49 (q, J = 7.1 Hz, 4H, $\underline{CH_2}CH_3$), 1.45 (t, J = 7.1 Hz, 6H, $CH_2\underline{CH_3}$).

^{13}C-NMR (126 MHz, $CDCl_3$) δ 163.68(CO), 149.65(C=N), 135.06(C-Br), 131.21(CH), 62.87(CH_2), 14.33(CH_3).

UPLC-MS (ESI): $C_{11}H_{13}BrNO_4$ $[M+H]^+$: m/z Calc.: 304.0; Found: 304.2

4-Bromo-2,6-pyridinedimethanol (102)

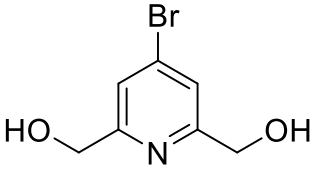

To a suspension of (1 g, 3.3 mmol, 1eq.) of bromo ester **101** in 50 ml of dry ethanol at ° C was added (626 mg, 16.5 mmol, 5 eq.) of $NaBH_4$ under stirring. After 1 h at 0°C and 1 h at room temperature, the mixture was heated to reflux for overnight, then 20 ml of acetone was added, and the mixture was again heated to reflux for 1 h. The solvents were distilled off, the gelatinous residue was mixed with 30 ml of a saturated Na_2Co_3 solution and the mixture was heated to reflux for 45 min. The solvent was distilled off, the white residue was extracted continuously with chloroform for one day (Soxhlet extraction). After the solution was cooled and concentrated, 505 mg (70% yield) of a white solid **2** precipitated.

^{1}H-NMR (500 MHz, $CDCl_3$) δ 7.42 (s, 2H, CH_{ar}), 4.76 (s, 4H, CH_2), 3.00 ((br. s, 2H, OH).

^{13}C-NMR (126 MHz, $CDCl_3/CD_3OD$) δ 161.30 (C=N), 134.92 (C-Br), 122.75 (CH), 64.27 (CH_2).

UPLC-MS (ESI): $C_7H_9BrNO_2$ $[M+H]^+$: m/z Calc.: 219.9; Found: 219.3

4-Bromo-2, 6-bis (bromomethyl) pyridine (103)

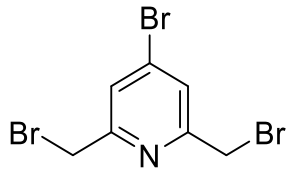

Phosphorous tribromide (176.9 mg, 0.65 mmol, 1.5 eq.) was added in one portion to a suspension of **102** (95 mg, 0.44 mmol, 1eq.) in chloroform (5ml). The reaction mixture was heated under reflux for 4 h. After cooling, the mixture was neutralized with 5% $NaHCO_3$. The aqueous layer was extracted with chloroform (6x). the combined organic phase was dried with Na_2SO_4 and evaporated in vacuo. The resulting residue was purified by flash SiO_2 column chromatography (5% Acetone in Cyclohexane) to obtain **3** (102 mg, 68%yield) as a white crystalline powder.

^{1}H NMR (500 MHz, $CDCl_3$) δ 7.55 (s, 2H, CH_{ar}), 4.48 (s, 4H, CH_2).

^{13}C NMR (126 MHz, $CDCl_3$) δ 157.87 (C=N), 134.49 (C-Br), 126.24 (CH), 32.49 (CH_2).

UPLC-MS (ESI): $C_7H_6Br_3NNa$ $[M+Na]^+$: m/z Calc.: 367.8; Found: 368.2

diethyl 2,2'-(((4-bromopyridine-2,6-diyl)bis(methylene))bis(methylazanediyl)) diacetate (104)

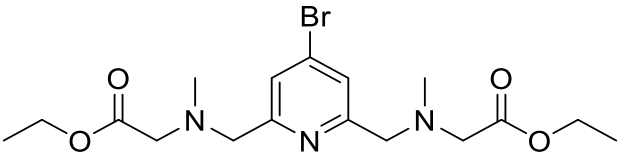

4-Bromo-2,6-bis(bromomethyl)pyridine **103** (1.15 g, 3.34 mmol, 1eq.), ethyl 2-(methylamino) acetate.HCl (2.05g, 13.37 mmol, 4 eq.) and K_2CO_3 (1.85g, 13.37 mmol, 4eq.) were dissolved in acetonitrile (50 mL), and the mixture was heated to reflux. The reaction was followed with TLC (acetone/cyclohexane, 1:2) and after 4 h the reactant was completely consumed. The mixture was filtered and the filtrate was evaporated to dryness. The oily residue was purified by column chromatography using (3:97→10:90 aceton/cyclohexane). Pure white powder of **104** (1 g, 72 %yield) was obtained.

^{1}H NMR (500 MHz, $CDCl_3$) δ 7.59 (s, 2H, CH_{ar}), 4.18 (q, J = 7.1 Hz, 4H, $\underline{CH_2}CH_3$), 3.80 (s, 4H, Pyr-CH_2), 3.34 (s, 4H, CH_2-Carbonyl), 2.42 (s, 6H, CH_3-N), 1.28 (t, J = 7.1 Hz, 6H, $CH_2\underline{CH_3}$).

^{13}C NMR (126 MHz, $CDCl_3$) δ 170.95 (C=O), 160.16 (C=N), 134.49 (C-Br), 124.69 (CH), 62.21 (Pyr-CH_2), 60.55 (CH_2-O), 58.32 (CH_2-Carbonyl), 42.45 (CH_3-N), 14.52(CH_3).

HRMS (ESI): $C_{17}H_{27}BrN_3O_4$ $[M+H]^+$: m/z Calc.: 418.1164, Found: 418.1165.

$C_{17}H_{26}BrN_3NaO_4[M+Na]^+$: m/z Calc.: 438.1004, Found: 438.1005.

Diethyl 2,2'-(((4-((4-(dimethylamino)phenyl)ethynyl)pyridine-2,6-diyl)bis (methylene)) bis(methylazanediyl))diacetate (105)

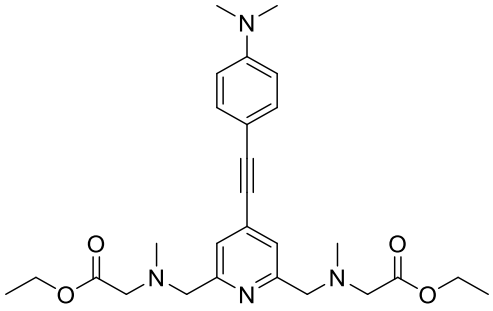

Compound **104** (500 mg, 1.2 mmol, 1eq.) was dissolved in dry THF (25ml) under argon atmosphere. Then 4-ethynyl-N,N-dimethylaniline (209 mg, 1.44 mmol, 1.2 eq.), $Pd(PPh_3)_2Cl_2$ (17 mg, 0.024 mmol, 0.02 eq.), Copper(I) iodide (10 mg, 0.05 mmol, 0.04 eq.), Et_3N (7.5 ml) were added. The mixture was stirred under Argon until the TLC (acetone/cyclohexane 30%) revealed complete consumption of **104** (4h). The reaction was quenched by washing with 1M NH_4Cl (2 x 30 ml), then with brine (2 x 30ml). The organic layer was collected and evaporated and the obtained crude residue was purified by column chromatography (10:90 → 50:50 acetone/cyclohexane) to yield a yellow crystalline powder of **105** (290 mg, 50 % yield).

^{1}H NMR (500 MHz, $CDCl_3$) δ 7.43 (s, 2H, CH_{Pyr}), 7.40 (d, J = 9.0 Hz, 2H, CH_{Ph}), 6.66 (d, J = 9.0 Hz, 2H, CH_{Ph}), 4.19 (q, J = 7.1 Hz, 4H, $\underline{CH_2}CH_3$), 3.82 (s, 4H, Pyr-CH_2), 3.35 (s, 4H, CH_2-Carbonyl), 3.00 (s, 6H, $N(CH_3)_2$), 2.44 (s, 6H, CH_3-N), 1.29 (t, J = 7.1 Hz, 6H, $CH_2\underline{CH_3}$).

^{13}C NMR (126 MHz, $CDCl_3$) δ 171.15 (C=O),158.37 (Pyr C=N), 150.69(PhC-N), 133.50 ($PyrC_4$), 133.32 ($PhC_{3,5}$), 123.03($PyrC_{3,5}$), 111.86 ($PhC_{2,6}$), 108.97 (PhC_1-Ethynyl), 95.56 (Ph-C≡), 85.96 (Pyr-C≡), 62.74 (Pyr-CH_2), 60.62 (CH_2-O), 58.43(CH_2-Carbonyl), 42.64 (CH_3-N), 40.27 $N(CH_3)_2$), 14.43(CH_3).

HRMS (ESI): $C_{27}H_{37}N_4O_4$ $[M+H]^+$: m/z Calc.: 481.2815, Found: 481.2815

$C_{27}H_{36}N_4NaO_4$ $[M+Na]^+$: m/z Calc.: 503.2634, Found: 503.2639

2,2'-(((4-((4-(dimethylamino)phenyl)ethynyl)pyridine-2,6-diyl)bis(methylene)) bis(methylazanediyl))diacetic acid (106)

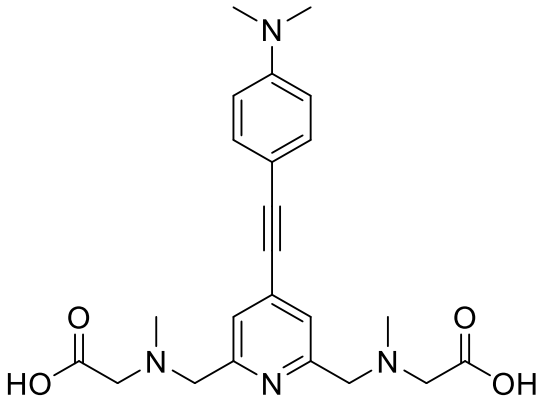

Potassium hydroxide (21mg, 0.37mmol, 3eq.) was added to a solution of Compound **105** (60 mg, 0.12 mmol, 1eq.) in methanol (2mL) and the solution was heated under reflux conditions for 3 h. The reaction was quenched with water (5ml) and the crude product was extracted with diethyl ether (3x 5ml). The aqueous portion was acidified with concentrated hydrochloric acid. The dicarboxylic acid precipitated on standing, was filtered off, and dried to give product **106** as a yellow crystalline powder (47 mg, 89 % yield).

UV-VIS: λ_{max} = 355 nm (ε = 7450 L cm^{-1} mol^{-1}).

^{1}H NMR (300 MHz, MeOD) δ 7.68 (s, 2H, CH_{Pyr}), 7.66 (d, J = 8.9 Hz, 2H, CH_{Ph}), 7.37 (d, J = 8.8 Hz, 2H, CH_{Ph}), 4.74 (s, 4H, Pyr-CH_2), 4.29 (s, 4H, CH_2-Carbonyl), 3.19 (s, 6H, N(CH_3)$_2$), 3.09 (s, 6H, CH_3-N).

^{13}C NMR (75 MHz, MeOD) δ 168.24 (C=O), 152.07 (Pyr C=N), 136.16 (PhC-N), 134.97 ($PhC_{3,5}$), 127.17 ($PyrC_{3,5}$), 118.74 ($PhC_{2,6}$), 87.09 (Pyr-C≡), 60.44 (Pyr-CH_2), 56.70 (CH_2-Carbonyl), 44.32 (CH_3-N), 43.06(N(CH_3)$_2$).

HRMS (ESI): $C_{23}H_{29}N_4O_4$ $[M+H]^+$: m/z Calc.: 425.2189, Found: 425.2188

$C_{23}H_{27}N_4O_4$ $[M-H]^-$: m/z Calc.: 423.2038, Found: 423.2044

Europium(III)-2,2'-(((4-((4-(dimethylamino)phenyl)ethynyl)pyridine-2,6-diyl)bis (methylene)) bis(methylazanediyl))diacetic acid (5-D^{+})

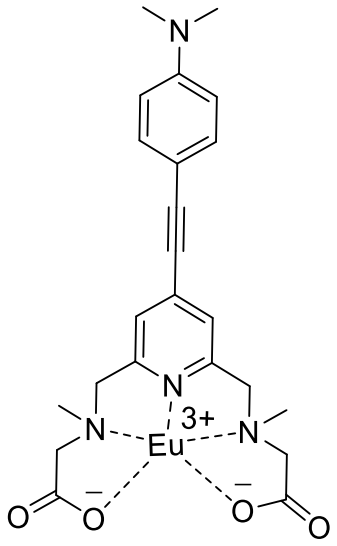

Saponified ligand **106** (849 µg, 0.0019mmol, 1eq.) was dissolved in water (1 mL), and the solution was neutralized with $NaHCO_3$ to pH 6.5. Afterwards, $EuCl_3 \cdot 6H_2O$ (732.8 µg, 0.0019mmol, 1eq.) dissolved in water (1 mL) was added over 15 minutes while the solution was kept at pH 5 - 6.5. Then the mixture was stirred for 2h at RT.

UV-VIS: λ_{max} = 365 nm (ε = 1790 L cm^{-1} mol^{-1}).

UPLC-MS (ESI): $C_{23}H_{27}EuN_4O_4$ [M+H]+ : m/z Calc.: 576.1, Found: 576.3

$C_{23}H_{27}N_4O_4$ [Ligand-H]$^{-}$: m/z Calc.: 423.2, Found: 423.1

4.10.2 Chemical Synthesis of the 4-dentate europium complex

Ethyl 4-bromo-6-(hydroxymethyl)picolinate (107)

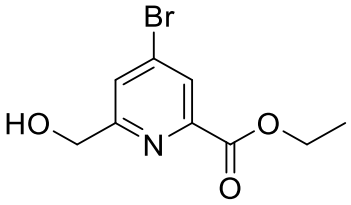

Compound **101** (1.037 g, 3.43 mmol, 1 eq.) was dissolved in dry ethanol (100ml) under argon atmosphere. Then, $NaBH_4$ (148 mg, 3.9 mmol, 1.14 eq.) was added and the mixture was stirred at RT for 1h. A white precipitate was observed. The solvent was evaporated under reduced pressure and then 10 ml water was added to the residue and stirred for 10 minutes. The mixture was extracted with dichloromethane till no product was observed in the aqueous layer. The organic fractions were collected and evaporated and the resulted residue was purified by SiO_2 column chromatography (0:100 to 2:98 MeOH/DCM). (339.2 mg, 38% yield) of **107** was obtained as a colorless oil.

^{1}H NMR (500 MHz, DMSO) δ 8.07 (m, 1H, CH_{ar}), 7.90 (d, J = 1.8 Hz, 1H, CH_{ar}), 5.71 (t, J = 5.9 Hz, 1H, OH), 4.62 (d, J = 5.9 Hz, 2H,$\underline{CH_2}$OH), 4.35 (q, J = 7.1 Hz, 2H, $\underline{CH_2}CH_3$), 1.33 (t, J = 7.1 Hz, 3H, CH_3).

^{13}C NMR (126 MHz, DMSO) δ 164.47 (C=O), 163.61 ($PyrC_6$), 148.24 ($PyrC_2$), 133.62 ($PyrC_4$), 126.42 ($PyrC_5$), 125.80 ($PyrC_3$), 63.52 (CH_2-OH), 61.65 ($\underline{CH_2}CH_3$), 14.09 (CH_3).

UPLC-MS (ESI): $C_9H_{11}BrNO_3$ $[M+H]^+$: m/z Calc.: 262.0, Found: 262.0

Ethyl 4-bromo-6-(bromomethyl) picolinate (108)

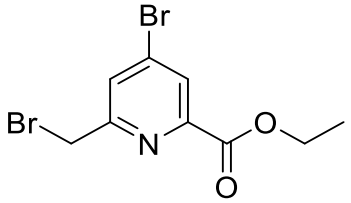

Phosphorous tribromide (952 mg, 3.5 mmol, 1.2 eq.) was dissolved in 5 ml DMF and added dropwisely to a solution of **107** (772mg, 2.96 mmol, 1eq.) in 15 ml DMF. A white precipitate was formed. The reaction mixture was stirred at room temperature for 3 h and the consumption of **107** was monitored by TLC. The mixture was neutralized with $NaHCO_3$ and then extracted by petroleum ether. The organic layer was evaporated and the residue was purified by short flash chromatography using DCM as eluent. The product was obtained as colorless oil (910 mg, 95% yield).

^{1}H NMR (300 MHz, $CDCl_3$) δ 8.17 (d, J = 1.7 Hz, 1H, CH_{ar}), 7.85 (d, J = 1.7 Hz, 1H, CH_{ar}), 4.59 (s, 2H, $\underline{CH_2}Br$), 4.48 (q, J = 7.1 Hz, 2H, $\underline{CH_2}CH_3$), 1.43 (t, J = 7.1 Hz, 3H, CH_3).

^{13}C NMR (75 MHz, $CDCl_3$) δ 163.79 (C=O), 158.72 ($PyrC_6$), 148.90 ($PyrC_2$), 134.66 ($PyrC_4$), 130.17 ($PyrC_5$), 127.88 ($PyrC_3$), 62.64 ($\underline{CH_2}CH_3$), 32.32 (CH_2-Br), 14.40 (CH_3).

HRMS (ESI): $C_9H_{10}Br_2NO_2$ $[M+H]^+$: m/z Calc.: 321.9073, Found: 321.9066.

$C_{18}H_{18}Br_4N_2NaO_4[2M+Na]^+$: m/z Calc.: 668.7892, Found: 668.7905.

Ethyl 4-bromo-6-(((2-ethoxy-2-oxoethyl)(methyl)amino)methyl)picolinate (109)

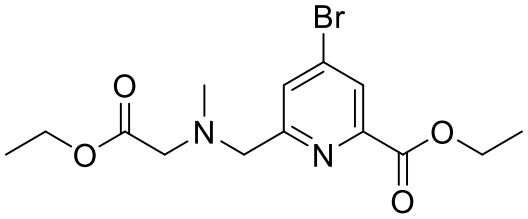

Ethyl 4-bromo-6-(bromomethyl)picolinate **108** (484 mg, 1.49 mmol, 1 eq.), ethyl 2-(methylamino) acetate.HCl (500 mg, 3.25 mmol, 2.2 eq.) and K_2CO_3 (450 mg, 3.25 mmol, 2.2 eq.) were dissolved in acetonitrile (50 mL), and the mixture was heated to reflux. The reaction was followed with TLC (acetone/cyclohexane 1:2) and after 18 h, the Starting compound **108** was completely consumed. The mixture was filtered and the filtrate was evaporated to dryness. The oily residue was purified by column chromatography using (0:100 to 0.5 :99.5 MeOH/DCM). Pure colorless oil of **109** (323 g, 60 %yield) was obtained.

^{1}H NMR (300 MHz, $CDCl_3$) δ 8.13 (d, J = 1.8 Hz, 1H, CH_{ar}), 7.99 (d, J = 1.8 Hz, 1H, CH_{ar}), 4.46 (q, J = 7.1 Hz, 2H, $\underline{CH_2}CH_3$), 4.19 (q, J = 7.1 Hz, 2H, $\underline{CH_2}CH_3$), 3.92 (s, 2H, Pyr-CH_2), 3.36 (s, 2H, CH_2-CO), 2.42 (s, 3H, N-CH_3), 1.42 (t, J = 7.1 Hz, 3H, $CH_2\underline{CH_3}$), 1.28 (t, J = 7.1 Hz, 3H, $CH_2\underline{CH_3}$).

^{13}C NMR (75 MHz, $CDCl_3$) δ 171.36 (C=O), 164.72 (Pyr-C=O), 162.30 ($PyrC_6$), 149.13 ($PyrC_2$), 135.01($PyrC_4$), 129.55 ($PyrC_5$), 127.60, ($PyrC_3$), 62.82 (Pyr-CH_2), 62.74 ($\underline{C}H_2CH_3$), 61.19 ($\underline{C}H_2CH_3$), 59.05 ($\underline{C}H_2$-CO), 43.07 (CH_3-N), 14.82 (CH_3).

HRMS (ESI): $C_{14}H_{20}BrN_2O_4$ $[M+H]^+$: m/z Calc.: 359.0606, Found: 359.0609.

$C_{14}H_{19}BrN_2NaO_4[M+Na]^+$: m/z Calc.: 381.0420 Found: 381.0430.

Ethyl 4-((4-(dimethylamino)phenyl)ethynyl)-6-(((2-ethoxy-2-oxoethyl) (methyl) amino) methyl)picolinate (110)

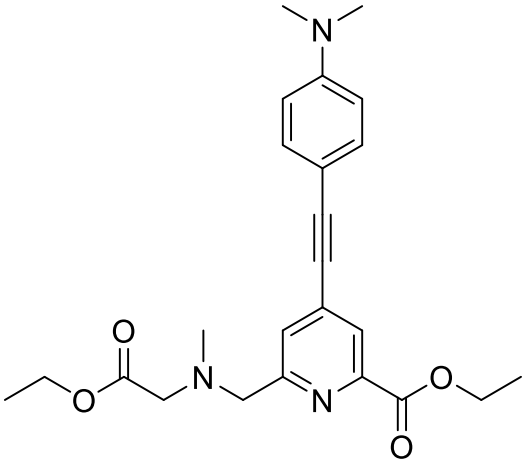

Compound **109** (220 mg, 0.61mmol, 1 eq.) was dissolved in dry THF (10 ml) under argon atmosphere. Then, 4-ethynyl-N, N-dimethylaniline (105.6 mg, 0.73 mmol, 1.2 eq.), $Pd(PPh_3)_2Cl_2$ (8.4 mg, 0.01 mmol, 0.02 eq.), Copper(I) iodide (4.8 mg, 0.025 mmol, 0.04 eq.), Et_3N (4 ml) were added. The mixture was stirred under Argon until the TLC (acetone/cyclohexane 30%) revealed complete consumption of **109** (5h). The reaction mixture was washed with 1M NH_4Cl (2 x 10 ml) and with brine (2 x 10 ml). The organic layer was collected and evaporated. The crude residue was purified by SiO_2 column chromatography (5:95 to 50:50 ethyl acetate/cyclohexane). A yellow crystalline powder of **110** (155 mg, 60 % yield) was obtained.

^{1}H NMR (300 MHz, MeOD) δ 7.94 (d, J = 1.5 Hz, 1H, CH_{pyr}), 7.79 (d, J = 1.5 Hz, 1H, CH_{pyr}), 7.40 (d, J = 9.0 Hz, 2H, CH_{ph}), 6.71 (d, J = 9.1 Hz, 2H, CH_{ph}), 4.43 (q, J = 7.1 Hz, 2H, $\underline{CH_2}CH_3$), 4.17 (q, J = 7.1 Hz, 2H, $\underline{CH_2}CH_3$), 3.86 (s, 2H, Pyr-CH_2), 3.39 (s, 2H, CH_2-CO), 3.00 (s, 6H, N-$(CH_3)_2$), 2.40 (s, 3H, CH_3-N), 1.42 (t, J = 7.1 Hz, 3H, $CH_2\underline{CH_3}$), 1.27 (t, J = 7.1 Hz, 3H, $CH_2\underline{CH_3}$).

^{13}C NMR (75 MHz, MeOD) δ 172.48 (C=O), 166.01(Pyr-C=O), 161.30 ($PyrC_6$), 152.59 (PhC_1), 148.61 ($PyrC_2$), 135.91($PyrC_4$), 134.41 ($PhC_{3,5}$), 128.72 ($PyrC_5$), 125.91($PyrC_3$), 112.90 ($PhC_{2,6}$), 109.11 (PhC_4), 98.93 (Ph-C≡), 85.66 (Pyr-C≡) , 63.05 (Pyr-CH_2), 62.73 (CH_2-O), 61.68 (CH_2-O), 58.99 ($\underline{C}H_2$-CO), 42.74 (CH_3-N), 40.23 (N-$(CH_3)_2$), 14.56 (CH_3), 14.53(CH_3).

HRMS (ESI): $C_{24}H_{30}N_3O_4$ $[M+H]^+$: m/z Calc.: 424.2231, Found: 424.2251.

$C_{24}H_{29}N_3NaO_4$ $[M+Na]^+$: m/z Calc.: 446.2050, Found: 446.2078.

6-(((carboxymethyl)(methyl)amino)methyl)-4-((4-(dimethylamino)phenyl)ethynyl) picolinic acid (111)

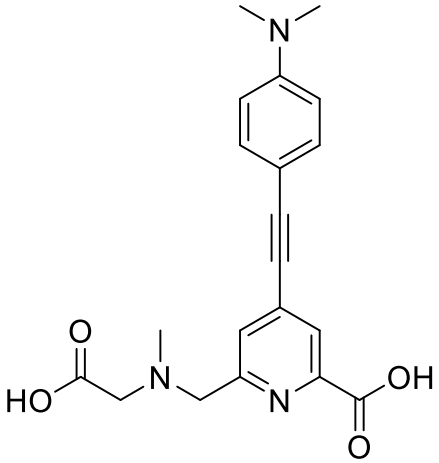

Compound **110** (25 mg, 0.059 mmol, 1eq.) was dissolved in methanol (1 mL). Potassium hydroxide (10 mg, 0.178 mmol, 3 eq.) was added, and the solution was heated under reflux conditions for 3 h. The reaction was quenched with water (2 ml) and extracted with diethyl ether (3 x 3 ml). The aqueous portion was acidified to pH = 2 with concentrated hydrochloric acid. The carboxylic acid precipitated on standing, was filtered off, and dried under vacuum to give product **111** as a yellow crystalline powder (19.5 mg, 90 % yield).

UV-VIS: λ_{max} = 361 nm (ε = 5200 L cm-¹ mol-¹).

^{1}H NMR (300 MHz, DMSO) δ 8.01 (s, 1H, CH_{pyr}), 7.87 (s, 1H, CH_{pyr}), 7.44 (d, J = 8.8 Hz, 2H, CH_{ph}), 6.74 (d, J = 9.0 Hz, 2H, CH_{ph}), 4.64 (s, 2H, Pyr-CH_2), 4.26 (s, 2H, CH_2-CO), 2.97 (s, 6H, N-$(CH_3)_2$), 2.90 (s, 3H, CH_3-N).

^{13}C NMR (75 MHz, DMSO) δ 167.63 (C=O), 165.50 (C=O), 151.56 ($PyrC_6$), 151.39 (PhC_1), 148.53 ($PyrC_2$), 134.32 ($PyrC_4$), 133.78 ($PhC_{3,5}$),129.18 ($PyrC_5$), 125.73 ($PyrC_3$), 112.36 ($PhC_{2,6}$), 106.83 (PhC_4), 99.07 (Ph-C≡), 85.21 (Pyr-C≡),58.93 (Pyr-CH_2), 55.36 ($\underline{C}H_2$-CO), 41.81 (CH_3-N), 40.12 (N-$(CH_3)_2$).

HRMS (ESI): $C_{20}H_{20}N_3O_4$ $[M-H]^-$: m/z Calc.: 366.1459, Found: 366.1463.

Europium(III)-6-(((carboxymethyl)(methyl)amino)methyl)-4-((4-(dimethylamino) phenyl)ethynyl)picolinic acid (4-D^{+})

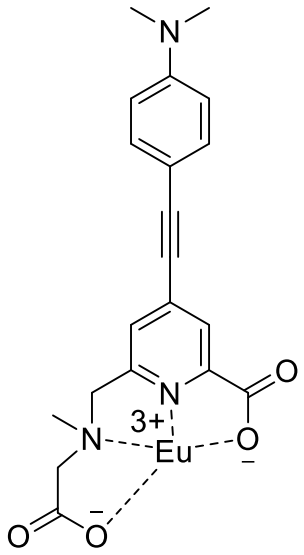

The saponified ligand **111** (848 µg, 0.0023) was dissolved in water (1 mL), and the solution was neutralized with $NaHCO_3$ to pH 6.5. Afterwards, $EuCl_3 \cdot 6H_2O$ (846 µg, 0.0019mmol, 1 eq.) dissolved in water (1 mL) was added over 15 minutes while the solution was kept at pH 5 - 6.5. Then, the mixture was stirred for 2h at room temperature.

UV-VIS: λ_{max} = 378 nm (ε = 3050 L cm^{-1} mol^{-1}).

UPLC-MS (ESI): $C_{20}H_{20}N_3O_4$ [Ligand-H]$^-$: m/z Calc.: 366.1, found: 366.0,
$C_{20}H_{22}N_3O_4$ [Ligand+H]$^+$: m/z Calc.: 368.2, found:368.2.

4.10.3 Chemical synthesis of Protected sphingosine

(S)-2-(tert-butoxycarbonyl)-3-hydroxypropanoic acid (201)

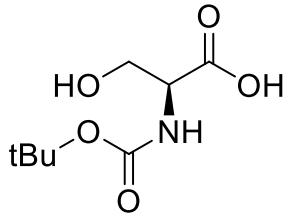

At 0°C, L-serine (3.15 g, 29.97 mmol, 1 eq.) was added to a solution of NaOH (1.26 g, 31.5 mmol, 1.05 eq.) in 35 mL H_2O. Di-*tert*-butyl dicarbonate (7.80 g, 35.74 mmol, 1.2 eq.) was dissolved in 30 mL 1,4-dioxane and added dropwise to the serine containing solution over 120 min keeping the temperature at 0°C. Stirring was continued for 1h at 0°C and additional 20 h at rt. Then, the reaction mixture was washed twice with cyclohexane (60 mL each). At 0°C, the pH was adjusted to 2 using 1 M aq. $NaHSO_4$. The mixture was extracted five times with EA (60 mL each). The combined organic layers were washed with 60 mL brine and dried over Na_2SO_4, filtered and evaporated to dryness. After drying in high vacuum, Boc-L-Serine **201** was obtained as colourless oil (5.60 g, 91% crude). the product was used in the next step without further purification.

(S)-tert-butyl 3-hydroxy-1-(methoxy(methyl)amino)-1-oxopropan-2-yl carbamate (202)

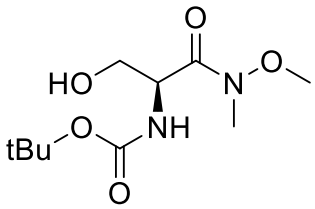

Under argon atmosphere, *N*-(*tert*-butoxycarbonyl)-L-serine **201** (5.60 g, 27.29 mmol, 1 eq.) was dissolved in dry CH_2Cl_2 (60 mL). *N*-Methylmorpholine (3.45 mL, 31.38 mmol, 1.15 eq.) and *N*, *O*-dimethylhydroxylamine hydrochloride (2.90 g, 30.02 mmol, 1.1 eq.) were added at -15°C. the mixture was stirred for 10 min. Then, EDC (6.20 g, 32.74 mmol, 1.2 eq.) was added to the mixture in 6 portions over 30 min. Stirring was continued at -15°C for 1.5 h. Then, the reaction was quenched by addition of 30 g ice and 80 mL 1 M aq. HCl. The organic layer was extracted with 4x 50 mL $CHCl_3$ and the combined organic layers were washed with sat. aq. $NaHCO_3$ and brine (50 mL each). The combined organic layers were dried over Na_2SO_4, filtered and evaporated to dryness. The title compound was obtained as a colourless solid (5.08 g, 75%).

^{1}H NMR (500 MHz, $CDCl_3$) δ 5.61 (s, 1H, NH), 4.79 (s, 1H, CH), 3.81 (s, 2H, CH_2), 3.77 (s, 3H, OCH_3), 3.22 (s, 3H, NCH_3), 2.72 (s, 1H, OH), 1.44 (s, 9H, $C(CH_3)_3$).

^{13}C NMR (101 MHz, $CDCl_3$) δ 171.00 (CON), 156.08 (COO), 80.24 (C), 63.89 (CH_2), 61.75 (CH_3), 52.51 (CH_3), 32.15 (CH), 28.45 ($C(CH_3)_3$).

(S)-N-methoxy-N-methyl-3-(tert-butyldiphenylsilyloxy)-2-(N-tert butyloxycarbonyl) amino propanamide (203)

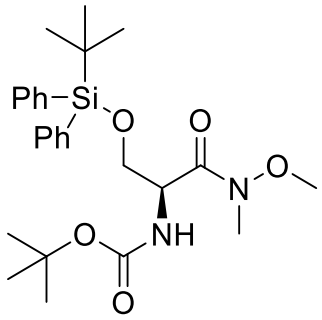

Under argon atmosphere, **202** (5.00 g, 20.14 mmol, 1 eq.), imidazole (4.10 g, 60.29 mmol, 3 eq.) and DMAP (0.123 g, 1 mmol, 0.05 eq.) were dissolved in dry CH_2Cl_2 (45mL). The mixture was cooled to 0°C and *tert*-butyldiphenylchlorsilane (5.76 mL, 22.15 mmol, 1.1 eq.) was added dropwise over 30 min. Stirring was continued at RT for 24 h. Then, the reaction was quenched by dropwise addition of 25 mL MeOH and diluted with 200 mL CH_2Cl_2. The organic layer was washed with 2x 0.1 M aq. HCl, sat. aq. $NaHCO_3$ and brine (100 mL each, backwash with 20 mL CH_2Cl_2). The combined organic layers were dried over Na_2SO_4, filtered and evaporated to dryness. Column chromatography (CH:EA 98:2 → 85:15) yielded the target compound as a colourless oil that solidified upon standing (8.515 g, 87%).

^{1}H NMR (500 MHz, $CDCl_3$) δ 7.70 – 7.56 (m, 4H, CH_{ar}), 7.49 – 7.31 (m, 6H, CH_{ar}), 5.41 (d, J = 8.8 Hz, 1H, NH), 4.83 (s, 1H, CH), 3.86 (d, J = 4.7 Hz, 2H, CH_2), 3.66 (s, 3H, OCH_3), 3.19 (s, 3H, NCH_3), 1.44 (s, 9H O-$C(CH_3)_3$), 1.04 (s, 9H, Si-$C(CH_3)_3$).

^{13}C NMR (126 MHz, CDCl3) δ 155.40 (CO), 135.62 (CH_{ar}), 133.17 (C_{ar}), 129.75 (CH_{ar}), 127.71 (CH_{ar}), 79.56 ($\underline{C}(CH_3)_3$), 64.14 (CH_2OSi), 61.43 (OCH_3), 52.48 ($\underline{C}HCO$), 28.39 ($OC(\underline{C}H_3)_3$), 26.72 ($SiC(\underline{C}H_3)_3$), 19.24 ($SiCMe_3$).

(S)-1-(tert-butyldiphenylsilyloxy)-2-(N-tert-butyloxycarbonyl)aminopent-4-en-3-on (204)

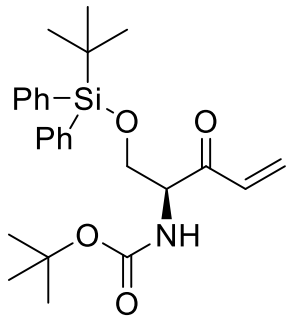

Under argon atmosphere, **203** (8.30 g, 17.05 mmol, 1 eq.) was dissolved in dry THF (57 mL). The mixture was cooled to -15°C using ice/NaCl mixture and vinyl magnesium bromide (1 M in THF, 57 mL, 56.27 mmol, 3.3 eq.) was added over 2 h so as to keep the reaction temperature below -15°C. Stirring was continued at the same temperature for 1 h then warmed to RT and stirred till TLC indicates complete conversion (about 2h). The reaction was quenched inversely by adding it dropwise into a mixture of ice/1 M HCl (150 g each) over a period of 30 min. The obtained aqueous mixture was extracted with EA (3x 100 mL). The combined organic layers were washed with sat. aq. $NaHCO_3$ and brine (75 mL each), dried over Na_2SO_4, filtered and evaporated to dryness. Column chromatography (CH:EA = 96:4 → 91:9) yielded the target compound as a colourless oil that solidified upon standing (5.04 g, 65%).

^{1}H NMR (500 MHz, $CDCl_3$) δ 7.65 – 7.53 (m, 4H, Har), 7.46 – 7.40 (m, 2H, Har), 7.37 (ddd, *J* = 8.1, 5.2, 2.1 Hz, 4H, Har), 6.51 (dd, *J* = 17.5, 10.6 Hz, 1H, =CH), 6.40 – 6.27 (m, 1H,=CHH), 5.82 (d, *J* = 10.7 Hz, 1H, =CHH), 5.55 (d, *J* = 7.69, 1H, NH), 4.67 (dt, *J* = 7.6, 3.7 Hz, 1H, CH), 4.00 (dd, *J* = 10.5, 3.5 Hz, 1H, C<u>H</u>HOSi), 3.93 (dd, *J* = 10.5, 4.0 Hz, 1H, CH<u>H</u>OSi), 1.45 (m, 9H, O-C(CH_3)$_3$), 1.01 (m, 9H, , Si-C(CH_3)$_3$).

^{13}C NMR (126 MHz, $CDCl_3$) δ 196.86 (CO), 155.14 (COO), 135.60 (CH_{ar}), 135.55 (CH_{ar}), 133.10 (<u>C</u>H=CH_2), 132.83(C_{ar}), 132.74 (C_{ar}), 129.86 (CH_{ar}), 129.60 (<u>C</u>H_2=CH), 127.77 (*C*H_{ar}),79.97 (CMe_3),64.19 (CHNH),59.44 (CH_2OSi), 28.38 ((*C*H_3)$_3$CO), 26.71 ((*C*H_3)$_3$CSi), 19.27 (SiCMe_3).

(2S,3R)-1-(tert-butyldiphenylsilyloxy)-2-(N-tert-butyloxycarbonyl) aminopent-4-en-3-ol (205)

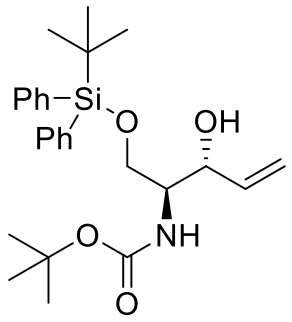

Under argon atmosphere, **204** (5.036 g, 11.10 mmol, 1 eq.) was dissolved in dry THF (4 mL). Dry EtOH (40 mL) was added under vigorous stirring and a white slurry was obtained. The mixture was cooled to -84°C using Ethyl acetate/liq. N_2 and TBLAH (5.65 g, 22.2 mmol, 2.0 eq.) was added over 20 min to keep the reaction temperature constant. Stirring was continued at the same temperature for 4 h. The reaction was quenched by dropwise addition of 49 mL 1 M 16 HCl at -84°C. The mixture was warmed to RT and Celite was added under stirring. The slurry was filtered and the Celite was washed with EA. The filtrate was extracted with EA. The combined organic layers were washed with sat. aq. $NaHCO_3$ and brine (75 mL each), dried (Na_2SO_4), filtered and evaporated to dryness. Column chromatography (CH:EA = 92:8) yielded the title compound as a colourless oil (4.04 g , 80%).

1H NMR (500 MHz, CDCl3) δ 7.73 – 7.59 (m, 4H, CH_{ar}), 7.52 – 7.33 (m, 6H, CH_{ar}), 5.91 (ddd, J = 17.2, 10.6, 5.0 Hz, 1H, =CH), 5.42 (dt, J = 17.2, 1.5 Hz, 1H, =CHH), 5.33 – 5.15 (m, 2H, =CHH+NH), 4.39 – 4.24 (m, 1H, CHOH), 3.91 (dd, J = 10.5, 3.6 Hz, 1H, C<u>H</u>HOSi), 3.76 (d, J = 10.5 Hz, 1H, CH<u>H</u>OSi), 3.71 (d, J = 4.0 Hz, 1H, C<u>H</u>NH), 3.34 (d, J = 7.8 Hz, 1H,OH), 1.43 (s, 9H, O-C$(CH_3)_3$), 1.07 (s, 9H, Si-C$(CH_3)_3$).

^{13}C NMR (126 MHz, CDCl3) δ 156.02 (NCOO), 137.80 (=CH), 135.67 (CHar), 132.62 (Car), 132.58 (Car), 130.16 (CHar), 130.14 (CHar), 130.12 (CHar), 128.04 (CHar), 128.01 (CHar), 116.21 (=CH2), 79.73 (Me3CO), 74.69 (CHOH), 64.32 (CH_2O), 54.86 (CHNH), 28.53 (($CH_3)_3$CO), 26.98 (($CH_3)_3$CSi), 19.29 ($SiCMe_3$).

UPLC-MS (ESI): $C_{26}H_{37}NO_4NaSi$ $[M+Na]^+$: m/z Calc.: 478.2, found: 478.3

(2*S*,3*R*,*E*)-1-(*tert*-butyldiphenylsilyloxy)-2-(*N*-*tert*butyloxycarbonyl) amino octadic -4-en-3-ol (206)

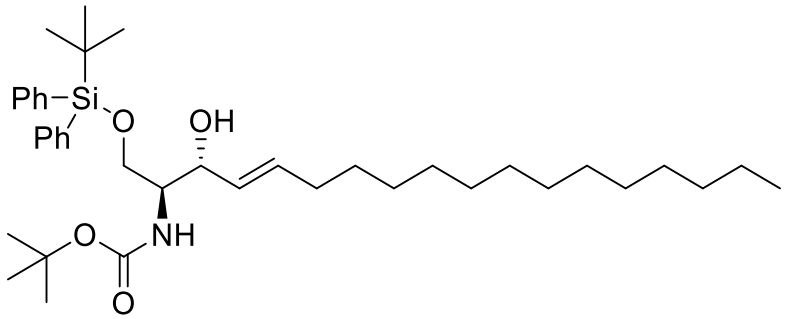

Under argon atmosphere, **205** (4.043 g, 8.87 mmol, 1 eq.) was dissolved in dry DCM (40 mL) and then 1-pentadecene (10.8 mL, 39.92 mmol, 4.5 eq.) was added. Grubbs 2nd catalyst (0.055 g, 0.0887 mmol, 0.01 eq.) was dissolved in 20 mL dry DCM and added to the mixture. The reaction mixture was heated at reflux for 4 h. Then potassium 2-isocyanoacetate (0.15 g, 1.153 mmol, 0.13 eq.) was dissolved in 1 mL MeOH and added and stirred for 30 minutes to quench the reaction. Celite was added and the volatiles were removed in vacuo. Column chromatography (CH:EA = 95:5→ 93:7→92:8→90:10) yielded the title compound as a colourless oil (3.6 g, 63.5%).

^{1}H NMR (500 MHz, $CDCl_3$) δ 7.68 (t, J = 6.9 Hz, 4H, CHar), 7.52 – 7.37 (m, 6H, CHar), 5.89 – 5.73 (m, 1H, =C<u>H</u>CH_2), 5.51 (dd, J = 15.4, 6.0 Hz, 1H, =C<u>H</u>CH), 5.25 (d, J = 8.1 Hz, 1H, NH), 4.28 (d, J = 4.4 Hz, 1H, CHOH), 3.94 (dd, J = 10.5, 3.6 Hz, 1H, CHHO), 3.79 (d, J = 10.1 Hz, 1H, CHHO), 3.69 (s, 1H, CHNH), 3.23 (s, 1H, OH), 2.07 (dd, J = 14.4, 6.9 Hz, 2H, CH2CH=), 1.48 (s, 9H, (CH3)3CO), 1.41 – 1.36 (m, 2H, CH2Me), 1.29 (s, 20H, 10x CH2), 1.10 (s, J = 5.9 Hz, 9H, (CH3)3CSi), 0.91 (t, J = 7.0 Hz, 3H, CH3).

^{13}C NMR (126 MHz, $CDCl_3$) δ 155.99 (COO), 135.68 (CH_{ar}),133.96 (=<u>C</u>HCH_2), 133.46 (C_{ar}), 132.72 (C_{ar}), 130.10 (CH_{ar}), 130.08 (CH_{ar}), 129.29(=CH<u>C</u>H) 127.99(CH_{ar}), 79.58 ($OCMe_3$), 74.48 (CHOH), 64.27 (CH_2OSi), 55.15 (CHNH), 32.26 (CH_2CH=), 32.07 (CH2Et), 29.84 (CH_2) , 29.81 (CH_2), 29.77 (CH_2), 29.67 (CH_2), 29.50 (CH_2), 29.43 (CH_2), 29.31 (CH_2), 28.54 ((CH_3)$_3$CO), 26.99 ((CH_3)$_3$CSi), 22.83 (CH_2Me), 19.29 ($SiCMe_3$), 14.26 (CH_3).

***tert*-butyl (2*S*,3*R*,*E*)-1-(*tert*-butyldiphenylsilyloxy)-3-(methoxymethoxy)octadec-4 en-2-ylcarbamate (207)**

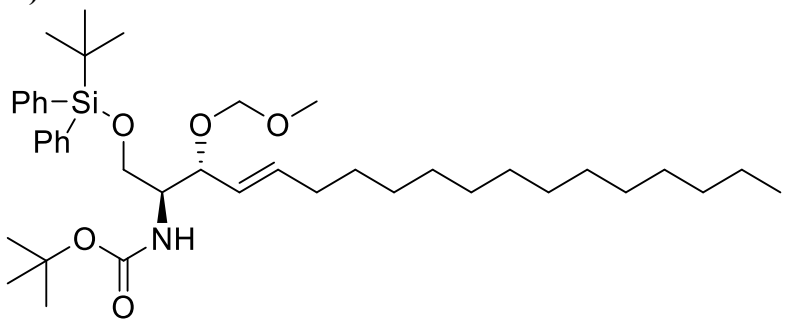

Under argon atmosphere, **206** (3.6 g, 5.64 mmol, 1 eq.) was dissolved in dry DCM (28 mL) and cooled to 0°C. At the same temperature, dry DIPEA (2.46 mL, 14.106 mmol, 2.5 eq.) was added and MOMCl (1.02 mL, 13.54 mmol, 2.4 eq.) was added dropwise. The reaction mixture was stirred at RT for overnight. Then, TLC indicated complete conversion of the starting material. The solution was diluted with 100 mL DCM and washed with 1 M aq. $NaHCO_3$, 1 M aq. NH_4Cl, H_2O, and brine (50 mL each). The organic layer was dried (Na_2SO4) and evaporated to dryness. Column chromatography (CH:EA = 99:1→96:4) yielded the title compound as a colourless oil (2.75 g, 72%).

^{1}H NMR (300 MHz, $CDCl_3$) δ 7.76 – 7.55 (m, 4H, CH_{ar}), 7.51 – 7.30 (m, 6H, CH_{ar}), 5.80 – 5.59 (m, 1H, =$CHCH_2$), 5.27 (dd, J = 15.4, 8.3 Hz, 1H, =CHCH), 4.74 (d, J = 8.1 Hz, 1H, NH), 4.66 (d, J = 6.6 Hz, 1H, CHHOMe), 4.49 (d, J = 6.6 Hz, 1H, CHHOMe), 4.22 – 4.11 (m, 1H, CHHOSi), 3.94 – 3.82 (m, 1H, CHHOSi), 3.77 (s, J = 8.4 Hz, 2H, OCHCHNH), 3.28 (s, J = 3.2 Hz, 3H, OCH_3), 2.08 – 1.93 (m, 2H, CH_2), 1.43 (s, 9H, $(CH_3)_3CO$), 1.26 (s, 22H, 11x CH2), 1.08 (s, J = 3.1 Hz, 9H, $(CH_3)_3CSi$), 0.88 (t, J = 6.7 Hz, 3H, CH_3).

^{13}C NMR (75 MHz, $CDCl_3$) δ = 155.54 (COO), 136.97 (=$CHCH_2$), 135.79 (CH_{ar}),, 133.53 (C_{ar}),, 129.85 (CH_{ar}), 127.83 (CH_{ar}), 126.61 (=CHCH), 93.85 (OCH_2O), 79.12 (($CH_3)_3CO$), 76.71 (CHO), 62.77 (CH_2OSi), 55.67 (OCH_3), 55.15 (CHNH), 32.49 (CH_2CH=), 32.07 (CH_2), 29.84 (CH_2), 29.81 (CH_2), 29.76 (CH_2), 29.64 (CH_2), 29.51 (CH_2), 29.39 (CH_2), 29.26 (CH_2), 28.55 ($C(CH_3)_3$), 27.06 (CH_2), 22.84 (CH_2CH_3), 19.45 (($CH_3)_3CSi$), 14.27 (CH_3).

UPLC-MS (ESI): $C_{41}H_{67}NO_5NaSi$ $[M+Na]^+$: m/z Calc.: 704.5, found: 704.5

***tert*-butyl (2*S*,3*R*,*E*)-1-hydroxy-3-(methoxymethoxy) octadec-4-en-2-ylcarbamate (208)**

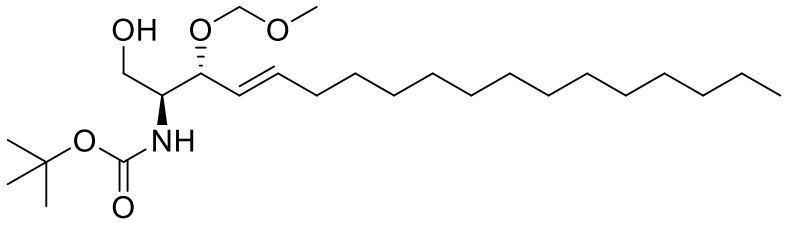

207 (0.391 g, 0.57 mmol, 1 eq.) was dissolved in 4 mL THF at rt. To the first solution tetrabutylammonium fluoride trihydrate (0.363 g, 1.149 mmol, 2 eq.), dissolved in 3 mL THF, was added dropwise with stirring. The reaction mixture was stirred at RT until complete conversion (3 h). 20 mL DCM were added and the mixture was washed with H_2O and 2x brine (20 mL each). The organic layer was dried (Na_2SO_4), filtered and evaporated to dryness. Using column chromatography (CH:EA =95:05 → 90:10 →80:20) the title product was obtained as a colorless waxy solid (0.224 g, 88%).

^{1}H NMR (300 MHz, $CDCl_3$) δ 5.82 – 5.68 (m, 1H; =C<u>H</u>CH$_2$), 5.35 (dd, J = 15.5, 7.9 Hz, 1H; =CHC<u>H</u>), 5.23 (d, J = 8.2 Hz, 1H, NH), 4.67 (d, J = 6.6 Hz, 1H, OC<u>H</u>HOMe), 4.52 (d, J = 6.6 Hz, 1H, OCH<u>H</u>OMe), 4.24 (dd, J = 7.7, 4.5 Hz, 1H, CHO), 3.95 (dd, J = 11.3, 3.4 Hz, 1H, C<u>H</u>HOH), 3.66 (d, J = 14.0 Hz, 2H, CH<u>H</u>OH+C<u>H</u>NH), 3.38 (s, 3H, OCH_3), 2.73 (bs, 1H, OH), 2.05 (dd, J = 13.6, 6.7 Hz, 2H, CH_2), 1.45 (s, 9H, $(CH_3)_3CO$), 1.36 (m, 2H, CH_2CH_3), 1.25 (m, 20H, 10x CH_2), 0.88 (t, J = 6.7 Hz, 3H, CH_3).

^{13}C NMR (126 MHz, $CDCl_3$) δ 162.60 (COO), 137.21 (=<u>C</u>HCH$_2$), 126.11 (=<u>C</u>HCH), 94.08 (OCH_2O), 78.83 ($(CH_3)_3CO$), 78.79 (CHO), 62.62 (CH_2OH), 55.88 (OCH_3), 55.14 (CHNH), 32.47 (CH_2), 32.07 (CH_2), 29.84 (CH_2), 29.82 (CH_2), 29.75 (CH_2), 29.60 (CH_2), 29.51 (CH_2), 29.31 (CH_2), 29.17 (CH_2), 28.53 (CH_2), 22.84 CH_2Me), 14.27 (CH_3).

UPLC-MS (ESI): $C_{25}H_{49}NO_5Na$ $[M+Na]^+$: m/z Calc.: 466.4, found: 466.2

4.10.4 Chemical Synthesis of the phosphodiesters

2-(2-hydroxyethyl)isoindoline-1,3-dione (209)

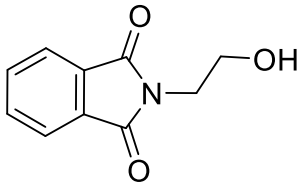

Phthalic anhydride (4.220 g, 28.00 mmol, 1 eq.) was dissolved in 30 mL DMF and 2-aminoethanol (1.70 mL, 28.00 mmol, 1 eq.) was added at rt. The reaction mixture was stirred under reflux for 24 h, cooled to RT and dissolved in 200 mL EA and 100 mL 0.1 M aq. HCl. The organic layer was separated and washed with brine (200 mL), dried (MgSO4) and evaporated to dryness. The obtained raw material was purified by crystallization from hot toluene yielding the title compound (4.2 g, 79%) as colourless crystals.

^{1}H NMR (300 MHz, $CDCl_3$) δ = 7.88 – 7.80 (m, 2H, CH_{ar}), 7.77 – 7.66 (m, 2H, CH_{ar}), 3.93 – 3.82 (m, 4H, 2x CH_2), 2.35 (s, 1H, OH).

^{13}C NMR (75 MHz, $CDCl_3$) δ 168.77 (CO), 134.14 (CH_{ar}), 132.12 (C_{ar}), 123.49 (CH_{ar}), 61.11 (CH_2), 40.66 (CH_2).

UPLC-MS (ESI): $C_{11}H_9NO_3$ $[M+H]^+$: m/z Calc.: 192.1, found: 192.1

***O*-2-phthalimidoethyl phosphorodichloridate (210)**

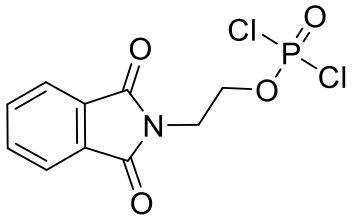

Under argon atmosphere, well dried **209** (1.800 g, 9.414 mmol, 1 eq.) was dissolved in dry toluene (15 mL). $POCl_3$ (2.89 mL, 31.066 mmol, 3.3 eq.) was added dropwise and the mixture was heated under reflux for 4 h. At 60°C, the volatiles were distilled off and the oily residue was dissolved in dry diethyl ether (10 mL). The material was left to crystallize at -20°C, and the supernatant was removed using a filtration cannula. After drying in vacuo, the title compound was obtained as an off-white solid (2.03 g, 70%).

^{1}H NMR (300 MHz, $CDCl_3$) δ = 7.92 – 7.82 (m, 2H, CH_{ar}), 7.80 – 7.69 (m, 2H, CH_{ar}), 4.57 (dt, J = 10.7, 5.4 Hz, 2H, CH_2OP), 4.09 (tt, J = 6.1, 3.0 Hz, 2H, CH_2N).

^{13}C NMR (75 MHz, $CDCl_3$) δ = 167.89 (Car), 134.65 (CHar), 131.86 (Car), 123.99 (CHar), 67.88 (d, *J* = 8.9 Hz, CH_2OP), 37.35 (d, *J* = 9.4 Hz, CH_2N).

^{31}P NMR (121 MHz, $CDCl_3$) δ= 8.64 .

tert-butyl ((2S,3R,E)-1-(((2-(1,3-dioxoisoindolin-2-yl)ethoxy)(hydroxy)phosphoryl) oxy)-3-(methoxymethoxy)octadec-4-en-2-yl)carbamate (211)

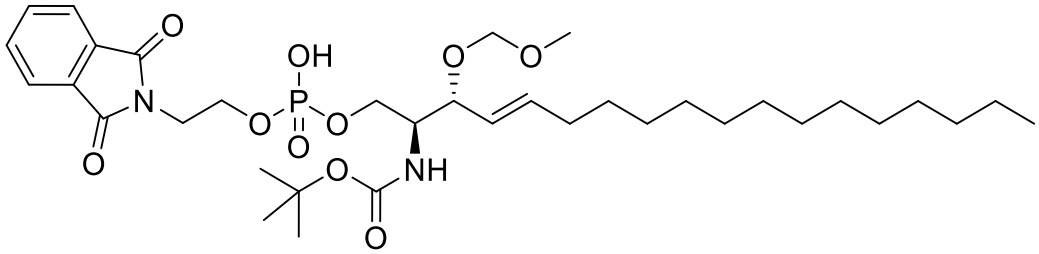

Under argon atmosphere, **210** (555 mg, 1.80 mmol, 4 eq.) was dissolved in dry DCM (20 mL) containing 1 mL of dry pyridine. At 0°C, a solution of **208** (200 mg, 0.45 mmol, 1 eq.) in 20 mL dry DCM was added dropwise over 1h. Stirring was continued at RT until complete conversion detected by TLC (CH:EA 1:1) (4 h) . The reaction was quenched by the addition of 20 mL sat. aq. $NaHCO_3$ and stirred for 20 min.$CHCl_3$ (300 mL), MeOH (150 mL) and H_2O (300 mL) were added. The organic layer was separated and evaporated to dryness. The crude material was purified by column chromatography (MeOH:$CHCl_3$ = 1:10→2:8) to yield the target compound as an off-white wax (267 mg, 85 %).

^{1}H NMR (500 MHz, $CDCl_3$/MeOD) δ =.12 – 8.06 (m, 2H, CHar), 8.05 – 7.98 (m, 2H, CHar), 6.05 – 5.85 (m, 1H, =CHCH2), 5.53 (dd, J = 15.4, 8.5 Hz, 1H, =CHCH), 4.75 (dd, J = 26.0, 6.8 Hz, 2H, CH2), 4.32 (dd, J = 12.6, 5.9 Hz, 2H, CH2), 4.29 – 4.24 (m, 1H, CH), 4.17 (t, J = 5.7 Hz, 4H, 2xCH_2), 3.98 (d, J = 6.6 Hz, 1H, CH), 3.57 (s, 3H, CH3), 2.28 (dd, J = 13.9, 7.0 Hz, 2H, CH2), 2.22 (s, 1H, OH), 1.67 – 1.59 (m, 9H, $C(CH_3)_3$), 1.49 (s, 22H, 11x CH_2), 1.11 (t, J = 7.0 Hz, 3H, CH_3).

^{13}C NMR (126 MHz, $CDCl_3$/MeOD) δ 169.19 (CON), 157.06 (COO), 138.24 (=$\underline{C}HCH_2$), 134.90 (CHar), 132.47 (Car), 126.60 (=$\underline{C}HCH$), 123.84 (CHar), 94.07 (OCH_2O), 80.01 (CMe_3), 77.12 (CHO), 65.02 (CH_2OP), 62.94 (CH_2OP), 55.88 (OCH3), 54.59 (NCH), 39.10 (CH_2), 39.04 (CH_2), 32.89 (CH_2), 32.43 (CH_2), 30.17 (CH_2), 30.14 (CH_2), 30.11 (CH_2), 30.00 (CH_2), 29.85 (CH_2), 29.76 (CH_2), 29.65 (CH_2), 28.64 ($C(CH_3)_3$), 23.16, 14.33 (CH_3). ^{31}P NMR (202 MHz, $CDCl_3$/MeOD) δ = -2.13.

UPLC-MS (ESI):$C_{35}H_{57}N_2O_{10}P[M+H]^+$: m/z Calc.: 697.4, found: 697.4

tert-butyl ((2S,3R,E)-1-(((2-aminoethoxy)(hydroxy)phosphoryl)oxy)-3-(methoxy methoxy)octadec-4-en-2-yl)carbamate (212)

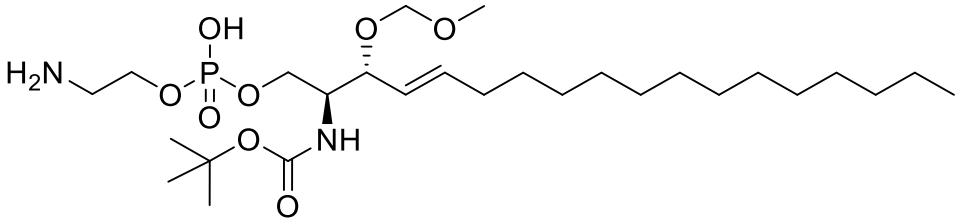

Compound **211** (110 mg, 0.16 mmol, 1 eq.) was dissolved in 6 mL MeOH/$CHCl_3$ (1:1). Hydrazine hydrate (64%, 30 µL, 0.63 mmol, 4 eq.) was added and the mixture stirred at RT for 4.5 h when TLC indicated complete consumption of the starting material. The solvent was evaporated and the crude material was dried under high vacuum. The material was adsorbed on Celite® and purified using short flash column chromatography ($CHCl_3$: MeOH: H_2O = 100:15:1→65:25:3). The title compound was isolated as a colorless solid (73.4 mg, 82%).

1H NMR (400 MHz, Pyr-d_5) δ 7.74 (s, 1H,NH), 5.82 (d, J = 15.1 Hz, 1H, =$CHCH_2$), 5.76 – 5.61 (m, 1H, =CHCH), 4.94 (d, J = 5.9 Hz, 1H, OCHHO), 4.76 (d, J = 5.9 Hz, 1H, OCHHO), 4.67 – 4.44 (m, 4H, 2 x CH_2OP), 4.39 (s, 1H, CHNH), 3.51 (s, 5H, CH_2NH_2, OCH_3), 2.08 (s, 2H, CH_2), 1.53 (d, J = 37.2 Hz, 9H, $OC(CH_3)_3$), 1.36 (d, J = 39.4 Hz, 20H, 10 x CH_2), 0.90 (t, J = 6.7 Hz,3H, CH_3).

^{13}C NMR (126 MHz, Pyr-d_5) δ 157.16 (COO), 137.40 (=$CHCH_2$), 128.15 (=CHCH), 94.38 (OCH_2O), 78.79($OC(CH_3)_3$), 77.44 (CHO), 65.81 (CH_2OP), 63.25 (CH_2OP), 56.11 (OCH_3), 55.77 ($NCHCH_2OP$), 33.17 (CH_2CH=), 32.60 (CH_2), 30.47 (CH_2), 30.43 (CH_2), 30.41 (CH_2), 30.31 (CH_2), 30.10 (CH_2), 30.06 (CH_2), 29.94 (CH_2), 29.15 (CH_2), 23.42 (CH_2), 14.76 (CH_3).

^{31}P NMR (202 MHz, pyr-d_5) δ = 2.82

UPLC-MS (ESI): $C_{27}H_{56}N_2O_8P$ $[M+H]^+$: m/z Calc.: 567.4, found: 567.4

(2S,3R,E)-2-(tert-butoxycarbonyl)-3-(methoxymethoxy)octadec-4-enyl 2-(dimethyl(prop-2-ynyl)ammonio)ethyl phosphate (214)

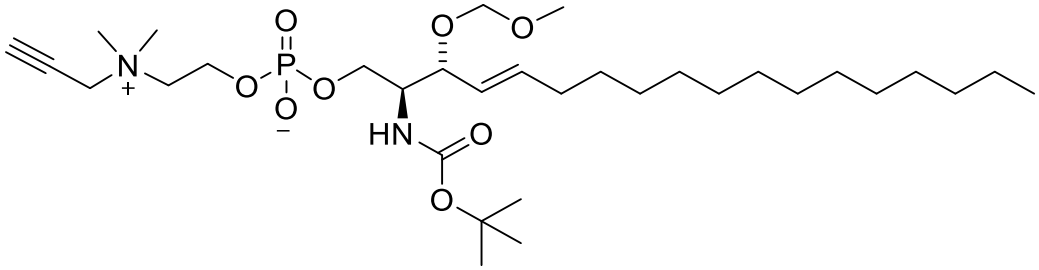

Under argon atmosphere, alcohol **208** (50 mg, 0.113 mmol, 1eq.) was dissolved in dry toluene (1.5 mL) and triethylamine (47 µL, 0.338 mmol, 3eq.) followed by DMAP (2.8 mg, 0.022 mmol, 0.2 eq.) were added. The reaction mixture was cooled to 0 °C before the addition of phospholane (2-chloro-2-oxo-1,2,3- dioxaphospholane) (32 µL, 0.338 mmol, 3eq.) Stirring at 0 °C continued till TLC showed disappearance of starting material (1 h). The mixture was transferred to a sealed reaction tube via cannula under positive argon pressure. The crude solution of intermediate **213** was diluted with dry MeCN (3 mL) before N,N-dimethylpropargylamine (0.5 mL) was added. The mixture was heated at 80 °C for 24 h. The reaction mixture was then concentrated in vacuo and purified by flash chromatography on silica (85/14/1 then 80/18/2 then 72/25/3 $CHCl_3$/MeOH/NH_4OH). The pure product was obtained as a white solid (35 mg, 50%).

^{1}H NMR (400 MHz, MeOD) δ 5.76 (dt, J = 15.1, 6.7 Hz, 1H), 5.35 (dd, J = 15.4, 8.6 Hz, 1H), 4.71 (d, J = 6.6 Hz, 1H), 4.54 (d, J = 6.6 Hz, 1H), 4.47 (d, J = 2.4 Hz, 2H), 4.33 (s, 2H), 4.21 (d, J = 10.3 Hz, 2H), 4.15 – 3.96 (m, 2H), 3.85 – 3.69 (m, 2H), 3.63 – 3.52 (m, 1H), 3.39 (s, 3H), 3.32 (d, J = 6.4 Hz, 6H), 2.19 – 1.98 (m, 2H), 1.53 – 1.40 (m, 11H), 1.32 (s, 20H), 0.93 (t, J = 6.9 Hz, 3H).

^{13}C NMR (101 MHz, MeOD) δ 158.00, 138.50, 127.94, 94.61, 83.24, 80.09, 77.72, 72.43, 65.91, 65.29, 60.22, 56.46, 56.08, 55.66, 52.03,33.42, 33.06, 30.75, 30.69, 30.59, 30.45, 30.30, 30.26, 28.88, 23.72, 14.44.

^{31}P NMR (162 MHz, MeOD) δ -0.04.

UPLC-MS (ESI): $C_{32}H_{62}N_2O_8P$ $[M+H]^+$: m/z Calc.: 633.4, found: 633.3

4.10.5 Chemical Synthesis of the bromo coumarin dye

Benzyl propiolate (301)

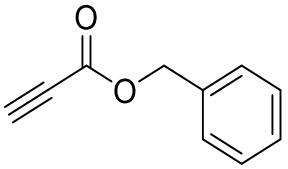

A solution of DMAP (30 mg, 0.24 mmol, 0.01 eq.) and DCC (5.16 g, 25 mmol, 1 eq.) in DCM (30 mL) was added slowly over 1.5 h to a solution of propiolic acid (1.54 mL, 24.84 mmol, 1 eq.) and benzyl alcohol (2.8 mL, 27.03 mmol, 1.1 eq.) in DCM (30 mL) at 0 °C. The suspension was then stirred for overnight at room temperature, monitoring through by TLC (EtOAc: Cyclohexan 1:2). Upon completion, the mixture was filtered through a layer of Celite and the filtrate concentrated in vacuo. The product was purified using column chromatography (7 % EtOAc in Cyclohexan) to yield a colorless oil (3.17 g, 80%).

^{1}H NMR (500 MHz, $CDCl_3$) δ : 7.41 – 7.33 (m, 5H, CH_{ar}), 5.23 (s, 2H, CH_2), 2.89 (s, 1H, CH).

^{13}C NMR (126 MHz, $CDCl_3$) δ : 152.43 (C=O), 134.35 (C_{ar}), 128.74 (CH_{ar}), 128.70 (CH_{ar}), 128.59 (CH_{ar}), 75.05(≡CH) , 74.56(≡C), 67.93(CH_2).

UPLC-MS (ESI): $C_{10}H_8O_2$ Na $[M+Na]^+$: m/z Calc.: 183.0, found: 183.1

Benzyl 2-(8-methyl-6-oxo-6H-[1,3]dioxolo[4,5-g]chromen-2-yl)acetate (302)

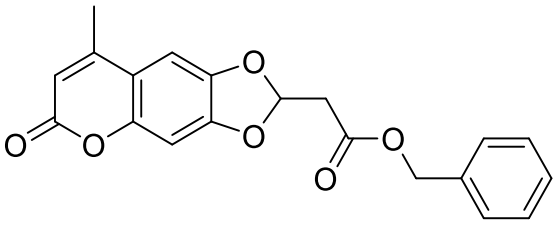

To a solution of 6,7-dihydroxy-coumarin (500 mg, 2.6 mmol, 1eq.) in dry DCM (25 mL), benzyl propiolate **301** (500 mg, 3.1 mmol, 1.2 eq.) and DMAP (507 mg, 4.15 mmol, 1.6 eq.) were added under argon atmosphere at room temperature. After being stirred for 7 h, the solvent was removed under reduced pressure. The product was purified using column chromatography (25 % EtOAc in Cyclohexan) afforded **302** (892 mg, 97%) as a white crystalline solid.

^{1}H NMR (500 MHz, $CDCl_3$) δ : 7.39 – 7.31 (m, 5H, CH_{ph}), 6.91 (s, 1H, CH_{cou}), 6.79 (s, 1H, CH_{cou}), 6.64 (t, J = 5.1 Hz, 1H, OCH), 6.16 (d, J = 1.2 Hz, 1H, C=CH), 5.19 (s, 2H, CH_2), 3.07 (d, J = 5.1 Hz, 2H, CH_2), 2.35 (d, J = 1.2 Hz, 3H, CH_3).

^{13}C NMR (126 MHz, CDCl3) δ : 167.70 (C=O), 161.32 (C=O), 152.51(C-Me), 150.69(C_{cou}), 150.59 (C_{cou}), 144.63 (C_{cou}), 135.20 (C_{ph}), 128.77 (CH_{ph}), 128.71 (CH_{ph}), 128.59 (CH_{ph}), 114.07 (C_{cou}), 112.48 (C=CH), 109.59 (CH_{cou}), 102.37 (CH_{cou}), 98.61 (OCH), 67.29 (CH_2), 40.22 (CH_2), 19.28 (CH_3).

UPLC-MS (ESI): $C_{20}H_{17}O_6$ $[M+H]^+$: m/z Calc.: 353.1, found: 353.1

Benzyl 2-(7-bromo-8-methyl-6-oxo-6H-[1,3]dioxolo[4,5-g]chromen-2-yl)acetate (303)

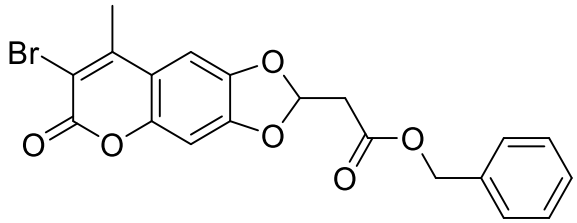

To a solution of **302** (600 mg, 1.70 mmol, 1 eq.) in dry ACN (20 mL) were added NBS (608 mg, 3.4 mmol, 2 eq.) and NaOAc (14 mg, 0.17 mmol, 0.1 eq.) under argon atmosphere at room temperature. The mixture was stirred till complete conversion of **302** monitored by TLC (30 % EtOAc in Cyclohexan). The organic layer was washed with brine solution and was extracted three times with DCM. The combined organic layers were dried over $MgSO_4$ and concentrated under reduced pressure. The resulting residue was purified by flash column chromatography (PE/EE 5:1) yielding **303** (730 mg, quant.)

^{1}H NMR (500 MHz, $CDCl_3$) δ : 7.51 – 7.30 (m, 5H, CH_{ph}), 6.96 (s, 1H, CH_{cou}), 6.79 (s, 1H, CH_{cou}), 6.66 (t, J = 5.0 Hz, 1H, OCH), 5.19 (s, 2H, CH_2), 3.08 (d, J = 5.0 Hz, 2H, CH_2), 2.55 (s, 3H, CH_3).

^{13}C NMR (126 MHz, $CDCl_3$) δ : 167.59 (C=O), 157.47 (C=O), 151.03 (C-Me), 150.76 (C_{cou}), 149.05 (C_{cou}), 145.20 (C_{cou}), 135.16 (C_{ph}), 128.78 (CH_{ph}), 128.74 (CH_{ph}), 128.63 (CH_{ph}), 113.93 (C_{cou}), 110.57 (C-Br), 109.90 (CH_{cou}), 102.76 (CH_{cou}), 98.42 (OCH), 67.33 (CH_2), 40.21 (CH_2), 20.17 (CH_3).

UPLC-MS (ESI): $C_{20}H_{16}BrO_6$ $[M+H]^+$: m/z Calc.: 431.0, found: 431.0

2-(7-Bromo-8-methyl-6-oxo-6H-[1,3]dioxolo[4,5-g]chromen-2-yl)acetic acid (304) / 2-(8-Methyl-6-oxo-6H-[1,3]dioxolo[4,5-g]chromen-2-yl)acetic acid (305) (3:1)

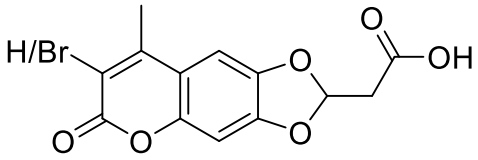

A suspension of **303** (541 mg, 1.25 mmol, 1 eq.) and Pd/C (10%, 13.8 mg, 0.012 mmol, 0.01 eq.) in dry THF (150 mL) was stirred under hydrogen atmosphere (p (H_2) = 1 atm) at room temperature overnight. After complete conversion of **303** the mixture was filtered over Celite and washed with MeOH. The solvent was removed under reduced pressure and the residue was purified by flash silica gel column chromatography (MeOH / DCM 10%) yielding a white solid of **304** (324 mg, 75%) as a 3:1 mixture with the debrominated product **305**.

^{1}H NMR (500 MHz, $(CD_3)_2CO$ δ : 7.69 (s, 1H, CH_{cou}), 7.58 (s, 1/3H, CH_{cou}), 7.34 (s, J = 2.4 Hz, 1H, CH_{cou}), 7.29 (s, 1/3H, CH_{cou}), 7.14 (t, J = 5.2 Hz, 1H, OCH), 7.11 (t, J = 5.2 Hz, 1/3H, OCH), 6.57 (d, J = 1.2 Hz, 1/3H, C=CH), 3.55 (d, J = 5.2 Hz, 2H,CH_2), 3.54 (d, J = 5.2 Hz, 2/3H, CH_2), 3.04 (s, 3H, CH_3).

^{13}C NMR (126 MHz, $(CD_3)_2CO$) δ 169.24 169.19 (C=O), (C=O), 160.85 (C=O), 157.16 (C=O), 153.79 (C-Me), 152.38 (C-Me), 151.93 (C_{cou}), 149.89 (C_{cou}), 146.12 (C_{cou}), 114.46 (C_{cou}), 112.61 (C=CH), 111.46 (CH_{cou}), 111.13 (CH_{cou}), 110.42 (C-Br) , 104.01 (CH_{cou}), 103.49 (CH_{cou}), 98.59 (OCH), 98.46 (OCH), 40.04 (CH_2), 40.00 (CH_2), 20.22 (CH_3), 19.03 (CH_3).

UPLC-MS (ESI): $C_{13}H_{10}BrO_6$ $[M+H]^+$: m/z Calc.: 341.0, found: 341.0

UPLC-MS (ESI): $C_{13}H_{11}O_6$ $[M+H]^+$: m/z Calc.: 263.1, found: 263.1

2-(8-Methyl-6-oxo-6H-[1,3]dioxolo[4,5-g]chromen-2-yl)acetic acid (305)

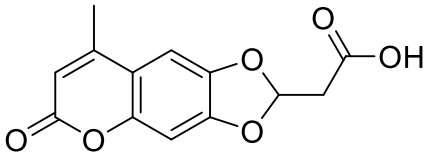

A suspension of **302** (1.1 g, 3.1 mmol, 1 eq.) and Pd/C (10%, 35.9 mg, 0.012 mmol, 0.01 eq.) in dry THF (375 mL) was stirred under hydrogen atmosphere (p(H_2) = 1 atm) at room temperature overnight. After complete conversion TLC (10% MeOH in DCM) of **302** the mixture was filtered through Celite and washed with MeOH. The solvent was removed under reduced pressure and the residue was purified by column chromatography (gradient from 1.5% MeOH to 8% MeOH in DCM) yielding (532 mg, 65%) of **305** as an orange solid.

^{1}H NMR (300 MHz, DMSO-d_6) δ 7.25 (s, 1H , CH_{cou}), 7.07 (s, 1H, CH_{cou}), 6.66 (t, J = 5.2 Hz, 1H, OCH), 6.22 (d, J = 1.1 Hz, 1H, C=CH), 3.04 (d, J = 5.2 Hz, 2H, CH_2), 2.35 (d, J = 1.1 Hz, 3H, CH_3).

^{13}C NMR (75 MHz, DMSO) δ 169.75 (C=O), 160.63 (C=O), 154.07 (C-Me), 150.86 (C_{cou}), 150.41 (C_{cou}), 144.74 (C_{cou}), 113.83 (C_{cou}), 111.67 (C=CH), 110.64 (CH_{cou}), 103.29 (CH_{cou}), 98.24 (OCH), 19.11 (CH_3).

UPLC-MS (ESI): $C_{13}H_{11}O_6$ $[M+H]^+$: m/z Calc.: 263.1, found: 263.1

2-(7-Bromo-8-methyl-6-oxo-6H-[1,3]dioxolo[4,5-g]chromen-2-yl)acetic acid (304)

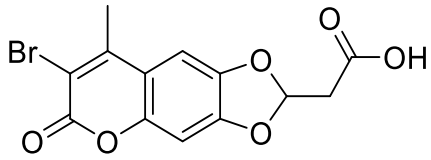

To a solution of **305** (250 mg, 0.95 mmol, 1 eq.) in dry DMF (10 mL) were added NBS (508 mg, 2.85 mmol, 3 eq.) and NaOAc (15.5 mg, 0.19 mmol, 0.1 eq.) under argon atmosphere at room temperature. The mixture was stirred (2d) till complete conversion of **305** monitored by TLC (0.5 % MeOH in DCM). The mixture was extracted three times with DCM. The combined organic layers were dried over $MgSO_4$ and concentrated under reduced pressure. The resulting residue was purified by column chromatography (gradient from 0.5% MeOH to 5% MeOH in DCM) yielding **304** (163 mg, 50 %.)

^{1}H NMR (500 MHz, $(CD_3)_2CO$) δ 7.23 (s, 1H, CH_{cou}), 6.88 (s, 1H, CH_{cou}), 6.68 (t, J = 5.2 Hz, 1H, OCH), 3.10 (d, J = 5.2 Hz, 2H,CH_2), 2.58 (s, 3H, CH_3).

^{13}C NMR (126 MHz, $(CD_3)_2CO$) δ 169.20 (C=O), 157.15 (C=O), 152.31 (C-Me), 151.87 (C_{cou}), 149.87 (C_{cou}), 146.10 (C_{cou}), 114.44 (C_{cou}), 111.44 (CH_{cou}), 110.42 (C-Br), 103.98 (CH_{cou}), 98.44 (OCH), 40.00 (CH_2), 20.21 (CH_3).

UPLC-MS (ESI): $C_{13}H_{10}BrO_6$ $[M+H]^+$: m/z Calc.: 341.0, found: 341.0

Methyl 6-(2-(7-bromo-8-methyl-6-oxo-6H-[1,3]dioxolo[4,5-g]chromen-2-yl)aceta mido) hexa noate (306)

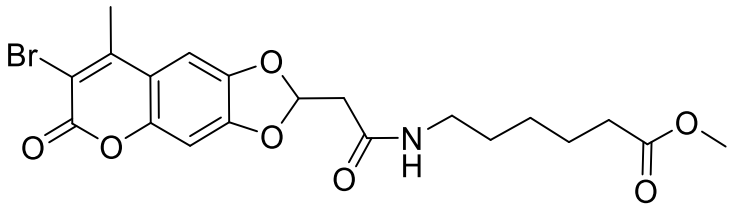

To a solution of **304** (380 mg, 1.11 mmol, 1eq.) and Methyl 6-aminohexanoate hydrochloride (405 mg, 2.23 mmol, 2 eq.) in dry DCM (50 mL) were added EDC.HCl (257 mg, 1.34 mmol, 1.2 eq.) and HOBt (175.7 mg, 1.34 mmol, 1.2 eq.) under argon atmosphere at room temperature. The reaction was monitored by TLC. After completion of the reaction (24 h), it was washed with 1N HCl and saturated NaCl solution, dried over MgSO4 and concentrated under reduced pressure. The resulting residue was purified by flash silica gel column chromatography (DCM/MeOH 99.5:0.5) yielding **306** (157 mg, 30%) as a white solid.

^{1}H NMR (500 MHz, $CDCl_3$) δ 6.92 (s, 1H, CH_{cou}), 6.71 (s, 1H, CH_{cou}), 6.58 (t, *J* = 5.2 Hz, 1H, OCH), 5.87 (s, 1H, NH), 3.59 (s, 3H, OCH_3), 3.33 – 3.17 (m, 2H,CH_2), 2.83 (d, *J* = 5.2 Hz, 2H, CH_2), 2.48 (s, 3H, CH_3), 2.25 (t, *J* = 7.3 Hz, 2H, CH_2), 1.58 (dd, *J* = 15.3, 7.5 Hz, 2H, CH_2), 1.48 (dt, *J* = 14.8, 7.2 Hz, 2H, CH_2), 1.34 – 1.26 (m, 2H, CH_2).

^{13}C NMR (126 MHz, CDCl3) δ 166.25 (C=O) , 157.33 (C=O), 150.96 (C-Me) , 150.74 (Ccou), 148.84 (Ccou), 145.18 (Ccou), 113.73 (Ccou), 110.93 (CHcou), 110.35 (C-Br), 102.65 (CHcou), 98.23 (OCH), 51.58 (CH3), 42.11 (CH2), 39.42 (CH2), 33.78 (CH2), 29.01 (CH2), 26.23 (CH2), 24.32 (CH2), 20.04 (CH3).

UPLC-MS (ESI): $C_{20}H_{21}BrNO_7[M-H]^-$: m/z Calc.: 466.1, found: 466.1

6-(2-(7-bromo-8-methyl-6-oxo-6H-[1,3]dioxolo[4,5-g]chromen-2-yl)acetamido)hexanoic acid (307)

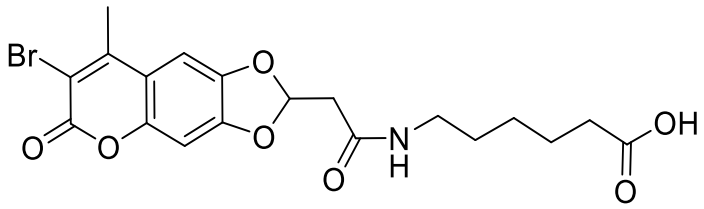

1st procedure:

To a solution of **306** (52 mg, 0.11 mmol, 1eq.) in dry THF (3 mL), LiOH (13.3 mg, 0.56 mmol, 5 eq.) solution in H_2O (3 mL) was added and stirred at room temperature. The reaction was monitored by TLC. After completion of the reaction (3 h), it was diluted with diethyl ether (10 mL) and washed with saturated $NaHCO_3$ solution .The aqueous layer was then acidified with 10% $KHSO_4$ solution and extracted with diethyl ether (5x ,15mL each), dried over MgSO4 and concentrated under reduced pressure. The resulting residue was purified by flash silica gel column chromatography (gradient from 0.5% MeOH to 5% MeOH in DCM) yielding **307** (15 mg, 30 %) as an off white solid.

2nd procedure:

In an argon atmosphere, **304** (0.320 g, 0.938 mmol, 1 eq.) was dissolved in dry DCM (50 mL) and DMAP (0.137 g, 1.13 mmol, 1.2 eq.), as well as N-hydroxysuccinimide (0.130 g, 1.13 mmol, 1.2 eq.) were added. At 0°C, EDC (0.360 g, 1.88 mmol, 2 eq.) was added and stirring was continued for 22 h with protection from light and gradual warming to rt. Then, TLC and UPLC-MS indicated complete conversion of the starting material. The reaction mixture was diluted with DCM (20 mL) and washed with 0.5 M $KHSO_4$ (2x 40 mL) and brine (20 mL). The organic layer was dried (Na_2SO4), filtered and evaporated to dryness. The obtained material was directly used without further purification.

UPLC-MS (ESI): $C_{17}H_{13}BrNO_8$ $[M+H]^+$: m/z calc.: 437.9, found: 438.0.

In an argon atmosphere, 6-aminohexanoic acid (0.136 g, 1.034 mmol, 1.1 eq.) was dissolved in dry DCM (20 mL) and dry DIPEA (197.5 µL, 1.13 mmol, 1.2 eq.) was added. At 0°C, the freshly prepared *N*-succinimidyl ester of **304** was added and stirring was continued 22 h with protection from light and gradual warming to rt. Then, TLC and UPLC-MS indicated complete conversion of the starting material. the mixture extracted with saturated $NaHCO_3$ solution .The aqueous layer was then acidified with Conc. HCl solution and extracted with ethyl acetate, dried over MgSO4 and concentrated under reduced pressure.

The resulting residue was purified by silica gel column chromatography (gradient from 0.5% MeOH to 5% MeOH in DCM) yielding **307** (192 mg, 45%) as an off white solid.

3rd procedure:

To a solution of **309** (279 mg, 0.55mmol, 1 eq.) in dry DCM (3 mL) was added dropwise at RT 1ml TFA. After stirring (3 h) at RT, TLC and UPLC-MS indicated complete deprotection of the t-butyl ester. the solvent and TFA residues were evaporated under reduced pressure to give the free acid **307** as a white pure solid (198.5 mg, 80 % yield).

^{1}H NMR (500 MHz, DMSO-d_6) δ 8.08 (t, *J* = 5.6 Hz, 1H, NH), 7.39 (s, 1H, CH_{cou}), 7.13 (s, 1H, CH_{cou}), 6.67 (t, *J* = 5.4 Hz, 1H, OCH), 3.06 (dd, *J* = 12.7, 6.8 Hz, 2H, CH_2), 2.85 (d, *J* = 5.4 Hz, 2H, CH_2), 2.54 (s, 3H, CH_3), 2.19 (t, *J* = 7.4 Hz, 2H, CH_2), 1.55 – 1.44 (m, 2H, CH_2), 1.44 – 1.35 (m, 2H, CH_2), 1.33 – 1.21 (m, 2H, CH_2).

^{13}C NMR (126 MHz, DMSO-d_6) δ 174.43 (C=O), 165.99 (C=O), 156.49 (C=O), 152.04 (C-Me), 150.67 (C_{cou}), 148.41 (C_{cou}), 144.85 (C_{cou}), 113.20 (C_{cou}) , 111.46 (CH_{cou}), 108.93 (C-Br), 103.45 (CH_{cou}), 97.70 (OCH), 40.77 (CH_2), 40.02 (CH_2), 38.36 (CH_2), 33.60 (CH_2), 28.70 (CH_2), 25.92 (CH_2), 24.18 (CH_2), 19.98 (CH_3),

UPLC-MS (ESI): $C_{19}H_{21}BrNO_7$ $[M+H]^+$: m/z Calc.: 454.1, found: 454.1

Tert-butyl 6-aminohexanoate (308)

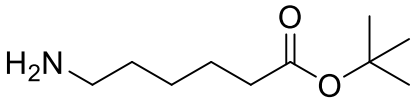

Aminohexanoic acid **(**2.0 g, 15.25 mmol, 1 eq.) was dissolved in thionyl chloride (5.0 mL, 68.6 mmol, 4.5 eq.). This solution was stirred at RT for 2 hours and concentrated *in vacuo* to dryness. To the reddish semi-solid product, a slurry of sodium bicarbonate (2.6 g, 30.4 mmol, 2.0 eq.) in *t*-BuOH (9.0 mL; 86.6 mmol; 5.7 eq.) was added and the slurry was stirred at RT for another 2 h. The residual *t*-BuOH was removed *in vacuo* at 40 0C. The thick white slurry was diluted with ethyl acetate and washed with of 1M NaOH (2x), H_2O (2x) and brine (1x). The organic layer was dried over Na_2SO_4 and concentrated to afford 8 (2.14 g, 75%) as a colorless oil.

^{1}H NMR (500 MHz, $CDCl_3$) δ 2.75 (s, 2H, NH_2), 2.20 (t, J = 7.5 Hz, 2H, CH_2), 1.58 (dt, J = 15.2, 7.5 Hz, 2H, CH_2), 1.46 (dd, J = 14.4, 7.1 Hz, 2H, CH_2), 1.42 (s, 9H, $C(CH_3)_3$), 1.33 (ddd, J = 15.7, 9.1, 6.1 Hz, 2H, CH_2).

^{13}C NMR (126 MHz, CDCl3) δ 173.28 (C=O), 80.12 ($C(Me)_3$), 35.64 (CH_2), 28.24 (CH_3), 26.51 (CH_2), 25.03 (CH_2).

UPLC-MS (ESI): $C_{10}H_{21}NO_2$ $[M+H]^+$: m/z Calc.: 188.2, found: 188.2

Tert-butyl 6-(2-(7-bromo-8-methyl-6-oxo-6H-[1,3]dioxolo[4,5-g]chromen-2-yl) acetamido) hexanoate (309)

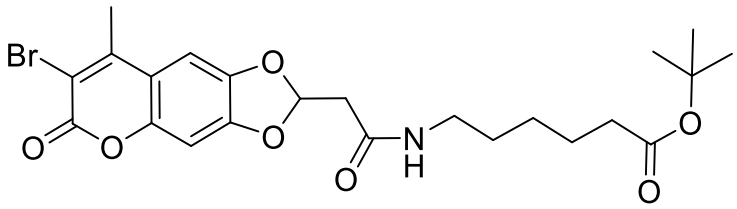

To a solution of **304** (175 mg, 0.51 mmol, 1eq.) and tert-butyl 6-aminohexanoate **308** (192.2 mg, 1.02 mmol, 2 eq.) in dry DCM (25 mL) were added EDC.HCl (118 mg, 0.61 mmol, 1.2 eq.) and HOBt (81 mg, 0.61 mmol, 1.2 eq.) under argon atmosphere at room temperature. The reaction was monitored by TLC. After completion of the reaction (20 h), it was washed with 1N HCl and saturated NaCl solution, dried over Na_2SO4 and concentrated under reduced pressure. The resulting residue was purified by silica gel column chromatography (gradient from 0.5% MeOH to 1% MeOH in DCM) yielding **309** (192 mg, 75%) as an off white solid.

^{1}H NMR (300 MHz, $CDCl_3$) δ 6.90 (s, 1H, CH_{cou}), 6.66 (s, 1H, CH_{cou}), 6.62 (t, J = 5.3 Hz, 1H, OCH), 6.43 (t, J = 5.5 Hz, 1H, NH), 3.28 (dd, J = 13.1, 6.7 Hz, 2H, CH_2), 2.90 (d, J = 5.3 Hz, 2H, CH_2), 2.48 (s, 3H, CH_3), 2.20 (t, J = 7.3 Hz, 2H, CH_2), 1.66 – 1.47 (m, 4H, 2x CH_2), 1.40 (s, 9H, $C(CH_3)_3$), 1.38 – 1.28 (m, 2H, CH_2).

^{13}C NMR (75 MHz, $CDCl_3$) δ 173.08 (C=O), 166.45 (C=O), 157.26 (C=O), 151.10 (C-Me), 150.82 (C_{cou}), 148.62 (C_{cou}), 145.23 (C_{cou}), 113.49 (C_{cou}), 111.21 (CH_{cou}), 109.98 (C-Br), 102.49 (CH_{cou}), 97.97 (OCH), 80.18 ($C(Me)_3$) , 42.06 (CH_2), 39.43 (CH_2), 35.30 (CH_2), 28.96 (CH_2), 28.10 (CH_3), 26.22 (CH_2), 24.49 (CH_2), 20.01 (CH_3).

UPLC-MS (ESI): $C_{23}H_{28}BrNO_7Na$ $[M+Na]^+$: m/z Calc.: 532.1, found: 532.1

2,5-dioxopyrrolidin-1-yl 6-(2-(7-bromo-8-methyl-6-oxo-6H-[1,3]dioxolo[4,5-g]chromen-2-yl)acetamido)hexanoate (310)

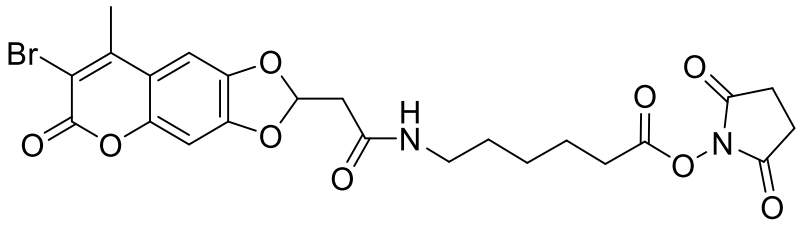

Under argon atmosphere, **307** (0.050 g, 0.11 mmol, 1 eq.) was dissolved in dry DCM (10 mL) and DMAP (26.9 mg, 0.22 mmol, 2 eq.), as well as N-hydroxysuccinimide (25.3 mg, 0.22 mmol, 2 eq) were added. At 0°C, EDC.HCl (46.4 mg, 0.242 mmol, 2.2 eq.) was added and the mixture was stirred for 1h at 0°C then at RT for overnight with protection from light. Then, TLC and UPLC-MS indicated complete conversion of the starting material.

The reaction mixture was diluted with DCM (25 mL) and washed with 0.5 M KHSO4 (2x 20 mL) and brine (20 mL). The organic layer was dried (Na_2SO_4), filtered and evaporated to dryness. The obtained material was directly used without further purification.
UPLC-MS (ESI): $C_{23}H_{23}BrN_2O_9$ $[M+H]^+$: m/z Calc.: 551.1, found: 551.1

4.10.6 Chemical synthesis of 7-methoxy-coumarin-3-carboxylic acid

2-hydroxy-4-methoxybenzaldehyde (311)

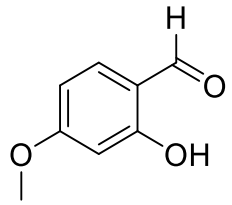

To a solution of 3-methoxyphenol (6.2g 50.0 mmol, 1 eq.), magnesium chloride (7.17 g, 75.0 mmol, 1.5 eq.) in dry THF (150 mL) was added triethylamine (27.2 µL, 112.5 mmol, 2.25 eq.). The mixture was stirred at room temperature for 15 min, and then was added dry Parafomaldehyde (7.50 g, 250.0 mmol, 5 eq.) in one portion. The mixture was heated to reflux overnight until the starting material consumed as monitored by TLC, cooled to ambient temperature, and quenched with diluted HCl (3N) until pH = 2. The resulting solution was extracted with ethyl acetate (2 × 50 mL), and the combined organic layers were washed with brine, dried over magnesium sulfate, filtered and concentrated under reduced pressure. The residue was purified by flash column chromatography on silica gel eluting with cyclohexane-ethyl acetate (95:5 to 75:25) to give the desired product as colorless oil (7.5 g, 98.5%).

^{1}H NMR (500 MHz, $CDCl_3$) δ 11.49 (s, 1H), 9.72 (s, 1H), 7.43 (d, J = 8.7 Hz, 1H), 6.54 (dd, J = 8.7, 2.4 Hz, 1H), 6.43 (d, J = 2.3 Hz, 1H), 3.86 (s, 3H).

^{13}C NMR (126 MHz, $CDCl_3$) δ 194.35, 166.89, 164.20, 135.05, 115.20, 108.34, 100.46, 55.26.
UPLC-MS (ESI): $C_8H_9O_3$ $[M+H]^+$: m/z Calc.: 153.1, found: 153.1

7-methoxy-2-oxo-2H-chromene-3-carboxylic acid (312)

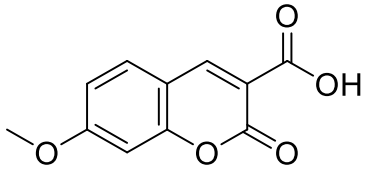

An oven-dried screw cap test tube was first charged with a magnetic stir bar, 2-hydroxy-4-methoxybenzaldehyde **311** (2.7g, 17.7 mmol, 1eq.), Meldrum's acid (2.6 g, 17.7 mmol 1eq.), distilled water (100 mL), and sodium azide (576.6 mg, 8.8mol, 0.5 eq.). The whole mixture was then stirred vigorously at room temperature for 1 h to complete the conversion. Upon completion, the resulting solution was acidified with chilled acid−water, when solid mass precipitated out, filtered off, and thoroughly washed with water to obtain the target product as pale yellow solid (3.9 g, Quantitative yield).

^{1}H NMR (500 MHz, DMSO) δ 8.71 (s, 1H), 7.82 (d, J = 8.7 Hz, 1H), 7.05 – 6.95 (m, 2H), 3.89 (s, 3H).

^{13}C NMR (126 MHz, DMSO) δ 164.18, 157.25, 156.91, 149.11, 131.58, 113.82, 113.32, 111.68, 100.29, 56.26.

UPLC-MS (ESI): $C_{11}H_9O_5$ $[M+H]^+$: m/z Calc.: 221.0, found: 221.1

2,5-dioxopyrrolidin-1-yl 7-methoxy-2-oxo-2H-chromene-3-carboxylate (313)

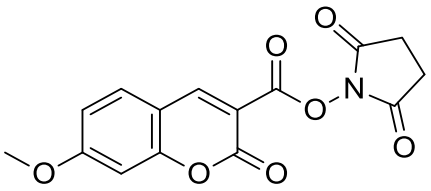

To a solution of 7-methoxycoumarin-3-carboxylic acid **312** (750 mg, 3.4 mmol, 1eq.) in dry DMF (10 ml) N-hydroxysuccinimide (392 mg, 3.4 mmol, 1eq.) was added. After dissolution, the reaction mixture was cooled at 0 °C for 1 h. DCC (771.7 mg, 3.74 mmol, 1.1 eq.) was added. After stirring for 30 min at this temperature, the reaction mixture was stirred at room temperature for 2.5 h. The solution was filtered off to remove dicyclohexylurea. An isopropanol–hexane solution (1: 20) was added to the filtrate to give product as a white solid (607 mg, 56%).

^{1}H NMR (500 MHz, $CDCl_3$) δ 8.70 (s, 1H), 7.50 (d, J = 8.8 Hz, 1H), 6.85 (dd, J = 8.7, 2.4 Hz, 1H), 6.75 (d, J = 2.3 Hz, 1H), 3.83 (s, 3H), 2.80 (s, 4H).

^{13}C NMR (126 MHz, $CDCl_3$) δ 169.66, 166.80, 158.23, 156.30, 152.34, 131.88, 114.79, 111.38, 107.92, 100.46, 56.23, 25.53.

UPLC-MS (ESI): $C_{15}H_{12}NO_7$ $[M+H]^+$: m/z Calc.: 318.0, found: 318.1

6-(7-methoxy-2-oxo-2H-chromene-3-carboxamido)hexanoic acid (314)

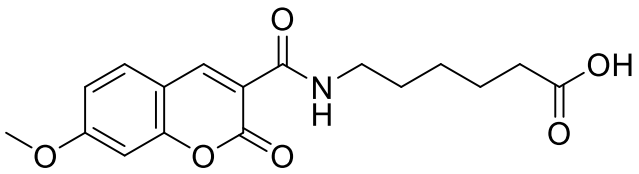

In an argon atmosphere, 6-aminohexanoic acid (82.7 g, 0.63 mmol, 1 eq.) was dissolved in dry DMF (6.5 mL) and dry DIPEA (128 µL, 0.757 mmol, 1.2 eq.) was added. At 0°C, 7-methoxycoumarin-3-carboxylic acid N-succinimidyl ester **313** (200mg, 0.63mmol, 1eq.) was added and stirring was continued overnight with protection from light at RT. Then, TLC and UPLC-MS indicated complete conversion of the starting material. The reaction mixture was diluted with 50 mL EA and washed with 10% acetic acid (3x 10 mL) and then with brine (10 mL). The organic layer was dried (Na_2SO_4), filtered and evaporated to dryness. the product was purified using column chromatography (DCM:MeOH= 9 :1) which yielded the title compound as a colorless solid (189 mg, 90%).

^{1}H NMR (500 MHz, $CDCl_3$) δ 8.85 (s, 1H), 8.81 (t, J = 5.4 Hz, 1H), 7.58 (d, J = 8.7 Hz, 1H), 6.93 (dd, J = 8.7, 2.4 Hz, 1H), 6.86 (d, J = 2.4 Hz, 1H), 3.91 (s, 3H), 3.45 (dd, J = 13.0, 7.1 Hz, 2H), 2.37 (t, J = 7.5 Hz, 2H), 1.67 (ddt, J = 19.5, 15.0, 7.5 Hz, 4H), 1.45 (tt, J = 10.2, 6.4 Hz, 2H).

^{13}C NMR (126 MHz, $CDCl_3$) δ 178.39, 164.83, 162.18, 161.92, 156.64, 148.40, 130.99, 114.72, 114.04, 112.47, 100.29, 56.03, 39.59, 33.76, 29.12, 26.43, 24.35.

UPLC-MS (ESI): $C_{17}H_{18}NO_6$ $[M-H]^-$: m/z Calc.: 332.1, found: 332.0

2,5-dioxopyrrolidin-1-yl 6-(7-methoxy-2-oxo-2H-chromene-3-carboxamido) hexanoate (315)

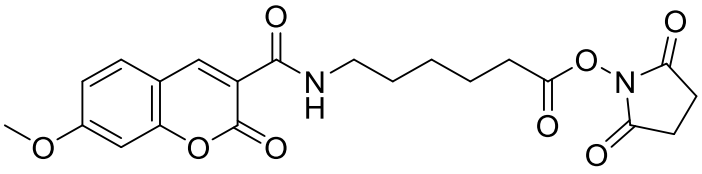

In an argon atmosphere, **314** (100 mg, 0.3 mmol, 1 eq.) was dissolved in dry DCM (14.5 ml) and DMAP (44 mg, 0.36 mmol, 1.2 eq.), as well as N-hydroxysuccinimide (41.5 mg, 0.36 mmol, 1.2 eq.) were added. At 0°C, EDC (115 mg, 0.6 mmol, 2 eq.) was added and stirring was continued for overnight with protection from light and gradual warming to RT. Then, TLC and UPLC-MS indicated complete conversion of the starting material. The reaction mixture was diluted with 40 mL DCM and washed with 0.5 M $KHSO_4$ (2x 50 mL) and brine (20 mL).

The organic layer was dried (Na_2SO_4), filtered and evaporated to dryness. The obtained material was directly used without further purification assuming complete conversion.
UPLC-MS (ESI): $C_{21}H_{23}N_2O_8$ $[M+H]^+$: m/z Calc.: 431.1, found: 431.1

4.10.7 Chemical synthesis of the NBD derivatives fluorophores

N-(2-(dimethylamino)ethyl)-7-nitrobenzo[c][1,2,5]oxadiazol-4-amine (316)

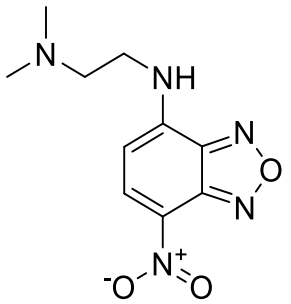

In a 50 mL round-bottom flask, N,N-dimethylethyl-1,2-diamine (0.276 ml, 2.52 mmol, 1.01 eq.) and $NaHCO_3$ (210 mg, 2.5 mmol, 1 eq.) were dissolved in 10 mL of MeCN. To the stirring mixture was added dropwise a solution of 4-chloro-7-nitrobenz-2-oxa-1,3-diazole (NBD) (500 mg, 2.5 mmol, 1 eq.) in 20 mL of MeCN over 1 h. The color turned dark brown. The mixture was heated at 60 °C for 15 min. The reaction mixture was cooled to room temperature, filtered to remove particulates, and concentrated in vacuo. The product was purified via chromatography on silica gel (1:9 MeOH/DCM) and concentrated in vacuo to yield a brown solid (400 mg, 64% yield).

^{1}H NMR (400 MHz, CD_3CN) δ 8.48 (d, J = 8.8 Hz, 1H), 6.28 (d, J = 8.8 Hz, 1H), 3.56 (s, 2H), 2.66 (t, J = 6.1 Hz, 2H), 2.29 (s, 6H).

^{13}C NMR (126 MHz, DMSO) δ 145.12, 137.92, 136.20, 120.85, 119.16, 99.35, 56.27, 44.89, 41.09.
UPLC-MS (ESI): $C_{10}H_{14}N_5O_3$ $[M+H]^+$: m/z Calc.: 252.1, found: 252.1

4-azido-7-nitrobenzo[c][1,2,5]oxadiazole ‘’azido-NBD’’ (317)

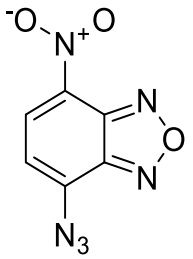

Sodium azide (486 mg, 7.474 mmol, 3.0 eq.) was dissolved in 50 mL of H_2O/acetone (1:1, v/v) in a 250 mL round bottom flask. Then a solution of NBD chloride (500 mg, 2.5 mmol, 1.0 eq.) in acetone (25 mL) was added into the flask dropwise at room temperature with stirring. The reaction mixture turned from light yellow to yellow-brown. After 15 min, TLC (EA: CH 1:2) monitoring revealed complete conversion. The reaction mixture was concentrated under vacuum to remove acetone. The yellow precipitates were filtered out and washed with water (15 mL X 3) and then dried to give **317** as yellow crystals (465 mg, 90%).

^{1}H NMR (500 MHz, $CDCl_3$) δ 8.50 (d, J = 8.1 Hz, 1H), 7.06 (d, J = 8.1 Hz, 1H).

^{13}C NMR (126 MHz, $CDCl_3$) δ 146.04, 143.70, 138.22, 132.22, 115.01.

UPLC-MS (ESI): $C_6H_3N_6O_3$ $[M+H]^+$: m/z Calc.: 207.0, found: 207.1

2-azidoethan-1-amine (318)

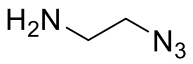

A mixture of 2-bromo-ethylamin hydrobromide (700 mg, 3.42 mmol, 1 eq.) and sodium azide (666.3 mg, 10.25 mmol, 3 eq.) in water (10 mL) was stirred at 75 °C overnight. Then the mixture was poured into 1 N NaOH (5 mL) and the resulting mixture was extracted with diethyl ether (20 mL × 3). The combined organic layers were washed with brine, dried over anhydrous $MgSO_4$ and concentrated smoothly to give the product as a light yellow oil (123 mg, 42%).

^{1}H NMR (500 MHz, $CDCl_3$) δ 3.38 – 3.30 (m, 2H), 2.89 – 2.82 (m, 2H), 1.42 (s, 2H).

^{13}C NMR (126 MHz, $CDCl_3$) δ 54.77, 41.46.

UPLC-MS (ESI): $C_2H_7N_4$ $[M+H]^+$: m/z Calc.: 87.1, found: 87.1

N-(2-bromoethyl)-7-nitrobenzo[c][1,2,5]oxadiazol-4-amine (319)

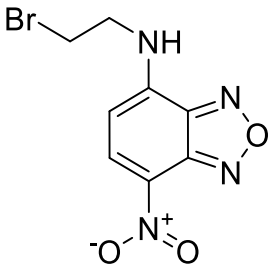

The ethanol solution of 2-bromoethylamine prepared by mixing 2-bromoethylamine hydrobromide (300 mg, 1.46 mmol, 1 eq.) with NaOH (131.7 mg, 3.29 mmol, 2.25 eq.) in 15 mL anhydrous ethanol was added dropwise into 15 mL of anhydrous ethanol containing 4-chloro-7-nitrobenz-2-oxa-1,3-diazole (NBD) (292 mg, 1.46 mmol,1 eq.) with stirring under reflux. TLC (EA: CH 1:2) monitoring found the reaction was finished in 4 h and the resulted green mixture was cooled to room temperature. The solvent was removed by evaporation in vacuo. The resulting residue was purified by column chromatography starting with 2:1 CH/EA to wash NBD residuals then 1:1 to get the product (291 mg, 70% yield).

^{1}H NMR (400 MHz, $CDCl_3$) δ 8.50 (d, J = 8.5 Hz, 1H), 6.43 (s, 1H), 6.26 (d, J = 8.5 Hz, 1H), 3.98 (q, J = 6.0 Hz, 2H), 3.70 (t, J = 6.0 Hz, 2H).

^{13}C NMR (101 MHz, $CDCl_3$) δ 144.54, 143.97, 143.11, 136.06, 125.40, 99.22, 45.11, 29.20.

UPLC-MS (ESI): $C_8H_8BrN_4O_3$ $[M+H]^+$: m/z Calc.: 287.0, found: 287.0

N-(2-azidoethyl)-7-nitrobenzo[c][1,2,5]oxadiazol-4-amine (320)

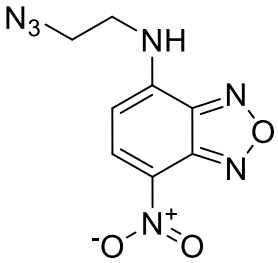

N- (2-Bromoethyl)-7-nitrobenzo[c][1,2,5]oxadiazol-4-amine **319** (100 mg, 0.35 mmol, 1.0 eq.) and NaN_3 (68 mg, 1.04 mmol, 3.0 eq.) were dissolved in DMF (5 mL). The mixture was stirred at 80 °C for 4 h and at RT for 15h. H_2O (20 mL) was added, the aqueous phase was extracted with Et_2O (3 × 50 mL), the combined organic layers were dried over $MgSO_4$ and the solvents were removed in vacuo to provided azide **320** as an orange solid (81 mg, 93% yield).

^{1}H NMR (400 MHz, DMSO) δ 9.49 (s, 1H), 8.51 (d, J = 8.9 Hz, 1H), 6.50 (d, J = 8.9 Hz, 1H), 3.67 (s, 4H).

UPLC-MS (ESI): $C_8H_8N_7O_3$ $[M+H]^+$: m/z Calc.: 250.1, found: 250.1

4.10.8 Chemical synthesis of the visible light range fluorophores

N-(2-azidoethyl)-5(6)-fluorescein-carboxoamide (321)

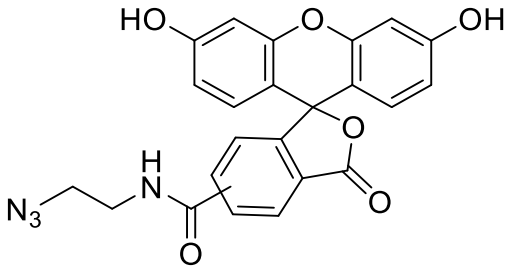

5(6)-carboxyfluorescein (50 mg, 0.13 mmol, 1 eq.) and triethylamine (30 µL, 0.2 mmol, 1.5 eq.) were dissolved in 1 mL of DMSO, followed by addition of TSTU (160 mg, 0.5 mmol, 4 eq.) The reaction mixture was stirred at RT for 30 min Then 2-azidoethanamine 318 (93.7 µl, 1.06 mmol, 8 eq.) was added and the mixture was stirred overnight at room temperature. Triethylamine and azidoaminoethane were evaporated under reduced pressure. Product was purified by column chromatography on silica gel using linear gradient of methanol in dichloromethane (3–10%) with the addition of 0.1ml acetic acid /100 ml mobile phase to give the product as an orange solid (47mg, 80%).

^{1}H NMR (500 MHz, MeOD) δ 8.35 (s, 1H), 8.11 (dd, J = 8.0, 1.6 Hz, 1H), 8.05 (dd, J = 8.1, 1.4 Hz, 1H), 8.00 (d, J = 8.1 Hz, 1H), 7.53 (s, 1H), 7.22 (d, J = 8.1 Hz, 1H), 6.62 (d, J = 1.8 Hz, 2H), 6.53 (dd, J = 8.6, 3.7 Hz, 2H), 6.46 (d, J = 8.7 Hz, 2H), 3.56 – 3.37 (m, 2H), 3.35 – 3.22 (m, 2H).

^{13}C NMR (126 MHz, MeOD) δ 168.73, 168.51, 154.30, 137.60, 135.24, 130.39, 130.35, 130.25, 129.86, 126.52, 126.03, 125.13, 124.33, 114.08, 111.19, 111.04, 103.64, 51.37, 51.16, 40.78, 40.63, 40.43.

UPLC-MS (ESI): $C_{23}H_{17}N_4O_6$ $[M+H]^+$: m/z Calc.: 445.1, found: 445.1

2,5-dioxopyrrolidin-1-yl 6-((9-(diethylamino)-5-oxo-5H-benzo[a]phenoxazin-2-yl)oxy) hexanoate (322)

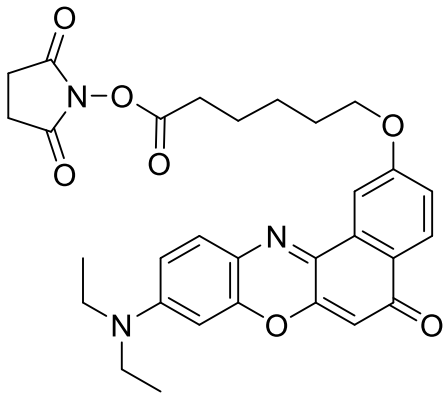

Under argon atmosphere, Nile red labeled Hexane acid (50 mg, 0.11 mmol, 1 eq.), HOSu (15.5 mg, 0.13 mmol, 1.2 eq.) and DMAP (15.9 mg, 0.13 mmol, 1.2 eq.) were dissolved in 2 ml dry DCM. EDC.HCl (42.2 mg, 0.22 mmol, 2 eq.) was added portionwise to the first mixture at 0°C. After 10 min the ice bath was removed and stirring was continued at RT for 4.5 h. Then, the reaction was quenched and the mixture was washed twice with 10 mL 0.5 M aq. KHSO4 and 10 mL H_2O. The organic layer was dried ($MgSO_4$), evaporated to dryness and the crude product was used directly for the next step without further purification.

UPLC-MS (ESI): $C_{30}H_{32}N_3O_7$ $[M+H]^+$: m/z Calc.: 546.2, found: 546.2

4.10.9 Chemical synthesis of the labeled sphingomyelin analogs

4-((2*S*,3*R*,*E*)-2-(*tert*-butyloxycarbonylamino)-3-(methoxymethoxy)octadec-4-en-1 phosphoethylamino)-7-nitrobenzo-2-oxa-1,3-diazol (401)

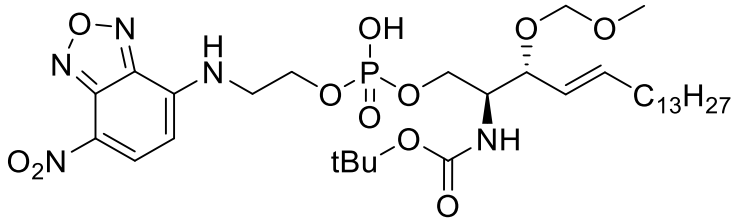

The primary amine **212** (250 g, 0.44 mmol, 1 eq.) was dissolved in 10 mL MeOH/$CHCl_3$ (1:3). DIPEA (300 µL, 1.76 mmol, 4 eq.) and. NBDCl (264 mg, 1.32 mmol, 3 eq.) were added and stirring was continued at RT away from light. After 4 h, all volatiles were evaporated under a stream of air and the residue was dissolved in 20 mL $CHCl_3$. The solution was washed twice with 0.1 M aq. HCl (25 mL each) with $CHCl_3$ backwash. The organic fractions were collected and evaporated in vacuo. The orange crude obtained was subjected to column chromatography ($CHCl_3$:MeOH:H_2O = 100:15:1 → 66:10:1 to afford (270 mg , 85%) of the title product as a yellowish brown solid.

^{1}H NMR (400 MHz, $CDCl_3$) δ 8.23 (d, *J* = 8.6 Hz, 1H), 6.05 (d, *J* = 8.0 Hz, 1H), 5.59 – 5.23 (m, 1H), 5.02 (dd, *J* = 14.8, 8.0 Hz, 1H), 4.38 (d, *J* = 6.4 Hz, 1H), 4.30 – 4.18 (m, 6H), 3.94 (s, 1H), 3.81 – 3.71 (m, 2H), 3.52 (s, 2H), 3.07 (s, *J* = 6.4 Hz, 3H), 1.77 (d, *J* = 6.6 Hz, 2H), 1.14 (s, 9H), 0.99 (s, 22H), 0.62 (t, *J* = 6.6 Hz, 3H).

^{13}C NMR (101 MHz, $CDCl_3$) δ 156.14, 144.12, 137.46, 136.93, 125.58, 98.50, 93.28, 79.24, 76.35, 64.39, 62.64, 55.09, 53.74, 32.05, 31.58, 29.32, 29.14, 29.01, 28.93, 28.79, 27.83, 22.31, 13.56.

^{31}P NMR (162 MHz, $CDCl_3$) δ -1.42.

UPLC-MS (ESI): $C_{33}H_{55}N_5O_{11}P$ $[M-H]^-$: m/z Calc.: 728.4, found: 728.2

(2S,3R,E)-2-(6-(2-(7-bromo-8-methyl-6-oxo-6H-[1,3]dioxolo[4,5-g]chromen-2-yl) acetamido)hexanamido)-3-hydroxyoctadec-4-en-1-yl(2-((7-nitrobenzo[c][1,2,5] oxadiazol-4-yl)amino)ethyl) hydrogen phosphate (ZP-403)

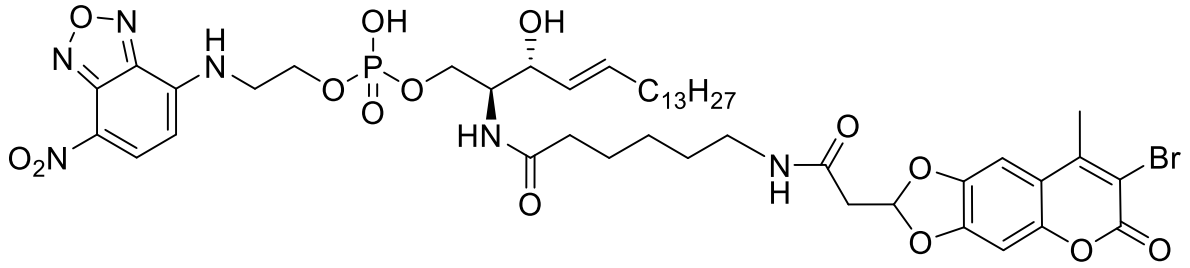

In an argon atmosphere, **401** (46 mg, 0.063 mmol, 1 eq.) was dissolved in MeOH (6 mL). At rt, 4 M HCl in 1,4-dioxan (081.5 µL, 1.56 mmol, 25 eq.) was added and the mixture was stirred at 70°C for 2 h with exclusion of light. Then, UPLC-MS and TLC indicated complete conversion of the starting material. The mixture was concentrated in a stream of air and dried under high vacuum. The orange residue **402** was dissolved in dry DCM (4 mL) and dry DIPEA (85 µL, 0.49 mmol, 8 eq.). **310** (0.045g, 0.08 mmol, 1.3 eq.) was dissolved in dry DCM (3 mL) and added dropwise to the first solution at 0°C. After 24 h stirring at RT, UPLC-MS and TLC showed complete conversion. MeOH (1 mL) was added to quench the reaction and left to stir for 1 h. The reaction mixture was diluted with CH_2Cl_2 (75 mL) and washed twice with 10 mL 0.1 M aq. HCl. The organic layer was dried (Na_2SO_4), and the volatiles were removed in vacuo. The material obtained was purified using preparative TLC ($CHCl_3$:MeOH:H_2O = 65:25:3) to give the final probe as an orange solid (25 mg, 39%).

^{1}H NMR (500 MHz, $CDCl_3$+CD_3OD+TMS) δ 8.48 (d, *J* = 8.5 Hz, 1H), 7.44 (s, 1H), 7.03 (d, *J* = 3.8 Hz, 1H), 6.80 (s, 1H), 6.65 (t, *J* = 4.9 Hz, 1H), 6.25 (s, 1H), 5.77 – 5.59 (m, 1H), 5.43 (dd, *J* = 15.3, 7.2 Hz, 1H), 4.20 (d, *J* = 3.3 Hz, 2H), 4.15 – 4.07 (m, 2H), 3.97 (s, 1H), 3.89 (s, 1H), 3.69 (s, 1H), 3.36 (s, 1H), 3.24 (s, 2H), 2.93 (d, *J* = 5.0 Hz, 2H), 2.57 (d, *J* = 3.6 Hz, 3H), 2.21 (dd, *J* = 14.3, 7.1 Hz, 2H), 2.08 – 1.87 (m, 2H), 1.65 – 1.58 (m, 2H), 1.55 – 1.45 (m, 2H), 1.25 (s, 26H), 0.89 (d, *J* = 6.6 Hz, 3H).

^{13}C NMR (126 MHz, $CDCl_3$+CD_3OD+TMS) δ 174.67, 167.81, 158.32, 152.23, 151.37, 149.01, 145.76, 134.63, 129.06, 114.00, 111.54, 109.92, 102.92, 98.19, 71.78, 64.67, 54.30, 41.66, 39.46, 36.21, 35.94, 32.62, 32.14, 32.08, 29.92, 29.88, 29.79, 29.67, 29.58, 29.54, 29.51, 28.85, 26.39, 25.89, 25.43, 22.89, 20.16, 14.19.

^{31}P NMR (202 MHz, $CDCl_3$+CD_3OD) δ = 5.64 (s, 1P).

UPLC-MS (ESI): $C_{45}H_{61}BrN_6O_{14}P$ $[M-H]^-$: m/z Calc.: 1019.3, found: 1019.1

(2S,3R,E)-3-hydroxy-2-(6-(7-methoxy-2-oxo-2H-chromene-3-carboxamido)hexanamido) octadec-4-enyl 2-(7-nitrobenzo[c][1,2,5]oxadiazol-4-yl amino) ethyl hydrogen phosphate (TP-366)

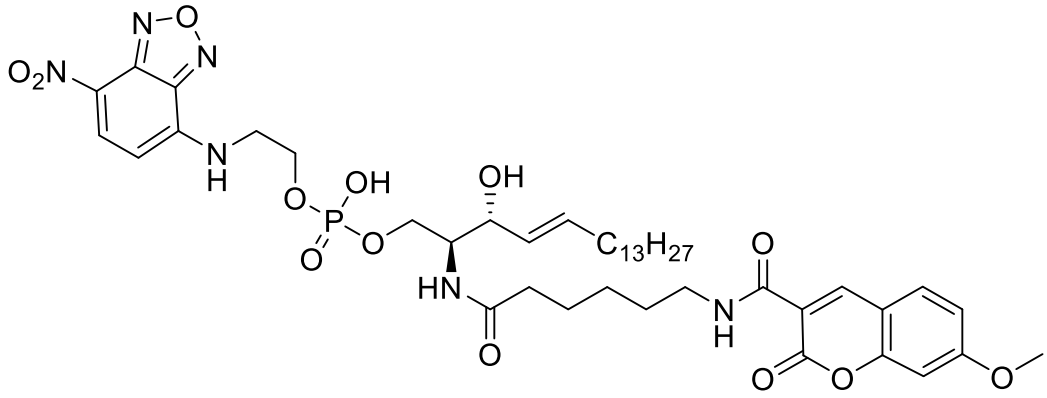

Under argon atmosphere, **401** (50 mg, 0.068 mmol, 1 eq.) was dissolved in MeOH (7 mL). At RT, 4 M HCl in dioxane (427 µL, 1.7 mmol, 25 eq.) was added and the mixture was stirred at 70°C for 2 h with exclusion of light. Then, UPLC-MS and TLC indicated complete deprotection of the starting material. The mixture was concentrated in a stream of air and dried under high vacuum. The orange residue **402** was dissolved in dry DCM (7 mL) and dry DIPEA (93.2 µL, 0.54 mmol, 8 eq.). The active ester **315** (68 mg, 0.016 mmol, 2.3 eq.) is added portion wise to the first solution at 0°C. After 20 h stirring at RT, UPLC-MS and TLC showed complete conversion. The reaction was quenched and worked up as reported. The material obtained was subjected to preparative TLC (DCM: MeOH: H_2O = 100:15:1) to get the title compound as an orange solid (15 mg, 24%). NMR spectra as reported[121].

UPLC-MS (ESI): $C_{43}H_{62}N_6O_{13}P$ $[M+H]^+$: m/z Calc.: 901.4, found: 901.2

(2S,3R,E)-2-dodecanamido-3-hydroxyoctadec-4-en-1-yl (2-((7-nitrobenzo[c][1,2, 5]oxadi -azol-4-yl)amino)ethyl) hydrogen phosphate (TP-367)

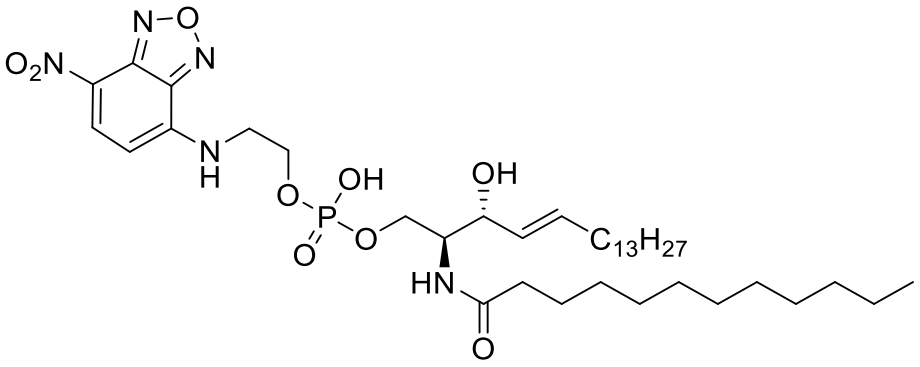

In an argon atmosphere, **401** (50 mg, 0.068 mmol, 1 eq.) was dissolved in MeOH (4 mL). At RT, 4 M HCl in dioxane (427 µL, 1.7 mmol, 25 eq.) was added and the mixture was stirred at 70°C for 3 h with exclusion of light. Then, UPLC-MS and TLC indicated complete deprotection of the starting material. The mixture was concentrated in a stream of air and dried under high vacuum. The orange residue **402** was dissolved in dry DCM (3 mL) and dry DIPEA (174.75 µL, 1.01 mmol, 15 eq.). Lauric acid N-hydroxysuccinimide ester (68 mg, 0.016 mmol, 2.3 eq.) was added portion wise to the first solution at 0°C. After 24 h stirring at RT, UPLC-MS and TLC showed complete conversion. MeOH (1 ml) was added to quench the reaction and left to stir for 1 h. The reaction mixture was diluted with DCM (40 mL) and washed twice with 10 mL 0.1 M aq. HCl then one time with brine. The organic layer was dried (Na_2SO_4), and the volatiles were removed in vacuo. The crude mixture was purified using column chromatography ($CHCl_3$:MeOH:H_2O = 100:15:1 →65:25:3) and the product was collected as an orange solid (23,8 mg, 45%).

^{1}H NMR (500 MHz, $CDCl_3$+CD_3OD) δ 8.51 (d, J = 8.0 Hz, 1H), 7.73 (dd, J = 5.7, 3.2 Hz, 1H), 7.59 (dd, J = 5.7, 3.2 Hz, 1H), 6.27 (s, 1H), 5.71 (dd, J = 14.4, 7.4 Hz, 1H), 5.45 (dd, J = 14.7, 6.8 Hz, 1H), 4.16 (s, 4H), 3.99 (s, 1H), 3.90 (s, 1H), 3.68 (dd, J = 18.2, 11.7 Hz, 2H), 2.18 (t, J = 7.5 Hz, 2H), 2.02 (d, J = 6.7 Hz, 2H), 1.58 (s, 2H), 1.27 (s, 39H), 0.91 – 0.88 (m, 6H).

^{13}C NMR (126 MHz, $CDCl_3$+CD_3OD) δ 168.41, 134.87, 131.40, 129.04, 68.46, 57.42, 54.07, 39.01, 36.67, 32.15, 29.94, 29.59, 29.17, 26.16, 24.04, 23.18, 22.89, 14.18.

^{31}P NMR (202 MHz, $CDCl_3$+CD_3OD) δ 3.95.

UPLC-MS (ESI): $C_{38}H_{65}N_5O_9P$ $[M-H]^-$: m/z Calc.: 766.5, found: 766.2

(2S,3R,E)-2-(tert-butoxycarbonyl)-3-(methoxymethoxy)octadec-4-enyl 2-(dimethyl((1-(2-(7-nitrobenzo[c][1,2,5]oxadiazol-4-ylamino)ethyl)-1H-1,2,3-triazol-4-yl)methyl) ammonio)ethyl phosphate (406)

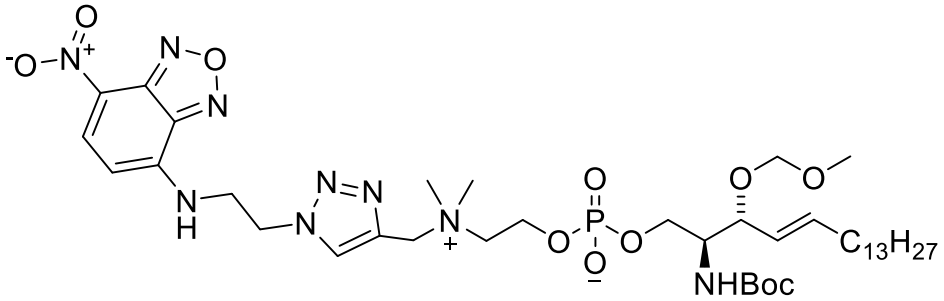

Propargyl-sphingomyelin **214** (10 mg, 0.016 mmol, 1eq.) was dissolved in a mixture of t-BuOH/H_2O 4:1 (1.25 ml) before azide **320** (4.7 mg, 0.019 mmol, 1.2eq.), sodium ascorbate (0.95 mg, 0.0048 mmol.0.3eq.) and copper sulfate hydrate (0.8 mg, 0.003 mmol,0.2 eq.) were successively added. The reaction mixture, covered with foil, was stirred 48 h at room temperature, concentrated in vacuo and purified by flash chromatography on silica (85/14/1 then 80/18/2 then 72/25/3 $CHCl_3$/MeOH/NH_4OH) to give the NBD-labeled sphingomyelin as a yellow solid (11.5 mg, 83%).

^{1}H NMR (500 MHz, MeOD) δ 8.40 (t, J = 9.0 Hz, 1H), 8.31 (s, 1H), 6.30 (d, J = 8.8 Hz, 1H), 5.63 (dt, J = 15.2, 6.7 Hz, 1H), 5.21 (dd, J = 15.4, 8.6 Hz, 1H), 4.75 (d, J = 6.0 Hz, 2H), 4.64 (s, 2H), 4.57 (d, J = 6.6 Hz, 1H), 4.40 (d, J = 6.6 Hz, 1H), 4.23 (s, 2H), 4.08 (d, J = 10.1 Hz, 4H), 4.04 (s, 2H), 3.95 (t, J = 8.1 Hz, 2H), 3.64 (s, J = 6.8 Hz, 1H), 3.45 (s, 2H), 3.25 (s, 3H), 3.08 (s, 6H), 1.95 (dd, J = 13.8, 6.8 Hz, 2H), 1.38 – 1.26 (m, 11H), 1.23 – 1.15 (m, 20H), 0.79 (t, J = 4.5 Hz, 3H).

^{13}C NMR (126 MHz, MeOD) δ 158.29, 158.01, 145.95, 145.47, 138.57, 138.08, 136.93, 130.53, 127.88, 124.42, 94.57, 80.08, 77.73, 65.91, 64.48, 60.36, 60.17, 56.08, 55.67, 52.11, 33.43, 33.08, 30.79, 30.77, 30.71, 30.61, 30.47, 30.32, 30.26, 28.85, 23.74, 14.44.

^{31}P NMR (202 MHz, MeOD) δ -0.93.

UPLC-MS (ESI): $C_{40}H_{69}N_9O_{11}P$ $[M]^+$: m/z Calc.: 882.5, found: 882.3

2-(dimethyl((1-(2-(7-nitrobenzo[c][1,2,5]oxadiazol-4-ylamino)ethyl)-1H-1,2,3-triazol-4-yl)methyl)ammonio)ethyl (2S,3R,E)-3-hydroxy-2-(6-(7-methoxy-2-oxo-2H-chromene-3-carboxamido)hexanamido)octadec-4-enyl phosphate (ZQP-407)

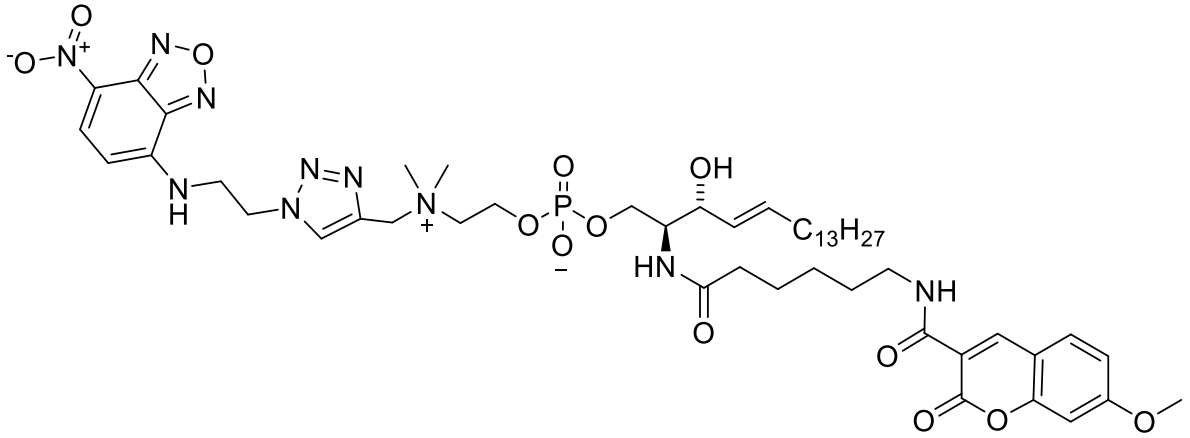

In an argon atmosphere, **406** (11.5 mg, 0.013 mmol, 1 eq.) was dissolved in MeOH (3 mL). At rt, 4 M HCl in 1,4-dioxan (081.5 µL, 0.325 mmol, 25 eq.) was added and the mixture was stirred at 70°C for 2 h with exclusion of light. Then, UPLC-MS and TLC indicated complete conversion of the starting material. The mixture was concentrated in a stream of air and dried under high vacuum. The orange residue was dissolved in dry CH_2Cl_2 (2 mL) and dry DIPEA (22.5 µL, 0.13 mmol, 10 eq.). **315** (0.0073g, 0.017 mmol, 1.3 eq.) was dissolved in dry CH_2Cl_2 (2 mL) and added dropwise to the first solution at 0°C. After 48 h stirring at RT, UPLC-MS and TLC showed complete conversion. MeOH (0.5 mL) was added to quench the reaction and left to stir for 1 h. The reaction mixture was diluted with CH_2Cl_2 (40 mL) and washed twice with 5 mL 0.1 M aq. HCl. The organic layer was dried (Na_2SO_4), and the volatiles were removed in vacuo. The material obtained was subjected to column chromatography (85/14/1 then 80/18/2 then 72/25/3 $CHCl_3$/MeOH/NH_4OH) to give the NBD/Coumarin-labeled sphingomyelin as an orange solid (4.2 mg, 30%).

^{1}H NMR (500 MHz, MeOD) δ 8.74 (s, 1H), 8.47 (d, J = 8.7 Hz, 1H), 8.41 (s, 1H), 7.71 (d, J = 8.8 Hz, 1H), 6.99 (dd, J = 8.7, 2.4 Hz, 1H), 6.95 (d, J = 2.3 Hz, 1H), 6.37 (d, J = 8.8 Hz, 1H), 5.77 – 5.63 (m, 1H), 5.49 (s, 1H), 5.45 (dd, J = 15.3, 7.5 Hz, 1H), 4.84 (d, J = 6.1 Hz, 2H), 4.73 (d, J = 14.2 Hz, 2H), 4.32 (s, 2H), 4.18 – 4.09 (m, 2H), 4.09 – 4.03 (m, 2H), 4.03 – 3.95 (m, 2H), 3.93 (s, 3H), 3.55 (t, J = 4.3 Hz, 2H), 3.41 (t, J = 7.1 Hz, 2H), 3.18 (d, J = 3.6 Hz, 6H), 2.22 (t, J = 7.5 Hz, 2H), 2.01 (dd, J = 14.5, 7.0 Hz, 3H), 1.70 – 1.57 (m, 4H), 1.45 – 1.39 (m, 2H), 1.35 (d, J = 7.2 Hz, 2H), 1.32 – 1.19 (m, 22H), 0.88 (t, J = 7.0 Hz, 3H).

^{13}C NMR (126 MHz, MeOD) δ 175.74, 166.98, 166.81, 164.11, 162.54, 158.10, 149.35, 138.02, 136.96, 135.17, 132.49, 131.10, 130.55, 115.13, 113.58, 101.28, 72.77, 65.90, 65.85, 60.37, 60.18, 56.77, 52.16, 49.85, 40.54, 37.15, 33.44, 33.08, 30.83, 30.79, 30.73, 30.49, 30.42, 30.39, 30.15, 27.68, 26.73, 23.74, 14.44.

^{31}P NMR (202 MHz, MeOD) δ 0.15.

UPLC-MS (ESI): $C_{50}H_{74}N_{10}O_{13}P$ $[M]^+$: m/z Calc.: 1053.5, found: 1053.3

(2S,3R,E)-2-((tert-butoxycarbonyl)amino)-3-(methoxymethoxy)octadec-4-en-1-yl (2-(((1-(2-(3',6'-dihydroxy-3-oxo-3H-spiro[isobenzofuran-1,9'-xanthene]-5(6)-carboxamido) ethyl)-1H-1,2,3-triazol-4-yl)methyl)dimethylammonio) ethyl)phosphate (408)

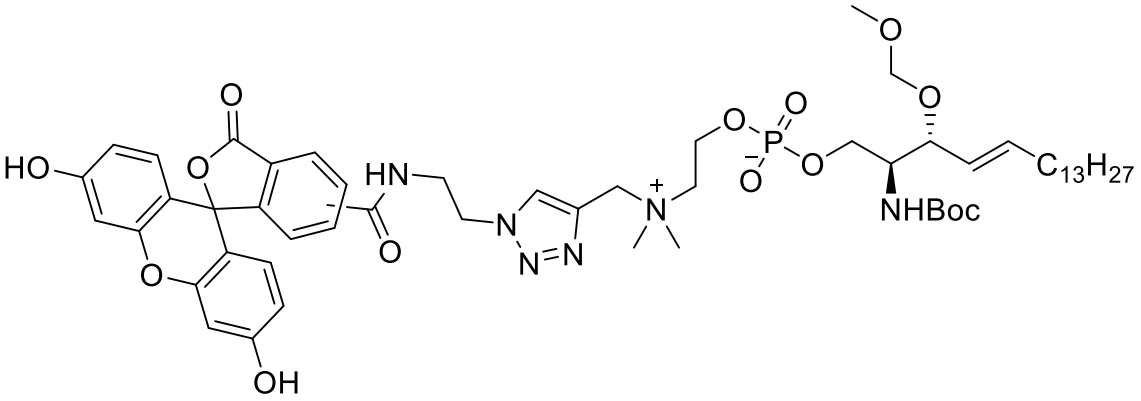

Propargyl-sphingomyelin **214** (6.5 mg, 0.01 mmol, 1eq.) was dissolved in a mixture of DMSO/H_2O 3:1 (1ml) before azide **321** (5.8 mg, 0.013 mmol, 1.3eq.), sodium ascorbate (0.6 mg, 0.003 mmol, 0.3 eq.) and copper sulfate hydrate (0.5 mg, 0.002 mmol,0.2 eq.) were successively added. The reaction mixture, covered with foil, was stirred 48 h at room temperature, concentrated in vacuo and the product was purified by column chromatography on silica gel starting with 5% of methanol in dichloromethane then 10% to elute the excess azide. 65/25/3 $CHCl_3$/MeOH/H_2O mixture* was used to elute the product which then collected as an orange solid (6.5 mg, 54%).

*0.1ml acetic acid /100 ml mobile phase used to avoid tailing on the column.

^{1}H NMR (500 MHz, MeOD) δ 8.49 (s, 0.5H), 8.42 (s, 0.5H), 8.37 (s, 0.5H), 8.13 – 8.06 (m, 0.5H), 8.01 (d, J = 7.6 Hz, 1H), 7.76 – 7.69 (m, 1H), 7.67 – 7.60 (m, 1H), 7.56 (s, 0.5H), 7.34 (d, J = 7.9 Hz, 0.5H), 6.94 (t, J = 9.2 Hz, 3H), 6.66 (t, J = 8.1 Hz, 4H), 6.61 (d, J = 9.8 Hz, 3H), 5.71 (dq, J = 13.0, 6.5 Hz, 1H), 5.37 – 5.24 (m, 1H), 4.79 (s, 2H), 4.77 – 4.74 (m, 12H), 4.72 (s, 2H), 4.70 – 4.64 (m, 4H), 4.49 (t, J = 6.7 Hz, 2H), 4.41 (s, 2H), 4.35 (s, 2H), 4.24 – 4.21 (m, 2H), 4.10 – 3.99 (m, 6H), 3.95 (s, 2H), 3.86 (s, 2H), 3.75 (s, 2H), 3.66 (dd, J = 3.2, 1.8 Hz, 3H), 3.60 – 3.56 (m, 2H), 3.24 (s, 6H), 3.12 (d, J = 3.1 Hz, 3H),

2.38 – 2.28 (m, 2H), 2.22 (d, J = 3.4 Hz, 1H),2.04 (dd, J = 13.3, 6.6 Hz, 4H), 1.74 – 1.66 (m, 2H), 1.65 – 1.57 (m, 4H), 1.30 (s, 9H), 1.29 (s, 22H), 0.96 (t, J = 7.5 Hz, 3H).

^{13}C NMR (126 MHz, MeOD) δ 138.56, 133.59, 132.41, 129.83, 127.92, 104.09, 94.52, 77.69, 69.11, 65.91, 56.09, 51.98,40.18, 33.42, 33.07, 31.62, 31.51, 30.78, 30.76, 30.70, 30.60, 30.46, 30.31, 30.25, 30.14, 28.87, 24.94, 24.03, 23.73, 14.44, 11.40.

^{31}P NMR (202 MHz, MeOD) δ 19.02.

UPLC-MS (ESI): $C_{55}H_{78}N_6O_{14}P$ $[M]^+$: m/z Calc.: 1077.5, found: 1077.3

(*2S,3R,E*)-2-(6-((9-(diethylamino)-5-oxo-5H-benzo[a]phenoxazin-2-yl)oxy) hexanamido)-3-hydroxyoctadec-4-en-1-yl (2-(((1-(2-(3',6'-dihydroxy -3-oxo-3H-spiro[isobenzofuran-1,9'-xanthene]-5(6)-carboxamido)ethyl)-1H-1,2,3-triazol-4-yl)methyl)dimethylammonio) ethyl) phosphate (ZQ_2P-410)

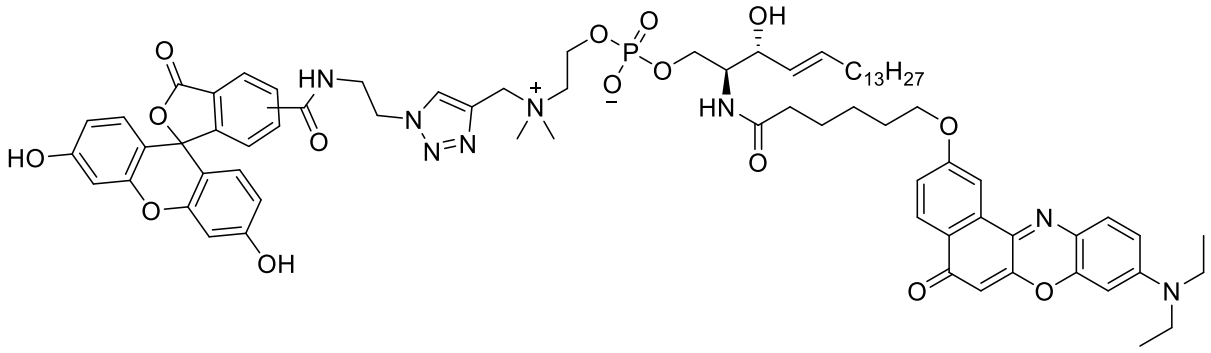

In an argon atmosphere, **408** (5.4 mg, 0.005 mmol, 1 eq.) was dissolved in MeOH/$CHCl_3$ (1.5 mL). At rt, 4 M HCl in 1,4-dioxan (31.5 µL, 0.126 mmol, 25 eq.) was added and the mixture was stirred at 70°C for 3 h with exclusion of light. Then, UPLC-MS and TLC indicated complete conversion of the starting material. The mixture was concentrated in a stream of air and dried under high vacuum. The orange residue **409** was dissolved in dry CH_2Cl_2 (2 mL) and dry DIPEA (17.6 µL, 0.1 mmol, 20 eq.). **322** (4.1 mg, 0.0075 mmol, 1.5 eq.) was dissolved in dry CH_2Cl_2 (1 mL) and added dropwise to the first solution at 0°C. After 48 h stirring at RT, UPLC-MS and TLC showed complete conversion. MeOH (0.5 mL) was added to quench the reaction and left to stir for 1 h. The reaction mixture was diluted with CH_2Cl_2 (10 mL) and washed twice with 5 mL 0.1 M aq. HCl. The organic layer was dried (Na_2SO_4), and the volatiles were removed in vacuo. The crude mixture obtained was subjected to column chromatography ($CHCl_3$/MeOH 95/5 to 90/10) to elute the residual active ester then ($CHCl_3$/MeOH/H_2O* 65/25/3) to give the target product as a violet solid (4.7 mg, 69%).

R_f ($CHCl_3$:MeOH:H_2O^* = 65:25:3) = 0.56

*0.1ml acetic acid /100 ml mobile phase used to avoid tailing on the column or TLC.

^{1}H NMR (500 MHz, DMSO) δ 8.79 (s, 0.5H), 8.48 (s, 0.5H), 8.34 (s, 0.5H), 8.29 (s, 0.5H), 8.06 (d, J = 5.3 Hz, 0.5H), 8.05 – 7.96 (m, 1H), 7.92 (d, J = 2.6 Hz, 0.5H), 7.82 (d, J = 8.7 Hz, 0.5H), 7.73 – 7.62 (m, 1H), 7.59 (dd, J = 9.0, 3.7 Hz, 0.5H), 7.40 (d, J = 17.4 Hz, 0.5H), 7.30 – 7.19 (m, 1H), 6.80 (d, J = 9.3 Hz, 1H), 6.63 (d, J = 2.4 Hz, 1H), 6.54 (d, J = 8.2 Hz, 2H), 6.17 (s, 1H), 5.73 (s, 1H), 5.63 – 5.41 (m, 1H), 5.39 – 5.22 (m, 1H), 4.60 (dd, J = 48.3, 23.7 Hz, 2H), 4.40 (d, J = 33.3 Hz, 1H), 4.19 (ddd, J = 25.6, 12.7, 8.7 Hz, 2H), 4.14 – 4.01 (m, 3H), 3.82 (ddd, J = 147.0, 58.9, 25.6 Hz, 6H), 3.56 – 3.43 (m, 6H), 2.15 – 1.92 (m, 2H), 1.88 – 1.70 (m, 2H), 1.55 (ddd, J = 24.8, 15.8, 6.3 Hz, 2H), 1.43 – 1.30 (m, 2H), 1.30 – 0.96 (m, 22H), 0.91 – 0.68 (m, 9H).

^{31}P NMR (202 MHz, DMSO) δ -0.57.

UPLC-MS (ESI): $C_{74}H_{92}N_8O_{15}P$ $[M]^+$: m/z Calc.: 1363.6, found: 1363.3

2-(((1-(2-(3',6'-dihydroxy-3-oxo-3H-spiro[isobenzofuran-1,9'-xanthene]-5(6)-carboxamido)ethyl)-1H-1,2,3-triazol-4-yl)methyl)dimethylammonio) ethyl ((2S,3R,E)-2-dodecanamido-3-hydroxyoctadec-4-en-1-yl) phosphate (ZQ$_3$P-411)

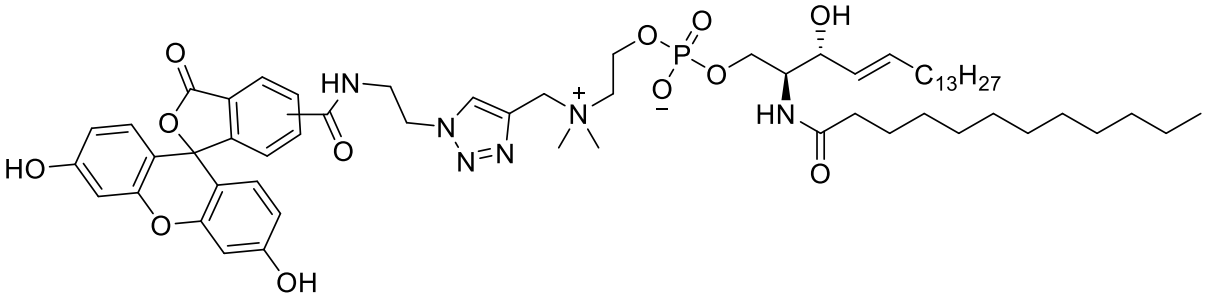

In an argon atmosphere, **408** (5.3 mg, 0.0049 mmol, 1 eq.) was dissolved in MeOH/$CHCl_3$ (1.5 mL). At rt, 4 M HCl in 1,4-dioxan (32 µL, 0.128 mmol, 25 eq.) was added and the mixture was stirred at 70°C for 3 h with exclusion of light. Then, UPLC-MS and TLC indicated complete conversion of the starting material. The mixture was concentrated in a stream of air and dried under high vacuum. The orange residue was dissolved in dry CH_2Cl_2 (2 mL) and dry DIPEA (18 µL, 0.1 mmol, 20 eq.). Lauric acid N-hydroxysuccinimide ester (4.1 mg, 0.0098 mmol, 2 eq.) was dissolved in dry DMF (1 mL) and added dropwise to the first solution at 0°C. After 24 h stirring at RT, UPLC-MS and TLC showed complete conversion. MeOH (0.5 mL) was added to quench the reaction and left to stir for 1 h. The reaction mixture was diluted with CH_2Cl_2 (10 mL) and washed twice with 5 mL 0.1 M aq. HCl. The organic layer was dried (Na_2SO_4), and the volatiles were removed in vacuo. The crude mixture obtained was subjected to preparative TLC (CH_3Cl_3: MeOH: H_2O* = 65:25:3) to get the title compound as an orange solid (3.7 mg, 68%).

R_f ($CHCl_3$:MeOH:H_2O^* = 65:25:3) = 0.57

*0.1ml acetic acid /100 ml mobile phase used to avoid tailing on the column or TLC.

^{31}P NMR (202 MHz, DMSO) δ 0.52, 0.28.

UPLC-MS (ESI): $C_{60}H_{88}N_6O_{12}P$ $[M]^+$: m/z Calc.: 1115.6, found: 1115.4

4.10.10 Synthesis of the reference coumarin labeled ceramide analog

6-(2-(7-bromo-8-methyl-6-oxo-6H-[1,3]dioxolo[4,5-g]chromen-2-yl)acetamido)-N-((2S,3R,E)-1,3-dihydroxyoctadec-4-en-2-yl)hexanamide (413)

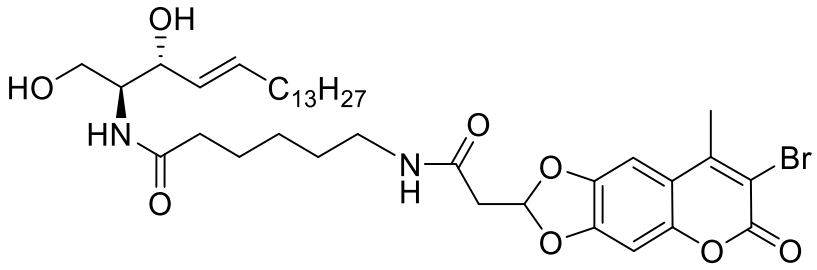

The intermediate **208** (0.020 g, 0.045 mmol, 1 eq.) was dissolved in 5 mL MeOH and 4 M HCl in 1,4-dioxane (281 µL, 1.13 mmol, 25 eq.) was added dropwise. The mixture was heated at 70°C for 120 min and then concentrated in a stream of air and dried in vacuo. The residue **412** was dissolved in 6 mL of dry DCM and dry DIPEA (61 µL, 0.360 mmol, 8 eq.) was added. At 0°C, **310** (0.030 mg, 0.054 mmol, 1.2 eq.) was added. The reaction was protected from light and stirred at RT overnight. Then, MeOH (1 mL) was added and the mixture was stirred for another 1 h to quench the active ester. 30 mL DCM were added and the reaction mixture was washed with 25 mL 0.5 M KHSO4, dried (Na2SO4), filtered an evaporated to dryness. The crude mixture was purified using column chromatography (EA:MeOH=100:0→99:1) yielding the title compound (0.030 g, 0.082 mmol, 90% over two steps) as a white solid.

^{1}H NMR (300 MHz, $CDCl_3$) δ 7.02 (s, 1H), 6.80 (s, 1H), 6.62 (dd, J = 5.1, 4.4 Hz, 1H), 6.41 (d, J = 7.6 Hz, 1H), 6.21 (s, 1H), 5.87 – 5.67 (m, 1H), 5.63 – 5.39 (m, 1H), 4.32 (s, 1H), 4.03 – 3.84 (m, 2H), 3.69 (s, 1H), 3.37 – 3.22 (m, 3H), 3.14 (s, 1H), 2.89 (d, J = 5.1 Hz, 2H), 2.56 (s, 3H), 2.25 (t, J = 6.9 Hz, 2H), 2.12 – 1.96 (m, 2H), 1.51 (dd, J = 14.3, 7.2 Hz, 2H), 1.45 – 1.16 (m, 22H), 0.87 (t, J = 6.7 Hz, 3H).

^{13}C NMR (75 MHz, $CDCl_3$) δ 166.75, 163.62, 157.46, 139.91, 133.93, 113.79, 110.82, 102.79, 98.23, 74.71, 54.07, 31.93, 29.70, 29.51, 29.42, 29.37, 28.24, 22.70, 20.07, 14.14.

UPLC-MS (ESI): $C_{37}H_{56}BrN_2O_8$ $[M]^+$: m/z Calc.: 735.3, found: 735.2

5 Appendix

5.1 Supplementary Tables

Europium Chelate	5-D^+	4-D^+
Absorption maximum [nm]	365	378
ε [L cm^{-1} mol^{-1}]	1790	3050
Luminescence Lifetime* (H_2O) [µs]	49 (49.8) 390 (50.2)	52 (15.2) 203 (84.8)
Luminescence Lifetime* (D_2O) [µs]	232 (19.6) 1065 (80.4)	- 1279 (100)
q (H_2O) **	3.5	4.9
* 617 nm emission, 345 nm excitation, data were fitted with a biexponential decay, in brackets: relative amplitudes (%); ** according to Supkowski-Horrocks equation[184]		

Table S 1. Spectral properties of the europium complexes.

5.2 Supplementary Figures

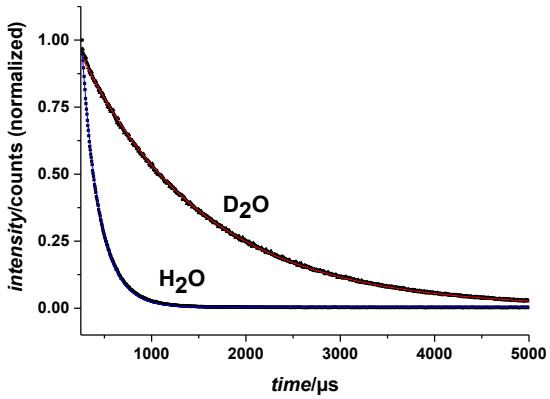

Figure S 1. Normalized luminescence decay profile of **4-D^+** (c = 100 µmol L^{-1}) and monoexponential fits in H_2O (blue) and D_2O (red). λ_{ex} = 345 nm, λ_{em}= 617 nm, delay time = 200 µs. Fitting parameter for y = exp (-t/τ) see **Table S 1**. $R^2 > 0.999$.

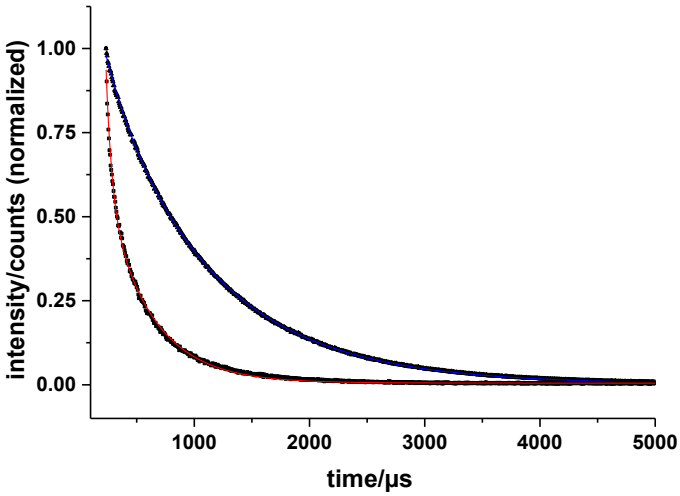

Figure S 2. Normalized luminescence decay profile of **5-D**$^{+}$ (c = 100 µmol L^{-1}) in TRIS buffer in absence (red bi-exponential fit) and presence of 75 µmol L^{-1} of ATP (blue bi-exponential fit). λ_{ex} = 345 nm, λ_{em}= 617 nm, delay time = 200 µs. Fitting parameter for y = A_1 exp (-t/τ_1) + A_2 exp (-t/τ_2) **5-D**$^{+}$ see **Table S 1**; **5-D**$^{+}$ + ATP: τ_1 = 218 µs (A_1 = 6.4 %), τ_2 = 926 µs (A_2 = 93.6 %); R^2 = 0.99993.

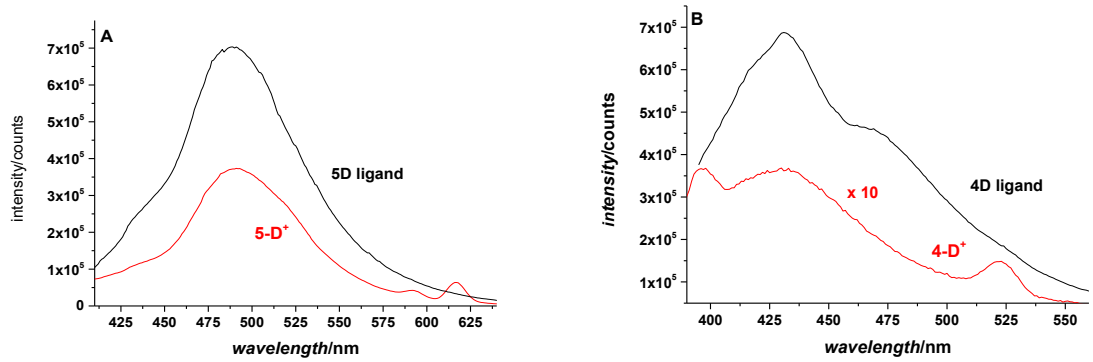

Figure S 3. Steady state fluorescence spectra of dentate ligands (c = 50 µmol L^{-1}) before (black lines) and after complexation of an equimolar amount of Eu^{3+} (red lines). (**A**) Five-dentate ligand, **(B)** four-dentate ligand . λ_{ex}= 345 nm.

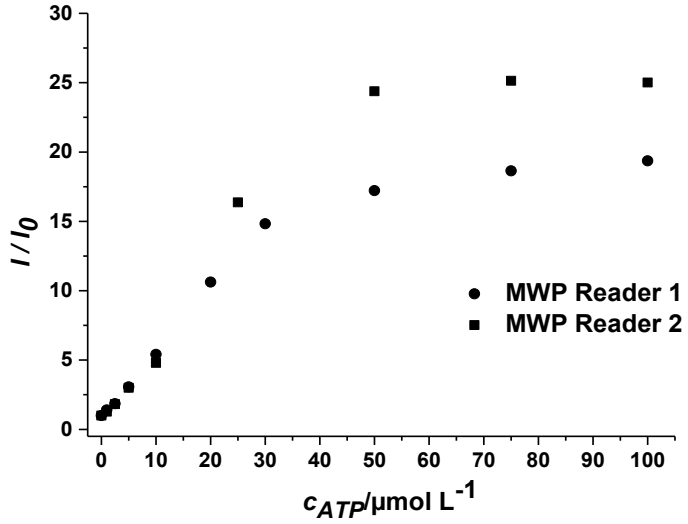

Figure S 4. Normalized luminescence responses (I/I_0) of **5-D**$^+$ (c=50 µmol L^{-1}) to ATP, in TRIS buffer (pH 7.4) using two different microwell plate (MWP) readers (MWP 1: Tecan, MWP 2: Victor). I_0 is the luminescence intensity in the absence of phosphate; λ_{ex}=345 nm, λ_{em}=618 nm; time-resolved measurement, Lag time: 100 ms, signal integration time: 400 ms.

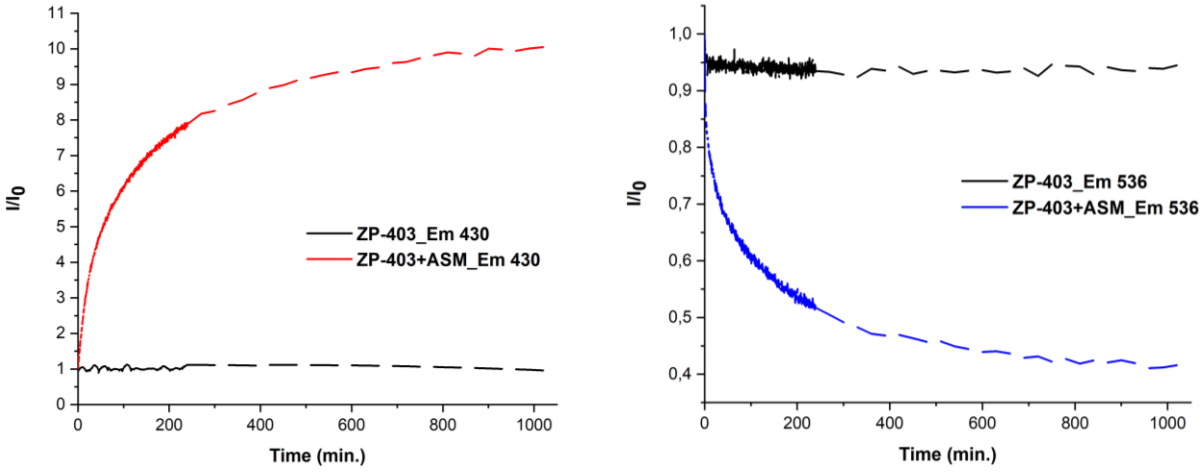

Figure S 5. Real time normalized fluorescence intensity changes of **ZP-403** during the enzymatic reaction; **left**: Bromo-coumarin fluorescence intensity change; **right**: NBD fluorescence intensity change. Probe concentration= 1µM, ASM buffer.

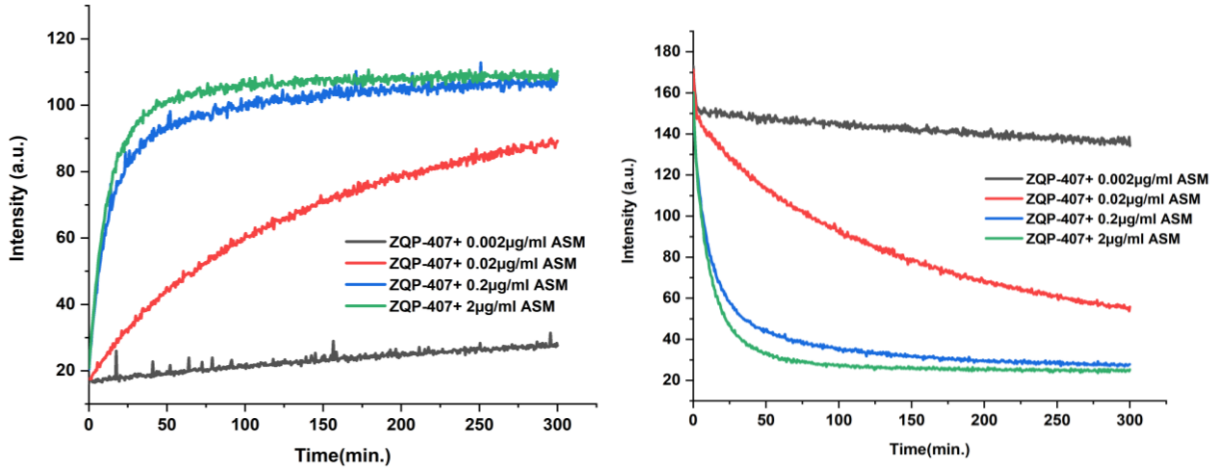

Figure S 6. Effect of different ASM concentrations on the cleavage rate of the FRET probe **ZQP-407**; **Left**: kinetic study, Ex_347, Em_405; **Right**: kinetic study, Ex_347, Em_536. ASM buffer, Probe concentration= 1μM.

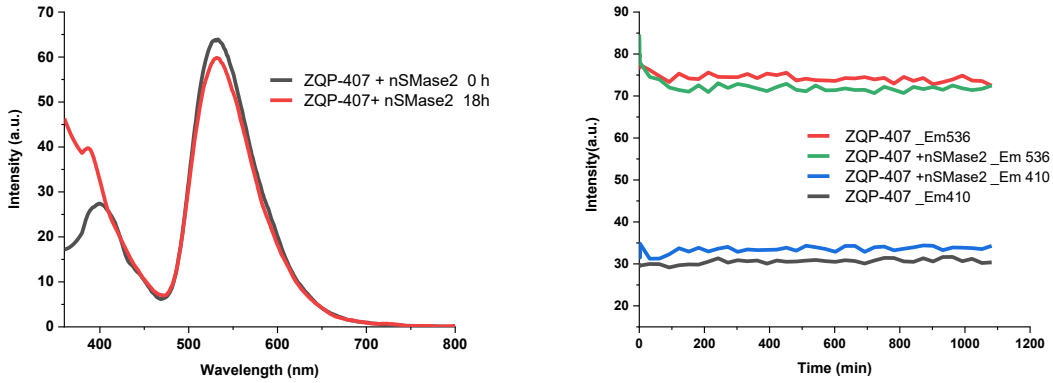

Figure S 7. ZQP-407 FRET Probe cleavage study by nSMase 2 enzyme. Left: Scanning before and after incubation; Right: kinetic study. ASM buffer, Probe concentration= 1μM.

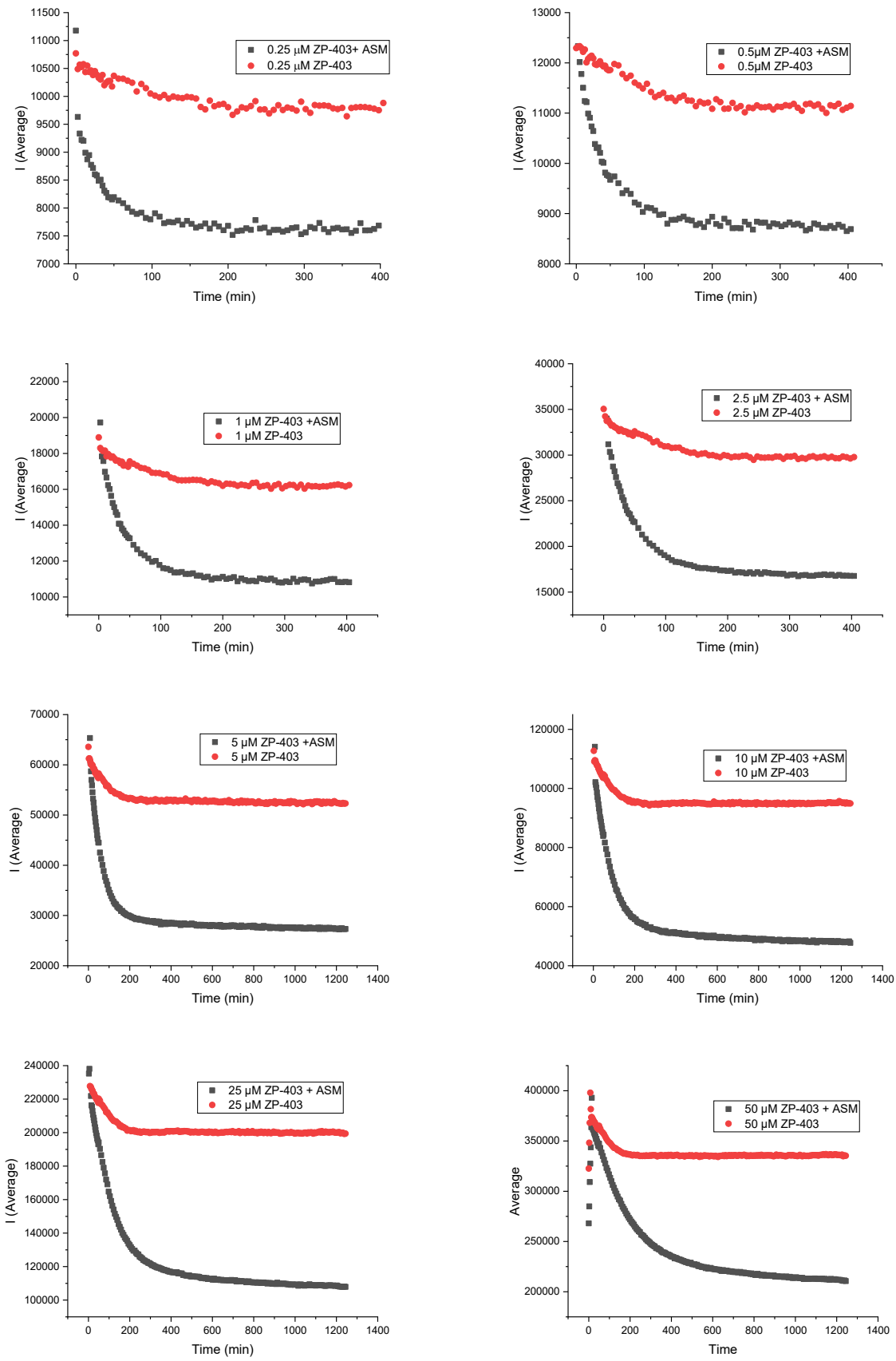

Figure S 8. FRET probe **ZP-403** with 0.6 µg/ml ASM: cleavage kinetics.

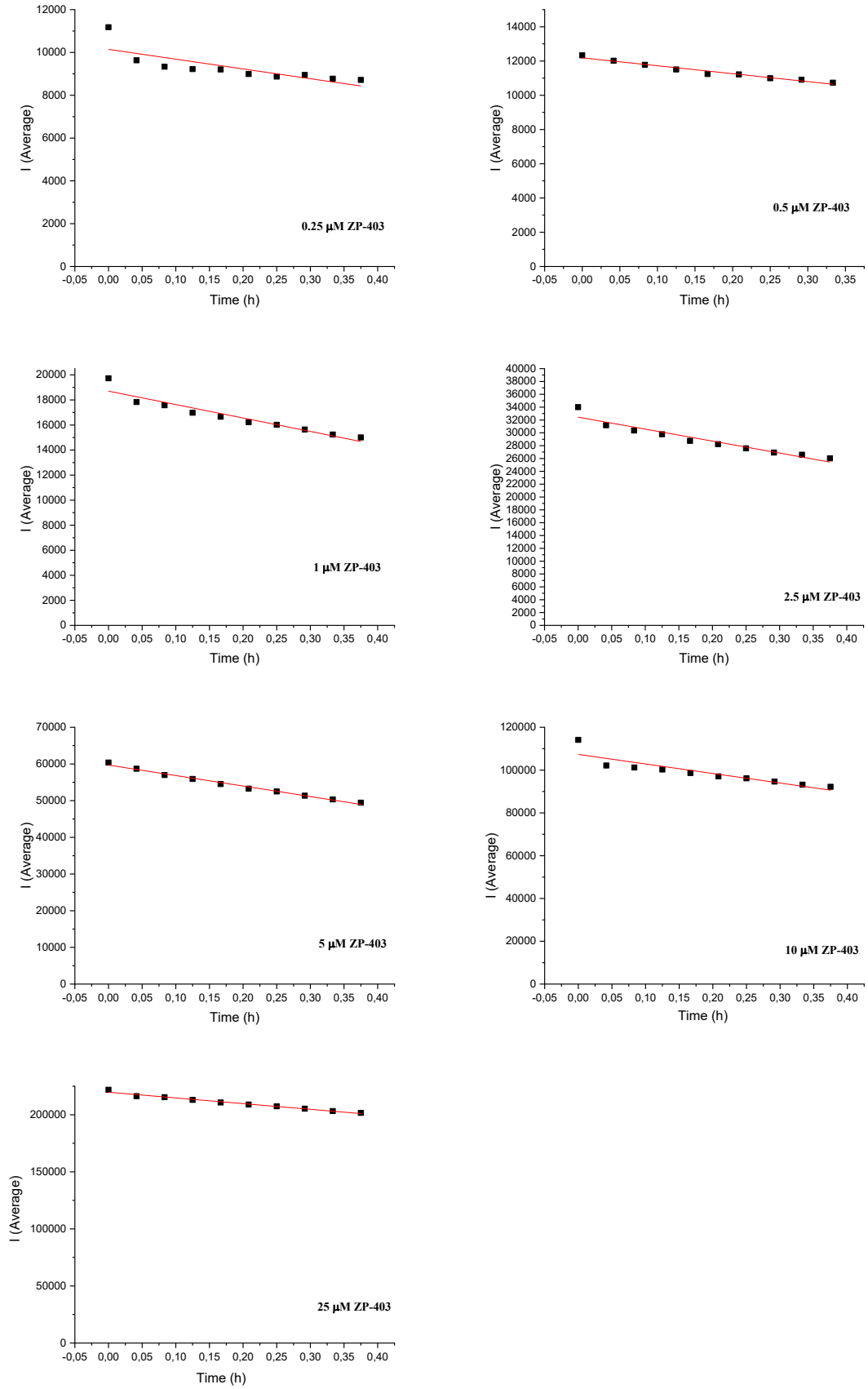

Figure S 9. Iinitial slopes determination of FRET probe **ZP-403** with 0.6 µg/ml ASM

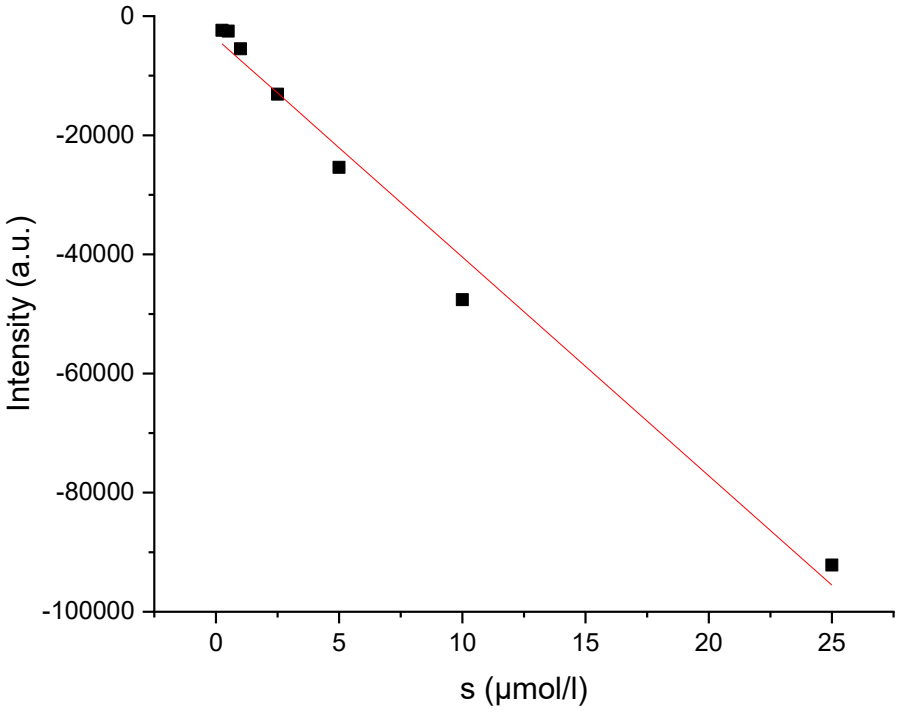

Figure S 10. Calibration curve for the FRET probe **ZP-403**, derived from the plateau values observed in **Figure S 8**.

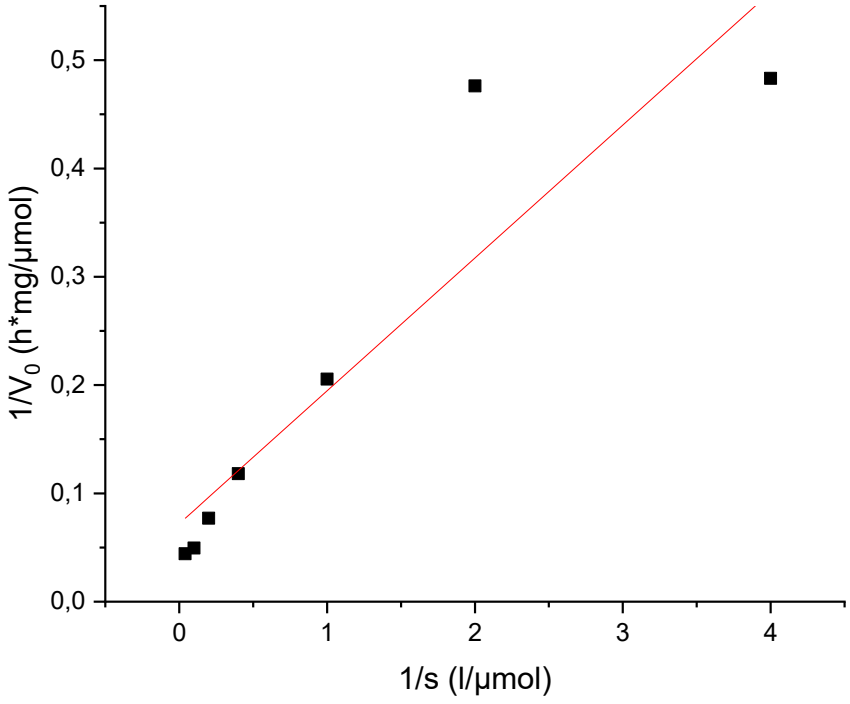

Figure S 11. lineweaver burk plot for the FRET probe **ZP-403**

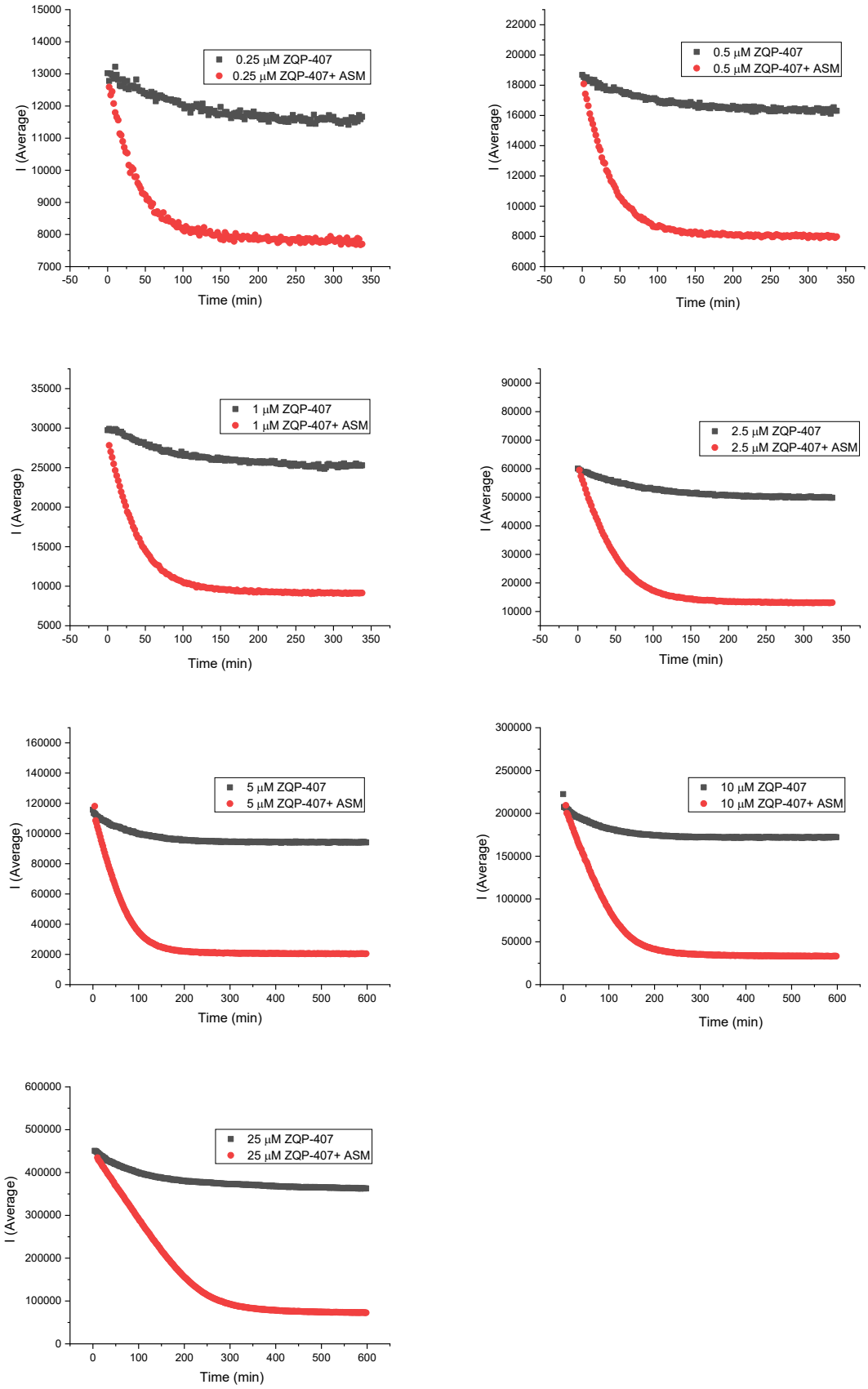

Figure S 12. Cleavage kinetics of the FRET probe **ZQP-407** with 0.2 μg/ml ASM.

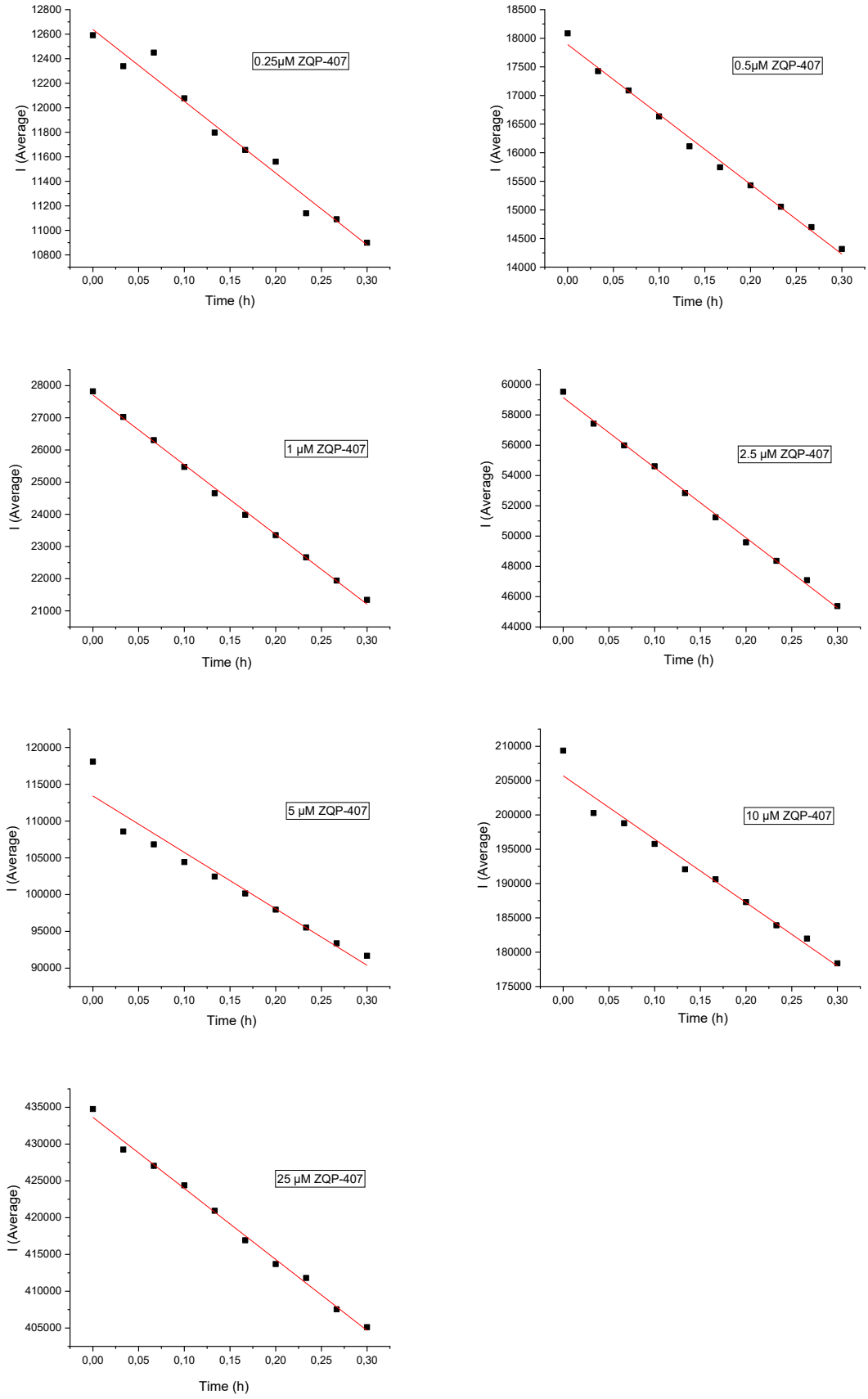

Figure S 13. Initial slopes determination of FRET probe ZQP-407 with 0.2 µg/ml ASM

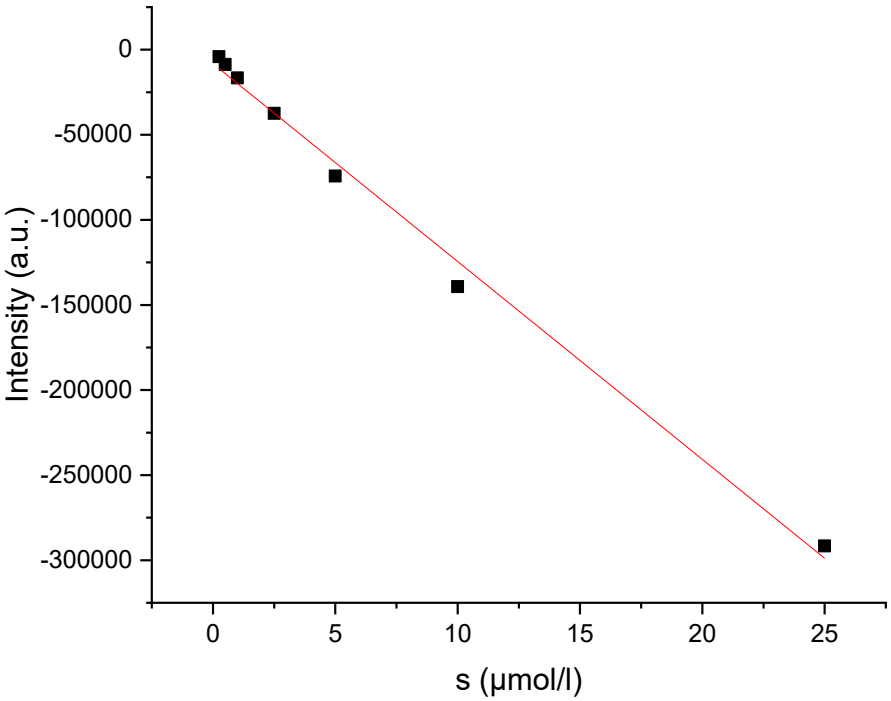

Figure S 14. Calibration curve for the FRET probe **ZQP-407**, derived from the plateau values observed in **Figure S 12**.

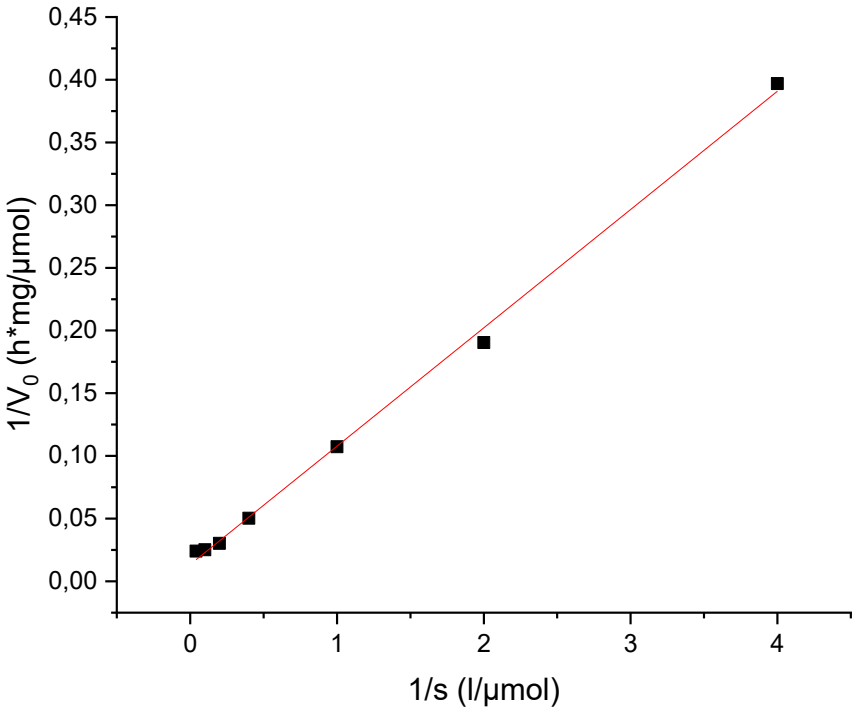

Figure S 15. lineweaver burk plot for the FRET probe **ZQP-407**

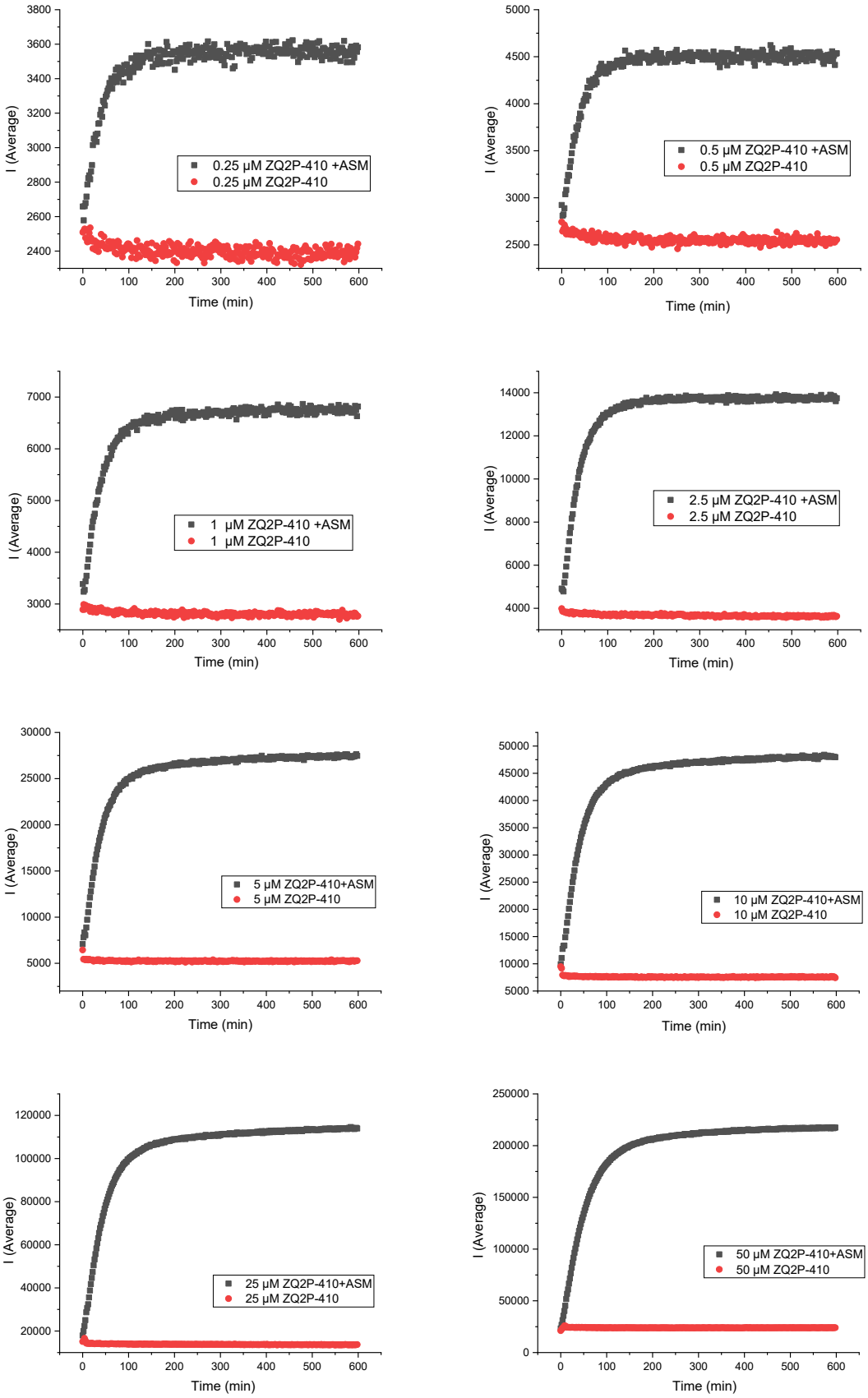

Figure S 16. Cleavage kinetics of the FRET probe **ZQ$_2$P-410** with 0.2 μg/ml ASM.

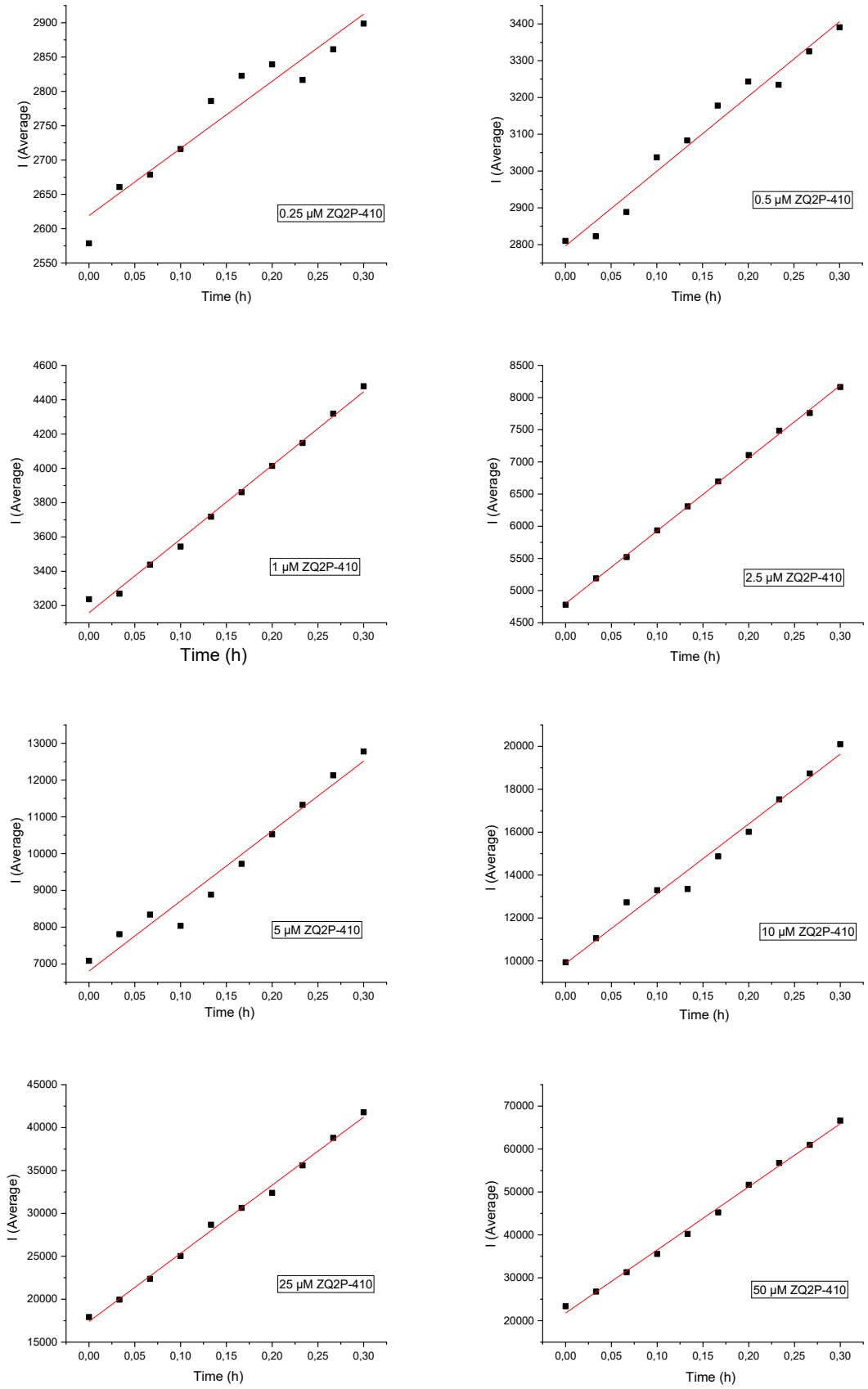

Figure S 17. Initial slopes determination of FRET probe **ZQ$_2$P-410** with 0.2 µg/ml ASM.

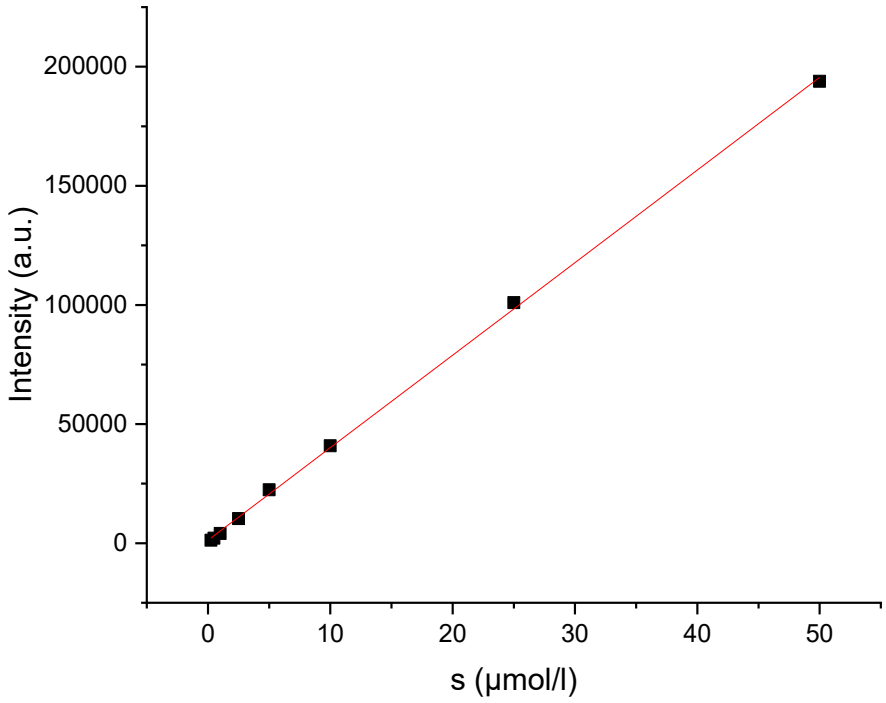

Figure S 18. Calibration curve for the FRET probe **ZQ$_2$P-410**, derived from the plateau values observed in **Figure S 16**.

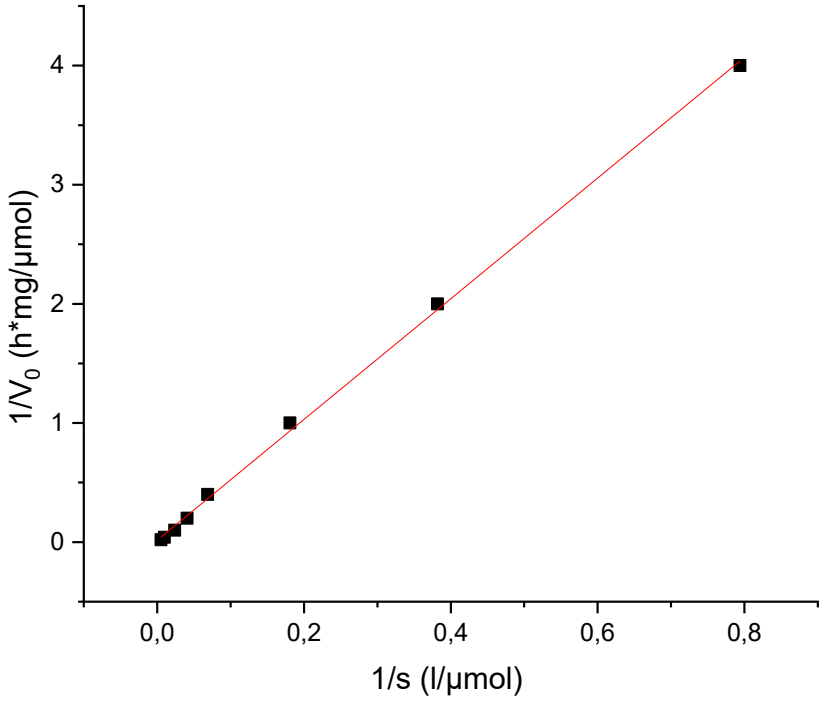

Figure S 19. lineweaver burk plot for the FRET probe **ZQ$_2$P-410.**

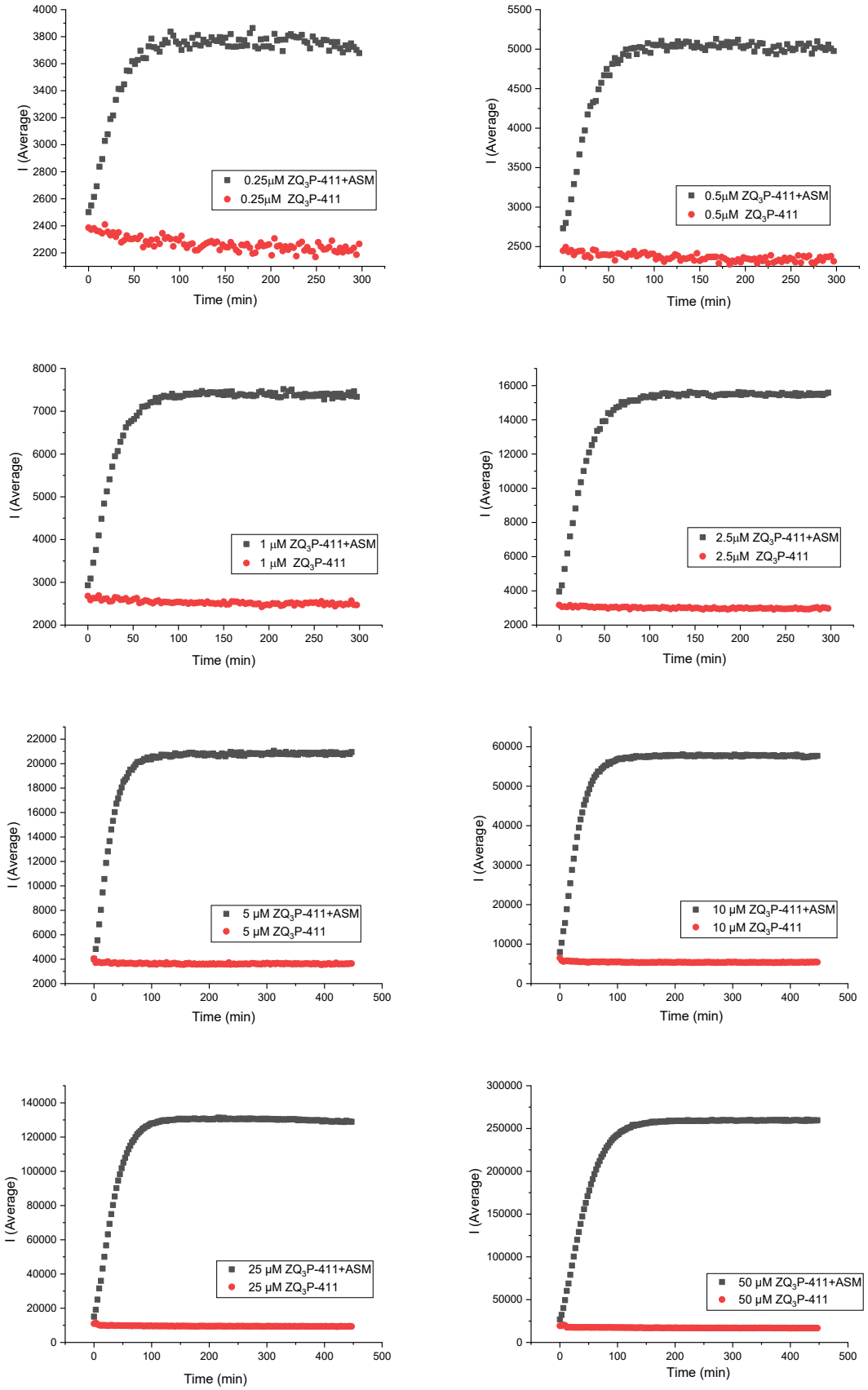

Figure S 20. Cleavage kinetics of the FRET probe **ZQ₃P-411** with 0.2 μg/ml ASM.

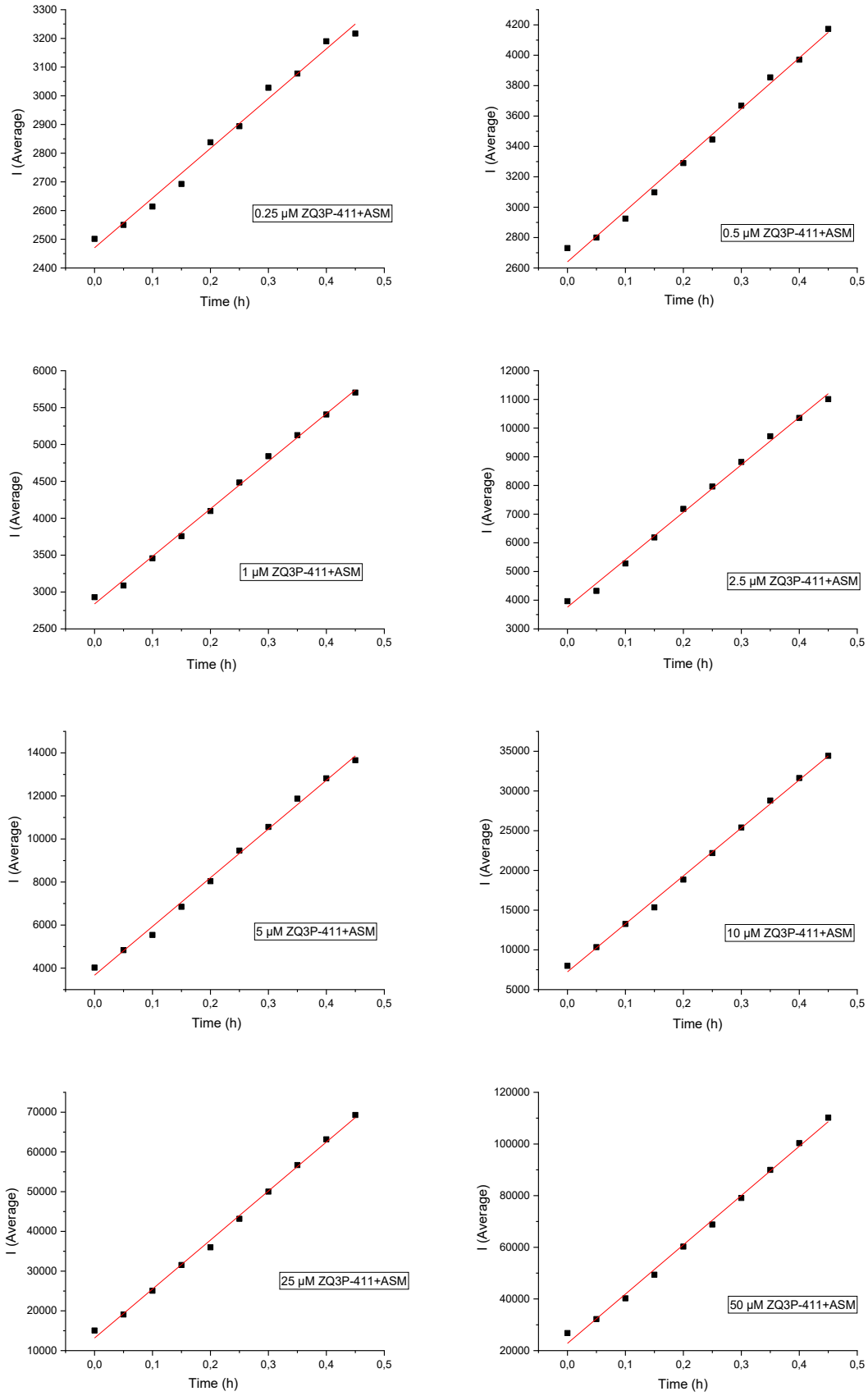

Figure S 21. Initial slopes determination of FRET probe **ZQ$_3$P-411** with 0.2 µg/ml ASM.

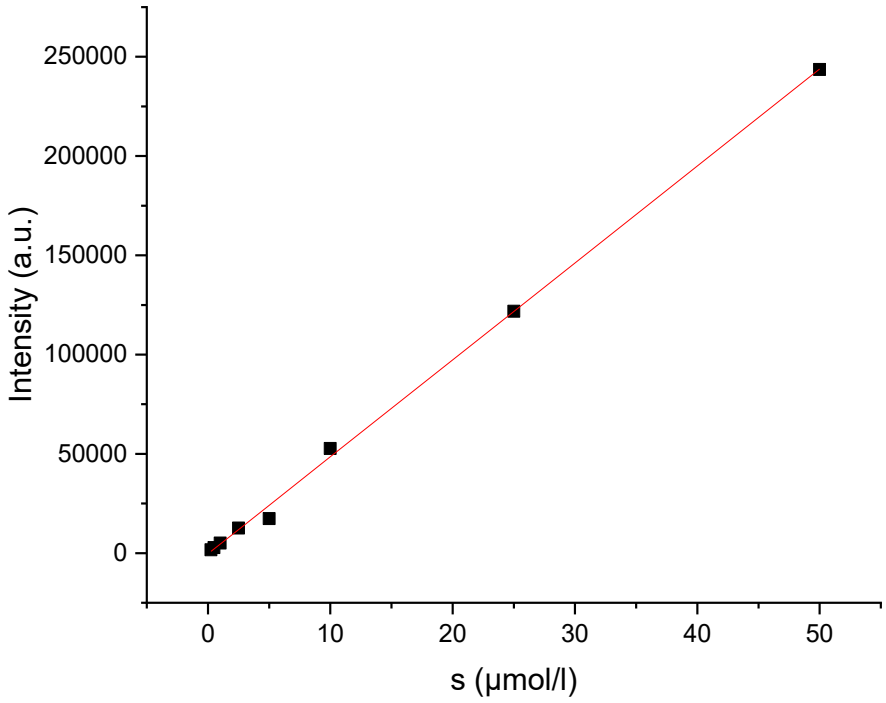

Figure S 22. Calibration curve for the FRET probe **ZQ$_3$P-411**, derived from the plateau values observed in **Figure S 20**.

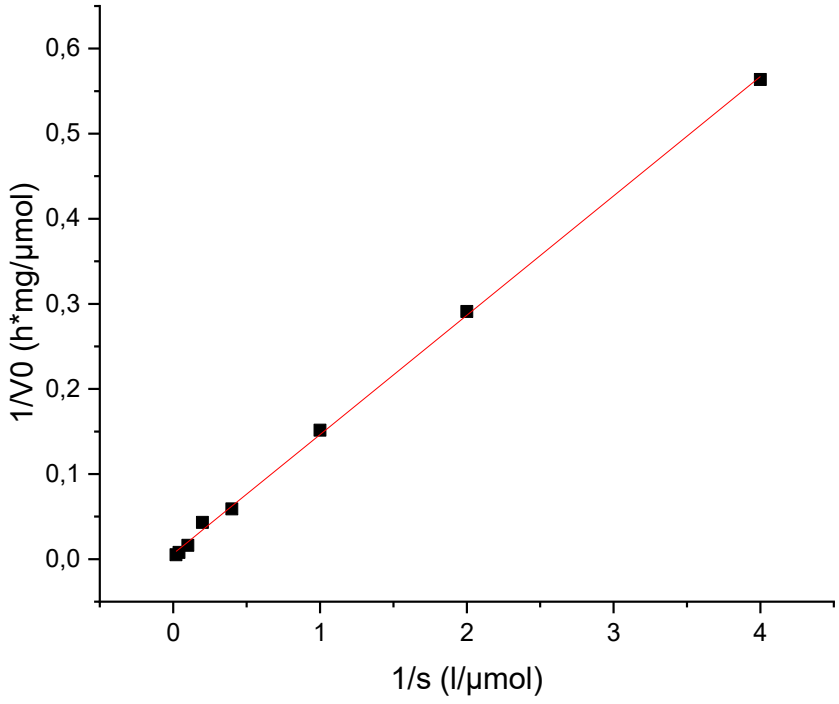

Figure S 23. lineweaver burk plot for the FRET probe **ZQ$_3$P-411**.

5.3 Supplementary NMR spectra

Diethyl 4-bromo-2,6-pyridinedicarboxylate (**101**) ($CDCl_3$)

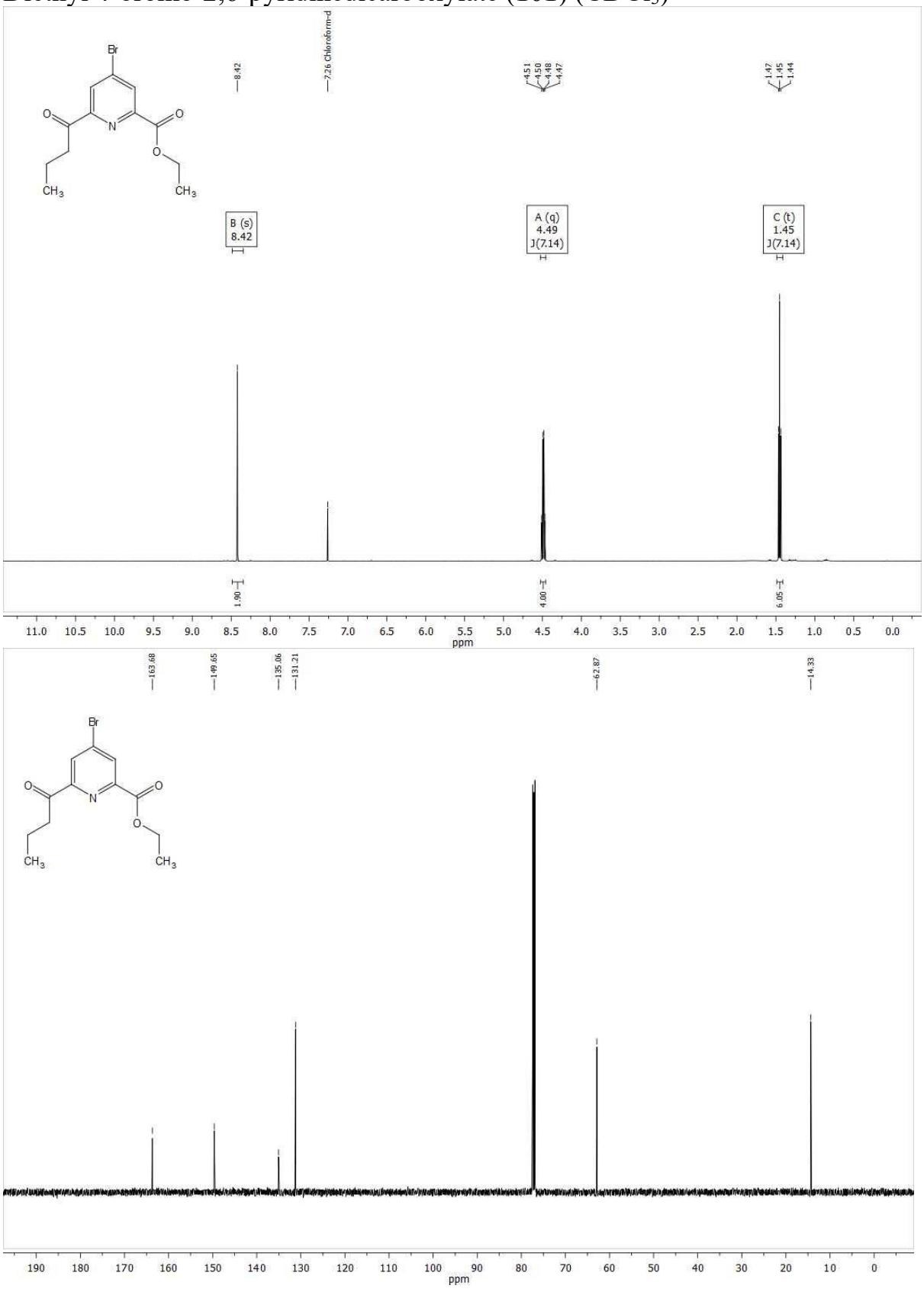

4-Bromo-2,6-pyridinedimethanol (**102**) ($CDCl_3$)

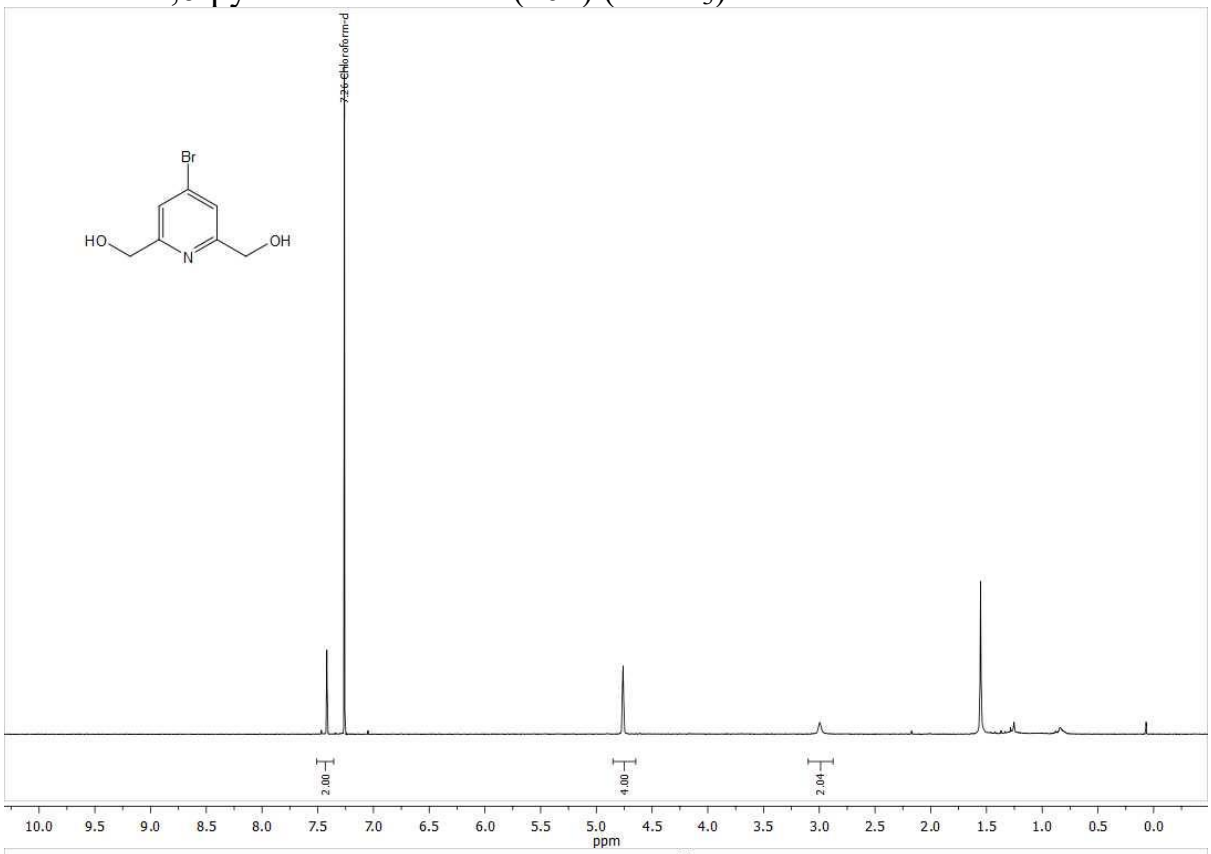

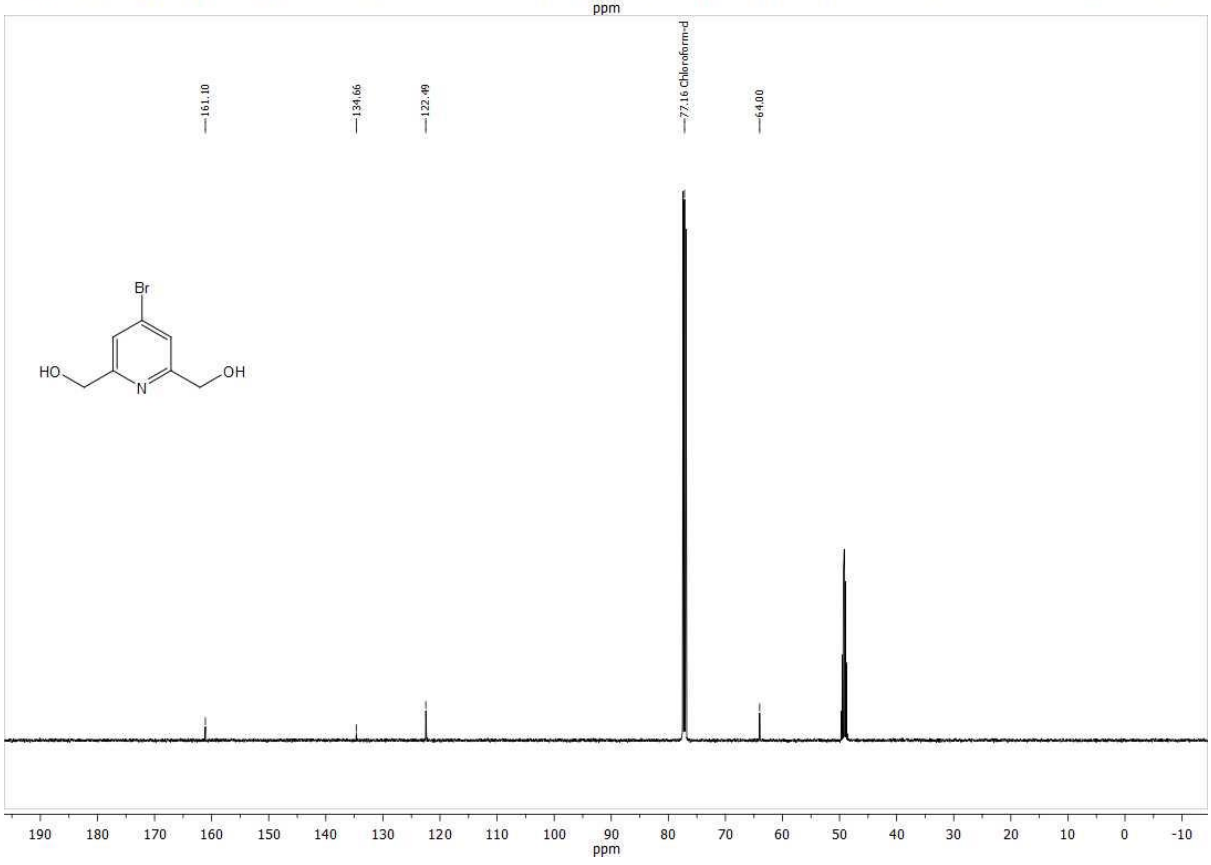

4-Bromo-2, 6-bis (bromomethyl) pyridine (**103**) ($CDCl_3$)

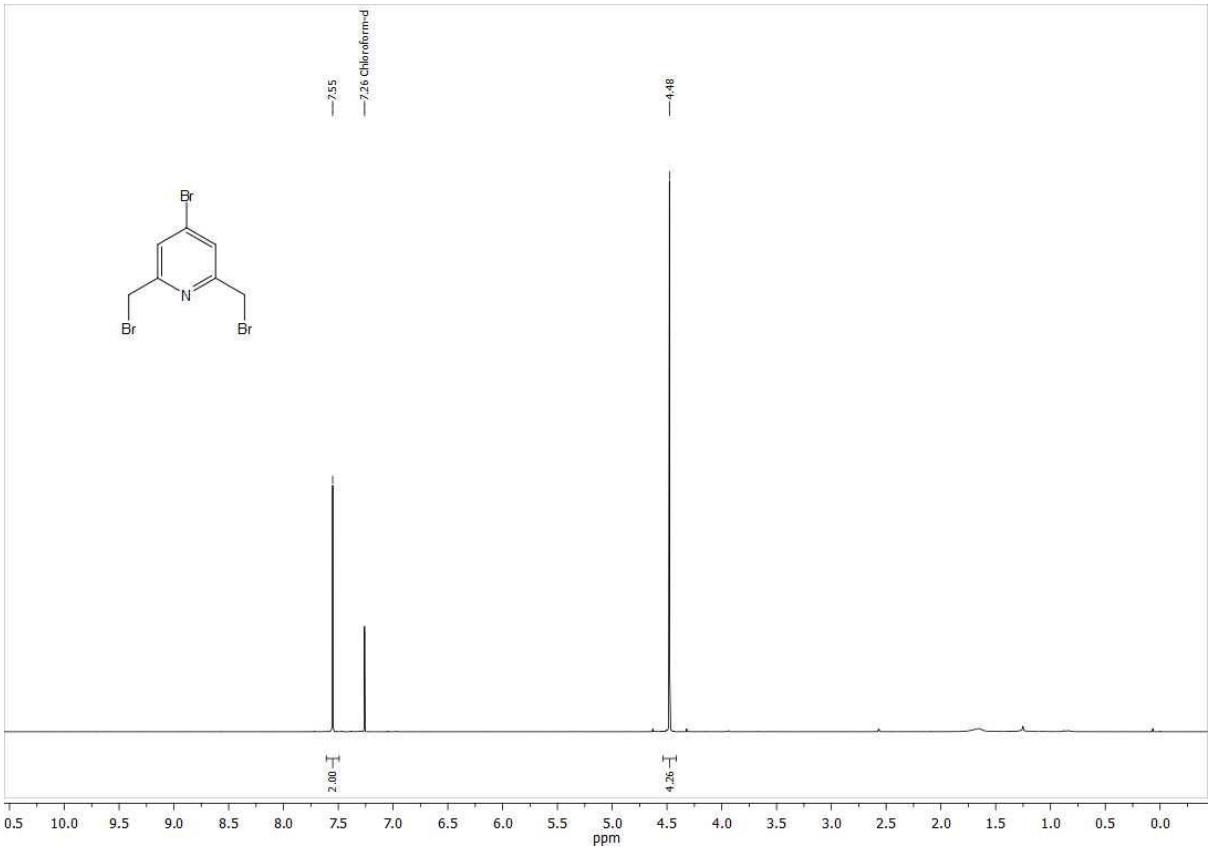

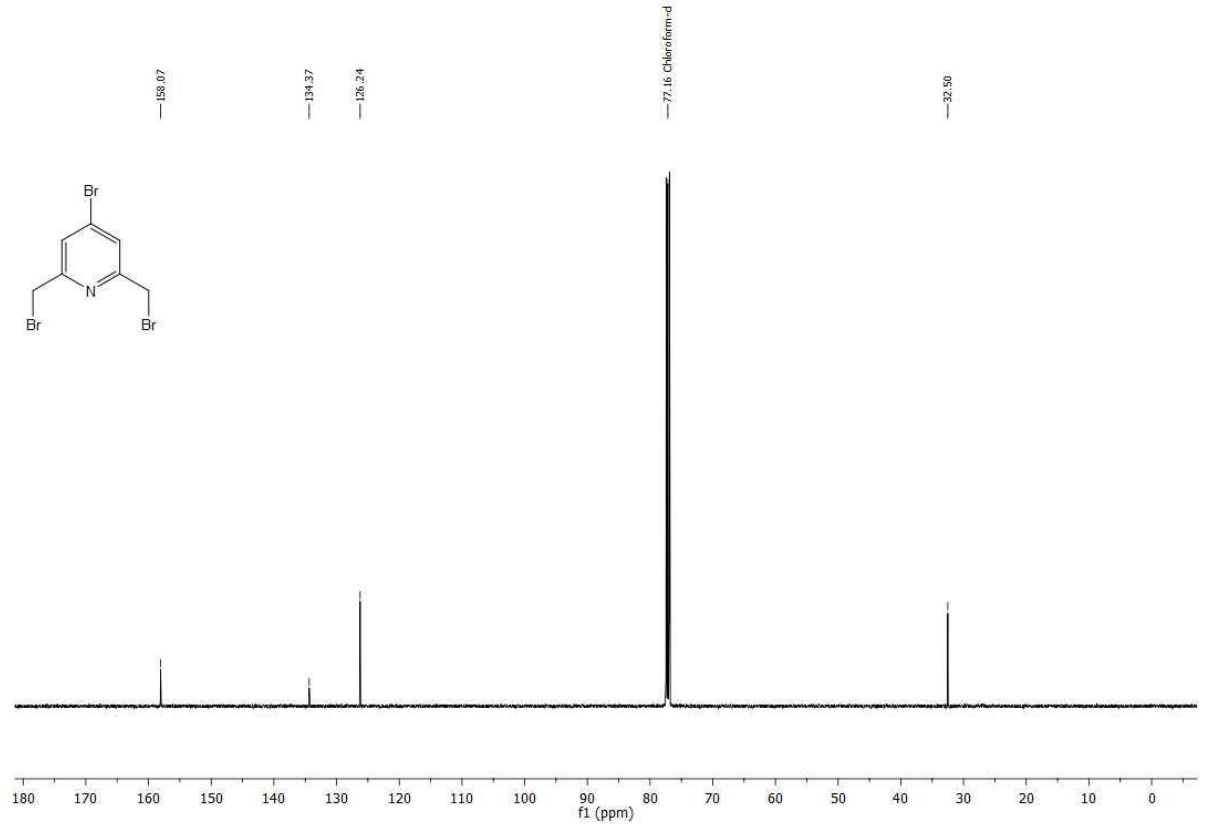

diethyl 2,2'-(((4-bromopyridine-2,6-diyl)bis(methylene))bis (methylazanedi -yl)) diacetate (**104**) ($CDCl_3$)

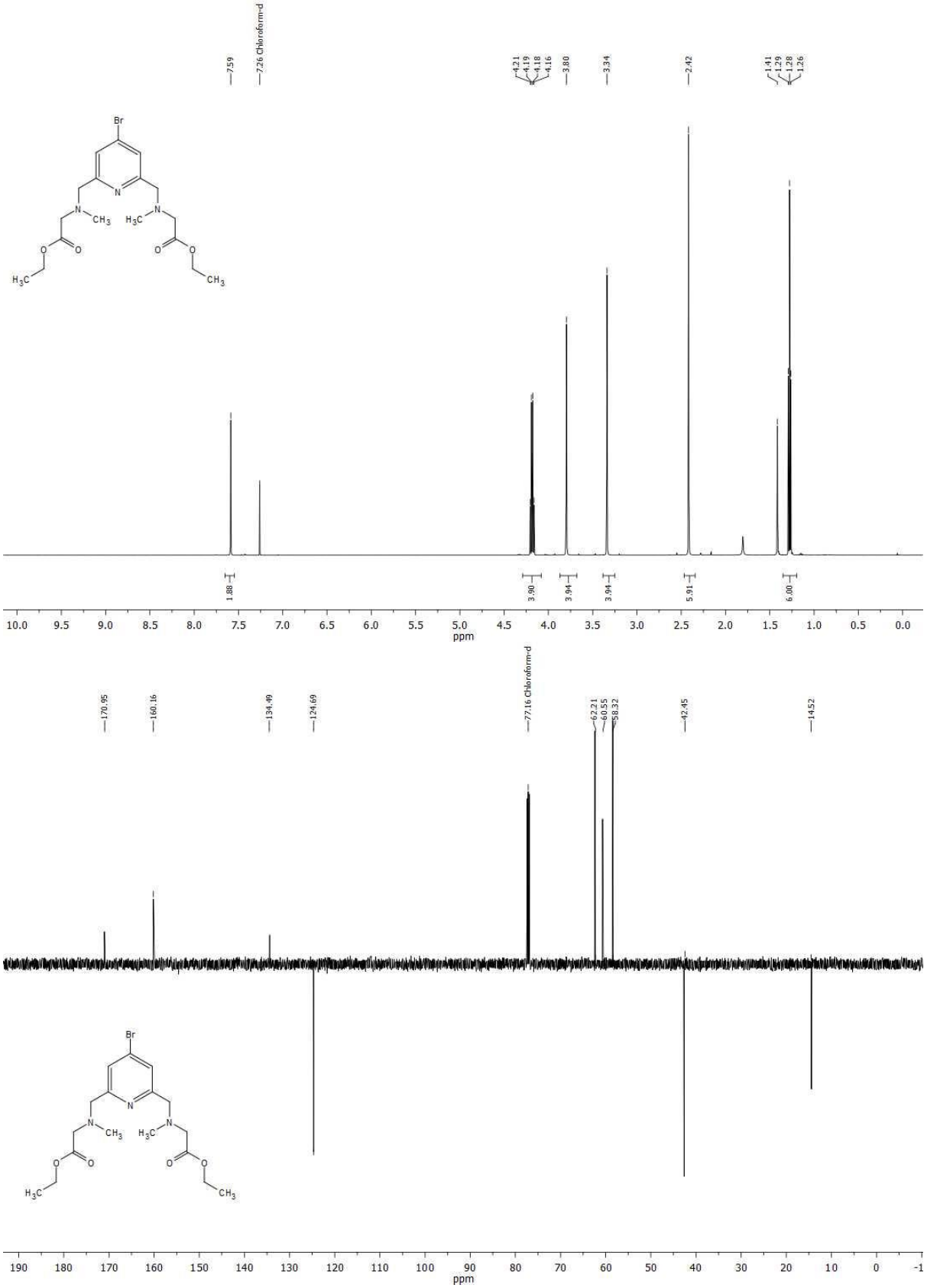

Diethyl 2,2'-(((4-((4-(dimethylamino)phenyl)ethynyl)pyridine-2,6-diyl)bis (meth ylene))bis(methylazanediyl))diacetate (**105**) ($CDCl_3$)

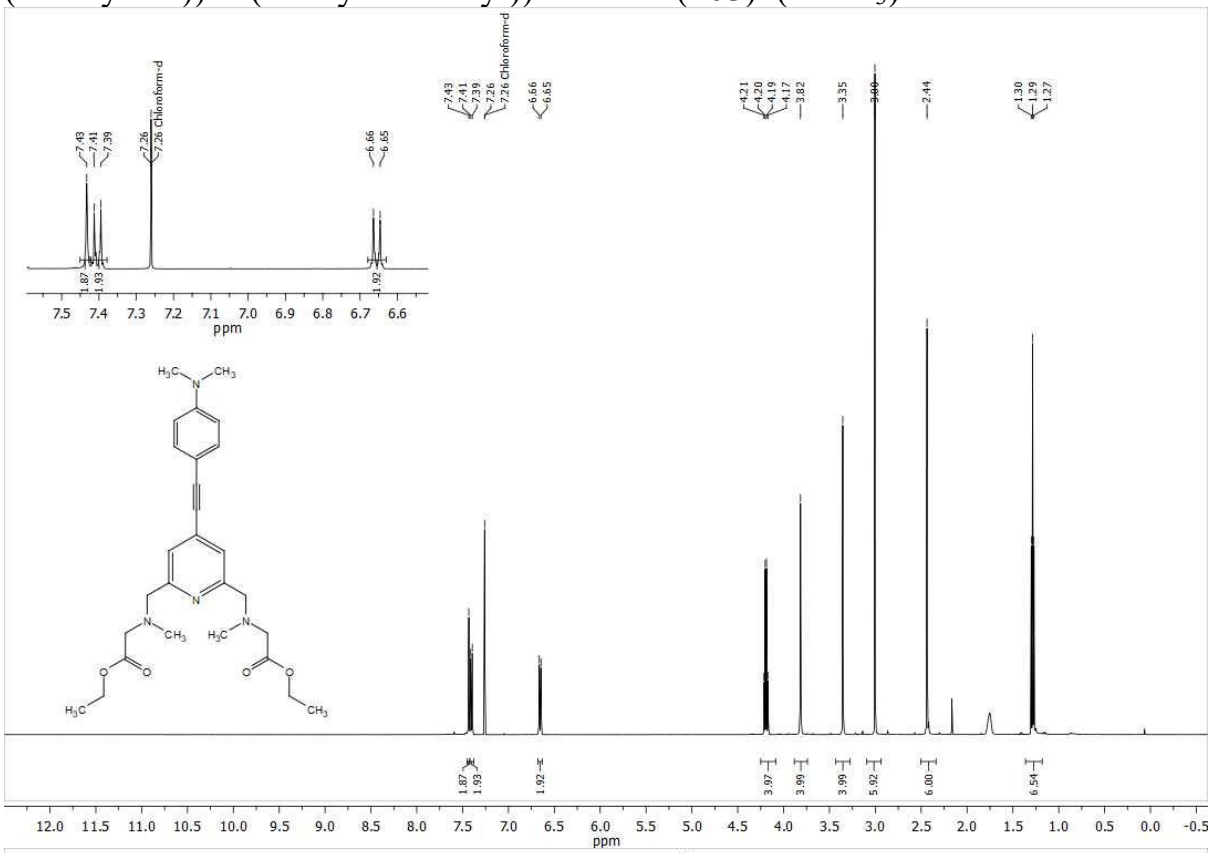

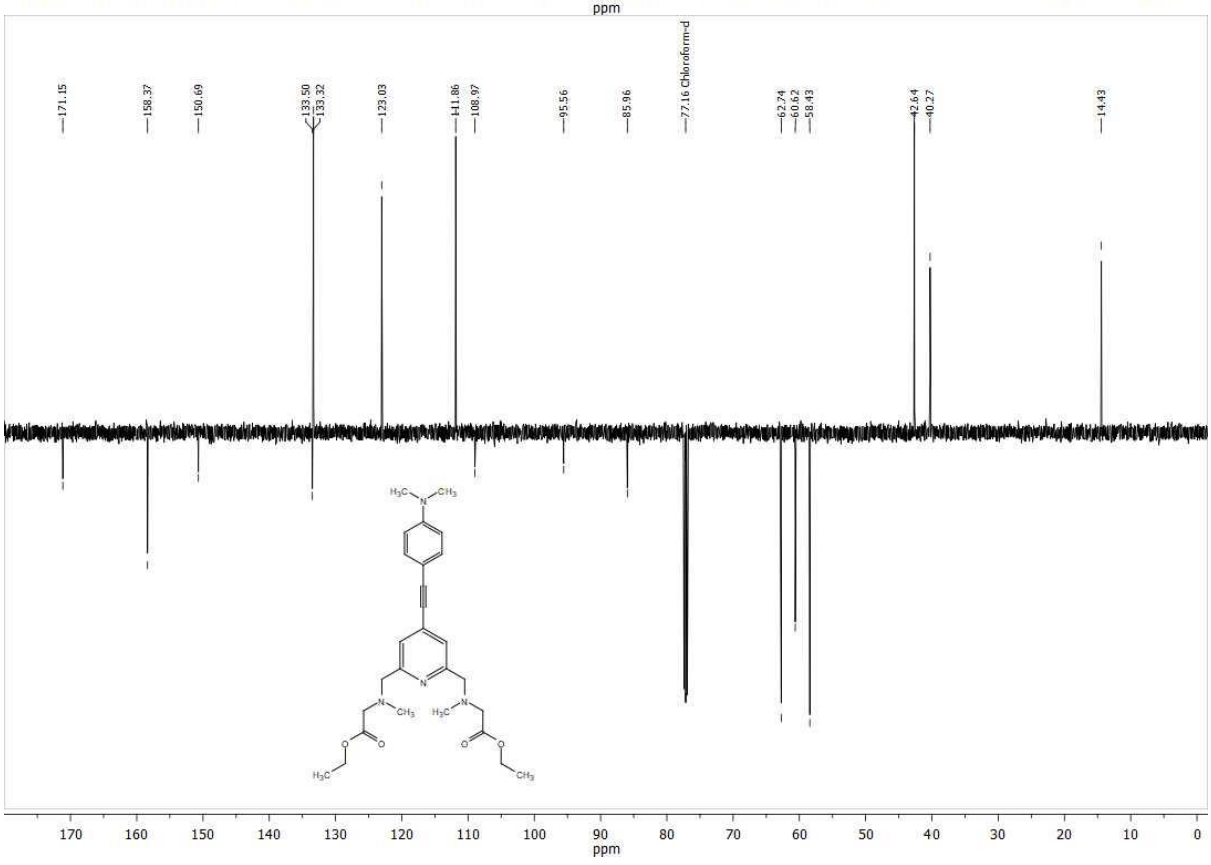

2,2'-(((4-((4-(dimethylamino)phenyl)ethynyl)pyridine-2,6-diyl)bis(methylene))bis(methylazanediyl))diacetic acid (**106**) (CD_3OD)

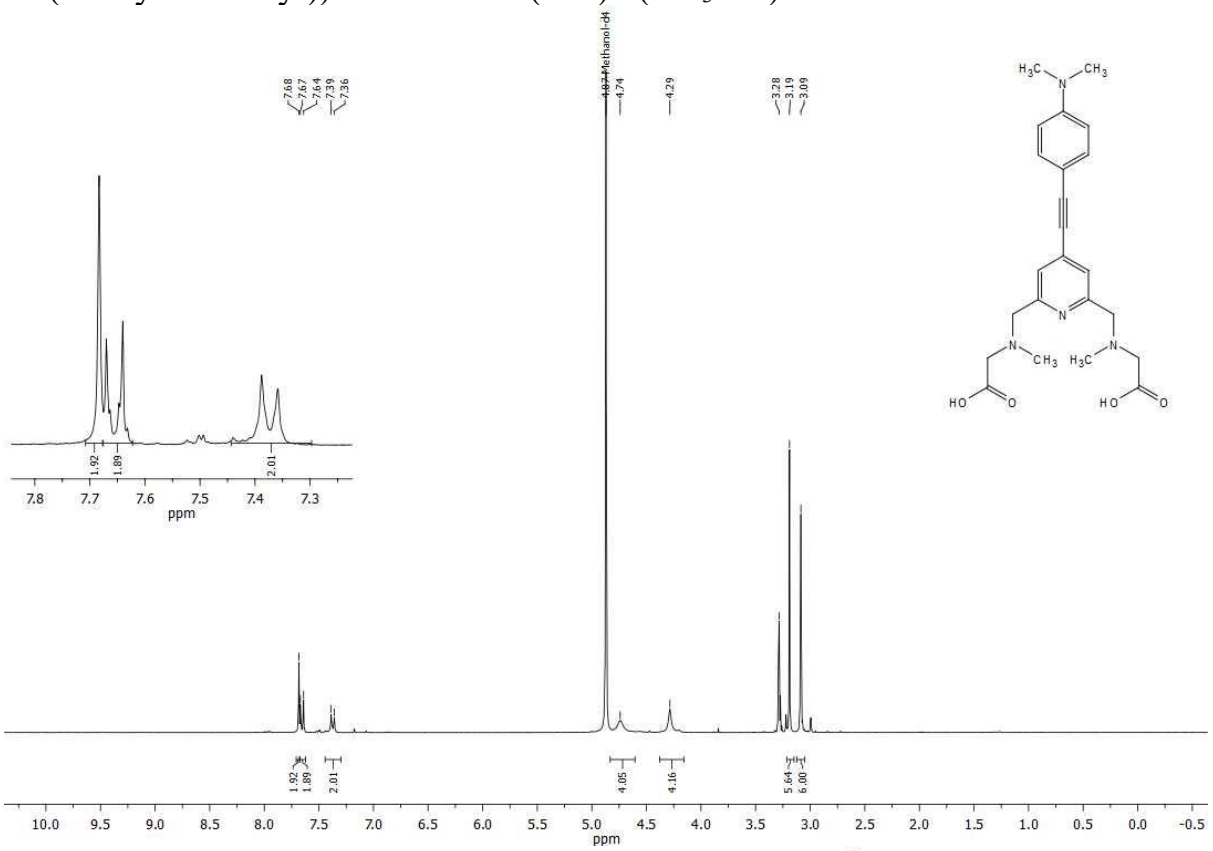

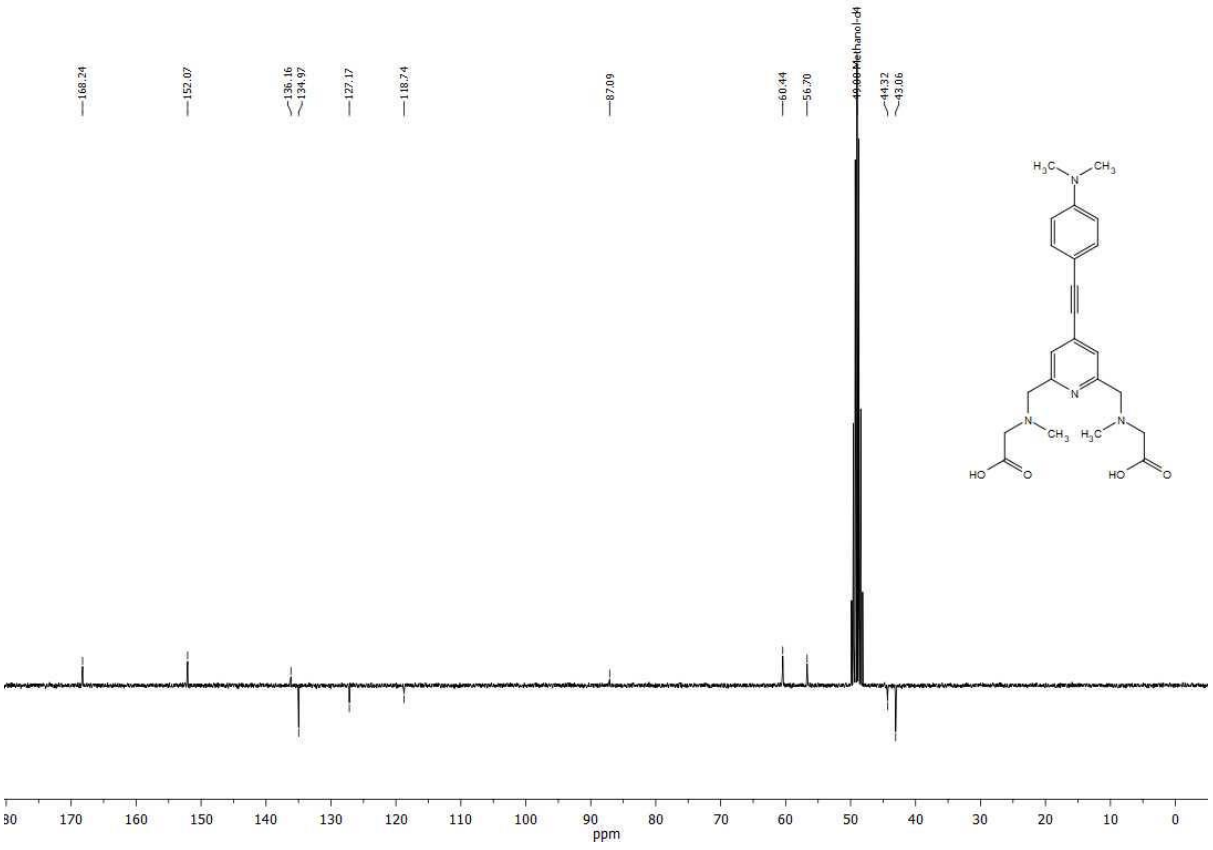

Ethyl 4-bromo-6-(hydroxymethyl)picolinate (**107**) (DMSO-D6)

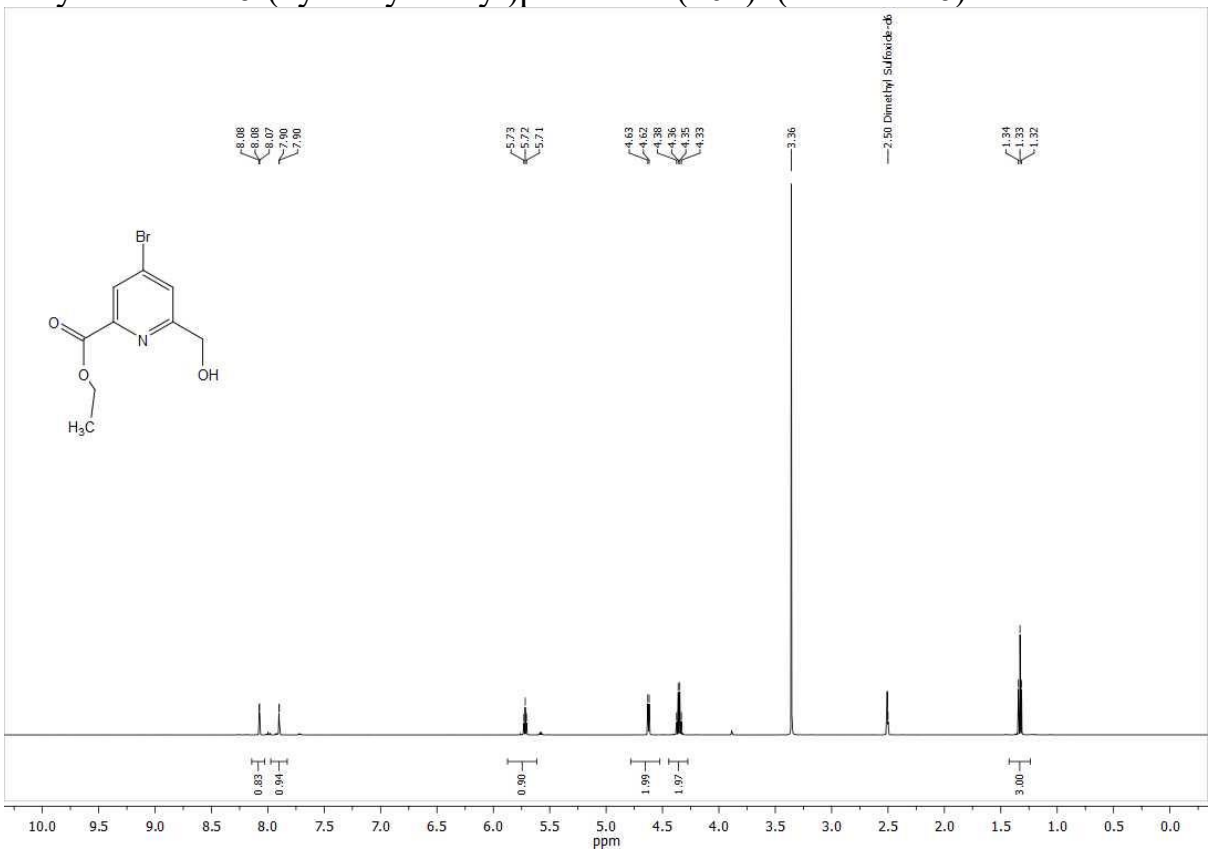

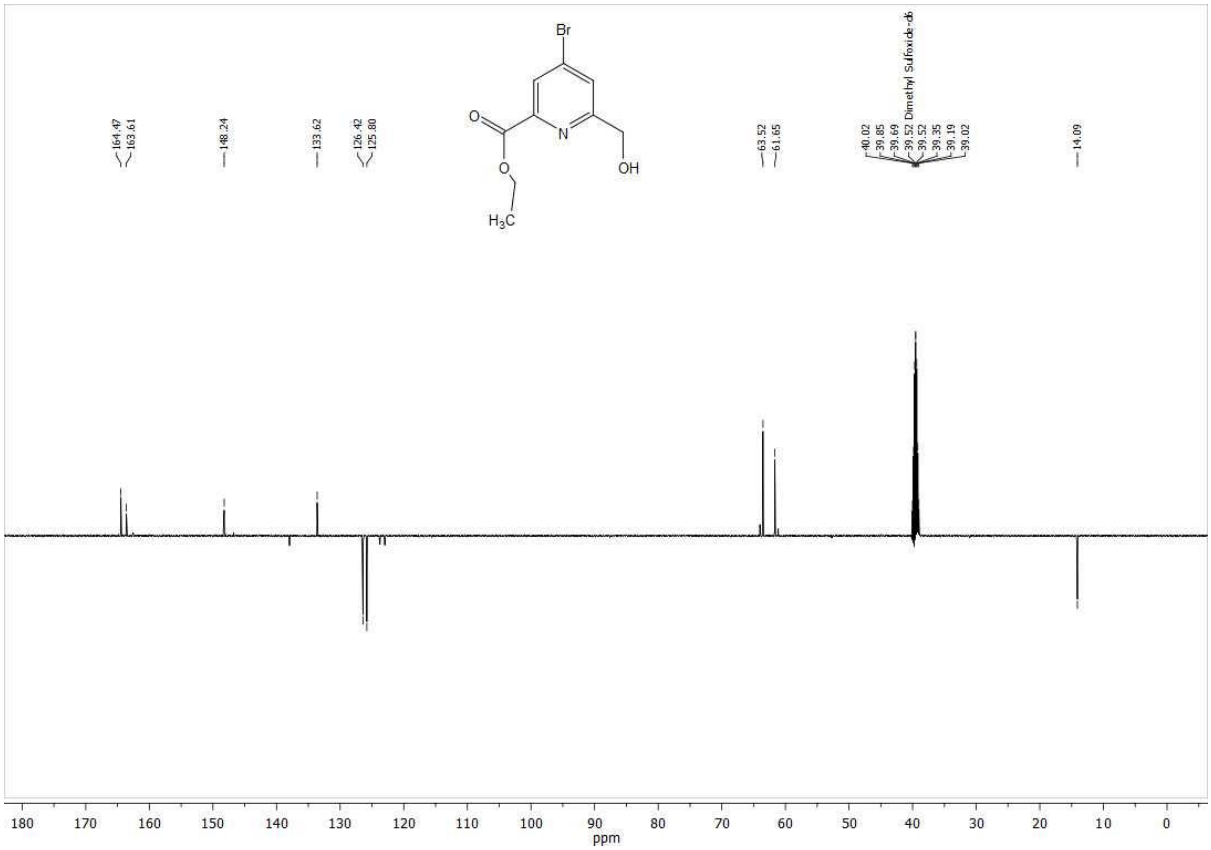

Ethyl 4-bromo-6-(bromomethyl) picolinate (**108**) ($CDCl_3$)

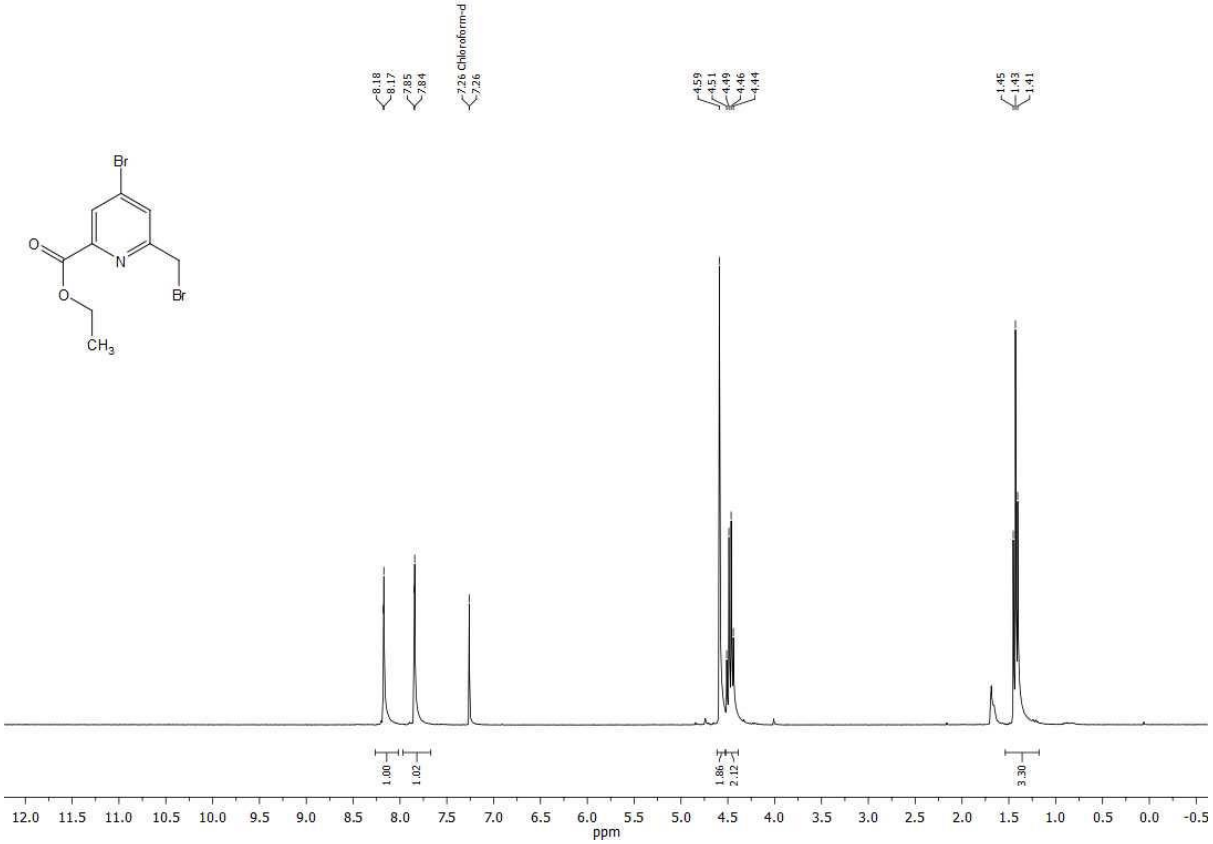

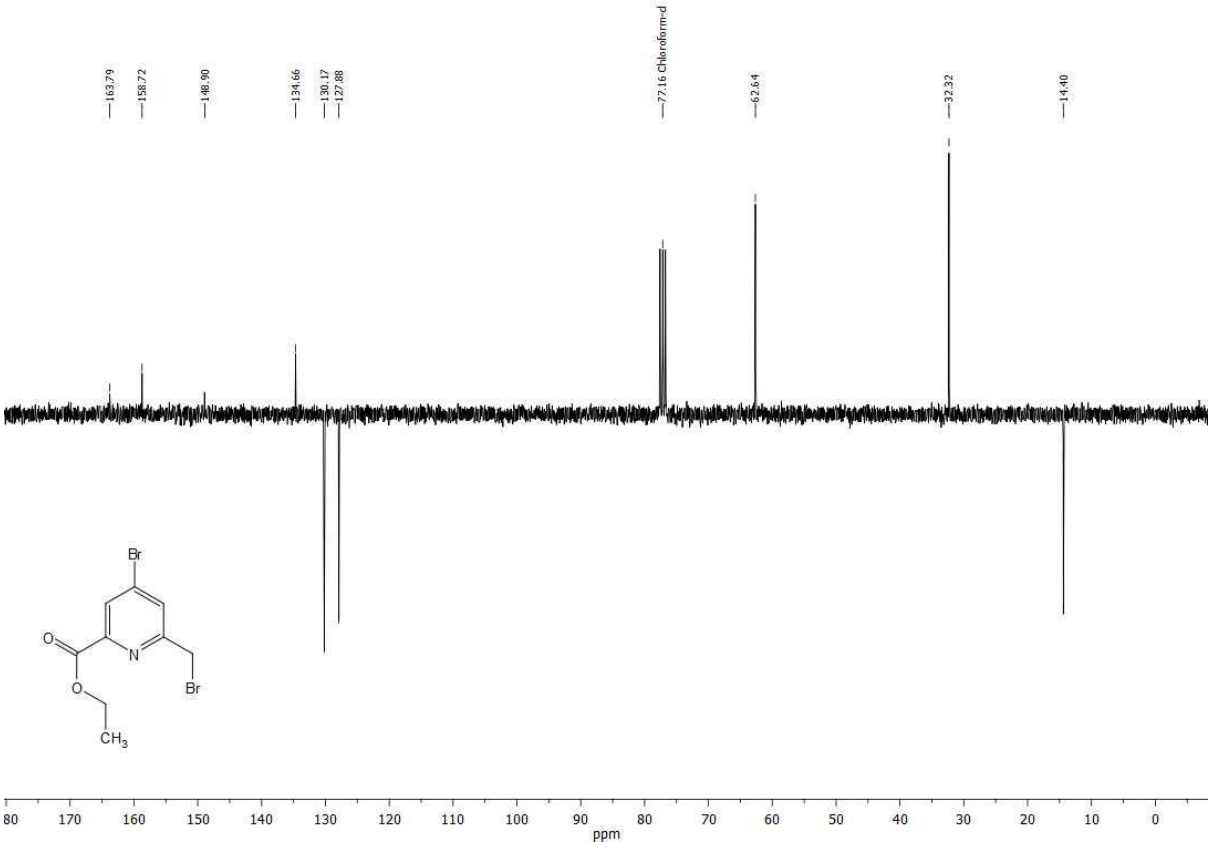

Ethyl 4-bromo-6-(((2-ethoxy-2-oxoethyl)(methyl)amino)methyl)picolinate (**109**) ($CDCl_3$)

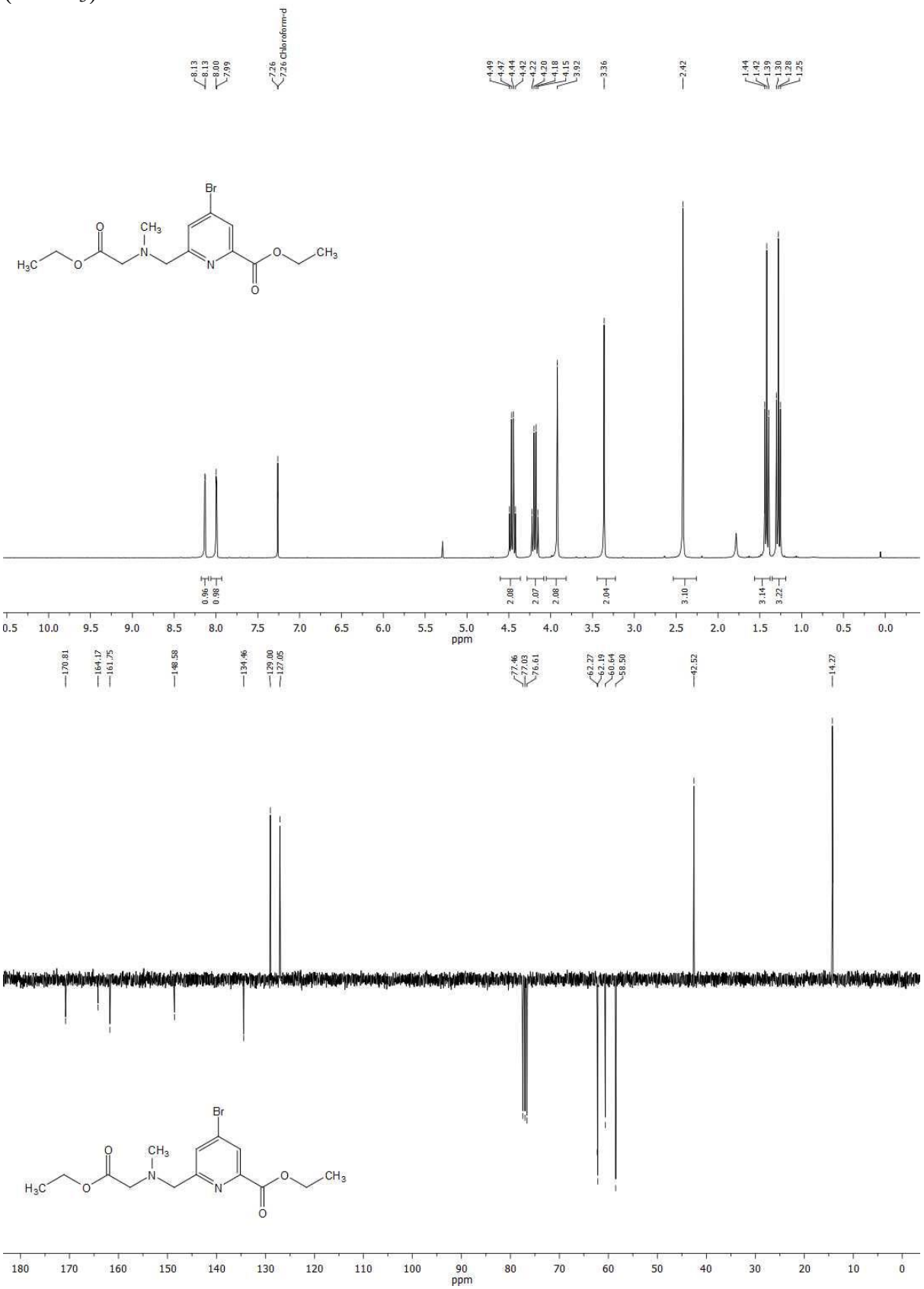

Ethyl 4-((4-(dimethylamino)phenyl)ethynyl)-6-(((2-ethoxy-2-oxoethyl) (methyl) amino)methyl)picolinate (**110**) (CD_3OD)

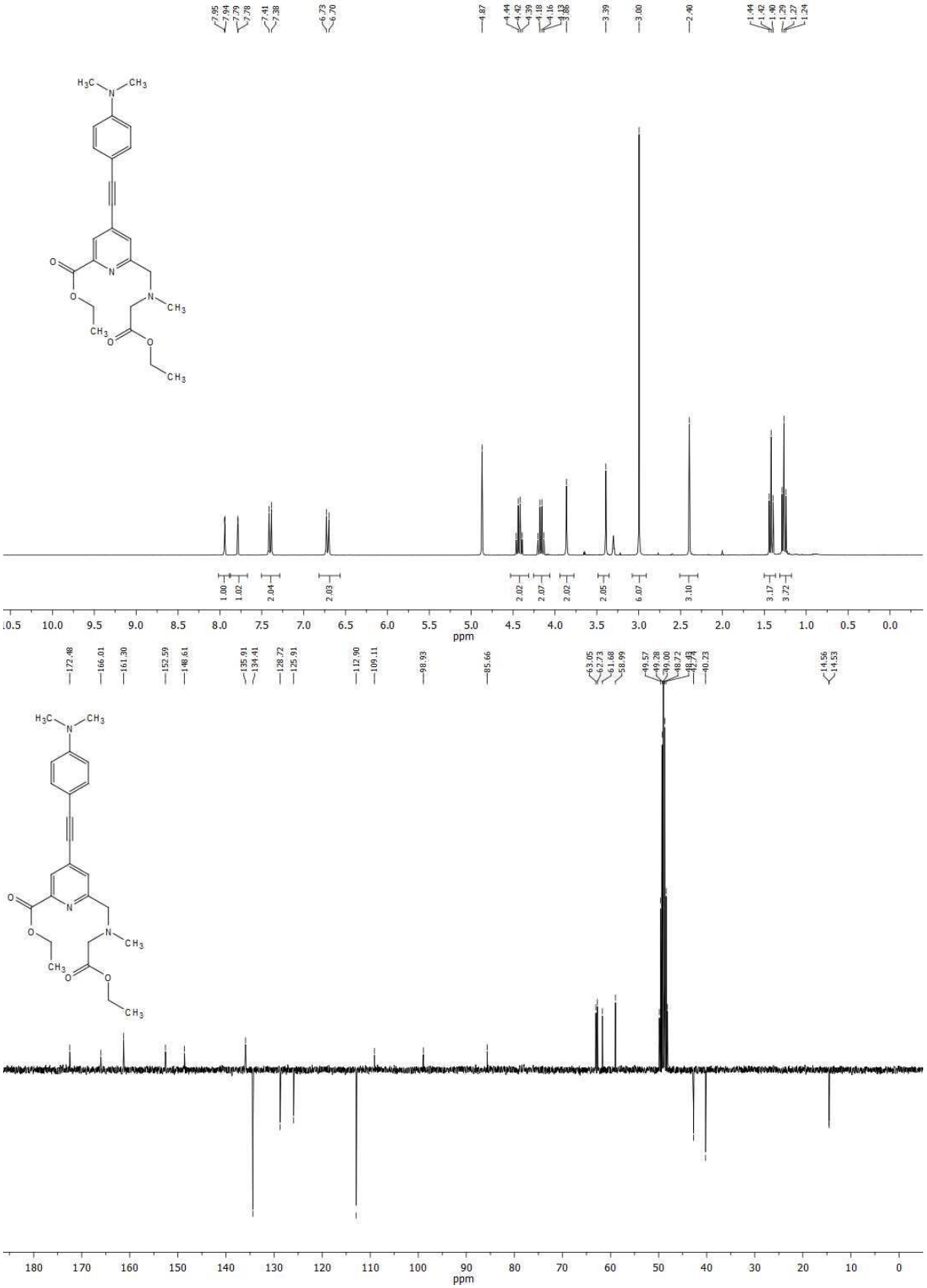

6-(((carboxymethyl)(methyl)amino)methyl)-4-((4-(dimethylamino)phenyl) ethynyl)picolinic acid (**111**) (DMSO-D6)

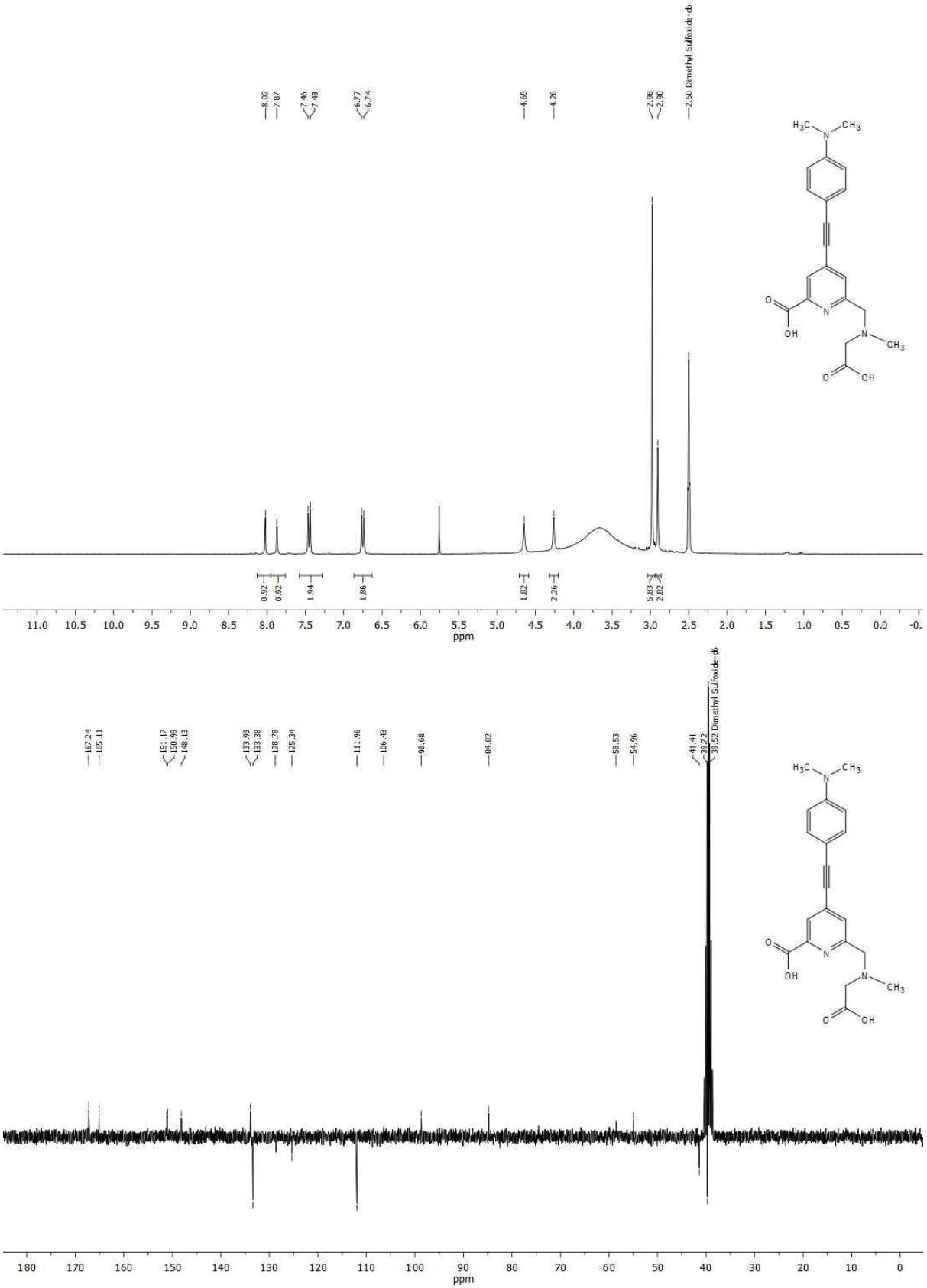

(S)-tert-butyl 3-hydroxy-1-(methoxy(methyl)amino)-1-oxopropan-2-yl carbamate (**202**) ($CDCl_3$)

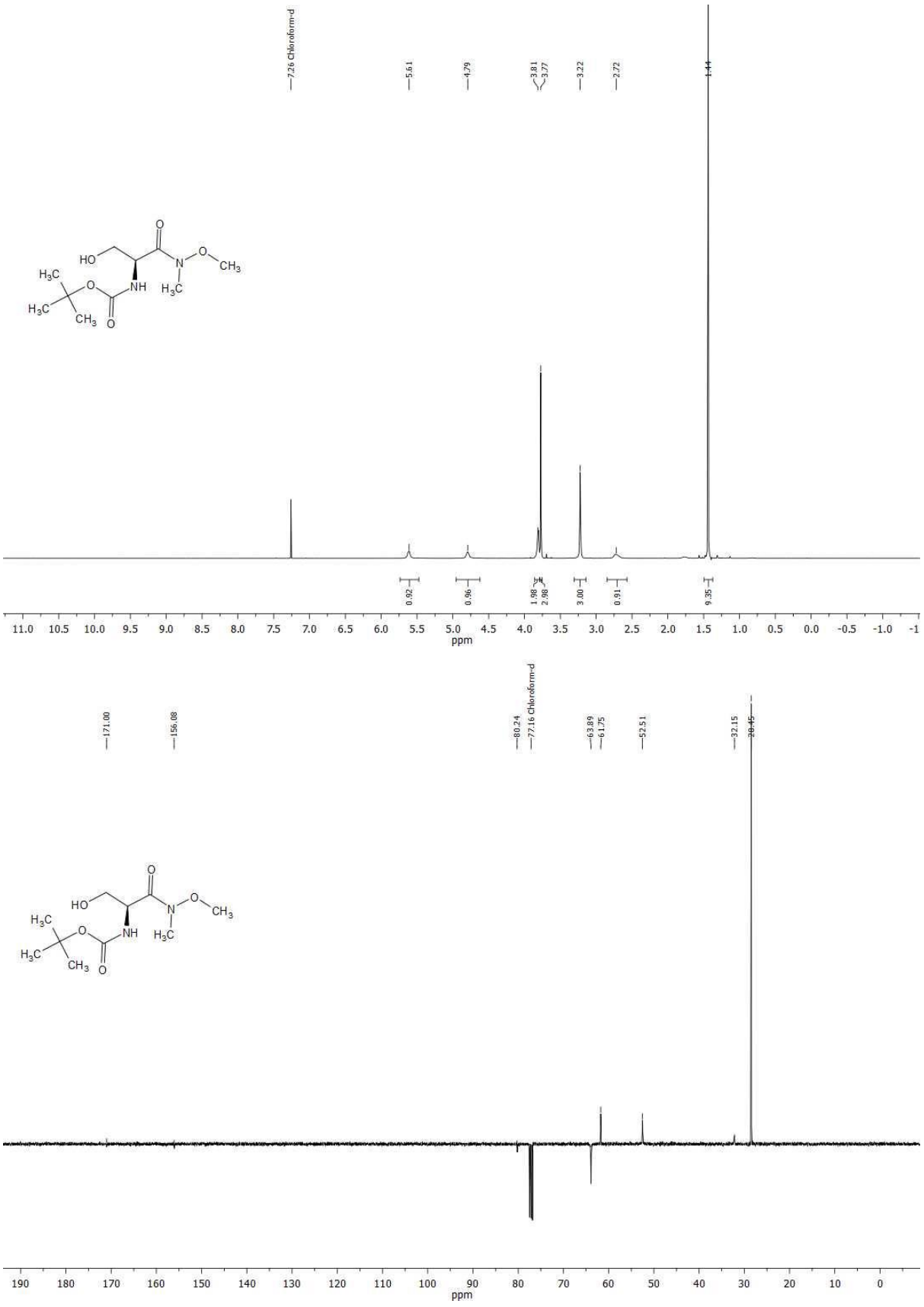

(S)-N-methoxy-N-methyl-3-(tert-butyldiphenylsilyloxy)-2-(N-tert butyloxy carbonyl) amino propanamide (**203**) ($CDCl_3$)

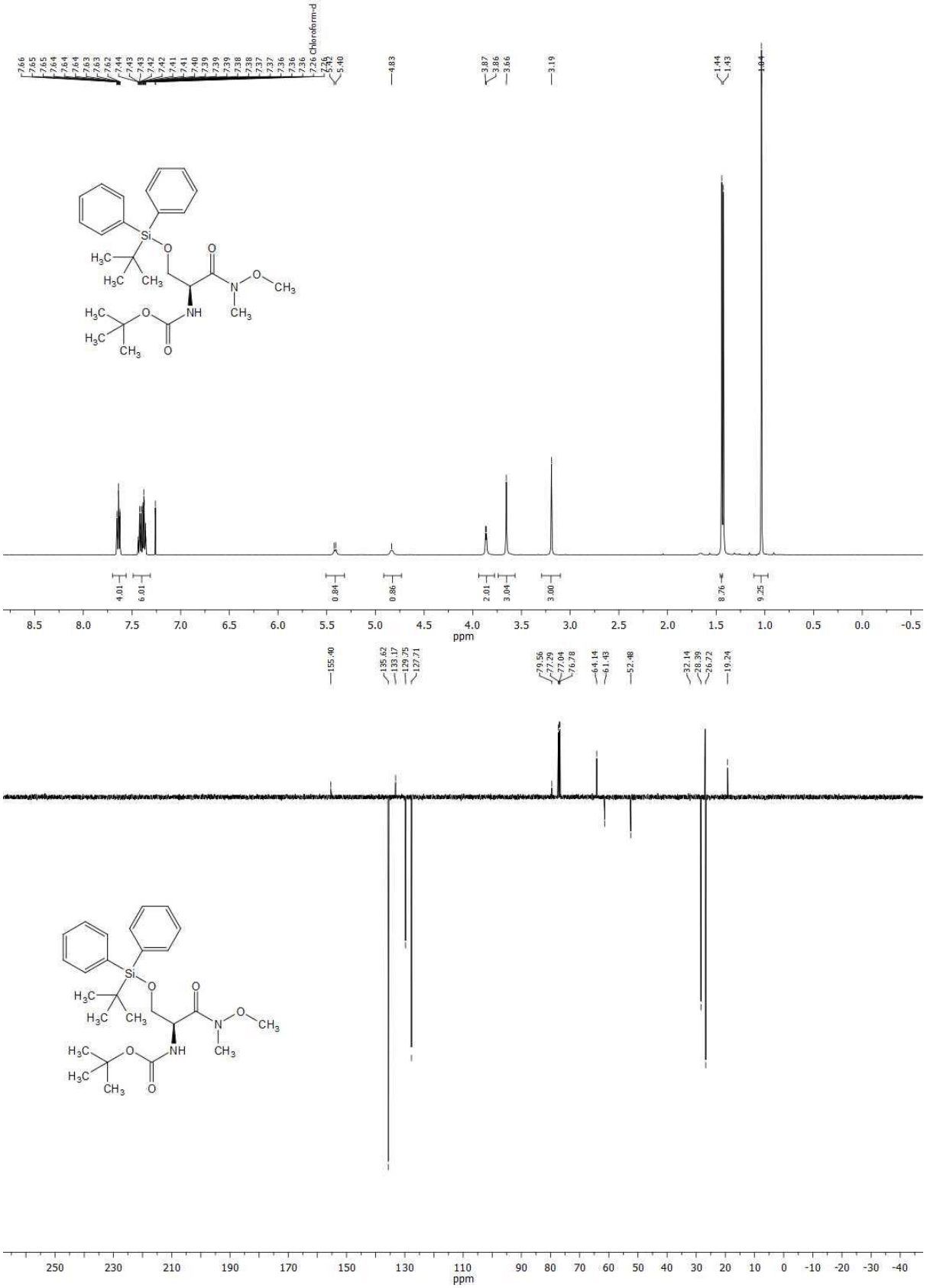

(S)-1-(tert-butyldiphenylsilyloxy)-2-(N-tert-butyloxycarbonyl)aminopent-4-en-3-on (**204**) ($CDCl_3$)

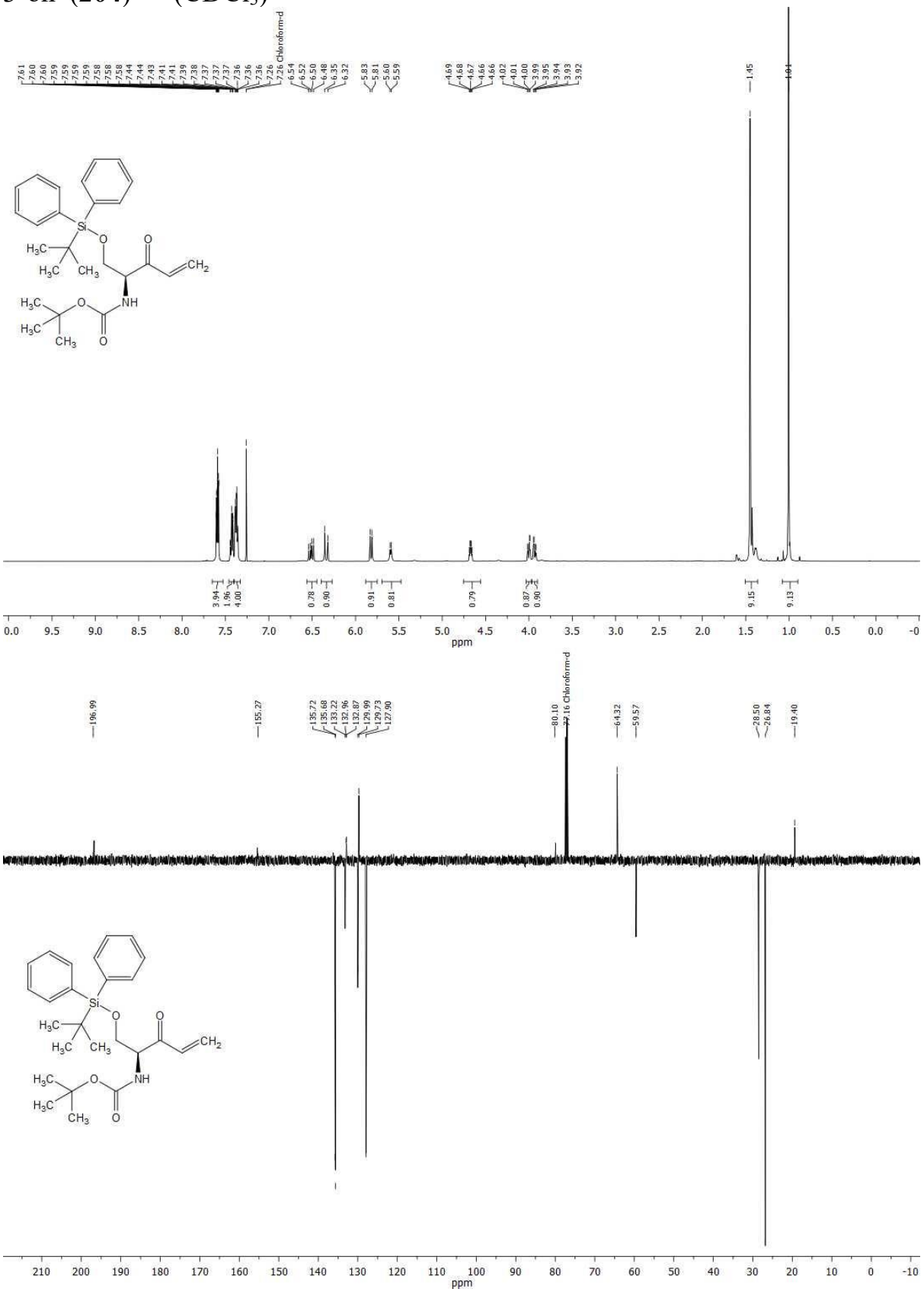

(2S,3R)-1-(tert-butyldiphenylsilyloxy)-2-(N-tert-butyloxycarbonyl) aminopent-4-en-3-ol (**205**) ($CDCl_3$)

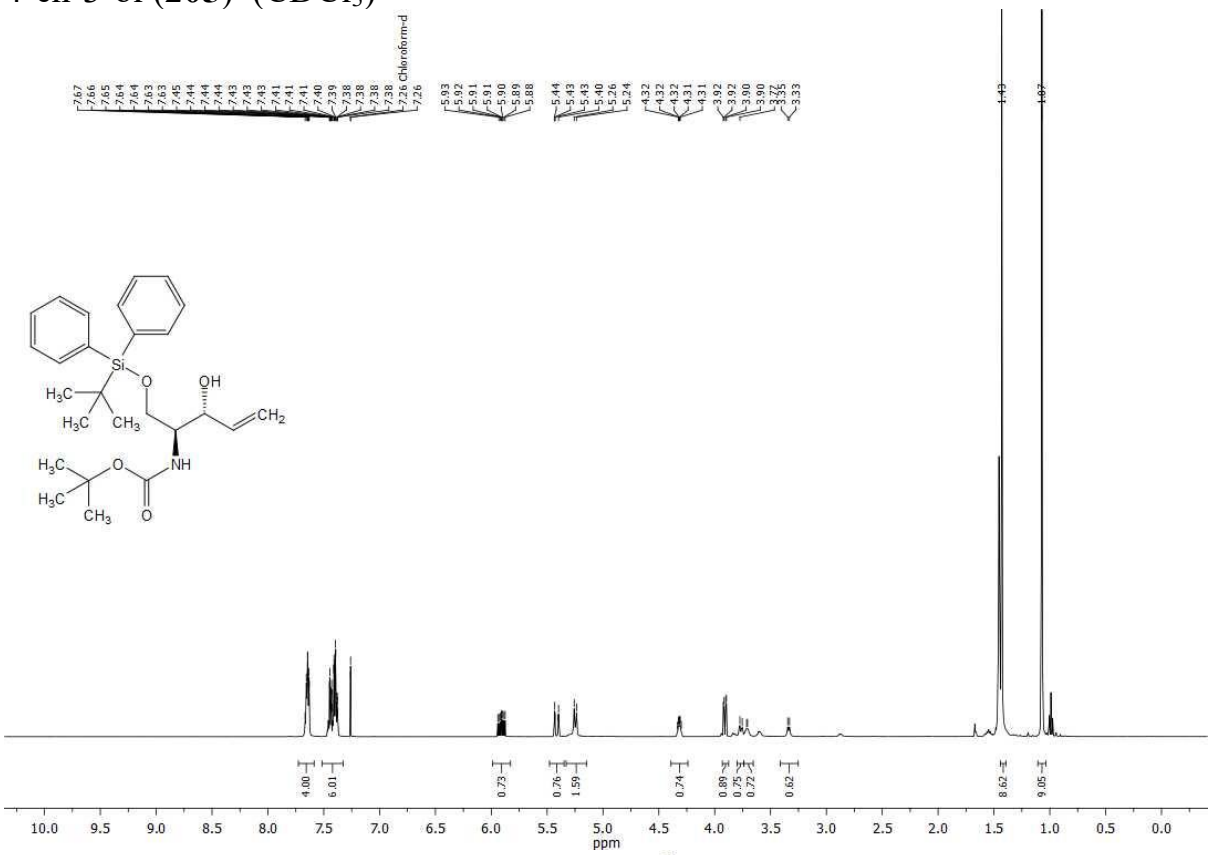

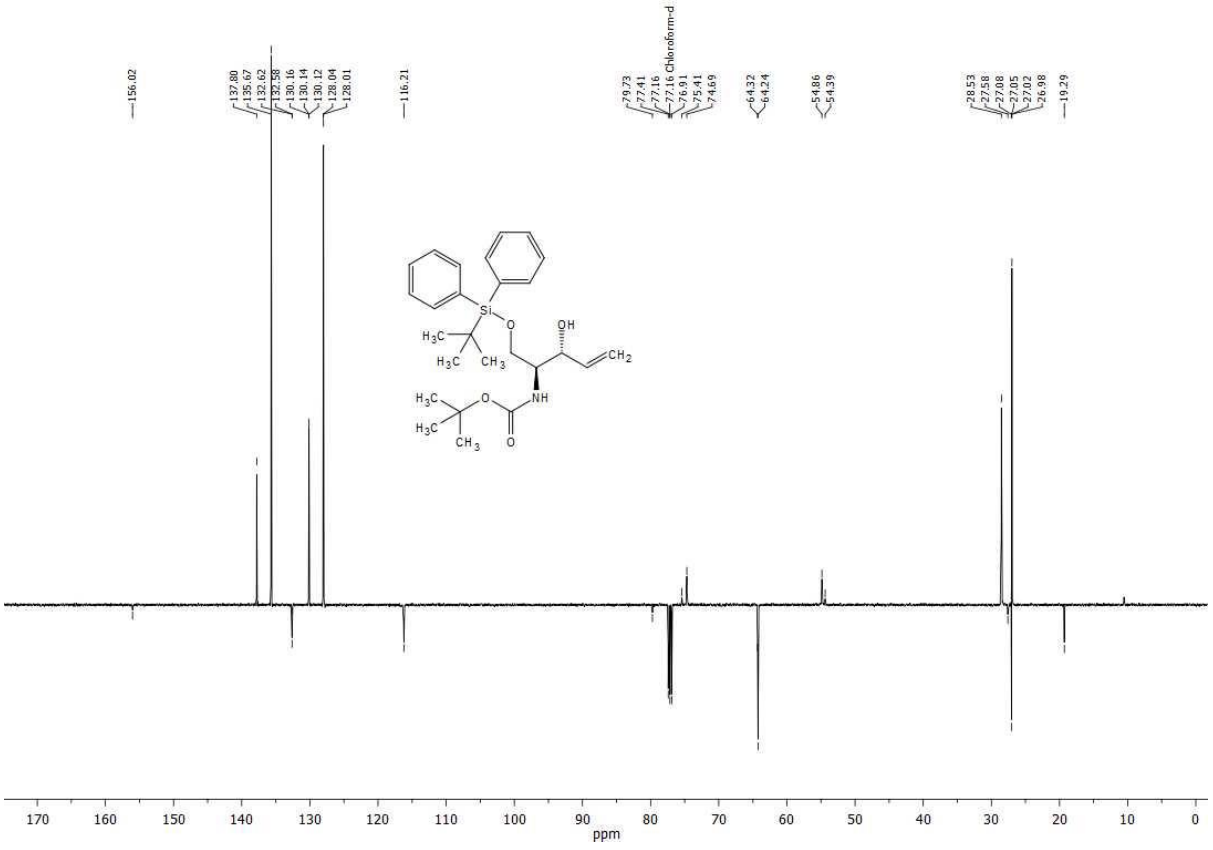

(2S,3R,E)-1-(tert-butyldiphenylsilyloxy)-2-(N-tertbutyloxycarbonyl) amino octadic-4-en-3-ol (**206**) ($CDCl_3$)

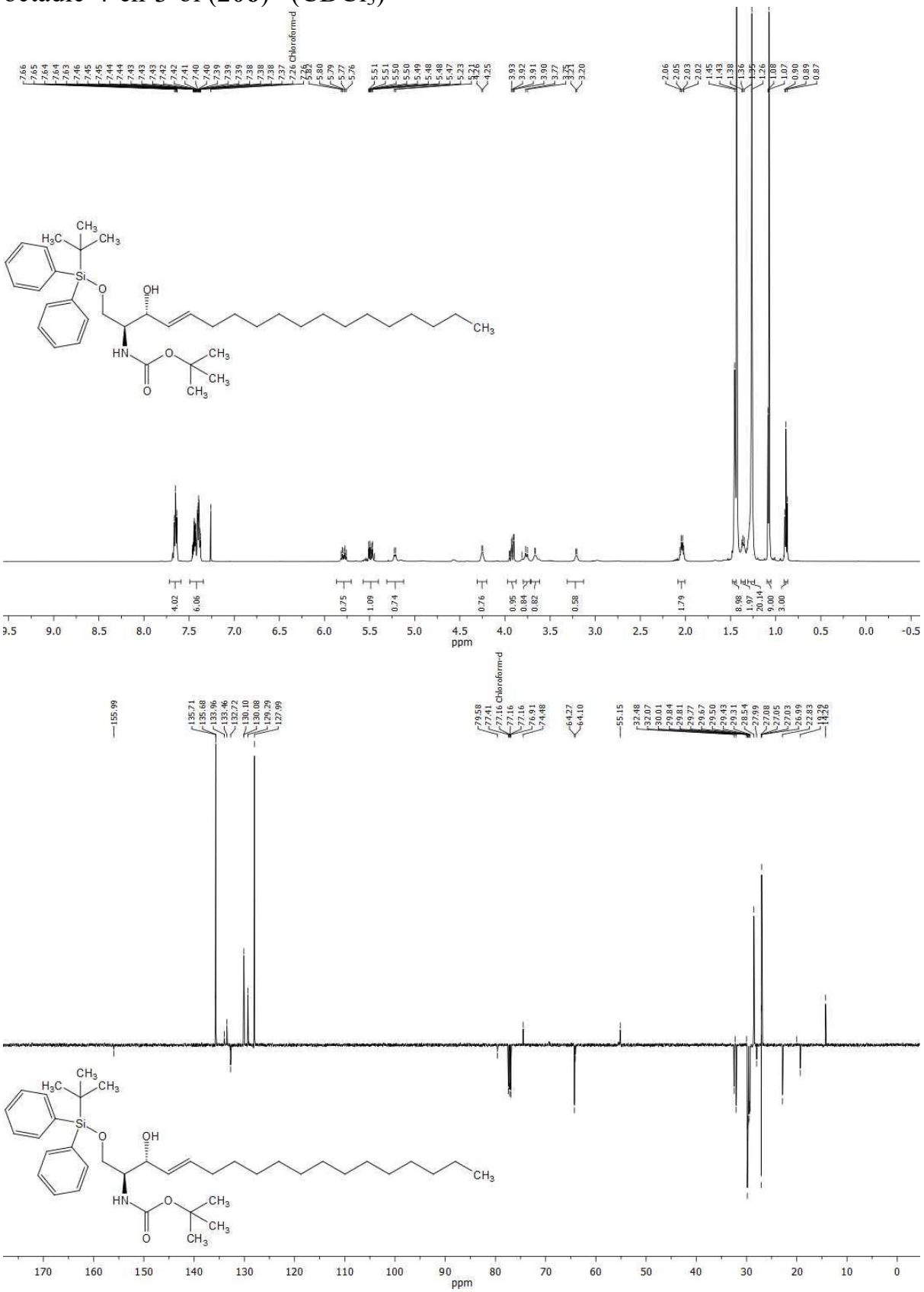

tert-butyl(2S,3R,E)-1-(tert-butyldiphenylsilyloxy)-3-(methoxymethoxy)octadec-4 en-2-ylcarbamate (**207**) ($CDCl_3$)

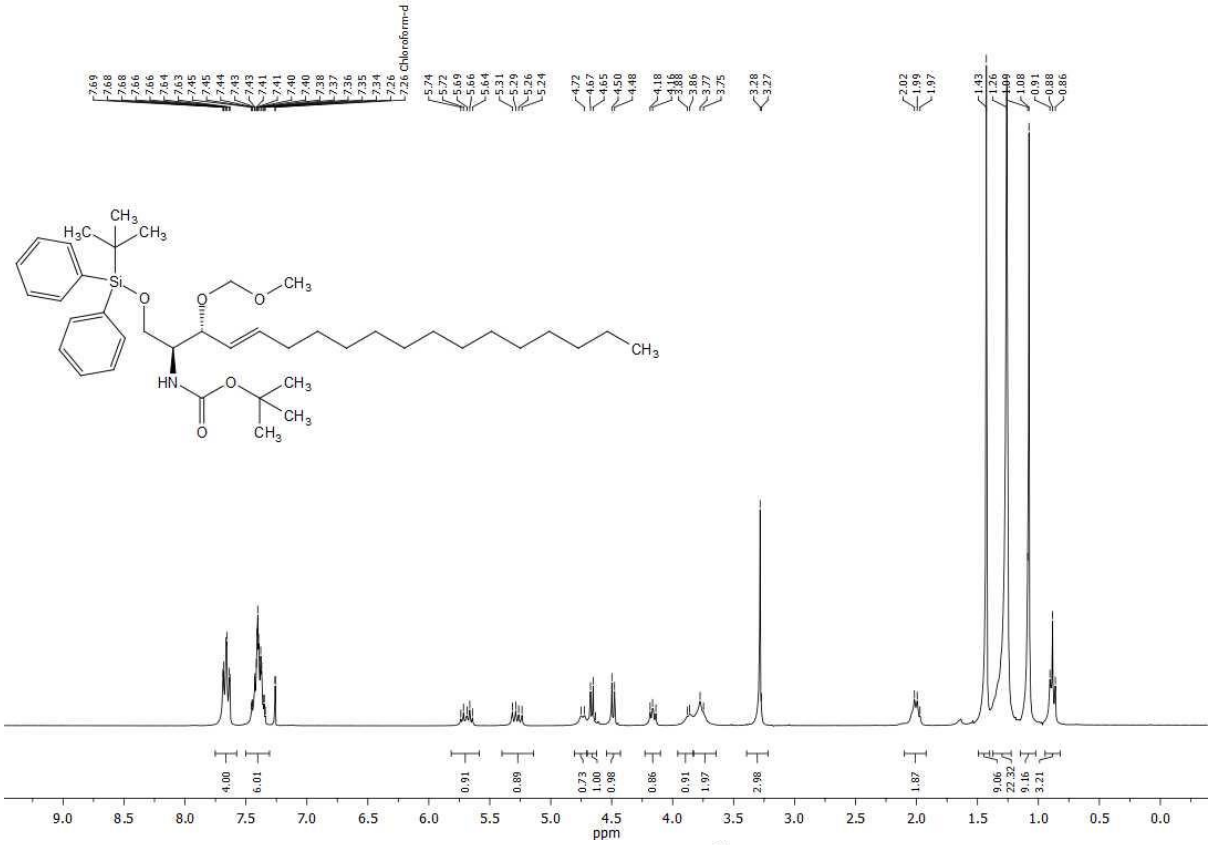

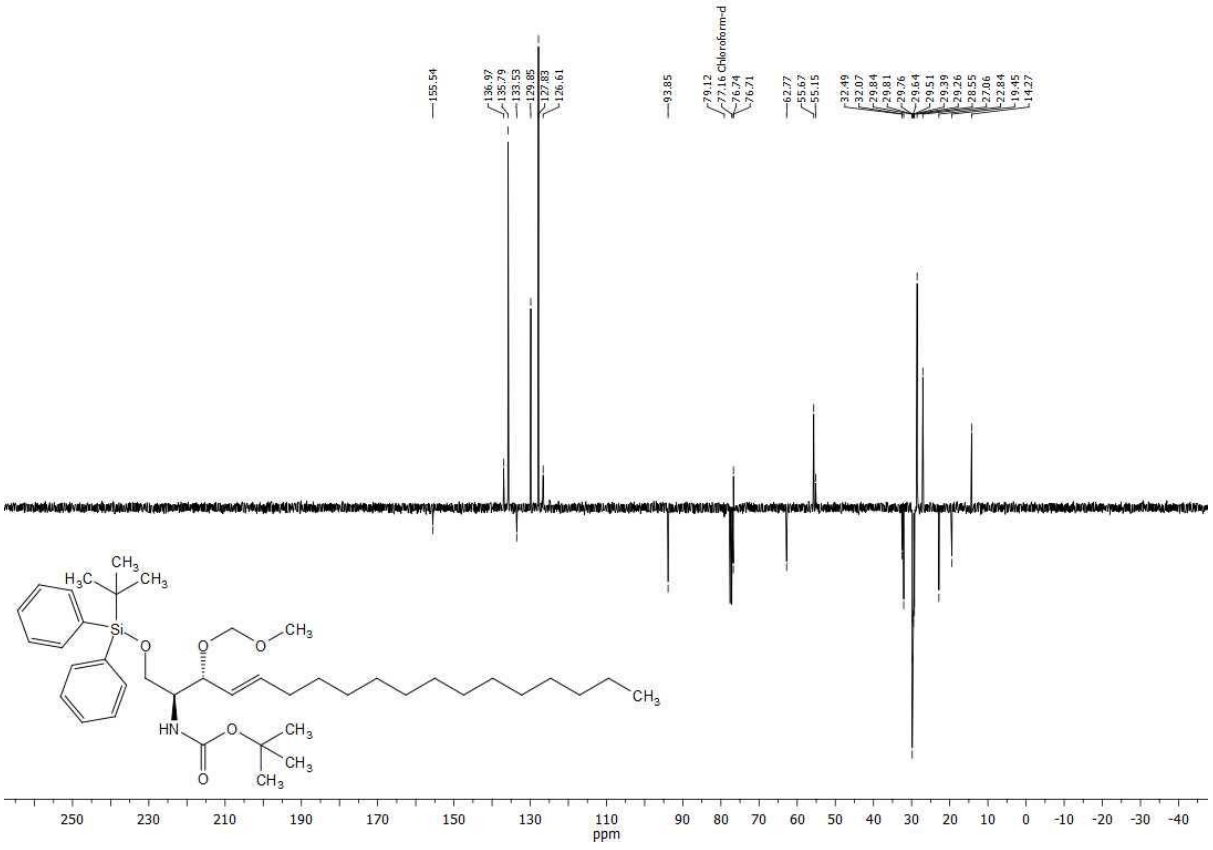

tert-butyl (2*S*,3*R*,*E*)-1-hydroxy-3-(methoxymethoxy)octadec-4-en-2-yl carbamate (**208**) ($CDCl_3$)

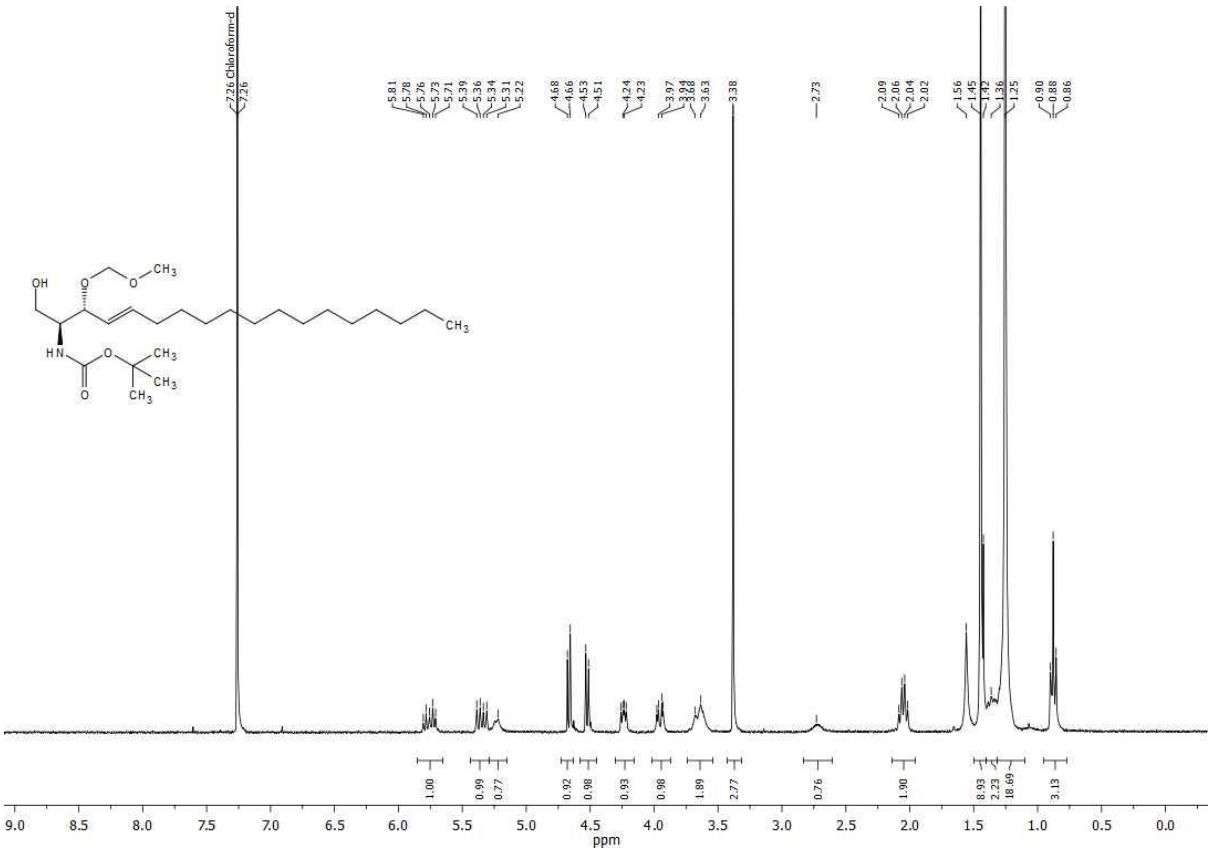

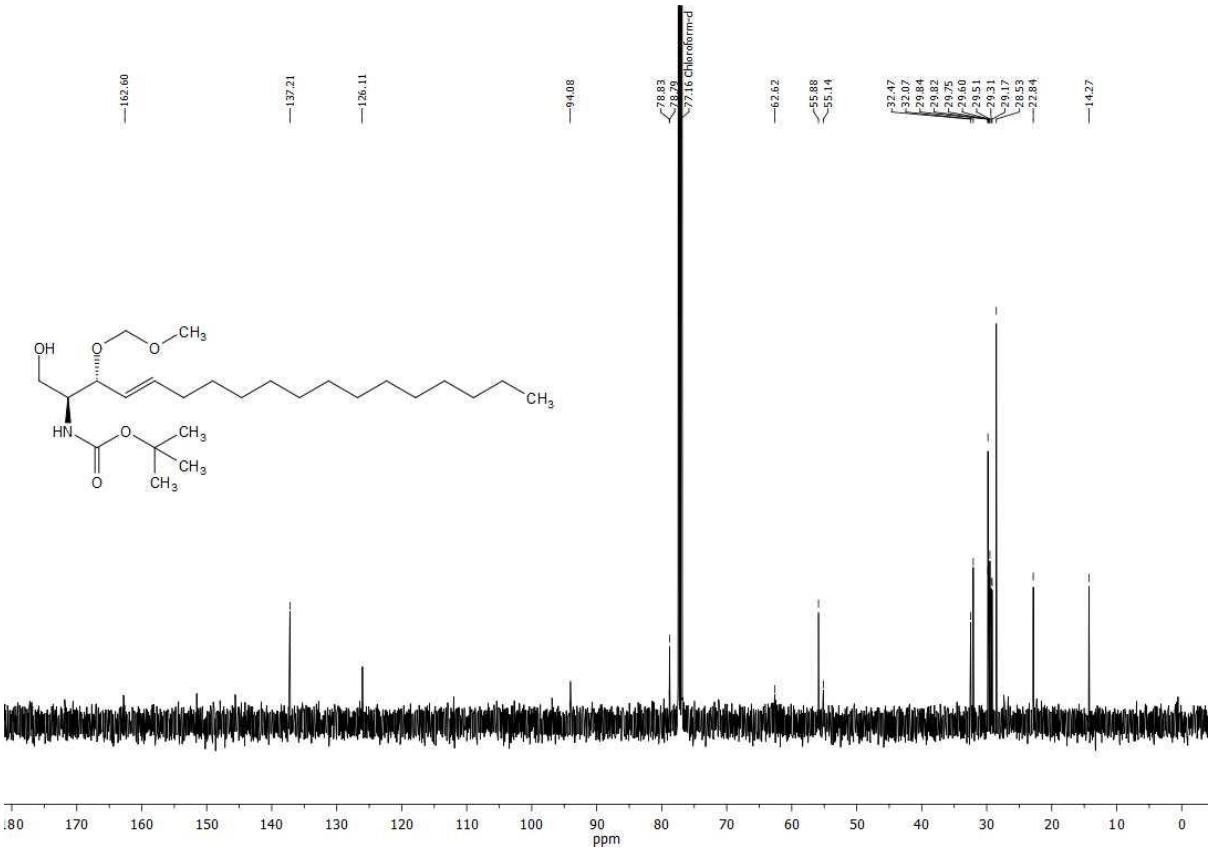

2-(2-hydroxyethyl)isoindoline-1,3-dione (**209**) ($CDCl_3$)

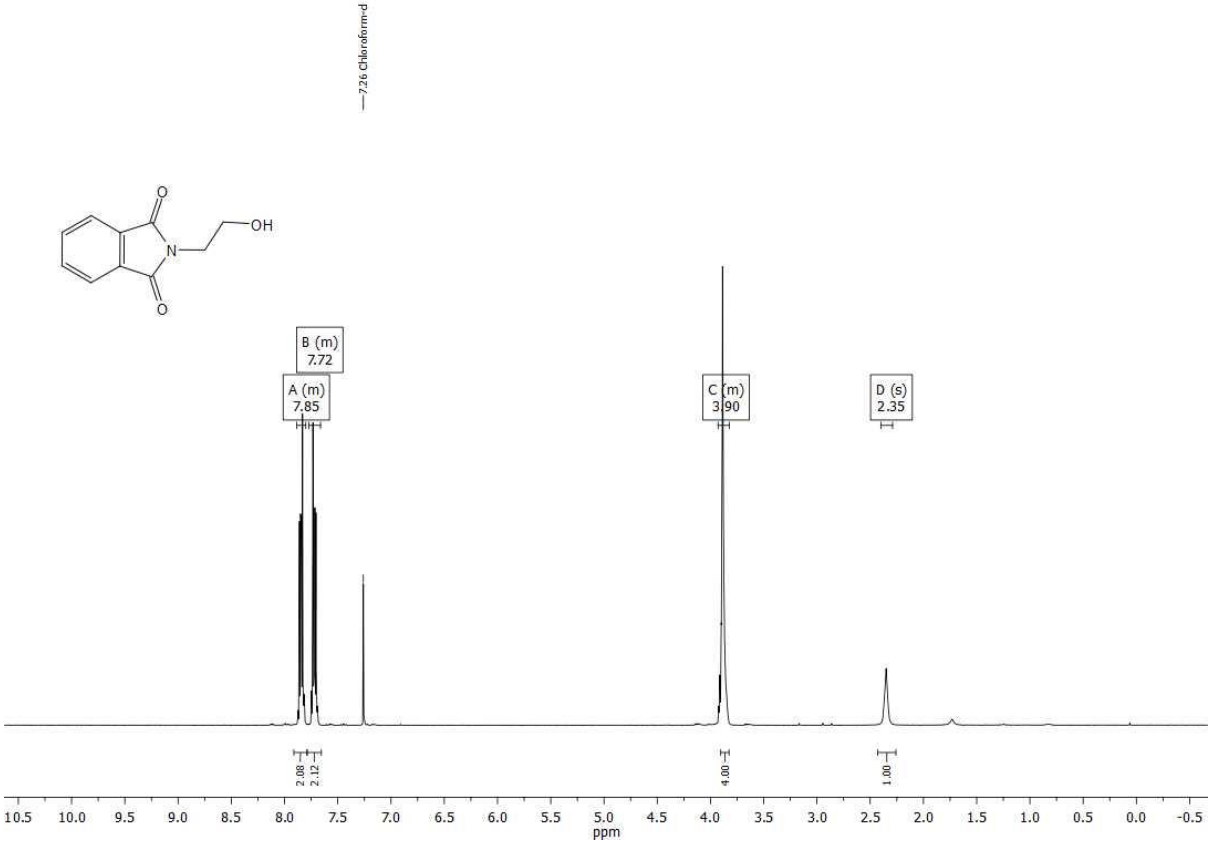

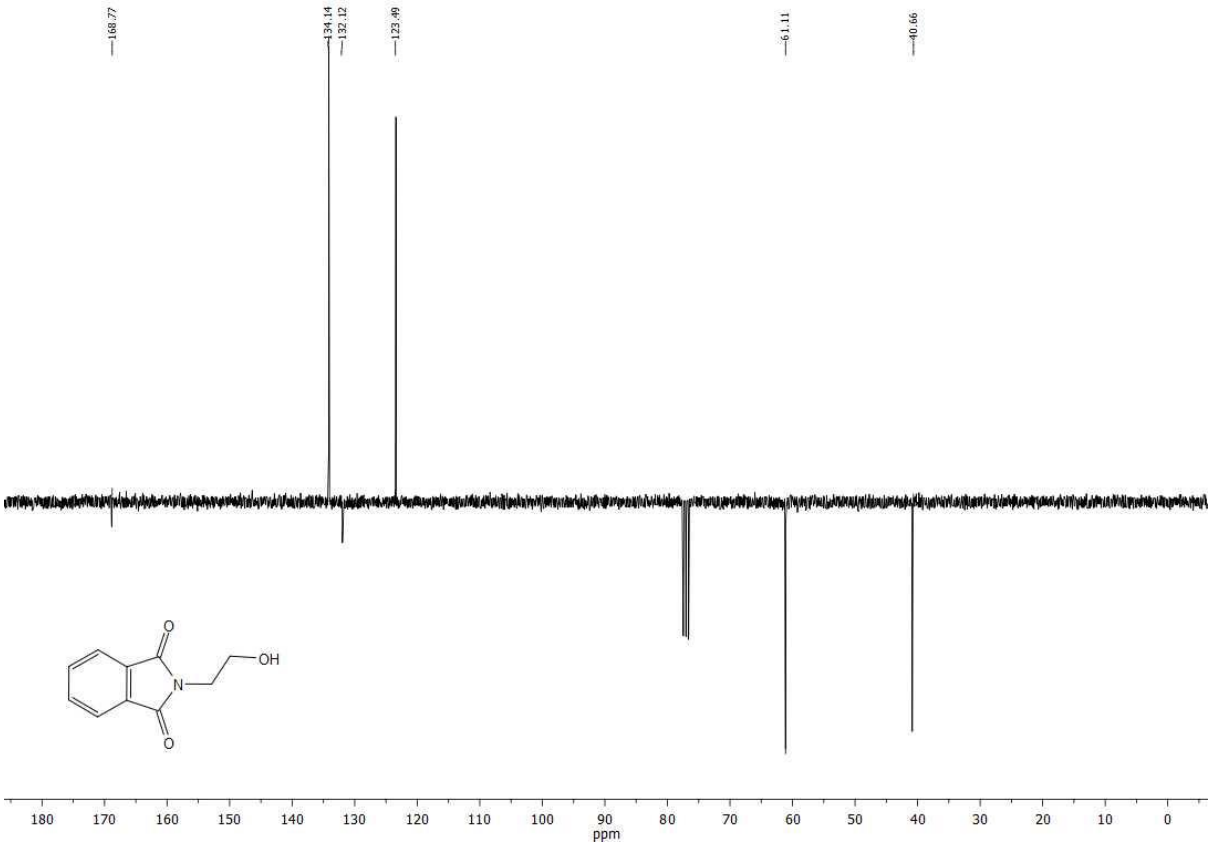

O-2-phthalimidoethyl phosphorodichloridate (**210**) ($CDCl_3$)

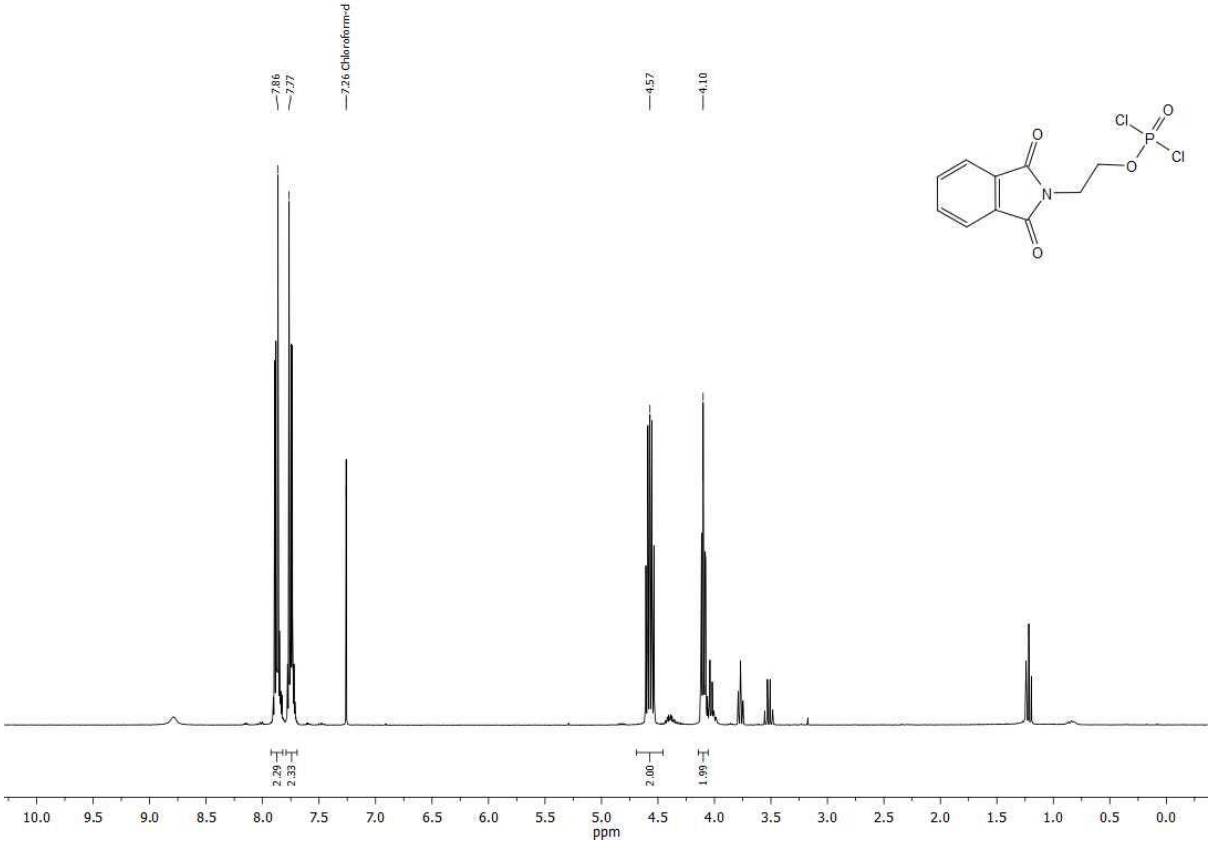

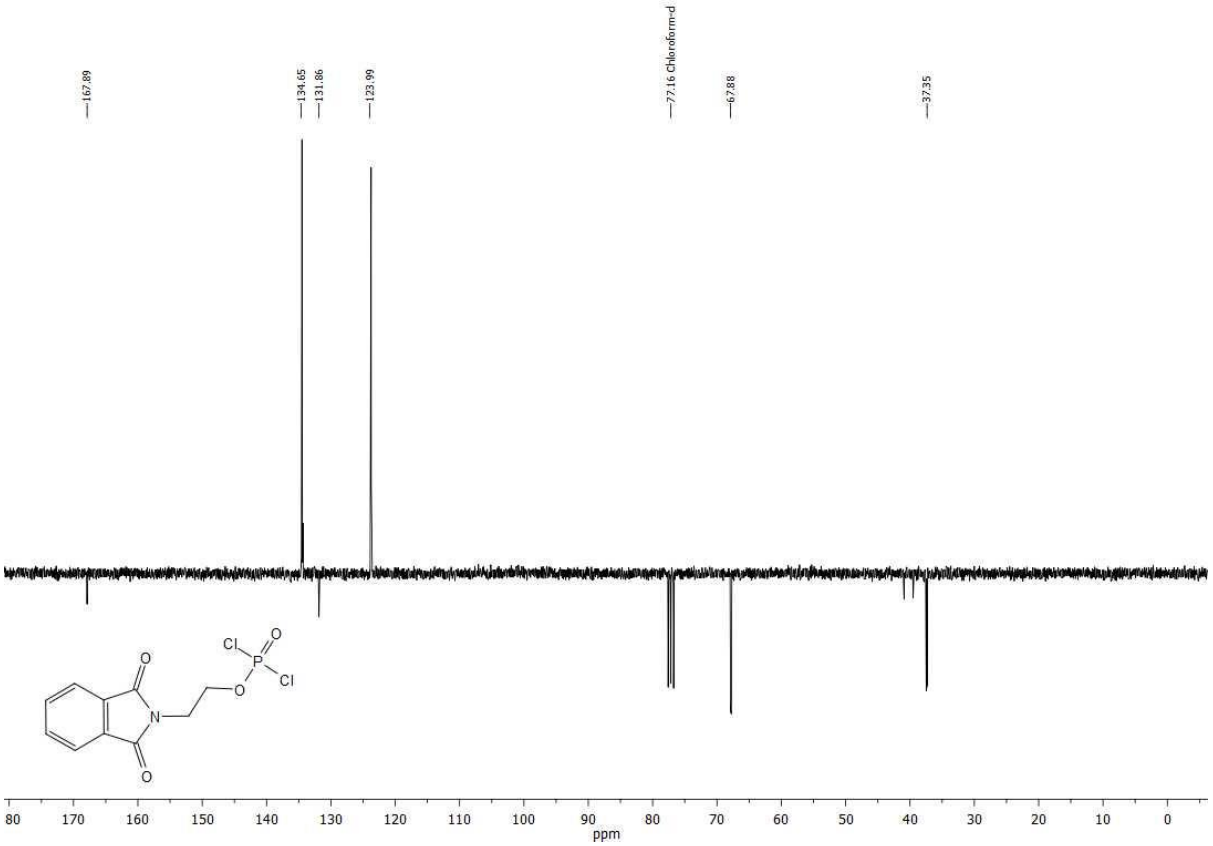

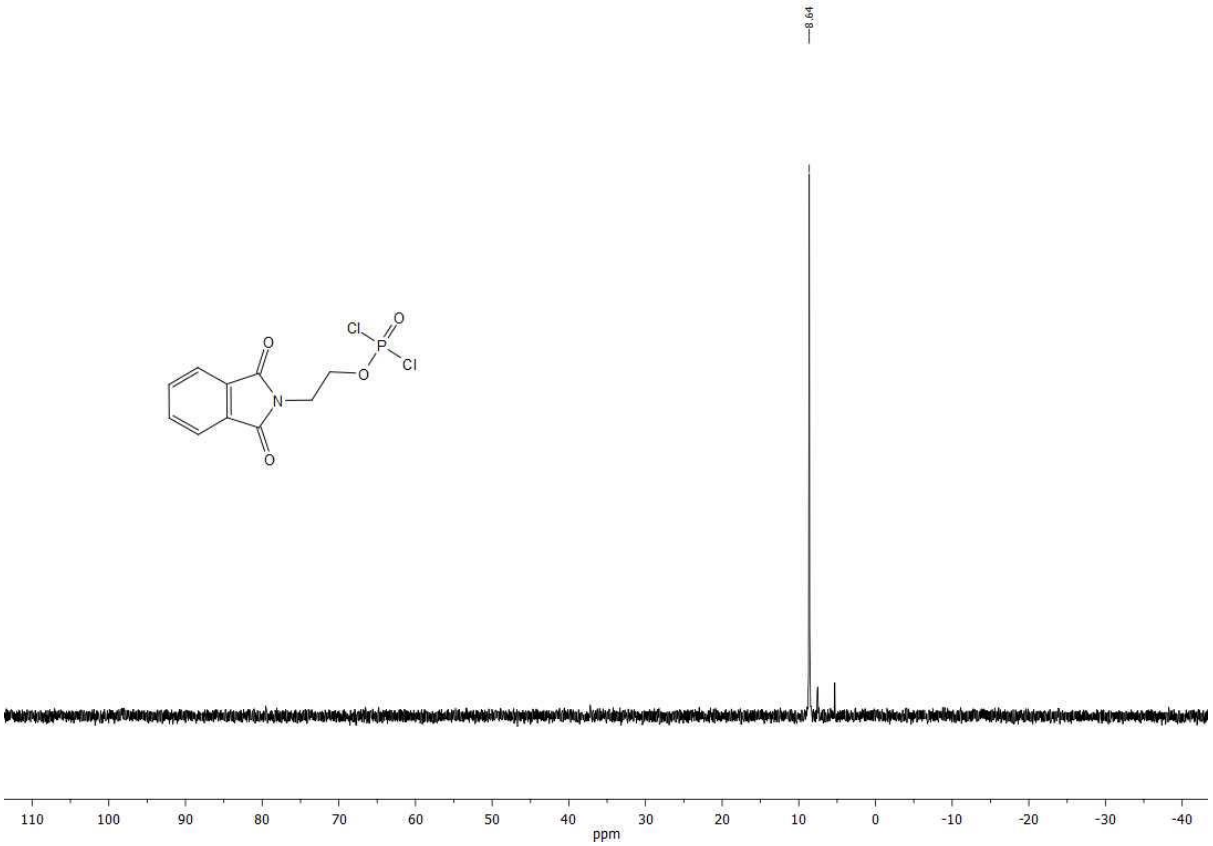

tert-butyl ((2S,3R,E)-1-(((2-(1,3-dioxoisoindolin-2-yl)ethoxy) (hydroxy) phosphoryl) oxy)-3-(methoxymethoxy)octadec-4-en-2-yl)carbamate (**211**) ($CDCl_3$/MeOD)

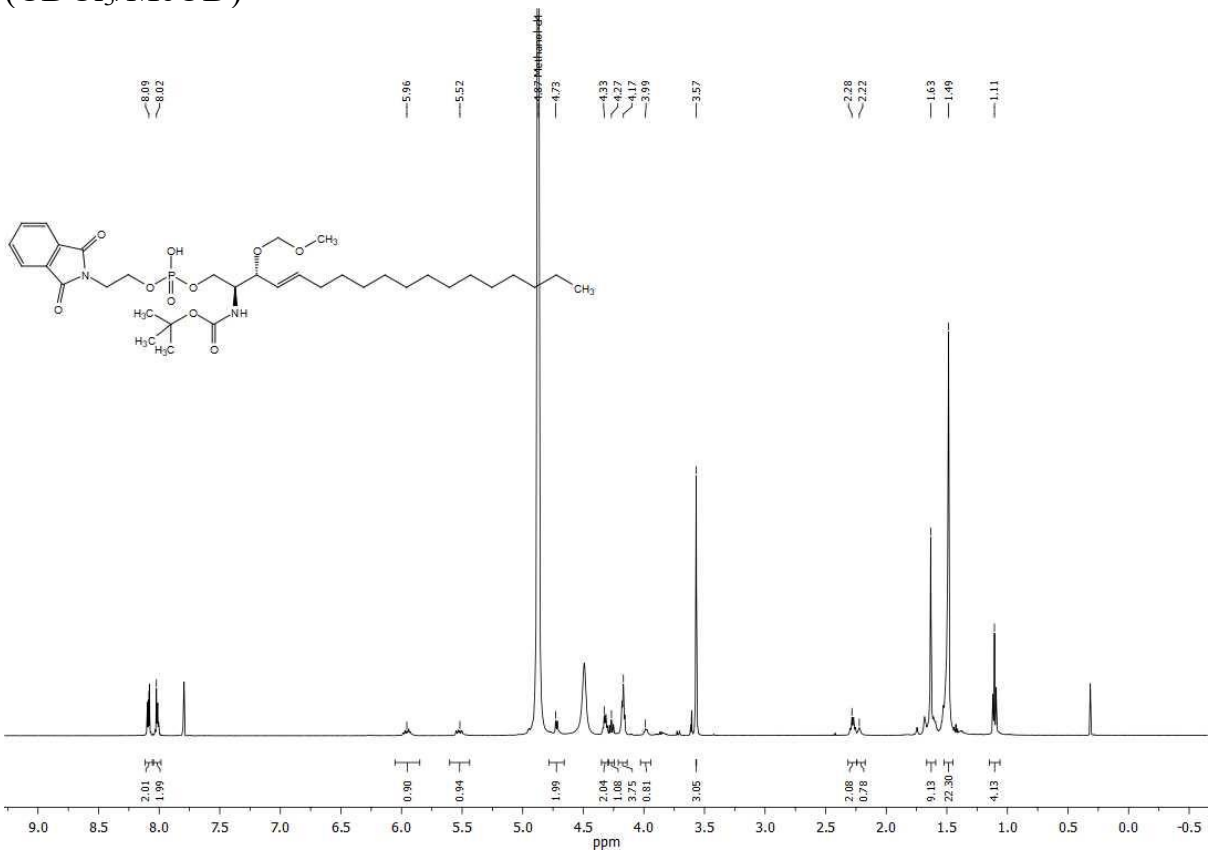

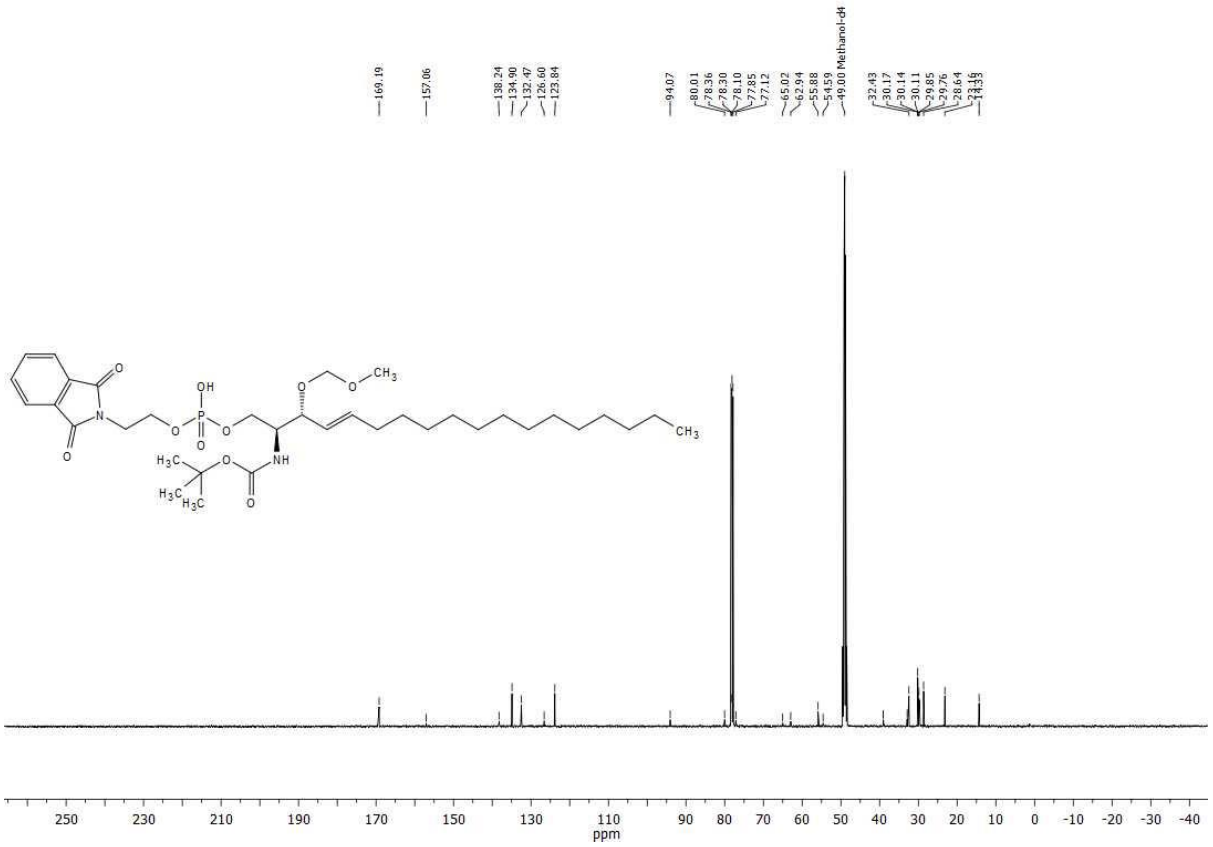
169.19
157.06
138.24
134.90
132.47
126.60
123.64
94.07
80.01
78.36
78.30
78.10
77.85
77.12
65.02
62.94
55.88
54.59
49.00 Methanol-d4
32.43
30.17
30.14
30.11
29.85
29.76
28.64
23.16
14.13
250 230 210 190 170 150 130 110 90 80 70 60 50 40 30 20 10 0 -10 -20 -30 -40
ppm

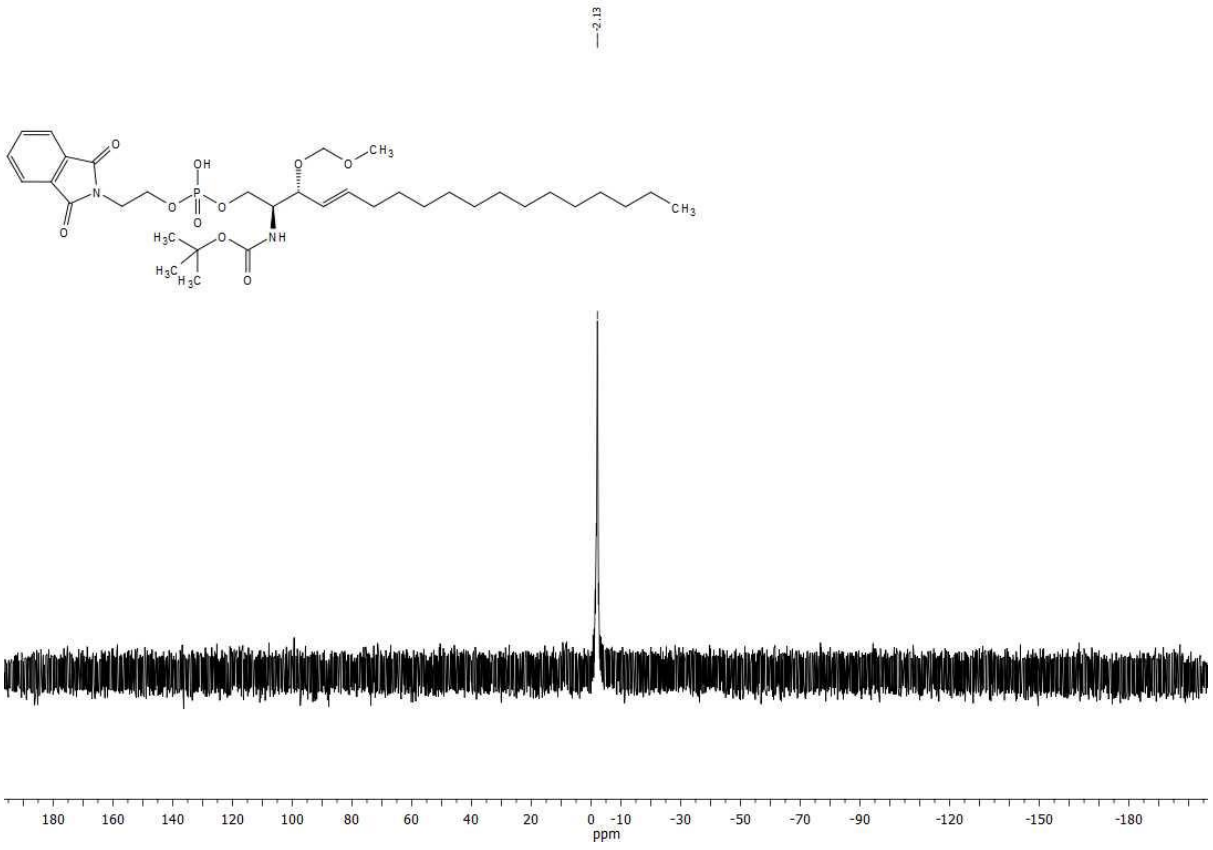
2.13
180 160 140 120 100 80 60 40 20 0 -10 -30 -50 -70 -90 -120 -150 -180
ppm

2-ammonioethyl ((2S,3R,E)-2-((tert-butoxycarbonyl)amino)-3-(methoxymethox
-y)octadec-4-en-1-yl) phosphate (**212**)

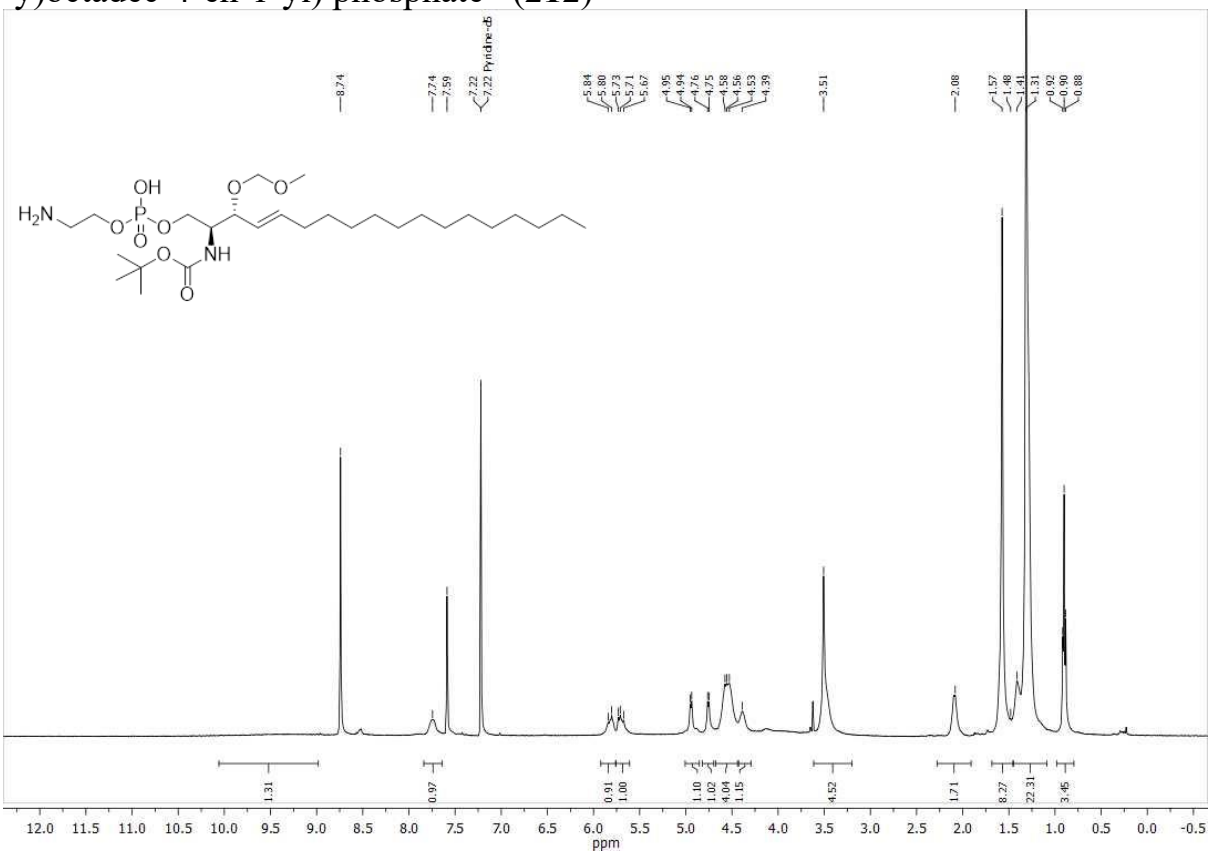

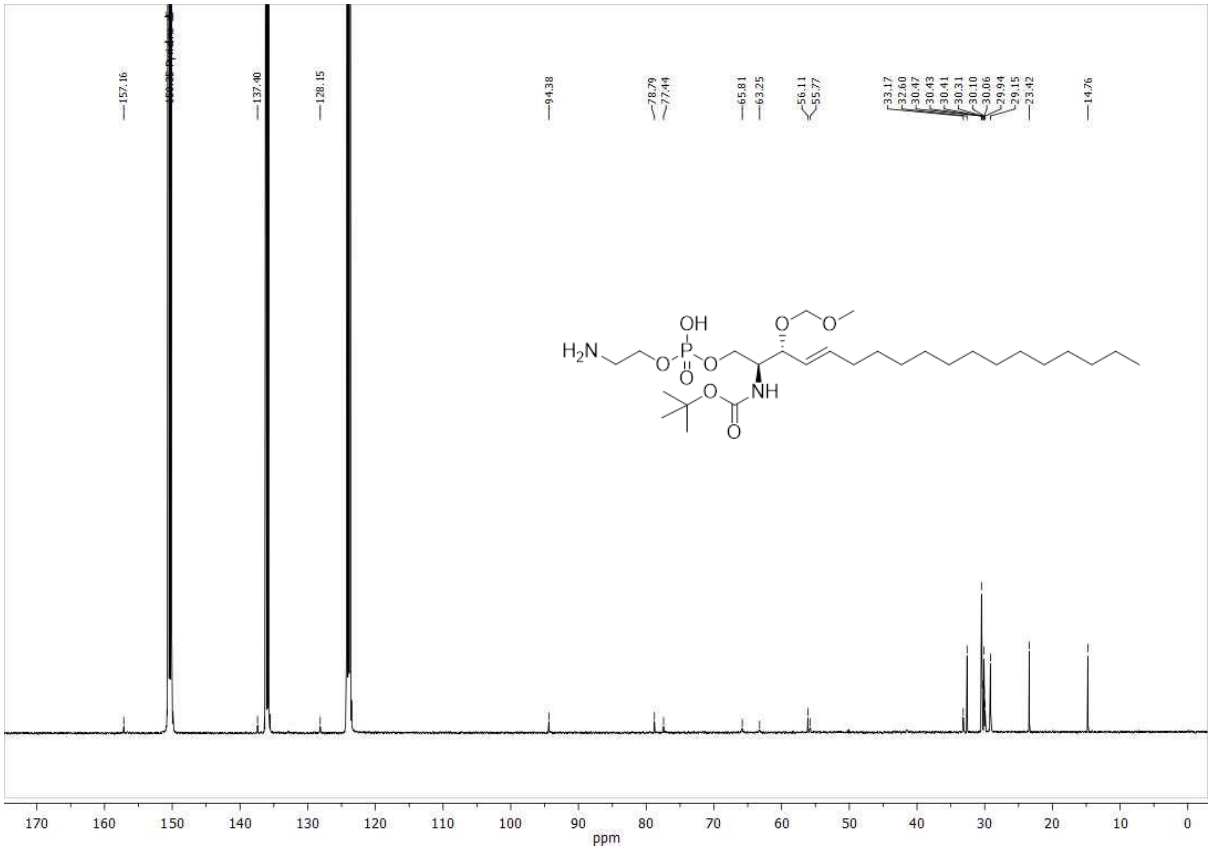

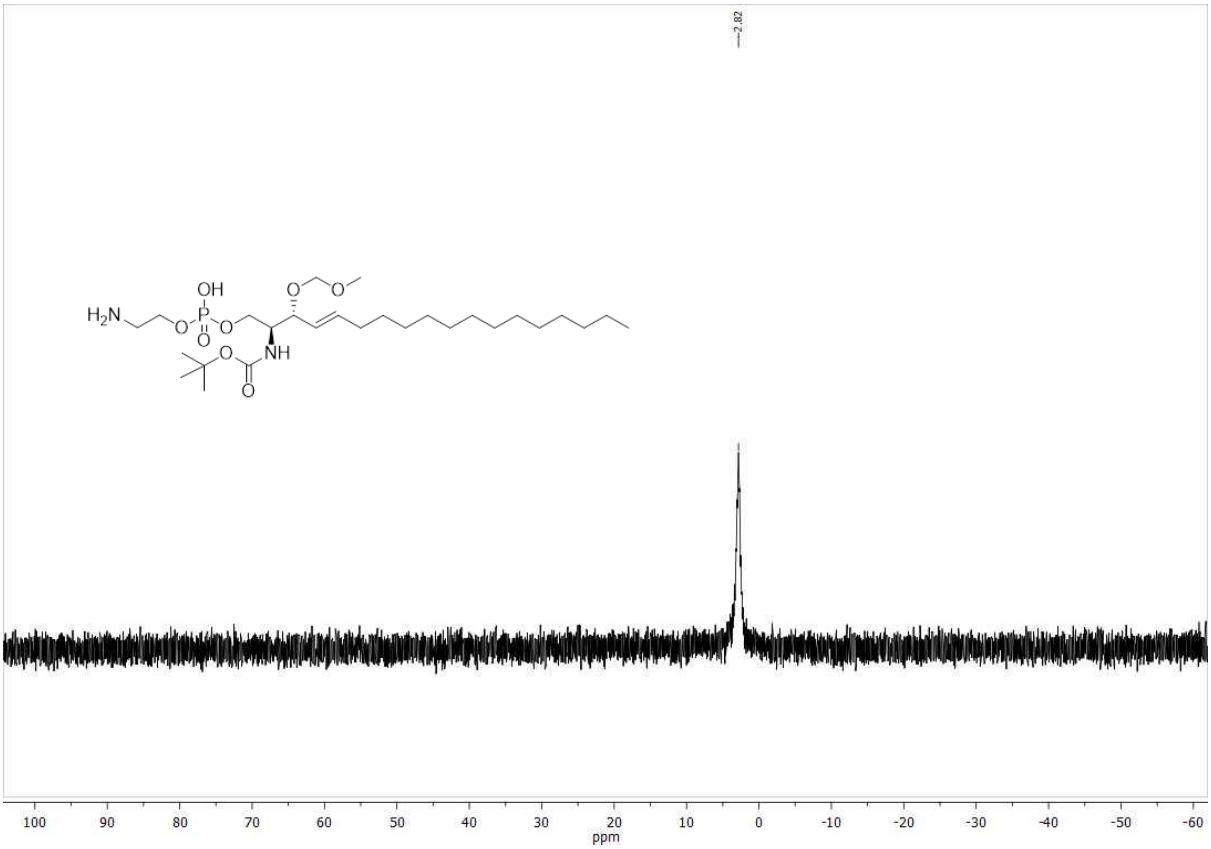

(2S,3R,E)-2-(tert-butoxycarbonyl)-3-(methoxymethoxy)octadec-4-enyl 2 (dimethyl(prop-2-ynyl) ammonio)ethyl phosphate (**214**) (CD_3OD)

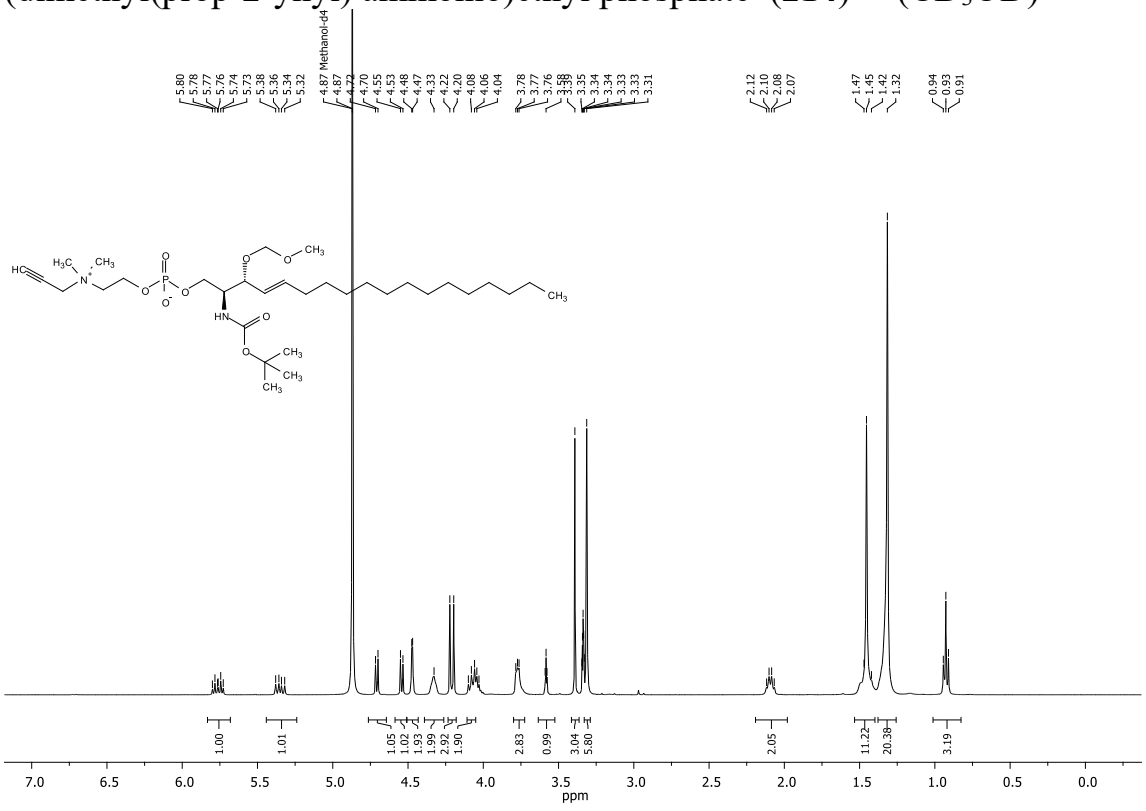

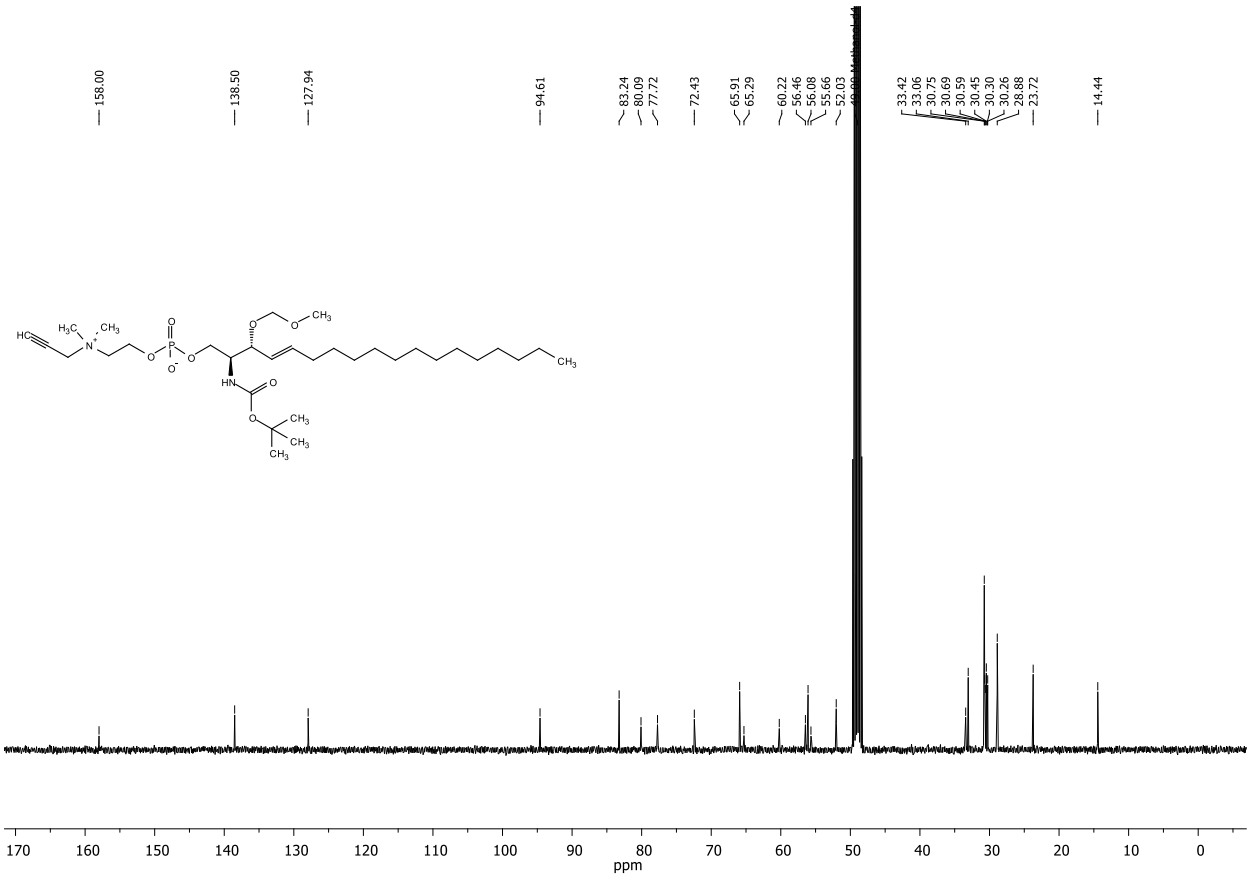
158.00
138.50
127.94
94.61
83.24
80.09
77.72
72.43
65.91
65.29
60.22
56.46
56.08
55.66
52.03
33.42
33.06
30.75
30.69
30.59
30.45
30.30
30.26
28.88
23.72
14.44
170 160 150 140 130 120 110 100 90 80 70 60 50 40 30 20 10 0
ppm

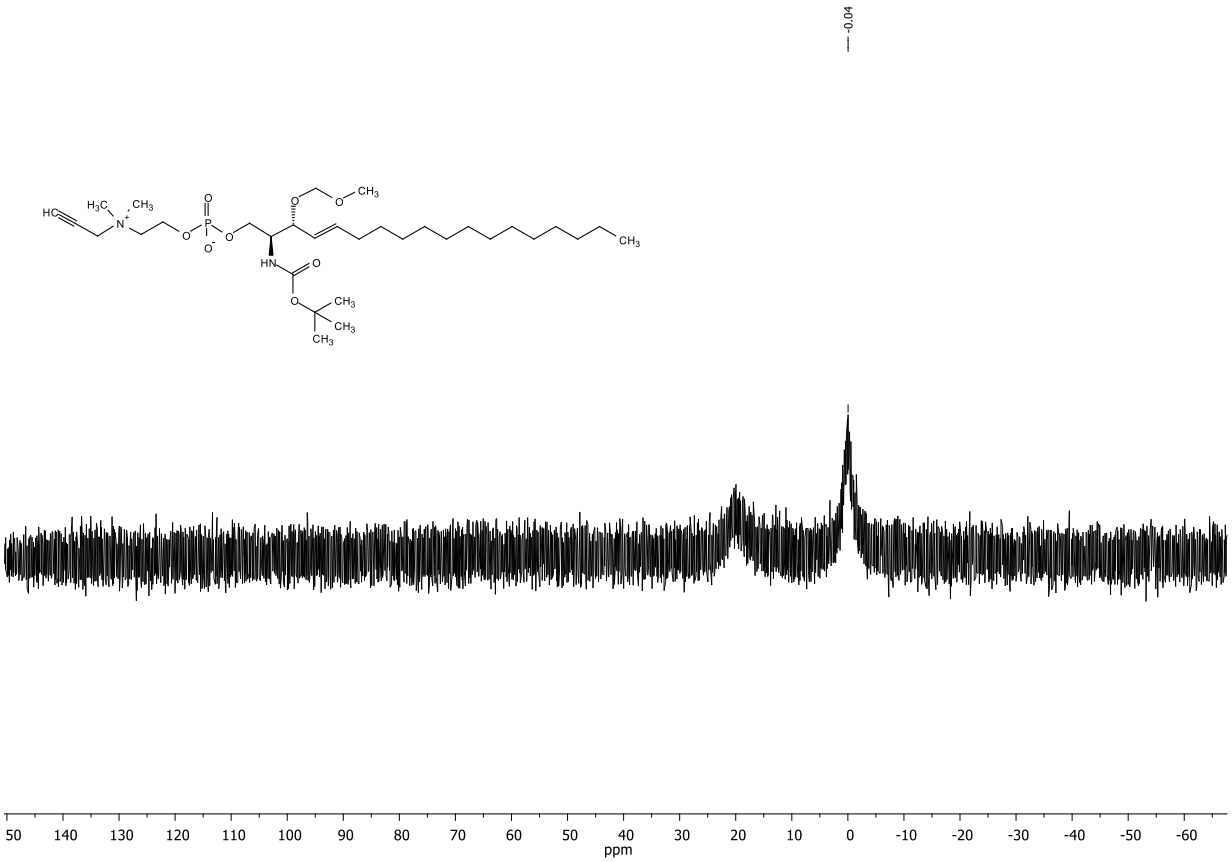
-0.04
50 140 130 120 110 100 90 80 70 60 50 40 30 20 10 0 -10 -20 -30 -40 -50 -60
ppm

Benzyl propiolate (**301**) ($CDCl_3$)

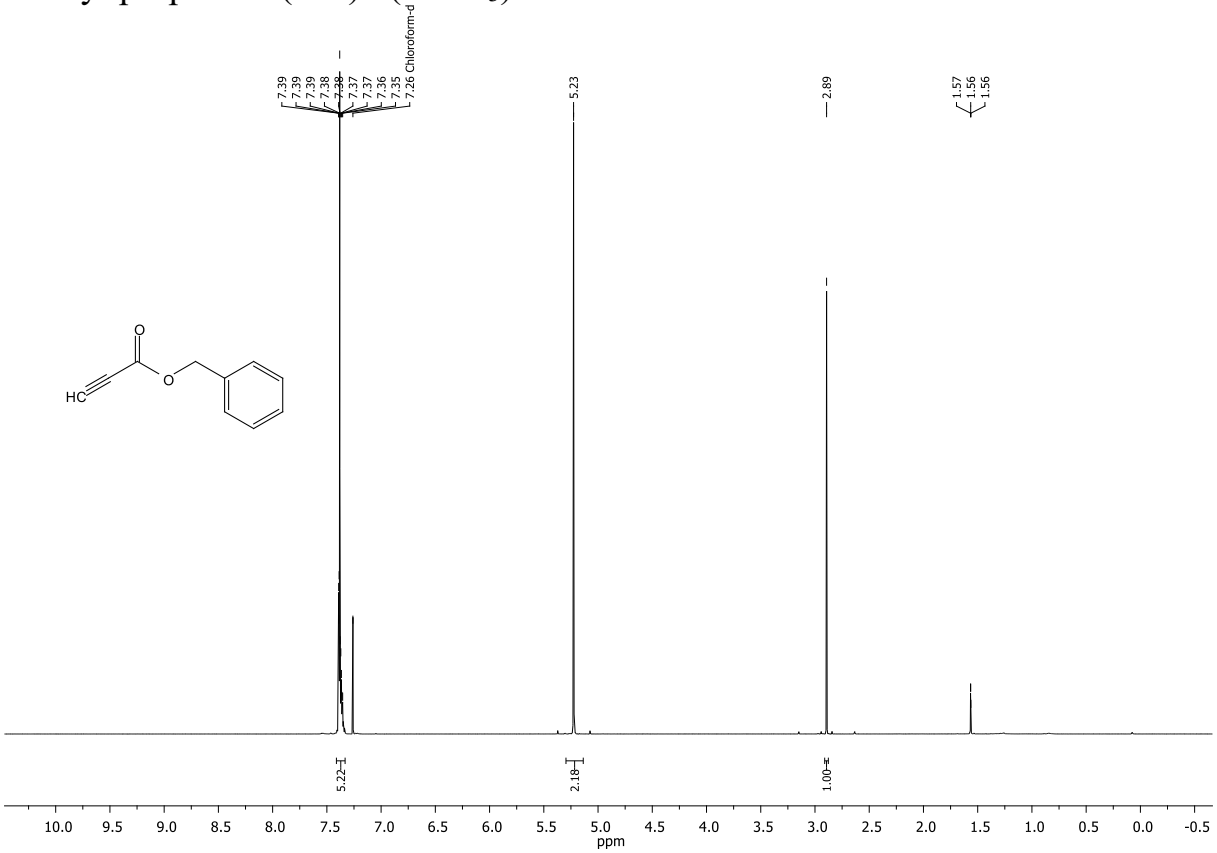

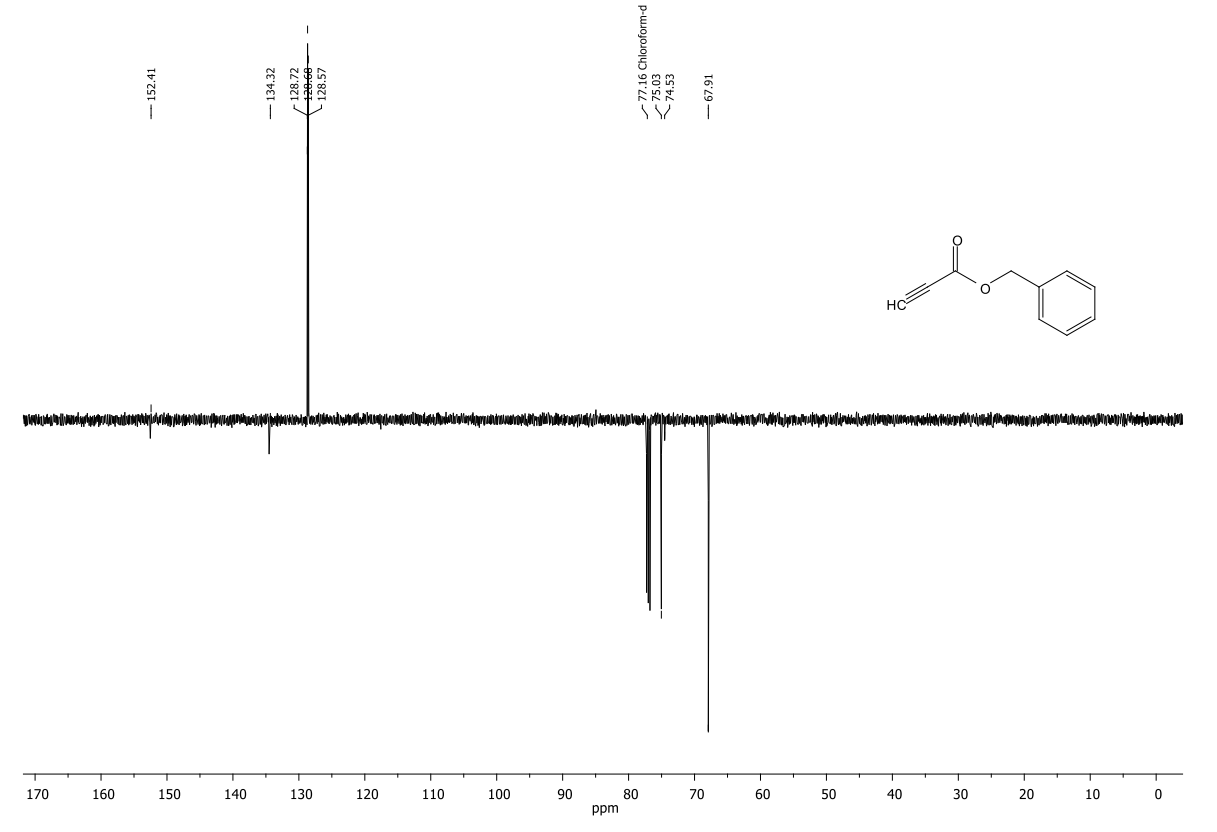

Benzyl 2-(8-methyl-6-oxo-6H-[1,3]dioxolo[4,5-g]chromen-2-yl)acetate (**302**) ($CDCl_3$)

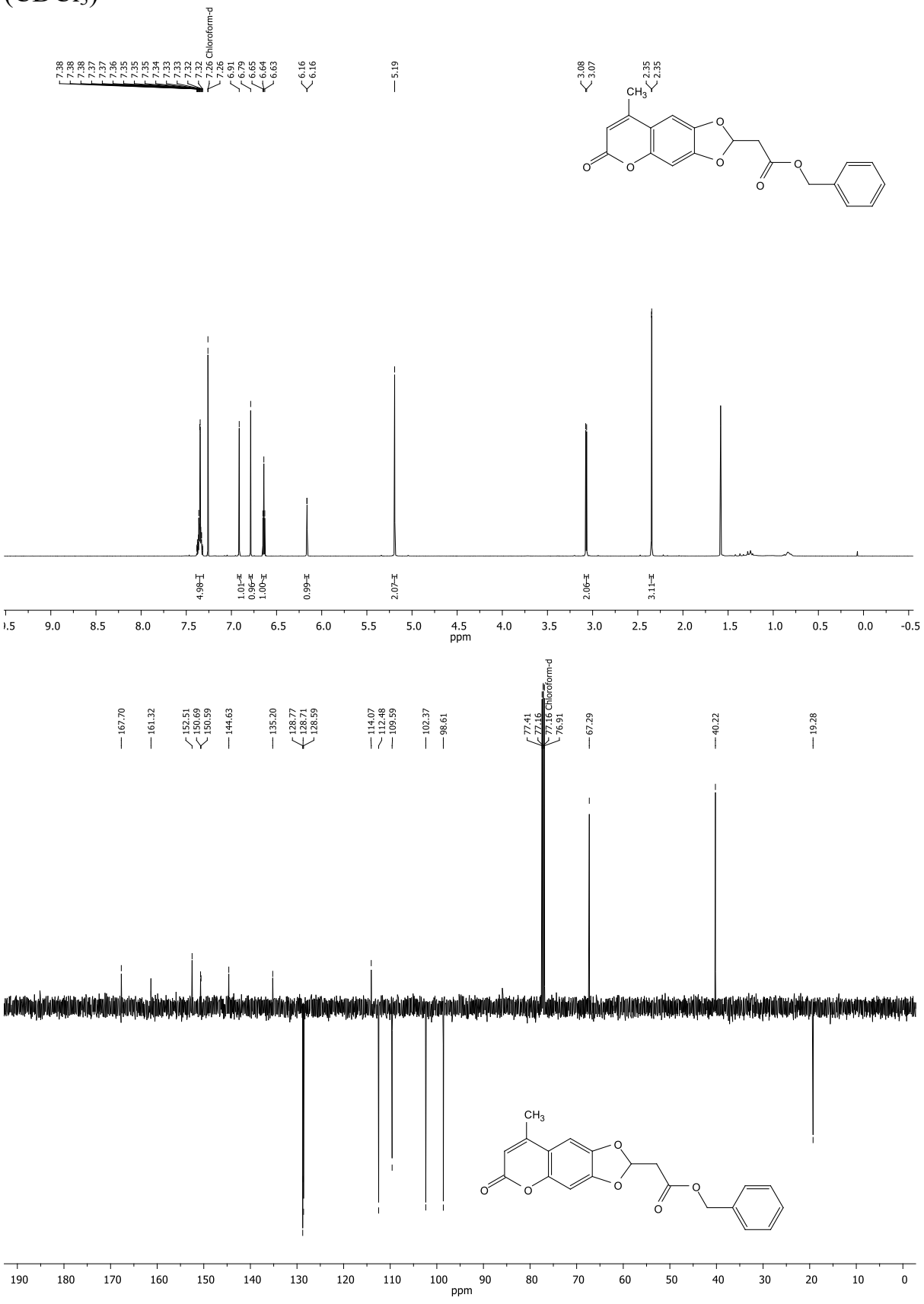

Benzyl 2-(7-bromo-8-methyl-6-oxo-6H-[1,3]dioxolo[4,5-g]chromen-2-yl)acetate (**303**) ($CDCl_3$)

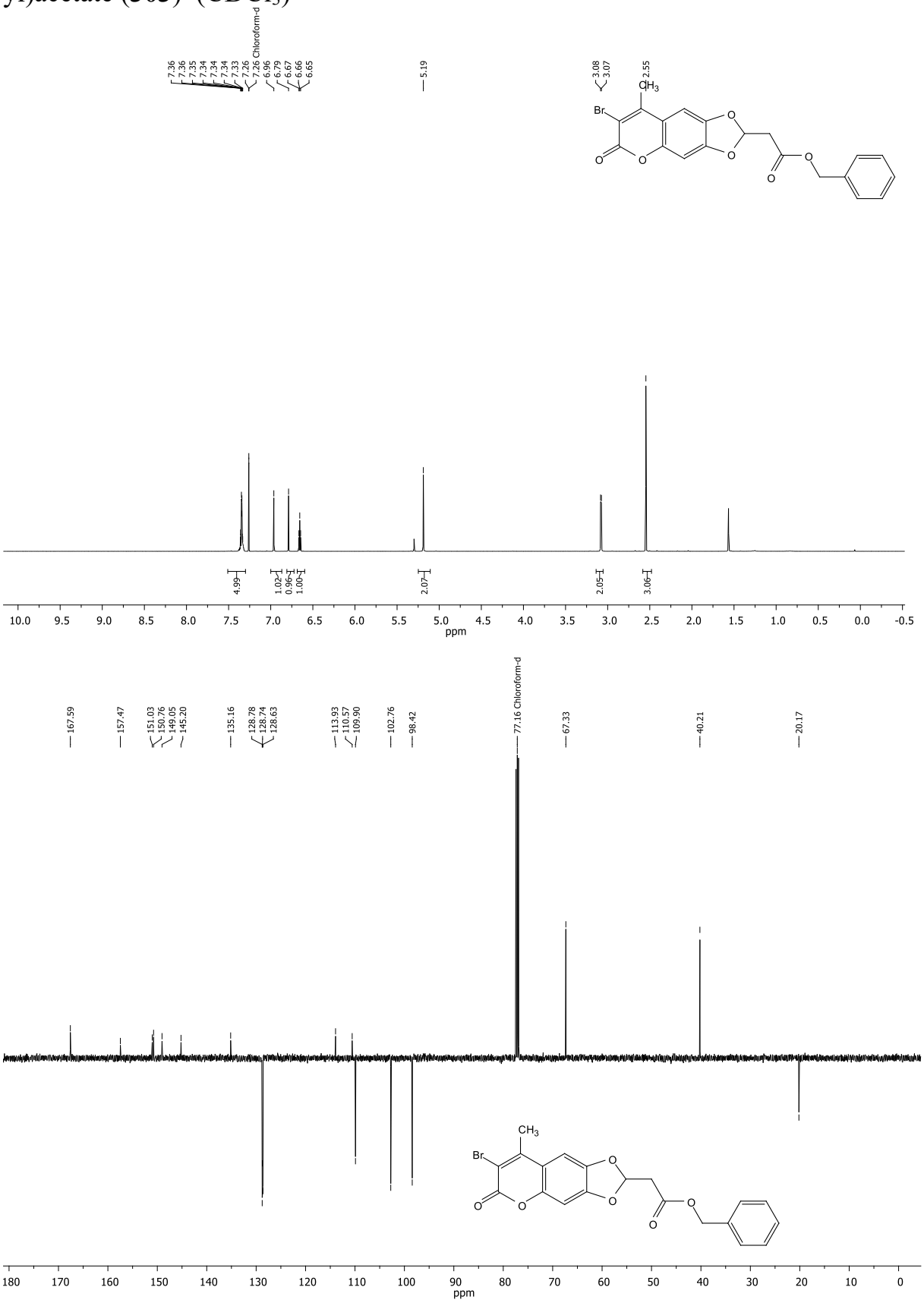

2-(7-Bromo-8-methyl-6-oxo-6H-[1,3]dioxolo[4,5-g]chromen-2-yl)acetic acid (**304**) / 2-(8-Methyl-6-oxo-6H-[1,3]dioxolo[4,5-g]chromen-2-yl)acetic acid (**305**) (3:1) ($(CD_3)_2CO$)

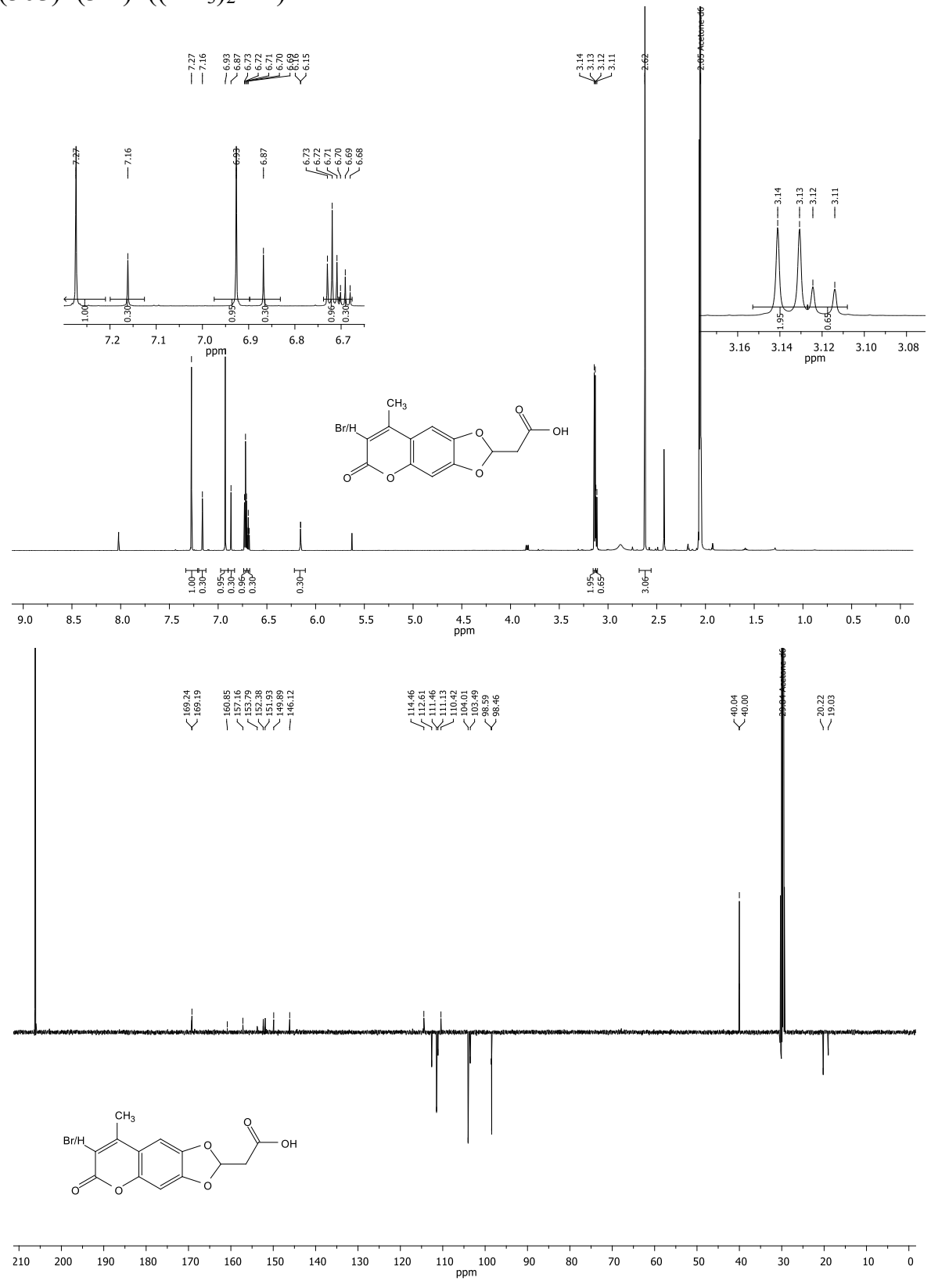

2-(8-Methyl-6-oxo-6H-[1,3]dioxolo[4,5-g]chromen-2-yl)acetic acid (**305**) (DMSO-d_6)

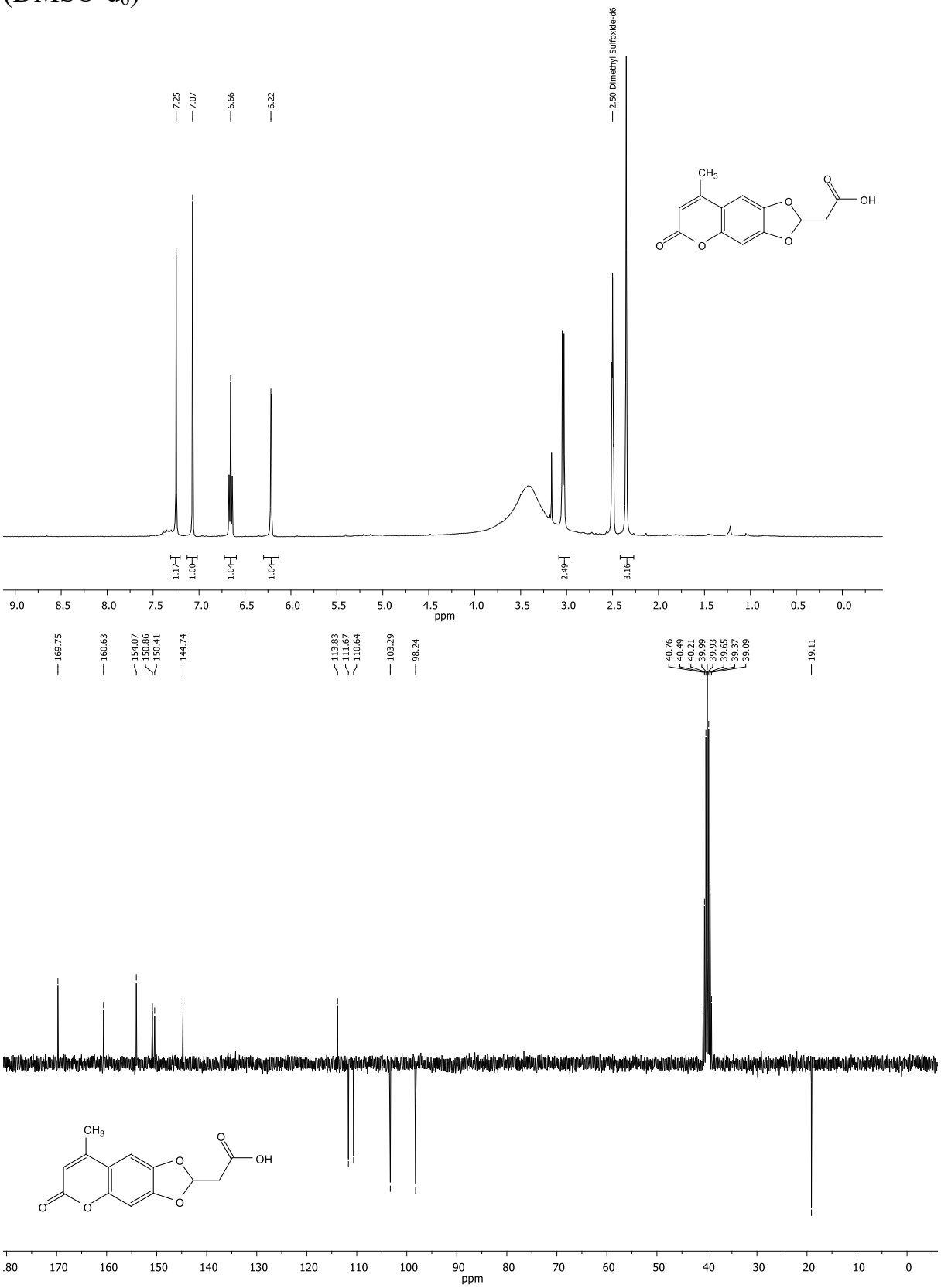

2-(7-Bromo-8-methyl-6-oxo-6H-[1,3]dioxolo[4,5-g]chromen-2-yl)acetic acid (**304**) ($(CD_3)_2CO$)

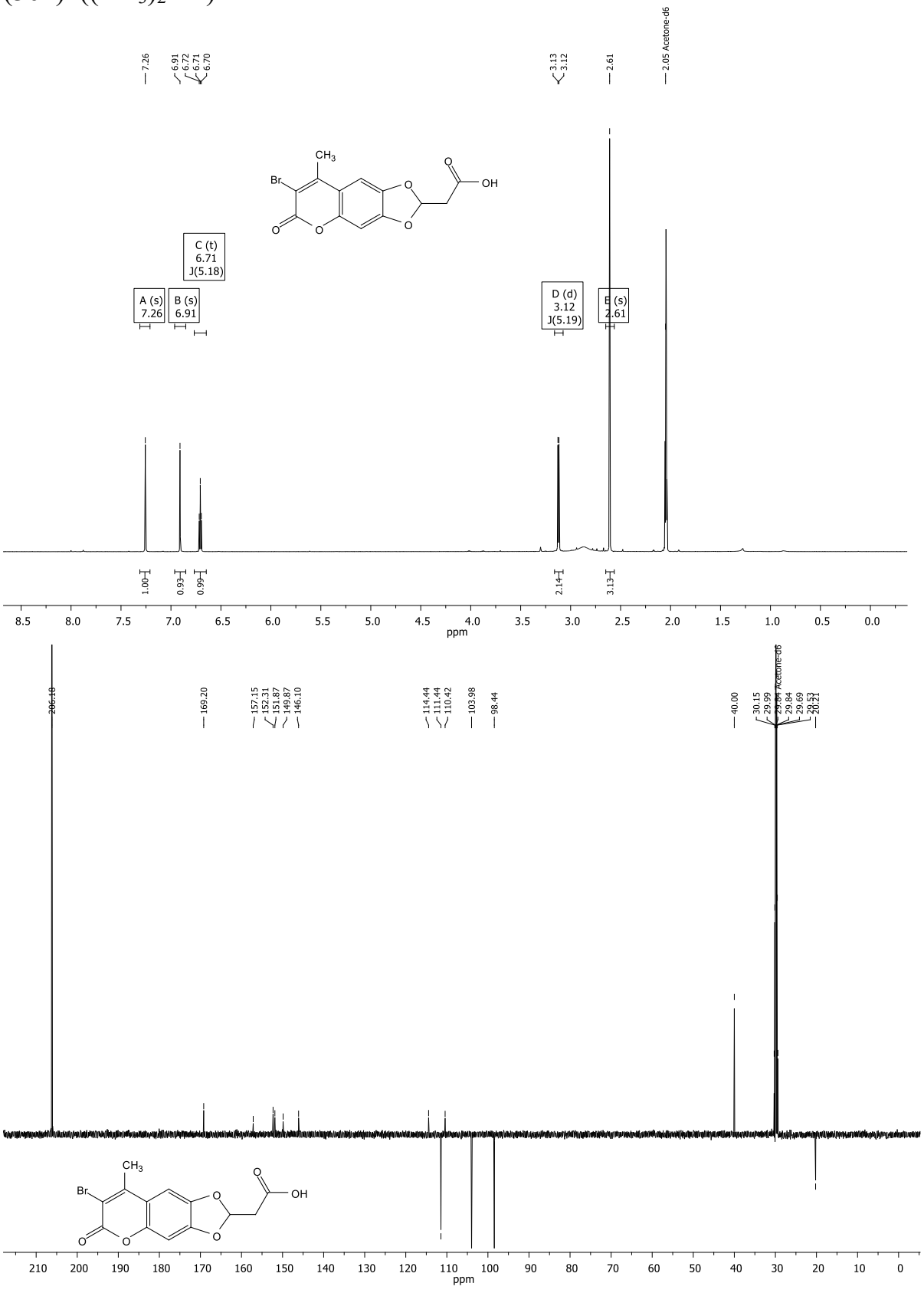

Methyl 6-(2-(7-bromo-8-methyl-6-oxo-6H-[1,3]dioxolo[4,5-g]chromen-2-yl) aceta mido)hexa noate (**306**) (CD_3Cl)

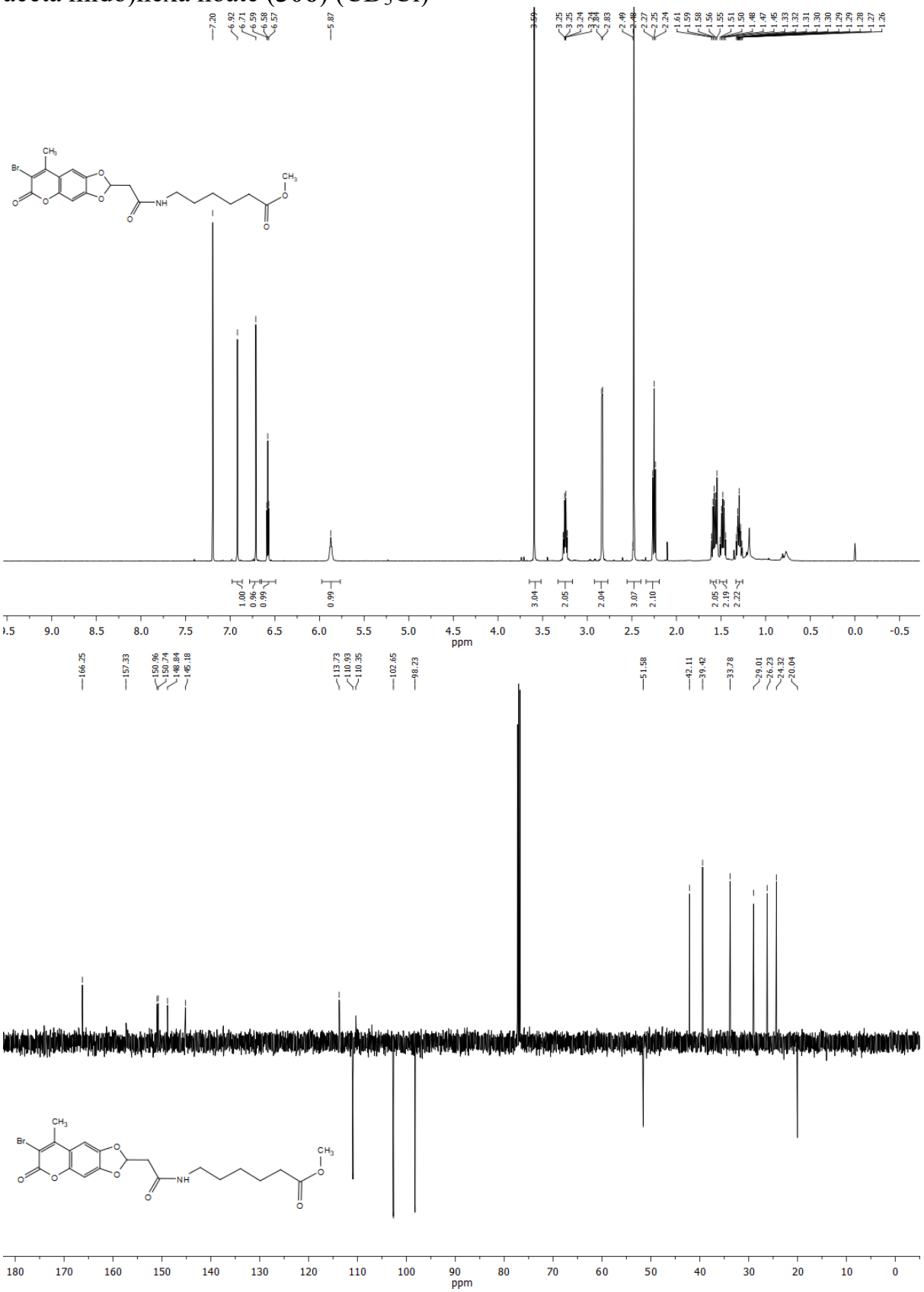

6-(2-(7-bromo-8-methyl-6-oxo-6H-[1,3]dioxolo[4,5-g]chromen-2-yl)acetamido) hexanoic acid (**307**) (DMSO-d_6)

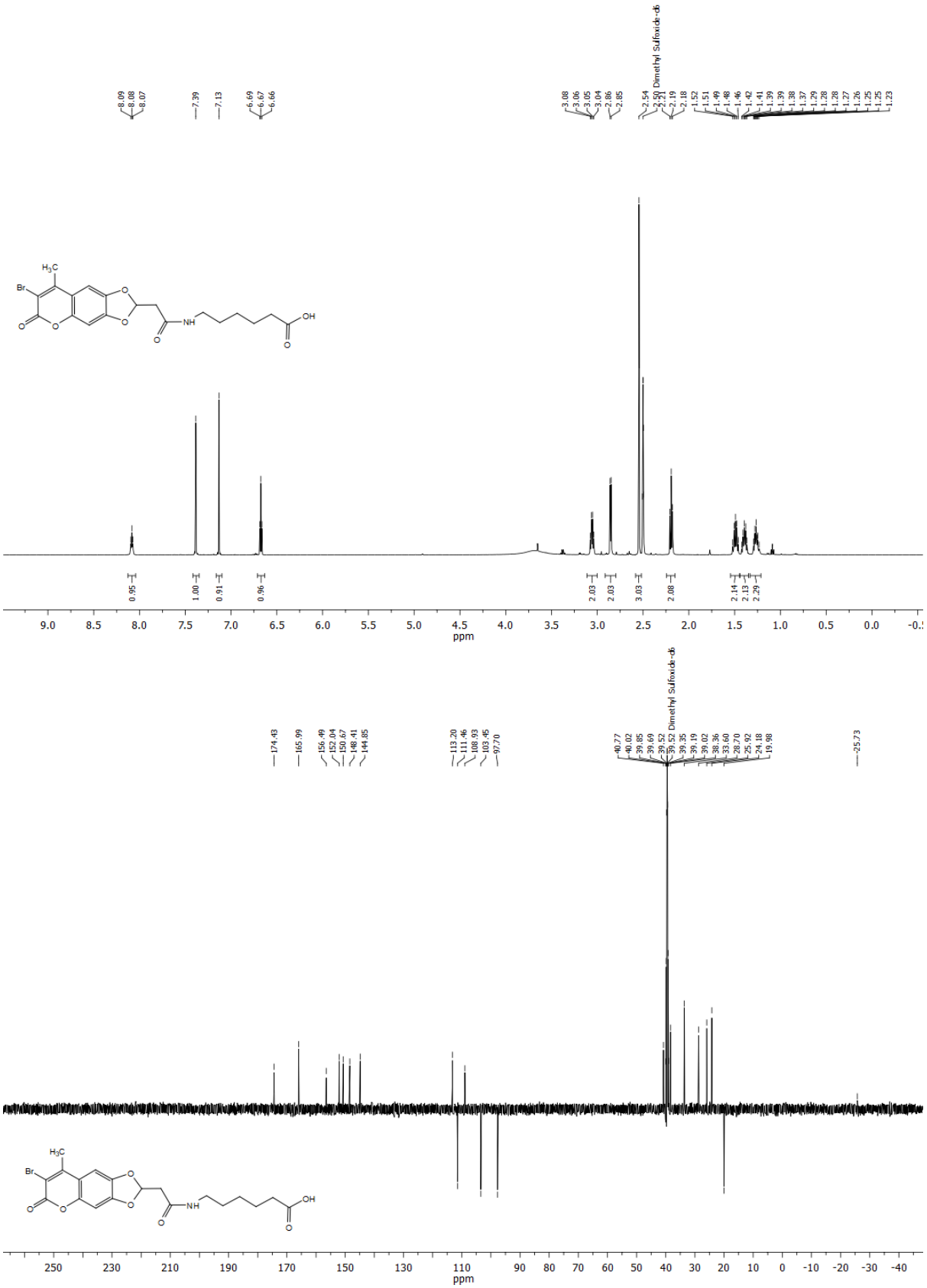

Tert-butyl 6-aminohexanoate (**308**) ($CDCl_3$)

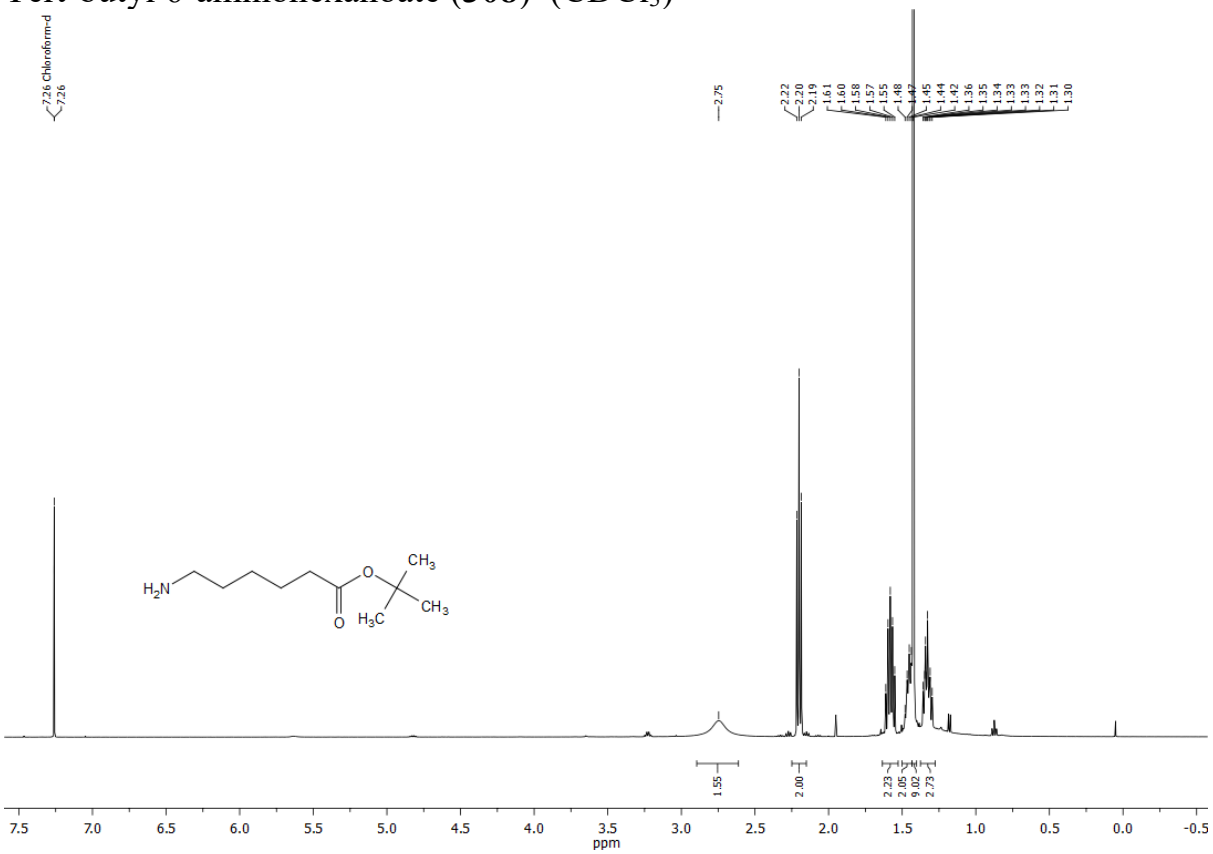

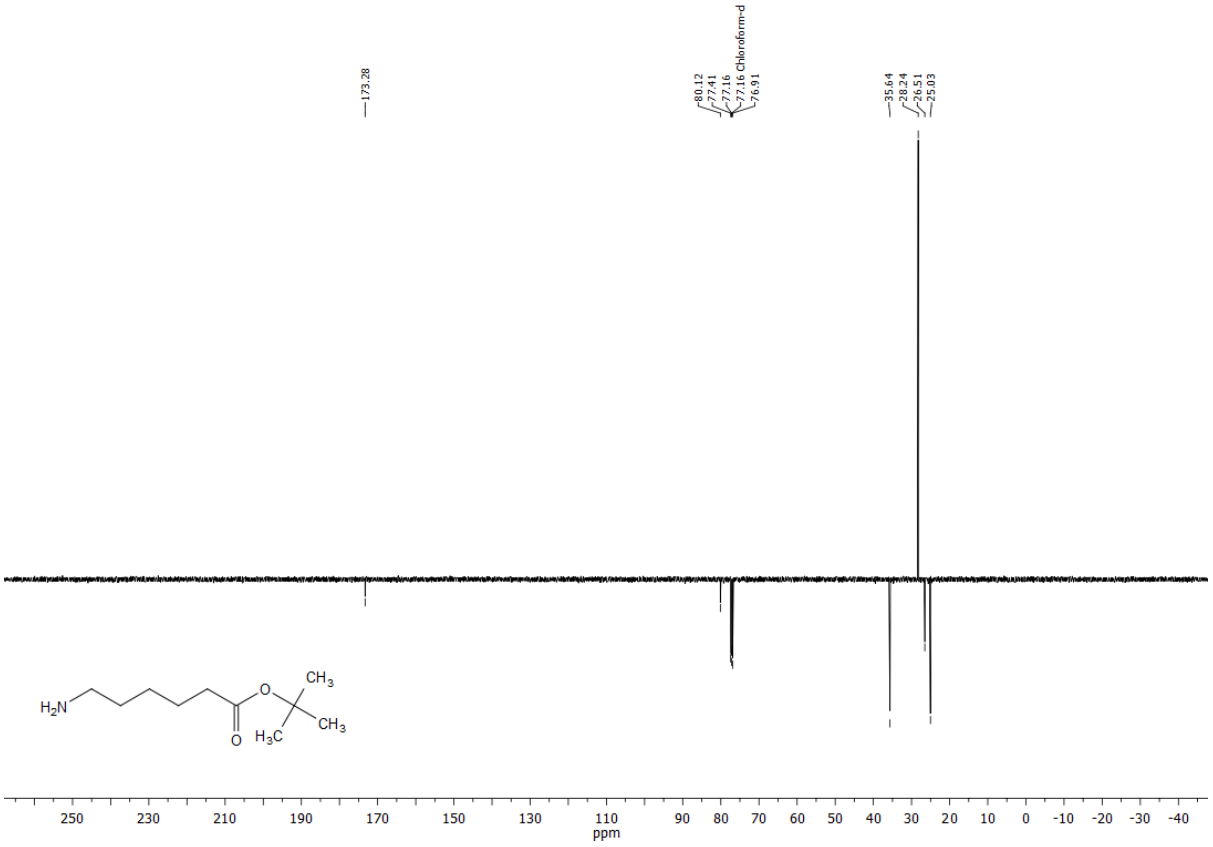

Tert-butyl 6-(2-(7-bromo-8-methyl-6-oxo-6H-[1,3]dioxolo[4,5-g]chromen-2-yl)acetamido) hexanoate (**309**) ($CDCl_3$)

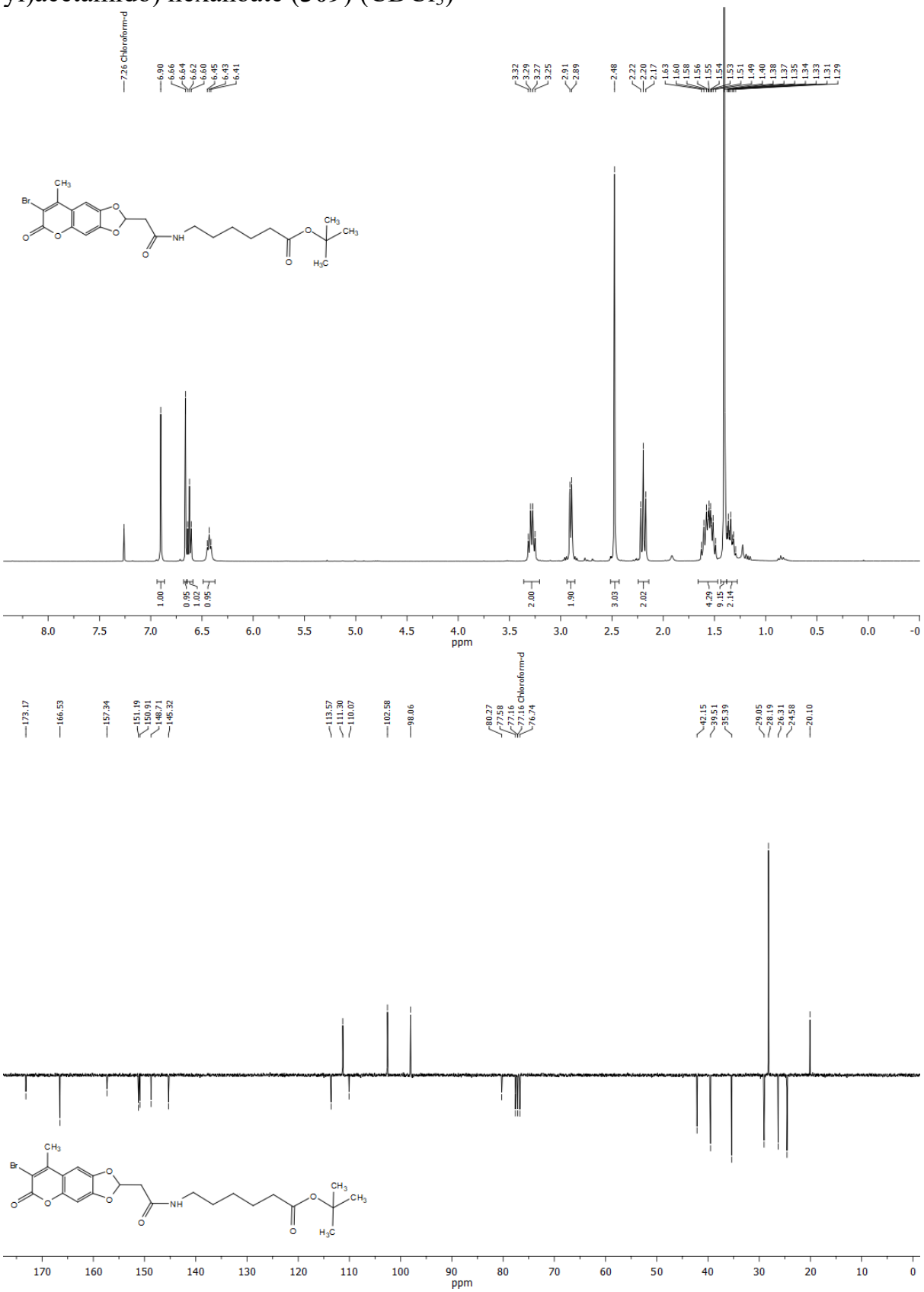

2-hydroxy-4-methoxybenzaldehyde (**311**) ($CDCl_3$)

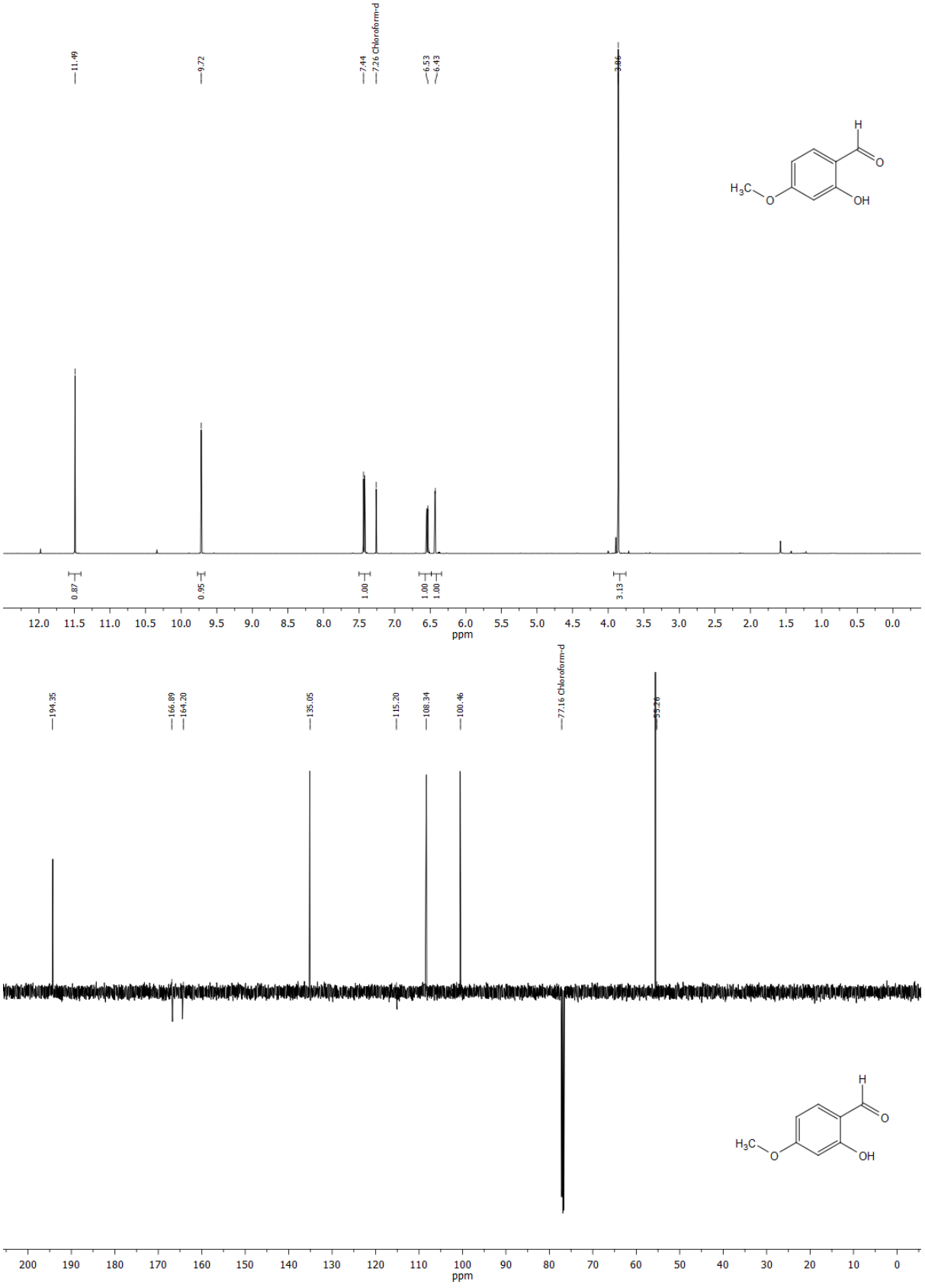

7-methoxy-2-oxo-2H-chromene-3-carboxylic acid (**312**) (DMSO-d_6)

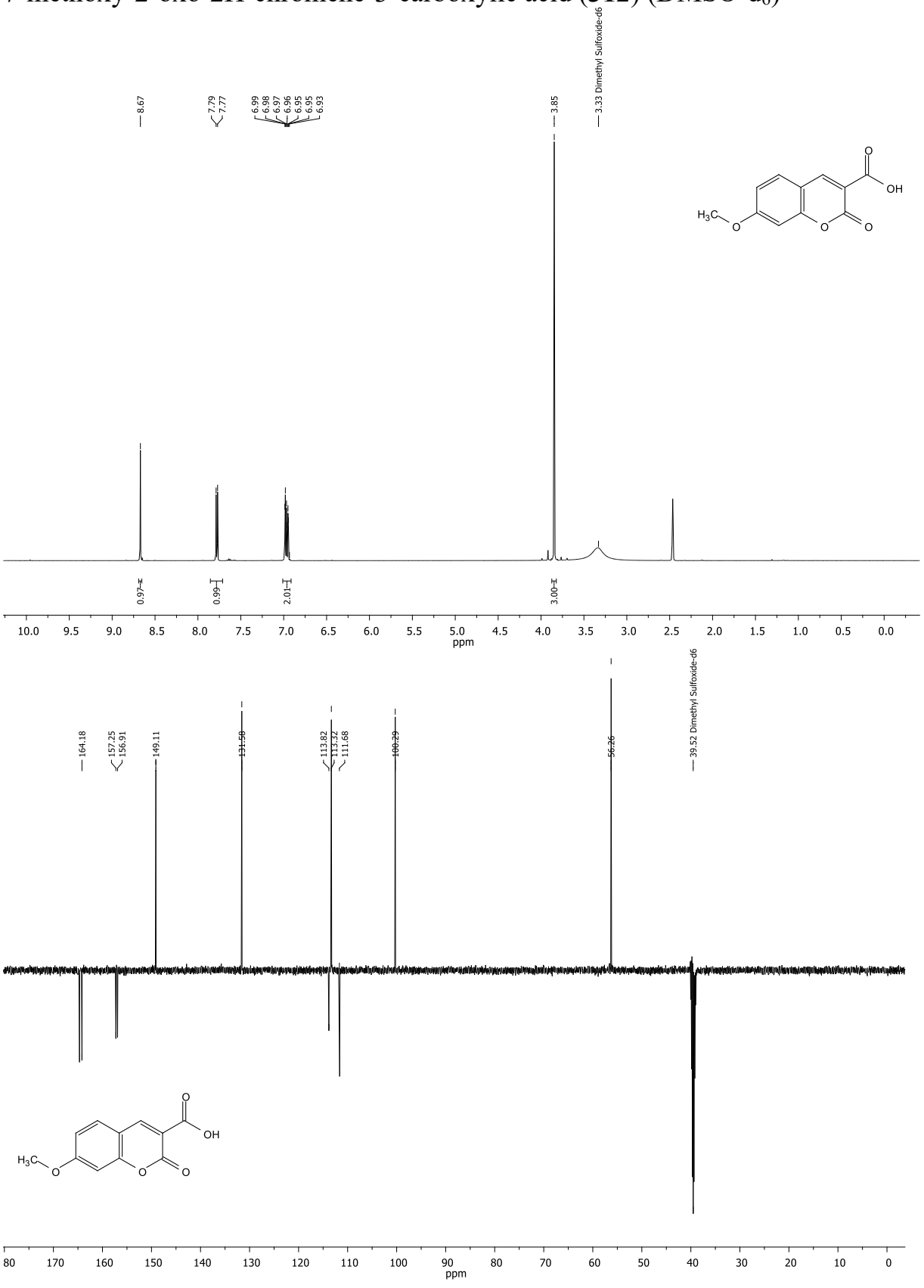

2,5-dioxopyrrolidin-1-yl 7-methoxy-2-oxo-2H-chromene-3-carboxylate (**313**) ($CDCl_3$)

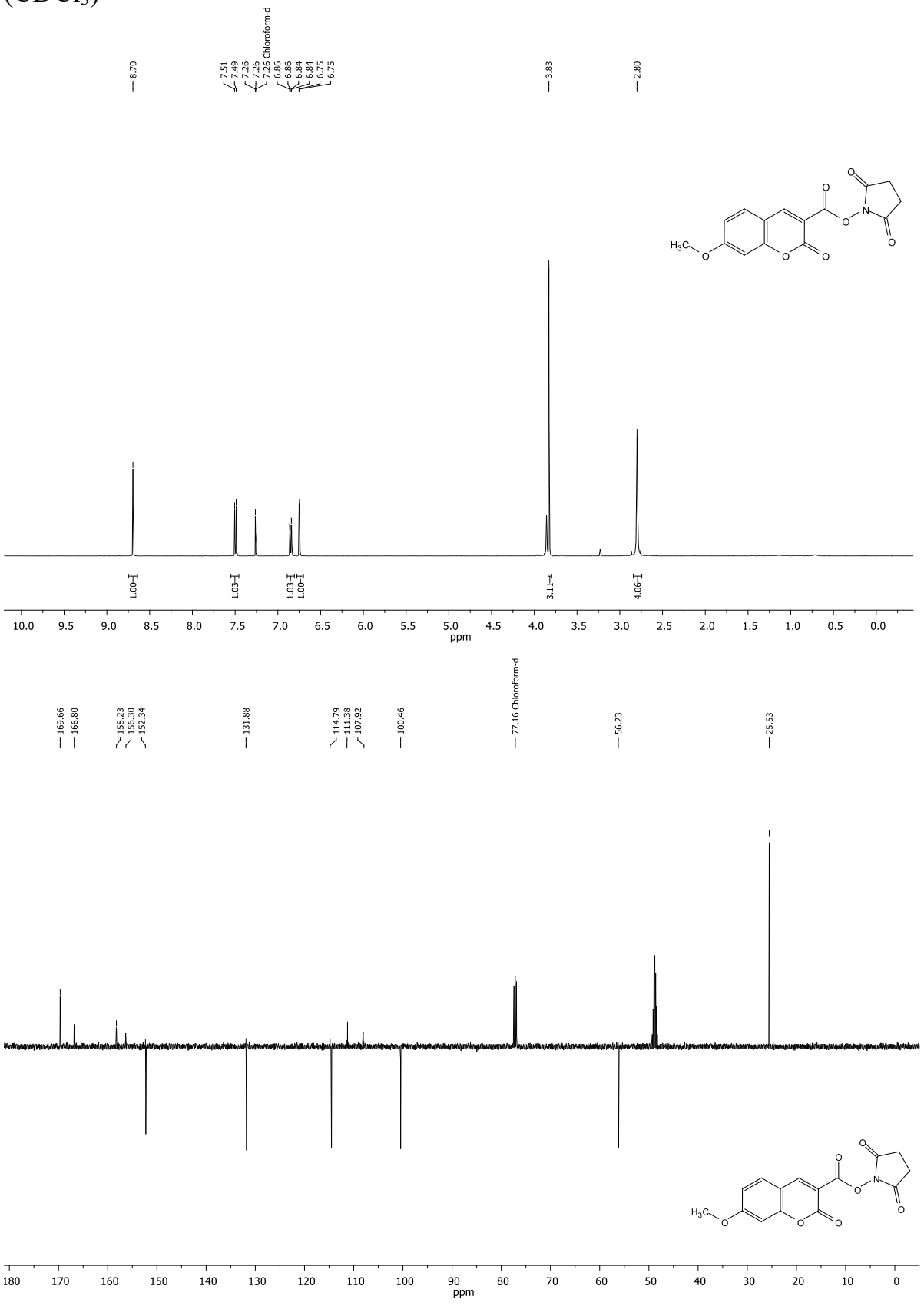

6-(7-methoxy-2-oxo-2H-chromene-3-carboxamido)hexanoic acid (**314**) ($CDCl_3$)

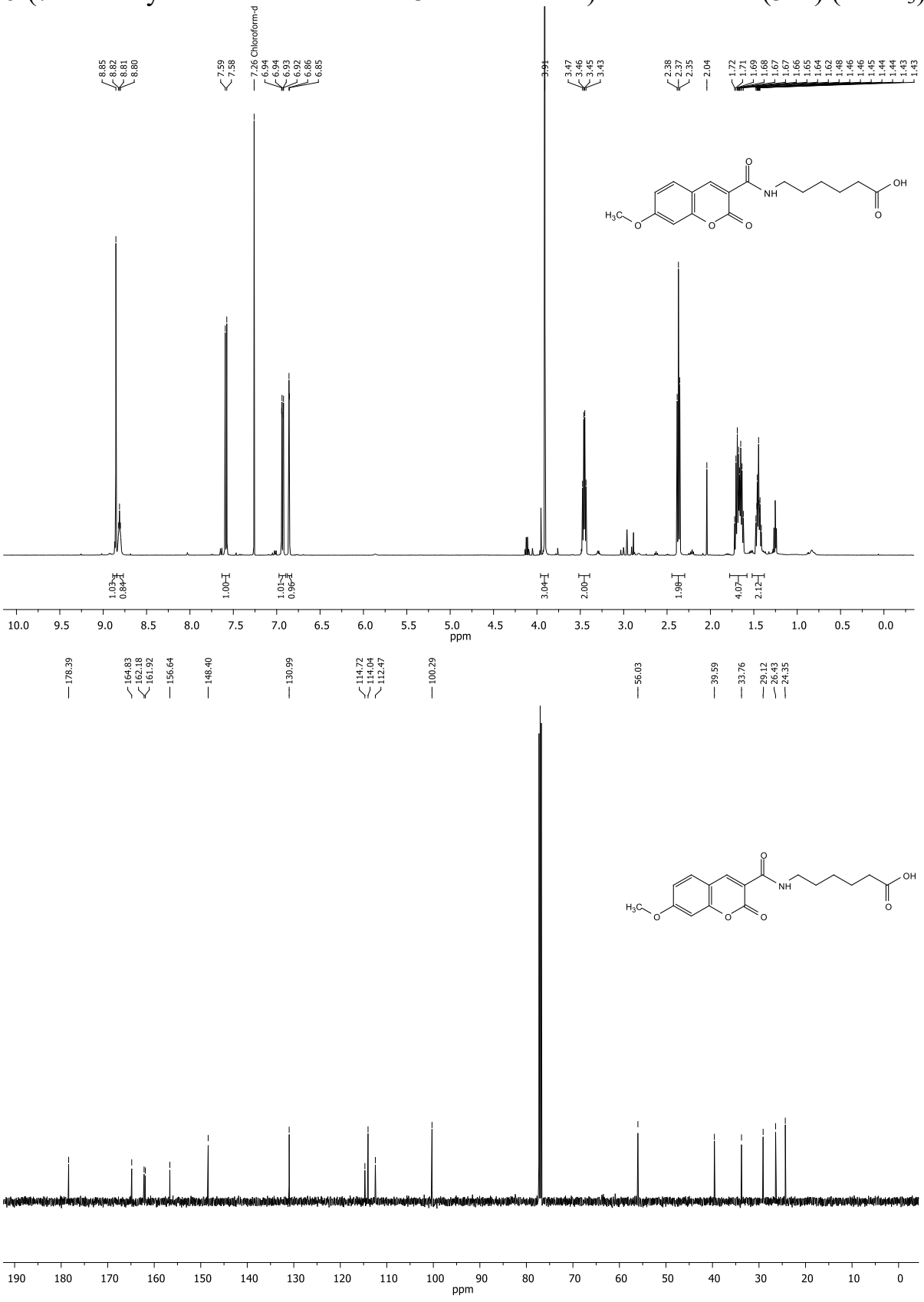

N-(2-(dimethylamino)ethyl)-7-nitrobenzo[c][1,2,5]oxadiazol-4-amine (**316**)
(CD_3CN) & (DMSO-d_6)

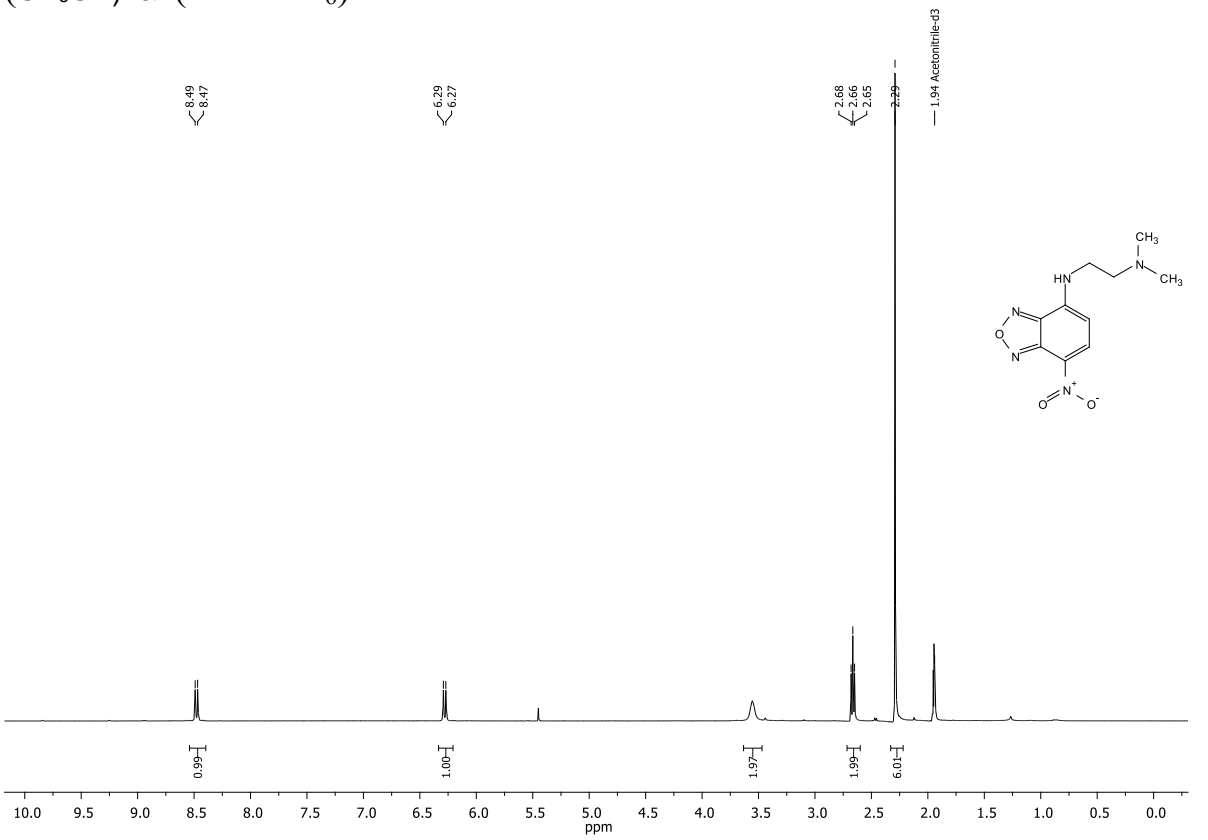

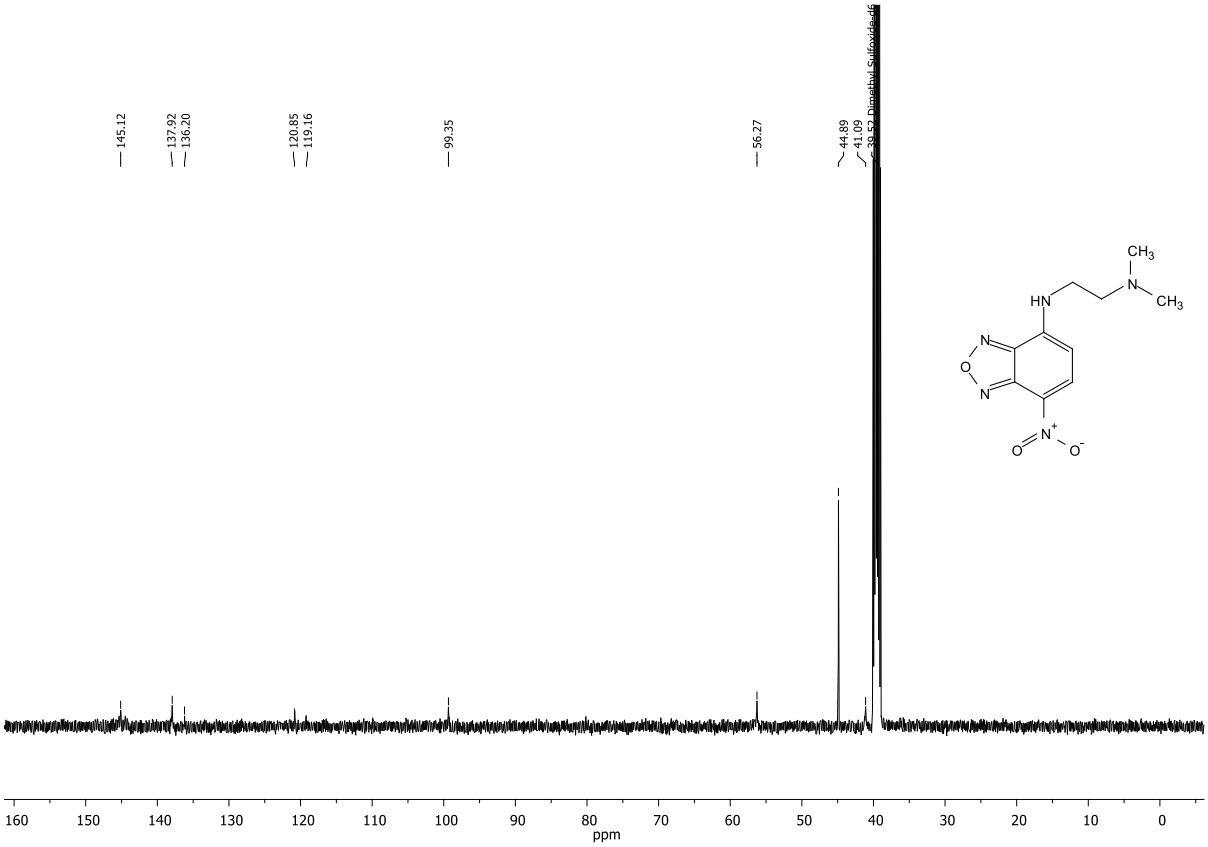

4-azido-7-nitrobenzo[c][1,2,5]oxadiazole ‘’azido-NBD’’ (**317**) ($CDCl_3$)

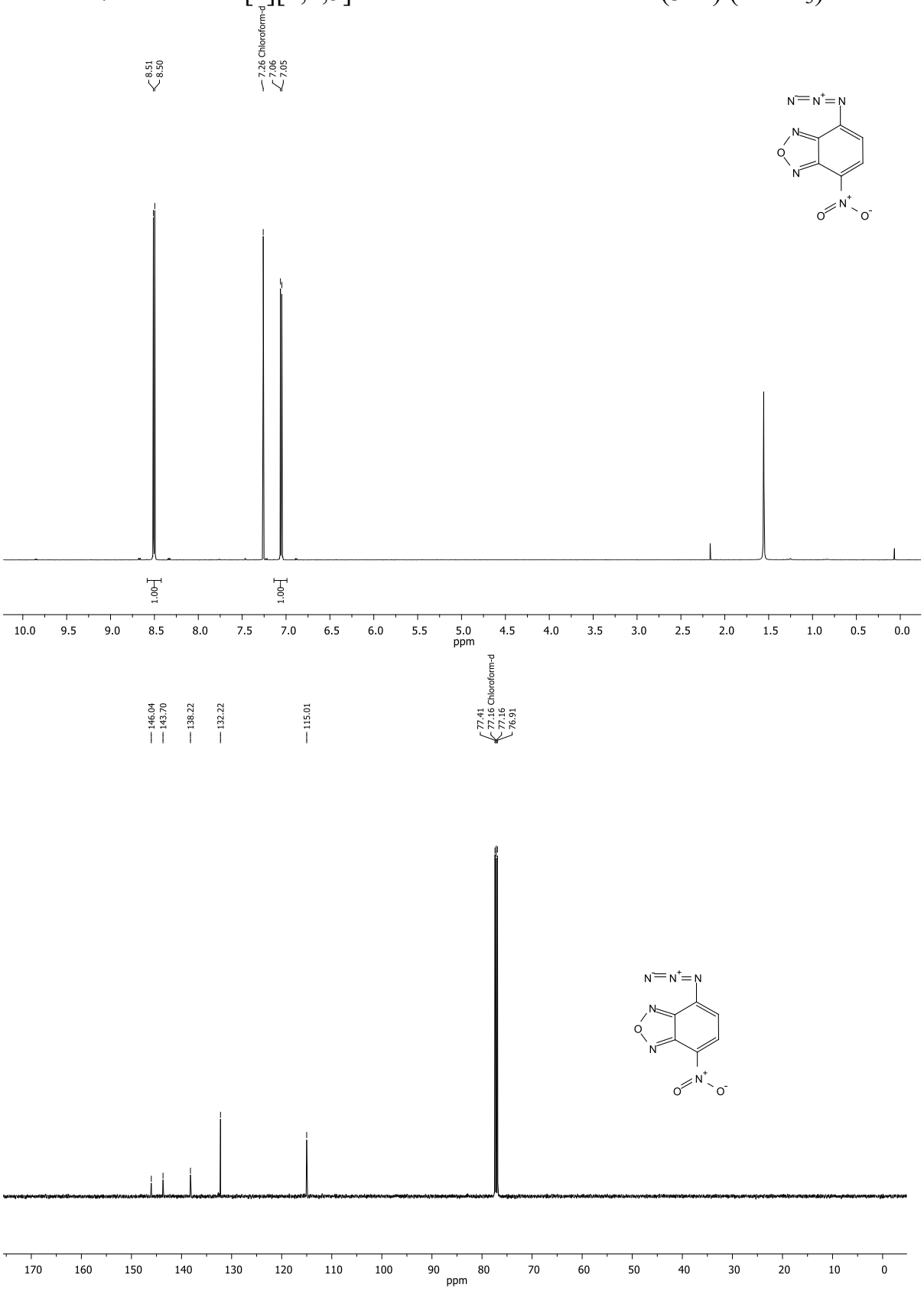

2-azidoethan-1-amine (**318**) ($CDCl_3$)

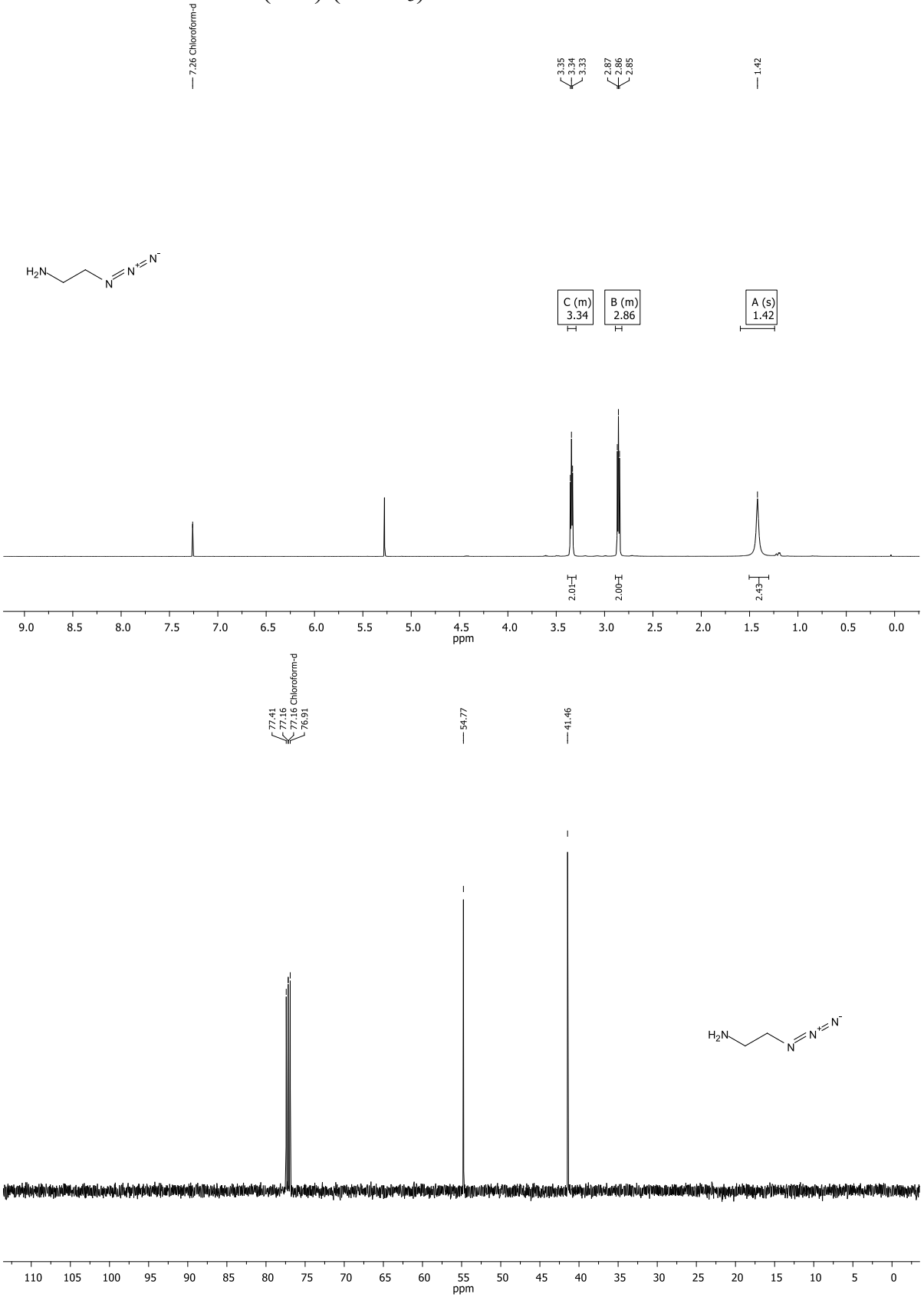

N-(2-bromoethyl)-7-nitrobenzo[c][1,2,5]oxadiazol-4-amine (**319**) ($CDCl_3$)

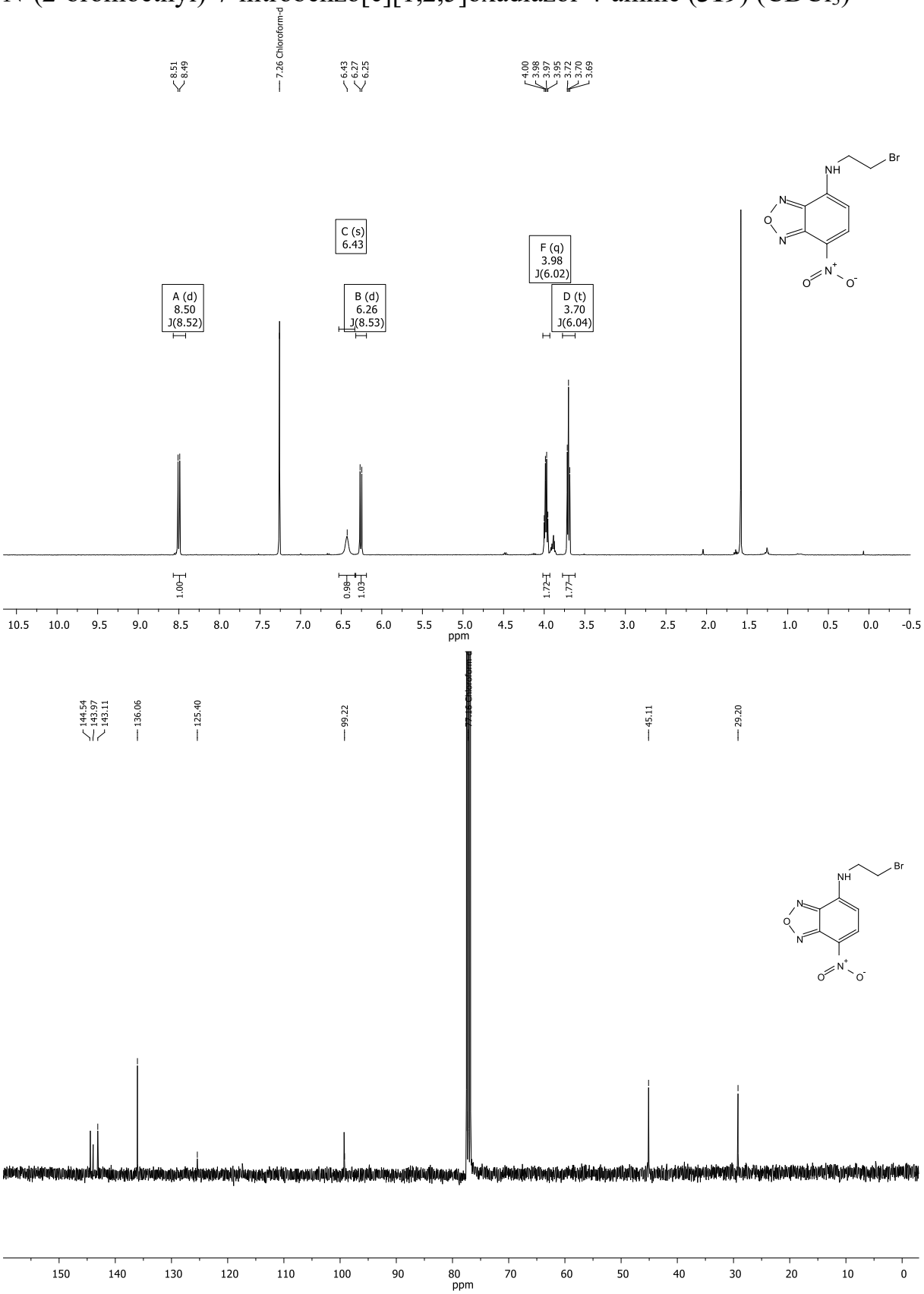

N-(2-azidoethyl)-7-nitrobenzo[c][1,2,5]oxadiazol-4-amine (**320**) (DMSO-d_6)

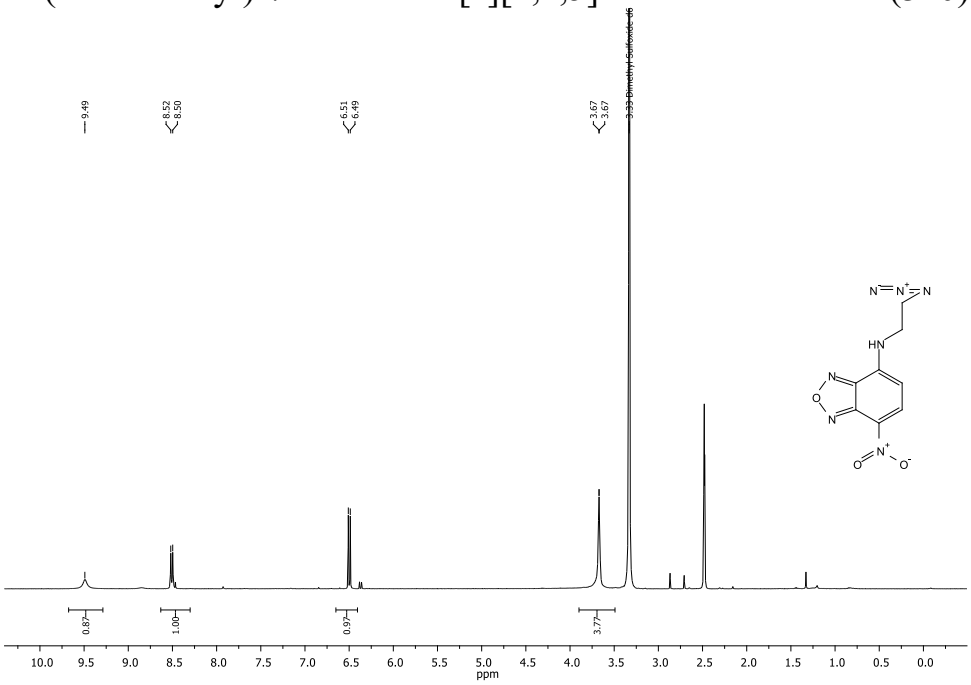

N-(2-azidoethyl)-5(6)-fluorescein-carboxoamide (**321**) (CD_3OD)

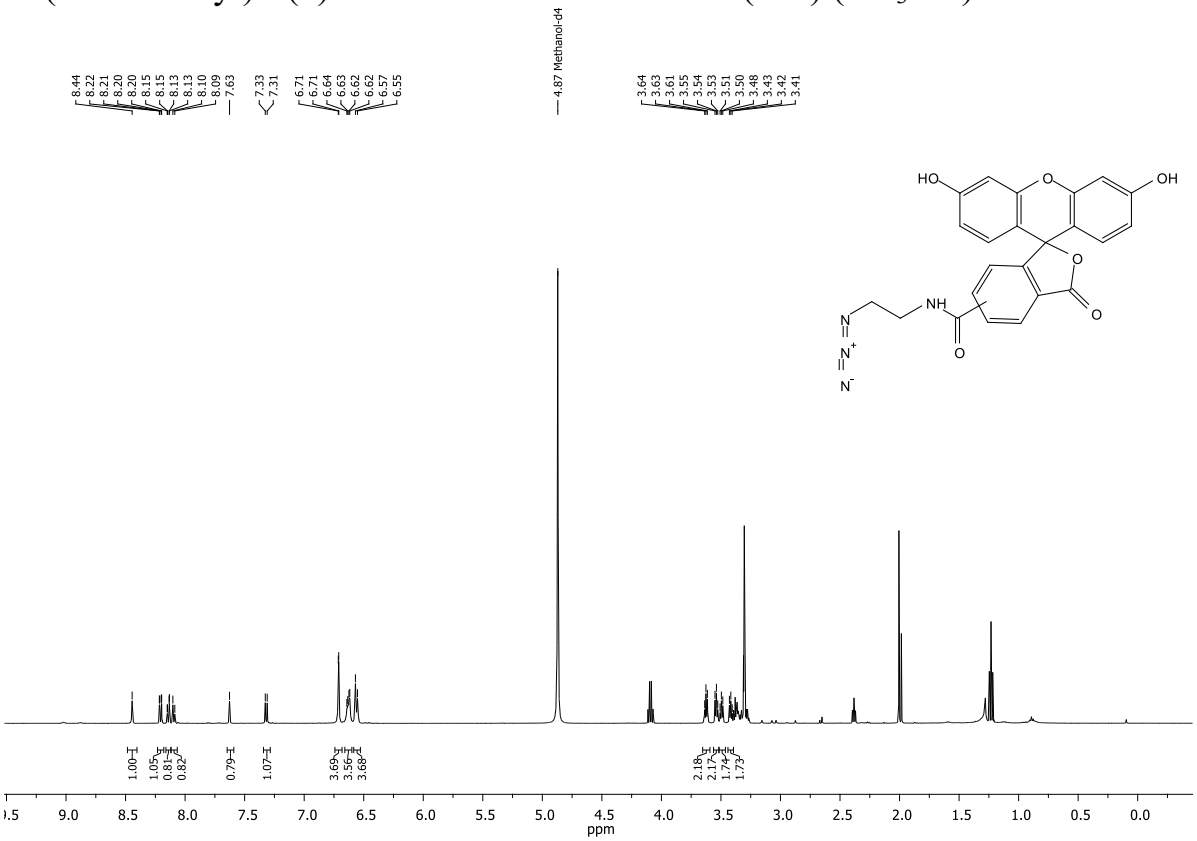

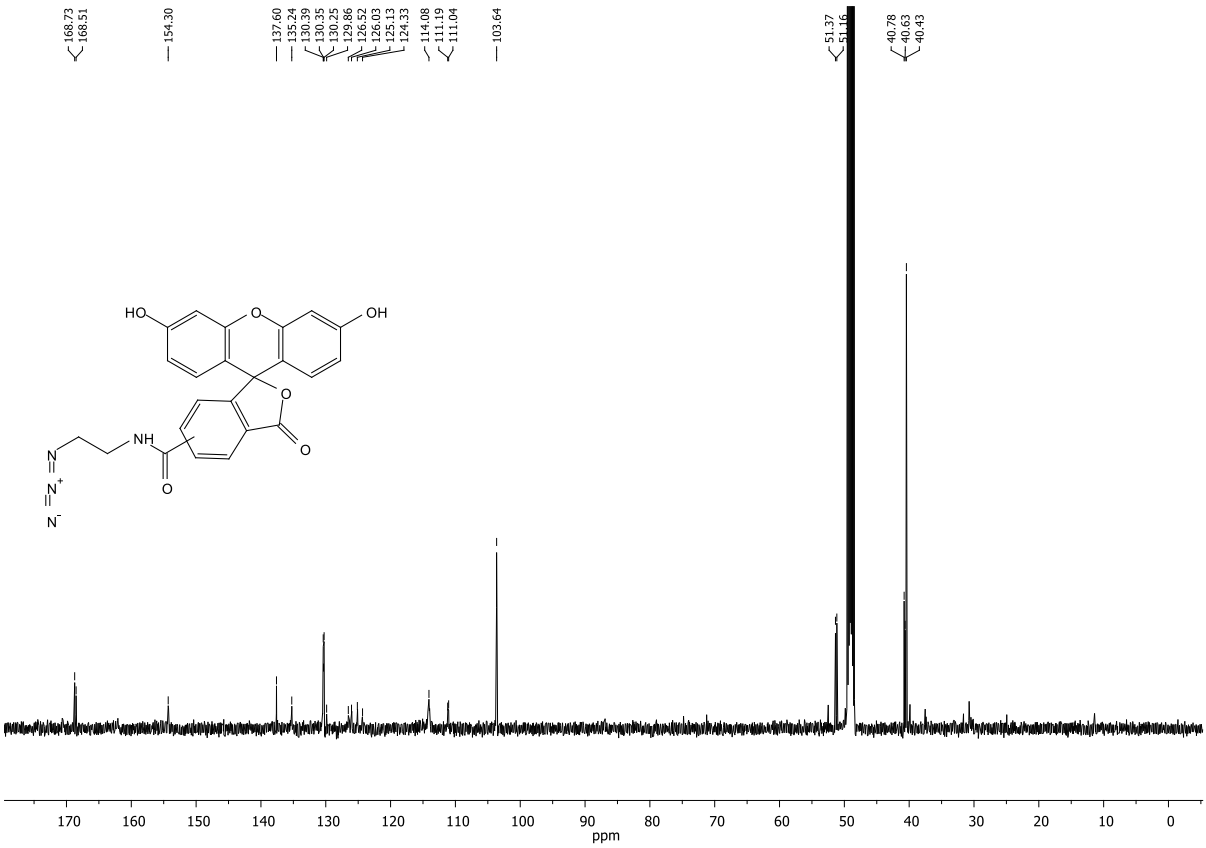

4-((2S,3R,E)-2-(tert-butyloxycarbonylamino)-3-(methoxymethoxy)octadec-4-en-1 phosphoethylamino)-7-nitrobenzo-2-oxa-1,3-diazol (**401**) ($CDCl_3$)

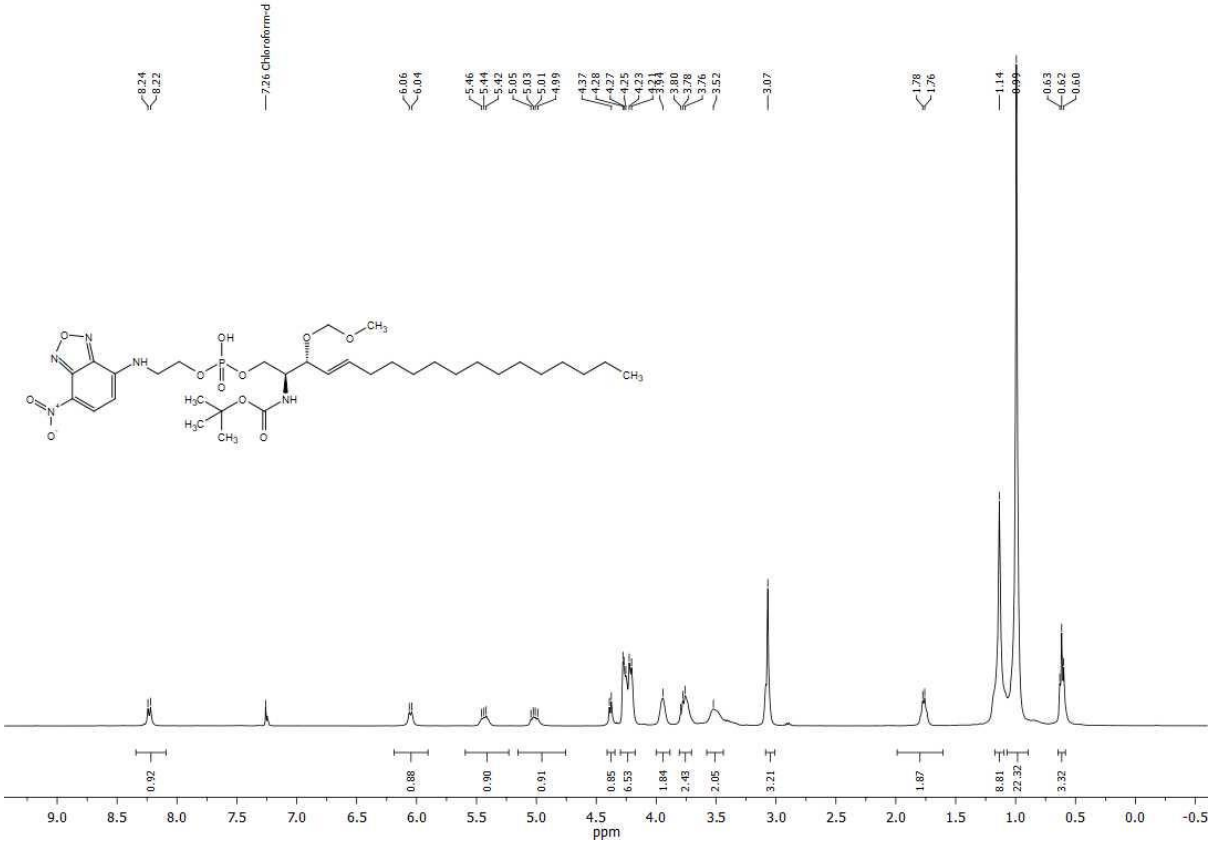

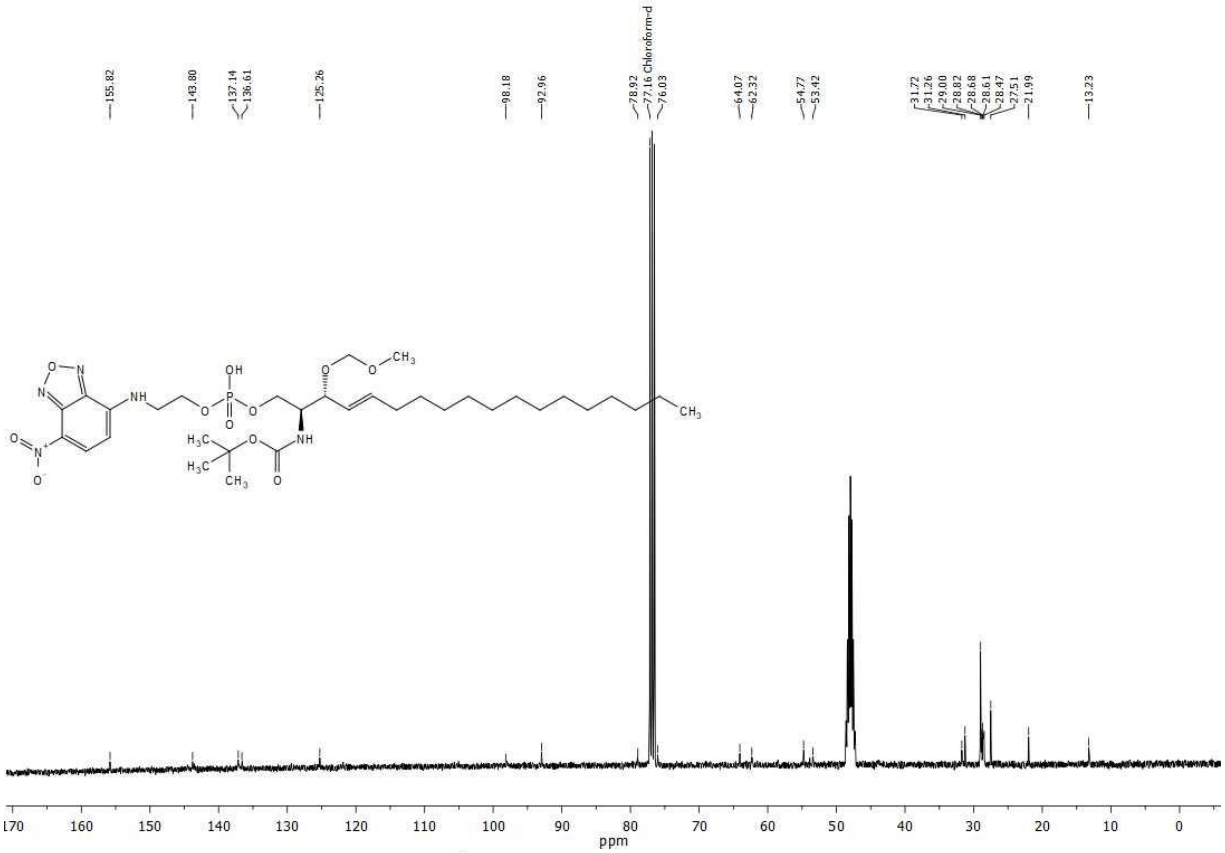
155.82
149.80
137.14
136.61
125.26
98.18
92.96
78.92
77.16 Chloroform-d
76.03
64.07
62.32
54.77
53.42
31.72
31.26
29.00
28.82
28.68
28.61
28.47
27.51
21.99
13.23
ppm

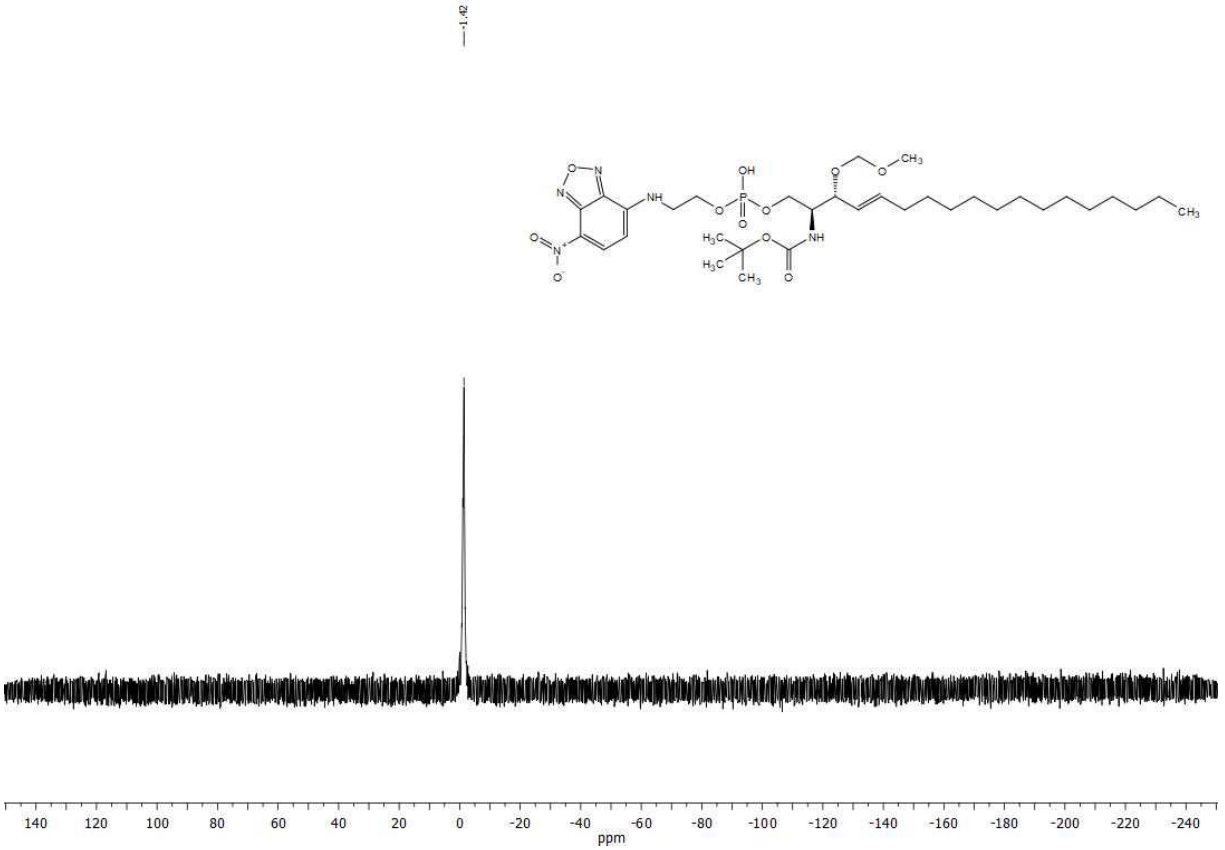
1.42
ppm

(2S,3R,E)-2-(6-(2-(7-bromo-8-methyl-6-oxo-6H-[1,3]dioxolo[4,5-g]chromen-2-yl) acetamido)hexanamido)-3-hydroxyoctadec-4-en-1-yl(2-((7-nitrobenzo[c] [1,2,5] oxadiazol-4-yl)amino)ethyl) hydrogen phosphate (**ZP-403**) ($CDCl_3$+CD_3OD

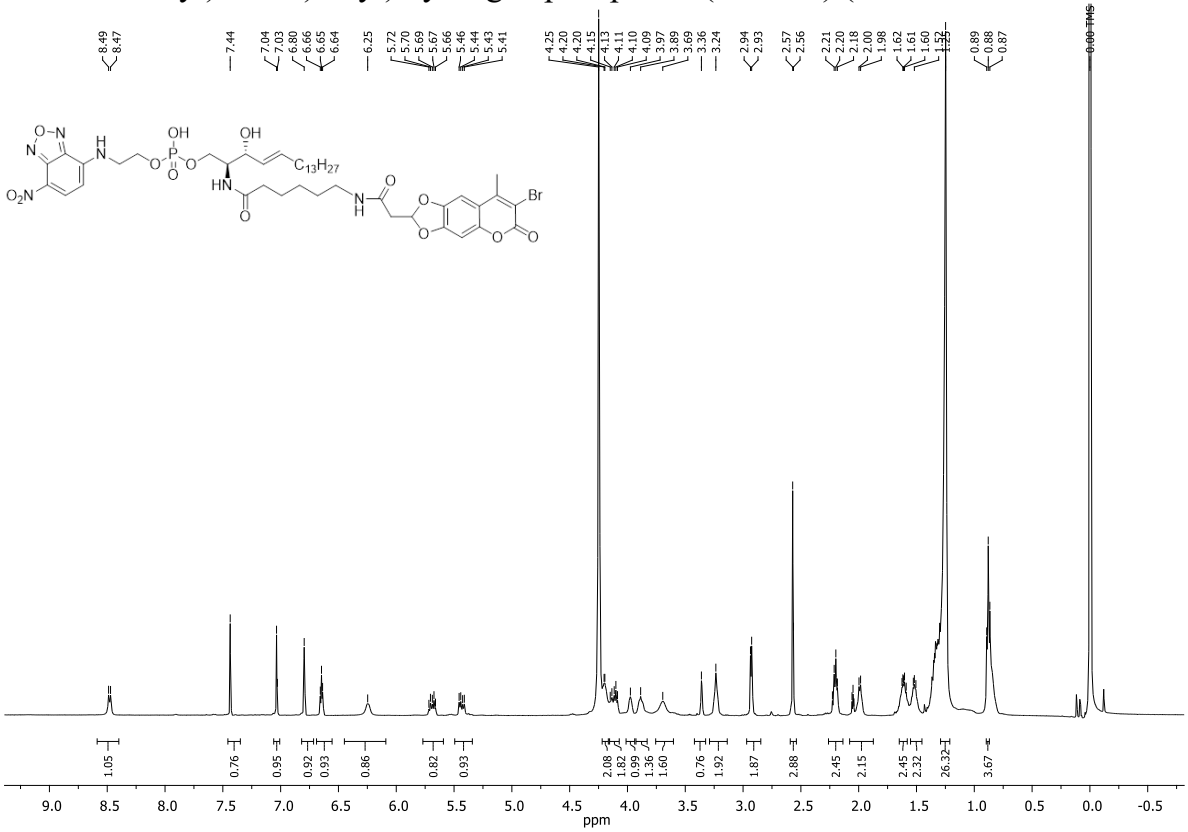

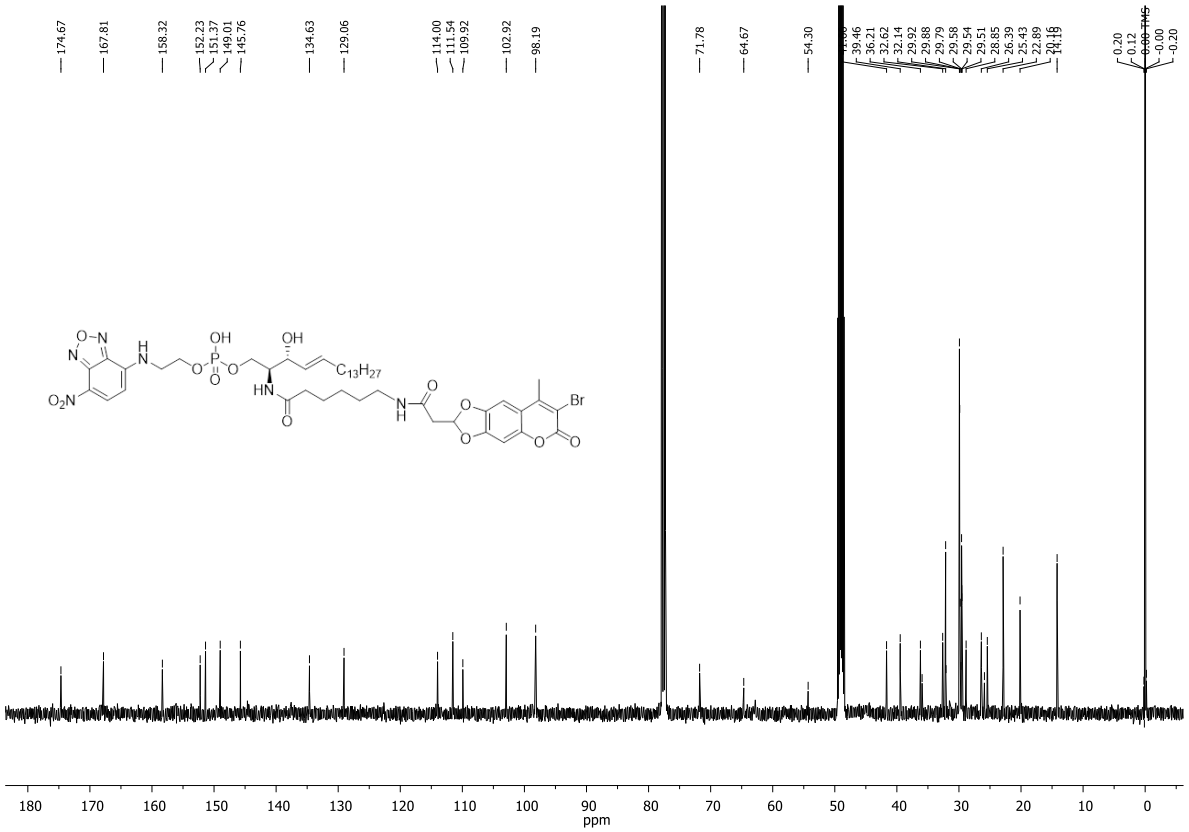

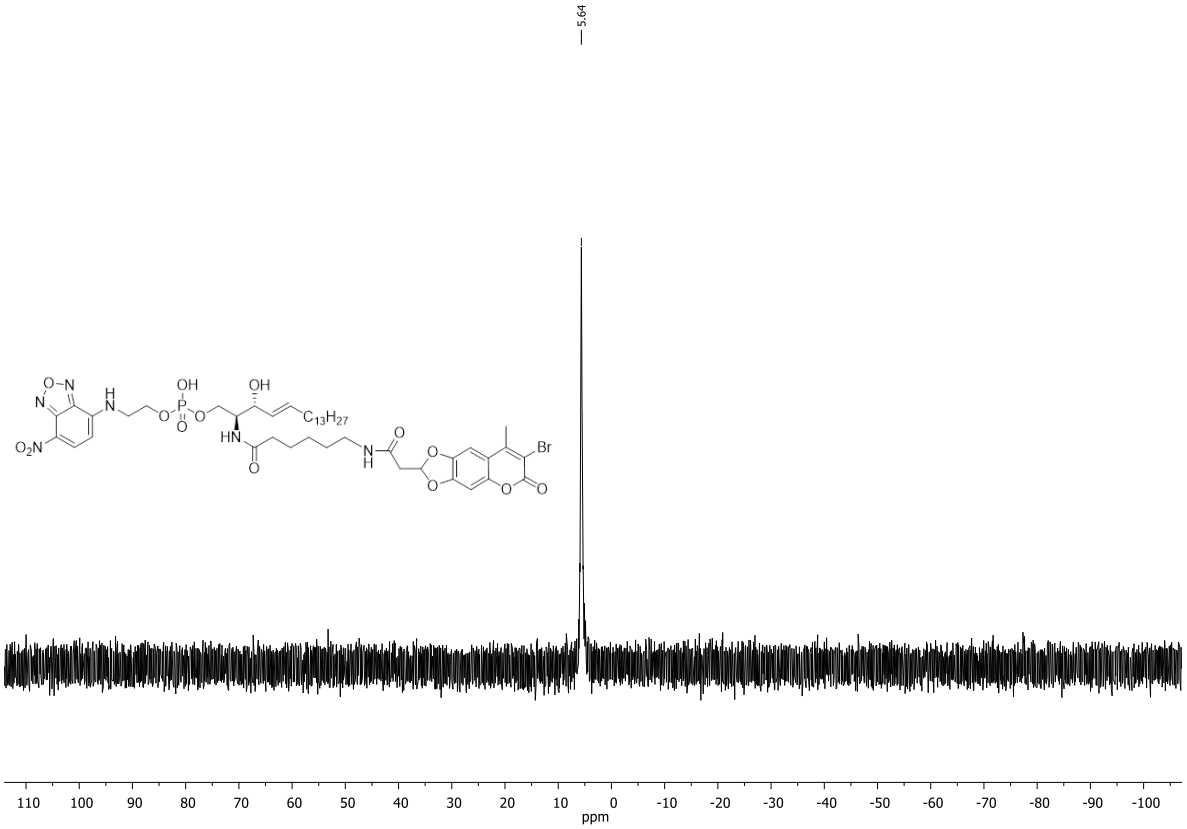

(2S,3R,E)-2-dodecanamido-3-hydroxyoctadec-4-en-1-yl (2-((7-nitrobenzo[c][1, 2, 5]oxadiazol-4-yl)amino)ethyl) hydrogen phosphate (**TP-367**) ($CDCl_3$+CD_3OD)

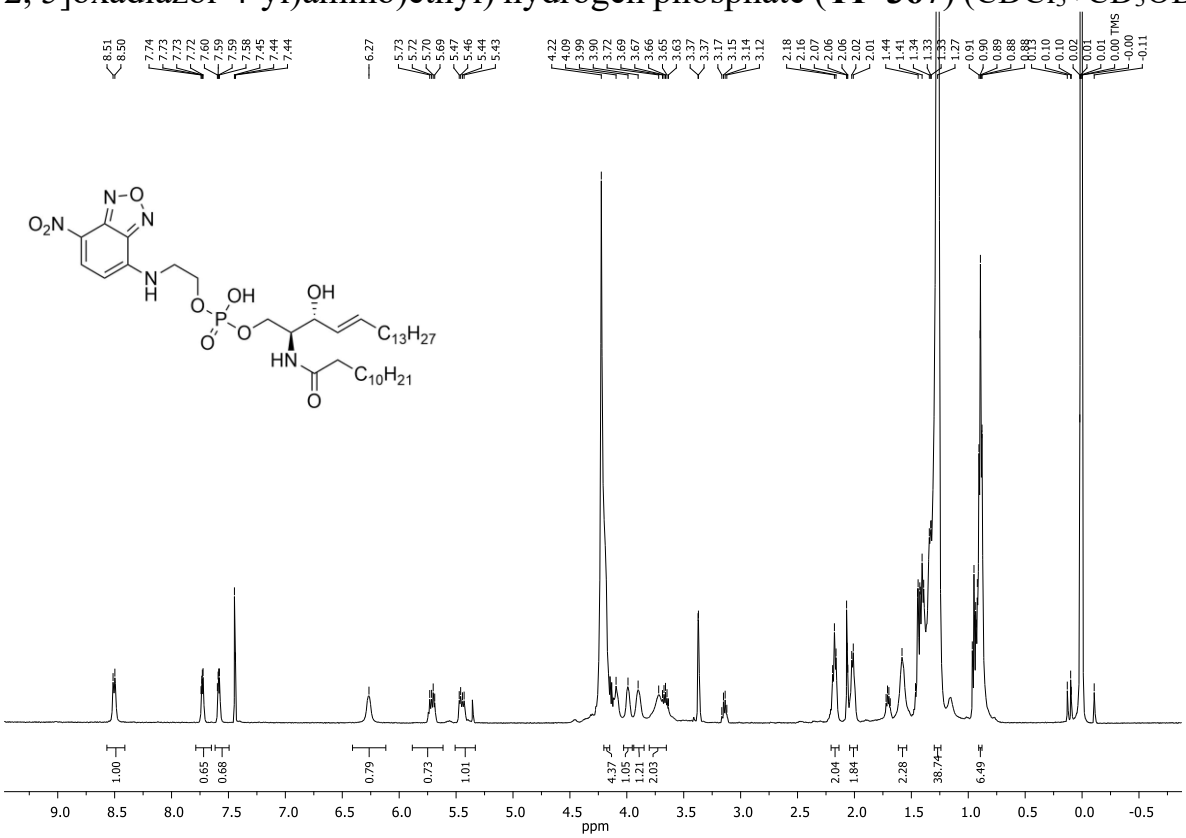

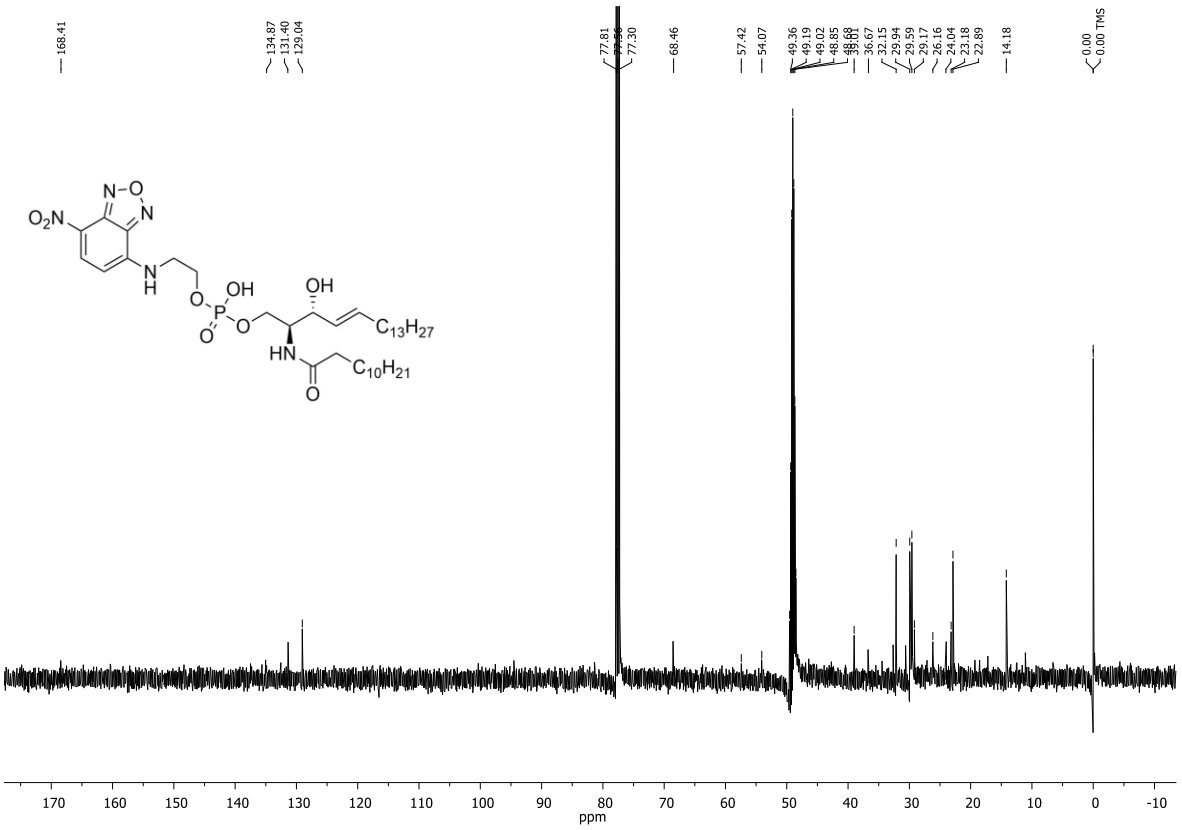
168.41
134.87
131.40
129.04
77.81
77.56
77.30
68.46
57.42
54.07
49.36
49.19
49.02
48.85
39.68
39.51
36.67
32.15
29.94
29.59
29.17
26.16
24.04
23.18
22.89
14.18
0.00
0.00 TMS
ppm

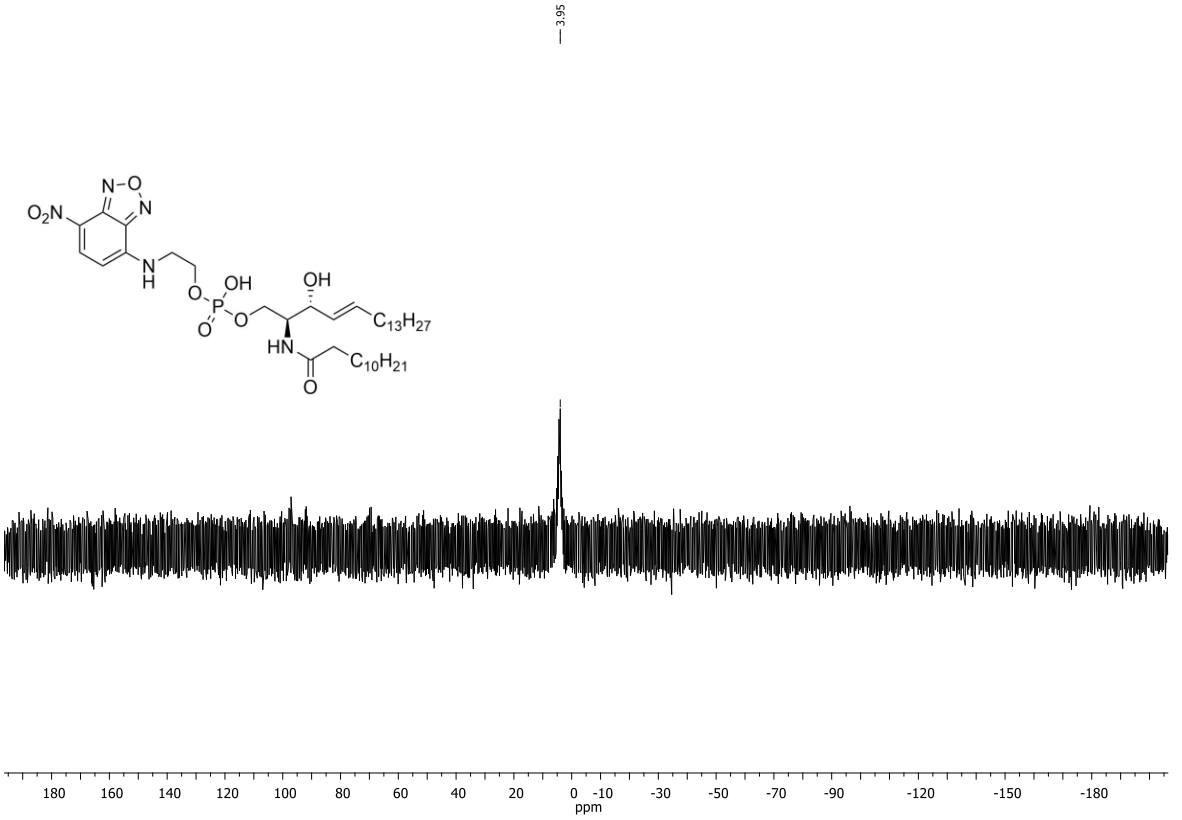
3.95
ppm

(2S,3R,E)-2-(tert-butoxycarbonyl)-3-(methoxymethoxy)octadec-4-enyl 2-(dimet-hyl((1-(2-(7-nitrobenzo[c][1,2,5]oxadiazol-4-ylamino)ethyl)-1H-1,2,3-triazol-4-yl)methyl)ammonio)ethyl phosphate (**406**) (MeOD)

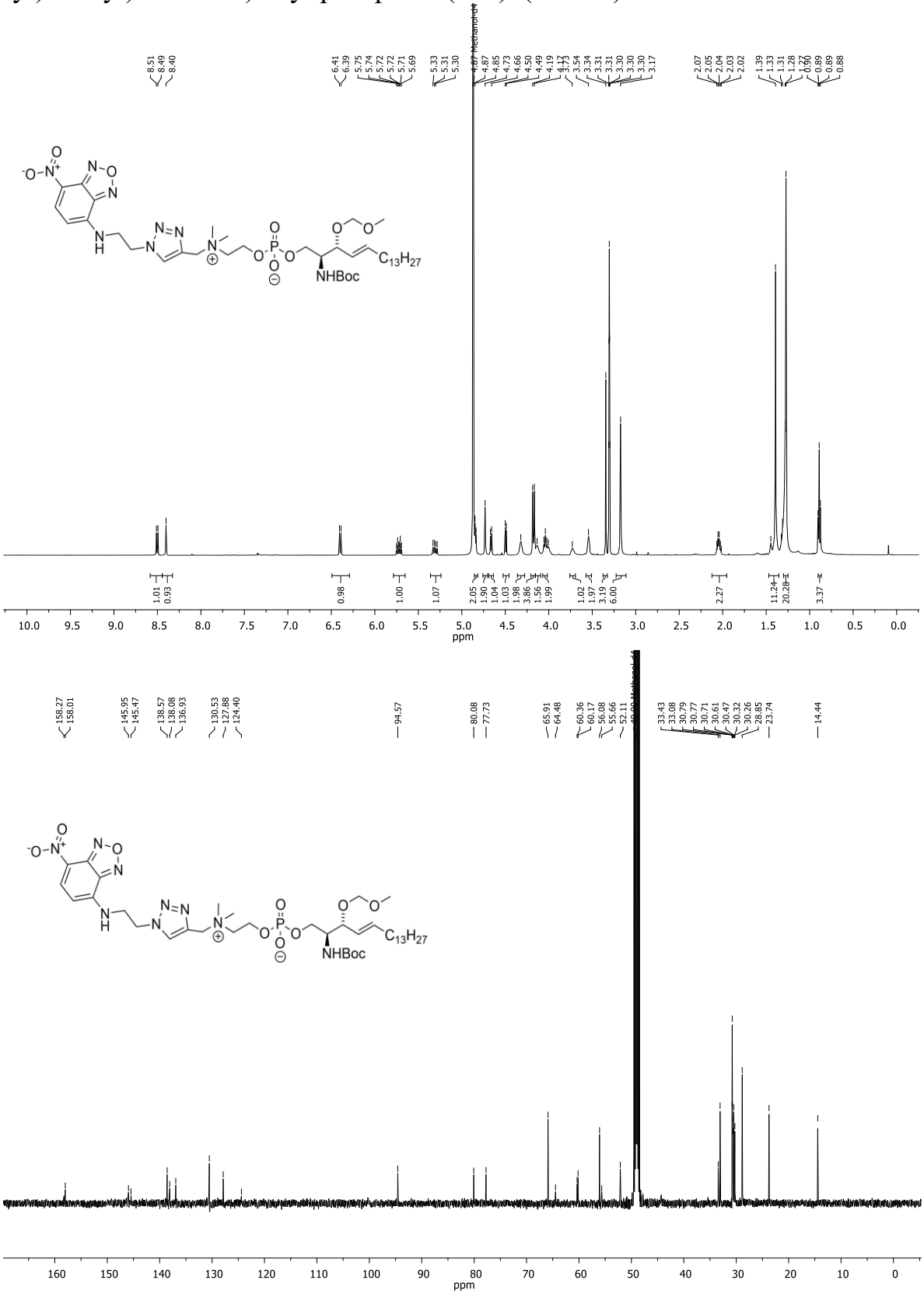

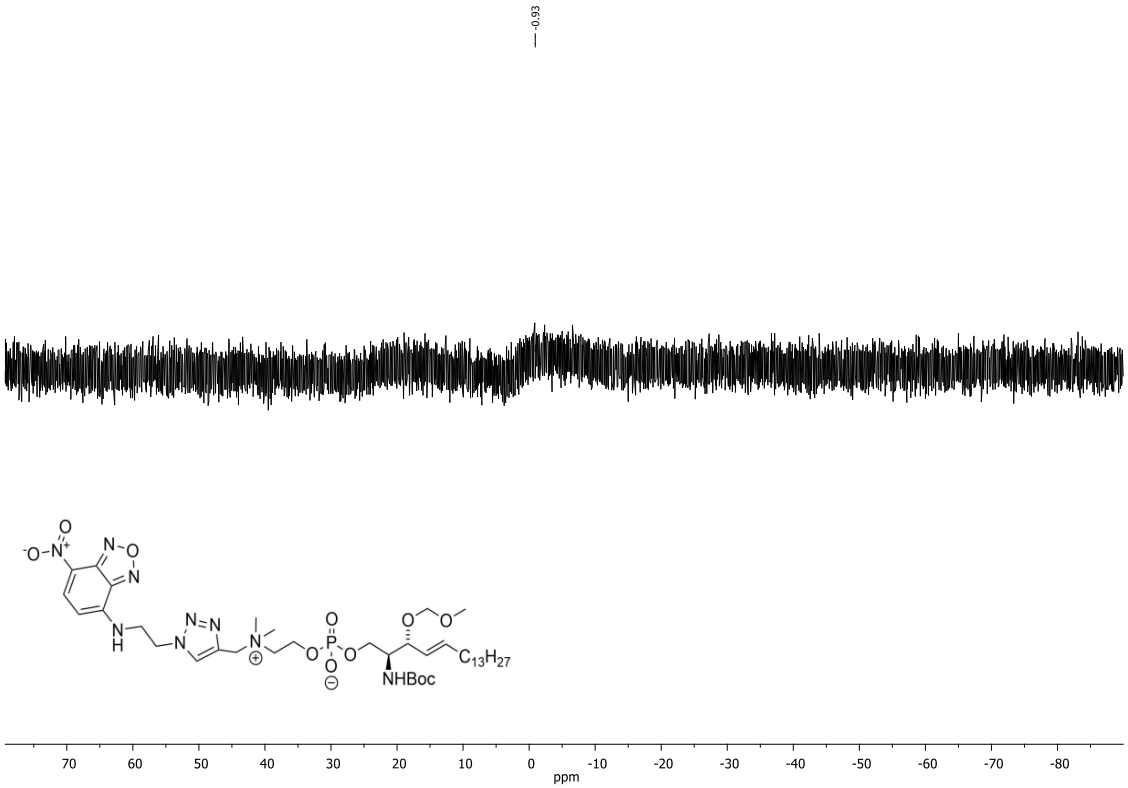

2-(dimethyl((1-(2-(7-nitrobenzo[c][1,2,5]oxadiazol-4-ylamino)ethyl)-1H-1,2,3-triazol-4-yl)methyl)ammonio)ethyl (2S,3R,E)-3-hydroxy-2-(6-(7-methoxy-2-oxo-2H-chromene-3-carboxamido)hexanamido)octadec-4-enyl phosphate (**ZQP-407**) (MeOD)

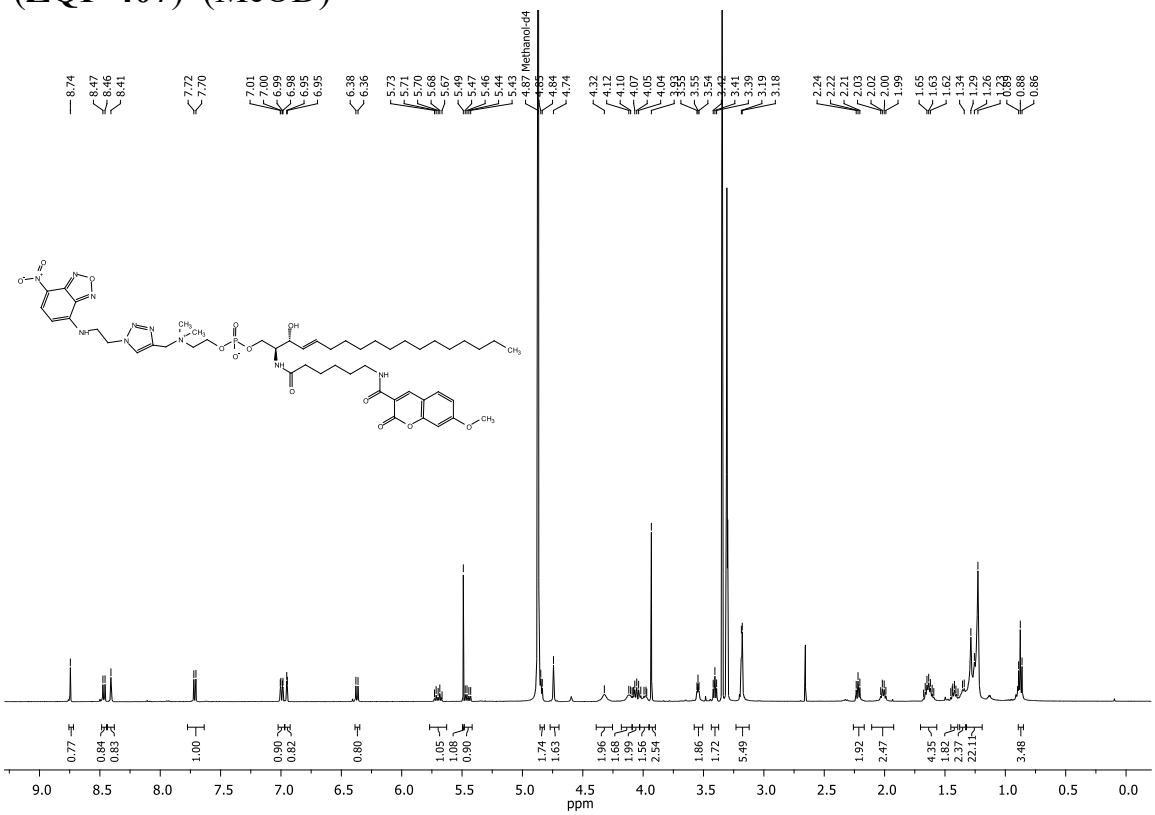

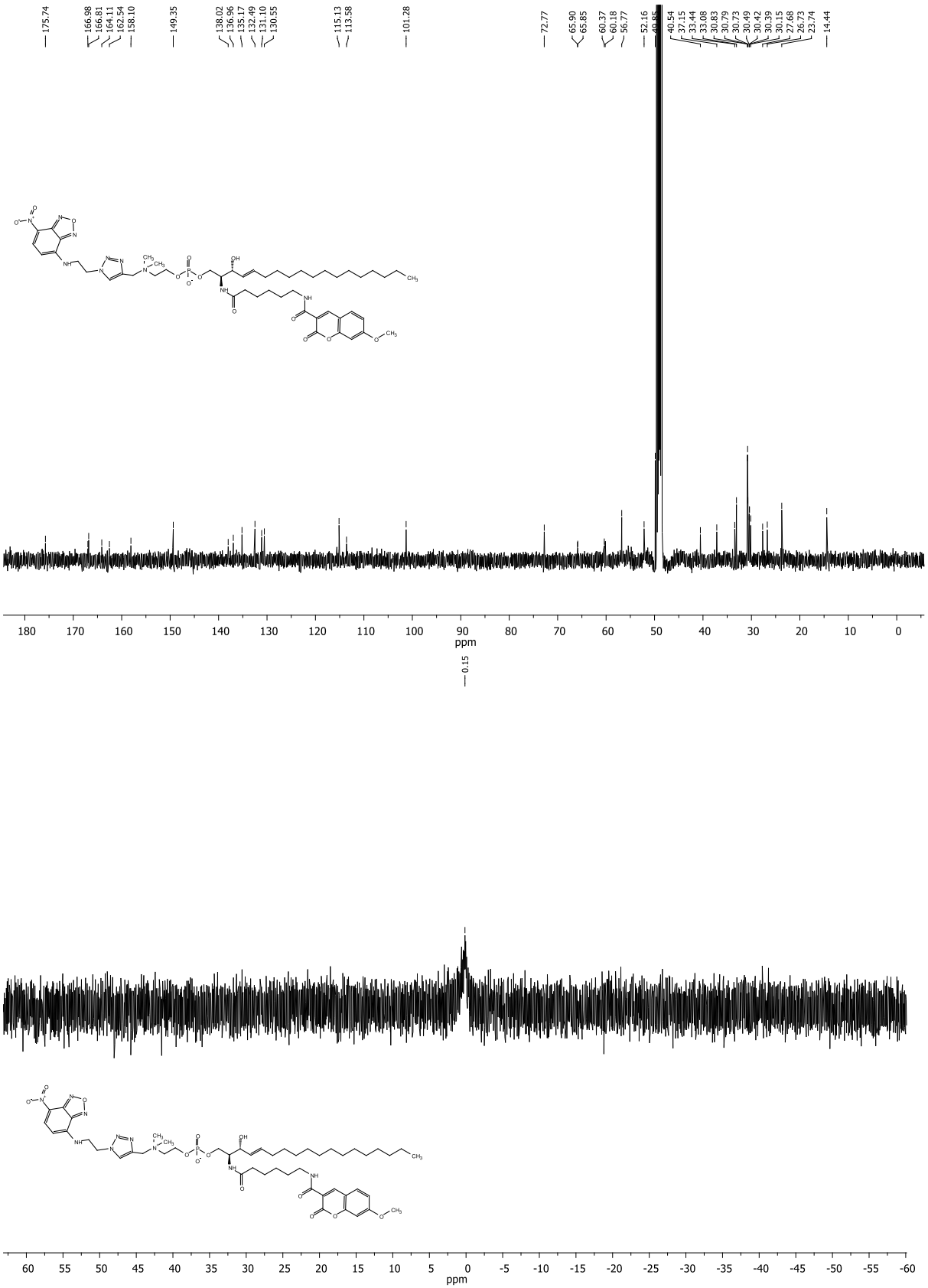
175.74
166.98
166.81
164.11
162.54
158.10
149.35
138.02
136.96
135.17
132.49
131.10
130.55
115.13
113.58
101.28
72.77
65.90
65.85
60.37
60.18
56.77
52.16
40.54
37.15
33.44
33.08
30.83
30.79
30.73
30.49
30.42
30.39
30.15
27.68
26.73
23.74
14.44
180 170 160 150 140 130 120 110 100 90 80 70 60 50 40 30 20 10 0
ppm
0.15
60 55 50 45 40 35 30 25 20 15 10 5 0 -5 -10 -15 -20 -25 -30 -35 -40 -45 -50 -55 -60
ppm

(E)-2-(tert-butoxycarbonyl)-3-(methoxymethoxy)octadec-4-enyl 2-(((1-(2-(3-carboxy-3(4)-(3-hydroxy-6-oxo-6H-xanthen-9-yl)benzamido)ethyl)-1H-1,2,3-triazol-4-yl)methyl)dimethylammonio)ethyl phosphate (**408**) (MeOD)

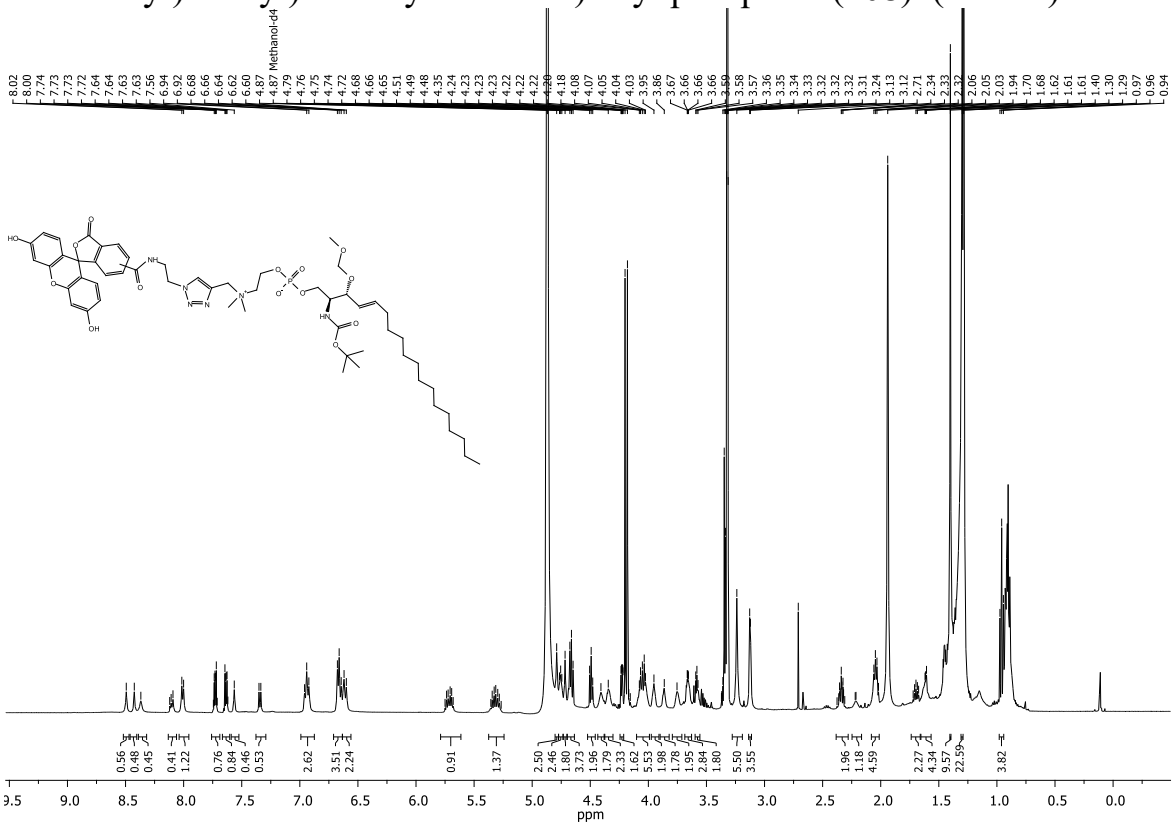

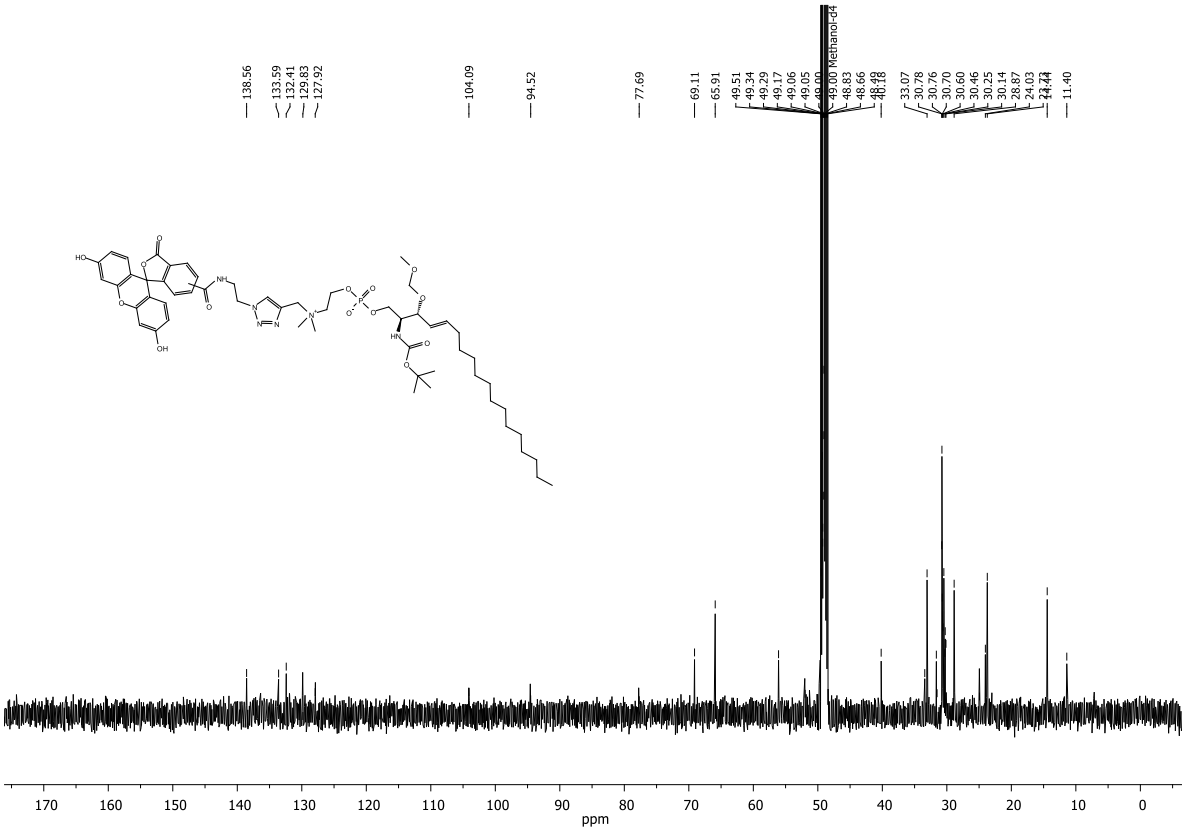

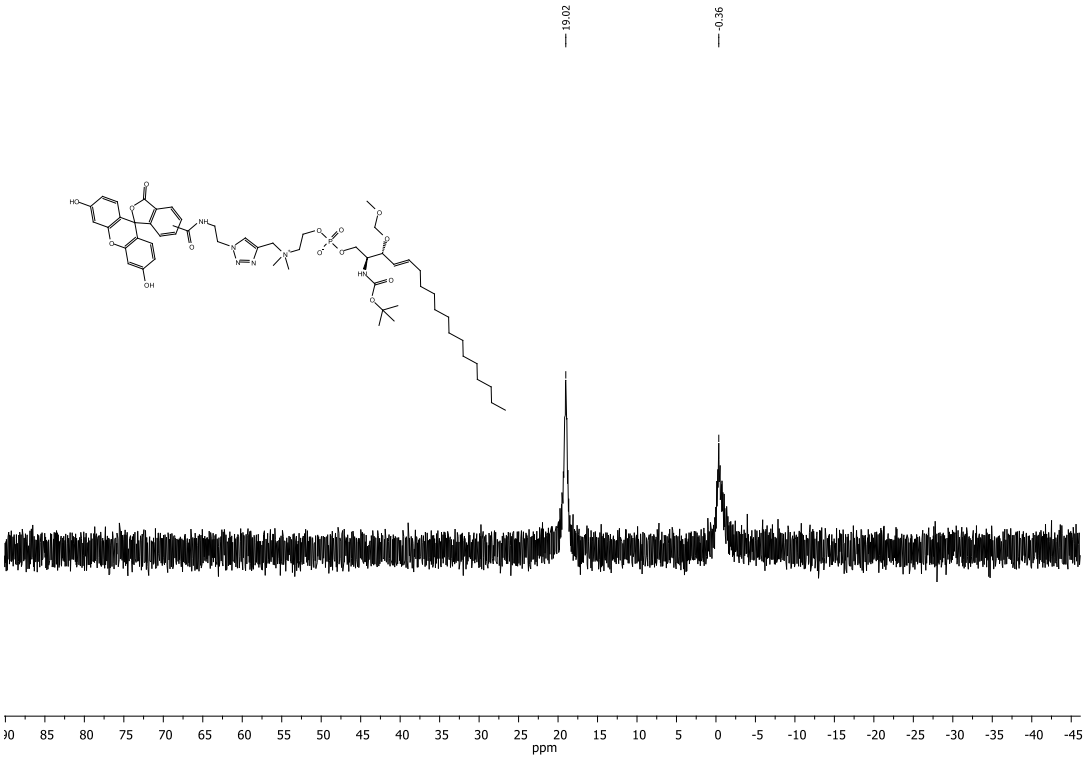

(2S,3R,E)-2-(6-((9-(diethylamino)-5-oxo-5H-benzo[a]phenoxazin-2-yl)oxy) hexanamido)-3-hydroxyoctadec-4-en-1-yl (2-(((1-(2-(3',6'-dihydroxy -3-oxo-3H-spiro[isobenzofuran-1,9'-xanthene]-5(6)-carboxamido)ethyl)-1H-1,2,3-triazol-4-yl)methyl)dimethylammonio) ethyl) phosphate (**ZQ$_2$P-410**)(DMSO-d$_6$)

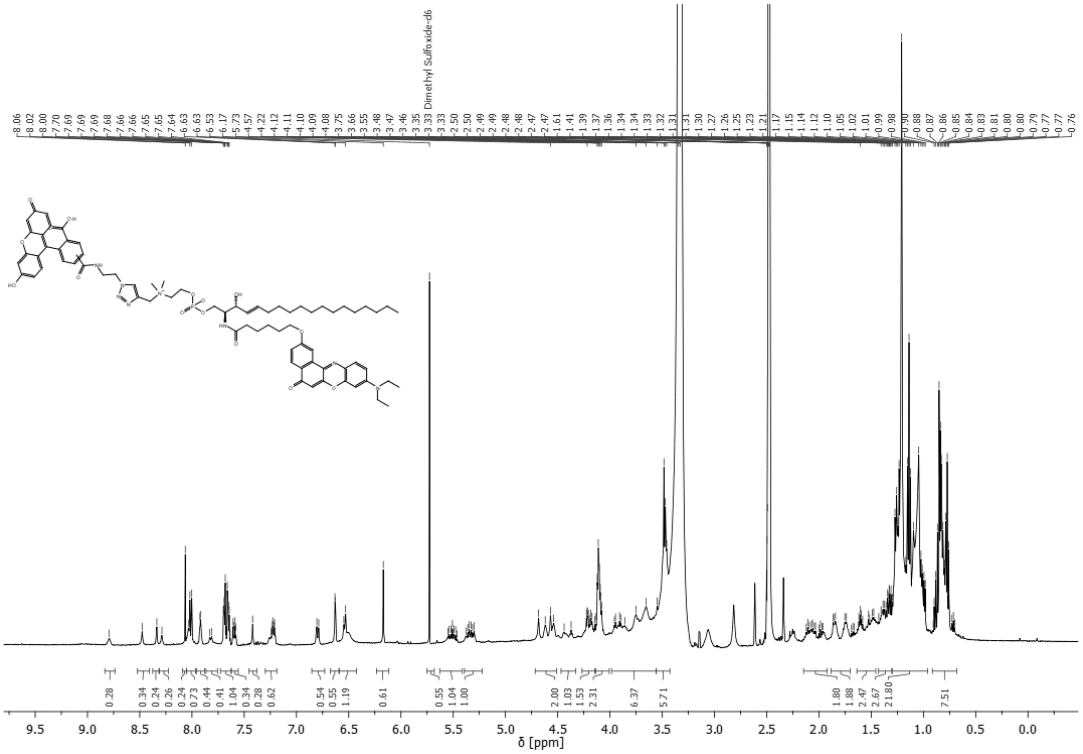

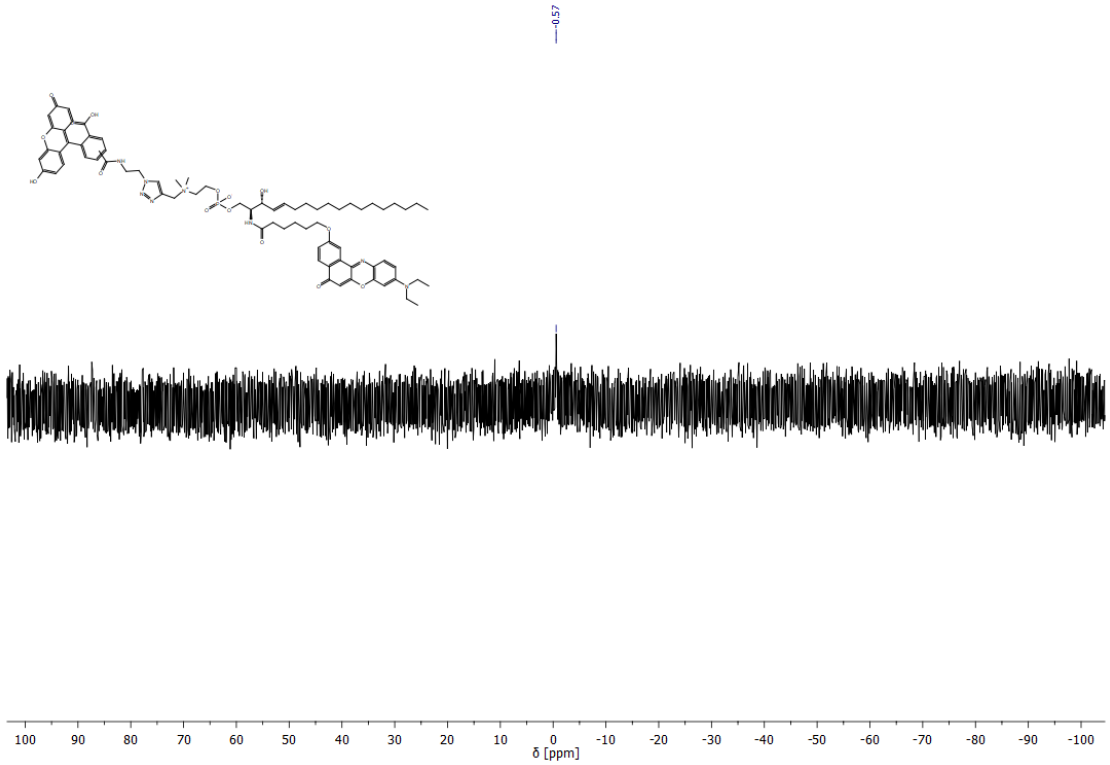

2-(((1-(2-(3',6'-dihydroxy-3-oxo-3H-spiro[isobenzofuran-1,9'-xanthene]-5(6)-carboxamido)ethyl)-1H-1,2,3-triazol-4-yl)methyl)dimethylammonio) ethyl ((2S,3R,E)-2-dodecanamido-3-hydroxyoctadec-4-en-1-yl) phosphate (**ZQ_3P-411**) (DMSO-d_6)

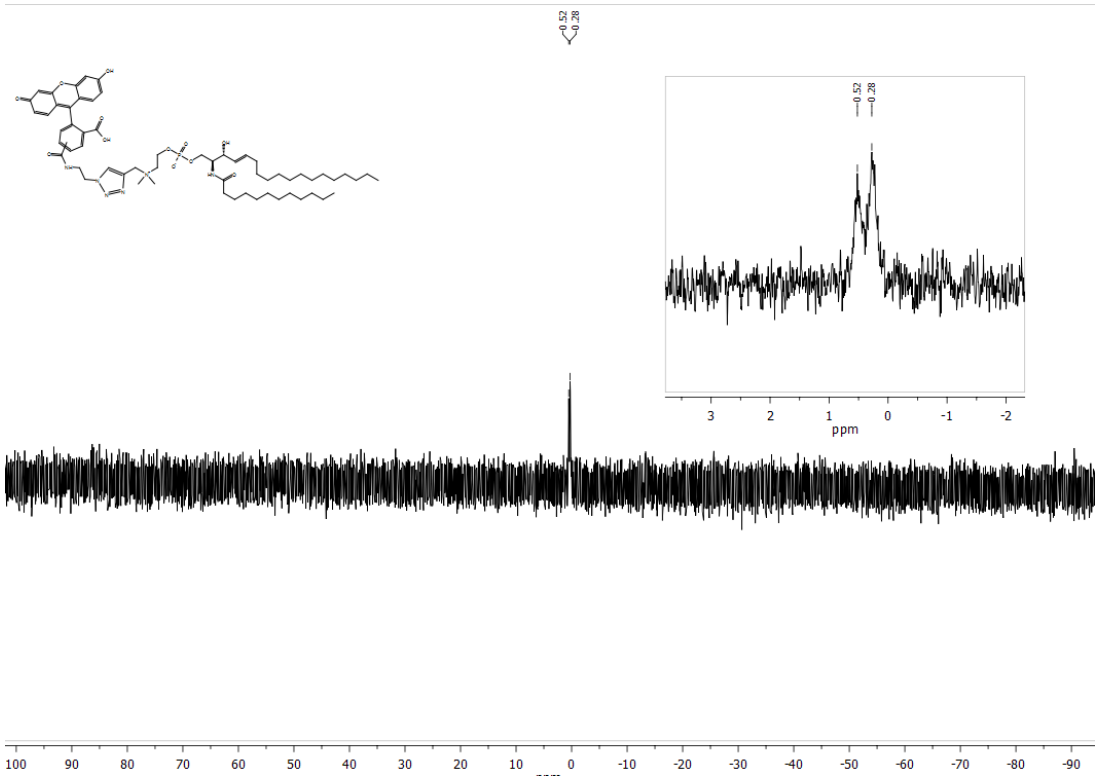

6-(2-(7-bromo-8-methyl-6-oxo-6H-[1,3]dioxolo[4,5-g]chromen-2-yl)acetamido)-N-((2S,3R,E)-1,3-dihydroxyoctadec-4-en-2-yl)hexanamide (**413**) ($CDCl_3$)

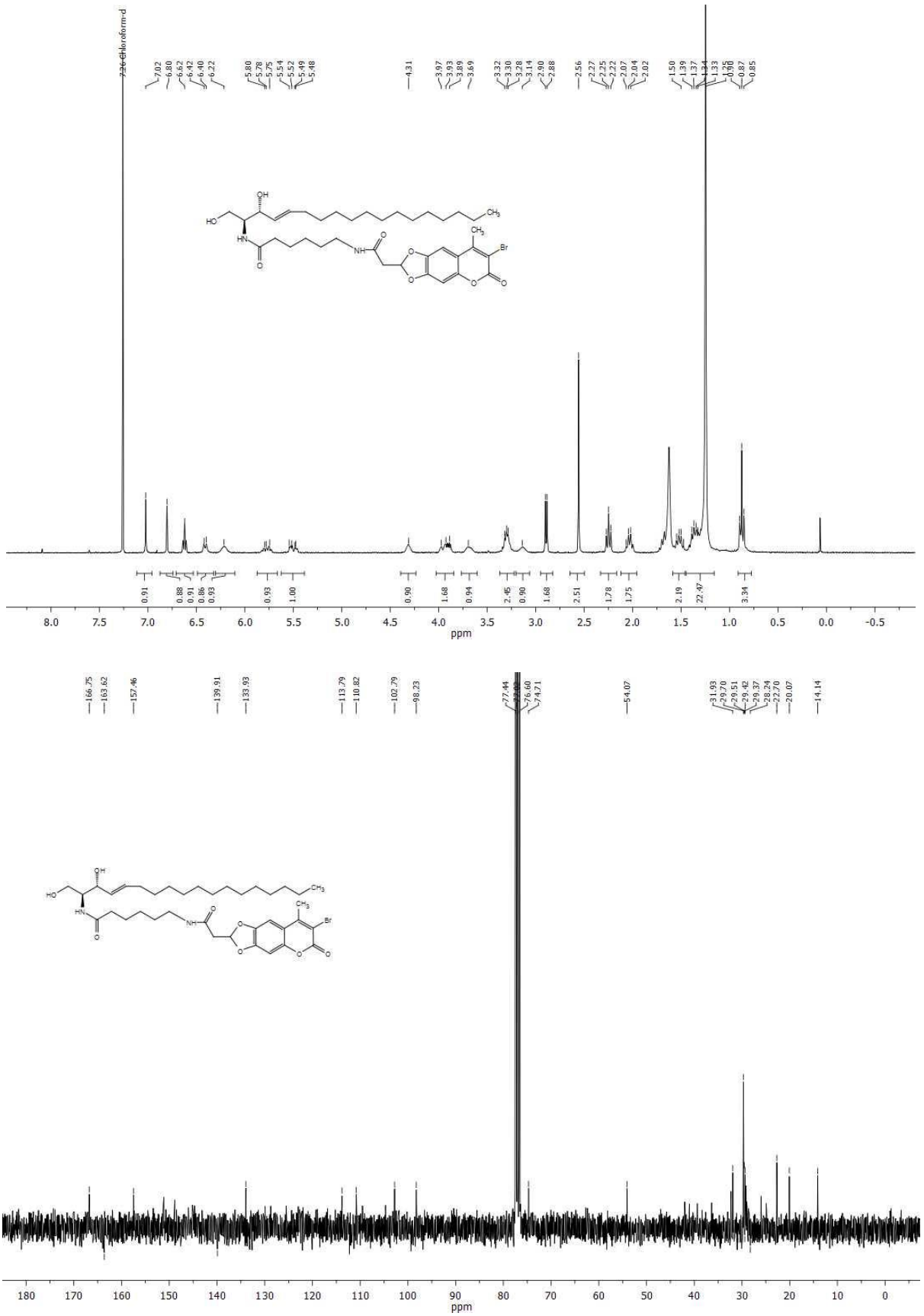

6 References

1. van Echten-Deckert, G. & Herget, T. Sphingolipid metabolism in neural cells. *Biochim. Biophys. Acta - Biomembr.* **1758**, 1978–1994 (2006).
2. Merrill Jr., A. H. *et al.* Importance of Sphingolipids and Inhibitors of Sphingolipid Metabolism as Components of Animal Diets. *J. Nutr.* **127**, 830S-833S (1997).
3. Hussain, G. *et al.* Role of cholesterol and sphingolipids in brain development and neurological diseases. *Lipids Health Dis.* **18**, 26 (2019).
4. Heung, L. J., Luberto, C. & Del Poeta, M. Role of Sphingolipids in Microbial Pathogenesis. *Infect. Immun.* **74**, 28 LP – 39 (2006).
5. Karlsson, K.-A. Aspects on Structure and Function of Sphingolipids in Cell Surface Membranes BT - Structure of Biological Membranes. in (eds. Abrahamsson, S. & Pascher, I.) 245–274 (Springer US, 1977). doi:10.1007/978-1-4684-8127-3_14
6. Bartke, N. & Hannun, Y. A. Bioactive sphingolipids: metabolism and function. *J. Lipid Res.* **50 Suppl**, S91–S96 (2009).
7. Hannun, Y. A. & Obeid, L. M. Principles of bioactive lipid signalling: lessons from sphingolipids. *Nat. Rev. Mol. Cell Biol.* **9**, 139–150 (2008).
8. Huang, F.-C. The Role of Sphingolipids on Innate Immunity to Intestinal Salmonella Infection. *Int. J. Mol. Sci.* **18**, 1720 (2017).
9. Grassmé, H. *et al.* Host defense against Pseudomonas aeruginosa requires ceramide-rich membrane rafts. *Nat. Med.* **9**, 322–330 (2003).
10. Gulbins, E., Dreschers, S., Wilker, B. & Grassmé, H. Ceramide, membrane rafts and infections. *J. Mol. Med.* **82**, 357–363 (2004).
11. Hanada, K. Sphingolipids in infectious diseases. *Japanese Journal of Infectious Diseases* (2005).
12. Jernigan, P. L. *et al.* Sphingolipids in Major Depression. *Neurosignals* **23**, 49–58 (2015).
13. Mühle, C., Reichel, M., Gulbins, E. & Kornhuber, J. Sphingolipids in Psychiatric Disorders and Pain Syndromes BT - Sphingolipids in Disease. in (eds. Gulbins, E. & Petrache, I.) 431–456 (Springer Vienna, 2013). doi:10.1007/978-3-7091-1511-4_22
14. Hannun, Y. A. & Obeid, L. M. Sphingolipids and their metabolism in physiology and disease. *Nat. Rev. Mol. Cell Biol.* **19**, 175–191 (2018).
15. Merscher, S. & Fornoni, A. Podocyte Pathology and Nephropathy – Sphingolipids in Glomerular Diseases. *Front. Endocrinol. (Lausanne).* **5**, 127 (2014).
16. Merrill, A. H. De novo sphingolipid biosynthesis: A necessary, but dangerous, pathway. *Journal of Biological Chemistry* (2002). doi:10.1074/jbc.R200009200
17. Chen, Y., Liu, Y., Sullards, M. C. & Merrill Jr, A. H. An introduction to sphingolipid metabolism and analysis by new technologies. *Neuromolecular Med.* **12**, 306–319 (2010).
18. Merrill, A. H., Wang, M. D., Park, M. & Sullards, M. C. (Glyco)sphingolipidology: an amazing challenge and opportunity for systems biology. *Trends Biochem. Sci.* **32**, 457–468 (2007).
19. Garrido, M. New sphingolipid probes for metabolism and trafficking studies. ' '. (Universitat de Barcelona, 2012).
20. Obeid, T. D. M. and L. M. Ceramide and Apoptosis: Exploring the Enigmatic Connections between Sphingolipid Metabolism and Programmed Cell Death. *Anti-Cancer Agents in Medicinal Chemistry* **12**, 340–363 (2012).
21. Cingolani, F., Futerman, A. H. & Casas, J. Ceramide synthases in biomedical research. *Chem. Phys. Lipids* **197**, 25–32 (2016).
22. Saied, E. M. Synthesis and Characterization of Inhibitors of Sphingolipid Metabolism ,Dissertation,. (Humboldt-Universität zu Berlin, 2017).

23. Adada, M., Luberto, C. & Canals, D. Inhibitors of the sphingomyelin cycle: Sphingomyelin synthases and sphingomyelinases. *Chem. Phys. Lipids* **197**, 45–59 (2016).
24. Kitatani, K., Idkowiak-Baldys, J. & Hannun, Y. A. The sphingolipid salvage pathway in ceramide metabolism and signaling. *Cell. Signal.* **20**, 1010–1018 (2008).
25. Yamaji, T., Kumagai, K., Tomishige, N. & Hanada, K. Two sphingolipid transfer proteins, CERT and FAPP2: Their roles in sphingolipid metabolism. *IUBMB Life* **60**, 511–518 (2008).
26. Gault, C. R., Obeid, L. M. & Hannun, Y. A. An overview of sphingolipid metabolism: from synthesis to breakdown. *Adv. Exp. Med. Biol.* **688**, 1–23 (2010).
27. Huitema, K., van den Dikkenberg, J., Brouwers, J. F. H. M. & Holthuis, J. C. M. Identification of a family of animal sphingomyelin synthases. *EMBO J.* **23**, 33–44 (2004).
28. Slotte, J. P. & Ramstedt, B. The functional role of sphingomyelin in cell membranes. *Eur. J. Lipid Sci. Technol.* **109**, 977–981 (2007).
29. Furland, N. E., Zanetti, S. R., Oresti, G. M., Maldonado, E. N. & Aveldaño, M. I. Ceramides and Sphingomyelins with High Proportions of Very Long-chain Polyunsaturated Fatty acids in Mammalian Germ Cells. *J. Biol. Chem.* **282**, 18141–18150 (2007).
30. Bienias, K., Fiedorowicz, A., Sadowska, A., Prokopiuk, S. & Car, H. Regulation of sphingomyelin metabolism. *Pharmacol. Reports* **68**, 570–581 (2016).
31. Goñi, F. M. & Alonso, A. Sphingomyelinases: enzymology and membrane activity. *FEBS Lett.* **531**, 38–46 (2002).
32. Pavoine, C. & Pecker, F. Sphingomyelinases: their regulation and roles in cardiovascular pathophysiology. *Cardiovasc. Res.* **82**, 175–183 (2009).
33. Smith, E. L. & Schuchman, E. H. The unexpected role of acid sphingomyelinase in cell death and the pathophysiology of common diseases. *FASEB J.* **22**, 3419–3431 (2008).
34. Gatt, S. Enzymic Hydrolysis and Synthesis of Ceramides. *J. Biol. Chem.* **238**, PC3131–PC3133 (1963).
35. Schneider, P. B. & Kennedy, E. P. Sphingomyelinase in normal human spleens and in spleens from subjects with Niemann-Pick disease. *J. Lipid Res.* **8**, 202–209 (1967).
36. Quintern, L. E. *et al.* Acid sphingomyelinase from human urine: purification and characterization. *Biochim. Biophys. Acta - Lipids Lipid Metab.* **922**, 323–336 (1987).
37. Human Placental Sphingomyelinase. Purification to Homogeneity, Antigenic Properties and Partial Amino-Acid Sequences of the Enzyme . *Biological Chemistry Hoppe-Seyler* **372**, 215 (1991).
38. Jones, C. S., Shankaran, P. & Callahan, J. W. Purification of sphingomyelinase to apparent homogeneity by using hydrophobic chromatography. *Biochem. J.* **195**, 373–382 (1981).
39. Fowler, S. Lysosomal localization of sphingomyelinase in rat liver. *Biochim. Biophys. Acta - Enzymol.* **191**, 481–484 (1969).
40. Quintern, L. E. *et al.* Isolation of cDNA clones encoding human acid sphingomyelinase: occurrence of alternatively processed transcripts. *EMBO J.* (1989). doi:10.1002/j.1460-2075.1989.tb08382.x
41. Schuchman, E. H., Levran, O., Pereira, L. V & Desnick, R. J. Structural organization and complete nucleotide sequence of the gene encoding human acid sphingomyelinase (SMPD1). *Genomics* **12**, 197–205 (1992).
42. Spence, M. W., Byers, D. M., Palmer, F. B. & Cook, H. W. A new Zn2+-stimulated sphingomyelinase in fetal bovine serum. *J. Biol. Chem.* **264**, 5358–5363 (1989).

43. Schissel, S. L., Schuchman, E. H., Williams, K. J. & Tabas, I. Zn2+-stimulated Sphingomyelinase Is Secreted by Many Cell Types and Is a Product of the Acid Sphingomyelinase Gene. *J. Biol. Chem.* **271**, 18431–18436 (1996).
44. Jenkins, R. W., Canals, D. & Hannun, Y. A. Roles and regulation of secretory and lysosomal acid sphingomyelinase. *Cell. Signal.* **21**, 836–846 (2009).
45. Tabas, I. Secretory sphingomyelinase. *Chem. Phys. Lipids* **102**, 123–130 (1999).
46. Zhang, Y. *et al.* Crucial role of alkaline sphingomyelinase in sphingomyelin digestion: a study on enzyme knockout mice. *J. Lipid Res.* **52**, 771–781 (2011).
47. Fotoulaki, M. *et al.* Acid sphingomyelinase-deficient Niemann–Pick disease: Novel findings in a Greek child. *J. Inherit. Metab. Dis.* **30**, 986 (2007).
48. Lallemand, T. *et al.* nSMase2 (Type 2-Neutral Sphingomyelinase) Deficiency or Inhibition by GW4869 Reduces Inflammation and Atherosclerosis in Apoe−/− Mice. *Arterioscler. Thromb. Vasc. Biol.* **38**, 1479–1492 (2018).
49. Hertervig, E., Nilsson, Å., Nyberg, L. & Duan, R.-D. Alkaline sphingomyelinase activity is decreased in human colorectal carcinoma. *Cancer* **79**, 448–453 (1997).
50. Beckmann, N., Sharma, D., Gulbins, E., Becker, K. A. & Edelmann, B. Inhibition of acid sphingomyelinase by tricyclic antidepressants and analogons. *Front. Physiol.* **5**, 331 (2014).
51. Liu, B. & Hannun, Y. A. Inhibition of the Neutral Magnesium-dependent Sphingomyelinase by Glutathione. *J. Biol. Chem.* **272**, 16281–16287 (1997).
52. Figuera-Losada, M. *et al.* Cambinol, a Novel Inhibitor of Neutral Sphingomyelinase 2 Shows Neuroprotective Properties. *PLoS One* **10**, e0124481 (2015).
53. Tabatadze, N. *et al.* Inhibition of neutral sphingomyelinase-2 perturbs brain sphingolipid balance and spatial memory in mice. *J. Neurosci. Res.* **88**, 2940–2951 (2010).
54. Cheng, Y., Nilsson, Å., Tömquist, E. & Duan, R.-D. Purification, characterization, and expression of rat intestinal alkaline sphingomyelinase. *J. Lipid Res.* **43**, 316–324 (2002).
55. Liu, J.-J., Nilsson, Å. & Duan, R.-D. Effects of phospholipids on sphingomyelin hydrolysis induced by intestinal alkaline sphingomyelinase: an in vitro study. *J. Nutr. Biochem.* **11**, 192–197 (2000).
56. Pinkert, T. Entwicklung molekularer Werkzeuge zur Erforschung des Lipidstoffwechsels. (Humboldt-Universität zu Berlin, Mathematisch-Naturwissenschaftliche Fakultät, 2017). doi:http://dx.doi.org/10.18452/18034
57. Schissel, S. L. *et al.* Secretory Sphingomyelinase, a Product of the Acid Sphingomyelinase Gene, Can Hydrolyze Atherogenic Lipoproteins at Neutral pH: IMPLICATIONS FOR ATHEROSCLEROTIC LESION DEVELOPMENT . *J. Biol. Chem.* **273**, 2738–2746 (1998).
58. Gulbins, E. Regulation of death receptor signaling and apoptosis by ceramide. *Pharmacol. Res.* **47**, 393–399 (2003).
59. Schissel, S. L., Keesler, G. A., Schuchman, E. H., Williams, K. J. & Tabas, I. The Cellular Trafficking and Zinc Dependence of Secretory and Lysosomal Sphingomyelinase, Two Products of the Acid Sphingomyelinase Gene. *J. Biol. Chem.* **273**, 18250–18259 (1998).
60. Schuchman, E. H. Acid sphingomyelinase, cell membranes and human disease: Lessons from Niemann–Pick disease. *FEBS Lett.* **584**, 1895–1900 (2010).
61. Gabandé-Rodríguez, E., Boya, P., Labrador, V., Dotti, C. G. & Ledesma, M. D. High sphingomyelin levels induce lysosomal damage and autophagy dysfunction in Niemann Pick disease type A. *Cell Death Differ.* **21**, 864–875 (2014).
62. Irun, P. *et al.* Identification of seven novel SMPD1 mutations causing Niemann–Pick disease types A and B. *Clin. Genet.* **84**, 356–361 (2013).

63. McGovern, M. M., Aron, A., Brodie, S. E., Desnick, R. J. & Wasserstein, M. P. Natural history of Type A Niemann-Pick disease. *Neurology* **66**, 228 LP – 232 (2006).
64. Wasserstein, M. P. *et al.* The Natural History of Type B Niemann-Pick Disease: Results From a 10-Year Longitudinal Study. *Pediatrics* **114**, e672--e677 (2004).
65. Papandreou, A. & Gissen, P. Diagnostic workup and management of patients with suspected Niemann-Pick type C disease. *Ther. Adv. Neurol. Disord.* **9**, 216–229 (2016).
66. Pineda, M. *et al.* A Suspicion Index to aid screening of early-onset Niemann-Pick disease Type C (NP-C). *BMC Pediatr.* **16**, 107 (2016).
67. Walkley, S. U. *et al.* Fostering collaborative research for rare genetic disease: the example of niemann-pick type C disease. *Orphanet J. Rare Dis.* **11**, 161 (2016).
68. Sturley, S. L., Patterson, M. C., Balch, W. & Liscum, L. The pathophysiology and mechanisms of NP-C disease. *Biochim. Biophys. Acta - Mol. Cell Biol. Lipids* **1685**, 83–87 (2004).
69. Pentchev, P. G. *et al.* Group C Niemann-Pick disease: faulty regulation of low-density lipoprotein uptake and cholesterol storage in cultured fibroblasts. *FASEB J.* **1**, 40–45 (1987).
70. Reagan, J. W., Hubbert, M. L. & Shelness, G. S. Posttranslational Regulation of Acid Sphingomyelinase in Niemann-Pick Type C1 Fibroblasts and Free Cholesterol-enriched Chinese Hamster Ovary Cells. *J. Biol. Chem.* **275**, 38104–38110 (2000).
71. Gorelik, A., Illes, K., Heinz, L. X., Superti-Furga, G. & Nagar, B. Crystal structure of mammalian acid sphingomyelinase. *Nat. Commun.* **7**, 12196 (2016).
72. Ferlinz, K., Hurwitz, R., Vielhaber, G., Suzuki, K. & Sandhoff, K. Occurrence of two molecular forms of human acid sphingomyelinase. *Biochem. J.* **301 (Pt 3**, 855–862 (1994).
73. Ponting, C. P. Acid sphingomyelinase possesses a domain homologous to its activator proteins: Saposins B and D. *Protein Sci.* **3**, 359–361 (1994).
74. Kolter, T. & Sandhoff, K. PRINCIPLES OF LYSOSOMAL MEMBRANE DIGESTION: Stimulation of Sphingolipid Degradation by Sphingolipid Activator Proteins and Anionic Lysosomal Lipids. *Annu. Rev. Cell Dev. Biol.* **21**, 81–103 (2005).
75. Zhou, Y.-F. *et al.* Human acid sphingomyelinase structures provide insight to molecular basis of Niemann–Pick disease. *Nat. Commun.* **7**, 13082 (2016).
76. Xiong, Z.-J., Huang, J., Poda, G., Pomès, R. & Privé, G. G. Structure of Human Acid Sphingomyelinase Reveals the Role of the Saposin Domain in Activating Substrate Hydrolysis. *J. Mol. Biol.* **428**, 3026–3042 (2016).
77. Sikora, J., Pavlu-Pereira, H., Elleder, M., Roelofs, H. & Wevers, R. A. Seven Novel Acid Sphingomyelinase Gene Mutations in Niemann-Pick Type A and B Patients. *Ann. Hum. Genet.* **67**, 63–70 (2003).
78. Seto, M. *et al.* A model of the acid sphingomyelinase phosphoesterase domain based on its remote structural homolog purple acid phosphatase. *Protein Sci.* **13**, 3172–3186 (2004).
79. Qiu, H. *et al.* Activation of Human Acid Sphingomyelinase through Modification or Deletion of C-terminal Cysteine. *J. Biol. Chem.* **278**, 32744–32752 (2003).
80. Lansmann, S. *et al.* Human acid sphingomyelinase. *Eur. J. Biochem.* **270**, 1076–1088 (2003).
81. Ferlinz, K. *et al.* Functional Characterization of the N-glycosylation Sites of Human Acid Sphingomyelinase by Site-Directed Mutagenesis. *Eur. J. Biochem.* **243**, 511–517 (1997).
82. Bartelsen, O. *et al.* Expression of recombinant human acid sphingomyelinase in insect Sf21 cells: purification, processing and enzymatic characterization. *J. Biotechnol.* **63**, 29–40 (1998).

83. Newrzella, D. & Stoffel, W. Functional Analysis of the Glycosylation of Murine Acid Sphingomyelinase. *J. Biol. Chem.* **271**, 32089–32095 (1996).
84. Loidl, A., Claus, R., Deigner, H. P. & Hermetter, A. High-precision fluorescence assay for sphingomyelinase activity of isolated enzymes and cell lysates. *J. Lipid Res.* **43**, 815–823 (2002).
85. Xu, M. *et al.* A high-throughput sphingomyelinase assay using natural substrate. *Anal. Bioanal. Chem.* **404**, 407–414 (2012).
86. Chuang, W.-L. *et al.* Improved sensitivity of an acid sphingomyelinase activity assay using a C6:0 sphingomyelin substrate. *Mol. Genet. Metab. Reports* **3**, 55–57 (2015).
87. Mintzer, R. J. *et al.* A Novel High-Throughput Screening Format to Identify Inhibitors of Secreted Acid Sphingomyelinase. *J. Biomol. Screen.* **10**, 225–234 (2005).
88. Liu, B. & Hannun, Y. A. B. T.-M. in E. [18] Sphingomyelinase assay using radiolabeled substrate. in *Sphingolipid Metabolism and Cell Signaling Part A* **311**, 164–167 (Academic Press, 2000).
89. Liu, F., Cheng, Y., Wu, J., Tauschel, H.-D. & Duan, R.-D. Ursodeoxycholic acid differentially affects three types of sphingomyelinase in human colon cancer Caco 2 cells. *Cancer Lett.* **235**, 141–146 (2006).
90. Duan, R.-D. & Nilsson, åke B. T.-M. in E. [30] Sphingolipid hydrolyzing enzymes in the gastrointestinal tract. in *Sphingolipid Metabolism and Cell Signaling Part A* **311**, 276–286 (Academic Press, 2000).
91. Mühle, C. & Kornhuber, J. Assay to measure sphingomyelinase and ceramidase activities efficiently and safely. *J. Chromatogr. A* **1481**, 137–144 (2017).
92. Kanfer, J. N., Young, O. M., Shapiro, D. & Brady, R. O. The Metabolism of Sphingomyelin: I. PURIFICATION AND PROPERTIES OF A SPHINGOMYELIN-CLEAVING ENZYME FROM RAT LIVER TISSUE . *J. Biol. Chem.* **241**, 1081–1084 (1966).
93. Stoffel, W. B. T.-M. in E. [50] Chemical synthesis of choline-labeled lecithins and sphingomyelins. in *Lipids Part B* **35**, 533–541 (Academic Press, 1975).
94. Barbone, A. G., Jackson, A. C., Ritchie, D. M. & Argentieri, D. C. [19] Robotic assay of sphingomyelinase activity for high throughput screening. in *Sphingolipid Metabolism and Cell Signaling Part A* **311**, 168–176 (Academic Press, 2000).
95. Harzer, K. & Benz, H. U. A simple sphingomyelinase determination for Niemann-Pick disease: differential diagnosis of types A, B and C. *J. Neurochem.* **21**, 999–1001 (1973).
96. Levade, T. *et al.* In situ assay of acid sphingomyelinase and ceramidase based on LDL-mediated lysosomal targeting of ceramide-labeled sphingomyelin. *J. Lipid Res.* **37**, 2525–2538 (1996).
97. Shan, G. *et al.* Isotope-labeled immunoassays without radiation waste. *Proc. Natl. Acad. Sci. U. S. A.* **97**, 2445–2449 (2000).
98. Santos, M. C. D., Morais, C. L. M., Nascimento, Y. M., Araujo, J. M. G. & Lima, K. M. G. Spectroscopy with computational analysis in virological studies: A decade (2006–2016). *TrAC Trends Anal. Chem.* **97**, 244–256 (2017).
99. Hajare, A. A. *et al.* High-throughput screening is an approach to drug discovery. *Am. J. Pharmtech Res.* (2014).
100. Chai, S. C. Assay Validation in High Throughput Screening – from Concept to Application. in (ed. Goktug, A. N.) Ch. 10 (IntechOpen, 2015). doi:10.5772/59765
101. Gal, A. E., Brady, R. O., Hibbert, S. R. & Pentchev, P. G. A Practical Chromogenic Procedure for the Detection of Homozygotes and Heterozygous Carriers of Niemann-Pick Disease. *N. Engl. J. Med.* **293**, 632–636 (1975).

102. Brady, R. O., Johnson, W. G. & Uhlendorf, B. W. Identification of heterozygous carriers of lipid storage diseases: Current status and clinical applications. *Am. J. Med.* **51**, 423–431 (1971).
103. Gal, A. E. & Fash, F. J. Synthesis of 2-N-(Hexadecanoyl)-amino-4-nitrophenyl phosphorylcholine-hydroxide, a chromogenic substrate for assaying sphingomyelinase activity. *Chem. Phys. Lipids* **16**, 71–79 (1976).
104. Harzer, K. *et al.* Niemann-Pick Disease Type A and B are Clinically but also Enzymatically Heterogeneous: Pitfall in the Laboratory Diagnosis of Sphingomyelinase Deficiency Associated with the Mutation Q292 K. *Neuropediatrics* **34**, 301–306 (2003).
105. van Diggelen, O. P. *et al.* A new fluorimetric enzyme assay for the diagnosis of Niemann–Pick A/B, with specificity of natural sphingomyelinase substrate. *J. Inherit. Metab. Dis.* **28**, 733–741 (2005).
106. Rojas, C. *et al.* DPTIP, a newly identified potent brain penetrant neutral sphingomyelinase 2 inhibitor, regulates astrocyte-peripheral immune communication following brain inflammation. *Sci. Rep.* **8**, 17715 (2018).
107. He, X., Chen, F., McGovern, M. M. & Schuchman, E. H. A Fluorescence-Based, High-Throughput Sphingomyelin Assay for the Analysis of Niemann–Pick Disease and Other Disorders of Sphingomyelin Metabolism. *Anal. Biochem.* **306**, 115–123 (2002).
108. Zhang, Y. *et al.* Involvement of the acid sphingomyelinase pathway in uva-induced apoptosis. *J. Biol. Chem.* **276**, 11775–11782 (2001).
109. Gaudino, J. J., Bjergarde, K., Chan-Hui, P.-Y., Wright, C. D. & Thomson, D. S. Synthesis of novel fluorescently labeled sphingomyelin derivatives useful for sphingomyelinase assay. *Bioorg. Med. Chem. Lett.* **7**, 1127–1132 (1997).
110. Gatt, S., Dinur, T. & Barenholz, Y. A fluorometric determination of sphingomyelinase by use of fluorescent derivatives of sphingomyelin, and its application to diagnosis of Niemann-Pick disease. *Clin. Chem.* **26**, 93–96 (1980).
111. Mohamed, Z. H., Rhein, C., Saied, E. M., Kornhuber, J. & Arenz, C. FRET probes for measuring sphingolipid metabolizing enzyme activity. *Chem. Phys. Lipids* **216**, 152–161 (2018).
112. Legnini, E. *et al.* Analysis of Acid Sphingomyelinase Activity in Dried Blood Spots Using Tandem Mass Spectrometry. *Ann Lab Med* **32**, 319–323 (2012).
113. Zhou, X., Tureček, F., Scott, C. R. & Gelb, M. H. Quantification of Cellular Acid Sphingomyelinase and Galactocerebroside β-Galactosidase Activities by Electrospray Ionization Mass Spectrometry. *Clin. Chem.* **47**, 874–881 (2001).
114. Ghomashchi, F., Barcenas, M., Turecek, F., Scott, C. R. & Gelb, M. H. Reliable Assay of Acid Sphingomyelinase Deficiency with the Mutation Q292K by Tandem Mass Spectrometry. *Clin. Chem.* **61**, 771–772 (2015).
115. Mohamed, Z. H., Rhein, C., Saied, E. M., Kornhuber, J. & Arenz, C. FRET probes for measuring sphingolipid metabolizing enzyme activity. *Chemistry and Physics of Lipids* **216**, 152–161 (2018).
116. Miyawaki, A. *et al.* Fluorescent indicators for Ca2+based on green fluorescent proteins and calmodulin. *Nature* **388**, 882–887 (1997).
117. Yi, L. *et al.* A Highly Sensitive Fluorescence Probe for Fast Thiol-Quantification Assay of Glutathione Reductase. *Angew. Chemie Int. Ed.* **48**, 4034–4037 (2009).
118. Wichmann, O., Wittbrodt, J. & Schultz, C. A Small-Molecule FRET Probe To Monitor Phospholipase A2 Activity in Cells and Organisms. *Angew. Chemie Int. Ed.* **45**, 508–512 (2006).
119. Takakusa, H. *et al.* Design and Synthesis of an Enzyme-Cleavable Sensor Molecule for Phosphodiesterase Activity Based on Fluorescence Resonance Energy Transfer. *J. Am. Chem. Soc.* **124**, 1653–1657 (2002).

120. Wichmann, O. & Schultz, C. FRET probes to monitor phospholipase A2 activity. *Chem. Commun.* 2500–2501 (2001). doi:10.1039/B107670C
121. Pinkert, T., Furkert, D., Korte, T., Herrmann, A. & Arenz, C. Amplification of a FRET Probe by Lipid–Water Partition for the Detection of Acid Sphingomyelinase in Live Cells. *Angew. Chemie Int. Ed.* **56**, 2790–2794 (2017).
122. Bhabak, K. P. *et al.* Development of a Novel FRET Probe for the Real-Time Determination of Ceramidase Activity. *ChemBioChem* **14**, 1049–1052 (2013).
123. Roth, A. G., Redmer, S. & Arenz, C. Potent Inhibition of Acid Sphingomyelinase by Phosphoinositide Analogues. *ChemBioChem* **10**, 2367–2374 (2009).
124. Roth, A. G. *et al.* Potent and Selective Inhibition of Acid Sphingomyelinase by Bisphosphonates. *Angew. Chemie Int. Ed.* **48**, 7560–7563 (2009).
125. Kappe, C., Mohamed, Z. H., Naser, E., Carpinteiro, A. & Arenz, C. A Novel Visible Range FRET Probe for Monitoring Acid Sphingomyelinase Activity in Living Cells. *Chem. - A Eur. J.* **26**, 5780–5783 (2020).
126. Jensen, E. C. Types of Imaging, Part 2: An Overview of Fluorescence Microscopy. *Anat. Rec.* **295**, 1621–1627 (2012).
127. Benninger, R. K. P. & Piston, D. W. Two-Photon Excitation Microscopy for the Study of Living Cells and Tissues. *Curr. Protoc. Cell Biol.* **59**, 4.11.1-4.11.24 (2013).
128. St. Croix, C. M., Shand, S. H. & Watkins, S. C. Confocal microscopy: comparisons, applications, and problems. *Biotechniques* **39**, S2–S5 (2005).
129. Xi, P. Scanning and Image Reconstruction Techniques in Confocal Laser Scanning Microscopy. in (ed. Liu, Y.) Ch. 27 (IntechOpen, 2011). doi:10.5772/14545
130. Diaspro, A., Chirico, G. & Collini, M. Two-photon fluorescence excitation and related techniques in biological microscopy. *Q. Rev. Biophys.* **38**, 97–166 (2005).
131. Schießl, I. M. & Castrop, H. Deep insights: intravital imaging with two-photon microscopy. *Pflügers Arch. - Eur. J. Physiol.* **468**, 1505–1516 (2016).
132. Göppert-Mayer, M. Über Elementarakte mit zwei Quantensprüngen. *Ann. Phys.* **401**, 273–294 (1931).
133. Kogej, T. *et al.* Mechanisms for enhancement of two-photon absorption in donor–acceptor conjugated chromophores. *Chem. Phys. Lett.* **298**, 1–6 (1998).
134. Albota, M. *et al.* Design of Organic Molecules with Large Two-Photon Absorption Cross Sections. *Science (80-.).* **281**, 1653–1656 (1998).
135. Zhou, F.-X. *et al.* A new 2{,}2′:6′{,}2″-terpyridine-based ligand and its complexes: structures{,} photophysical properties and DFT calculations to evaluate the halogen effect on the TPA. *CrystEngComm* **14**, 5613–5621 (2012).
136. Karatay, A. *et al.* The effect of heavy atom to two photon absorption properties and intersystem crossing mechanism in aza-boron-dipyrromethene compounds. *Dye. Pigment.* **122**, 286–294 (2015).
137. Küçüköz, B. *et al.* Enhancement of two photon absorption properties and intersystem crossing by charge transfer in pentaaryl boron-dipyrromethene (BODIPY) derivatives. *Phys. Chem. Chem. Phys.* **18**, 13546–13553 (2016).
138. Morone, M. *et al.* Enhancement of Two-Photon Absorption Cross-Section and Singlet-Oxygen Generation in Porphyrins upon β-Functionalization with Donor−Acceptor Substituents. *Org. Lett.* **8**, 2719–2722 (2006).
139. Ventelon, L., Charier, S., Moreaux, L., Mertz, J. & Blanchard-Desce, M. Nanoscale Push–Push Dihydrophenanthrene Derivatives as Novel Fluorophores for Two-Photon-Excited Fluorescence. *Angew. Chemie Int. Ed.* **40**, 2098–2101 (2001).
140. Iwase, Y., Kamada, K., Ohta, K. & Kondo, K. Synthesis and photophysical properties of new two-photon absorption chromophores containing a diacetylene moiety as the central π-bridge. *J. Mater. Chem.* **13**, 1575–1581 (2003).

141. Kamada, K. *et al.* Strong Two-Photon Absorption of Singlet Diradical Hydrocarbons. *Angew. Chemie Int. Ed.* **46**, 3544–3546 (2007).
142. Zhang, Q., Tian, X., Zhou, H., Wu, J. & Tian, Y. Lighting the Way to See Inside Two-Photon Absorption Materials: Structure-Property Relationship and Biological Imaging. *Mater. (Basel, Switzerland)* **10**, 223 (2017).
143. Heffern, M. C., Matosziuk, L. M. & Meade, T. J. Lanthanide Probes for Bioresponsive Imaging. *Chem. Rev.* **114**, 4496–4539 (2014).
144. Hewitt, S. H. & Butler, S. J. Application of lanthanide luminescence in probing enzyme activity. *Chem. Commun.* **54**, 6635–6647 (2018).
145. Parker, D. Excitement in f block : structure{,} dynamics and function of nine-coordinate chiral lanthanide complexes in aqueous media. *Chem. Soc. Rev.* **33**, 156–165 (2004).
146. Geiβler, D. & Hildebrandt, N. Lanthanide Complexes in FRET Applications. *Curr. Inorg. Chem.* (2011). doi:10.2174/1877944111101010017
147. Waleed Nafea Al-Qaysi, W. New Luminescent Europium Complexes as Indicators and in Sensors for pH in Biosamples and Water Samples. (University of Regensburg, 2018).
148. Weissman, S. I. Intramolecular Energy Transfer The Fluorescence of Complexes of Europium. *J. Chem. Phys.* **10**, 214–217 (1942).
149. Lis, S. Factors Affecting Luminescence Intensity of Lanthanide Ions. Analytical Applications of Lanthanide Luminescence in Solution. *Acta Phys. Pol. A* (1993). doi:10.12693/aphyspola.84.1003
150. Lis, S. Luminescence spectroscopy of lanthanide(III) ions in solution. *J. Alloys Compd.* **341**, 45–50 (2002).
151. Thibon, A. & Pierre, V. C. Principles of responsive lanthanide-based luminescent probes for cellular imaging. *Anal. Bioanal. Chem.* **394**, 107–120 (2009).
152. Lee, K., Dzubeck, V., Latshaw, L. & Schneider, J. P. De Novo Designed Peptidic Redox Potential Probe: Linking Sensitized Emission to Disulfide Bond Formation. *J. Am. Chem. Soc.* **126**, 13616–13617 (2004).
153. Viguier, R. F. H. & Hulme, A. N. A Sensitized Europium Complex Generated by Micromolar Concentrations of Copper(I): Toward the Detection of Copper(I) in Biology. *J. Am. Chem. Soc.* **128**, 11370–11371 (2006).
154. Leonard, J. P., dos Santos, C. M. G., Plush, S. E., McCabe, T. & Gunnlaugsson, T. pH driven self-assembly of a ternary lanthanide luminescence complex: the sensing of anions using a β-diketonate-Eu(iii) displacement assay. *Chem. Commun.* 129–131 (2007). doi:10.1039/B611487C
155. Schäferling, M. The Art of Fluorescence Imaging with Chemical Sensors. *Angew. Chemie Int. Ed.* **51**, 3532–3554 (2012).
156. Mohamed, Z. H., Soukka, T., Arenz, C. & Schäferling, M. Five-, Four- and Three-Dentate Europium Chelates for Anion Sensing and Their Applicability to Enzymatic Dephosphorylation Reactions. *ChemistrySelect* (2018). doi:10.1002/slct.201803287
157. Beer, P. D. & Gale, P. A. Anion Recognition and Sensing: The State of the Art and Future Perspectives. *Angew. Chemie Int. Ed.* **40**, 486–516 (2001).
158. Gunnlaugsson, T., Glynn, M., Hussey, G., Kruger, P. & Pfeffer, F. Anion recognition and sensing in organic and aqueous media using luminescent and colorimetric sensors. *Coord. Chem. Rev.* **250**, 3094–3117 (2006).
159. Spangler, C., Schaeferling, M. & Wolfbeis, O. Fluorescent probes for microdetermination of inorganic phosphates and biophosphates. *Microchim. Acta* **161**, 1–39 (2007).
160. Gale, P. A. & Caltagirone, C. Anion sensing by small molecules and molecular ensembles. *Chem. Soc. Rev.* (2015). doi:10.1039/c4cs00179f

161. Butler, S. J. Quantitative determination of fluoride in pure water using luminescent europium complexes. *Chem. Commun.* **51**, 10879–10882 (2015).
162. Plush, S. E. & Gunnlaugsson, T. Luminescent Sensing of Dicarboxylates in Water by a Bismacrocyclic Dinuclear Eu(III) Conjugate. *Org. Lett.* **9**, 1919–1922 (2007).
163. Smith, D. G., McMahon, B. K., Pal, R. & Parker, D. Live cell imaging of lysosomal pH changes with pH responsive ratiometric lanthanide probes. *Chem. Commun.* **48**, 8520–8522 (2012).
164. Shuvaev, S., Starck, M. & Parker, D. Responsive, Water-Soluble Europium(III) Luminescent Probes. *Chem. – A Eur. J.* **23**, 9974–9989 (2017).
165. Haufe, H., Muschter, K., Siegert, J. & Böttcher, H. dd_EndNote. *Scientia Horticulturae* **239**, 26–34 (2018).
166. Schäferling, M., Grögel, D. B. M. & Schreml, S. Luminescent probes for detection and imaging of hydrogen peroxide. *Microchim. Acta* **174**, 1 (2011).
167. Butler, S. J. & Parker, D. Anion binding in water at lanthanide centres: from structure and selectivity to signalling and sensing. *Chem. Soc. Rev.* **42**, 1652–1666 (2013).
168. Gunnlaugsson, T., Harte, A. J., Leonard, J. P. & Nieuwenhuyzen, M. Delayed lanthanide luminescence sensing of aromatic carboxylates using heptadentate triamide Tb(iii) cyclen complexes: the recognition of salicylic acid in water. *Chem. Commun.* 2134–2135 (2002). doi:10.1039/B204888D
169. Lippert, A. R., Gschneidtner, T. & Chang, C. J. Lanthanide-based luminescent probes for selective time-gated detection of hydrogen peroxide in water and in living cells. *Chem. Commun.* **46**, 7510–7512 (2010).
170. Parker, D., Kanthi Senanayake, P. & A. Gareth Williams, J. Luminescent sensors for pH{,} pO2{,} halide and hydroxide ions using phenanthridine as a photosensitiser in macrocyclic europium and terbium complexes. *J. Chem. Soc.{,} Perkin Trans. 2* 2129–2140 (1998). doi:10.1039/A801270I
171. Wessig, P. *et al.* Two-photon FRET pairs based on coumarin and DBD dyes. *RSC Adv.* **6**, 33510–33513 (2016).
172. Demay-Drouhard, P., Chamoreau, L.-M., Guillot, R., Policar, C. & Bertrand, H. C. Synthesis of Homoditopic Ligands with an Incrementable Rodlike Backbone. *European J. Org. Chem.* **2017**, 131–137 (2017).
173. Kleoff, M. *et al.* Efficient Syntheses of New Super Lewis Basic Tris(dialkylamino)-Substituted Terpyridines and Comparison of Their Methyl Cation Affinities. *Chem. – A Eur. J.* **25**, 7526–7533 (2019).
174. Li, Q.-F. *et al.* Highly luminescent hydrogels synthesized by covalent grafting of lanthanide complexes onto PNIPAM via one-pot free radical polymerization. *J. Mater. Chem. C* **4**, 3195–3201 (2016).
175. Nettekoven, M. & Jenny, C. The Development of a Practical and Reliable Large-Scale Synthesis of 2,6-Diamino-4-bromopyridine. *Org. Process Res. Dev.* **7**, 38–43 (2003).
176. Georgiades, S. N. & Rizeq, N. Synthesis of a 'Propeller-Like' Oligoheteroaryl with Alternating Pyridine and Oxazole Motifs. *Synlett* **26**, 489–493 (2015).
177. Rizeq, N. & Georgiades, S. N. Linear and Branched Pyridyl–Oxazole Oligomers: Synthesis and Circular Dichroism Detectable Effect on c-Myc G-Quadruplex Helicity. *European J. Org. Chem.* **2016**, 122–131 (2016).
178. Rasheed, O. K. *et al.* The assembly of "S3N"-ligands decorated with an azo-dye as potential sensors for heavy metal ions. *Dalt. Trans.* **46**, 5229–5239 (2017).
179. Therrien, J. A. & Wolf, M. O. The Influence of para Substituents in Bis(N-Heterocyclic Carbene) Palladium Pincer Complexes for Electrocatalytic CO2 Reduction. *Inorg. Chem.* **56**, 1161–1172 (2017).

180. Ziessel, R., Steffen, A. & Starck, M. Design and synthesis of phosphorylated pyridine-based ligands for lanthanide complexation. Part 1. *Tetrahedron Lett.* **53**, 3713–3716 (2012).
181. Schäferling, M., Ääritalo, T. & Soukka, T. Multidentate Europium Chelates as Luminoionophores for Anion Recognition: Impact of Ligand Design on Sensitivity and Selectivity, and Applicability to Enzymatic Assays. *Chem. – A Eur. J.* **20**, 5298–5308 (2014).
182. Picot, A. *et al.* Design of pyridine-dicarboxamide ligands for the sensitization of europium(III) by two photon antenna effect. in *Optical Materials in Defence Systems Technology III* (eds. Grote, J. G., Kajzar, F. & Lindgren, M.) **6401**, 75–82 (SPIE, 2006).
183. Picot, A. *et al.* Synthesis, structures, optical properties, and TD-DFT studies of donor-π-conjugated dipicolinic acid/ester/amide ligands. *Tetrahedron* **64**, 399–411 (2008).
184. Supkowski, R. M. & Horrocks, W. D. On the determination of the number of water molecules, q, coordinated to europium(III) ions in solution from luminescence decay lifetimes. *Inorganica Chim. Acta* **340**, 44–48 (2002).
185. Parker, D., Dickins, R. S., Puschmann, H., Crossland, C. & Howard, J. A. K. Being Excited by Lanthanide Coordination Complexes: Aqua Species, Chirality, Excited-State Chemistry, and Exchange Dynamics. *Chem. Rev.* **102**, 1977–2010 (2002).
186. Structure and thermodynamics of lanthanide and actinide complexes in solution . *Pure and Applied Chemistry* **27**, 23 (1971).
187. Gale, P. A. & Caltagirone, C. Anion sensing by small molecules and molecular ensembles. *Chem. Soc. Rev.* **44**, 4212–4227 (2015).
188. Spangler, C., Schaeferling, M. & Wolfbeis, O. S. Fluorescent probes for microdetermination of inorganic phosphates and biophosphates. *Microchim. Acta* **161**, 1–39 (2008).
189. Rama Mohana Rao, D. *et al.* Thermodynamic study of Eu(III) complexation by pyridine monocarboxylates. *J. Chem. Thermodyn.* **55**, 67–74 (2012).
190. Hasegawa, Y., Saitou, S., Tamaki, S., Yajima, H. & Tadokoro, M. Effects of Zinc(II) on the Luminescence of Europium(III) in Complexes Containing β-Diketone and Schiff Bases. *Helv. Chim. Acta* **92**, 2565–2575 (2009).
191. Yang, J.-H., Zhu, G.-Y. & Wang, H. Application of the co-luminescence effect of rare earths: simultaneous determination of trace amounts of samarium and europium in solution. *Analyst* **114**, 1417–1419 (1989).
192. Zeidan, Y. H. *et al.* Acid Ceramidase but Not Acid Sphingomyelinase Is Required for Tumor Necrosis Factor-α-induced PGE2 Production. *J. Biol. Chem.* **281**, 24695–24703 (2006).
193. Madry, C. *et al.* Effects of the ecto-ATPase apyrase on microglial ramification and surveillance reflect cell depolarization, not ATP depletion. *Proc. Natl. Acad. Sci.* **115**, E1608--E1617 (2018).
194. Li, P., Cao, J., Chen, Y., Wang, W. & Yang, J. Apyrase protects against allergic airway inflammation by decreasing the chemotactic migration of dendritic cells in mice. *Int. J. Mol. Med.* (2014). doi:10.3892/ijmm.2014.1771
195. Veloria, J. R., Devkota, A. K., Cho, E. J. & Dalby, K. N. Optimization of a Luminescence-Based High-Throughput Screening Assay for Detecting Apyrase Activity. *SLAS Discov. Adv. Sci. Drug Discov.* **22**, 94–101 (2016).
196. Veloria, J. R., Devkota, A. K., Cho, E. J. & Dalby, K. N. Optimization of a Luminescence-Based High-Throughput Screening Assay for Detecting Apyrase Activity. *SLAS Discov. Adv. Life Sci. R&D* **22**, 94–101 (2017).

197. Yamamoto, T., Hasegawa, H., Hakogi, T. & Katsumura, S. Versatile Synthetic Method for Sphingolipids and Functionalized Sphingosine Derivatives via Olefin Cross Metathesis. *Org. Lett.* **8**, 5569–5572 (2006).
198. Kotha, S. & Dipak, M. K. Strategies and tactics in olefin metathesis. *Tetrahedron* **68**, 397–421 (2012).
199. Dong, Z. & Butcher, J. A. A useful synthesis of d-erythro-sphingomyelins. *Tetrahedron Lett.* **32**, 5291–5294 (1991).
200. Sandbhor, M. S., Key, J. A., Strelkov, I. S. & Cairo, C. W. A Modular Synthesis of Alkynyl-Phosphocholine Headgroups for Labeling Sphingomyelin and Phosphatidylcholine. *J. Org. Chem.* **74**, 8669–8674 (2009).
201. Goretta, S. A. *et al.* Effects of chemical modification of sphingomyelin ammonium group on formation of liquid-ordered phase. *Bioorg. Med. Chem.* **20**, 4012–4019 (2012).
202. Balas, L., Jousseaume, B. & Langwost, B. Improved preparation of aliphatic propynoic esters. *Tetrahedron Lett.* **30**, 4525–4526 (1989).
203. Fan, Y. C. & Kwon, O. Phosphine/Palladium-Catalyzed Syntheses of Alkylidene Phthalans, 3-Deoxyisoochracinic Acid, Isoochracinic Acid, and Isoochracinol. *Org. Lett.* **14**, 3264–3267 (2012).
204. Liu, L. *et al.* Palladium-Catalyzed Regio- and Stereoselective Coupling–Addition of Propiolates with Arylsulfonyl Hydrazides: A Pattern for Difunctionalization of Alkynes. *Org. Lett.* **20**, 4023–4027 (2018).
205. Li, M. & Hua, R. Ru3(CO)12-Catalyzed Reactions of Catechols with Alkynes: An Atom-Economic Process for the Synthesis of 2,2-Disubstituted 1,3-Benzodioxoles from the Double Addition of the O−H Bond Across a Triple Bond. *J. Org. Chem.* **73**, 8658–8660 (2008).
206. Chaudhuri, S. K., Roy, S. & Bhar, S. Dioxane dibromide mediated bromination of substituted coumarins under solvent-free conditions. *Beilstein J. Org. Chem.* **8**, 323–329 (2012).
207. Kelkar, R. M., Joshi, U. K. & Paradkar, M. V. A Novel Synthesis of 4-Aminomethylcoumarins. *Synthesis (Stuttg).* **1986**, 214–216 (1986).
208. Léger, B., Nowicki, A., Roucoux, A. & Rolland, J.-P. Competitive hydrogenation/dehalogenation of halogenoarenes with surfactant-stabilized aqueous suspensions of rhodium and palladium colloids: A major effect of the metal nature. *J. Mol. Catal. A Chem.* **266**, 221–225 (2007).
209. Jourdant, A., González-Zamora, E. & Zhu, J. Wilkinson's Catalyst Catalyzed Selective Hydrogenation of Olefin in the Presence of an Aromatic Nitro Function: A Remarkable Solvent Effect. *J. Org. Chem.* **67**, 3163–3164 (2002).
210. Dyson, P. J. & Jessop, P. G. Solvent effects in catalysis: rational improvements of catalysts via manipulation of solvent interactions. *Catal. Sci. Technol.* **6**, 3302–3316 (2016).
211. David, A. & Vannice, M. A. Control of catalytic debenzylation and dehalogenation reactions during liquid-phase reduction by H2. *J. Catal.* **237**, 349–358 (2006).
212. Nittoli, T. & Markotan, T. P. Maytansinoid derivatives, conjugates thereof, and methods of use.
213. Phan, D. H. T., Kim, B. & Dong, V. M. Phthalides by Rhodium-Catalyzed Ketone Hydroacylation. *J. Am. Chem. Soc.* **131**, 15608–15609 (2009).
214. Hofslokken, N. U. & Skatteboel, L. Convenient Method for the ortho-Formylation of Phenols. *ACTA Chem. Scand.* **53**, 258–262 (1999).
215. Brahmachari, G. Room Temperature One-Pot Green Synthesis of Coumarin-3-carboxylic Acids in Water: A Practical Method for the Large-Scale Synthesis. *ACS Sustain. Chem. Eng.* **3**, 2350–2358 (2015).

216. Berthelot, T., Talbot, J.-C., Laïn, G., Déleris, G. & Latxague, L. Synthesis of Nε-(7-diethylaminocoumarin-3-carboxyl)- and Nε-(7-methoxycoumarin-3-carboxyl)-L-fmoc lysine as tools for protease cleavage detection by fluorescence. *J. Pept. Sci.* **11**, 153–160 (2005).
217. Greene, N. T. & Shimizu, K. D. Colorimetric Molecularly Imprinted Polymer Sensor Array using Dye Displacement. *J. Am. Chem. Soc.* **127**, 5695–5700 (2005).
218. Peng, H. *et al.* An unexpected copper catalyzed 'reduction' of an arylazide to amine through the formation of a nitrene intermediate. *Tetrahedron* **69**, 5079–5085 (2013).
219. Li, C. *et al.* Click Chemistry to Fluorescent Amino Esters: Synthesis and Spectroscopic Studies. *European J. Org. Chem.* **2010**, 2395–2405 (2010).
220. Buscher, T., Barroso, Á., Denz, C. & Studer, A. Synthesis and photo-postmodification of zeolite L based polymer brushes. *Polym. Chem.* **6**, 4221–4229 (2015).
221. Wanat, P. *et al.* Ethynyl, 2-Propynyl, and 3-Butynyl C-Phosphonate Analogues of Nucleoside Di- and Triphosphates: Synthesis and Reactivity in CuAAC. *Org. Lett.* **17**, 3062–3065 (2015).
222. Gadek, T. R. Trimethylsilyl triflate mediated introduction of phospholipid head groups. *Tetrahedron Lett.* **30**, 915–918 (1989).
223. Chan, T. R., Hilgraf, R., Sharpless, K. B. & Fokin, V. V. Polytriazoles as Copper(I)-Stabilizing Ligands in Catalysis. *Org. Lett.* **6**, 2853–2855 (2004).
224. Key, J. A. & Cairo, C. W. Identification of fluorogenic and quenched benzoxadiazole reactive chromophores. *Dye. Pigment.* **88**, 95–102 (2011).
225. Liu, B. & Thayumanavan, S. Substituent Effects on the pH Sensitivity of Acetals and Ketals and Their Correlation with Encapsulation Stability in Polymeric Nanogels. *J. Am. Chem. Soc.* **139**, 2306–2317 (2017).
226. Copeland, R. A., Harpel, M. R. & Tummino, P. J. Targeting enzyme inhibitors in drug discovery. *Expert Opin. Ther. Targets* **11**, 967–978 (2007).
227. Arenz, C. Small Molecule Inhibitors of Acid Sphingomyelinase. *Cell. Physiol. Biochem.* **26**, 1–8 (2010).
228. Mühle, C. *et al.* Characterization of Acid Sphingomyelinase Activity in Human Cerebrospinal Fluid. *PLoS One* **8**, 1–9 (2013).
229. Vanier, M. T. Niemann-Pick disease type C. *Orphanet J. Rare Dis.* **5**, 16 (2010).
230. Bhabak, K. P., Proksch, D., Redmer, S. & Arenz, C. Novel fluorescent ceramide derivatives for probing ceramidase substrate specificity. *Bioorganic Med. Chem.* (2012). doi:10.1016/j.bmc.2012.08.035
231. Greenspan, P., Mayer, E. P. & Fowler, S. D. Nile red: a selective fluorescent stain for intracellular lipid droplets. *J. Cell Biol.* **100**, 965–973 (1985).
232. Folch, J., Lees, M. & Stanley, G. H. S. A SIMPLE METHOD FOR THE ISOLATION AND PURIFICATION OF TOTAL LIPIDES FROM ANIMAL TISSUES. *J. Biol. Chem.* **226**, 497–509 (1957).
233. Lansmann, S. *et al.* Purification of acid sphingomyelinase from human placenta: Characterization and N-terminal sequence. *FEBS Lett.* **399**, 227–231 (1996).

List of publications

Journal Articles:

Mohamed, Z. H., El-Koussi, N. A., Mahfouz, N. M., Youssef, A. F., Abdel Jaleel, G. A., & Shouman, S. A., Cu (I) catalyzed alkyne-azide 1,3-dipolar cycloaddition (CuAAC): Synthesis of 17α-[1-(substituted phenyl)-1,2,3-triazol-4-yl]-19-nor-testosterone-17β-yl acetates targeting progestational and antipro-liferative activities, *European Journal of Medicinal Chemistry*, 2015, 97, 75–82.

Mohamed, Z. H., Soukka, T., Arenz, C., & Schäferling, M., Five-, Four- and Three-Dentate Europium Chelates for Anion Sensing and Their Applicability to Enzymatic Dephosphorylation Reactions, *ChemistrySelect*, 2018, 3(44), 12430–12439.

Mohamed, Z. H., Rhein, C., Saied, E. M., Kornhuber, J., & Arenz, C. (2018, November 1). FRET probes for measuring sphingolipid metabolizing enzyme activity, *Chemistry and Physics of Lipids*, 2018, 216**,** 152–161.

Naser E., Kadow S., Schumacher F., **Mohamed Z. H.**, Kappe C., Hessler G., Pollmeier B., Kleuser B., Arenz C., Becker K., Gulbins E., Carpinteiro A., Characterization of the small molecule ARC39, a direct and specific inhibitor of acid sphingomyelinase in vitro, *Journal of Lipid Research*, 2020, 61(6), 896–910.

Kappe, C., **Mohamed, Z. H.**, Naser, E., Carpinteiro, A., & Arenz, C., A Novel Visible Range FRET Probe for Monitoring Acid Sphingomyelinase Activity in Living Cells. *Chemistry - A European Journal*, 2020, 26(26), 5780–5783.

Poster contributions:

Z. H. Mohamed, Nawal A. El-Koussi, Nadia M. Mahfouz, Adel F. Youssef ''Design and Synthesis of 17α-(1-Substituted-1,2,3–Triazol-4-yl)-19- Nortestosterone Acetate Derivatives Using Click Chemistry'' Assiut University eighth Pharmaceutical Sciences Conference, 14 Mars 2012, Assiut, Egypt.

Z.H. Mohamed and Christoph Arenz'' Design and Synthesis of Novel FRET Probes for The Functional Analysis of The Acid Sphingomyelinase'' FEBS Special Meeting 2019 Sphingolipid Biology: Sphingolipids in Physiology and Pathology 6-10 May 2019, Cascais, Portugal.

Z.H. Mohamed and Christoph Arenz'' Probing the Activity of Sphingomyelinases by Fluorescence Resonance Energy Transfer (FRET)'' Euroanalysis XX Conference, September 1 st to 5 th, 2019, Istanbul, Turkey.

Curriculum Vitae

Removed for online publication.

Acknowledgements

All praises and thanks are to Allah, the Lord of all the worlds, the Most Beneficent, the Most Merciful for giving me the power to start and successfully complete this work.

While this thesis is presented in my name, I am indebted to many peoples and organizations who made the completion of this work possible. First of all, I'd like to thank my supervisor Prof. Dr. Christoph Arenz a lot for introducing me to this interesting area of Organic and Bioorganic Chemistry, for his readiness at all times to help and his critical suggestions, inspiring advices, scientific discussions, as well as for his tireless support and encouragement to participate in different fruitful collaborations. I must also mention the high degree of respect that he has been treating me throughout this period. I'm highly grateful for his readiness to financially support me in the last year until I have accomplished my projects. Moreover, I thank Dr. rer. nat. Ute Resch-Genger for her encouragement, valuable guidance and support. Furthermore, I thank Prof. Dr. Michael Schäferling for his co-supervising of my first project and providing me the opportunity to work independently and develop my scientific background in this research area in addition to his reputed reviewing of my thesis.

I am highly grateful to my group colleagues Essa Saied, Thomas Pinkert, Christian Kimmich Alexandra Klose-Stier, Christiane Schöniger, Susanne Plötz , Marcel Geufke, Fernando de Leon, Christian Kappe, Kevin Prause, Max Wilde, Doaa Samaha, Dr. Housam Haj Hamdo and Dr. Gita Naseri for the highly friendly working atmosphere and the helpful discussions. My thanks are also to Stephanie Diederich, Laura Marongiu, Danny Jeske for their technical assistance and help in biological experiments. My sincere thanks to Mrs. Sabine Herrmann for her support and administrative help throughout my stay time. Furthermore, I would like also to thank all the colleagues of the Seitz group, for helping with the use of different machines and provided useful scientific discussions regarding my work. Many thanks to all the colleagues of the Institute of Chemistry, Humboldt University of Berlin, for the excellent atmosphere and their help. I am grateful also for the colleagues of the Biophotonics department at the Federal Institute for Materials Research and Testing (BAM) for their valuable assistance and useful discussions as well as for the valuable experiments performed with their help.

My special thanks are dedicated to Mrs. Angela Thiesies, K. Pfaff, J. Hildebrandt and H. Steingräber for the NMR-measurements. Deep thanks also directed to Mr. Lutz Pospisil for his help in providing solvents, gases and technical supports.

I am very grateful to our collaborator Dr. Cosima Rhein at At Universitätsklinikum Erlangen, for the fluorescence microscopy studies of our probes. My deepest appreciation is also dedicated to our cooperating group of Dr. med. Alexander Carpinteiro, at University Hospital Essen. My deep thanks are directed to Eyad Naser for his efforts in *in vivo* characterization of our chemical tools.

My special thanks are also dedicated to the committee of my thesis: Prof. Dorothea Fiedler for reviewing my thesis, Prof. Rüdiger Tiemann the committee chairman, and Prof. Michael W. Linscheid the committee member.

I would like also to express my thanks to "SALSA, the Graduate School of Analytical Sciences Adlershof" for offering me their reputed scholarship. Special thanks directed to Mrs. Katharina Schultens, Esther Santel for the honest advices and continuous support throughout my fellowship. I am also highly grateful for the financial support of the Federal Institute for Materials Research and Testing (BAM) and my home university, Assiut university.

My heartfelt thanks to my beloved family. My *Mother* and older brother *Hassan* who I lost during this journey; my heart does not stop praying for you. Thanks to my brothers and sisters for their continuous support and encouragement. My invaluable gratefulness and love to my small family, my lovely wife *Doaa*, my son *Ali*, my daughter *Arwa* and my 8 months years old daughter *Fatima*.

Eidesstattliche Erklärung

Ich, Zainelabdeen H. M. Ahmed, erkläre, dass ich die Dissertation selbständig und nur unter Verwendung der von mir gemäß § 7 Abs. 3 der Promotionsordnung der Mathematisch-Naturwissenschaftlichen Fakultät, veröffentlicht im Amtlichen Mitteilungsblatt der Humboldt-Universität zu Berlin Nr. 42/2018 am 11.07.2018 angegebenen Hilfsmittel angefertigt habe.

Ort | Datum	Unterschrift
10.11.2020	
_____	_____